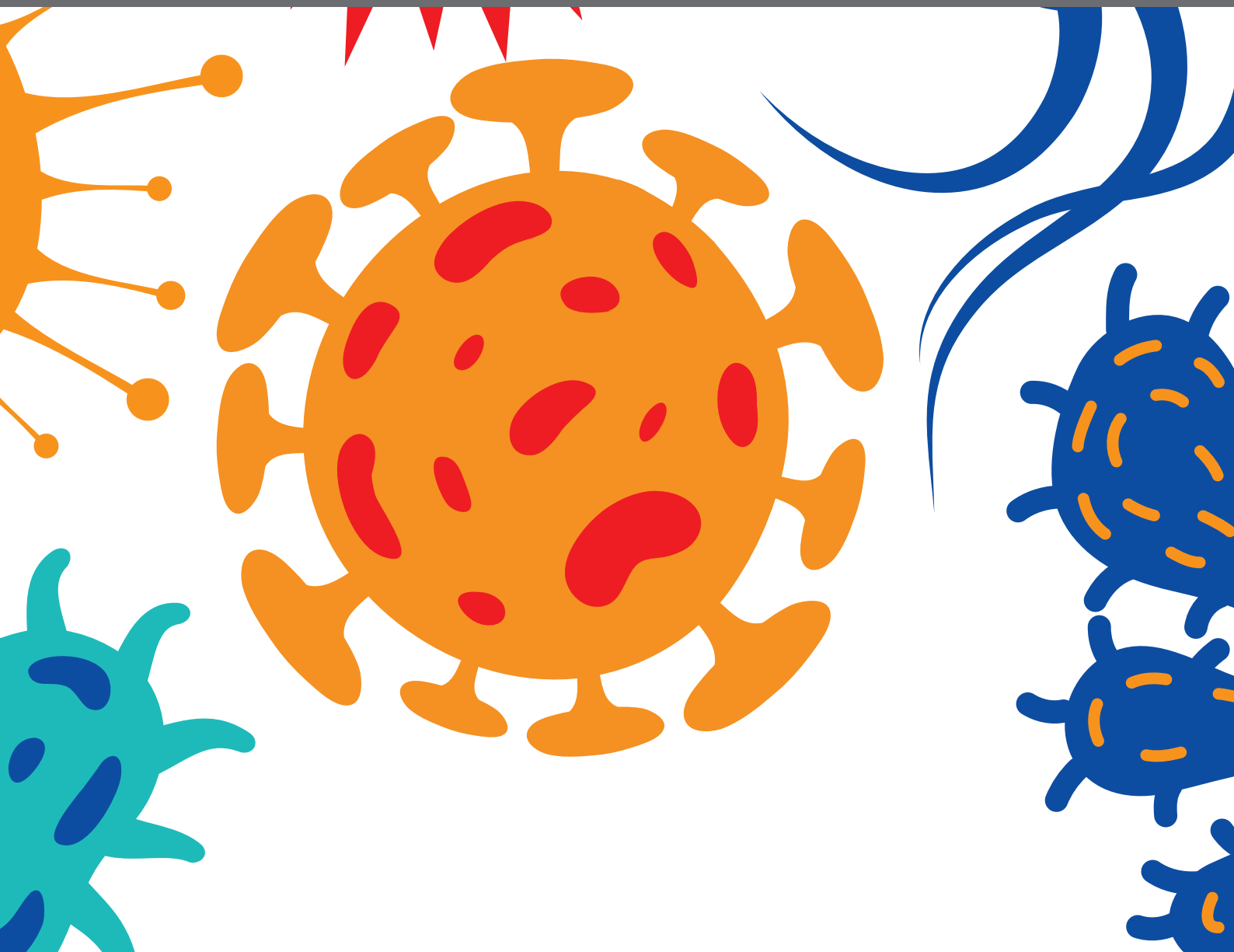


HOST/PARASITE MOLECULAR AND CELLULAR INTERACTIONS IN THE ESTABLISHMENT AND MAINTENANCE OF PROTOZOAN INFECTIONS

EDITED BY: Martin M. Edreira, Maria E. Francia and Natalia de Miguel
PUBLISHED IN: *Frontiers in Cellular and Infection Microbiology*





frontiers

Frontiers eBook Copyright Statement

The copyright in the text of individual articles in this eBook is the property of their respective authors or their respective institutions or funders. The copyright in graphics and images within each article may be subject to copyright of other parties. In both cases this is subject to a license granted to Frontiers.

The compilation of articles constituting this eBook is the property of Frontiers.

Each article within this eBook, and the eBook itself, are published under the most recent version of the Creative Commons CC-BY licence.

The version current at the date of publication of this eBook is CC-BY 4.0. If the CC-BY licence is updated, the licence granted by Frontiers is automatically updated to the new version.

When exercising any right under the CC-BY licence, Frontiers must be attributed as the original publisher of the article or eBook, as applicable.

Authors have the responsibility of ensuring that any graphics or other materials which are the property of others may be included in the CC-BY licence, but this should be checked before relying on the CC-BY licence to reproduce those materials. Any copyright notices relating to those materials must be complied with.

Copyright and source acknowledgement notices may not be removed and must be displayed in any copy, derivative work or partial copy which includes the elements in question.

All copyright, and all rights therein, are protected by national and international copyright laws. The above represents a summary only. For further information please read Frontiers' Conditions for Website Use and Copyright Statement, and the applicable CC-BY licence.

ISSN 1664-8714

ISBN 978-2-88976-367-2

DOI 10.3389/978-2-88976-367-2

About Frontiers

Frontiers is more than just an open-access publisher of scholarly articles: it is a pioneering approach to the world of academia, radically improving the way scholarly research is managed. The grand vision of Frontiers is a world where all people have an equal opportunity to seek, share and generate knowledge. Frontiers provides immediate and permanent online open access to all its publications, but this alone is not enough to realize our grand goals.

Frontiers Journal Series

The Frontiers Journal Series is a multi-tier and interdisciplinary set of open-access, online journals, promising a paradigm shift from the current review, selection and dissemination processes in academic publishing. All Frontiers journals are driven by researchers for researchers; therefore, they constitute a service to the scholarly community. At the same time, the Frontiers Journal Series operates on a revolutionary invention, the tiered publishing system, initially addressing specific communities of scholars, and gradually climbing up to broader public understanding, thus serving the interests of the lay society, too.

Dedication to Quality

Each Frontiers article is a landmark of the highest quality, thanks to genuinely collaborative interactions between authors and review editors, who include some of the world's best academicians. Research must be certified by peers before entering a stream of knowledge that may eventually reach the public - and shape society; therefore, Frontiers only applies the most rigorous and unbiased reviews.

Frontiers revolutionizes research publishing by freely delivering the most outstanding research, evaluated with no bias from both the academic and social point of view. By applying the most advanced information technologies, Frontiers is catapulting scholarly publishing into a new generation.

What are Frontiers Research Topics?

Frontiers Research Topics are very popular trademarks of the Frontiers Journals Series: they are collections of at least ten articles, all centered on a particular subject. With their unique mix of varied contributions from Original Research to Review Articles, Frontiers Research Topics unify the most influential researchers, the latest key findings and historical advances in a hot research area! Find out more on how to host your own Frontiers Research Topic or contribute to one as an author by contacting the Frontiers Editorial Office: frontiersin.org/about/contact

HOST/PARASITE MOLECULAR AND CELLULAR INTERACTIONS IN THE ESTABLISHMENT AND MAINTENANCE OF PROTOZOAN INFECTIONS

Topic Editors:

Martin M. Edreira, Universidad de Buenos Aires, Argentina

Maria E. Francia, Institut Pasteur de Montevideo, Uruguay

Natalia de Miguel, CONICET Instituto Tecnológico de Chascomús (INTECH), Argentina

Citation: Edreira, M. M., Francia, M. E., de Miguel, N., eds. (2022). Host/Parasite Molecular and Cellular Interactions in the Establishment and Maintenance of Protozoan Infections. Lausanne: Frontiers Media SA.
doi: 10.3389/978-2-88976-367-2

Table of Contents

- 05 Editorial: Host/Parasite Molecular and Cellular Interactions in the Establishment and Maintenance of Protozoan Infections**
Martin M. Edreira, Maria E. Francia and Natalia de Miguel
- 08 The Host Protein Aquaporin-9 is Required for Efficient Plasmodium falciparum Sporozoite Entry into Human Hepatocytes**
Nadia Amanzougaghene, Shahin Tajeri, Samir Yalaoui, Audrey Lorthiois, Valérie Soulard, Audrey Gego, Armelle Rametti, Véronica Risco-Castillo, Alicia Moreno, Maurel Tefit, Geert-Jan van Gemert, Robert W. Sauerwein, Jean-Christophe Vaillant, Philippe Ravassard, Jean-Louis Pérignon, Patrick Froissard, Dominique Mazier and Jean-François Franetich
- 20 The NF- κ B Pathway: Modulation by Entamoeba histolytica and Other Protozoan Parasites**
Attinder Chadha and Kris Chadee
- 32 Targeting Host Glycolysis as a Strategy for Antimalarial Development**
Andrew J. Jezewski, Yu-Hsi Lin, Julie A. Reisz, Rachel Culp-Hill, Yasaman Barekatain, Victoria C. Yan, Angelo D'Alessandro, Florian L. Muller and Audrey R. Odom John
- 46 Interaction With the Extracellular Matrix Triggers Calcium Signaling in Trypanosoma cruzi Prior to Cell Invasion**
Nubia Carolina Manchola Varón, Guilherme Rodrigo R. M. dos Santos, Walter Colli and Maria Julia M. Alves
- 59 Stage-Specific Class I Nucleases of Leishmania Play Important Roles in Parasite Infection and Survival**
Anita Leocadio Freitas-Mesquita and José Roberto Meyer-Fernandes
- 68 Leishmania Parasites Differently Regulate Antioxidant Genes in Macrophages Derived From Resistant and Susceptible Mice**
Haifa Bichiou, Sameh Rabhi, Cherif Ben Hamda, Cyrine Bouabid, Meriam Belghith, David Piquemal, Bernadette Trentin, Imen Rabhi and Lamia Guizani-Tabbane
- 79 Shedding of Trypanosoma cruzi Surface Molecules That Regulate Host Cell Invasion Involves Phospholipase C and Increases Upon Sterol Depletion**
Leonardo Loch, Thiago Souza Onofre, João Paulo Ferreira Rodrigues and Nobuko Yoshida
- 90 "Immunoinformatic Identification of T-Cell and B-Cell Epitopes From Giardia lamblia Immunogenic Proteins as Candidates to Develop Peptide-Based Vaccines Against Giardiasis"**
Thania Garzon, David Ortega-Tirado, Gloria Lopez-Romero, Efrain Alday, Ramón Enrique Robles-Zepeda, Adriana Garibay-Escobar and Carlos Velazquez
- 109 EhVps23: A Component of ESCRT-I That Participates in Vesicular Trafficking and Phagocytosis of Entamoeba histolytica**
Ausencio Galindo, Rosario Javier-Reyna, Guillermina García-Rivera, Cecilia Bañuelos, Sarita Montañó, Jaime Ortega-Lopez, Bibiana Chávez-Munguía, Lizbeth Salazar-Villatoro and Esther Orozco

- 125 *E-NTPDases: Possible Roles on Host-Parasite Interactions and Therapeutic Opportunities***
Lisvane Paes-Vieira, André Luiz Gomes-Vieira and
José Roberto Meyer-Fernandes
- 136 *Trypanosoma cruzi Induces B Cells That Regulate the CD4⁺ T Cell Response***
Martín Somoza, Adriano Bertelli, Cecilia A. Pratto, Ramiro E. Verdun,
Oscar Campetella and Juan Mucci
- 150 *Biological and Molecular Effects of Trypanosoma cruzi Residence in a LAMP-Deficient Intracellular Environment***
Anny Carolline Silva Oliveira, Luisa Rezende, Vladimir Gorshkov,
Marcella Nunes Melo-Braga, Thiago Verano-Braga,
Wesley Fernandes-Braga, Jorge Luís de Melo Guadalupe,
Gustavo Batista de Menezes, Frank Kjeldsen, Héliida Monteiro de Andrade
and Luciana de Oliveira Andrade
- 168 *TNF-TNFR1 Signaling Enhances the Protection Against Neospora caninum Infection***
Flávia Batista Ferreira França, Murilo Vieira Silva, Mariana Ferreira Silva,
Eliézer Lucas Pires Ramos, Vanessa dos Santos Miranda,
Caroline Martins Mota, Fernanda Maria Santiago, José Roberto Mineo and
Tiago Wilson Patriarca Mineo
- 179 *An Iron Transporter Is Involved in Iron Homeostasis, Energy Metabolism, Oxidative Stress, and Metacyclogenesis in Trypanosoma cruzi***
Claudia F. Dick, Nathália Rocco-Machado, André L. A. Dos-Santos,
Luiz F. Carvalho-Kelly, Carolina L. Alcantara, Narcisa L. Cunha-E-Silva,
José R. Meyer-Fernandes and Adalberto Vieyra
- 194 *Ablation of the P21 Gene of Trypanosoma cruzi Provides Evidence of P21 as a Mediator in the Control of Epimastigote and Intracellular Amastigote Replication***
Thaise Lara Teixeira, Miguel Angel Chiurillo, Noelia Lander,
Cassiano Costa Rodrigues, Thiago Souza Onofre, Éden Ramalho Ferreira,
Camila Miyagui Yonamine, Júlia de Gouveia Santos, Renato Arruda Mortara,
Claudio Vieira da Silva and José Franco da Silveira
- 205 *Trypanosoma cruzi Genomic Variability: Array Comparative Genomic Hybridization Analysis of Clone and Parental Strain***
Danielle Rodrigues Cortez, Fabio Mitsuo Lima, João Luís Reis-Cunha,
Daniella Castanheira Bartholomeu, Rolando Andre Rios Villacis,
Silvia Regina Rogatto, André Guilherme Costa-Martins,
Fernanda Sycko Marchiano, Rafaela Andrade do Carmo,
Jose Franco da Silveira and Marjorie Mendes Marini



Editorial: Host/Parasite Molecular and Cellular Interactions in the Establishment and Maintenance of Protozoan Infections

Martin M. Edreira^{1,2,3*}, Maria E. Francia^{4,5*} and Natalia de Miguel^{6,7*}

¹ Laboratorio de Biología Molecular de Trypanosomas, IQUIBICEN, CONICET-Universidad de Buenos Aires, Ciudad de Buenos Aires, Argentina, ² Departamento de Química Biológica, Facultad de Ciencias Exactas y Naturales, Universidad de Buenos Aires, Ciudad de Buenos Aires, Argentina, ³ Department of Pharmacology and Chemical Biology, School of Medicine, University of Pittsburgh, Pittsburgh, PA, United States, ⁴ Laboratory of Apicomplexan Biology, Institut Pasteur de Montevideo, Montevideo, Uruguay, ⁵ Departamento de Parasitología y Micología, Facultad de Medicina, Universidad de la República, Montevideo, Uruguay, ⁶ Laboratorio de Parásitos Anaerobios, Instituto Tecnológico de Chascomús (CONICET-UNSAM), Chascomús, Argentina, ⁷ Escuela de Bio y Nanotecnologías, Universidad Nacional de San Martín (UNSAM), Buenos Aires, Argentina

Keywords: Apicomplexa, Kinetoplastid, Anaerobic parasites, host-pathogen interaction, immune evasion, host cell subversion

Editorial on the Research Topic

Host/Parasite Molecular and Cellular Interactions in the Establishment and Maintenance of Protozoan Infections

OPEN ACCESS

Edited and reviewed by:

Tania F. De Koning-Ward,
Deakin University, Australia

*Correspondence:

Martin M. Edreira
mme2@pitt.edu
Maria E. Francia
mfrancia@pasteur.edu.uy
Natalia de Miguel
ndemiguel@intech.gov.ar

Specialty section:

This article was submitted to
Parasite and Host,
a section of the journal
Frontiers in Cellular and
Infection Microbiology

Received: 27 April 2022

Accepted: 06 May 2022

Published: 24 May 2022

Citation:

Edreira MM, Francia ME and
de Miguel N (2022) Editorial:
Host/Parasite Molecular and Cellular
Interactions in the Establishment and
Maintenance of Protozoan Infections.
Front. Cell. Infect. Microbiol. 12:930073.
doi: 10.3389/fcimb.2022.930073

INTRODUCTION

Protozoan parasites cause several human and veterinary diseases such as leishmaniasis, malaria, trypanosomiasis, toxoplasmosis, trichomoniasis and amebiasis, resulting in considerable morbidity and mortality worldwide, particularly affecting low-income countries. To establish successful infections in their hosts, protozoan parasites have developed a wide range of strategies. However, despite being of critical importance, the cellular and molecular mechanisms underlying host/parasite interactions are still not well understood.

Herein we briefly introduce a collection of 16 original research articles and literature reviews written by over 100 authors, reflecting the state of the art in host-pathogen interactions, highlighting different cellular and molecular mechanisms employed by protozoan parasites to establish a successful infection and thrive within their hosts

MULTI-SPECIES HOST- PARASITES INTERACTION

Parasite encoded Nucleotidases or NTPDases catalyze the hydrolysis of ATP to ADP. These cell-surface hydrolases have been shown to play multiple roles in parasite's infectivity and virulence by impacting purine salvage pathways and parasite adhesion to the host cell. The roles of NTPDases in parasite biology and their potential as drug targets in multiple species, including *Leishmania* spp., *Trypanosoma* spp., *Trichomonas vaginalis*, *Toxoplasma gondii* and *Schistosoma*, are reviewed by Paes-Vieira et al. This review highlights the promise of devoting efforts to improving the selectivity and specificity of compounds assayed against E-NTPDases from different parasites, as promising roads to elimination.

HOST-APICOMPLEXAN PARASITES INTERACTIONS

Apicomplexans, including parasites of the *Plasmodium* genus are obligate intracellular parasites. Different life forms of the *Plasmodium* parasites bear cell type specificity, with sporozoites invading liver cells and merozoites red blood cells, but it's unknown how the parasite distinguishes between cell types. Based on transcriptome analysis of hepatoma cells, which are refractory to parasite invasion, Amanzougaghene et al. postulate that the transmembrane protein Aquaporin-9 (AQP9) plays a significant role in facilitating *Plasmodium*'s invasion. AQP9 overexpression in hepatocytes increases their permissiveness to *P. falciparum*, while its downregulation increases their refractoriness. Interestingly, the dependence on AQP9 for invasion was shown to be species-specific.

While specific parasite proteins play essential roles in the invasion and survival within the host, metabolic pathways present in the host, which have co-evolved with the parasites, provide unexplored opportunities for intervention. It is well established that the outcome of clinical malaria is interdependent on erythrocyte metabolism. Chronic metabolic disorders affecting erythrocytes are positively selected in malaria endemic areas. However, the role of acute inhibition of metabolic pathways as plausible treatment strategies have not been extensively evaluated. Erythrocytes particularly rely on the enolase isozyme ENO2 for glycolytic function. Jezewskiet al., explore the effects of specific ENO2 inhibition by non-prodrugged phosphonates on parasite viability. They show that the significant antimalarial potency of each of three assayed compounds was highly correlated to their individual capacity to disrupt erythrocyte redox balance *in vitro*, and their degree of inhibitor-induced anemia *in vivo* in mice. Interestingly multi-resistant strains to antimalarials are sensitive to ENO2 inhibition).

Tumor necrosis factor (TNF) is a major inflammatory cytokine known to play pivotal roles in the responses mounted to parasitic infections, including those caused by apicomplexan and kinetoplastids parasites. Batista Ferreira França et al. evaluate the role of TNF in the cellular and humoral immune responses to the bovine abortigenic parasite *Neospora caninum*. Using mice lacking the TNF receptor, TNFR1, the authors demonstrate that lack of TNF induced signaling causes increased inflammation, increased parasite burden in the brain, whilst it reduces nitric oxide (NO) levels and IgG1 production. Overall, this study highlights the importance of TNF - TNF receptor 1 signaling during *N. caninum* infection.

HOST-KINETOPLASTID PARASITES INTERACTIONS

The molecular underpinnings of host immune response subversion are highlighted in many studies included in this topic. Freitas-Mesquita and Meyer-Fernandes review the multiple roles of stage-specific class I nucleases of the

Leishmania genus in subverting the host-cell defense. In addition, Bichiou et al. explore how *Leishmania* infection modulates macrophage response. Downstream targets of nuclear erythroid related factor 2 (Nrf2) are enzymes related to tolerance of the oxidative stress produced by the oxidative burst required to fight pathogens. The authors analyze the expression levels of NRF2 and its target genes in bone marrow derived macrophages isolated from *Leishmania*-resistant and *Leishmania*-susceptible mice (BMdMs), infected with *L. major* promastigotes. The study uncovers that *Leishmania* infection strongly induces the expression of NRF2 but does not affect the expression of heme oxygenase 1 (HO-1), a factor whose levels are known to affect parasite survival, in mice of different genetic backgrounds. Despite the induction of NRF2, Bichiou et al., report that the transcription of glutathione reductase (Gsr) and cysteine/glutamate exchange transporter (Slc7a11), involved in glutathione accumulation, are actively repressed in infected (susceptible) Balb/c BMdMs. In line with this observation, the study shows that silencing of NRF2 increases the survival and multiplication of the parasite, weakening the cell's ability to control the infection (Bichiou et al., 2021). In the case of *T. cruzi*, Somoza et al., demonstrate that trypomastigotes directly stimulated B cells that can modulate the development of a proinflammatory response by impairing their proliferation and inducing an apoptotic process in T CD4+ cells.

In addition to overcoming the immune system, and in order to establish a productive infection, different signaling pathways are activated by *T. cruzi* prior host cell invasion. Manchola Varón, et al., describe the involvement of calcium signaling in parasite interaction with the extracellular matrix at an early stage, and the organelles involved in calcium homeostasis during this interaction.

Extracellular vesicles, secreted surface proteins and enzymes involved in metabolism of *T. cruzi* have been shown to influence virulence and host cell invasion. Four original articles in this series tackle the roles of several *T. cruzi* encoded proteins, assaying their role in parasite survival. Loch et al., examine the differential release of gp82 and gp90 as well as their involvement in the shedding process and regulation of host cell invasion. Texeira et al., demonstrate that P21, a secreted protein with immunomodulatory properties, plays a role in facilitating invasion, but appears to negatively regulate amastigote proliferation in mammalian cells. Dick et al., have identified TcIT, a putative 39-kDa Fe transporter, and present evidence regarding its participation in Fe metabolism, proliferation/differentiation, virulence, and maintenance of *T. cruzi* infection. Finally, Silva Oliveira et al. reveal that changes in *T. cruzi* surface molecules are induced by the intracellular environment, which could confer adaptability to the parasite allowing it to infect specific tissues.

It is interesting to note that *T. cruzi* has shown to be a remarkably heterogeneous taxon, presenting extensive inter- and intrastrain genetic diversity and differential infectivity. Rodrigues Cortez et al., designed intraspecific array-based on comparative genomic hybridization to identify chromosomal regions harboring copy-number variations between two strains. The

authors discuss the genome plasticity which responds to environmental stress by varying gene copy number and generating segmental aneuploidy.

HOST-ANAEROBIC PARASITES INTERACTIONS

Protozoan parasites that reside extracellularly and in oxygen-deprived environments (anaerobic) within their hosts include enteric human pathogens such as *Giardia intestinalis*, *Entamoeba histolytica*, and the human and bovine urogenital tract parasites *Trichomonas vaginalis* and *Trichomonas foetus*, respectively. In this Research Topic, Chadha and Chadee present an update of the current situation regarding *Entamoeba histolytica* and other protozoan parasites that induce outside-in and inside-out signaling to modulate NF- κ B in disease pathogenesis and survival in the host. Additionally, Galindo et al., describe the role of *E. histolytica* ESCRT-I complex in vesicular trafficking and phagocytosis, as well as, the relationship between molecules involved in phagocytosis. The authors also demonstrate that phagocytosis is an important step in the mechanism of aggression by *E. histolytica* trophozoites during tissue invasion. Finally, Garzon et al., introduce the use of immunoinformatic approaches to identify and characterize potential T-cell and B-cell epitopes of *Giardia* immunogenic proteins. This bioinformatics analysis provides a deeper understanding of the *Giardia* immunogens that might bind to critical molecules of the host immune system. This approach could help develop novel strategies of peptide-based vaccines against giardiasis.

CLOSING REMARKS

We hope that the research showcased in this Research Topic highlights the importance of conceiving parasitic infections comprehensively within their natural context. The understanding of the mechanisms of pathogenesis is essential to unravel the complex co-evolved host-parasite biology underlying the deadly diseases highlighted herein, and could lead to effective rational strategies for the design of new and much needed therapies. Host-parasite interactions should remain a research priority in veterinary medicine and public health.

AUTHOR CONTRIBUTIONS

ME, MF, and ND drafted the manuscript. All authors contributed to manuscript revision, read, and approved the submitted version.

Conflict of Interest: The authors declare that the research was conducted in the absence of any commercial or financial relationships that could be construed as a potential conflict of interest.

Publisher's Note: All claims expressed in this article are solely those of the authors and do not necessarily represent those of their affiliated organizations, or those of the publisher, the editors and the reviewers. Any product that may be evaluated in this article, or claim that may be made by its manufacturer, is not guaranteed or endorsed by the publisher.

Copyright © 2022 Edreira, Francia and de Miguel. This is an open-access article distributed under the terms of the Creative Commons Attribution License (CC BY). The use, distribution or reproduction in other forums is permitted, provided the original author(s) and the copyright owner(s) are credited and that the original publication in this journal is cited, in accordance with accepted academic practice. No use, distribution or reproduction is permitted which does not comply with these terms.



The Host Protein Aquaporin-9 is Required for Efficient *Plasmodium falciparum* Sporozoite Entry into Human Hepatocytes

Nadia Amanzougaghene¹, Shahin Tajeri¹, Samir Yalaoui^{2,3}, Audrey Lorthiois^{2,3}, Valérie Soulard¹, Audrey Gego^{2,3}, Armelle Rametti^{2,3}, Véronica Risco-Castillo⁴, Alicia Moreno¹, Maurel Tefit¹, Geert-Jan van Gemert⁵, Robert W. Sauerwein⁵, Jean-Christophe Vaillant⁶, Philippe Ravassard⁷, Jean-Louis Pérignon^{2,3}, Patrick Froissard^{2,3†}, Dominique Mazier¹ and Jean-François Franetich^{1*}

OPEN ACCESS

Edited by:

Martin M. Edreira,
Universidad de Buenos Aires,
Argentina

Reviewed by:

Manuel Elkin Patarroyo,
Colombian Institute of Immunology
Foundation, Colombia
Gavin Wright,
Wellcome Sanger Institute (WT),
United Kingdom

*Correspondence:

Jean-François Franetich
jean-francois.franetich@upmc.fr

[†]Deceased

Specialty section:

This article was submitted to
Parasite and Host,
a section of the journal
Frontiers in Cellular and
Infection Microbiology

Received: 03 May 2021

Accepted: 02 June 2021

Published: 29 June 2021

Citation:

Amanzougaghene N, Tajeri S,
Yalaoui S, Lorthiois A, Soulard V,
Gego A, Rametti A, Risco-Castillo V,
Moreno A, Tefit M, van Gemert G-J,
Sauerwein RW, Vaillant J-C,
Ravassard P, Pérignon J-L,
Froissard P, Mazier D and
Franetich J-F (2021) The Host
Protein Aquaporin-9 Is Required
for Efficient *Plasmodium*
falciparum Sporozoite Entry
Into Human Hepatocytes.
Front. Cell. Infect. Microbiol. 11:704662.
doi: 10.3389/fcimb.2021.704662

¹ Sorbonne Université, INSERM, CNRS, Centre d'Immunologie et des Maladies Infectieuses, CIMI-Paris, Paris, France, ² Université Pierre et Marie Curie-Paris 6, UMR S945, Paris, France, ³ INSERM, U945, Paris, France, ⁴ Enva, UPEC, Anses, Dynamyc research group EA 7380, Maisons-Alfort, France, ⁵ Department of Medical Microbiology, Radboud University Nijmegen Medical Centre, MMB-NCMLS, Nijmegen, Netherlands, ⁶ AP-HP, Service de Chirurgie Digestive, Hépatobillo-Pancréatique et Transplantation Hépatique, Centre Hospitalo-Universitaire Pitié-Salpêtrière, Paris, France, ⁷ CR-ICM - LGN CNRS UMR-7991, IFR des Neurosciences, Groupe Hospitalier Pitié-Salpêtrière, Paris, France

Hepatocyte invasion by *Plasmodium* sporozoites represents a promising target for innovative antimalarial therapy, but the molecular events mediating this process are still largely uncharacterized. We previously showed that *Plasmodium falciparum* sporozoite entry into hepatocytes strictly requires CD81. However, CD81-overexpressing human hepatoma cells remain refractory to *P. falciparum* infection, suggesting the existence of additional host factors necessary for sporozoite entry. Here, through differential transcriptomic analysis of human hepatocytes and hepatoma HepG2-CD81 cells, the transmembrane protein Aquaporin-9 (AQP9) was found to be among the most downregulated genes in hepatoma cells. RNA silencing showed that sporozoite invasion of hepatocytes requires AQP9 expression. AQP9 overexpression in hepatocytes increased their permissiveness to *P. falciparum*. Moreover, chemical disruption with the AQP9 inhibitor phloretin markedly inhibited hepatocyte infection. Our findings identify AQP9 as a novel host factor required for *P. falciparum* sporozoite hepatocyte-entry and indicate that AQP9 could be a potential therapeutic target.

Keywords: *Plasmodium falciparum*, sporozoites, liver stage, hepatocytes, Aquaporin-9, CD81

INTRODUCTION

Of the protozoan parasites of humans, *Plasmodium falciparum* is the deadliest, accounting for an estimated 228 million cases of malaria and causing 405 000 deaths in 2018 (WHO | World malaria report 2018). After being inoculated in the skin of a host during the bite of an infected *Anopheles* mosquito, the sporozoite form of the parasite is quickly conveyed by the blood to the liver. Once there, it is sequestered *via* interactions with heparan sulphate proteoglycans (HSPGs), crosses the

endothelial barrier, and then migrates through several parenchymal cells before invading a hepatocyte by forming a membrane-bound compartment called the parasitophorous vacuole membrane (PVM), where it can develop and multiply to form merozoites that initiate the pathogenic erythrocytic cycle (Mota et al., 2001).

Sporozoite entry into hepatocytes is a highly complex process that involves coordinated interaction of sporozoite and host factors for initiation of infection, which may offer a multitude of promising therapeutic targets (Dundas et al., 2019). Currently, two major host cell surface proteins are well known to be involved in sporozoite invasion, the tetraspanin CD81 and the scavenger receptor class B type I (SR-BI) (Silvie et al., 2003; Rodrigues et al., 2008; Yalaoui et al., 2008a), but how they interact with specific parasite ligands remains largely unknown (Silvie et al., 2007). Moreover, the molecular events involved in sporozoite invasion are further complicated because they depend on the plasmodial species and the host cell type (Risco-Castillo et al., 2014). Indeed, CD81 is essential for *P. falciparum* and *P. yoelii* sporozoite invasion (Silvie et al., 2003) but is not required by *P. vivax*, which depends only on SR-BI. On the other hand, SR-BI is not required for *P. falciparum* and *P. yoelii* infections (Manzoni et al., 2017). However, *P. berghei* sporozoites can enter cells alternatively *via* either CD81 or SR-BI (Manzoni et al., 2017). The choice of route by which sporozoites invade hepatocytes has been shown to be determined by the parasite 6-cysteine domain protein P36 in a species-specific manner (Manzoni et al., 2017). In addition, SR-BI has been found to be essential for subsequent parasite development inside hepatocytes but not CD81 (Silvie et al., 2003; Rodrigues et al., 2008). Most recently, another host factor, aquaporin 3 (AQP3), which is a water and glycerol channel belonging to the aquaglyceroporin subfamily, has been implicated in the maturation of parasites after invasion (Posfai et al., 2018; Posfai et al., 2020).

Previous studies have shown that the human hepatocarcinoma HepG2 cells express SR-BI but not CD81, and as a consequence, they support infection by *P. berghei* but not by *P. falciparum* or *P. yoelii* sporozoites (Silvie et al., 2006b; Manzoni et al., 2017). Interestingly, ectopic expression of CD81 in HepG2 cells is sufficient to confer susceptibility to *P. yoelii* but not to *P. falciparum* sporozoites (Silvie et al., 2006b), implying the existence of additional host factors that are critical for *P. falciparum* infection.

The aim of this study was to identify host proteins required for successful infection of human hepatocytes by *P. falciparum* sporozoites. The approach adopted was that of a differential transcriptome analysis of naturally permissive human hepatocytes *versus* non-permissive hepatoma HepG2-CD81 cells. Among the most downregulated genes in the non-permissive cells, we focused on that coding for aquaporin-9 (AQP9), a water and glycerol channel previously shown to be involved in mice susceptibility to *P. berghei* blood stage infection (Liu et al., 2007). The contribution of AQP9 to the *Plasmodium* liver stage of *P. falciparum*, *P. yoelii* and *P. berghei* was investigated using primary human hepatocytes, human hepatoma cells and primary murine hepatocytes.

MATERIALS AND METHODS

Ethics Statement

Human hepatocytes were isolated from liver segments taken after oral informed consent was obtained from adult patients undergoing partial hepatectomy as part of their medical treatment (Service de Chirurgie Digestive, Hépatobilio-Pancréatique et Transplantation Hépatique, Hôpital Pitié-Salpêtrière, Paris, France). The collection and use of this material for the purposes of the study presented here were undertaken in accordance with French national ethical guidelines under Article L. 1121-1 of the “Code de la Santé Publique”. Given that the tissue samples were classed as surgical waste, they were used anonymously. Moreover, because they were not in any way genetically manipulated, article L. 1211-2 stipulates that their use for research purposes is allowed provided that the patient does not express any opposition to this to the surgeon prior to surgery after being informed of the nature of the research in which they might be potentially employed. The collection and use of this material were furthermore approved by the Institutional Review Board (Comité de Protection des Personnes) of the Centre Hospitalo-Universitaire Pitié-Salpêtrière, Assistance Publique-Hôpitaux de Paris, France. All animal care and procedures were carried out in strict accordance with the recommendations of the Guide for the Care and Use of Laboratory Animals of the European Union “European directive 86/609/EEC”. The protocol was approved by the Ethics Committee for Animal Experiments of University Pierre et Marie Curie, Paris 6, France (Permit Number: 75-1087).

RNA Isolation, Microarray Protocol and Differential Analysis of Transcriptomes

Three sets of human primary hepatocytes (**Supplementary Table 1**) were cultured for one week in a differentiation maintenance medium (complete medium for hepatocyte culture supplemented with 2% DMSO) (Isom et al., 1985). Hepatoma-derived HepG2-CD81 cells (Silvie et al., 2006b) from three different cultures were grown to subconfluence in 75 cm² flasks. Cells were lysed with TRIzol (Invitrogen, Life Technologies), and RNA was purified according to the manufacturer's instructions. RNA was equally purified from 1 g of human liver for use as a reference in all the microarray hybridizations. RNA concentration and purity were assessed using a NanoDropND-1000 Spectrophotometer (Thermo Scientific) and the Agilent 2100 Bioanalyser.

Transcriptomes of *P. falciparum* permissive human hepatocytes (HHs) and refractory HepG2-CD81 hepatoma cells (HCs) were analysed using a human 1A oligoarray kit (pangenomic human 22K DNA microarrays from Agilent Technologies, Les Ulis, France). Cyanine-labelled cDNA probes were synthesized from 20 µg of HH, HC, or total liver RNA using a CyScribe Post-Labeling kit (GE Healthcare Life Sciences, Vélizy, France). cDNA probes synthesized from cell RNAs were labelled with cyanine 3 (Cy3), while probes synthesized from the liver reference RNA were labelled with cyanine 5 (Cy5). Cy3- and Cy5-labelled probes were then co-hybridized to spots

on the same microarray. Signals were extracted using a Genepix 4000B scanner (Axon Instruments) and Genepix Pro 6.0 software and normalized with VARAN software (<http://www.bionet.espci.fr/varan/>), allowing calculation of the HH/HC intensity ratio for each targeted gene spotted on the microarray as the ratio of (HH/reference intensity ratio) *versus* (HC/reference intensity ratio). All microarray procedures were performed in accordance with the manufacturer's instructions. The CD81 synthetic oligonucleotide probe used here is complementary to the endogenous 5'-untranslated region of wild type CD81 but not to the ectopic CD81 expressed by the HepG2-CD81 cell line, therefore the probe recognizes only endogenous CD81 mRNA.

Hepatocytes, Hepatoma Cells and Cell Culture

Primary human hepatocytes were isolated from healthy parts of the liver fragments as previously described (Yalaoui et al., 2008a). Primary mouse hepatocytes were isolated as previously described (Yalaoui et al., 2008a) from AQP9^{-/-} mice backcrossed onto a C57BL/6J background and their AQP9^{+/+} littermate controls aged 7 to 10 weeks and gender matched (Rojek et al., 2007). These mice were kindly provided by Pr. S. Nielsen (Aarhus University, Aarhus, Denmark) and Pr. M. Amiry-Moghaddam (University of Oslo, Oslo, Norway). Human and mouse hepatocytes were seeded at a density of 8×10^4 cells and 4×10^4 cells, respectively, in 96-well microplates precoated with rat tail collagen I (Becton Dickinson) and cultured at 37°C in 5% CO₂ in William's E medium (Gibco, Life Technologies, Saint Aubin, France) supplemented with 2% penicillin-streptomycin, 1% sodium pyruvate, 1% L-glutamine, 1% insulin-transferrin-selenium, 1% non-essential amino acids (solutions for cell culture, Gibco) and 10% foetal bovine serum (FBS, Gibco). For human hepatocyte, the culture medium was also supplemented with 10^{-7} M dexamethasone (Sigma) and 2% DMSO. HepG2-CD81 (Bartosch et al., 2003; Silvie et al., 2006b) human hepatoma cells were cultured in DMEM (Gibco) supplemented with 10% FBS, 1% glutamine and 1% penicillin-streptomycin (Gibco). HepaRG human hepatoma cells, a gift from Pr. C. Guillouzo (INSERM, Rennes, France), were cultured in William's E medium (Gibco) supplemented with 1% penicillin-streptomycin, 1% L-glutamine, insulin (5 µg/ml), 5×10^{-5} M hydrocortisone and 10% FBS (Thermo Scientific, Villebon-sur-Yvette, France). Mouse and human hepatocytes as well as human hepatoma cells were cultured for at least 24 hours before further studies.

Plasmodium Parasites and In Vitro Infection

P. yoelii (265BY strain), *P. berghei* (PbGFPCON, ANKA strain) (Franke-Fayard et al., 2004) and *P. falciparum* (NF54 strain) sporozoites were obtained by dissection of salivary glands from infected *Anopheles stephensi* mosquitoes bred and infected in the insectary facilities of UMRS 945 (Paris, France) for rodent *Plasmodium*-infected mosquitoes and the Department of Medical Microbiology, Radboud University (Nijmegen,

Holland) for *P. falciparum*-infected mosquitoes. Infection assays were performed in 96-well plates. Cells were inoculated with 3×10^4 *P. falciparum* or 2×10^4 *P. berghei* or *P. yoelii* *Plasmodium* sporozoites per well and then centrifuged for 10 min at 2000 rpm to allow fast parasite sedimentation onto the target cells. After 3 hours at 37°C/5% CO₂, thus allowing sporozoite penetration into hepatocytes, cultures were washed and further incubated in fresh medium for 2 or 4 days (for *P. yoelii* and *P. berghei* or *P. falciparum*, respectively) until quantification of EEFs or directly fixed in PFA for quantification of parasite entry.

Gene Knockdown Using Small Interfering RNAs

For gene knockdown, we used small double-stranded RNA oligonucleotides (siRNAs) targeting human CD81 (sihCD81; 5'- GCA CCA AGT GCA TCA AGT A -3'), human AQP3 (AQP3_5 siRNA from Qiagen HP GenomeWide), human AQP9 (sihAQP9¹; 5'-CTG CTG ATC GTG GGA GAA A-3' and sihAQP9s^{2 to 5} corresponding respectively to siRNAs from Qiagen HP GenomeWide - AQP9_1 HP siRNA; AQP9_2 HP siRNA; AQP9_4 HP siRNA; AQP9_5 HP siRNA), and hCD92 (sihCD92; 5'- AAG GCA AGA ACT GAA AAC T -3'), used as a negative control. Primary hepatocytes were transfected with 30 nM siRNA in 96-well microplates using Lipofectamine RNAi MAX (Invitrogen) according to the manufacturer's recommendations. HepaRG cells (5×10^6 cells in 400 µl of RPMI) were transfected with 200 pmol of siRNA *via* electroporation (300 V, 500 µF) (Silvie et al., 2006a) using a Gene Pulser apparatus (Bio-Rad, Ivry, France). siRNA-transfected hepatoma cells or hepatocytes were then cultured for 48 hours before mRNA expression analysis or for 72 hours before protein expression or sporozoite infection efficiency analysis.

Lentiviral Vector Constructs and Cell Transduction

The lentiviral constructs pTRIP-CMV-hAQP9 ΔU3 and pTRIP-CMV-hCD81 ΔU3 were generated *via* gateway recombination cloning (Invitrogen). Briefly, hAQP9 and hCD81 coding sequences were PCR amplified and cloned into a pENTR/D/TOPO plasmid (Invitrogen) to generate entry clones. LR clonase II recombination was performed using the entry clones and the pTRIP-CMV-rfa Gateway ΔU3 destination vector as described previously (Russ et al., 2008). The pTRIP-CMV-GFP ΔU3 vector (Castaing et al., 2005) was used as a control. Lentiviral vector stocks were produced by transient transfection of 293T cells with the p8.91 encapsidation plasmid (Zufferey et al., 1997), the VSV glycoprotein-G encoding pHCMV-G plasmid (Yee et al., 1994), and the pTripΔU3 lentiviral vector as previously described (Zennou et al., 2000). Supernatants were treated with DNase I (Roche Diagnostics) prior to ultracentrifugation, and the resulting pellet was resuspended in PBS, separated into aliquots and frozen at 80°C until use. Primary human hepatocytes and hepatoma cells were transduced through addition of a 1:1000 concentrated lentiviral preparation. After an incubation period

of three hours, the cells were washed. Three days later, the cultures were processed for protein expression analysis as described in western blotting procedures or infected with sporozoites and cultured for four days until exo-erythrocytic forms (EEFs) quantification to evaluate hepatocyte permissiveness to *Plasmodium* infection.

Quantification of hAQP9 and hCD81 Transcripts via Real-Time PCR

RNA extractions were performed with a PureLink RNA Mini Kit (Ambion, Life Technologies) according to the manufacturer's recommendations. DNase treatment (PureLink DNase Set; Ambion, Life Technologies) was performed during the extraction. The quality and purity of RNAs were assessed with the Agilent 2100 Bioanalyser. Reverse transcription was realized with a SuperScript VILO cDNA Synthesis Kit (Invitrogen) according to the manufacturer's instructions, using 1 µg of RNA in a 20 µL final volume and duplicates for all samples. Quantitative real-time PCRs (qPCRs) were carried out using the SYBR Green method (SYBR GreenER qPCR SuperMix Universal, Invitrogen) with a MX3005P qPCR System (Agilent Technologies). The volume of cDNA used was equivalent to 100 ng of RNA per reaction, and the primers were used at a final concentration of 200 nM. Primer pairs based on the cDNA sequence were specifically designed for hAQP9 (5'-ttgcaacataccagctccgtatc-3' and 5'-accaaaggccctactacaggaat-3') and for hCD81 (5'-tcattcctgtttgcctgtgaggt-3' and 5'-tgagggtggtcaaagcagtcagt-3'). All samples were run in duplicate with the two different cDNAs synthesized, and gene expression data were normalized according to the level of *TBP* (TATA box-binding protein) (Ceelen et al., 2011).

Protein Expression Analysis via Western Blotting and Cell Immunofluorescence

Primary human hepatocytes were lysed at 4°C for 30 minutes in 30 mM Tris (pH 7.4), 150 mM NaCl, 0.02% NaN₃, protease inhibitors (PMSE, INH) and 1% Triton X-100. *CD81* and *AQP9* expression was analysed via western blotting using a mouse anti-hCD81 mAb (1:1000) and a mouse anti-m/hAQP9 mAb (G3, Santa Cruz) (1:100), respectively, followed by a goat anti-mouse Alexa Fluor 680 conjugate (Molecular Probes, Life Technologies) (1:15000). Monoclonal mouse anti-tubulin (Abcam) (1:5000) was used as a standard. Data were acquired and quantified with an Odyssey Infrared Imaging System (LI-COR Biosciences, Lincoln, NE).

Quantification of hCD81 and *AQP9* expression at the surface of human hepatocytes was performed as previously described for murine hepatocytes (Yalaoui et al., 2008a). Cells were washed with PBS, and immunolabelled for human AQP9 using a goat anti-hAQP9 (C18, Santa Cruz) antibody and a donkey anti-goat IgG-Alexa 488 conjugate antibody (Molecular Probes). CD81 was labelled with a mouse anti-hCD81 antibody (TS81, provided by Dr. E. Rubinstein, INSERM, Villejuif, France) and revealed with donkey anti-mouse IgG-Alexa 568 (Molecular Probes). Cell density was evaluated with diamidino-phenyl-indole (DAPI, Sigma) and used to normalize *CD81* expression. Fluorescence

intensity was acquired with a Flexstation Universal Microplate Reader (Molecular Devices, St Grégoire, France).

Quantification of Parasite Infection or Invasion via Immunofluorescence

After fixation of cultures with cold methanol, EEFs were identified using anti-HSP70 serum, prepared from mice immunized with a recombinant HSP70 protein (a gift from Pr. D. Mattei, Institut Pasteur, Paris, France), stained with an Alexa 488-conjugated or Alexa Fluor 680-conjugated goat anti-mouse immunoglobulin (Molecular Probes) and counted under a fluorescence microscope or using the Odyssey Infrared Imaging System as described previously (Gego et al., 2006). Nuclei were stained with 1 µg/ml DAPI. Quantification of parasite entry was carried out using double immunostaining with the appropriate mouse monoclonal anti-CSP antibody for *P. falciparum* CSP^{P. falciparum} and *P. yoelii* (CSP^{P. yoelii}) (Dr. Y. Charoenvit, Naval Medical Research Center; Silver Spring, MD), or a TRAP antibody for *P. berghei* (Dr. A. Crisanti, Imperial College, London, UK), thus allowing discrimination of intracellular and extracellular sporozoites, as previously described (Rénia et al., 1988; Silvie et al., 2002).

Sporozoite Cell Traversal Assay

Hepatocytic cell traversal was analysed using a dextran incorporation FACS assay (Prudêncio et al., 2008). Immediately after electroporation in the presence of siAQP9, siCD81, or siCD92, HepaRG cells were plated and cultivated in a 25 cm² culture flask at 37°C/5% CO₂. Forty-eight hours later, the cells were trypsinized for direct mRNA expression analysis or seeded in 48-well plates (8 × 10⁴ cells/well) for a cell traversal assay. After 24 hours, they were incubated with 10⁵ *P. yoelii* or *P. berghei* sporozoites for 2 hours or with 10⁵ *P. falciparum* sporozoites for 3 hours in the presence of rhodamine-dextran lysine fixable (10000 MW, Molecular Probes). After washing, the cells were trypsinized, fixed with 1% glutaraldehyde and analysed via FACS using an LSR Fortessa flow cytometer (BD Biosciences); 10⁴ cells were analysed (van Schaijk et al., 2008).

Infection Inhibition Assay With the AQP9 Inhibitor Phloretin

To assess the function of AQP9 in *Plasmodium* parasite infection, we tested the effect of phloretin (Sigma, Saint Quentin Fallavier, France), an inhibitor that restricts the solute permeability of AQP9 (Tsukaguchi et al., 1998; Yang and Verkman, 2002; Liu et al., 2007), on infection of human primary hepatocytes by *P. falciparum*. Phloretin was co-incubated with the sporozoites in the first 2 hours of the invasion step. Thereafter, the cells were incubated with fresh complete medium for three additional days until EEF quantification. Phloretin concentrations up to 500 µM were tested because this concentration has previously been shown to inhibit 60% of urea and glycerol transport (Tsukaguchi et al., 1998) and to not affect rat hepatocyte viability (Mosmann, 1983; Huebert et al., 2002). Using an MTT toxicity assay (Mosmann, 1983), we assessed that phloretin was not toxic to primary

human hepatocytes under the assay conditions (**Supplementary Figure 1**). We also assessed that phloretin was not toxic on *Plasmodium* sporozoites preincubated with different concentrations of phloretin (**Supplementary Figure 2**).

Data Analysis

GraphPad Prism 7 statistical Software (GraphPad. Software, San Diego, CA, USA) was used for data analysis and graphing. All values were expressed as means and standard deviations (SD). A *p*-value of 0.05 or less was considered as statistically significant.

RESULTS

Comparative Transcriptomics of *Plasmodium falciparum* Permissive and Non-Permissive Hepatocytes Identified AQP9 as a Candidate Host Protein Involved in Sporozoite Invasion

To identify novel host factors and further understand human hepatocyte susceptibility to *P. falciparum* sporozoite invasion, we performed differential transcriptomic analysis of naturally *P. falciparum*-permissive human hepatocytes (HHs) and refractory human hepatoma HepG2-CD81 cells (HCs) using microarray technology. Only genes downregulated in non-permissive hepatoma cells were taken into account. Our results showed that a total of 276 genes were downregulated in non-permissive hepatoma cells compared to the permissive hepatocytes, with HH/HC ratios higher than 3. A list of the top 30 downregulated genes with the highest ratios is presented in (**Supplementary Table 2**). As expected, *CD81* (with an HH/HC ratio of 14.7) was found to be among the most downregulated genes in hepatoma cells (**Figure 1A** and **Supplementary Figure 3A**). It should be noted that the *CD81* cDNA probe used on the DNA chips was designed to detect only endogenous *CD81* mRNA but not ectopic *CD81*. *SR-BI* (HH/HC=6) was also found amid the downregulated genes in hepatoma cells (**Figure 1A** and **Supplementary Figure 3A**). In contrast, the expression ratio of the irrelevant *CD9* gene (HH/HC=1.06), which is known as not involved in hepatocyte permissiveness to *Plasmodium* infection (Yalaoui et al., 2008b), was not changed (**Figure 1A** and **Supplementary Figure 3A**).

From evaluation of each candidate gene, *AQP9* which belongs to the aquaglyceroporin subfamily, a transmembrane channel protein that conducts water and glycerol (Liu et al., 2007), was selected for functional investigations, because it was among the most downregulated genes in the non-permissive HepG2 cells (**Figure 1A** and **Supplementary Figure 3A**), and evidence from a previous study showed it to be involved in mouse susceptibility to *P. berghei* blood stage infection (Liu et al., 2007). Interestingly, another aquaglyceroporin, *AQP3*, which was reported to be involved in *P. berghei* development within human hepatoma cells and in *P. vivax* development within human primary hepatocytes but is not essential for sporozoite invasion (Posfai et al., 2018; Posfai et al., 2020), was not found to be significantly differentially expressed between the two cell types (HH/HC ratio

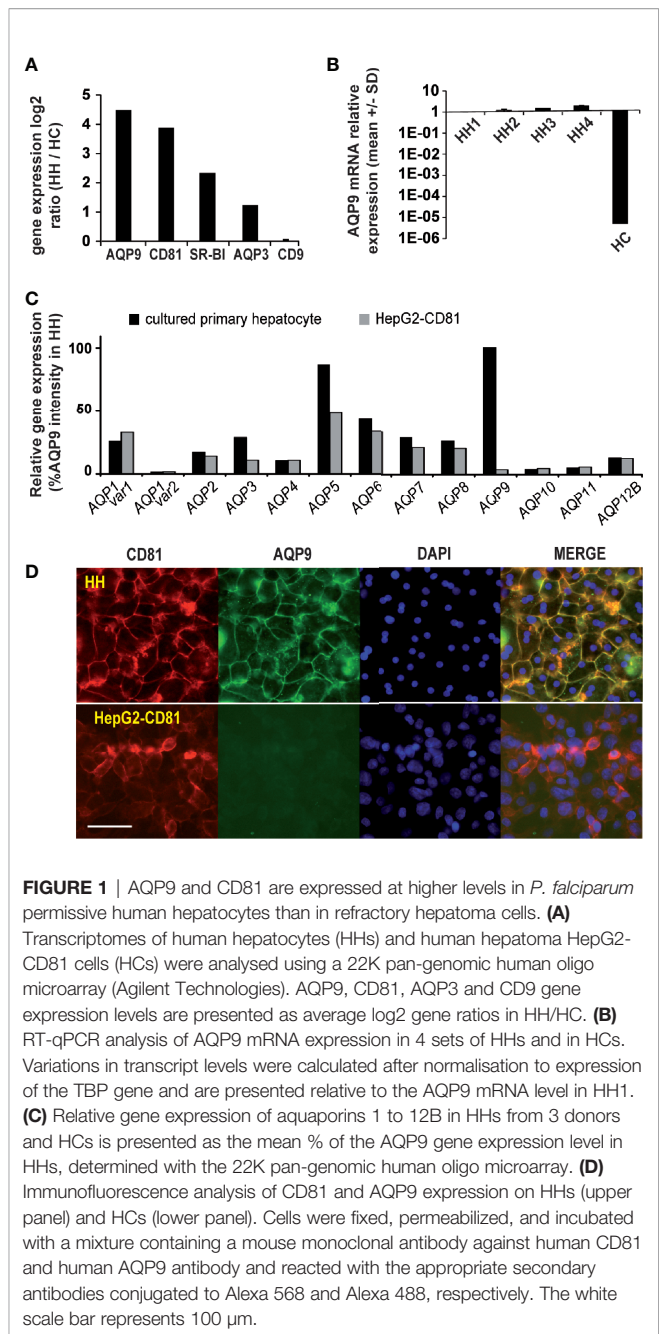


FIGURE 1 | AQP9 and CD81 are expressed at higher levels in *P. falciparum* permissive human hepatocytes than in refractory hepatoma cells. **(A)** Transcriptomes of human hepatocytes (HHs) and human hepatoma HepG2-CD81 cells (HCs) were analysed using a 22K pan-genomic human oligo microarray (Agilent Technologies). AQP9, CD81, AQP3 and CD9 gene expression levels are presented as average log2 gene ratios in HH/HC. **(B)** RT-qPCR analysis of AQP9 mRNA expression in 4 sets of HHs and in HCs. Variations in transcript levels were calculated after normalisation to expression of the TBP gene and are presented relative to the AQP9 mRNA level in HH1. **(C)** Relative gene expression of aquaporins 1 to 12B in HHs from 3 donors and HCs is presented as the mean % of the AQP9 gene expression level in HHs, determined with the 22K pan-genomic human oligo microarray. **(D)** Immunofluorescence analysis of CD81 and AQP9 expression on HHs (upper panel) and HCs (lower panel). Cells were fixed, permeabilized, and incubated with a mixture containing a mouse monoclonal antibody against human CD81 and human AQP9 antibody and reacted with the appropriate secondary antibodies conjugated to Alexa 568 and Alexa 488, respectively. The white scale bar represents 100 μ m.

of 2.3) (**Figure 1A**). The relatively high *AQP9* gene expression in primary hepatocytes was further confirmed in hepatocytes isolated from 4 additional donors using qPCR (**Figure 1B**; **Supplementary Table 1**). The expression of other aquaporin genes was not or was only moderately downregulated (**Figure 1C** and **Supplementary Figure 3B**). Moreover, immunofluorescence experiments showed that the drastic downregulation of the *AQP9* transcript in HepG2-CD81 cells was accompanied by a near total lack of protein expression (**Figure 1D**). Overall, as a membrane-bound protein highly expressed in infection-permissive cells and almost silent in non-permissive cells (**Figure 1D** and **Supplementary Figure 4**),

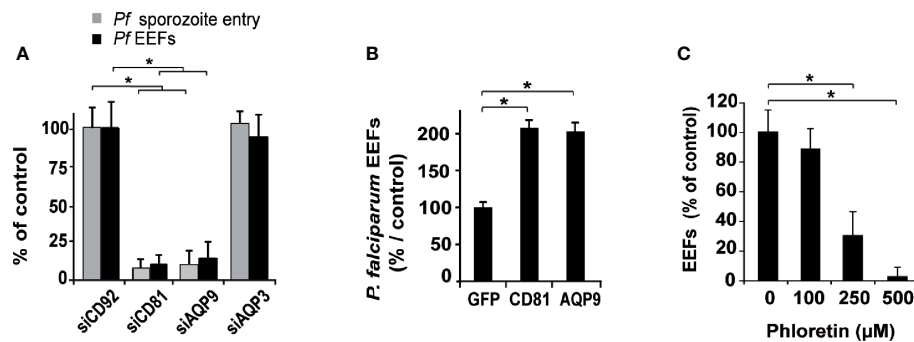


FIGURE 2 | Human hepatocyte permissiveness to *P. falciparum* sporozoite infection depends on AQP9 expression. **(A)** Hepatocytes were transfected with siRNAs and tested for their permissiveness to *P. falciparum* sporozoite infection: sihCD92-, sihCD81-, sihAQP9¹- and sihAQP3-transfected human hepatocytes were infected three days after transfection with *P. falciparum* sporozoites and cultured for 3 hours to evaluate sporozoite entry via double immunostaining for PICSP protein (grey bars) or for four days to evaluate cell infection after immunolabelling of EEFs using HSP70 antibody (black bars). Sporozoite and EEF numbers are expressed as a percentage of those in sihCD92-transfected control hepatocytes. $p = 0.0006$. **(B)** Hepatocytes overexpressing CD81 or AQP9 were tested for their permissiveness to *P. falciparum* infection: hepatocytes transduced with a lentiviral vector expressing GFP protein, as a control, hCD81, or hAQP9 were infected three days later with sporozoites and cultured for four days until EEF quantification. EEF numbers are expressed as a percentage of those in GFP-transduced control hepatocytes. The mean schizont numbers per well in controls of three independent experiments were 141, 203, and 314. $p = 0.05$. **(C)** Hepatocytes were treated for the first two hours following sporozoite inoculation with three doses of phloretin. Hepatocytes were then washed and incubated with fresh complete medium for three additional days until EEF quantification. EEF rates are relative to those in untreated hepatocytes. $p = 0.0009$. All analyses were carried out in triplicate wells, and the results are expressed as the mean \pm standard deviation. p values were determined by Mann-Whitney U test.

hepatocyte AQP9 is a candidate protein that could be involved in sporozoite entry into cells.

Aquaporin-9 Is Required for Efficient *P. falciparum* Sporozoite Entry Into Human Hepatocytes

To investigate the potential role of AQP9 in human hepatocyte infection by *P. falciparum* sporozoites, we performed AQP9 gene silencing using five small interfering RNAs (siRNAs). These siRNAs were first tested for their ability to ablate AQP9 gene expression in hepatocytes (Supplementary Figure 5A). sihCD92 and sihCD81 were used as negative and positive controls, respectively. Gene silencing procedure as well as sihCD92 which are routinely used in our laboratory have no impact on *Plasmodium* infection. Next, using western blotting and quantitative immunofluorescence, we confirmed that siAQP9 does not affect CD81 protein levels (Supplementary Figures 5A, B). Microscopic observation of the cultures transfected with either sihAQP9, sihCD81 or sihCD92 showed no obvious morphological alteration of the cells nor of the cell layer integrity (Supplementary Figure 6). Finally, we checked the efficiency of the five siRNAs in blocking sporozoite infection of hepatocytes (Supplementary Figure 5C). Silencing with sihAQP9^{1,3,5} resulted in an ~70% reduction in hepatocyte permissiveness to *P. falciparum* compared to the control sihCD92-treated hepatocytes. This reduction was similar to that obtained with sihCD81. sihAQP9⁴ caused an ~35% reduction in hepatocyte permissiveness, while sihAQP9² had no effect. The reduction in hepatocyte infectivity observed with sihAQP9s was proportional to the inhibition of AQP9 expression. Together, these results show that AQP9 and CD81 are individually required for *Plasmodium* infection but that neither is able to compensate for silencing of the other. We choose siAQP9¹ among the 3 siRNA

(siAQP9^{1,3} and ⁵) showing a potent and comparable silencing of AQP9 protein to be used for the rest of our experiments.

To further define the role of AQP9, we investigated its specific contribution to sporozoite entry into hepatocytes. Hepatocytes were inoculated with *P. falciparum* sporozoites three days after transfection, and their entry was evaluated by double immunostaining three hours post-sporozoite infection (Rénia et al., 1988; Silvie et al., 2002). The entry of parasites into sihAQP9- and sihCD81-treated hepatocytes was decreased by 90% and 92%, respectively, compared to sihCD92-treated cells (Figure 2A and Supplementary Figure 7A), and this inhibitory effect was similar to that observed for infection efficiency. In contrast, AQP3 gene silencing did not affect *Plasmodium* sporozoite infection or entry (Figure 2A and Supplementary Figure 7A), corroborating results obtained elsewhere (Posfai et al., 2018).

We then examined whether AQP9 overexpression might improve cell permissiveness to *P. falciparum* sporozoite infection, as overexpression of CD81 in hepatocytic cell lines did for rodent *Plasmodium* species (Silvie et al., 2006b). To this end, we transduced human hepatocytes that naturally express endogenous CD81 and AQP9 with a lentiviral vector allowing expression of CD81 or AQP9, and then cultured the hepatocytes for three days prior to *Plasmodium* sporozoite infection. Cells transduced with a vector encoding the irrelevant GFP protein were used as a control (GFP expression in liver cells was previously reported to not alter *Plasmodium* infection efficiency (Yalaoui et al., 2008b)). Overexpression of AQP9 (as assessed by western blotting, Supplementary Figure 8) induced a two-fold increase in hepatocyte permissiveness to *P. falciparum* infection compared with GFP-transduced hepatocytes, comparable to that of CD81 (Figure 2B). Pharmacologic inhibition of AQP9 by phloretin during the first two hours of

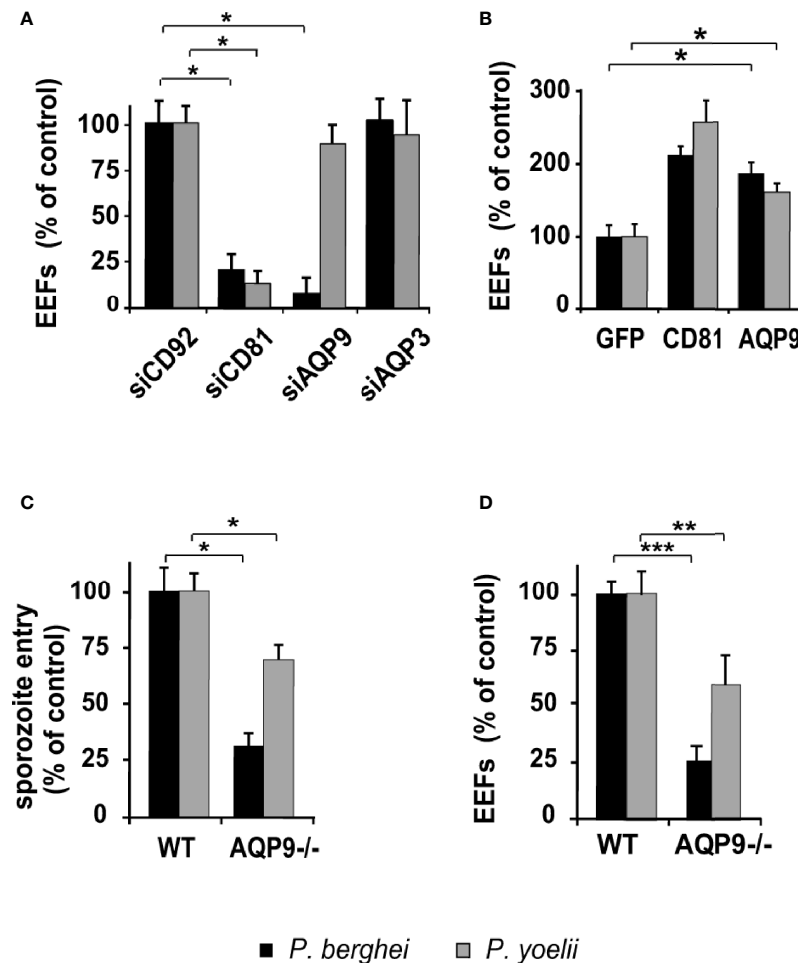


FIGURE 3 | Hepatocyte permissiveness to rodent parasites differentially depends on AQP9 according to parasite/host cell combinations. **(A)** siRNA-transfected human hepatocytes (HHs) were infected with sporozoites three days post-transfection and cultured for two days until EEf quantification. EEf values are expressed as a percentage of those in control siCD92-transfected hepatocytes. $*p = 0.0001$. **(B)** Three days post lentiviral transduction, HHs overexpressing GFP protein, hCD81, or hAQP9 were cultured for two days until EEf quantification. EEf numbers are expressed as a percentage of those in control GFP-transduced hepatocytes. $*p = 0.0079$. **(C, D)** Primary hepatocytes isolated from wild-type (WT) and AQP9 knockout (AQP9^{-/-}) mice were infected with *P. berghei* or *P. yoelii*. Sporozoite cell entry was evaluated 3 h post-infection using double immunostaining **(C)**, whereas EEf quantification was performed after 48 h of culture **(D)**. Penetration rates and EEf numbers are expressed as a percentage of those in control WT hepatocytes. $*p = 0.05$; $**p = 0.0018$; $***p = 0.0004$. The results are expressed as the mean \pm standard deviation. p values were determined by Mann-Whitney U test.

hepatocyte co-incubation with sporozoites resulted in a significant reduction in hepatocyte infection in a dose-dependent manner (Figure 2C). We also found that cell traversal of *P. falciparum* sporozoites was not affected by either CD81 or AQP9 silencing (Supplementary Figure 9A).

Since AQP9 RNA silencing induced a major, but incomplete, inhibition of *P. falciparum* infection, with 10 to 30% residual development of liver schizonts, we could assess whether AQP9 might play a role in the maturation of the parasite. SiAQP9¹-treated human hepatocytes infected by *P. falciparum* sporozoites were labelled four days post-inoculation with an anti-PfHSP70 antibody in order to measure the size of the schizonts.

Fluorescence microscopy analysis revealed that schizont diameters were similar in siCD92, siCD81 and siAQP9¹-treated hepatocytes (Supplementary Figure 10A).

Taken together, these data clearly provide evidence that AQP9 expression is important for *P. falciparum* sporozoite entry into human hepatocytes but have no influence on parasite development at the liver stage. Interestingly, the magnitude of the effect of AQP9 silencing in human hepatocytes on infection by *P. falciparum*, either on parasite entry or on the number of schizonts, is comparable to that of CD81 silencing. Similarly, both AQP9 overexpression and CD81 overexpression significantly enhance *P. falciparum* infection of human hepatocytes.

The Rodent Parasites *P. yoelii* and *P. berghei* Differentially Depend on AQP9 for Infection of Liver Cells

We further extended our experiments to study liver infection by the rodent malaria parasites *P. yoelii* and *P. berghei*. Given that the requirement for host proteins that confer permissiveness to *Plasmodium* infection may differ according to the species of the target cell (Silvie et al., 2007) and that *P. yoelii* and *P. berghei* sporozoites are capable of infecting human hepatocytes *in vitro* (Silvie et al., 2006b), the role of AQP9 was investigated in infection of human hepatocytes by these rodent *Plasmodium* species. The permissiveness of sihCD81- and sihAQP9¹-treated human hepatocytes to *P. berghei* infection was reduced by ~79% and ~92%, respectively. As expected, silencing of *CD81* reduced *P. yoelii* infection by ~87%, but surprisingly, silencing of *AQP9* did not affect *P. yoelii* infection (**Figure 3A** and **Supplementary Figure 7B**). In fact, the dramatic effect of *AQP9* silencing on infection by *P. berghei* was also somewhat unexpected, because it is well known that human HepG2 hepatoma cells can be readily infected by this parasite, despite undetectable *AQP9* expression. This paradox was further investigated in HepaRG cells that express *AQP9*. *P. berghei* infection of these cells was markedly decreased by *AQP9* RNA silencing (**Supplementary Figures 11A, B**), which suggests that this parasite uses *AQP9*-dependent pathways to invade human liver cells naturally expressing *AQP9* but is able to use alternative pathways in hepatoma cells that do not express *AQP9* (see **Table 1**). *CD81* or *AQP9* overexpression in human hepatocytes transduced with *CD81*- or *AQP9*-expressing lentiviral vectors led to an increase in the number of liver schizonts in each rodent species (**Figure 3B**). Finally, the availability of *AQP9* knockout mice prompted us to test permissiveness of primary hepatocytes isolated from wild-type or *AQP9* knockout mice to rodent *Plasmodium* sporozoites. The total lack of *AQP9* resulted in a reduction in hepatocyte permissiveness to *P. berghei* and *P. yoelii* infection by ~77% and ~34%, respectively (**Figure 3C**). Sporozoite entry was reduced by ~69% and ~30% for *P. berghei* and *P. yoelii* sporozoites, respectively (**Figure 3D**). Similar to *P. falciparum*, *AQP9* silencing had no effect on cell traversal (**Supplementary Figure 9B**). *P. berghei* schizont diameters measured two days post-infection were similar in *AQP9*-knockout and wild type hepatocytes (**Supplementary Figure 10B**) thus confirming that *AQP9* is not involved in parasite development at the liver stage.

Altogether, these results indicate that *P. berghei* and *P. yoelii* display differential dependence on *AQP9* for entry into hepatocytes. Indeed, *P. yoelii* invasion is found to not be or be poorly *AQP9*-dependent, whereas for *P. berghei*, invasion depends mainly on *AQP9*, at least in human liver cells that express this protein.

DISCUSSION

The first multiplicative stage of malaria parasites within their human host occurs exclusively in the hepatocyte *in vivo*, and this development can also be obtained *in vitro*. It is interesting that *CD81*-expressing human hepatoma HepG2 cells are permissive to productive infection by sporozoites of the rodent parasites *P. berghei* and *P. yoelii*, but not to productive infection by *P. falciparum* (Silvie et al., 2006a). This differential susceptibility was exploited to search for proteins responsible for the exclusive permissiveness of human hepatocytes to *P. falciparum* sporozoites. Comparison of the transcriptome of human hepatocytes with that of human hepatoma HepG2-*CD81* cells, which do not support *P. falciparum* sporozoite infection, led to identification of genes whose expression is downregulated in hepatoma cells. We focused our functional studies on *AQP9*, a membrane protein already suspected to be involved in the virulence of the rodent parasite *P. berghei* (Liu et al., 2007) and whose gene expression was one of those most downregulated in hepatoma cells. Our results demonstrate that *AQP9* is required for efficient *P. falciparum* sporozoite entry into human hepatocytes. Furthermore, we found that the rodent parasites *P. yoelii* and *P. berghei* differentially depend on *AQP9* and that this difference varies depending on the host cell type.

AQP9 is a member of the AQPs family, which consists of 13 distinct small hydrophobic membrane proteins with predominant roles in trans-cellular water transport in response to osmotic gradients (Verkman, 2005). Among the aquaporins, AQPs 3, 7, 9 and 10, referred to as aquaglyceroporins, also transport glycerol and other small uncharged solutes (Verkman, 2005). Human *AQP9* is widely expressed in the liver but also in other tissues, including the lung, spleen and leukocytes, whereas rodent *AQP9* has mainly been found at the basolateral hepatocyte plasma membrane facing the sinusoids (Huebert et al., 2002; Mazzone et al., 2006) and in a less abundant manner in other tissues, such as the testis, epididymis, spleen,

TABLE 1 | Summary of the role of *AQP9* in susceptibility to *Plasmodium* infection according to the different cell types and plasmodial species tested on the basis of RNA silencing experiments.

	Human				Mouse
	Human hepatocytes (CD81+/AQP9+)	HepG2 (CD81-/AQP9)	HepG2/CD81 (CD81+/AQP9)	HepaRG (CD81+/AQP9+)	Mouse hepatocytes (CD81+/AQP9+)
<i>P. falciparum</i>	AQP9-dependent	no infection	no infection	infection (role of AQP9 not tested)	no infection
<i>P. yoelii</i>	AQP9-independent	no infection	AQP9-independent	infection (role of AQP9 not tested)	AQP9-independent
<i>P. berghei</i>	AQP9-dependent	AQP9-independent	AQP9-independent	AQP9-dependent	AQP9-dependent

brain and lung (Ishibashi et al., 1998; Tsukaguchi et al., 1998; Elkjaer et al., 2000). By regulating water entry or entry of other small uncharged solutes and interacting with cytoskeleton elements and signalling cascades, the AQPs can influence cell morphology, volume, motility and migration (Saadoun et al., 2005; Holm et al., 2016). Therefore, they are considered potential therapeutic targets (Saadoun et al., 2005).

The results of our gene silencing experiments demonstrate that AQP9 expression is required for *P. falciparum* sporozoite infection of human hepatocytes, and this requirement appears to be of the same order of magnitude as it is for CD81, which thus far is the only hepatocyte surface molecule known to be strictly required for *P. falciparum* sporozoite infectivity (Silvie et al., 2003). Moreover, overexpression of AQP9, as well as of CD81, in human hepatocytes led to increased *P. falciparum* infection. From our previous studies on CD81 (Silvie et al., 2003) and the current results presented in this paper, one can conclude that *P. falciparum* require both CD81 and AQP9 to invade hepatocytes as the invasion is drastically hampered in the absence of one or other. There are two arguments that support this conclusion. First, diminishing expression levels of one does not impact on the other one. Second, the reduction in hepatocyte infectivity observed with the inhibition of the expression of either protein was proportional to its inhibition level, as none is able to compensate for silencing of the other, suggesting that these two proteins are operating independently and/or sequentially. While not tested here, it would be interesting to test whether simultaneous silencing of both AQP9 and CD81 proteins could result in a complete invasion-inhibition.

Additional experiments using the rodent parasites *P. yoelii* and *P. berghei* showed that the requirement for AQP9 varies with the species of the parasite and of the host cell. Thus, invasion of *P. berghei* sporozoites was more dependent on the presence of AQP9 than invasion of *P. yoelii* sporozoite in murine hepatocytes, and this effect was more pronounced when human hepatocytes were used. These findings differ from those obtained for CD81 dependence (Silvie et al., 2007). Indeed, when human hepatocytes are used, *P. yoelii* invasion is strictly dependent on CD81 but only poorly dependent on AQP9, whereas for *P. berghei*, invasion is mainly dependent on AQP9, at least in human liver cells that express this protein, as it is on CD81. It should be noted that *P. berghei* is strictly CD81-dependent for invasion of the mouse cell line Hepa 1.6 but CD81-independent when human hepatoma cell lines are used (Silvie et al., 2007).

Taken together, our results showed that AQP9 and CD81 are individually required for *Plasmodium* sporozoite infection, but that neither is able to compensate for the absence of the other. Moreover, the species specificity for *P. falciparum* and *P. berghei*, with a lesser impact on *P. yoelii*, suggest a distinct role for AQP9 to the functions of previously described CD81 or SR-BI (Silvie et al., 2003; Yalaoui et al., 2008a; Risco-Castillo et al., 2014; Manzoni et al., 2017), probably acting downstream to the events requiring both these host proteins. Furthermore, our findings strengthen previous observations that sporozoite entry into liver cells is a complex phenomenon and suggest that extrapolation of

results obtained with rodent models to human parasites should be carried out with caution. This complexity is consistent with the general view that entry of intracellular pathogens relies on plastic and dynamic interactions between various molecules at the cell surfaces of the pathogen and host, as illustrated for HIV, HCV, and *P. falciparum* merozoites (Cosset and Lavillette, 2011; Bartholdson et al., 2013) and for the role of CD81, SR-BI and CD9P-1 in hepatocyte invasion by *Plasmodium* sporozoites (Yalaoui et al., 2008a; Charrin et al., 2009).

Our experiments with human and rodent parasites showed that AQP9 plays a crucial role in sporozoite invasion but not in the cell traversal that precedes it. Similar results were reported for CD81, which was also found to not be required for migration of *P. falciparum* and *P. yoelii* sporozoites through cells (Silvie et al., 2003). Internalization of the *Plasmodium* sporozoite and the associated PVM formation through invagination of the host cell plasma membrane involves a series of finely orchestrated events, including gliding motility, moving junction formation, and penetration (Dundas et al., 2019). Several studies have shown that this invasion process, as is the case in other Apicomplexa parasites, requires not only the parasite's actin-myosin motor but also membrane reorganization and *de novo* polymerization of host actin at the entry site for anchoring the junction on which the parasite pulls to penetrate the host cell (Gonzalez et al., 2009; Gomes-Santos et al., 2012; Gaji et al., 2013). Interestingly, previous studies have shown that AQP9 plays a major role in processes involving dynamic membrane reorganization and actin polymerization (Loitto et al., 2002; Loitto et al., 2007). More importantly, studies of AQP9 inhibition have shown that it promotes cell membrane protrusions through its water transport function. It has been proposed that AQP9-induced water influx results in a pressure-driven forward push of the membrane, creating a gap that allows diffusion and polymerization of actin monomers (Loitto et al., 2009; Karlsson et al., 2013). In our study, the inhibitory effect observed with phloretin strongly suggests an important role for the transport of water, and possibly of other small molecules, in liver cell invasion by *Plasmodium* sporozoites. Although it is not clear how AQP9 functions to promote sporozoite invasion into hepatocytes, one could speculate that AQP9 might play an indirect role through actin polymerization, possibly through its water transport function. Interestingly, a similar mechanism has been reported for *Cryptosporidium parvum*, another intracellular apicomplexan parasite, in which the host aquaporin AQP1 has been shown to be crucial for entry of the parasite into cholangiocytes (Chen et al., 2005). More specifically, it was shown that AQP1 mediates the localized water influx that leads to the increase in cell volume and actin polymerization accompanying the membrane protrusion that allows *C. parvum* entry and PVM formation (Chen et al., 2005). Collectively, these data support a model in which AQP9, through its water permeation function and possibly permeation of other small molecules, induces the membrane reorganization and actin polymerization, likely at the entry site, required to permit invagination of the PVM and entry of the sporozoite. Additional studies will be necessary to confirm this hypothesis.

In conclusion, the present study demonstrates that the host protein AQP9 is involved in entry of *P. falciparum* (and of *P. berghei*) sporozoites into hepatocytes and suggests that this process may involve water transport and possibly other small molecules. Our findings also suggest that *P. falciparum* sporozoites are able to hijack hepatocyte membrane machinery to achieve internalization into the parasitophorous vacuole. Collectively, our data provide new insights into the complex cellular process required for *Plasmodium* infection of liver cells and may assist in the development of host factor-directed antimalarial therapies.

DATA AVAILABILITY STATEMENT

The original contributions presented in the study are included in the article/**Supplementary Material**. Further inquiries can be directed to the corresponding author.

ETHICS STATEMENT

The protocol was approved by the Ethics Committee for Animal Experiments of University Pierre et Marie Curie, Paris 6, France (Permit Number: 75-1087).

AUTHOR CONTRIBUTIONS

NA, J-FF, ST, SY, PF, and DM conceived, planned, and designed experiments. NA, J-FF, ST, SY, AL, VS, AR, AG, VR-C and MT conducted experiments. NA, J-FF, ST, SY, AL, VS, AG, AR, VR-C, AM, MT, G-JG, RS, J-CV, PR, J-LP, PF, and DM analyzed the data. J-FF, PF, G-JG, RS, J-CV, PR and DM provided essential materials. NA, J-FF, ST, SY, PF, J-LP and DM wrote the manuscript. All authors contributed to the article and approved the submitted version.

REFERENCES

- Bartholdson, S. J., Crosnier, C., Bustamante, L. Y., Rayner, J. C., and Wright, G. J. (2013). Identifying Novel Plasmodium Falciparum Erythrocyte Invasion Receptors Using Systematic Extracellular Protein Interaction Screens. *Cell. Microbiol.* 15, 1304–1312. doi: 10.1111/cmi.12151
- Bartosch, B., Vitelli, A., Granier, C., Goujon, C., Dubuisson, J., Pascale, S., et al. (2003). Cell Entry of Hepatitis C Virus Requires a Set of Co-Receptors That Include the CD81 Tetraspanin and the SR-B1 Scavenger Receptor. *J. Biol. Chem.* 278, 41624–41630. doi: 10.1074/jbc.M305289200
- Castaing, M., Guerci, A., Mallet, J., Czernichow, P., Ravassard, P., and Scharfmann, R. (2005). Efficient Restricted Gene Expression in Beta Cells by Lentivirus-Mediated Gene Transfer Into Pancreatic Stem/Progenitor Cells. *Diabetologia* 48, 709–719. doi: 10.1007/s00125-005-1694-6
- Ceelen, L., De Spiegelaere, W., David, M., De Craene, J., Vinken, M., Vanhaecke, T., et al. (2011). Critical Selection of Reliable Reference Genes for Gene Expression Study in the HepaRG Cell Line. *Biochem. Pharmacol.* 81, 1255–1261. doi: 10.1016/j.bcp.2011.03.004
- Charrin, S., Yalaoui, S., Bartosch, B., Cocquerel, L., Franetich, J.-F., Boucheix, C., et al. (2009). The Ig Domain Protein CD9P-1 Down-Regulates CD81 Ability to Support Plasmodium Yoelii Infection. *J. Biol. Chem.* 284, 31572–31578. doi: 10.1074/jbc.M109.057927
- Chen, X.-M., O'Hara, S. P., Huang, B. Q., Splinter, P. L., Nelson, J. B., and LaRusso, N. F. (2005). Localized Glucose and Water Influx Facilitates Cryptosporidium Parvum Cellular Invasion by Means of Modulation of Host-Cell Membrane Protrusion. *Proc. Natl. Acad. Sci. U. S. A.* 102, 6338–6343. doi: 10.1073/pnas.0408563102
- Cosset, F.-L., and Lavillette, D. (2011). Cell Entry of Enveloped Viruses. *Adv. Genet.* 73, 121–183. doi: 10.1016/B978-0-12-380860-8.00004-5
- Dundas, K., Shears, M. J., Sinnis, P., and Wright, G. J. (2019). Important Extracellular Interactions Between Plasmodium Sporozoites and Host Cells Required for Infection. *Trends Parasitol.* 35, 129–139. doi: 10.1016/j.pt.2018.11.008
- Elkjaer, M., Vajda, Z., Nejsum, L. N., Kwon, T., Jensen, U. B., Amiry-Moghaddam, M., et al. (2000). Immunolocalization of AQP9 in Liver, Epididymis, Testis, Spleen, and Brain. *Biochem. Biophys. Res. Commun.* 276, 1118–1128. doi: 10.1006/bbrc.2000.3505
- Franke-Fayard, B., Trueman, H., Ramesar, J., Mendoza, J., van der Keur, M., van der Linden, R., et al. (2004). A Plasmodium Berghei Reference Line That

FUNDING

SY was supported by a fellowship from the European Community. This work was supported in part by grants from the Agence Nationale pour la Recherche (ANR-6 BLAN-0378 and MaTuRe project) and the European Community (LSHP-CT-2005-012199/MALINV).

ACKNOWLEDGMENTS

The authors are indebted to Dr. Olivier Silvie for fruitful discussions and critical reading of the manuscript and to Dr. Georges Snounou for fruitful discussions. We are grateful to Mr. Thierry Houpert for his expertise and precious technical assistance with the maintenance of the Anopheles stephensi colony. Microarray hybridization and analysis were performed at the “Plateforme post-génomique de la Pitié-Salpêtrière”. We would like to thank Perrine Frere and Aurélien Dauphin for confocal microscopy assistance in the imaging facilities “Plateforme d’Imagerie Cellulaire Pitié-Salpêtrière (Shared Resource Facilities of CRICM, IFR14, IFR113, INSERM, UPMC). We also thank Catherine Blanc and Bénédicte Hoareau for flow cytometry assistance (Flow Cytometry Core CyPS, Université Pierre et Marie Curie & Groupe hospitalier Pitié-Salpêtrière).

In memory of Patrick Froissard who tragically left us during the course of this study.

SUPPLEMENTARY MATERIAL

The Supplementary Material for this article can be found online at: <https://www.frontiersin.org/articles/10.3389/fcimb.2021.704662/full#supplementary-material>

- Constitutively Expresses GFP at a High Level Throughout the Complete Life Cycle. *Mol. Biochem. Parasitol.* 137, 23–33. doi: 10.1016/j.molbiopara.2004.04.007
- Gaji, R. Y., Huynh, M.-H., and Carruthers, V. B. (2013). A Novel High Throughput Invasion Screen Identifies Host Actin Regulators Required for Efficient Cell Entry by *Toxoplasma Gondii*. *PLoS One* 8, e64693. doi: 10.1371/journal.pone.0064693
- Gego, A., Silvie, O., Franetich, J.-F., Farhati, K., Hannoun, L., Luty, A. J. F., et al. (2006). New Approach for High-Throughput Screening of Drug Activity on *Plasmodium* Liver Stages. *Antimicrob. Agents Chemother.* 50, 1586–1589. doi: 10.1128/AAC.50.4.1586-1589.2006
- Gomes-Santos, C. S. S., Itoe, M. A., Afonso, C., Henriques, R., Gardner, R., Sepúlveda, N., et al. (2012). Highly Dynamic Host Actin Reorganization Around Developing *Plasmodium* Inside Hepatocytes. *PLoS One* 7, e29408. doi: 10.1371/journal.pone.0029408
- Gonzalez, V., Combe, A., David, V., Malmquist, N. A., Delorme, V., Leroy, C., et al. (2009). Host Cell Entry by Apicomplexa Parasites Requires Actin Polymerization in the Host Cell. *Cell Host Microbe* 5, 259–272. doi: 10.1016/j.chom.2009.01.011
- Holm, A., Magnusson, K.-E., and Vikström, E. (2016). *Pseudomonas Aeruginosa* N-3-Oxo-Dodecanoyl-Homoserine Lactone Elicits Changes in Cell Volume, Morphology, and AQP9 Characteristics in Macrophages. *Front. Cell. Infect. Microbiol.* 6, 32. doi: 10.3389/fcimb.2016.00032
- Huebert, R. C., Splinter, P. L., Garcia, F., Marinelli, R. A., and LaRusso, N. F. (2002). Expression and Localization of Aquaporin Water Channels in Rat Hepatocytes. Evidence for a Role in Canalicular Bile Secretion. *J. Biol. Chem.* 277, 22710–22717. doi: 10.1074/jbc.M202394200
- Ishibashi, K., Kuwahara, M., Gu, Y., Tanaka, Y., Marumo, F., and Sasaki, S. (1998). Cloning and Functional Expression of a New Aquaporin (AQP9) Abundantly Expressed in the Peripheral Leukocytes Permeable to Water and Urea, But Not to Glycerol. *Biochem. Biophys. Res. Commun.* 244, 268–274. doi: 10.1006/bbrc.1998.8252
- Isom, H. C., Secott, T., Georgoff, I., Woodworth, C., and Mummaw, J. (1985). Maintenance of Differentiated Rat Hepatocytes in Primary Culture. *Proc. Natl. Acad. Sci. U. S. A.* 82, 3252–3256. doi: 10.1073/pnas.82.10.3252
- Karlsson, T., Bolshakova, A., Magalhães, M. A. O., Loitto, V. M., and Magnusson, K.-E. (2013). Fluxes of Water Through Aquaporin 9 Weaken Membrane-Cytoskeleton Anchorage and Promote Formation of Membrane Protrusions. *PLoS One* 8, e59901. doi: 10.1371/journal.pone.0059901
- Liu, Y., Promeneur, D., Rojek, A., Kumar, N., Frøkjaer, J., Nielsen, S., et al. (2007). Aquaporin 9 is the Major Pathway for Glycerol Uptake by Mouse Erythrocytes, With Implications for Malarial Virulence. *Proc. Natl. Acad. Sci. U. S. A.* 104, 12560–12564. doi: 10.1073/pnas.0705131104
- Loitto, V.-M., Forslund, T., Sundqvist, T., Magnusson, K.-E., and Gustafsson, M. (2002). Neutrophil Leukocyte Motility Requires Directed Water Influx. *J. Leukoc. Biol.* 71, 212–222.
- Loitto, V. M., Huang, C., Sigal, Y. J., and Jacobson, K. (2007). Filopodia Are Induced by Aquaporin-9 Expression. *Exp. Cell Res.* 313, 1295–1306. doi: 10.1016/j.yexcr.2007.01.023
- Loitto, V. M., Karlsson, T., and Magnusson, K.-E. (2009). Water Flux in Cell Motility: Expanding the Mechanisms of Membrane Protrusion. *Cell Motil. Cytoskeleton* 66, 237–247. doi: 10.1002/cm.20357
- Manzoni, G., Marinach, C., Topçu, S., Briquet, S., Grand, M., Tolle, M., et al. (2017). *Plasmodium* P36 Determines Host Cell Receptor Usage During Sporozoite Invasion. *eLife* 6, e25903. doi: 10.7554/eLife.25903
- Mazzone, A., Tietz, P., Jefferson, J., Pagano, R., and LaRusso, N. F. (2006). Isolation and Characterization of Lipid Microdomains From Apical and Basolateral Plasma Membranes of Rat Hepatocytes. *Hepatology* 43, 287–296. doi: 10.1002/hep.21039
- Mosmann, T. (1983). Rapid Colorimetric Assay for Cellular Growth and Survival: Application to Proliferation and Cytotoxicity Assays. *J. Immunol. Methods* 65, 55–63. doi: 10.1016/0022-1759(83)90303-4
- Mota, M. M., Pradel, G., Vandenberg, J. P., Hafalla, J. C., Frevert, U., Nussenzweig, R. S., et al. (2001). Migration of *Plasmodium* Sporozoites Through Cells Before Infection. *Science* 291, 141–144. doi: 10.1126/science.291.5501.141
- Posfai, D., Maher, S. P., Roesch, C., Vantaux, A., Sylvester, K., Péneau, J., et al. (2020). *Plasmodium* Vivax Liver and Blood Stages Recruit the Druggable Host Membrane Channel Aquaporin-3. *Cell Chem. Biol.* 27, 719–727. doi: 10.1016/j.chembiol.2020.03.009
- Posfai, D., Sylvester, K., Reddy, A., Ganley, J. G., Wirth, J., Cullen, Q. E., et al. (2018). *Plasmodium* Parasite Exploits Host Aquaporin-3 During Liver Stage Malaria Infection. *PLoS Pathog.* 14, e1007057. doi: 10.1371/journal.ppat.1007057
- Prudêncio, M., Rodrigues, C. D., Ataíde, R., and Mota, M. M. (2008). Dissecting In Vitro Host Cell Infection by *Plasmodium* Sporozoites Using Flow Cytometry. *Cell. Microbiol.* 10, 218–224. doi: 10.1111/j.1462-5822.2007.01032.x
- Rénia, L., Miltgen, F., Charoenvit, Y., Ponnudurai, T., Verhave, J. P., Collins, W. E., et al. (1988). Malaria Sporozoite Penetration. A New Approach by Double Staining. *J. Immunol. Methods* 112, 201–205. doi: 10.1016/0022-1759(88)90358-4
- Risco-Castillo, V., Topçu, S., Son, O., Briquet, S., Manzoni, G., and Silvie, O. (2014). CD81 Is Required for Rhoptry Discharge During Host Cell Invasion by *Plasmodium* Yoelii Sporozoites. *Cell. Microbiol.* 16, 1533–1548. doi: 10.1111/cmi.12309
- Rodrigues, C. D., Hannus, M., Prudêncio, M., Martin, C., Gonçalves, L. A., Portugal, S., et al. (2008). Host Scavenger Receptor SR-BI Plays a Dual Role in the Establishment of Malaria Parasite Liver Infection. *Cell Host Microbe* 4, 271–282. doi: 10.1016/j.chom.2008.07.012
- Rojek, A. M., Skowronski, M. T., Fuchtbauer, E.-M., Fuchtbauer, A. C., Fenton, R. A., Agre, P., et al. (2007). Defective Glycerol Metabolism in Aquaporin 9 (AQP9) Knockout Mice. *Proc. Natl. Acad. Sci. U. S. A.* 104, 3609–3614. doi: 10.1073/pnas.0610894104
- Russ, H. A., Bar, Y., Ravassard, P., and Efrat, S. (2008). In Vitro Proliferation of Cells Derived From Adult Human Beta-Cells Revealed by Cell-Lineage Tracing. *Diabetes* 57, 1575–1583. doi: 10.2337/db07-1283
- Saadoun, S., Papadopoulos, M. C., Hara-Chikuma, M., and Verkman, A. S. (2005). Impairment of Angiogenesis and Cell Migration by Targeted Aquaporin-1 Gene Disruption. *Nature* 434, 786–792. doi: 10.1038/nature03460
- Silvie, O., Charrin, S., Billard, M., Franetich, J.-F., Clark, K. L., van Gemert, G.-J., et al. (2006a). Cholesterol Contributes to the Organization of Tetraspanin-Enriched Microdomains and to CD81-Dependent Infection by Malaria Sporozoites. *J. Cell Sci.* 119, 1992–2002. doi: 10.1242/jcs.02911
- Silvie, O., Franetich, J.-F., Boucheix, C., Rubinstein, E., and Mazier, D. (2007). Alternative Invasion Pathways for *Plasmodium* Berghei Sporozoites. *Int. J. Parasitol.* 37, 173–182. doi: 10.1016/j.ijpara.2006.10.005
- Silvie, O., Greco, C., Franetich, J.-F., Dubart-Kupperschmitt, A., Hannoun, L., van Gemert, G.-J., et al. (2006b). Expression of Human CD81 Differently Affects Host Cell Susceptibility to Malaria Sporozoites Depending on the *Plasmodium* Species. *Cell. Microbiol.* 8, 1134–1146. doi: 10.1111/j.1462-5822.2006.00697.x
- Silvie, O., Rubinstein, E., Franetich, J.-F., Prenant, M., Belnoue, E., Renia, L., et al. (2003). Hepatocyte CD81 is Required for *Plasmodium falciparum* and *Plasmodium yoelii* Sporozoite Infectivity. *Nat. Med.* 9, 93–96. doi: 10.1038/nm0808
- Silvie, O., Semblat, J. P., Franetich, J. F., Hannoun, L., Eling, W., and Mazier, D. (2002). Effects of Irradiation on *Plasmodium falciparum* Sporozoite Hepatic Development: Implications for the Design of Pre-Erythrocytic Malaria Vaccines. *Parasite Immunol.* 24, 221–223. doi: 10.1046/j.1365-3024.2002.00450.x
- Tsukaguchi, H., Shayakul, C., Berger, U. V., Mackenzie, B., Devidas, S., Guggino, W. B., et al. (1998). Molecular Characterization of a Broad Selectivity Neutral Solute Channel. *J. Biol. Chem.* 273, 24737–24743. doi: 10.1074/jbc.273.38.24737
- van Schaijk, B. C. L., Janse, C. J., van Gemert, G.-J., van Dijk, M. R., Gego, A., Franetich, J.-F., et al. (2008). Gene Disruption of *Plasmodium falciparum* p52 Results in Attenuation of Malaria Liver Stage Development in Cultured Primary Human Hepatocytes. *PLoS One* 3, e3549. doi: 10.1371/journal.pone.0003549
- Verkman, A. S. (2005). More Than Just Water Channels: Unexpected Cellular Roles of Aquaporins. *J. Cell Sci.* 118, 3225–3232. doi: 10.1242/jcs.02519
- WHO | World Malaria Report 2018 WHO. Available at: <http://www.who.int/malaria/publications/world-malaria-report-2018/en/> (Accessed June 4, 2020).
- Yalaoui, S., Huby, T., Franetich, J.-F., Gego, A., Rametti, A., Moreau, M., et al. (2008a). Scavenger Receptor BI Boosts Hepatocyte Permissiveness to *Plasmodium* Infection. *Cell Host Microbe* 4, 283–292. doi: 10.1016/j.chom.2008.07.013
- Yalaoui, S., Zougbedé, S., Charrin, S., Silvie, O., Arduise, C., Farhati, K., et al. (2008b). Hepatocyte Permissiveness to *Plasmodium* Infection Is Conveyed by a Short and Structurally Conserved Region of the CD81 Large Extracellular Domain. *PLoS Pathog.* 4, e1000010. doi: 10.1371/journal.ppat.1000010
- Yang, B., and Verkman, A. S. (2002). Analysis of Double Knockout Mice Lacking Aquaporin-1 and Urea Transporter UT-B. Evidence for UT-B-Facilitated

- Water Transport in Erythrocytes. *J. Biol. Chem.* 277, 36782–36786. doi: 10.1074/jbc.M206948200
- Yee, J. K., Miyanohara, A., LaPorte, P., Bouic, K., Burns, J. C., and Friedmann, T. (1994). A General Method for the Generation of High-Titer, Pantropic Retroviral Vectors: Highly Efficient Infection of Primary Hepatocytes. *Proc. Natl. Acad. Sci. U. S. A.* 91, 9564–9568. doi: 10.1073/pnas.91.20.9564
- Zennou, V., Petit, C., Guetard, D., Nerhbass, U., Montagnier, L., and Charneau, P. (2000). HIV-1 Genome Nuclear Import is Mediated by a Central DNA Flap. *Cell* 101, 173–185. doi: 10.1016/S0092-8674(00)80828-4
- Zufferey, R., Nagy, D., Mandel, R. J., Naldini, L., and Trono, D. (1997). Multiply Attenuated Lentiviral Vector Achieves Efficient Gene Delivery *In Vivo*. *Nat. Biotechnol.* 15, 871–875. doi: 10.1038/nbt0997-871

Conflict of Interest: The authors declare that the research was conducted in the absence of any commercial or financial relationships that could be construed as a potential conflict of interest.

Copyright © 2021 Amanzougaghene, Tajeri, Yalaoui, Lorthiois, Soulard, Gego, Rametti, Risco-Castillo, Moreno, Tefit, van Gemert, Sauerwein, Vaillant, Ravassard, Pérignon, Froissard, Mazier and Franetich. This is an open-access article distributed under the terms of the Creative Commons Attribution License (CC BY). The use, distribution or reproduction in other forums is permitted, provided the original author(s) and the copyright owner(s) are credited and that the original publication in this journal is cited, in accordance with accepted academic practice. No use, distribution or reproduction is permitted which does not comply with these terms.



The NF- κ B Pathway: Modulation by *Entamoeba histolytica* and Other Protozoan Parasites

Attinder Chadha and Kris Chadee*

Departments of Microbiology, Immunology, and Infectious Diseases, Cumming School of Medicine, Snyder Institute for Chronic Diseases, University of Calgary, Calgary, AB, Canada

OPEN ACCESS

Edited by:

Martin M. Edreira,
Universidad de Buenos Aires,
Argentina

Reviewed by:

Carlos Rosales,
Universidad Nacional Autónoma de
México, Mexico

William Petri,
University of Virginia, United States

*Correspondence:

Kris Chadee
kchadee@ucalgary.ca

Specialty section:

This article was submitted to
Parasite and Host,
a section of the journal
Frontiers in Cellular and
Infection Microbiology

Received: 27 July 2021

Accepted: 27 August 2021

Published: 14 September 2021

Citation:

Chadha A and Chadee K (2021) The
NF- κ B Pathway: Modulation by
Entamoeba histolytica and
Other Protozoan Parasites.
Front. Cell. Infect. Microbiol. 11:748404.
doi: 10.3389/fcimb.2021.748404

Protozoan parasites have led to worldwide devastation because of their ability to cause infectious diseases. They have evolved as successful pathogens in part because of their remarkable and sophisticated ways to evade innate host defenses. This holds true for both intracellular and extracellular parasites that deploy multiple strategies to circumvent innate host defenses for their survival. The different strategies protozoan parasites use include hijacking the host cellular signaling pathways and transcription factors. In particular, the nuclear factor- κ B (NF- κ B) pathway seems to be an attractive target for different pathogens owing to their central role in regulating prompt innate immune responses in host defense. NF- κ B is a ubiquitous transcription factor that plays an indispensable role not only in regulating immediate immune responses against invading pathogens but is also a critical regulator of cell proliferation and survival. The major immunomodulatory components include parasite surface and secreted proteins/enzymes and stimulation of host cells intracellular pathways and inflammatory caspases that directly or indirectly interfere with the NF- κ B pathway to thwart immune responses that are directed for containment and/or elimination of the pathogen. To showcase how protozoan parasites exploits the NF- κ B signaling pathway, this review highlights recent advances from *Entamoeba histolytica* and other protozoan parasites in contact with host cells that induce outside-in and inside-out signaling to modulate NF- κ B in disease pathogenesis and survival in the host.

Keywords: *entamoeba histolytica*, macrophage, NF- κ B – nuclear factor kappa B, innate immunity, cytokine

INTRODUCTION

Protozoan parasites have been a major concern due to their ability to cause considerable mortality and morbidity in both humans and animals worldwide (Dorny et al., 2009; Dixon et al., 2011; Fletcher et al., 2012; Kelly, 2013). They are responsible for affecting more than 500 million people across the globe (Monzote and Siddiq, 2011). Although parasitic infection and death are a major cause of concern in developing countries, they are also responsible for causing significant illness in developed countries (Fletcher et al., 2012). The burden of human protozoan parasitic infections has been aggravated because of the lack of a licensed vaccine against any of the diseases these parasites cause. Moreover, prophylaxis and treatment are dependent on drugs, which are rendered ineffective in many cases due to the emergence of drug resistance warranting the search for replacements (Andrews et al., 2014).

Protozoan parasites are unicellular eukaryotic that either reside extracellularly or intracellularly in host cells. They have evolved as successful pathogens due to their remarkable ability to evade immune responses allowing them to escape adaptive humoral and cellular immunity (Sacks and Sher, 2002). For instance, *Toxoplasma gondii* (Lima and Lodoen, 2019), *Leishmania* (Gupta et al., 2013) and *Trypanosoma cruzi* (Cardoso et al., 2016) evade humoral antibody response by adopting an intracellular lifestyle, while antigenic variations, in the case of extracellular pathogens such as *Giardia* (Prucca and Lujan, 2009), African trypanosomes (Horn, 2014), and malarial parasites (Kyes et al., 2001) that express their antigens on the surface of red blood cells, help them overcome immune destruction.

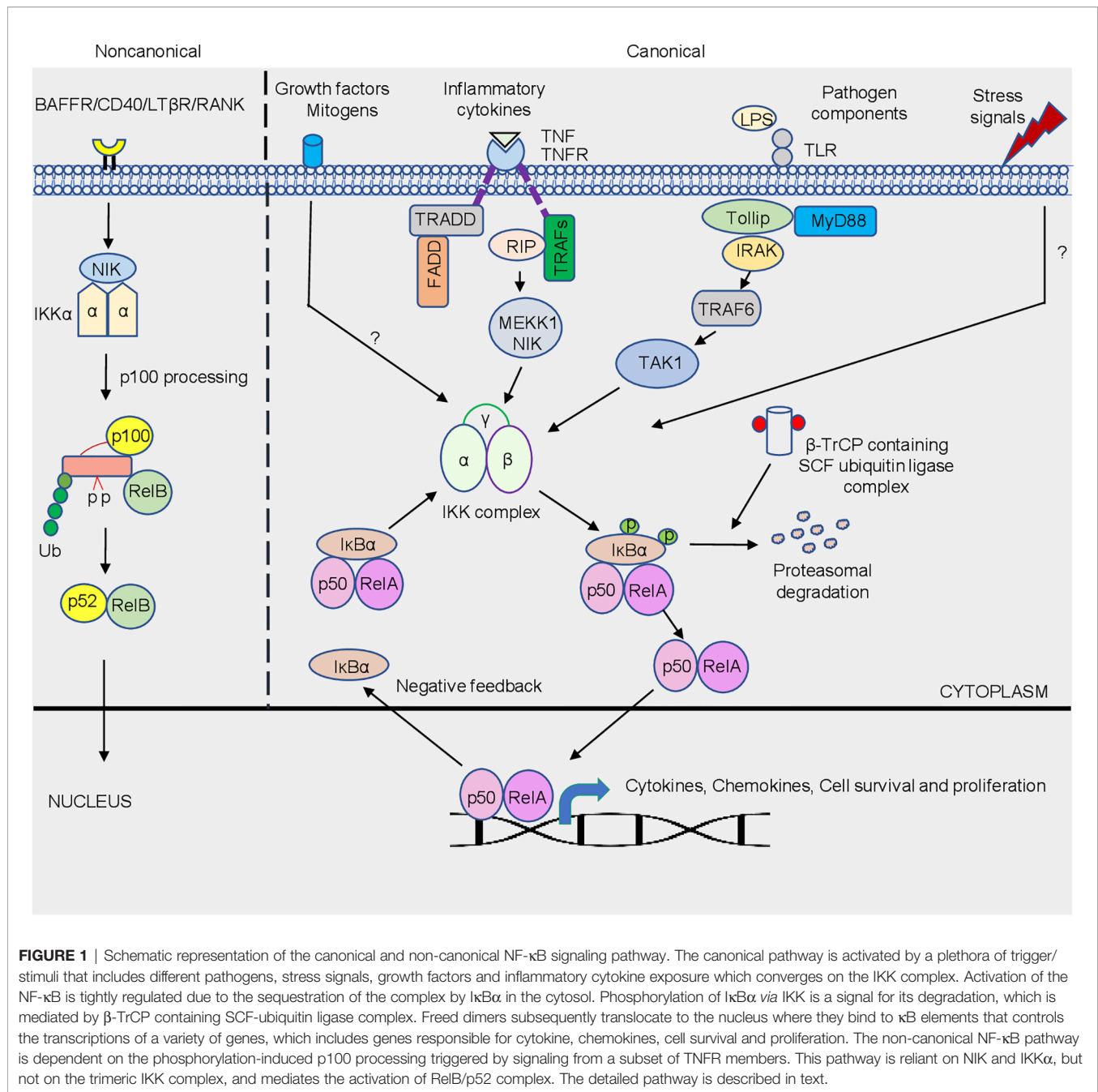
Although pathogens deploy different strategies for immune subversion, modulation of the NF- κ B pathway critical for generating an immune response seems to be a crucial target (Tato and Hunter, 2002). While the NF- κ B pathway is critical for mounting an immune response, pathogens have devised multiple ways to thwart this pathway to their advantage including, bacteria (Le Negrate, 2012), viruses (Santoro et al., 2003), and protozoan parasites (Heussler et al., 2001). Pathogens or their components have a remarkable ability for interfering with the NF- κ B pathway at multiple levels which includes, membrane-bound receptors to downstream signaling molecules of the pathway. Host-pathogen interaction can have multiple outcomes, but pathogens that circumvent signaling pathways seem to establish a successful niche for their replication and to cause disease. Both extracellular protozoan parasites *via* outside-in-signaling and intracellular protozoan parasites *via* inside-out-signaling have devised unique ways to overcome innate defense barriers by modulating the NF- κ B pathway at multiple levels. To understand the complex interaction whereby protozoan parasite interacts with the NF- κ B pathway, this review will focus on recent findings on modulation of NF- κ B signaling with the extracellular parasite *Entamoeba histolytica* (Eh) and the intracellular parasite, *T. gondii*.

THE NF- κ B PATHWAY

NF- κ B activation is a rapid event that occurs within minutes upon any trigger or stimulation that regulates a myriad of genes in host cells and does not require protein synthesis which makes this pathway an attractive target for invading pathogens (Santoro et al., 2003). NF- κ B regulates diverse cellular function (Figure 1) which includes, promoting inflammation, an early response to pathogen that plays an indispensable role in cell survival and proliferation (Karin et al., 2002; Li and Verma, 2002). It comprises of dimeric transcription factors belonging to the Rel family. Five Rel proteins belonging to two different classes have been identified in mammalian cells (Ghosh et al., 1998; Santoro et al., 2003). c-Rel, RelA (p65) and RelB belong to one class, that are synthesized as matured form, and contain an N-terminal Rel homology domain (RHD) responsible for dimerization and DNA binding, and C-terminus that possess transcription modulating domains (Verma et al., 1995; Santoro et al., 2003; Gilmore, 2006). Another class comprise of an N-terminal RHD and a C-terminal ankyrin repeat domain-containing p105 and

p100 precursor proteins that require ubiquitin-dependent processing at the C-terminus. Thus, the mature DNA-binding proteins of this class contain N-terminal RHD but lack C-terminus transcription modulating activity (Santoro et al., 2003; Gilmore, 2006). NF- κ B, whose predominant form p50 and RelA subunits, remains inactive in the cytoplasm because of its association with inhibitor proteins known as inhibitors of NF- κ B (I κ Bs), including I κ B α , I κ B β and I κ B ϵ (Verma et al., 1995; Ghosh et al., 1998; Santoro et al., 2003). The mechanism of NF- κ B activation is tightly regulated. Different stimuli or trigger, including bacterial, viral, and protozoan parasite infections may culminate in phosphorylation of I κ B proteins, leading to ubiquitination and proteasomal degradation of phosphorylated I κ B proteins (Figure 1). The degradation of I κ B sets free NF- κ B that translocates to the nucleus and binds to DNA to control the transcription of different genes including, cytokines, chemokines, antimicrobial peptides, anti-apoptotic proteins, and stress-response proteins. The NF- κ B pathway is activated by signaling through multiple receptors on the cell membrane. Amongst the different sensors, TLRs (Toll-like receptor) are important pathogen recognition receptors (PRR) that bind bacterial products and LPS (lipopolysaccharide) to initiate downstream signaling cascade culminating into NF- κ B activation. Binding of bacterial products/LPS to TLRs initiates downstream signaling leading to the recruitment of MyD88 (myeloid differentiation primary response gene 88), a death-domain containing adaptor protein and Toll-interacting protein Tollip (Silverman and Maniatis, 2001). The pro-inflammatory cytokine TNF (tumor necrosis factor)- α signals *via* the NF- κ B pathway. Cognate binding of TNF- α to type 1 TNF- α receptor (TNFR1) recruits the adaptor protein TNFR-associated death domain (TRADD) that acts as a docking site for the receptor interacting protein RIP and TNFR-associated factor TRAF2 that initiates downstream signaling (Chen and Goeddel, 2002). Further, downstream are MAP3K-related kinase which are thought to link receptor-complexes and stimulate an I κ B kinase (IKK) complex. TRADD also binds to Fas-associated death domain (FADD) that initiate a protease cascade culminating into apoptosis (Baud and Karin, 2001). Activation of the NF- κ B pathway (Figure 1) by different stimuli involves distinct scaffolding or signaling proteins, which, in addition to those mentioned above, include mitogen-activated protein kinase/extracellular signal-regulated kinase 1 (MEKK1), TNFR-associated factors (TRAFs), protein kinase C (PKC), transforming growth factor- β (TGF- β)-activated kinase (TAK1), NF- κ B-inducing kinase (NIK), interleukin (IL)-1-receptor-associated kinases (IRAKs), double-stranded (ds) RNA-dependent protein kinase (PKR) and several others (Silverman and Maniatis, 2001). Most of the above-mentioned proteins execute its effect by acting on another important downstream protein complex, the I κ B kinase (IKK) signalosome complex that plays an indispensable role in NF- κ B activation (Israël, 2000).

The IKK signalosome complex is a multi-subunit complex comprising of three distinctive subunits IKK- α , IKK- β , and IKK- γ (Figure 1). IKK- α and IKK- β form the catalytic center of the complex that exist either as a homo- or heterodimers, and with



IKK- γ or NEMO (NF- κ B essential modulator) forms the regulatory subunit, that acts as a docking site for the other signaling protein or IKK kinase (Rothwarf et al., 1998; Israël, 2000; Santoro et al., 2003). Integrity of IKK- γ is required for NF- κ B activation. The mechanism of NF- κ B activation is well orchestrated by serine phosphorylation of IKK- β subunit that is mediated by upstream kinases or through trans autophosphorylation of IKK subunits. Autophosphorylation of IKK- β at the C-terminal serine cluster prevents prolonged NF- κ B activation, thus acting as a negative feedback regulation (Delhase et al., 1999). The phosphorylation of I κ B at N-terminal Ser 32 and Ser 36 (Karin and Ben-Neriah, 2000), mediated by IKK, leads to

proteasomal degradation of the inhibitory subunit by 26S proteasome, resulting in NF- κ B activation. β -transducin repeat-containing protein (β -TrCP) containing SCF (Skp1, Cdc53/cullin, and F box protein) ubiquitin ligase mediates the ubiquitination of phosphorylated I κ B at Lys21 and Lys22 (Liang et al., 2004). In general, bacterial and viral infections triggered NF- κ B activation is mediated by IKK- β . In contrast, a unique regulatory mechanism of the NF- κ B pathway *via* the non-canonical arm predominantly targets activation of RelB/p52 subunit (Senftleben et al., 2001). Unlike the canonical pathway that responds to signals elicited by diverse receptors, the non-canonical pathway is targeted

by a specific set of receptors (Sun and Harhaj, 2006). The best-characterized non-canonical NF- κ B receptors include a subset of the TNFR superfamily members, including B-cell-activating factor belonging to the TNF family receptor (BAFFR; Claudio et al., 2002), lymphotoxin β -receptor (LT β R; Dejardin et al., 2002), receptor activator for NF- κ B (RANK; (Novack et al., 2003) and CD40 (Coope et al., 2002). In resting cells, RelB associates with NF- κ B2 p100 polypeptide in the cytoplasm whose C-terminal ankyrin repeat undergoes degradation upon stimulation, releasing RelB-p52 dimers that translocate to the nucleus (Senftleben et al., 2001; **Figure 1**). Activation of this process is mediated by the IKK- α subunit, unlike the canonical NF- κ B pathway which is primarily mediated by IKK- β . NIK is a central signaling component of the non-canonical pathway, which integrates signals from a subset of TNF receptor family members and activates a downstream kinase, IKK α , for triggering phosphorylation of p100 and its processing (Sun, 2011). Following activation, NF- κ B translocates to the nucleus where it binds to DNA consensus sequence 5'-GGGACTTCC-3' (κ B elements; **Figure 1**). NF- κ B transcriptional activity is greatly enhanced by the phosphorylation of RelA by protein kinase A (PKA) that facilitates its association with the transcriptional coactivator CBP/p300 (Zhong et al., 1998). Importantly, acetylation of NF- κ B was described as an additional regulatory mechanism for the activity of NF- κ B (Chen et al., 2001).

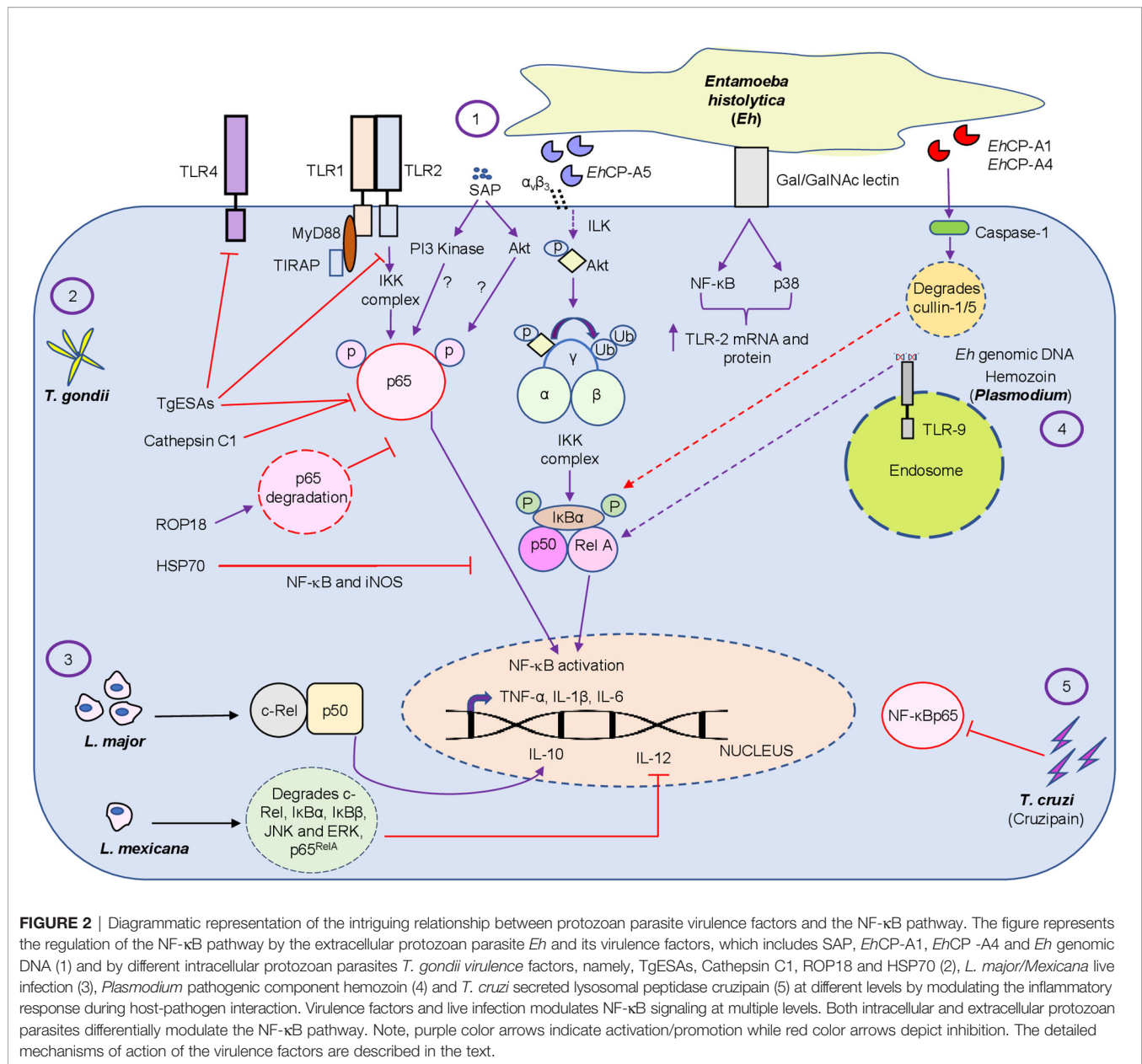
NF- κ B REGULATION DURING *ENTAMOEBA HISTOLYTICA* INFECTION

E. histolytica (*Eh*) is an extracellular protozoan parasite and the causative agent of the disease amebiasis. *Eh* infects ~10% of the world population leading to 100,000 deaths/year (Stanley Jr, 2003). Though the disease is a concern worldwide, it is more prevalent in developing countries due to poor sanitation and nutrition (Mahmud et al., 2013). Although multiple factors contribute to disease pathogenesis, it is primarily determined by the efficacy and quality of the host immune response. For undetermined reasons, ~10% of *Eh* infection sporadically breaches innate mucosal barriers and invades the lamina propria. *Eh* disease pathogenesis is the result of the dynamic interaction of *Eh* with different components of the immune system and the expression of *Eh* virulence factors (Faust and Guillen, 2012; Verkerke et al., 2012; Marie and Petri Jr, 2014; Ghosh et al., 2019; Rosales, 2021). When *Eh* breaches the innate protective mucus barrier (Moncada et al., 2003; Mortimer and Chadee, 2010; Begum et al., 2020a) it comes into direct contact with mucosal epithelial cells and subepithelial macrophages and dendritic cells. Here, NF- κ B signaling from epithelial and immune cells plays an indispensable role in shaping the pro-inflammatory landscape during infection (Kammanadiminti and Chadee, 2006; Kammanadiminti et al., 2007; Hou et al., 2010; Begum et al., 2020b). *Eh* components or live *Eh* in direct contact with epithelial cells or macrophages can modulate cellular functions. For example, Caco-2 and T84 human colonic epithelial cells cocultured with differentiated THP-1 macrophages for 24h, followed by stimulation with soluble

amebic proteins (SAP) augmented Hsp 27 and 72. In this interaction, Hsp27 played an important role in inhibiting the NF- κ B pathway because of its association with the IKK complex while Hsp72 inhibited apoptosis (Kammanadiminti and Chadee, 2006). This may in part, explain why colonic inflammation is not robust in the majority of individuals with intestinal amebiasis. This interaction is not unique to *Eh* as the inhibitory effects of heat shock proteins (Hsp) on NF- κ B activation was shown in T-cells (Guzhova et al., 1997). Curiously, the IKK complex seem to be a potential target for Hsp inhibition of the NF- κ B pathway (Yoo et al., 2000; Kohn et al., 2002). In another study (Kammanadiminti et al., 2007), *Eh* secreted proteins and SAP induced the expression of the NF- κ B dependent cytokine, monocyte chemotactic protein (MCP) from T84, LS174T and Caco-2 epithelial cells. Mechanistically, SAP-induced the phosphorylation of NF- κ B p65 subunit and enhanced transcriptional activity that was dependent on phosphatidylinositol 3-kinase (PI3 kinase) (**Figure 2** and **Table 1**). Inhibition of PI3 kinase abrogated the activation of Akt, p65, and MCP-1 mRNA induction. What remains unclear from these studies is whether PI3 kinase or Akt directly phosphorylates the p65 subunit in response to ameba components.

In vivo, the NF- κ B p50 subunit played a protective role, as *Eh* challenged C57BL/6 and 129/Sv mice with targeted deletion of the p50 subunit were more susceptible to *Eh* (Cho et al., 2010). A unique mechanism of epithelial cell death was also explored during *Eh* infection (Kim et al., 2014). Curiously, calpain, a calcium-dependent cysteine protease, induced protein degradation of pro-survival transcription factors, including NF- κ B p65, STAT3 and STAT5 that promoted cell death in response to *Eh* (Kim et al., 2014; **Table 1**). *Eh* invasion of the colonic mucosa leads to a pro-inflammatory cytokine burst and recruitment of different immune cells, which includes neutrophils and macrophages to the site of infection (Seydel et al., 1997; Mortimer and Chadee, 2010; Nakada-Tsukui and Nozaki, 2016).

Eh deploy an arsenal of virulence factors, which includes amoebapore, galactose/N-acetyl-D-galactosamine (Gal/GalNAc) lectin (Gal-lectin), cysteine proteinases and prostaglandin E₂ (Moonah et al., 2013; Marie and Petri Jr, 2014). *Eh* Gal-lectin is a major surface molecule that mediates the binding of *Eh* to host cells and to Gal and GalNAc colonic MUC2 mucin glycans (Chadee et al., 1987; Petri et al., 1987). Macrophages are innate immune cells that are instrumental in mounting a robust pro-inflammatory response. Stimulation of macrophages with native Gal-lectin activated NF- κ B and MAP kinase signaling pathway that culminated in the induction of TLR-2 mRNA and surface expression (Kammanadiminti et al., 2004; **Figure 2** and **Table 1**). The *Eh* Gal-lectin, a vaccine candidate for amebiasis, induces dendritic cell (DC) maturation and activation *via* MAPK and NF- κ B pathway leading to Th1 cytokine production (Ivory and Chadee, 2007). Amongst the different virulence factors, cysteine proteinases play a major role in the pathogenicity of amebiasis (Ankri et al., 1999; Tillack et al., 2006; Meléndez-López et al., 2007). *Eh*CP-A1, *Eh*CP-A2 and *Eh*CP-A5 are highly expressed cysteine proteinases in axenically cultured *Eh* (Bruchhaus et al., 1996; Tillack et al., 2007). The cysteine proteinases repertoire is



expressed spatially: *EhCP-A1* is confined to intracellular vesicles while *EhCP-A2* is expressed on the cell surface, and *EhCP-A5* is limited to the inner and outer cell membrane (Jacobs et al., 1998; Que et al., 2002; Meléndez-López et al., 2007). Pro-mature cysteine proteinase 5 (PCP5) is a major virulence factor of *Eh* that is secreted and/or present on the surface of ameba, binds *via* its RGD motif to $\alpha_v\beta_3$ integrins on colonic cells to trigger NF- κ B mediated pro-inflammatory responses (Hou et al., 2010). PCP5-RGD binding to $\alpha_v\beta_3$ integrins activated integrin-linked kinase (ILK) that mediated the phosphorylation of Akt-473 that subsequently bound and induced IKK activation *via* ubiquitination of NEMO that phosphorylates I κ B α triggering pro-inflammatory responses (Hou et al., 2010; **Figure 2**). The Gal-lectin and *EhCP-A5* together also play a central role in contact-dependent activation of the

NLRP3 inflammasome in macrophages for high output IL-1 β secretion (Mortimer et al., 2014; Mortimer et al., 2015). In this interaction, Gal-lectin activates the NF- κ B pathway for transcriptional activation of the NLRP3 inflammasome to stimulate TNF- α release (Mortimer et al., 2014). During primary *Eh* infection, macrophage secreted TNF- α has a detrimental outcome leading to increased diarrheal disease. However, naïve macrophages that are primed with TNF- α and IFN- γ produce high levels of nitric oxide (NO) that kills *Eh* (Lin et al., 1994; Seguin et al., 1995; Haque et al., 2007). Several *Eh* components can bind macrophage and epithelial TLR to activate the NF- κ B pathway to induce a raging pro-inflammatory response. Mouse macrophages stimulated with *Eh* genomic DNA signaled *via* TLR9 to activate NF- κ B and MAPK that was

dependent on MyD88 (Ivory et al., 2008; **Figure 2** and **Table 1**). Lipopeptidophosphoglycan (LPPG), a *Eh* associated molecular pattern, activated NF- κ B via TLR-2 and -4 resulting in the release of IL-12p40, TNF- α , IL-10, and IL-8 from human monocytes (**Table 1**). Mouse macrophages lacking TLR-2 (*TLR-2*^{-/-}) or deficient in TLR-4 (*TLR-4*^{d/d}) were unresponsive to LPPG stimulation (Maldonado-Bernal et al., 2005). *Eh* induced inflammation is characterized by the infiltration of neutrophils, which have been implicated in host defense against amebiasis. Interestingly, *Eh* activates neutrophils to induce extracellular traps that was dependent on the NF- κ B pathway (Fonseca et al., 2018). This suggests the if *Eh* can suppress the NF- κ B pathway in neutrophils like it does in macrophages, it can ward off potent innate host defenses.

The forgoing discussion elegantly demonstrates that *Eh* and its components can manipulate the NF- κ B pathway to elicit a florid pro-inflammatory response that may play a crucial role in *Eh* invasion and shape the outcome of disease. While detailed experimentations have uncovered many unanswered questions during *Eh*-host interaction, there are many questions that still need to be addressed. For instance, which specific NF- κ B protein subunits play a regulatory role during *Eh* pathogenesis and what will be the outcome of NF- κ B signaling from different cell types

upon contact with *Eh*. In this regard we recently (Chadha et al., 2021) uncovered a novel role for inflammatory caspase-1 that intersected NF- κ B signaling during *Eh*-macrophage contact. In this interaction, *Eh*-induced caspase-1 activation rapidly degraded cullin-1/5 proteins, a central scaffolding component of multi-subunit E3s ligase that attenuated NF- κ B signaling (**Figure 2**) inhibiting TNF- α production. Cullin-1/5 degradation was also observed from colonic epithelial cells following live *Eh* inoculated in proximal colonic loops of mice as a short-term infection model. Cullin-1/5 degradation was dependent on *Eh* surface cysteine proteinases *Eh*CP-A1 and *Eh*CP-A4, but not on *Eh*CP-A5, based on pharmacological inhibition of the cysteine proteinases and *Eh*CP-A5 deficient parasites. These findings highlight that *Eh* suppression of NF- κ B signaling induces a predominant NLRP3 dependent IL-1 β pro-inflammatory response that may contribute to disease pathogenesis. *Eh* in contact with macrophages is also known to induce the degradation of cytoskeletal-associated proteins talin, Pyk2 and paxillin that activated the NLRP3 inflammasome by an unknown mechanism (St-Pierre et al., 2017; **Table 1**). These findings suggest that *Eh* in contact with host cells at the intercellular junction uses several *Eh* ligands that couples to multiple putative receptors to activate inflammatory caspases and the NF- κ B pathway that regulates pro-inflammatory

TABLE 1 | Differential regulation of the NF- κ B pathway by protozoan parasites.

Parasite (Disease)	Pathogen component	Target	Result/outcome	Reference
<i>E. histolytica</i> (Amebiasis)	SAP	IKK Complex	NF- κ B inhibition	(Kammanadiminti and Chadee, 2006)
		Phosphorylation of p65	MCP-1 cytokine induction	(Kammanadiminti et al., 2007)
	Calpain	Degradation of p65, STAT3/5	Cell death	(Kim et al., 2014)
	Gal/GalNAc-lectin	NF- κ B and MAPK activation	TLR-2 m-RNA and protein expression	(Kammanadiminti et al., 2004)
	<i>Eh</i> CP-A5	IKK activation and I κ B phosphorylation	Enhanced pro-inflammatory response	(Hou et al., 2010)
	LPPG	TLR-2 and -4 activation	IL-12p40, TNF- α , IL-10, and IL-8 release	(Maldonado-Bernal et al., 2005)
	<i>Eh</i> genomic DNA	TLR9	NF- κ B and MAPK activation	(Ivory et al., 2008)
<i>Toxoplasma gondii</i> (Toxoplasmosis)	Live <i>Eh</i>	Cytoskeletal-associated proteins talin, Pyk2 and paxillin	NLRP3 inflammasome activation	(St-Pierre et al., 2017)
	TgESAs	Inhibits NF- κ Bp65 and TLR2/4 activation	Up-regulates IL-10 and TGF- β	(Wang et al., 2017)
	ROP18	p65 degradation	Aborted NF- κ B signaling	(Du et al., 2014)
	ROP16	Inhibits STAT3/6 and NF- κ B transcription	down-regulates TLR induced cytokines	(Saeij et al., 2007)
	Cathepsin C1	Inhibits p65 phosphorylation	Decrease TNF- α , IL-12, IL-6, IL-8, IL-1 production	(Liu et al., 2019)
<i>Plasmodium</i> (Malaria)	HSP70	Inhibits iNOS and NF- κ B	Decrease host parasitocidal mechanism	(Dobbin et al., 2002)
	GPI	NF- κ B/c-rel	iNOS expression	(Tachado et al., 1996)
<i>Trypanosoma cruzi</i> (Chagas)	Hemozoin	TLR-9 mediated NF- κ B activation	Up-regulates pro-IL-1 β and NLRP3 activation	(Coban et al., 2005; Parroche et al., 2007; Baccarella et al., 2013)
	GPI	Activates TLR2/MyD88, MAPK and NF- κ B	Induction of IL-12, TNF- α , and NO	(Campos et al., 2001)
<i>Leishmania</i> (Leishmaniasis)	Cruzipain	Interferes NF- κ Bp65 signaling	Hinders macrophage activation	(Watanabe Costa et al., 2016)
	<i>L. major</i> infection	Selectively translocate c-Rel/p50	Induces IL-10 expression	(Guizani-Tabbane et al., 2004)
	gp63	Cleaves NF- κ Bp65 RelA into p35RelA	Induces expression of MCP-1, MIP-1 α , MIP-1 β , MIP-2	(Gregory et al., 2008)
	<i>L. mexicana</i> infection	Degrades entire NF- κ B pathway (p65 ^{RelA} , c-Rel, I κ B α , I κ B β , JNK and ERK)	Inhibits IL-12 production	(Cameron et al., 2004)

responses. We are now beginning to decipher some of the salient features that regulates *Eh*-host parasite interaction in epithelial cells, macrophages and neutrophils by teasing out defined pathways that may be beneficial to the host and/or parasite in disease pathogenesis.

NF- κ B PATHWAY MODULATION DURING *TOXOPLASMA GONDII* INFECTION

Unlike extracellular *Eh*, intracellular protozoan parasites have devised unique ways to modulate the innate immune response *via* inside-out signaling by manipulating the NF- κ B pathway. *T. gondii*, the causative agent of toxoplasmosis, is an obligatory intracellular protozoan parasite that can infect all nucleated cells of warm-blooded animals (Hou et al., 2019; Li et al., 2019; de Faria Junior et al., 2021) including wild, domesticated and companion animals (Dubey et al., 2012). It infects about one-third of the world's human population (Sasai et al., 2018). Infection in immunocompromised individuals often leads to symptomatic and lethal toxoplasmosis (Tenter et al., 2000). Humans and other animals become infected due to consumption of under-cooked meat of infected animals or by ingesting water or food contaminated with oocysts (Jones et al., 2005; Dubey and Jones, 2008). *T. gondii* has three infectious stages known as tachyzoite, bradyzoite and sporozoites (within oocysts) (Dubey et al., 1998). Mouse models identified three different strains of *T. gondii* called type I, type II, and type III with different virulence factors. Amongst the three strains, type I is the most virulent strain, while type II and type III are avirulent (Howe et al., 1996; Mordue et al., 2001).

To counteract the host immune responses, *Toxoplasma* deploys multiple strategies to subvert the NF- κ B signaling pathway. Infection of bone marrow-macrophages with RH tachyzoites (RH strain of *T. gondii*, which is a type I representative strain) repressed NF- κ B activation by inhibiting nuclear localization of p65 or c-Rel, while *in-vivo* infection activated the NF- κ B pathway (Shapira et al., 2002). While the pathogen displays a repertoire of virulence factors, some play a crucial role in establishing the infection *via* immunomodulation of different immune cells. *T. gondii* excretory/secretory antigens (TgESAs), a virulence factor, inhibited nuclear translocation of NF- κ Bp65 and TLR-2 and -4 activation from LPS-stimulated Ana-1 murine macrophage that upregulated the anti-inflammatory cytokines IL-10 and TGF- β and downregulated the pro-inflammatory cytokines TNF- α and IL-1 β (Wang et al., 2017; **Figure 2** and **Table 1**). One of the strategies used by the parasite to subvert immune responses, is degradation of host proteins and transcription factors essential for regulating the immune response. *T. gondii* releases its protein into the host from organelles called dense granules and rhoptries (ROPs), thus manipulating host cell and their transcriptional responses (Lima and Lodoen, 2019; Tuladhar et al., 2019). ROP18, an effector of type I strains, is a serine/threonine kinase that modulates the phosphorylation of host proteins to circumvent cell signaling pathways. Surprisingly, ROP18 induced the phosphorylation of p65 at Ser-468 that led to ubiquitin-dependent degradation of p65

culminating in aborted NF- κ B signaling, thus conferring a survival advantage (Du et al., 2014; **Figure 2** and **Table 1**). Another protein ROP16, a putative protein kinase, suppressed IL-12 responses in infected macrophages stimulated with TLR agonist (Saeij et al., 2007) and inhibited NF- κ B transcriptional activity (Rosowski et al., 2011), possibly due to the activation of STAT3/6 (Saeij et al., 2007) that downregulated TLR-induced cytokine production (**Table 1**). In contrast, *T. gondii* strains that express dense granule protein GRA15 directly activates NF- κ B through a MyD88-independent mechanism (Melo et al., 2011). Recently (Liu et al., 2019), *T. gondii* cathepsin C1 (CPC1), a member of the GRA (dense granule) protein family, was shown to inhibit the phosphorylation of p65 subsequently leading to decreased production of pro-inflammatory cytokines TNF- α , IL-12, IL-6, IL-8 and IL-1 (**Figure 2** and **Table 1**). CPC1 inhibited NF- κ B activation through positive regulation of HIF (hypoxia-inducible factor)-1 α /EPO (erythropoietin) axis (Liu et al., 2019). While several studies have indicated the involvement of the NF- κ B pathway during *T. gondii* infection, it seems to be cell-specific regulation. Heat shock protein 70 (HSP70) of *T. gondii* inhibited parasitocidal activity by inhibiting iNOS, and NF- κ B activation from RAW 264.7 and splenocytes, respectively (Dobbin et al., 2002; **Figure 2** and **Table 1**). Surprisingly, *T. gondii* infected macrophage up-regulated the phosphorylation and degradation of I κ B and blocked the translocation of NF- κ B by inhibiting the phosphorylation of p65/RelA (Shapira et al., 2005) leading to aborted pro-inflammatory cytokine production (Butcher et al., 2001; Shapira et al., 2002). While these results are well documented in murine macrophages it is still debatable if a similar mechanism occurs in murine fibroblasts (Shapira et al., 2002; Molestina et al., 2003). LPS induced IL-1 β production inhibition from primary human neutrophils following type 1 strain infection was associated with inhibition of NF- κ B. Although neutrophils infected with *T. gondii* aborted NF- κ B signaling *via* reduced I κ B α degradation and p65/RelA phosphorylation, it also showed marked reduction in transcripts for NLRP3 inflammasome sensor and IL-1 β (Lima et al., 2018). To assess the importance of NF- κ B during the infection, mice deficient in specific genes belonging to the NF- κ B pathway have been assessed. Mice lacking RelB succumb to acute infection, due to inability to produce IFN- γ indicating an indispensable role of RelB in conferring resistance to *T. gondii* infection (Caamaño et al., 1999). During chronic infection, NF- κ B $^{-/-}$ mice have higher mortality when compared to wild-type (WT) mice due to global T-cell loss and apoptosis (Franzoso et al., 1998). Previous studies have shown altered microRNA expression profile by Apicomplexan parasites (Deng et al., 2004; McDonald et al., 2013; Hou et al., 2019) indicating the involvement of microRNA during infections. *T. gondii* infection perturbed the signaling pathways responsible for generating host defense responses (Hakimi and Ménard, 2010) by modulating the expression of host microRNAs, which contributes to efficient parasite replication (Cong et al., 2017). In agreement with these observations, *T. gondii* attenuated the NF- κ B pathway by inducing miR-146a in the host (Taganov et al., 2006). STAT3 and NF- κ B activation in response to *T. gondii* up-regulated the expression of miRNAs miR-125b-2, miR-30c-1, miR-17-92 and

miR-23b-27b-24-1 (Cai et al., 2013). Taken together, these observations suggest that *T. gondii* exploits the NF- κ B pathway for successful replication and to evade cell mediated immunity.

ROLE OF NF- κ B IN OTHER PROTOZOAN PARASITES

As NF- κ B signaling is crucial for mounting an immediate immune response against invading pathogens, its manipulation has been described at multiple levels in response to several protozoan parasites. *Plasmodium* is the etiologic agent of the disease malaria. According to the WHO report 2015, it infects over 200 million people annually and kills over 500,000 patients a year (World Health Organization (WHO), 2016). Glycosylphosphatidylinositol (GPI) of plasmodium activates macrophages and endothelial cells inducible NO synthase expression that involves NF- κ B/c-rel (Tachado et al., 1996; **Table 1**). Hemozoin, a malarial pigment, binds to TLR9 and activates NF- κ B and the NLRP3 inflammasome to increase the levels of pro-IL-1 β (Coban et al., 2005; Parroche et al., 2007; Baccarella et al., 2013; **Figure 2** and **Table 1**). A recent study (Toda et al., 2020) demonstrated a role for plasma-derived extracellular vesicles (EVs) from *P. vivax* patients (PvEVs) that activated NF- κ B translocation from human spleen fibroblasts (hSFs), which up-regulated the levels of ICAM-1 that resulted in specific adhesion properties of reticulocytes (from infected patients) to hSFs (Toda et al., 2020). *Trypanosoma cruzi* the causative agent of Chagas disease, infects over 5 million people across the globe and kills thousands of people each year (Pérez-Molina and Molina, 2018). Cytokines released by immune cells play a decisive role in disease pathogenesis and invasion by infectious agent. The Y strain of *T. cruzi* was shown to activate NF- κ B via the TNF pathway that increased invasion of non-professional phagocytic epithelial cells demonstrating a negative role for NF- κ B activation favoring the parasite (Pinto et al., 2011). *T. cruzi* GPI, a pathogen-associated molecular pattern, is recognized by TLR-2, which stimulates the TLR-2/Myd88 pathway, MAPK and NF- κ B transcription factor activation (Campos et al., 2001; Takeda and Akira, 2005; **Table 1**). In contrast, cruzipain, a *T. cruzi* secreted lysosomal peptidase, hindered macrophage activation during the initial stages of infection by interfering with NF- κ Bp65 mediated signaling (Watanabe Costa et al., 2016; **Figure 2** and **Table 1**). Leishmaniasis, caused by multiple *Leishmania* species, is responsible for an estimated 12 million infections across the globe and thousands of deaths per year (Lozano et al., 2012; Vos et al., 2016). Different *Leishmania* species differentially regulate the NF- κ B pathway. For instance, *L. major* infected monocytes (primary and PMA-differentiated U937 cells) inhibited nuclear localization of p65^{RelA}/p50 heterodimers, however, it selectively promoted the translocation of c-Rel/p50 heterodimers, which induced the anti-inflammatory cytokine, IL-10 (Guizani-Tabbane et al., 2004; **Figure 2** and **Table 1**). Infection of murine-BMDM with *L. mexicana* amastigotes degraded the entire NF- κ B pathway; degradation of p65^{RelA}, c-Rel, the upstream kinases JNK and ERK and the inhibitors I κ B α and I κ B β (Cameron et al., 2004; **Figure 2** and **Table 1**). In contrast, another group showed a novel subversion mechanism, wherein *Leishmania* protease, gp63, *in vitro* cleaved

NF- κ B p65RelA that resulted in a fragment p35RelA that dimerized with p50, which induced gene expression of the chemokines MCP-1, MIP-1 α , MIP-1 β and MIP-2 (Gregory et al., 2008; **Table 1**). A comprehensive view of the regulation of the NF- κ B pathway by protozoan parasites is listed in **Table 1** and **Figure 2** summarizes the differential regulation of the NF- κ B pathway by different protozoan parasites and their virulence factors.

CONCLUSION AND FUTURE DIRECTION

The immune system is armored with multiple receptors, which are recognized by invading pathogens culminating in gene expression associated with the development of an immune response. Parasite interaction with the innate immune response involves coupling through multiple receptors that activates the NF- κ B pathway. From an evolution point of view, multiple strategies reflect the selective pressure this pathway has imposed on different pathogens, while in turn evolution of different pathogens have led to the diversification of this pathway (Tato and Hunter, 2002). From the forgoing discussion it is apparent that parasites deploy multiple ways to circumvent signaling via the NF- κ B pathway. However, we know very little on the diverse array of parasite molecules and/or downstream signaling involved in NF- κ B activation and inhibition by extracellular and intracellular protozoan parasites. NF- κ B pathway diversification involves different protein subunits that form different hetero/homodimers (Gilmore, 2006). Intriguingly, different combination and permutation of these dimers have different functional consequence on gene expression responsible for immune activation/inhibition. At present, we still do not know which specific homo/heterodimer subunits are formed during contact and/or invasion by parasites, and what would be the functional consequence. The question that is still baffling and needs attention is, whether NF- κ B activation by different parasites favors the host or the pathogen or both. The dichotomy in NF- κ B activation and inhibition observed by extracellular and intracellular parasites, in part, may answer why intracellular parasites inhibit this pathway, while extracellular parasites activates it. It is essential to understand which specific NF- κ B subunit play an indispensable role during parasitic infection and how different receptor sense these parasites in a cell-type specific manner. Understanding these pathways could provide a better appreciation on the complexity of the disease and thus, help to develop better therapeutic approach for parasitic infections.

AUTHOR CONTRIBUTIONS

AC and KC conceived the review topic and wrote the manuscript. All authors contributed to the article and approved the submitted version.

FUNDING

This work was funded by a Discovery Grant (RGPIN-2019-04136) from the Natural Sciences and Engineering Research Council of Canada and a project grant from the Canadian Institutes of Health Research (PJT-407276) awarded to KC.

REFERENCES

- Andrews, K. T., Fisher, G., and Skinner-Adams, T. S. (2014). Drug Repurposing and Human Parasitic Protozoan Diseases. *Int. J. Parasitol. Drugs Drug Resistance* 4 (2), 95–111. doi: 10.1016/j.ijpddr.2014.02.002
- Ankri, S., Stolarsky, T., Bracha, R., Padilla-Vaca, F., and Mirelman, D. (1999). Antisense Inhibition of Expression of Cysteine Proteinases Affects Entamoeba Histolytica-Induced Formation of Liver Abscess in Hamsters. *Infection Immun.* 67 (1), 421–422. doi: 10.1128/IAI67.1.421-422.1999
- Baccarella, A., Fontana, M. F., Chen, E. C., and Kim, C. C. (2013). Toll-Like Receptor 7 Mediates Early Innate Immune Responses to Malaria. *Infection Immun.* 81 (12), 4431–4442. doi: 10.1128/IAI.00923-13
- Baud, V., and Karin, M. (2001). Signal Transduction by Tumor Necrosis Factor and its Relatives. *Trends Cell Biol.* 11 (9), 372–377. doi: 10.1016/S0962-8924(01)02064-5
- Begum, S., Gorman, H., Chadha, A., and Chadee, K. (2020a). Role of Inflammasomes in Innate Host Defense Against Entamoeba Histolytica. *J. Leukocyte Biol.* 108 (3), 801–812. doi: 10.1002/JLB.3MR0420-465R
- Begum, S., Moreau, F., Coria, A. L., and Chadee, K. (2020b). Entamoeba Histolytica Stimulates the Alarmin Molecule HMGB1 From Macrophages to Amplify Innate Host Defenses. *Mucosal Immunol.* 13 (2), 344–356. doi: 10.1038/s41385-019-0233-6
- Bruchhaus, I., Jacobs, T., Leippe, M., and Tannich, E. (1996). Entamoeba Histolytica and Entamoeba Dispar: Differences in Numbers and Expression of Cysteine Proteinase Genes. *Mol. Microbiol.* 22 (2), 255–263. doi: 10.1046/j.1365-2958.1996.00111.x
- Butcher, B. A., Kim, L., Johnson, P. F., and Denkers, E. Y. (2001). Toxoplasma Gondii Tachyzoites Inhibit Proinflammatory Cytokine Induction in Infected Macrophages by Preventing Nuclear Translocation of the Transcription Factor NF- κ B. *J. Immunol.* 167 (4), 2193–2201. doi: 10.4049/jimmunol.167.4.2193
- Caamaño, J., Alexander, J., Craig, L., Bravo, R., and Hunter, C. A. (1999). The NF- κ B Family Member RelB is Required for Innate and Adaptive Immunity to Toxoplasma gondii. *J. Immunol.* 163 (8), 4453–4461
- Cai, Y., Chen, H., Jin, L., You, Y., and Shen, J. (2013). STAT3-Dependent Transactivation of miRNA Genes Following Toxoplasma Gondii Infection in Macrophage. *Parasites Vectors* 6 (1), 1–9. doi: 10.1186/1756-3305-6-356
- Cameron, P., McGachy, A., Anderson, M., Paul, A., Coombs, G. H., Motttram, J. C., et al. (2004). Inhibition of Lipopolysaccharide-Induced Macrophage IL-12 Production by Leishmania Mexicana Amastigotes: The Role of Cysteine Peptidases and the NF- κ B Signaling Pathway. *J. Immunol.* 173 (5), 3297–3304. doi: 10.4049/jimmunol.173.5.3297
- Campos, M. A., Almeida, I. C., Takeuchi, O., Akira, S., Valente, E. P., Procópio, D. O., et al. (2001). Activation of Toll-Like Receptor-2 by Glycosylphosphatidylinositol Anchors From a Protozoan Parasite. *J. Immunol.* 167 (1), 416–423. doi: 10.4049/jimmunol.167.1.416
- Cardoso, M. S., Reis-Cunha, J. L., and Bartholomeu, D. C. (2016). Evasion of the Immune Response by Trypanosoma Cruzi During Acute Infection. *Front. Immunol.* 6, 659. doi: 10.3389/fimmu.2015.00659
- Chadee, K., Petri, W., Innes, D., and Ravdin, J. (1987). Rat and Human Colonic Mucins Bind to and Inhibit Adherence Lectin of Entamoeba Histolytica. *J. Clin. Invest.* 80 (5), 1245–1254. doi: 10.1172/JCI113199
- Chadha, A., Moreau, F., Wang, S., Dufour, A., and Chadee, K. (2021). Entamoeba histolytica Activation of Caspase-1 Degrades Cullin That Attenuates NF- κ B Dependent Signaling From Macrophages. *PLoS Pathogens*. doi: 10.1371/journal.ppat.1009936
- Chen, L.-f., Fischle, W., Verdine, E., and Greene, W. C. (2001). Duration of Nuclear NF- κ B Action Regulated by Reversible Acetylation. *Science* 293 (5535), 1653–1657. doi: 10.1126/science.1062374
- Chen, G., and Goeddel, D. V. (2002). TNF-R1 Signaling: A Beautiful Pathway. *Science* 296 (5573), 1634–1635. doi: 10.1126/science.1071924
- Cho, K.-N., Becker, S. M., and Hought, E. R. (2010). The NF- κ B P50 Subunit is Protective During Intestinal Entamoeba Histolytica Infection of 129 and C57BL/6 Mice. *Infection Immun.* 78 (4), 1475–1481. doi: 10.1128/IAI.00669-09
- Claudio, E., Brown, K., Park, S., Wang, H., and Siebenlist, U. (2002). BAF-Induced NEMO-Independent Processing of NF- κ B2 in Maturing B Cells. *Nat. Immunol.* 3 (10), 958–965. doi: 10.1038/ni842
- Coban, C., Ishii, K. J., Kawai, T., Hemmi, H., Sato, S., Uematsu, S., et al. (2005). Toll-Like Receptor 9 Mediates Innate Immune Activation by the Malaria Pigment Hemozoin. *J. Exp. Med.* 201 (1), 19–25. doi: 10.1084/jem.20041836
- Cong, W., Zhang, X.-X., He, J.-J., Li, F.-C., Elsheikha, H. M., and Zhu, X.-Q. (2017). Global miRNA Expression Profiling of Domestic Cat Livers Following Acute Toxoplasma Gondii Infection. *Oncotarget* 8 (15), 25599. doi: 10.18632/oncotarget.16108
- Coope, H., Atkinson, P., Huhse, B., Belich, M., Janzen, J., Holman, M., et al. (2002). CD40 Regulates the Processing of NF- κ B2 P100 to P52. *EMBO J.* 21 (20), 5375–5385. doi: 10.1093/emboj/cdf542
- de Faria Junior, G. M., Murata, F. H. A., Lorenzi, H. A., Castro, B. B. P., Assoni, L. C. P., Ayo, C. M., et al. (2021). The Role of microRNAs in the Infection by T. Gondii in Humans. *Front. Cell. Infect. Microbiol.* 11, 1–11. doi: 10.3389/fcimb.2021.670548
- Dejardin, E., Droin, N. M., Delhase, M., Haas, E., Cao, Y., Makris, C., et al. (2002). The Lymphotoxin- β Receptor Induces Different Patterns of Gene Expression via Two NF- κ B Pathways. *Immunity* 17 (4), 525–535. doi: 10.1016/S1074-7613(02)00423-5
- Delhase, M., Hayakawa, M., Chen, Y., and Karin, M. (1999). Positive and Negative Regulation of I κ B Kinase Activity Through I κ B Subunit Phosphorylation. *Science* 284 (5412), 309–313. doi: 10.1126/science.284.5412.309
- Deng, M., Lancto, C. A., and Abrahamson, M. S. (2004). Cryptosporidium Parvum Regulation of Human Epithelial Cell Gene Expression. *Int. J. Parasitol.* 34 (1), 73–82. doi: 10.1016/j.ijpara.2003.10.001
- Dixon, B., Parrington, L., Cook, A., Pintar, K., Pollari, F., Kelton, D., et al. (2011). The Potential for Zoonotic Transmission of Giardia Duodenalis and Cryptosporidium Spp. From Beef and Dairy Cattle in Ontario, Canada. *Veterinary Parasitol.* 175 (1–2), 20–26. doi: 10.1016/j.vetpar.2010.09.032
- Dobbin, C. A., Smith, N. C., and Johnson, A. M. (2002). Heat Shock Protein 70 is a Potential Virulence Factor in Murine Toxoplasma Infection via Immunomodulation of Host NF- κ B and Nitric Oxide. *J. Immunol.* 169 (2), 958–965. doi: 10.4049/jimmunol.169.2.958
- Dorny, P., Praet, N., Deckers, N., and Gabriël, S. (2009). Emerging Food-Borne Parasites. *Veterinary Parasitol.* 163 (3), 196–206. doi: 10.1016/j.vetpar.2009.05.026
- Du, J., An, R., Chen, L., Shen, Y., Chen, Y., Cheng, L., et al. (2014). Toxoplasma Gondii Virulence Factor ROP18 Inhibits the Host NF- κ B Pathway by Promoting P65 Degradation. *J. Biol. Chem.* 289 (18), 12578–12592. doi: 10.1074/jbc.M113.544718
- Dubey, J., and Jones, J. (2008). Toxoplasma Gondii Infection in Humans and Animals in the United States. *Int. J. Parasitol.* 38 (11), 1257–1278. doi: 10.1016/j.ijpara.2008.03.007
- Dubey, J., Lindsay, D., and Speer, C. (1998). Structures of Toxoplasma Gondii Tachyzoites, Bradyzoites, and Sporozoites and Biology and Development of Tissue Cysts. *Clin. Microbiol. Rev.* 11 (2), 267–299. doi: 10.1128/CMR.11.2.267
- Dubey, J., Tiao, N., Gebreyes, W., and Jones, J. (2012). A Review of Toxoplasmosis in Humans and Animals in Ethiopia. *Epidemiol. Infect.* 140 (11), 1935–1938. doi: 10.1017/S0950268812001392
- Faust, D. M., and Guillen, N. (2012). Virulence and Virulence Factors in Entamoeba Histolytica, the Agent of Human Amoebiasis. *Microbes Infect.* 14 (15), 1428–1441. doi: 10.1016/j.micinf.2012.05.013
- Fletcher, S. M., Stark, D., Harkness, J., and Ellis, J. (2012). Enteric Protozoa in the Developed World: A Public Health Perspective. *Clin. Microbiol. Rev.* 25 (3), 420–449. doi: 10.1128/CMR.05038-11
- Fonseca, Z., Diaz-Godínez, C., Mora, N., Alemán, O. R., Uribe-Querol, E., Carrero, J. C., et al. (2018). Entamoeba Histolytica Induce Signaling via Raf/MEK/ERK for Neutrophil Extracellular Trap (NET) Formation. *Front. Cell. Infect. Microbiol.* 8:226. doi: 10.3389/fcimb.2018.00226
- Franzoso, G., Carlson, L., Poljak, L., Shores, E. W., Epstein, S., Leonardi, A., et al. (1998). Mice Deficient in Nuclear Factor (NF)- κ B/P52 Present With Defects in Humoral Responses, Germinal Center Reactions, and Splenic Microarchitecture. *J. Exp. Med.* 187 (2), 147–159. doi: 10.1084/jem.187.2.147
- Ghosh, S., May, M. J., and Kopp, E. B. (1998). NF- κ B and Rel Proteins: Evolutionarily Conserved Mediators of Immune Responses. *Annu. Rev. Immunol.* 16 (1), 225–260. doi: 10.1146/annurev.immunol.16.1.225
- Ghosh, S., Padalia, J., and Moonah, S. (2019). Tissue Destruction Caused by Entamoeba Histolytica Parasite: Cell Death, Inflammation, Invasion, and the Gut Microbiome. *Curr. Clin. Microbiol. Rep.* 6 (1), 51–57. doi: 10.1007/s40588-019-0113-6
- Gilmore, T. D. (2006). Introduction to NF- κ B: Players, Pathways, Perspectives. *Oncogene* 25 (51), 6680–6684. doi: 10.1038/sj.onc.1209954
- Gregory, D. J., Godbout, M., Contreras, I., Forget, G., and Olivier, M. (2008). A Novel Form of NF- κ B is Induced by Leishmania Infection: Involvement in

- Macrophage Gene Expression. *Eur. J. Immunol.* 38 (4), 1071–1081. doi: 10.1002/eji.200737586
- Guizani-Tabbane, L., Ben-Aissa, K., Belghith, M., Sassi, A., and Dellagi, K. (2004). Leishmania Major Amastigotes Induce P50/C-Rel NF- κ B Transcription Factor in Human Macrophages: Involvement in Cytokine Synthesis. *Infect. Immun.* 72 (5), 2582–2589. doi: 10.1128/IAI.72.5.2582-2589.2004
- Gupta, G., Oghumu, S., and Satoskar, A. R. (2013). Mechanisms of Immune Evasion in Leishmaniasis. *Adv. Appl. Microbiol.* 82, 155–184. doi: 10.1016/B978-0-12-407679-2.00005-3
- Guzhova, I. V., Darieva, Z. A., Melo, A. R., and Margulis, B. A. (1997). Major Stress Protein Hsp70 Interacts With NF- κ B Regulatory Complex in Human T-Lymphoma Cells. *Cell Stress Chaperones* 2 (2), 132. doi: 10.1379/1466-1268 (1997)002<0132:msphiw>2.3.co;2
- Hakimi, M.-A., and Ménard, R. (2010). Do Apicomplexan Parasites Hijack the Host Cell microRNA Pathway for Their Intracellular Development? *F1000 Biol. Rep.* 2. doi: 10.3410/B2-42
- Haque, R., Mondal, D., Shu, J., Roy, S., Kabir, M., Davis, A. N., et al. (2007). Correlation of Interferon- γ Production by Peripheral Blood Mononuclear Cells With Childhood Malnutrition and Susceptibility to Amebiasis. *Am. J. Trop. Med. Hygiene* 76 (2), 340–344. doi: 10.4269/ajtmh.2007.76.340
- Heussler, V. T., Küenzi, P., and Rottenberg, S. (2001). Inhibition of Apoptosis by Intracellular Protozoan Parasites. *Int. J. Parasitol.* 31 (11), 1166–1176. doi: 10.1016/S0020-7519(01)00271-5
- Horn, D. (2014). Antigenic Variation in African Trypanosomes. *Mol. Biochem. Parasitol.* 195 (2), 123–129. doi: 10.1016/j.molbiopara.2014.05.001
- Hou, Z., Liu, D., Su, S., Wang, L., Zhao, Z., Ma, Y., et al. (2019). Comparison of Splenocyte microRNA Expression Profiles of Pigs During Acute and Chronic Toxoplasmosis. *BMC Genomics* 20 (1), 1–15. doi: 10.1186/s12864-019-5458-y
- Hou, Y., Mortimer, L., and Chadee, K. (2010). Entamoeba Histolytica Cysteine Proteinase 5 Binds Integrin on Colonic Cells and Stimulates Nfkb-Mediated Pro-Inflammatory Responses. *J. Biol. Chem.* 285 (46), 35497–35504. doi: 10.1074/jbc.M109.066035
- Howe, D. K., Summers, B. C., and Sibley, L. D. (1996). Acute Virulence in Mice is Associated With Markers on Chromosome VIII in Toxoplasma gondii. *Infect. Immun.* 64 (12), 5193–5198. doi: 10.1128/iai.64.12.5193-5198.1996
- Israël, A. (2000). The IKK Complex: An Integrator of All Signals That Activate NF- κ B? *Trends Cell Biol.* 10 (4), 129–133. doi: 10.1016/S0962-8924(00)01729-3
- Ivory, C. P., and Chadee, K. (2007). Activation of Dendritic Cells by the Gal-Lectin of Entamoeba Histolytica Drives Th1 Responses In Vitro and In Vivo. *Eur. J. Immunol.* 37 (2), 385–394. doi: 10.1002/eji.200636476
- Ivory, C. P., Prystajek, M., Jobin, C., and Chadee, K. (2008). Toll-Like Receptor 9-Dependent Macrophage Activation by Entamoeba Histolytica DNA. *Infection Immun.* 76 (1), 289–297. doi: 10.1128/IAI.01217-07
- Jacobs, T., Bruchhaus, I., Dandekar, T., Tannich, E., and Leippe, M. (1998). Isolation and Molecular Characterization of a Surface-Bound Proteinase of Entamoeba Histolytica. *Mol. Microbiol.* 27 (2), 269–276. doi: 10.1046/j.1365-2958.1998.00662.x
- Jones, J. L., Lopez, B., Murry, M. A., Wilson, M., Klein, R., Luby, S., et al. (2005). Toxoplasma Gondii Infection in Rural Guatemalan Children. *Am. J. Trop. Med. Hygiene* 72 (3), 295–300. doi: 10.4269/ajtmh.2005.72.295
- Kammanadiminti, S. J., and Chadee, K. (2006). Suppression of NF- κ B Activation by Entamoeba Histolytica in Intestinal Epithelial Cells is Mediated by Heat Shock Protein 27. *J. Biol. Chem.* 281 (36), 26112–26120. doi: 10.1074/jbc.M601988200
- Kammanadiminti, S. J., Dey, I., and Chadee, K. (2007). Induction of Monocyte Chemotactic Protein 1 in Colonic Epithelial Cells by Entamoeba Histolytica is Mediated via the Phosphatidylinositol 3-Kinase/P65 Pathway. *Infect. Immun.* 75 (4), 1765–1770. doi: 10.1128/IAI.01442-06
- Kammanadiminti, S. J., Mann, B. J., Dutil, L., and Chadee, K. (2004). Regulation of Toll-Like Receptor-2 Expression by the Gal-Lectin of Entamoeba Histolytica. *FASEB J.* 18 (1), 155–157. doi: 10.1096/fj.03-0578fj
- Karin, M., and Ben-Neriah, Y. (2000). Phosphorylation Meets Ubiquitination: The Control of NF- κ B Activity. *Annu. Rev. Immunol.* 18 (1), 621–663. doi: 10.1146/annurev.immunol.18.1.621
- Karin, M., Cao, Y., Greten, F. R., and Li, Z.-W. (2002). NF- κ B in Cancer: From Innocent Bystander to Major Culprit. *Nat. Rev. Cancer* 2 (4), 301–310. doi: 10.1038/nrc780
- Kelly, P. (2013). Protozoal Gastrointestinal Infections. *Medicine* 41 (12), 705–708. doi: 10.1016/j.mpmed.2013.09.003
- Kim, K. A., Min, A., Lee, Y. A., and Shin, M. H. (2014). Degradation of the Transcription Factors NF- κ B, STAT3, and STAT5 is Involved in Entamoeba Histolytica-Induced Cell Death in Caco-2 Colonic Epithelial Cells. *Korean J. Parasitol.* 52 (5), 459. doi: 10.3347/kjp.2014.52.5.459
- Kohn, G., Wong, H. R., Bshesh, K., Zhao, B., Vasi, N., Denenberg, A., et al. (2002). Heat Shock Inhibits Tnf-Induced ICAM-1 Expression in Human Endothelial Cells via I Kappa Kinase Inhibition. *Shock* 17 (2), 91–97. doi: 10.1097/00024382-200202000-00002
- Kyes, S., Horrocks, P., and Newbold, C. (2001). Antigenic Variation at the Infected Red Cell Surface in Malaria. *Annu. Rev. Microbiol.* 55, 673. doi: 10.1146/annurev.micro.55.1.673
- Le Negrate, G. (2012). Subversion of Innate Immune Responses by Bacterial Hindrance of NF- κ B Pathway. *Cell. Microbiol.* 14 (2), 155–167. doi: 10.1111/j.1462-5822.2011.01719
- Liang, Y., Zhou, Y., and Shen, P. (2004). NF- κ B and its Regulation on the Immune System. *Cell Mol. Immunol.* 1 (5), 343–350.
- Lima, T. S., Gov, L., and Lodoen, M. B. (2018). Evasion of Human Neutrophil-Mediated Host Defense During Toxoplasma Gondii Infection. *MBio* 9 (1), e02027–e02017. doi: 10.1128/mBio.02027-17
- Lima, T. S., and Lodoen, M. B. (2019). Mechanisms of Human Innate Immune Evasion by Toxoplasma Gondii. *Front. Cell. Infect. Microbiol.* 9:103. doi: 10.3389/fcimb.2019.00103
- Lin, J.-Y., Seguin, R., Keller, K., and Chadee, K. (1994). Tumor Necrosis Factor Alpha Augments Nitric Oxide-Dependent Macrophage Cytotoxicity Against Entamoeba Histolytica by Enhanced Expression of the Nitric Oxide Synthase Gene. *Infect. Immun.* 62 (5), 1534–1541. doi: 10.1128/iai.62.5.1534-1541.1994
- Liu, Y., Zou, X., Ou, M., Ye, X., Zhang, B., Wu, T., et al. (2019). Toxoplasma Gondii Cathepsin C1 Inhibits NF- κ B Signalling Through the Positive Regulation of the HIF-1 α /EPO Axis. *Acta Tropica* 195, 35–43. doi: 10.1016/j.actatropica.2019.04.018
- Li, Q., and Verma, I. M. (2002). NF- κ B Regulation in the Immune System. *Nat. Rev. Immunol.* 2 (10), 725–734. doi: 10.1038/nri910
- Li, S., Yang, J., Wang, L., Du, F., Zhao, J., and Fang, R. (2019). Expression Profile of microRNAs in Porcine Alveolar Macrophages After Toxoplasma Gondii Infection. *Parasites Vectors* 12 (1), 1–11. doi: 10.1186/s13071-019-3297-y
- Lozano, R., Naghavi, M., Foreman, K., Lim, S., Shibuya, K., Aboyans, V., et al. (2012). Global and Regional Mortality From 235 Causes of Death for 20 Age Groups in 1990 and 2010: A Systematic Analysis for the Global Burden of Disease Study 2010. *Lancet* 380 (9859), 2095–2128. doi: 10.1016/S0140-6736 (12)61728-0
- Mahmud, R., Ibrahim, J., Moktar, N., and Anuar, T.-S. (2013). “Entamoeba Histolytica in Southeast Asia,” in *Parasites and Their Vectors*. Eds. Y. Lim and I. Vythilingam (Vienna: Springer), 103–129.
- Maldonado-Bernal, C., Kirschning, C., Rosenstein, Y., Rocha, L., Rios-Sarabia, N., Espinosa-Cantellano, M., et al. (2005). The Innate Immune Response to Entamoeba Histolytica Lipopeptidophosphoglycan is Mediated by Toll-Like Receptors 2 and 4. *Parasite Immunol.* 27 (4), 127–137. doi: 10.1111/j.1365-3024.2005.00754.x
- Marie, C., and Petri, J. W. A. (2014). Regulation of Virulence of Entamoeba histolytica. *Annu. Rev. Microbiol.* 68, 493–520. doi: 10.1146/annurev-micro-091313-103550
- McDonald, V., Korbel, D., Barakat, F., Choudhry, N., and Petry, F. (2013). Innate Immune Responses Against Cryptosporidium Parvum Infection. *Parasite Immunol.* 35 (2), 55–64. doi: 10.1111/pim.12020
- Meléndez-López, S. G., Herdman, S., Hirata, K., Choi, M.-H., Choe, Y., Craik, C., et al. (2007). Use of Recombinant Entamoeba Histolytica Cysteine Proteinase 1 to Identify a Potent Inhibitor of Amebic Invasion in a Human Colonic Model. *Eukaryotic Cell* 6 (7), 1130–1136. doi: 10.1128/EC.00094-07
- Melo, M. B., Jensen, K. D., and Saeij, J. P. (2011). Toxoplasma Gondii Effectors are Master Regulators of the Inflammatory Response. *Trends Parasitol.* 27 (11), 487–495. doi: 10.1016/j.pt.2011.08.001
- Molestina, R. E., Payne, T. M., Coppens, I., and Sinai, A. P. (2003). Activation of NF- κ B by Toxoplasma Gondii Correlates With Increased Expression of Antiapoptotic Genes and Localization of Phosphorylated Ikb to the Parasitophorous Vacuole Membrane. *J. Cell Sci.* 116 (21), 4359–4371. doi: 10.1242/jcs.00683

- Moncada, D. M., Kammanadiminti, S. J., and Chadee, K. (2003). Mucin and Toll-Like Receptors in Host Defense Against Intestinal Parasites. *Trends Parasitol.* 19 (7), 305–311. doi: 10.1016/S1471-4922(03)00122-3
- Monzote, L., and Siddiq, A. (2011). Drug Development to Protozoan Diseases. *Open Medicinal Chem. J.* 5:1. doi: 10.2174/1874104501105010001
- Moonah, S. N., Jiang, N. M., and Petri, J. W. A. (2013). Host Immune Response to Intestinal Amebiasis. *PLoS Pathog.* 9 (8), e1003489. doi: 10.1371/journal.ppat.1003489
- Mordue, D. G., Monroy, F., La Regina, M., Dinarello, C. A., and Sibley, L. D. (2001). Acute Toxoplasmosis Leads to Lethal Overproduction of Th1 Cytokines. *J. Immunol.* 167 (8), 4574–4584. doi: 10.4049/jimmunol.167.8.4574
- Mortimer, L., and Chadee, K. (2010). The Immunopathogenesis of Entamoeba Histolytica. *Exp. Parasitol.* 126 (3), 366–380. doi: 10.1016/j.exppara.2010.03.005
- Mortimer, L., Moreau, F., Cornick, S., and Chadee, K. (2014). Gal-Lectin-Dependent Contact Activates the Inflammasome by Invasive Entamoeba histolytica. *Mucosal Immunol.* 4, 829–841. doi: 10.1038/mi.2013.100
- Mortimer, L., Moreau, F., Cornick, S., and Chadee, K. (2015). The NLRP3 Inflammasome Is a Pathogen Sensor for Invasive Entamoeba histolytica via Activation of $\alpha 5\beta 1$ Integrin at the Macrophage-Amebae Intercellular Junction. *PLoS Pathog.* 11 (5), e1004887. doi: 10.1371/journal.ppat.1004887
- Nakada-Tsukui, K., and Nozaki, T. (2016). Immune Response of Amebiasis and Immune Evasion by Entamoeba Histolytica. *Front. Immunol.* 7, 175. doi: 10.3389/fimmu.2016.00175
- Novack, D. V., Yin, L., Hagen-Stapleton, A., Schreiber, R. D., Goeddel, D. V., Ross, F. P., et al. (2003). The I κ B Function of NF- κ B2 P100 Controls Stimulated Osteoclastogenesis. *J. Exp. Med.* 198 (5), 771–781. doi: 10.1084/jem.20030116
- Parroche, P., Lauw, F. N., Goutagny, N., Latz, E., Monks, B. G., Visintin, A., et al. (2007). Malaria Hemozoin is Immunologically Inert But Radically Enhances Innate Responses by Presenting Malaria DNA to Toll-Like Receptor 9. *Proc. Natl. Acad. Sci.* 104 (6), 1919–1924. doi: 10.1073/pnas.0608745104
- Pérez-Molina, J. A., and Molina, I. (2018). Chagas Disease. *Lancet* 391 (10115), 82–94. doi: 10.1016/S0140-6736(17)31612-4
- Petri, W. A., Smith, R., Schlesinger, P., Murphy, C., and Ravdin, J. (1987). Isolation of the Galactose-Binding Lectin That Mediates the In Vitro Adherence of Entamoeba histolytica. *J. Clin. Invest.* 80 (5), 1238–1244. doi: 10.1172/JCI113198
- Pinto, A. M., Sales, P. C., Camargos, E. R., and Silva, A. M. (2011). Tumour Necrosis Factor (TNF)-Mediated NF- κ B Activation Facilitates Cellular Invasion of non-Professional Phagocytic Epithelial Cell Lines by Trypanosoma Cruzi. *Cell. Microbiol.* 13 (10), 1518–1529. doi: 10.1111/j.1462-5822.2011.01636.x
- Prucca, C. G., and Lujan, H. D. (2009). Antigenic Variation in Giardia Lamblia. *Cell. Microbiol.* 11 (12), 1706–1715. doi: 10.1111/j.1462-5822.2009.01367.x
- Que, X., Brinen, L. S., Perkins, P., Herdman, S., Hirata, K., Torian, B. E., et al. (2002). Cysteine Proteinases From Distinct Cellular Compartments are Recruited to Phagocytic Vesicles by Entamoeba Histolytica. *Mol. Biochem. Parasitol.* 119 (1), 23–32. doi: 10.1016/S0166-6851(01)00387-5
- Rosales, C. (2021). Neutrophils vs. Amoebas: Immunity Against the Protozoan Parasite Entamoeba histolytica. *J. Leukocyte Biol.* 1–12. doi: 10.1002/JLB.4MR0521-849RR
- Rosowski, E. E., Lu, D., Julien, L., Rodda, L., Gaiser, R. A., Jensen, K. D., et al. (2011). Strain-Specific Activation of the NF- κ B Pathway by GRA15, a Novel Toxoplasma Gondii Dense Granule Protein. *J. Exp. Med.* 208 (1), 195–212. doi: 10.1084/jem.20100717
- Rothwarf, D. M., Zandi, E., Natoli, G., and Karin, M. (1998). IKK- γ is an Essential Regulatory Subunit of the I κ B Kinase Complex. *Nature* 395 (6699), 297–300. doi: 10.1038/26261
- Sacks, D., and Sher, A. (2002). Evasion of Innate Immunity by Parasitic Protozoa. *Nat. Immunol.* 3 (11), 1041–1047. doi: 10.1038/ni1102-1041
- Saeij, J., Collier, S., Boyle, J., Jerome, M., White, M., and Boothroyd, J. (2007). Toxoplasma Co-opts Host Gene Expression by Injection of a Polymorphic Kinase Homologue. *Nature* 445 (7125), 324–327. doi: 10.1038/nature05395
- Santoro, M. G., Rossi, A., and Amici, C. (2003). NF- κ B and Virus Infection: Who Controls Whom. *EMBO J.* 22 (11), 2552–2560. doi: 10.1093/emboj/cdg267
- Sasai, M., Pradipta, A., and Yamamoto, M. (2018). Host Immune Responses to Toxoplasma Gondii. *Int. Immunol.* 30 (3), 113–119. doi: 10.1093/intimm/dxy004
- Seguin, R., Mann, B. J., Keller, K., and Chadee, K. (1995). Identification of the Galactose-Adherence Lectin Epitopes of Entamoeba Histolytica That Stimulate Tumour Necrosis Factor-Alpha Production by Macrophages. *Proc. Natl. Acad. Sci.* 92 (26), 12175–12179. doi: 10.1073/pnas.92.26.12175
- Senfleben, U., Cao, Y., Xiao, G., Greten, F. R., Krähn, G., Bonizzi, G., et al. (2001). Activation by I κ B α of a Second, Evolutionary Conserved, NF- κ B Signaling Pathway. *Science* 293 (5534), 1495–1499. doi: 10.1126/science.1062677
- Seydel, K. B., Li, E., Swanson, P. E., and Stanley, J. S. L. (1997). Human Intestinal Epithelial Cells Produce Proinflammatory Cytokines in Response to Infection in a SCID Mouse-Human Intestinal Xenograft Model of Amebiasis. *Infect. Immun.* 65 (5), 1631–1639. doi: 10.1128/iai.65.5.1631-1639.1997
- Shapira, S., Harb, O. S., Margarit, J., Matrajt, M., Han, J., Hoffmann, A., et al. (2005). Initiation and Termination of NF- κ B Signaling by the Intracellular Protozoan Parasite Toxoplasma Gondii. *J. Cell Sci.* 118 (15), 3501–3508. doi: 10.1242/jcs.02428
- Shapira, S., Speirs, K., Gerstein, A., Caamano, J., and Hunter, C. (2002). Suppression of NF- κ B Activation by Infection With Toxoplasma Gondii. *J. Infect. Dis.* 185 (Supplement_1), S66–S72. doi: 10.1086/338000
- Silverman, N., and Maniatis, T. (2001). NF- κ B Signaling Pathways in Mammalian and Insect Innate Immunity. *Genes Dev.* 15 (18), 2321–2342. doi: 10.1101/gad.909001
- Stanley, J. S. L. (2003). Amoebiasis. *Lancet* 361 (9362), 1025–1034. doi: 10.1016/S0140-6736(03)12830-9
- St-Pierre, J., Moreau, F., Cornick, S., Quach, J., Begum, S., Aracely Fernandez, L., et al. (2017). The Macrophage Cytoskeleton Acts as a Contact Sensor Upon Interaction With Entamoeba Histolytica to Trigger IL-1 β Secretion. *PLoS Pathog.* 13 (8), e1006592. doi: 10.1371/journal.ppat.1006592
- Sun, S. -C. (2011). Non-Canonical NF- κ B Signaling Pathway. *Cell Res.* 21 (1), 71–85. doi: 10.1038/cr.2010.177
- Sun, S. C., and Harhaj, E. W. (2006). Receptors and Adaptors for NF- κ B Signaling, ed. Liou HC. in: NF- κ B/Rel Transcription Factor Family. *Molecular Biology Intelligence Unit* (Boston, MA: Springer), 26–40. doi: 10.1007/0-387-33573-0_3
- Tachado, S. D., Gerold, P., McConville, M. J., Baldwin, T., Quilici, D., Schwarz, R. T., et al. (1996). Glycosylphosphatidylinositol Toxin of Plasmodium Induces Nitric Oxide Synthase Expression in Macrophages and Vascular Endothelial Cells by a Protein Tyrosine Kinase-Dependent and Protein Kinase C-Dependent Signaling Pathway. *J. Immunol.* 156 (5), 1897–1907.
- Taganov, K. D., Boldin, M. P., Chang, K.-J., and Baltimore, D. (2006). NF- κ B-Dependent Induction of microRNA miR-146, an Inhibitor Targeted to Signaling Proteins of Innate Immune Responses. *Proc. Natl. Acad. Sci.* 103 (33), 12481–12486. doi: 10.1073/pnas.0605298103
- Takeda, K., and Akira, S. (2005). Toll-Like Receptors in Innate Immunity. *Int. Immunol.* 17 (1), 1–14. doi: 10.1093/intimm/dxh186
- Tato, C., and Hunter, C. (2002). Host-Pathogen Interactions: Subversion and Utilization of the NF- κ B Pathway During Infection. *Infection Immun.* 70 (7), 3311–3317. doi: 10.1128/IAI.70.7.3311-3317.2002
- Tenter, A. M., Heckeroth, A. R., and Weiss, L. M. (2000). Toxoplasma Gondii: From Animals to Humans. *Int. J. Parasitol.* 30 (12–13), 1217–1258. doi: 10.1016/S0020-7519(00)00124-7
- Tillack, M., Biller, L., Irmer, H., Freitas, M., Gomes, M. A., Tannich, E., et al. (2007). The Entamoeba Histolytica Genome: Primary Structure and Expression of Proteolytic Enzymes. *BMC Genomics* 8 (1), 1–15. doi: 10.1186/1471-2164-8-170
- Tillack, M., Nowak, N., Lotter, H., Bracha, R., Mirelman, D., Tannich, E., et al. (2006). Increased Expression of the Major Cysteine Proteinases by Stable Episomal Transfection Underlines the Important Role of EhCP5 for the Pathogenicity of Entamoeba Histolytica. *Mol. Biochem. Parasitol.* 149 (1), 58–64. doi: 10.1016/j.molbiopara.2006.04.009
- Toda, H., Diaz-Varela, M., Segui-Barber, J., Roobsoong, W., Baro, B., Garcia-Silva, S., et al. (2020). Plasma-Derived Extracellular Vesicles From Plasmodium Vivax Patients Signal Spleen Fibroblasts via NF- κ B Facilitating Parasite Cytoadherence. *Nat. Commun.* 11 (1), 1–12. doi: 10.1038/s41467-020-16337-y
- Tuladhar, S., Kochanowsky, J. A., Bhaskara, A., Ghotmi, Y., Chandrasekaran, S., and Koshy, A. A. (2019). The ROP16III-Dependent Early Immune Response Determines the Subacute CNS Immune Response and Type III Toxoplasma Gondii Survival. *PLoS Pathog.* 15 (10), e1007856. doi: 10.1371/journal.ppat.1007856
- Verkerke, H. P., Petri, W. A., and Marie, C. S. (2012). The Dynamic Interdependence of Amebiasis, Innate Immunity, and Undernutrition. *Semin. Immunopathol.* 34, 771–785. doi: 10.1007/s00281-012-0349-1

- Verma, I. M., Stevenson, J. K., Schwarz, E. M., Van Antwerp, D., and Miyamoto, S. (1995). Rel/NF-Kappa B/I Kappa B Family: Intimate Tales of Association and Dissociation. *Genes Dev.* 9 (22), 2723–2735. doi: 10.1101/gad.9.22.2723
- Vos, T., Allen, C., Arora, M., Barber, R. M., Bhutta, Z. A., Brown, A., et al. (2016). Global, Regional, and National Incidence, Prevalence, and Years Lived With Disability for 310 Diseases and Injuries 1990–2015: A Systematic Analysis for the Global Burden of Disease Study 2015. *Lancet* 388 (10053), 1545–1602. doi: 10.1016/S0140-6736(16)31678-6
- Wang, S., Zhang, Z., Wang, Y., Gadahi, J. A., Xie, Q., Xu, L., et al. (2017). *Toxoplasma Gondii* Excretory/Secretory Antigens (TgESAs) Suppress Pro-Inflammatory Cytokine Secretion by Inhibiting TLR-Induced NF- κ B Activation in LPS-Stimulated Murine Macrophages. *Oncotarget* 8 (51), 88351. doi: 10.18632/oncotarget.19362
- Watanabe Costa, R., da Silveira, J. F., and Bahia, D. (2016). Interactions Between Trypanosoma Cruzi Secreted Proteins and Host Cell Signaling Pathways. *Front. Microbiol.* 7, 388. doi: 10.3389/fmicb.2016.00388
- World Health Organization (2016). *World Malaria Report 2015* (Geneva, Switzerland: World Health Organization), 1–181.
- Yoo, C.-G., Lee, S., Lee, C.-T., Kim, Y. W., Han, S. K., and Shim, Y.-S. (2000). Anti-Inflammatory Effect of Heat Shock Protein Induction is Related to Stabilization of I κ B α Through Preventing I κ B Kinase Activation in Respiratory Epithelial Cells. *J. Immunol.* 164 (10), 5416–5423. doi: 10.4049/jimmunol.164.10.5416
- Zhong, H., Voll, R. E., and Ghosh, S. (1998). Phosphorylation of NF- κ B P65 by PKA Stimulates Transcriptional Activity by Promoting a Novel Bivalent Interaction With the Coactivator CBP/P300. *Mol. Cell* 1 (5), 661–671. doi: 10.1016/S1097-2765(00)80066-0

Conflict of Interest: The authors declare that the research was conducted in the absence of any commercial or financial relationships that could be construed as a potential conflict of interest.

Publisher's Note: All claims expressed in this article are solely those of the authors and do not necessarily represent those of their affiliated organizations, or those of the publisher, the editors and the reviewers. Any product that may be evaluated in this article, or claim that may be made by its manufacturer, is not guaranteed or endorsed by the publisher.

Copyright © 2021 Chadha and Chadee. This is an open-access article distributed under the terms of the Creative Commons Attribution License (CC BY). The use, distribution or reproduction in other forums is permitted, provided the original author(s) and the copyright owner(s) are credited and that the original publication in this journal is cited, in accordance with accepted academic practice. No use, distribution or reproduction is permitted which does not comply with these terms.



Targeting Host Glycolysis as a Strategy for Antimalarial Development

Andrew J. Jezewski^{1,2†}, Yu-Hsi Lin³, Julie A. Reisz⁴, Rachel Culp-Hill⁴, Yasaman Barekatain³, Victoria C. Yan³, Angelo D'Alessandro⁴, Florian L. Muller^{3,5} and Audrey R. Odom John^{1,2*†}

OPEN ACCESS

Edited by:

Martin M. Edreira,
Universidad de Buenos Aires,
Argentina

Reviewed by:

Jennifer L. Guler,
University of Virginia, United States
Maria Cassera,
University of Georgia, United States

*Correspondence:

Audrey R. Odom John
johna3@chop.edu

†Present Address:

Andrew J. Jezewski,
Department of Pediatrics, University of
Iowa, Iowa City, IA, United States
Audrey R. Odom John,
Department of Pediatrics, Children's
Hospital of Philadelphia, and the
Perelman School of Medicine at the
University of Pennsylvania,
Philadelphia, PA, United States

Specialty section:

This article was submitted to
Parasite and Host,
a section of the journal
Frontiers in Cellular
and Infection Microbiology

Received: 24 June 2021

Accepted: 17 August 2021

Published: 16 September 2021

Citation:

Jezewski AJ, Lin Y-H, Reisz JA,
Culp-Hill R, Barekatain Y, Yan VC,
D'Alessandro A, Muller FL and
Odom John AR (2021) Targeting Host
Glycolysis as a Strategy for
Antimalarial Development.
Front. Cell. Infect. Microbiol. 11:730413.
doi: 10.3389/fcimb.2021.730413

¹ Department of Pediatrics, Washington University School of Medicine, St. Louis, MO, United States, ² Department of Molecular Microbiology, Washington University School of Medicine, St. Louis, MO, United States, ³ Department of Cancer Systems Imaging, Division of Diagnostic Imaging, The University of Texas MD Anderson Cancer Center, Houston, TX, United States, ⁴ Department of Biochemistry and Molecular Genetics, Aurora, CO, United States, ⁵ Department of Neuro-Oncology, Division of Cancer Medicine, The University of Texas MD Anderson Cancer Center, Houston, TX, United States

Glycolysis controls cellular energy, redox balance, and biosynthesis. Antiglycolytic therapies are under investigation for treatment of obesity, cancer, aging, autoimmunity, and microbial diseases. Interrupting glycolysis is highly valued as a therapeutic strategy, because glycolytic disruption is generally tolerated in mammals. Unfortunately, anemia is a known dose-limiting side effect of these inhibitors and presents a major caveat to development of antiglycolytic therapies. We developed specific inhibitors of enolase – a critical enzyme in glycolysis – and validated their metabolic and cellular effects on human erythrocytes. Enolase inhibition increases erythrocyte susceptibility to oxidative damage and induces rapid and premature erythrocyte senescence, rather than direct hemolysis. We apply our model of red cell toxicity to address questions regarding erythrocyte glycolytic disruption in the context of *Plasmodium falciparum* malaria pathogenesis. Our study provides a framework for understanding red blood cell homeostasis under normal and disease states and clarifies the importance of erythrocyte reductive capacity in malaria parasite growth.

Keywords: *Plasmodium*, antimalarial, red blood cells, erythrocyte, enolase, glycolysis, oxidative stress, malaria

INTRODUCTION

Infection with *Plasmodium* spp. malaria parasites contributes to over 400,000 deaths annually. Chemotherapeutic resistance remains a central roadblock to malaria control, and novel antimalarials are urgently required. One approach to circumvent resistance is through targeting host, rather than parasitic, processes essential for parasite survival. As the pathogenic stage of *Plasmodium* spp. develops within erythrocytes, the red cell niche presents a unique set of potential host targets that are needed to maintain erythrocyte metabolic homeostasis. The promise of erythrocyte-targeted antimalarial therapies is underscored by the prevalence of hereditary erythrocyte metabolic disorders in humans. These include glucose-6-phosphate dehydrogenase deficiency (G6PDd, the most common inherited enzymopathy of humans), pyruvate kinase

deficiency (PKd), and sickle cell trait, all of which are under positive selection in malaria-endemic geographic regions (Verra et al., 2009; Driss et al., 2011; Hedrick, 2011; Rogers et al., 2013; Tzounakas et al., 2016). These prevalent genetic disorders reveal the evolutionary pressure on hosts to modulate the metabolic state of the red cell to improve survival during malaria, suggesting that acute, specific targeting of red cell glycolysis, the sole energy-generating pathway in mature erythrocytes, is a promising antimalarial approach.

Previous studies on hereditary erythrocyte enzymopathies suggest a complex interplay with malaria survival and do not provide definitive evidence as to whether acute, rather than chronic, metabolic disruption in erythrocytes indeed improves malaria clinical outcomes. For example, while reduced enzyme activity in G6PDd and PKd individuals correlates with protection from severe malaria, no specific genetic variants are associated with survival (Driss et al., 2011). In addition, severe malaria has diverse clinical presentations: while G6PDd may protect during cerebral malaria, it appears to worsen malaria-associated severe anemia, although this model is itself controversial (Network et al., 2014; Watson et al., 2019). Finally, acute glycolytic inhibition is distinct from the phenotype arising from hereditary enzymopathies and their complex long-term physiologic adaptations, which include increased red cell production, decreased half-life of circulating erythrocytes, and a tendency toward an overall increase of the metabolic robustness in circulating red cells (due to reticulocytosis). Similarly, caloric restriction has been proposed as a sub-acute “anti-glycolytic” state that is malaria-protective, but this intervention has pleiotropic physiologic and immunologic effects (Mejia et al., 2015).

Efforts to study red cell glycolytic homeostasis using a chemical approach have been similarly complicated due to a lack of specificity. Several compounds, including sodium fluoride, arsenic, 6-aminonicotinamide, oxythiamine, and 3-bromopyruvate, are used experimentally as glycolytic inhibitors despite known off-target cellular effects (Lange and Proft, 1970; Tylicki et al., 2005; Shoshan, 2012). While commonly deployed as a metabolic inhibitor, 2-deoxyglucose (2-DG) is likewise complex. First, 2-DG does not completely recapitulate low glucose conditions or glycolytic inhibition, because, like glucose itself, 2-DG is processed in erythrocytes (through hexokinase and glucose 6-phosphate dehydrogenase) toward NADPH production (Suzuki et al., 1983; Sandulache et al., 2011; Miwa et al., 2013; Oburoglu et al., 2014). Second, use of 2-DG in animal models impacts all cell types, including immunocytes. Metabolic reprogramming is essential to the function of immune cells, including macrophages and natural killer cells, which themselves are well-recognized mediators of malaria-induced anemia (Brinkmann et al., 1984; Baratin et al., 2005; Stegmann et al., 2015; Arora et al., 2018; Burrack et al., 2018; Fu et al., 2019).

Enolase (phosphopyruvate hydratase; E.C. 4.2.1.11) catalyzes the eighth step in glycolysis. Humans express three isozymes of enolase (α , β , γ) that comprise multiple dimer configurations: ENO1 ($\alpha\alpha$), found in all cell types; ENO2 ($\gamma\gamma$), primarily in neurons; and ENO3 ($\beta\beta$), a muscle-specific isoform (Pearce et al., 1976). Like neurons, erythrocytes particularly rely on ENO2 for glycolytic function (Kato et al., 1983). While red blood cells predominantly express the α isozyme they rely on the γ

isozyme to a larger extent than any other non-nervous tissue (Marangos et al., 1980). Thus, enolase presents a unique opportunity to achieve cellular specificity of glycolytic inhibition. In recent years, enolase inhibitors have been developed with compelling subtype specificity and enhanced potency *via* prodrug strategies (Leonard et al., 2016; Satani et al., 2016; Lin et al., 2020). This newly developed class of phosphonate enolase inhibitors (some of which are ENO2-specific) and their cognate pro-drugs represent novel reagents to evaluate the role of specific and acute glycolytic disruption in erythrocytes during malaria infection. Neurons, which express both ENO1 and ENO2, withstand ENO2 specific inhibition, while erythrocytes do not (Lin et al., 2020). Here we query and define the signature of disrupted red cell glycolytic homeostasis, validate tools to investigate antiglycolytic approaches to human disease states, and use these tools to establish the impact of acute and specific glycolytic inhibition of erythrocytes on *Plasmodium* spp. infection.

RESULTS

Metabolic Profile of Acute Glycolytic Inhibition in Human Erythrocytes

Enolase (E.C. 4.2.1.11) catalyzes the penultimate glycolytic step, the conversion of 2-phosphoglycerate (2-PG) to phosphoenolpyruvate (PEP). The phosphonate natural product SF-2312 inhibits human enolase with high micromolar potency but is charged and relatively excluded from cells (Leonard et al., 2016; Satani et al., 2016). The more permeable lipophilic ester prodrugs, POM-SF and POM-HEX, are converted intracellularly to the direct enolase inhibitors SF-2312 and HEX, respectively, and have substantially increased cellular potencies over their cognate phosphonates (Lin et al., 2020). To validate POM-SF and POM-HEX as specific inhibitors of erythrocyte enolase, we performed untargeted metabolomics. Principal component analysis (PCA) and orthogonal projections of latent structures discriminant analysis (OPLS-DA) establish that POM-SF and POM-HEX-treated human erythrocytes rapidly develop distinct metabolic profiles from untreated controls. This divergence increases during prolonged exposure (**Supplemental Figure 1** and **Supplemental Table 2**).

Importantly, the observed metabolic profiles (**Supplemental Table 1**) are consistent with acute and specific inhibition of glycolysis at the level of enolase, such that metabolites immediately upstream of enolase accumulate and metabolites immediately downstream are depleted (**Figure 1A**). Hierarchical clustering yields two prominent clusters: in the first, glycolytic inhibition slows or prevents metabolite accumulation, and in the second, glycolytic inhibition accelerates metabolite depletion (**Figure 1B**).

Acute Glycolytic Inhibition Disrupts Erythrocytic Glutathione Homeostasis

Metabolite-pathway analysis reveals that acute inhibition of glycolysis leads to significant alterations in metabolites associated with glutathione metabolism (FDR adj. $p = 4.21E-03$), alanine, aspartate, glutamate metabolism (FDR adj. $p = 3.97E-05$), and glycine, serine, threonine metabolism (FDR adj. $p = 8.34E-04$)

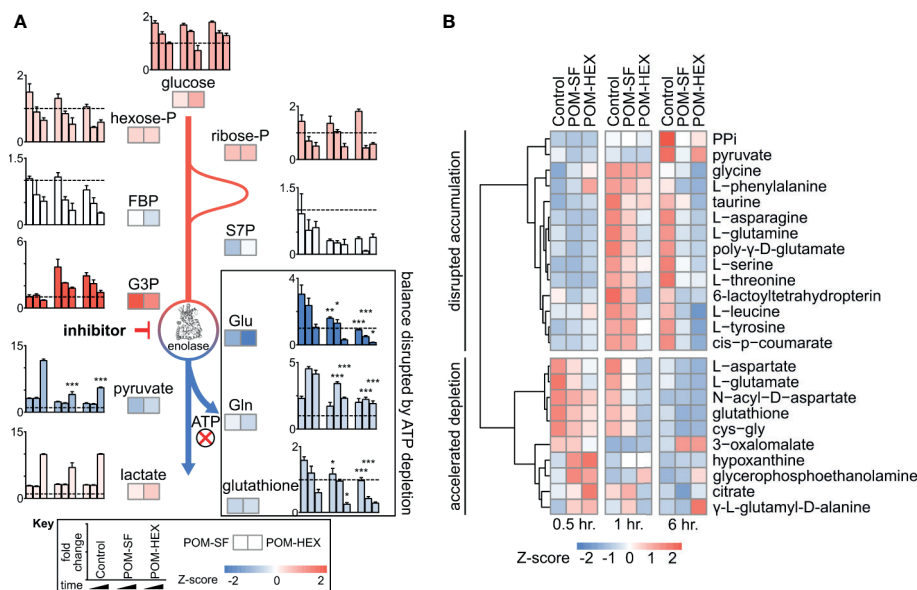


FIGURE 1 | Untargeted RBC metabolomics supports on-target inhibition of enolase and establishes a signature of enolase inhibition. Enolase inhibitor treated and untreated freshly harvested RBCs were collected for metabolite detection. **(A)** Metabolic changes proximal and distal to enolase indicate a characteristic pattern of inhibition. Key metabolites are plotted at 0.5, 1, and 6-hr. time points normalized to 0hr. controls, for untreated, POM-SF, and POM-HEX RBCs. Z-scores of key metabolites for each drug treatment were calculated from fold changes over control samples at $t = \dagger$ hr. FBP = fructose-1,6-bisphosphate, S7P = sedoheptulose-7-phosphate, G3P = glyceraldehyde-3-phosphate. Colors of bar graphs represent the average of z-scores for the two drug treatments. **(B)** Hierarchical clustering and time course for Z-scores of metabolites significantly different with respect to treatment and/or the interaction of time and treatment as calculated from the mean peak intensities from three biological replicates normalized to initial ($t = 0$ hr.) samples. PPI = inorganic pyrophosphate, cys-gly = L-cysteine-L-glycine. All samples were collected in experimental triplicate ($n=3$). * $p < 0.05$; ** $p < 0.05$; *** $p < 0.005$.

(Figure 2A and Supplemental Table 3) (Zhou and Xia, 2018). In addition, metabolite-protein nodal analysis reveals a high degree of interconnectedness of enolase inhibitor-responsive metabolites and protein interactions. Functional analysis supports an enrichment in glutathione metabolism ($p = 4.84E-52$), alanine, aspartate, glutamate metabolism ($p = 2.11E-34$), and pyruvate metabolism ($p = 7.61E-20$) (Figure 2B and Supplemental Table 3). Altogether, these metabolite characterizations indicate that acute glycolytic inhibition leads to a collapse in cellular reductive capacity. As glutathione synthesis is an ATP-dependent phenomenon, inhibition of glycolysis thus decreases total red cell antioxidant capacity. In corroboration, we also find a reduction in the total glutathione pool (reduced [GSH] + oxidized [GSSG]), driven by a depletion of GSH upon enolase inhibitor treatment (Figures 1A, 2C, D). Given that glutathione is a tripeptide made of cysteine, glutamate, glycine, it is likely that the reduced availability of glutathione component amino acids further compounds this effect. As GSH is the most abundant low molecular weight cellular antioxidant, we expected that acute glycolytic disruption in erythrocytes would cause a profound susceptibility to oxidative insults.

Acute Glycolytic Inhibition Causes Erythrocyte Senescence

To evaluate oxidative susceptibility during acute glycolytic inhibition in erythrocytes, we quantified methemoglobin (MetHb), in which the heme iron of hemoglobin is oxidized to

the ferric (Fe^{3+}), rather than ferrous (Fe^{2+}) form. While MetHb forms spontaneously under normoxic conditions, it is typically reduced by cellular protective mechanisms, some of which are dependent on reduced glutathione (Wright et al., 1996; Wright et al., 1999). As MetHb reductase is fueled by NADH (and, to a lesser extent, NADPH), we hypothesized that inhibition of late glycolysis would result in a metabolic bottleneck causing decreased NADH availability and thus impaired capacity to reduce ferric iron (Figure 3A). In keeping with this hypothesis, $1,2,3-^{13}C_3$ -glucose tracing highlights significant decreases in $^{13}C_3$ -pyruvate labeling and the ratio of $^{13}C_3$ -pyruvate/ $^{13}C_3$ -lactate, while flux through glycolysis versus the pentose phosphate pathway is unaltered – as gleaned by the ratios of isotopologues M+2/M+3 of lactate (Figure 3B). Both MetHb and antiparasitic effects appear in part driven by pyruvate availability (Figure 3C). We observed a consistent dose-dependent increase in MetHb formation upon inhibitor treatment (Figure 4A), confirming a functional loss of reductive capacity.

Cellular insults, including oxidative damage, cause erythrocytes to be marked for removal from circulation. Senescent erythrocytes are characterized by a loss of membrane asymmetry that results in extracellular exposure of phosphatidylserine (PS), detected by annexin-V staining (Andree et al., 1990; Koopman et al., 1994; Maćczak et al., 2016). While normal cells would respond by promoting PS internalization by ATP-dependent flippases, inhibition of glycolysis is expected to disrupt such repair. As with MetHb

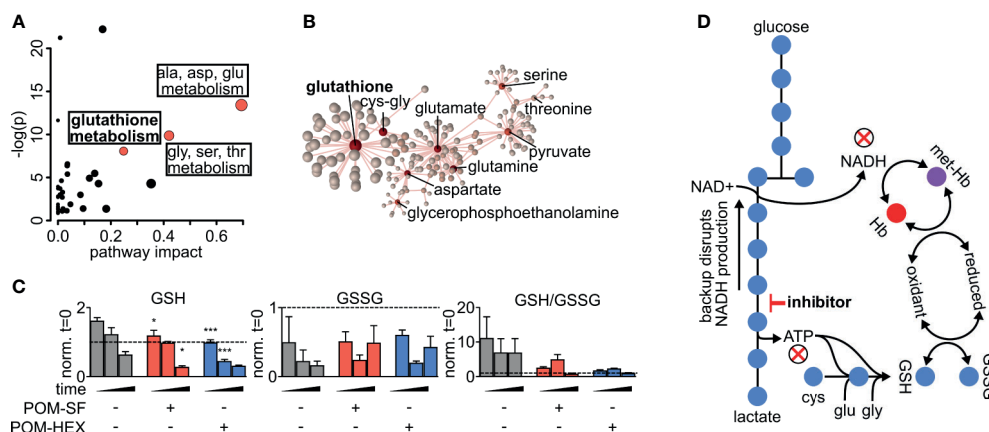


FIGURE 2 | Altered glutathione metabolism in erythrocytes following inhibition of glycolysis. **(A)** Metabolites significantly different with respect to treatment and/or the interaction of time and treatment show an enrichment in amino acid metabolism and glutathione metabolism as highlighted in red. Pathway impact is determined by the taking the total centrality score of significantly different metabolites compared to the total centrality score of all metabolites within the pathway as described in methods. A full list of metabolic pathways associated with significantly affected metabolites and the likelihood those metabolite changes impact their associated pathway is displayed in **Supplemental Table 3**. **(B)** Nodal analysis performed as described in methods of the same metabolites as in **(A)** depicts a high degree of interrelatedness through their predicted metabolite-protein interactions based on the KEGG database, and this interrelatedness is enriched for glutathione production. A full list of metabolite-protein interactions is displayed in **Supplemental Table 3**. **(C)** The depletion in total glutathione is driven via a depletion in reduced glutathione during enolase inhibitor treatment. **(D)** Model of glycolytic inhibition disrupting glutathione metabolism. **(A–C)** Statistics were performed such that metabolites found to be significant following two-way repeated measures ANOVA omnibus tests adjusted for multiple comparisons using a false discovery rate of 0.05 were followed up with post-hoc t-test analyses, treatment vs. control at each time point and adjusted for multiple comparisons, Dunnett method, $*p \leq 0.05$, $**p \leq 0.01$, $***p \leq 0.001$. All samples were collected in experimental triplicate ($n=3$). cys-gly, cysteine-glycine; GSH, reduced glutathione; GSSG, oxidized glutathione; Hb, hemoglobin; met-Hb, methemoglobin.

formation, we find that glycolytic inhibition of human erythrocytes leads to a dose-dependent increase in annexin V positivity (**Figure 4B**). Together, these results establish that glycolysis is essential to erythrocyte homeostasis. In addition, these studies reveal a likely mechanism by which genetic erythrocyte enzymopathies that impair central carbon metabolism reduce the circulatory half-life of erythrocytes (Cappadoro et al., 1998; van Wijk and van Solinge, 2005; Lutz and Bogdanova, 2013).

Acute Glycolytic Inhibition Does Not Directly Cause Erythrocyte Lysis

In parallel, we evaluated whether acute glycolytic inhibition also leads directly to hemolysis. To our surprise, continuous exposure to high concentrations of enolase inhibitors does not lead to erythrocyte lysis in static culture (**Figure 4C**). These results indicate that senescence and premature splenic clearance and destruction, rather than direct hemolysis, are the most likely mechanism for the decreased circulating half-life and anemia associated with interrupted glycolysis in erythrocytes *in vivo*.

Antimalarial Effects of Acute Inhibition of Erythrocyte Glycolysis

Plasmodium spp. induce host oxidative stress upon erythrocyte infection (Mohan et al., 1992; Becker et al., 2004; Cyrklaff et al., 2016). Therefore, inhibitors that impair erythrocyte reductive capacity may result in malaria protection. Erythrocyte-targeted antimalarials would be highly desirable as “resistance-proof”

antiparasitics (Prudêncio and Mota M, 2013; Lang et al., 2015; Lelliott et al., 2015). We therefore evaluated whether acute inhibition of erythrocyte glycolysis was directly antiparasitic to cultured *P. falciparum* (**Figure 4D**, **Table 1**). Treatment of asexual *P. falciparum* with phosphonates (SF-2312 and HEX) directly reduces parasite growth, with half maximal effective concentrations (EC_{50} s) $> 15\mu M$. Lipophilic ester pro-drugs, which likely exhibit improved cellular penetration (Krise and Stella, 1996; Pradere et al., 2014; Wiemer and Wiemer, 2014), exhibit 20- to 160-fold increased antimalarial potencies, compared to their cognate phosphonates (**Figure 4D**, **Table 1**). The most potent of these, POM-SF ($EC_{50} = 250 \pm 10 nM$), exhibits an *in vitro* potency in the submicromolar range as compared to other antimalarial compounds under development, such as the dihydroorotate dehydrogenase inhibitor DSM265 ($EC_{50} = 53 nM$) and the recently FDA-approved tafenoquine ($EC_{50} = 436 nM$) (Vennerstrom et al., 1999; Phillips et al., 2015).

Related phosphonate and pro-drug enolase inhibitors were evaluated for their antimalarial potency and their erythrotoxicity. We find that the antimalarial potency of each compound was highly correlated ($r^2 = 0.94$) to its capacity to disrupt erythrocyte redox balance (MetHb EC_{50}) (**Figure 4E**). This strict correlation indicates that both effects are likely mediated through a single common target, host erythrocyte enolase. In addition, the degree of inhibitor-induced anemia *in vivo* in mice also correlates with the antimalarial potency *in vitro* ($r^2 = 0.67$), suggesting that both anemia and antimalarial potency are mediated by a disruption in host cell redox balance (**Figure 4F**).

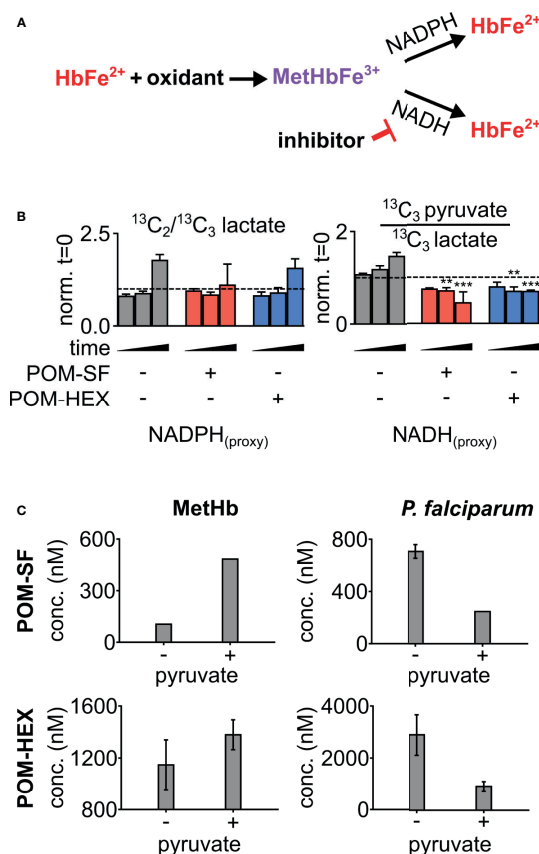


FIGURE 3 | Loss in reductive capacity induces erythrotoxic oxidative damage and antiparasitic effects. **(A)** Schematic showing two predominate mechanisms of methemoglobin (MetHb) reduction with **(B)** glucose labeling revealing a collapse in cellular redox potential with pyruvate M+3/lactate M+3 as a proxy for the cellular NAD⁺/NADH ratio, coupled without an increase in flux through the pentose phosphate pathway as shown via lactate M+2/lactate M+3 (n=3). **(C)** On the left, half-maximal inhibitory concentrations (EC₅₀) for MetHb formation in cultured human erythrocytes, with and without 1 mM supplemental pyruvate. On the right, EC₅₀ of *P. falciparum* growth, with and without 1 mM supplemental pyruvate. Representative dose-response curves for can be found in **Figure 4** and **Supplemental Figure 2**. All values are determined from three biological replicates, some error bars are below limit of visualization.

POM-SF and POM-HEX Are Effective Against Multi-Drug Resistant *P. falciparum*

We further evaluated the antimalarial activity of POM-SF and POM-HEX against parasites with reduced sensitivity to multiple classes of antimalarials, including chloroquine, sulfadoxine-pyrimethamine, mefloquine, and artemisinin. As expected, when targeting erythrocyte biology, multi-drug-resistant parasite lines remain sensitive to both POM-HEX and POM-SF, although there is a modest decrease in POM-SF sensitivity (**Supplemental Table 5**). While the antimalarial mechanisms of actions are likely entirely different than host enolase inhibition for these other frontline antimalarials we did want to rule out the possibility that these strains were somehow insensitive to enolase inhibition.

Chemical Complementation With Pyruvate Improves Antiparasitic Selectivity

To confirm the mechanism of enolase inhibitor-mediated erythrotoxicity, we evaluated strategies to rescue the erythrotoxicity of enolase inhibition. Pyruvate is a metabolic product immediately downstream of enolase and has been successfully and safely used in humans as a clinical antioxidant, including as a cardio- and neuro-protectant (Mallet et al., 2005; Zilberter et al., 2015; Ramos-Ibeas et al., 2017). We find that exogenous pyruvate ameliorates MetHb formation caused by glycolytic inhibition of erythrocytes. In contrast, we find pyruvate potentiates parasite growth inhibition (**Figure 3C**). As a result, pyruvate supplementation markedly improves the therapeutic index of glycolytic inhibitors (**Table 1**).

Parasite-Selective Enolase Inhibition Ameliorates Cerebral Malaria

Previous studies indicate that the glucose mimetic 2-deoxyglucose (2-DG) does not reduce parasitemia in acute malaria infection, but yet improves survival in a murine model of cerebral malaria (Cumnock et al., 2018; Wang et al., 2018). We took advantage of the fact that 2-DG inhibits glycolysis non-specifically in all cell types, while enolase inhibitors (HEX and POM-HEX) specifically target erythrocytes, to evaluate the role of erythrocyte glycolysis in outcomes of malaria infection (**Figures 5A–C**). As previously observed, 2-DG treatment does not reduce parasitemia; indeed, 2-DG causes a moderate increase in parasite burden [d4, control parasitemia of $7.8 \pm 3.3\%$ versus $13.3 \pm 3.9\%$ in 2-DG-treated animals, adj. p-value (Bonferroni method) = 0.011] (Cumnock et al., 2018; Wang et al., 2018). In our hands, 2-DG did not improve the clinical score or overall survival due to cerebral malaria.

Our *in vitro* studies predicted that erythrocyte toxicity would limit the antimalarial efficacy of the prodrug POM-HEX, which penetrates cells easily, leading to comparable erythrotoxic and antimalarial potencies (**Table 1**). In contrast, *Plasmodium*-infected erythrocytes actively transport charged molecules. For this reason, the phosphonate parent compound, HEX, is substantially less toxic to uninfected erythrocytes but retains antiparasitic activity (**Table 1**), predicting a wider therapeutic index *in vivo*. Indeed, in murine *Plasmodium berghei* infection, we find that HEX treatment reduced overall parasite burden [d4, control parasitemia $7.8 \pm 3.3\%$ versus $3.5 \pm 1.3\%$ in HEX-treated animals; adj. p-value (Bonferroni method) = 0.009], improved clinical scores [d6, vehicle 15.0 ± 7.3 versus 3.8 ± 2.0 in HEX-treated animals; adj. p-value (Bonferroni method) = 0.039], and significantly improved survival [14 days, compared to \dagger days for vehicle-treated animals; adj. p-value (Bonferroni method) = 0.0069 (Mantel-Cox)]. In contrast, POM-HEX, which is non-selectively toxic to both uninfected and infected erythrocytes, was no more effective than 2-DG. These data support the use of *in vitro* comparisons of erythrotoxicity versus antiparasitic potencies in order to predict *in vivo* preclinical efficacy. We find that the *in vitro* therapeutic index better predicts *in vivo* success compared to *in vitro* antimalarial potency alone.

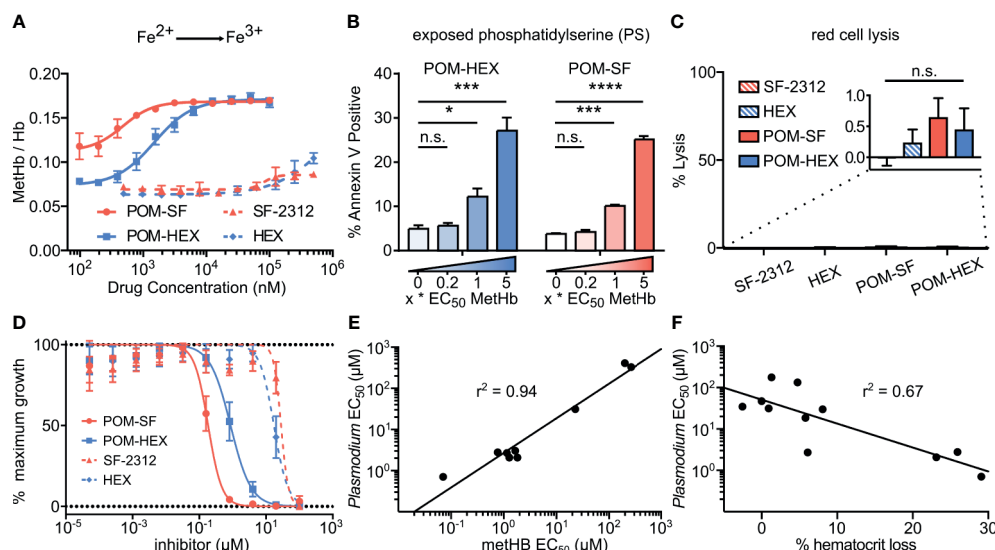
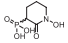
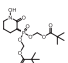
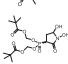


FIGURE 4 | Oxidative damage and erythrocyte senescence upon glycolytic inhibition without hemolysis offers potent antimalarial effects *in vitro*. **(A)** Dose-dependent increase in the proportion of oxidized (ferric) heme compared to reduce (ferrous) heme following treatment with indicated enolase inhibitors. Half-maximal effective concentrations are as indicated in **Supplemental Table 4** (n=3). **(B)** Dose-dependent increase in a marker of erythrocyte senescence (exposed phosphatidylserine), characterized via annexin V staining. Concentrations tested are in relation to the EC₅₀ of MetHb formation for each compound respectively (n=3). **(C)** Hemoglobin absorption (normalized to 100% detergent-mediated lysis) in freshly cultured human erythrocytes for indicated inhibitors (>100μM for 3 days) (n=3). **(D)** EC₅₀s were performed against *P. falciparum* strain 3D7. Displayed are representative curves for a subset of the most potent prodrugs and their respective parent compounds. EC₅₀s against parasite growth for all tested compounds are displayed in **Supplemental Table 4**. **(E, F)** A high correlation between parasite killing and host toxicity indicates shared mechanism. A linear regression was performed on all compounds for which an EC₅₀ for **(E)** MetHb or **(F)** *in vivo* mouse hematocrit loss and parasite growth inhibition could be determined (GraphPad Prism). **(A, D)** The respective EC₅₀s are calculated using non-linear regression from each of the independent biological replicates (GraphPad Prism). Hb, hemoglobin; met-Hb, methemoglobin. *p < 0.05; ***p < 0.005.

TABLE 1 | Table of parasite EC₅₀s and methemoglobin EC₅₀s for all tested compounds and their structures.

Compound	Structure	Parasite EC ₅₀ (μM)	MetHb EC ₅₀ (μM)	T.I.	- pyruvate		T.I.	T.I. Fold change
					Parasite EC ₅₀ (μM)	MetHb EC ₅₀ (μM)		
HEX		19 ± 1.0	500	26.3	18 ± 2.2	500	27.8	1.1
POM-HEX		2.9 ± 0.64	1.2 ± 0.19	0.4	0.91 ± 0.15	1.4 ± 0.11	1.5	3.7
POM-SF		0.71 ± 0.04	0.1 ± 0.002	0.1	0.25 ± 0.01	0.48 ± 0.01	1.9	13.6

Displayed are the means ± s.e.m from three or more independent biological replicates in the presence or absence of 1mM pyruvate. EC₅₀s are displayed at the highest concentration tested (500 μM) for instances where regression calculations cannot be resolved due to full inhibition extending beyond the highest doses tested. A therapeutic index (T.I.) was calculated as follows: [EC₅₀ for MetHb formation]/[EC₅₀ for parasite growth inhibition]. The change in T.I. was determined as follows: [T.I. without pyruvate]/[T.I. with pyruvate].

Non-Human Primates Tolerate High Doses of HEX With Longer Half Life

Because HEX treatment improves survival in mice with cerebral malaria, we sought to investigate its pharmacokinetic properties in non-human primates as a model for human application. We determined the serum half-life of HEX in cynomolgus monkeys and mice following sub-cutaneous injections. Although mice were treated with higher doses [400mg/kg], HEX-treated non-human primates [100mg/kg] display a higher serum concentration throughout the experiment and a markedly prolonged serum half-life [mice, minutes vs. non-human primates, 1 hour] (**Figure 6**). Compellingly, we find that the serum concentrations

of HEX remain above the *in vitro* EC₅₀ concentrations against *Plasmodium* for at least four hours. Prolonged bioavailability above the efficacious dose may be required for parasite clearance as this may be why only prolonged survival in the murine model was achieved. Improved drug exposure in non-human primates bodes well for enhanced antimalarial efficacy in humans.

DISCUSSION

As the central backbone of cellular metabolism, glycolysis controls energy production, redox balance, and biosynthesis. Antiglycolytic

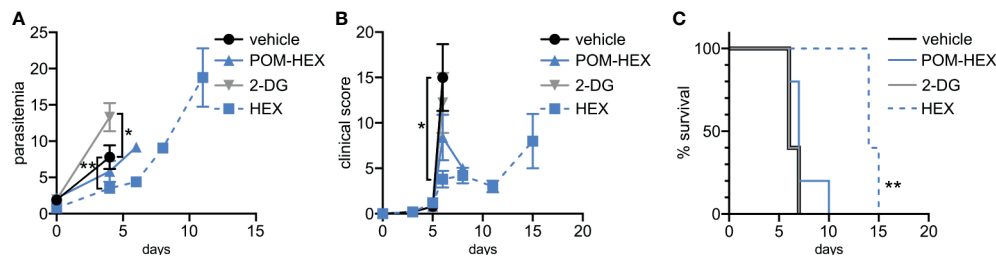


FIGURE 5 | Positive clinical impacts on murine severe malaria following glycolytic inhibition despite high parasitemias. 2-deoxyglucose (2DG) has pleiotropic effects beyond glycolytic inhibition and effects all cell types, while POM-HEX and HEX are specific to ENO2 isozyme expressing cell types like erythrocytes. **(A–C)** Swiss Webster mice ($n=5$) were infected with *P. berghei* ANKA strain parasites expressing a luciferase reporter and treated daily from day 2 onwards with either vehicle, 2DG (200 mg/kg), or enolase inhibitors POM-HEX (30 mg/kg), or HEX (100 mg/kg). **(A)** Mice were monitored for parasitemia via blood smear Giemsa staining on indicated days, * = $p \leq 0.05$, ** = $p \leq 0.01$. **(B)** Mice were also assessed for clinical signs of cerebral malaria as determined by signs of neurological symptoms such as paralysis, deviation of the head, ataxia, convulsions, and coma on indicated days, * = $p \leq 0.05$. **(C)** Survival was determined over 15 days, two mice remained alive in the Hex treated group on day 15 but were sacrificed due to high parasitemia concomitant with elevated clinical score as depicted by Kaplan-Meier survival curve, ** = $p \leq 0.01$.

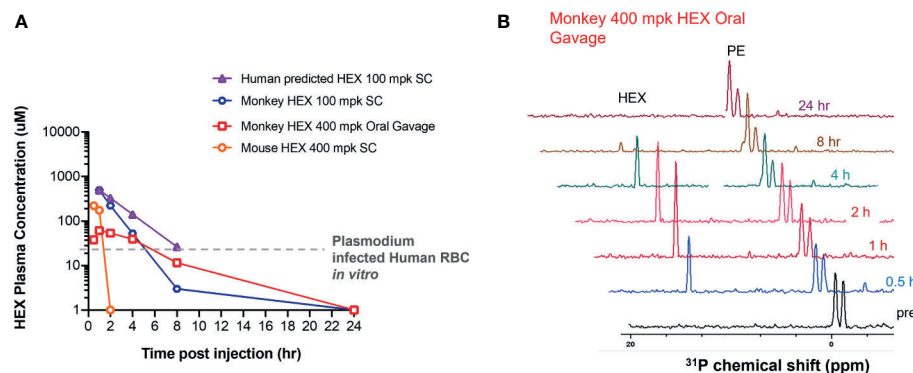


FIGURE 6 | High plasma exposures of HEX are tolerated in Non-human Primates. **(A)** HEX concentrations in plasma were measured by ^{31}P - ^1H HSQC (NS = 128) with a detection limit of $\sim 1 \mu\text{M}$. A 400 mg/kg dose SC in mice yielded $\sim 170 \mu\text{M}$ HEX 1 hr after injection, becoming undetectable at the 2 hr time point. In contrast, a dose of just 100 mpk (the blue tracer, replotted from Lin et al., 2020) yielded plasma concentrations of $>500 \mu\text{M}$ in cynomolgus monkeys at 1 hr, which remained significant for several hours thereafter. Approximate IC_{50} concentrations for RBC infected with *Plasmodium* shown as a grey trace, indicating that in mice, sufficient drug concentrations are for killing *Plasmodium* infected RBC are only maintained shortly after injection. The half-lives for HEX in monkey is around 1 hr, whilst in mice it is ~ 1 minutes, well in line with values obtained for fosmidomycin. Purple trace, predicted PK of HEX in human at a 100 mpk S.C. dose, based on monkey/human fosmidomycin comparison. The red trace, 400 mpk HEX administered by oral gavage in monkey, indicates HEX is orally bioavailable. **(B)**, NMR ^{31}P - ^1H HSQC 1D read outs at different time points post S.C. HEX (1 ppm chemical shift) and endogenous phosphate esters (PE), indicated.

inhibitors—so-called “starvation mimetics”—are under increasing consideration as potential therapies for conditions including obesity, cancer, aging, autoimmunity, and infectious diseases (Krieger and Landsberg, 1989; Bakker et al., 1999; Pelicano et al., 2006; Patel et al., 2008; Chang and Wei, 2011). Most recently, it has been reported that host glycolytic inhibition markedly reduced replication of SARS-CoV-2 (Krishnan et al., 2021). While glycolytic disruption is generally well tolerated, glycolysis is critical to metabolic homeostasis in erythrocytes, which exclusively rely on the Embden-Meyerhof-Parnas pathway for ATP generation. As such, anemia is a key dose-limiting side effect and presents a major threat to otherwise promising antiglycolytic therapies (Laszlo et al., 1960; Lin et al., 2020). Our work provides a mechanistic model through which to understand acute inhibition of erythrocyte glycolysis.

Inhibition of erythrocyte glycolysis is a particularly compelling target for antimalarial therapies. Not only are the symptomatic asexual stages of *Plasmodium* spp. housed within the red cell niche, but long-standing evidence suggests that the outcome of clinical malaria is intertwined with red cell metabolism. Most notably, heritable erythrocyte disorders that appear to reduce malaria severity, including enzymopathies such as G6PDd and PKd, dysregulate glycolytic function and antioxidant capacity (Driss et al., 2011; Rogers et al., 2013). Because hemoglobin binds and competes for band 3 sequestration of glycolytic enzymes, malaria-protective hemoglobinopathies such as sickle cell trait also disrupt glycolytic regulation and sensitize erythrocytes to oxidative stress (Rogers et al., 2013). These natural genetic experiments suggest that modulating erythrocyte metabolism successfully improves malaria

outcomes, and underscore that long-standing disruptions in erythrocyte metabolic homeostasis can be reasonably well tolerated. Although several antimalarials are contraindicated by glycolytic enzymopathies and novel anti-glycolytic therapies such as the reported enolase inhibitors should consider this in future development. As *Plasmodium* spp. have a remarkable capacity for drug resistance, targeting host factors for antimalarial discovery is highly attractive to slow emergence of resistance.

However, our data demonstrate that non-discriminately disrupting glycolysis in infected and uninfected erythrocytes neither drives antiparasitic activity nor improves the outcome of acute malaria infection. Potent enolase inhibition does not forestall a lethal parasite burden (POM-SF and POM-HEX) and does not prevent cerebral malaria (POM-HEX). Rather, our non-prodruged phosphonates (e.g., HEX) reduce parasite burden, extend survival, and decrease clinical symptoms of malaria. A possible explanation for the discrepancy in antimalarial efficacy of POM-HEX *in vitro* vs *in vivo* is that POM-HEX is rapidly converted to Hemi-POM-HEX in mouse plasma, such that effective plasma exposure to POM-HEX itself is quite low (Lin et al., 2020). The high carboxylesterase activity in mouse (compared to human) plasma has been a recurrent complication for modeling the effects of POM-containing pro-drugs and suggests that the performance of POM-HEX in mice likely underestimates its efficacy in humans (Bahar et al., 2012). The discrepancy between mouse pharmacokinetics and primates is further highlighted in our study, in which the half-life of POM-HEX in primates is 10-fold longer than that in mice. This observation is combined with the likelihood that the reticulocyte tropism of the *P. berghei* model reduces enolase inhibitor efficacy due to increased metabolic plasticity of reticulocytes. These assumptions would need to hold true for enolase inhibitors to be near the bioavailability and efficacy of artemisinin as the current frontline antimalarial. The deadliest form of human malaria *P. falciparum* preferentially infects mature erythrocytes.

Because our compounds exhibit a tight correlation between antiparasitic and erythrotoxic potencies, both phenotypes are likely due to inhibition of a single common cellular target, human enolase. Our studies cannot unequivocally rule out other potential secondary targets, including the *P. falciparum* enolase, which itself is likely essential for intraerythrocytic parasite development. Because *Plasmodium falciparum* is an obligate intracellular parasite, it is challenging to evaluate cellular parasite enolase inhibition in isolation. In support of human enolase as the primary antimalarial target of these compounds, however, we also find little or no antiparasitic selectivity for most inhibitors in this series. Nonetheless, multiple-target agents that simultaneously inhibit the host and parasite enzymes would be expected to have durable, resistance-resistant antiparasitic activity (Oldfield and Feng, 2014).

Among our enolase inhibitors, two compounds are notably selective for antiparasitic activity over erythrocyte toxicity, the unmodified parent phosphonates, specifically HEX and DeoxySF-2312. During intraerythrocytic development, *Plasmodium* spp. parasites establish new permeability pathways on the host erythrocyte membrane and are thus relatively

permissive to small anions, specifically including phosphonates (Ginsburg et al., 1983; Baumeister et al., 2006; Baumeister et al., 2011). Compared to uninfected red cells that lack these transporters, *Plasmodium*-infected red cells are thus more susceptible to enolase inhibition with charged phosphonate inhibitors. Therefore, we suggest that small molecule inhibitors designed to take advantage of the increased permeability of infected erythrocytes to specifically target glycolysis in *Plasmodium*-infected—but not uninfected—erythrocytes may represent a novel, successful, “resistance-proof” antimalarial strategy (Figure 7). However, one can imagine that even host targeted antiparasitic mechanisms could be circumvented by the parasite, especially host-rescuing anti-oxidant parasite driven processes. Additionally, due to the obligate intracellular asexual stage of the parasite, we cannot rule out some parasite targeting effects of these enolase inhibitors. Rapid compound clearance likely ameliorates the therapeutic effect of phosphonates such as HEX in mice, and our studies suggest that primates may represent a better pre-clinical model due to increased circulating half-life.

Our studies also establish a mechanistic model for anemia caused by acute antiglycolytic therapeutics through rapid premature erythrocyte senescence, rather than direct hemolysis. Targeted enolase inhibitor treatment of erythrocytes leads to a metabolic signature characterized by a collapse in glutathione homeostasis. The antioxidant capacity of erythrocytes is dependent on energy production, as erythrocytes, lacking mitochondria, are uniquely dependent on aerobic glycolysis. Enolase inhibition reduces the net ATP per glucose molecule by half, thus hampering production of the energy-expensive cellular antioxidant, glutathione. The production of this tripeptide (glutamate, cysteine, and glycine) requires ATP at each assembly step. Thus, enolase inhibition globally disturbs amino acid metabolism and leads to a state of energy depletion and the onset of oxidative stress. The depletion of glutathione likely results in an accumulation of oxidative insults over time that results in the metHb formation observed.

Depletion of reduced glutathione establishes the molecular mechanism of MetHb formation and senescence in inhibitor-treated erythrocytes. Lacking organelles, erythrocytes undergo a distinct cell death known as eryptosis. Like apoptosis, eryptosis causes cell shrinkage, membrane blebbing, protease activation, and loss of membrane asymmetry. Changing membrane phospholipids (e.g., phosphatidylserine) serves as a removal signal for circulating macrophages and splenic clearance. Our investigations thus explain the features of anemia observed in enolase-inhibitor-treated mice, who develop profound splenomegaly but not circulating extracellular hemoglobin (as would be expected by hemolysis).

As antiglycolytic therapies proceed through development, strategies to ameliorate erythrotoxicity will be required. We find that exogenous pyruvate supplementation restores reductive capacity to inhibitor-treated erythrocytes. This agrees with previous findings that pyruvate alone maintains erythrocyte ATP levels and 2,3-diphosphoglycerate (2,3-DPG) levels during long-term storage (Paniker and Beutler, 1971; Dawson et al., 1980). In contrast, pyruvate potentiates the antiparasitic effect of enolase inhibition,

perhaps through a feed-back inhibition of parasite glycolysis. These data suggest a profound biological difference in glycolytic regulation between *Plasmodium*-infected and uninfected erythrocytes that may be harnessed for future antimalarial therapeutics. In addition, well-tolerated oral pyruvate supplementation may represent a useful erythroprotective strategy alongside antiglycolytic “starvation-mimetic” therapies—to have one’s cake, and eat it, too (Stanko et al., 1994; Kalman et al., 1999; Koh-Banerjee et al., 2005).

METHODS

Compounds

Phosphonoacetohydroxamate (Sigma), SF2312 (Chem Space), DeoxySF2312, HEX, POM-HEX, and POM-SF were synthesized per previously published procedures (Leonard et al., 2016; Lin et al., 2020). Synthesis of novel SF2312 derivatives and HEX-pro drugs was performed as described (Muller et al., 2019). Compounds were resuspended in DMSO unless otherwise indicated.

Washing, Storage, and *In Vitro* Culture Conditions of Erythrocytes

Banked blood (Saint Louis Children’s Hospital) and fresh blood [healthy donors] was washed and stored at 50% hematocrit at 4°C up to 1 month past the clinical expiration date and collection date, respectively. Parasite strains provided by the Malaria Research and Reference Reagent Resource Center (MR4) as follows: 3D7 (MRA-102); K1 (MRA-159); D10 (MRA-201); and IPC-5202 (MRA-1240). Unless indicated, erythrocytes were cultured as previously described at 2% hematocrit in complete media (incomplete media supplemented with 27mM sodium bicarbonate, 11mM glucose, 5mM HEPES, 1mM sodium pyruvate, 0.37mM hypoxanthine, 0.01mM thymidine, 10µg/mL gentamicin, and 0.5% Albumax I (Thermo-Fisher) under 5% O₂/5% CO₂/90% N₂ atmosphere at 37°C (Guggisberg et al., 2014).

Plasmodium falciparum Growth Inhibition Assays

Asynchronous cultures diluted to 1% parasitemia in 100µL wells were subjected to drug dilutions, solvent controls, and untreated uninfected erythrocyte controls in technical duplicates. Following a three-day incubation, DNA content was quantified using Picogreen (Life Technologies), as previously described (Corbett et al., 2004). Half-maximal effective concentrations (EC₅₀) were determined from nonlinear regression of three biological replicates (GraphPad Prism).

Detection and Quantification of *In Vitro* Erythrocyte Hemolysis

Erythrocytes were treated with 100µM of each compound for 72 hours. Supernatants were collected and erythrocytes were resuspended in 100µL complete media containing 0.1% saponin and diluted 1:10. Hemoglobin (Hb) content of fully lysed erythrocytes and supernatants were determined *via* Abs 404nm. Percent lysis was defined (from four replicates across three separate blood donors) as the ratio of [supernatant Hb content]/[Hb content of fully lysed cultures] X 100.

Detection and Quantification of MetHb Formation

MetHb was detected by measuring absorbance in the 630–640nm range, which is specific from other hemoglobin subforms (oxyhemoglobin, deoxyhemoglobin, and carboxyhemoglobin). Supernatants were removed and erythrocyte pellets were fully lysed and diluted, as described above. The absorption peak for oxyhemoglobin (575nm) and MetHb (630nm) were measured and the EC₅₀ of MetHb formation was determined using non-linear regression analysis (GraphPad Prism).

Determination of Erythrocyte Membrane Asymmetry

Membrane asymmetry was determined by measuring Annexin-V labeling on day three of compound treatment. Erythrocytes washed with 200µL Annexin-V Binding Buffer (140mM sodium chloride, 2.5mM calcium chloride, 10mM HEPES pH 7.4) were briefly spun, supernatants removed, and resuspended in buffer containing Annexin-V conjugated to Alexa-FluorTM 488 (Invitrogen A13201). Annexin-V positivity was determined using an LSR-II BD FACS analyzer containing a 488nm laser. Eryptotic erythrocytes were compared to a 5µM ionomycin-treated positive control and an untreated negative control.

Retro-Orbital Bleeding and Hematocrit Determination

Mice were anesthetized using isoflurane. Blood was collected using heparinized microhematocrit capillary tubes (Fisherbrand #22-362574) *via* retro-orbital approach and was sealed with hemato-seal capillary tube sealant (Fisherbrand #02-678). After spinning at 1,500xg for 10 min, hematocrit was calculated by dividing the measured height of red blood cell layer by the total height of the blood.

Sample Collection for Untargeted Metabolomics

Freshly collected erythrocytes were washed, resuspended to 10% hematocrit in buffer [25mM HEPES (pH 7.4), 120mM NaCl, 5.4mM KCl, 1.8mM CaCl₂, and 1mM NaH₂PO₄], incubated for 1 hour at 37°C, then centrifuged at 2000xg for 5 minutes at 4°C, resuspended in fresh wash buffer to 30–40% hematocrit, and split into 210µL aliquots of packed erythrocytes. Erythrocytes were resuspended in 253µL of RPMI containing 11.9mM D-[1,2,3-¹³C] glucose (Millipore-Sigma) and either treated with POM-SF or POM-HEX at five times the EC₅₀s for MetHb formation, or an untreated solvent control with the balance volume to 550µL using washing buffer. All samples were incubated at 37°C shaking at 500 RPM. Triplicate samples of supernatants and packed erythrocytes were collected at 0, 0.5, 1, and 6-hour intervals and snap-frozen in liquid N₂.

Sample Processing, Metabolite Extraction, and Metabolite Detection

RBC and media samples were extracted at 1:10 and 1:20 dilutions, respectively, in 5:3:2 MeOH : MeCN:H₂O v/v/v, and supernatants analyzed on a Thermo Vanquish UHPLC coupled to a Thermo Q

Exact mass spectrometer, as extensively described (Nemkov et al., 2015; Nemkov et al., 2017). The extraction buffer was supplemented with 40uM 3- ^{13}C lactate to allow absolute quantification of lactate isotopologues, including lactate generated *via* glycolysis ([1,2,3- $^{13}\text{C}_3$] enriched) vs. the pentose phosphate pathway ([2,3- $^{13}\text{C}_2$] enriched), as described (Reisz et al., 2016). Metabolite assignments, peak area integration and isotopologues distributions were determined using Maven (Princeton University) (Nemkov et al., 2015; Nemkov et al., 2017).

Metabolite Data Processing and Analysis

Data were auto-scaled and normalized to zero-hour time points. Metabolites were removed from the dataset if greater than 50% of the samples contained missing values or the relative standard deviation among replicates exceeded 25%. Additionally, data was filtered using the interquartile range to reduce near-constant values from the experiment by 5%.

A principal component analysis of preprocessed data was plotted with the 95% confidence interval minimum volume enclosing ellipsoid for each respective group (MetaboAnalyst, cluster, plotly). A two-way repeated measures analysis of variance (ANOVA) was performed with multiple comparisons corrected for using a false discovery rate p-value cutoff of 0.05. Metabolite-Pathway analysis was performed using the R package of MetaboAnalyst, as previously described (Xia and Wishart, 2010). Metabolite-Protein nodal analysis was performed using omicsnet.ca and as previously described (Zhou and Xia, 2018).

Determining *In Vivo* Efficacy of Enolase Inhibitors Against Blood Stage Parasite Burden

Groups of five female Swiss-Webster mice were injected intraperitoneally (i.p.) with 10^3 luciferase-expressing *P. berghei* ANKA parasites (Franke-Fayard et al., 2008). Forty-eight hours

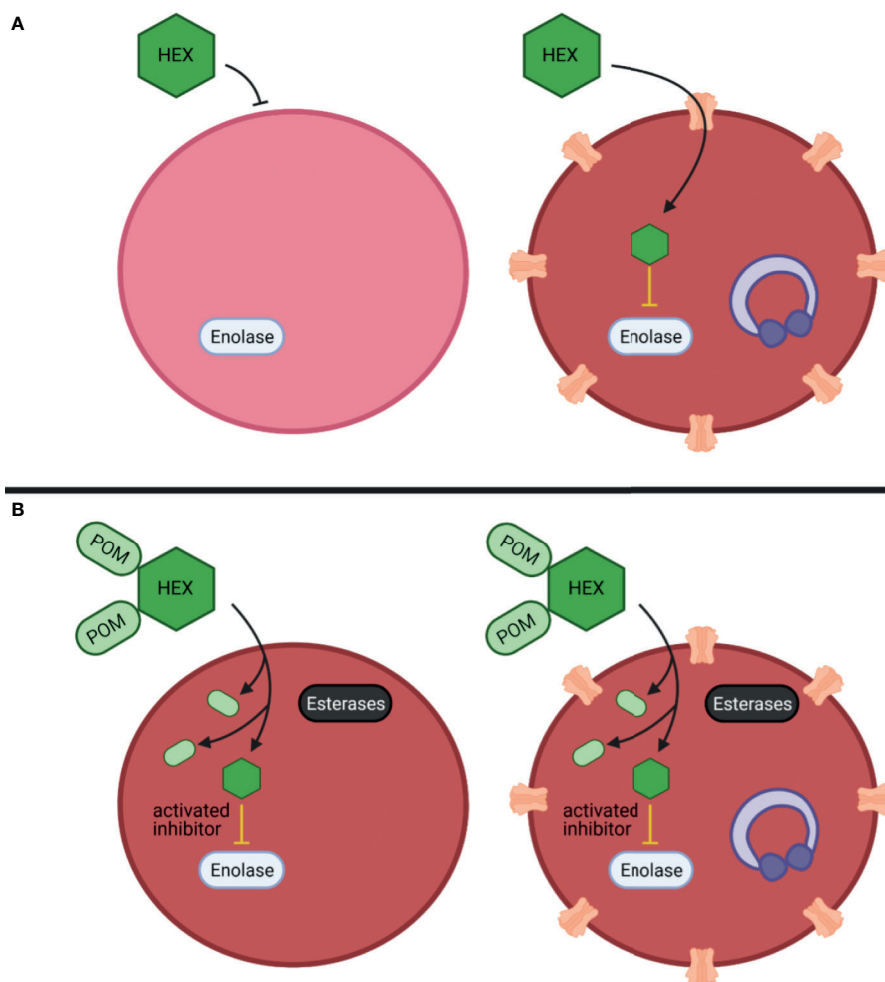


FIGURE 7 | Mechanistic model of anti-parasitic selectivity of a host target. **(A, B)** Darker red indicates increased methHB formation, infected red cells are indicated by purple ring-stage parasites, erythrocyte membrane channels are plasmodium derived low selectivity permeability pathways, prodrug processing is indicated by cytosolic esterases (black) **(A)** The enolase inhibitor HEX exhibits low potency but is selectively targeted to host infected red blood cells to generate a therapeutic index. **(B)** The prodrug cognate POM-HEX increases potency but eliminates any therapeutic window.

post infection, mice were injected i.p. daily for five days with either 200 μ L of 2% methylcellulose/0.5% Tween80, 40mg/kg chloroquine, 100mg/kg HEX, 30mg/kg POM-HEX, or 5mg/kg POM-SF. Enolase inhibitors dosing were selected as approximately 3-fold lower than the maximum acutely tolerated dose for each compound by i.p. injection. Day 7 post-infection, mice were injected with 150mg/kg D-luciferin potassium salt in PBS (GoldBio) and imaged on an IVIS 100 and parasite burden assessed (Xenogen LivingImage).

Determining *In Vivo* Efficacy of Enolase Inhibitors Against Cerebral Malaria

The glucose mimetic 2-DG and enolase inhibitors POM-HEX, and HEX were evaluated in the *P. berghei* mouse model of cerebral malaria, as previously described (Wang et al., 2018). Briefly, in addition to groups of mice ($n = 5$) dosed as described above for POM-HEX and HEX, 2-DG was administered to an additional group ($n = 5$) at 200mg/kg twice daily and all were monitored for survival, parasitemia (blood smear Giemsa), and clinical signs of cerebral malaria (paralysis, deviation of the head, ataxia, convulsions, and coma) over 15 days.

Pharmacokinetics Studies of HEX in Non-Human Primates

Adult male cynomolgus monkeys (*Macaca fascicularis*) with weight of 2.5–3.5 kg were used for PK studies ($n = 1$). To prepare HEX for injection, a stock solution of 150 mg/mL HEX in water with final pH of 7.2–7.4 was prepared. Just prior to injection, this stock was diluted with saline to desired concentration and filtered with 0.22 μ m filter. A dose of 100 mg/Kg of HEX was injected subcutaneously in an overnight fasted monkey. Blood samples were collected at the following time points: before injection, 1 hr, 2 hrs, 4 hrs (when food was also given to a monkey), 8 hrs, and 24 hrs after injection. Also, a dose of 400 mg/Kg of HEX was administered through oral gavage. To compare the PK studies in non-human primates with rodents, a 400 mg/kg dose of HEX was also injected subcutaneously in female mice ($n = 1$), and blood was collected before, 1 hr, and 2 hrs after injection. HEX concentrations in plasma were measured by using nuclear magnetic resonance (NMR) spectroscopy. Two hundred microliters of plasma were extracted with four hundred microliters of -20°C precooled methanol and incubated in -20°C for 45 minutes followed by spinning down in 4°C at $17,000 \times g$ for 30 min to separate supernatant. The supernatant then was concentrated by speedvac for 4 hours and dissolved in 470 μ L D₂O (Sigma Aldrich, 151882) and 30 μ L D₂O with 3%TPS as an internal standard (Sigma Aldrich, 450510) for NMR studies. NMR experiments were performed on Bruker Avance III HD 500 MHz spectrometer equipped with cryoprobe and Bruker 300 MHz with broad band observe probe. For each sample, we obtained one-dimensional (1D) proton (1H) spectrum using zg30 pulse program, 1D 1H spectrum with inverse gated 31-phosphate (31P) decoupling using zgig pulse program and (two-dimensional) 2D 1H-31P heteronuclear single quantum correlation (HSQC) using hsqcetgp pulse program (with scan parameters of 128 scans, gpz2%=32.40, 31P SW= 40 ppm, O2p=0 ppm, cnst2 = 22.95 which is adjusted for

HEX J2 coupling). NMR spectra were analyzed using 3.1 version of TopSpin. HEX was quantified in the sample with high concentration of the drug (100 mpk, 1 hr after SC injection) by comparing integrals of HEX and TSP (reference) in 1H spectra. To calculate HEX concentration for other time points, we obtained the 1D projections of 2D 1H-31P HSQC spectrum using the “proj” command in TopSpin. In the projected spectra, the peak at 1 δ ppm chemical shift appeared only in HEX treated samples which we used to calculate HEX concentration. We took the ratio of integral of 1 δ ppm peak for samples with unknown concentration of HEX versus one with known concentration.

Lead Contact and Materials Availability

Further information and requests for resources and reagents should be directed to and will be fulfilled by the Lead Contact, Audrey Odom John (johna3@email.chop.edu).

Statistics

All statistics represent a minimum of three biological replicates and all analyses were adjusted for multiple comparisons when necessary. Each statistical analysis is described in the respective figure legend and/or methods section. A minimum P-value threshold of $p < 0.05$ was required for statistical significance.

Study Approval

Experiments and procedures on non-human primates were performed as fee-for-service by Charles River Laboratories with approval of Charles River's Institutional Animal Care and Use Committee (IACUC). Mice experiments were performed at University of Texas MD Anderson Cancer Center with approval of MD Anderson's IACUC. The *P. berghei* mice experiments were performed as fee-for-service by the Anti-infectives core at New York University with approval of the NYU IACUC. Fresh human blood was acquired under Washington University protocol (IRB ID #: 201012782) with written informed consent.

DATA AVAILABILITY STATEMENT

This data is available at the NIH Common Fund's National Metabolomics Data Repository (NMDR) website, the Metabolomics Workbench, <http://dx.doi.org/10.21228/M8K41X>, where it has been assigned Project IDPR001177. The data can be accessed directly via its Project DOI: 10.21228/M8K41X.

ETHICS STATEMENT

The studies involving human participants were reviewed and approved by Washington University protocol (IRB ID #: 201012782) with written informed consent. The patients/participants provided their written informed consent to participate in this study. The animal study was reviewed and approved by the respective committees as fee-for-service experiments as indicated in methods section.

AUTHOR CONTRIBUTIONS

All authors contributed to the article and approved the submitted version. AJ performed metabolite sample preparation, red cell and parasite toxicity studies, data analysis, experimental design, data interpretation and manuscript preparation. RC-H performed metabolomics analysis. JR and AD'A performed metabolomics data analysis, data interpretation and manuscript preparation. AO conceived the study, contributed to experimental design, data interpretation, and manuscript preparation. FM conceived and synthesized enolase inhibitors. VY synthesized inhibitors and critical review of the manuscript. Y-HL carried out hematocrit and toxicity studies. YB performed and analyzed PK studies.

ACKNOWLEDGMENTS

The authors are grateful to Stephen Rodgers and Allan Doctor for helpful discussion. We thank Sudhir Ragavan and Pijus

Mandal for technical assistance in chemical synthesis. We thank Dimitra Georgiou for compliance support. This work is supported by the following: AJ is supported by NIH T32GM007067. AD'A was supported by funds from the Webb-Waring Early Career award 2017 by the Boettcher Foundation. FM is an Andrew Sabine family fellow and is supported by The Research Scholar award, RSG-15-145-01-CDD from the American Cancer Society and The Young Investigator Award YIA170032 from the National Comprehensive Cancer Network. AO is supported by NIH/NIAID R01-AI103280, R21-AI123808, and R21-AI130584, and AO is an Investigator in the Pathogenesis of Infectious Diseases (PATH) of the Burroughs Wellcome Fund.

SUPPLEMENTARY MATERIAL

The Supplementary Material for this article can be found online at: <https://www.frontiersin.org/articles/10.3389/fcimb.2021.730413/full#supplementary-material>

REFERENCES

- Andree, H. A., Reutelingsperger, C. P., Hauptmann, R., Hemker, H. C., Hermens, W. T., and Willems, G. M. (1990). Binding of Vascular Anticoagulant Alpha (VAC Alpha) to Planar Phospholipid Bilayers. *J. Biol. Chem.* 265 (9), 4923–4928. doi: 10.1016/S0021-9258(19)34062-1
- Arora, G., Hart, G. T., Manzella-Lapeira, J., Doritchamou, J. Y., Narum, D. L., Thomas, L. M., et al. (2018). NK Cells Inhibit Plasmodium Falciparum Growth in Red Blood Cells via Antibody-Dependent Cellular Cytotoxicity. *Elife* 7, e36806. doi: 10.7554/eLife.36806
- Bahar, F. G., Ohura, K., Ogihara, T., and Imai, T. (2012). Species Difference of Esterase Expression and Hydrolase Activity in Plasma. *J. Pharm. Sci.* 101 (10), 3979–3988. doi: 10.1002/jps.23258
- Bakker, B. M., Michels, P. A. M., Opperdoes, F. R., and Westerhoff, H. V. (1999). What Controls Glycolysis in Bloodstream Form Trypanosoma Brucei? *J. Biol. Chem.* 274 (21), 14551–14559. doi: 10.1074/jbc.274.21.14551
- Baratin, M., Roetynck, S., Lépolard, C., Falk, C., Sawadogo, S., Uematsu, S., et al. (2005). Natural Killer Cell and Macrophage Cooperation in MyD88-Dependent Innate Responses to Plasmodium Falciparum. *Proc. Natl. Acad. Sci.* 102 (41), 14747–14752. doi: 10.1073/pnas.0507355102
- Baumeister, S., Wiesner, J., Reichenberg, A., Hintz, M., Bietz, S., Harb, O. S., et al. (2011). Fosmidomycin Uptake Into Plasmodium and Babesia-Infected Erythrocytes Is Facilitated by Parasite-Induced New Permeability Pathways. *PLoS One* 6 (5), e19334. doi: 10.1371/journal.pone.0019334
- Baumeister, S., Winterberg, M., Duranton, C., Huber, S. M., Lang, F., Kirk, K., et al. (2006). Evidence for the Involvement of Plasmodium Falciparum Proteins in the Formation of New Permeability Pathways in the Erythrocyte Membrane. *Mol. Microbiol.* 60 (2), 493–504. doi: 10.1111/j.1365-2958.2006.05112.x
- Becker, K., Tilley, L., Vennerstrom, J. L., Roberts, D., Rogerson, S., and Ginsburg, H. (2004). Oxidative Stress in Malaria Parasite-Infected Erythrocytes: Host-Parasite Interactions. *Int. J. Parasitol.* 34 (2), 163–189. doi: 10.1016/j.ijpara.2003.09.011
- Brinkmann, V., Kaufmann, S. H., Simon, M. M., and Fischer, H. (1984). Role of Macrophages in Malaria: O₂ Metabolite Production and Phagocytosis by Splenic Macrophages During Lethal Plasmodium Berghei and Self-Limiting Plasmodium Yoelii Infection in Mice. *Infect. Immun.* 44 (3), 743–746. doi: 10.1128/iai.44.3.743-746.1984
- Burrack, K. S., Huggins, M. A., Taras, E., Dougherty, P., Henzler, C. M., Yang, R., et al. (2018). Interleukin-15 Complex Treatment Protects Mice From Cerebral Malaria by Inducing Interleukin-10-Producing Natural Killer Cells. *Immunity* 48 (4), 760–772.e4. doi: 10.1016/j.immuni.2018.03.012
- Cappadoro, M., Giribaldi, G., O'Brien, E., Turrini, F., Mannu, F., Ulliers, D., et al. (1998). Early Phagocytosis of Glucose-6-Phosphate Dehydrogenase (G6PD)-Deficient Erythrocytes Parasitized by Plasmodium Falciparum may Explain Malaria Protection in G6PD Deficiency. *Blood* 92 (7), 2527–2534.
- Chang, X., and Wei, C. (2011). Glycolysis and Rheumatoid Arthritis. *Int. J. Rheumatol. Dis.* 14 (3), 217–222. doi: 10.1111/j.1756-185X.2011.01598.x
- Corbett, Y., Herrera, L., Gonzalez, J., Cubilla, L., Capson, T. L., Coley, P. D., et al. (2004). A Novel DNA-Based Microfluorimetric Method to Evaluate Antimalarial Drug Activity. *Am. J. Trop. Med. Hyg.* 70 (2), 119–124. doi: 10.4269/ajtmh.2004.70.119
- Cummock, K., Gupta, A. S., Lissner, M., Chevee, V., Davis, N. M., and Schneider, D. S. (2018). Host Energy Source Is Important for Disease Tolerance to Malaria. *Curr. Biol.* 28 (10), 1635–1642.e3. doi: 10.1016/j.cub.2018.04.009
- Cyrklaff, M., Srsmith, S., Nyboer, B., Burda, K., Hoffmann, A., Lasitschka, F., et al. (2016). Oxidative Insult can Induce Malaria-Protective Trait of Sick and Fetal Erythrocytes. *Nat. Commun.* 7, 13401. doi: 10.1038/ncomms13401
- Dawson, R. B., Hershey, R. T., and Myers, C. S. (1980). Blood Preservation XXIX. Pyruvate Maintains Normal Red Cell 2, 3-DPG for Six Weeks of Storage in CPD-Adenine. *Transfusion* 20 (2), 218–223. doi: 10.1046/j.1537-2995.1980.20280169965.x
- Driss, A., Hibbert, J. M., Wilson, N. O., Iqbal, S. A., Adamkiewicz, T. V., and Stiles, J. K. (2011). Genetic Polymorphisms Linked to Susceptibility to Malaria. *Malar. J.* 10 (1), 271. doi: 10.1186/1475-2875-10-271
- Franke-Fayard, B., Djokovic, D., Dooren, M. W., Ramesar, J., Waters, A. P., Falade, M. O., et al. (2008). Simple and Sensitive Antimalarial Drug Screening In Vitro and In Vivo Using Transgenic Luciferase Expressing Plasmodium Berghei Parasites. *Int. J. Parasitol.* 38 (14), 1651–1662. doi: 10.1016/j.ijpara.2008.05.012
- Fu, S., Zhu, S., Tian, C., Bai, S., Zhang, J., Zhan, C., et al. (2019). Immunometabolism Regulates TCR Recycling and iNKT Cell Functions. *Sci. Signal.* 12 (570), eaau1788. doi: 10.1126/scisignal.aau1788
- Ginsburg, H., Krugliak, M., Eidelman, O., and Cabantchik, Z. I. (1983). New Permeability Pathways Induced in Membranes of Plasmodium Falciparum Infected Erythrocytes. *Mol. Biochem. Parasitol.* 8 (2), 177–190. doi: 10.1016/0166-6851(83)90008-7
- Guggisberg, A. M., Park, J., Edwards, R. L., Kelly, M. L., Hodge, D. M., Tolia, N. H., et al. (2014). A Sugar Phosphatase Regulates the Methylerythritol Phosphate (MEP) Pathway in Malaria Parasites. *Nat. Commun.* 5, 4467. doi: 10.1038/ncomms5467
- Hedrick, P. W. (2011). Population Genetics of Malaria Resistance in Humans. *Hered. (Edinb.)* 107 (4), 283–304. doi: 10.1038/hdy.2011.16

- Kalman, D., Colker, C. M., Wilets, I., Roufs, J. B., and Antonio, J. (1999). The Effects of Pyruvate Supplementation on Body Composition in Overweight Individuals. *Nutrition* 15 (5), 337–340. doi: 10.1016/S0899-9007(99)00034-9
- Kato, K., Asai, R., Shimizu, A., Suzuki, F., and Ariyoshi, Y. (1983). Immunoassay of Three Enolase Isozymes in Human Serum and in Blood Cells. *Clin. Chim. Acta* 127 (3), 353–363. doi: 10.1016/0009-8981(83)90162-6
- Koh-Banerjee, P. K., Ferreira, M. P., Greenwood, M., Bowden, R. G., Cowan, P. N., Almada, A. L., et al. (2005). Effects of Calcium Pyruvate Supplementation During Training on Body Composition, Exercise Capacity, and Metabolic Responses to Exercise. *Nutrition* 21 (3), 312–319. doi: 10.1016/j.nut.2004.06.026
- Koopman, G., Reutelingsperger, C. P., Kuijten, G. A., Keehnen, R. M., Pals, S. T., and van de Oers, M. H. (1994). Annexin V for Flow Cytometric Detection of Phosphatidylserine Expression on B Cells Undergoing Apoptosis. *Blood* 84 (5), 1415–1420.
- Krieger, D. R., and Landsberg, L. (1989). Obesity, Metabolism, and the Sympathetic Nervous System. *Am. J. Hypertens.* 2 (3 Pt 2), 125S–132S. doi: 10.1093/ajh/2.3.125S
- Krise, J. P., and Stella, V. J. (1996). Prodrugs of Phosphates, Phosphonates, and Phosphinates. *Adv. Drug Deliv. Rev.* 19 (2), 287–310. doi: 10.1016/0169-409X(95)00111-J
- Krishnan, S., Nordqvist, H., Ambikan, A. T., Gupta, S., Sperk, M., Svensson-Akusjarvi, S., et al. (2021). Implications of Central Carbon Metabolism in SARS-CoV-2 Replication and Disease Severity. *bioRxiv*, 432759. doi: 10.1101/2021.02.24.432759
- Lange, K., and Proft, E. R. (1970). Inhibition of the 6-Phosphogluconate Dehydrogenase in the Rat Kidney by 6-Aminonicotinamide. *Naunyn. Schmiedeberg's Arch. Pharmacol.* 267 (2), 177–180. doi: 10.1007/BF00999399
- Lang, F., Jilani, K., and Lang, E. (2015). Therapeutic Potential of Manipulating Suicidal Erythrocyte Death. *Expert Opin. Ther. Targets* 19 (9), 1219–1227. doi: 10.1517/14728222.2015.1051306
- Laszlo, J., Humphreys, S. R., and Goldin, A. (1960). Effects of Glucose Analogues (2-Deoxy-D-Glucose, 2-Deoxy-D-Galactose) on Experimental Tumors. *JNCI J. Natl. Cancer Inst.* 24 (2), 267–281.
- Lelliott, P. M., McMorran, B. J., Foote, S. J., and Burgio, G. (2015). The Influence of Host Genetics on Erythrocytes and Malaria Infection: Is There Therapeutic Potential? *Malar. J.* 14 (1), 289. doi: 10.1186/s12936-015-0809-x
- Leonard, P. G., Satani, N., Maxwell, D., Lin, Y. H., Hammoudi, N., Peng, Z., et al. (2016). SF2312 is a Natural Phosphonate Inhibitor of Enolase. *Nat. Chem. Biol.* 12 (12), 1053. doi: 10.1038/nchembio.2195
- Lin, Y.-H., Satani, N., Hammoudi, N., Yan, V. C., Barekatain, Y., Khadka, S., et al. (2020). An Enolase Inhibitor for the Targeted Treatment of ENO1-Deleted Cancers. *Nat. Metab.* 2, 1413–1426. doi: 10.1038/s42255-020-00313-3
- Lutz, H. U., and Bogdanova, A. (2013). Mechanisms Tagging Senescent Red Blood Cells for Clearance in Healthy Humans. *Front. Physiol.* 4 (December), 387. doi: 10.3389/fphys.2013.00387
- Maćczak, A., Cyrkler, M., Bukowska, B., and Michałowicz, J. (2016). Eryptosis-Inducing Activity of Bisphenol A and its Analogs in Human Red Blood Cells (*In Vitro* Study). *J. Hazard. Mater.* 307, 328–335. doi: 10.1016/j.jhazmat.2015.12.057
- Malaria Genomic Epidemiology Network and Malaria Genomic Epidemiology Network (2014). Reappraisal of Known Malaria Resistance Loci in a Large Multicenter Study. *Nat. Genet.* 46 (11), 1197–1204. doi: 10.1038/ng.3107
- Mallet, R. T., Sun, J., Knott, E. M., Sharma, A. B., and Olivencia-Yurvati, A. H. (2005). Metabolic Cardioprotection by Pyruvate: Recent Progress. *Exp. Biol. Med.* 230 (7), 435–443. doi: 10.1177/153537020523000701
- Marangos, P. J., Campbell, I. C., Schmechel, D. E., Murphy, D. L., and Goodwin, F. K. (1980). Blood Platelets Contain a Neuron-Specific Enolase Subunit. *J. Neurochem.* 34 (5), 1254–1258. doi: 10.1111/j.1471-4159.1980.tb09967.x
- Mejia, P., Treviño-Villareal, J. H., Hine, C., Harputlugil, E., Lang, S., Calay, E., et al. (2015). Dietary Restriction Protects Against Experimental Cerebral Malaria via Leptin Modulation and T-Cell Mtorc1 Suppression. *Nat. Commun.* 6, 6050. doi: 10.1038/ncomms7050
- Miwa, H., Shikami, M., Goto, M., Mizuno, S., Takahashi, M., Tsunekawa-Imai, N., et al. (2013). Leukemia Cells Demonstrate a Different Metabolic Perturbation Provoked by 2-Deoxyglucose. *Oncol. Rep.* 29 (5), 2053–2057. doi: 10.3892/or.2013.2299
- Mohan, K., Ganguly, N. K., Dubey, M. L., and Mahajan, R. C. (1992). Oxidative Damage of Erythrocytes Infected With Plasmodium Falciparum. *Ann. Hematol.* 65 (3), 131–134. doi: 10.1007/BF01695812
- Muller, F., Maxwell, D. S., Bornmann, W. G., Yu-Hsi, L. I., PRASAD, B. A., and Peng, Z. (2019). *Enolase Inhibitors and Methods of Treatment Therewith*. United States Patent US 10,363,261.
- Nemkov, T., D'Alessandro, A., and Hansen, K. C. (2015). Three-Minute Method for Amino Acid Analysis by UHPLC and High-Resolution Quadrupole Orbitrap Mass Spectrometry. *Amino Acids* 47 (11), 2345–2357. doi: 10.1007/s00726-015-2019-9
- Nemkov, T., Hansen, K. C., and D'Alessandro, A. (2017). A Three-Minute Method for High-Throughput Quantitative Metabolomics and Quantitative Tracing Experiments of Central Carbon and Nitrogen Pathways. *Rapid Commun. Mass. Spectrom.* 31 (8), 663–673. doi: 10.1002/rcm.7834
- Oburoglu, L., Tardito, S., Fritz, V., de Barros, S. C., Merida, P., Craveiro, M., et al. (2014). Glucose and Glutamine Metabolism Regulate Human Hematopoietic Stem Cell Lineage Specification. *Cell Stem Cell* 15 (2), 169–184. doi: 10.1016/j.stem.2014.06.002
- Oldfield, E., and Feng, X. (2014). Resistance-Resistant Antibiotics. *Trends Pharmacol. Sci.* 35 (12), 664–674. doi: 10.1016/j.tips.2014.10.007
- Paniker, N. V., and Beutler, E. (1971). Pyruvate Effect in Maintenance of ATP and 2, 3-DPG of Stored Blood. *J. Lab. Clin. Med.* 78 (3), 472–482.
- Patel, A. P., Staines, H. M., and Krishna, S. (2008). New Antimalarial Targets: The Example of Glucose Transport. *Travel Med. Infect. Dis.* 6 (1), 58–66. doi: 10.1016/j.tmaid.2008.01.005
- Pearce, J. M., Edwards, Y. H., and Harris, H. (1976). Human Enolase Isozymes: Electrophoretic and Biochemical Evidence for Three Loci. *Ann. Hum. Genet.* 39 (3), 263–276. doi: 10.1111/j.1469-1809.1976.tb00130.x
- Pelicano, H., Martin, D. S., Xu, R.-H., and Huang, P. (2006). Glycolysis Inhibition for Anticancer Treatment. *Oncogene* 25 (34), 4633–4646. doi: 10.1038/sj.onc.1209597
- Phillips, M. A., Lotharius, J., Marsh, K., White, J., Dayan, A., White, K. L., et al. (2015). A Long-Duration Dihydroorotate Dehydrogenase Inhibitor (DSM265) for Prevention and Treatment of Malaria. *Sci. Transl. Med.* 7 (296), 296ra111. doi: 10.1126/scitranslmed.aaa6645
- Pradere, U., Garnier-amblard, E. C., Coats, S. J., Amblard, F., and Schinazi, R. F. (2014). Synthesis of Nucleoside Phosphate and Phosphonate Prodrugs. *Chem. Rev.* 114 (18), 9154–9218. doi: 10.1021/cr5002035
- Prudêncio, M., and Mota M, M. (2013). Targeting Host Factors to Circumvent Anti-Malarial Drug Resistance. *Curr. Pharm. Des.* 19 (2), 290–299. doi: 10.2174/138161213804070276
- Ramos-Ibeas, P., Barandalla, M., Colleoni, S., and Lazzari, G. (2017). Pyruvate Antioxidant Roles in Human Fibroblasts and Embryonic Stem Cells. *Mol. Cell. Biochem.* 429 (1–2), 137–150. doi: 10.1007/s11010-017-2942-z
- Reisz, J. A., Wither, M. J., Dzieciatkowska, M., Nemkov, T., Issaian, A., Yoshida, T., et al. (2016). Oxidative Modifications of Glyceraldehyde 3-Phosphate Dehydrogenase Regulate Metabolic Reprogramming of Stored Red Blood Cells. *Blood* 128 (12), e32–e42. doi: 10.1182/blood-2016-05-714816
- Rogers, S. C., Ross, J. G., d'Avignon, A., Gibbons, L. B., Gazit, V., Hassan, M. N., et al. (2013). Sick Hemoglobin Disturbs Normal Coupling Among Erythrocyte O₂ Content, Glycolysis, and Antioxidant Capacity. *Blood* 121 (9), 1651 LP – 1662. doi: 10.1182/blood-2012-02-414037
- Sandulache, V. C., Ow, T. J., Pickering, C. R., Frederick, M. J., Zhou, G., Fokt, I., et al. (2011). Glucose, Not Glutamine, is the Dominant Energy Source Required for Proliferation and Survival of Head and Neck Squamous Carcinoma Cells. *Cancer* 117 (13), 2926–2938. doi: 10.1002/cncr.25868
- Satani, N., Lin, Y.-H., Hammoudi, N., Raghavan, S., Georgiou, D. L., and Muller, F. L. (2016). ENOblock Does Not Inhibit the Activity of the Glycolytic Enzyme Enolase. *PLoS One* 11 (12), e0168739. doi: 10.1371/journal.pone.0168739
- Shoshan, M. C. (2012). 3-Bromopyruvate: Targets and Outcomes. *J. Bioenerg. Biomembr.* 44 (1), 7–15. doi: 10.1007/s10863-012-9419-2
- Stanko, R. T., Reynolds, H. R., Hoyson, R., Janosky, J. E., and Wolf, R. (1994). Pyruvate Supplementation of a Low-Cholesterol, Low-Fat Diet: Effects on Plasma Lipid Concentrations and Body Composition in Hyperlipidemic Patients. *Am. J. Clin. Nutr.* 59 (2), 423–427. doi: 10.1093/ajcn/59.2.423
- Stegmann, K. A., De Souza, J. B., and Riley, E. M. (2015). IL-18-Induced Expression of High-Affinity IL-2R on Murine NK Cells is Essential for NK-Cell IFN- γ Production During Murine Plasmodium Yoelii Infection. *Eur. J. Immunol.* 45 (12), 3431–3440. doi: 10.1002/eji.201546018
- Suzuki, M., O'Dea, J. D., Suzuki, T., and Agar, N. S. (1983). 2-Deoxyglucose as a Substrate for Glutathione Regeneration in Human and Ruminant Red Blood

- Cells. *Comp. Biochem. Physiol. Part B Comp. Biochem.* 75 (2), 195–197. doi: 10.1016/0305-0491(83)90312-7
- Tylicki, A., Czerniecki, J., Dobrzyn, P., Matanowska, A., Olechno, A., and Strumilo, S. (2005). Modification of Thiamine Pyrophosphate Dependent Enzyme Activity by Oxythiamine in *Saccharomyces Cerevisiae* Cells. *Can. J. Microbiol.* 51 (10), 833–839. doi: 10.1139/w05-072
- Tzounakas, V. L., Kriebardis, A. G., Georgatzakou, H. T., Foudoulaki-Paparizos, L. E., Dzieciatkowska, M., Wither, M. J., et al. (2016). Glucose 6-Phosphate Dehydrogenase Deficient Subjects may be Better “Storers” Than Donors of Red Blood Cells. *Free Radic. Biol. Med.* 96, 152–165. doi: 10.1016/j.freeradbiomed.2016.04.005
- van Wijk, R., and van Solinge, W. W. (2005). The Energy-Less Red Blood Cell is Lost: Erythrocyte Enzyme Abnormalities of Glycolysis. *Blood* 106 (13), 4034–4042. doi: 10.1182/blood-2005-04-1622
- Vennerstrom, J. L., Nuzum, E. O., Miller, R. E., Dorn, A., Gerena, L., Dande, P. A., et al. (1999). 8-Aminoquinolines Active Against Blood Stage *Plasmodium Falciparum* *In Vitro* Inhibit Hematin Polymerization. *Antimicrob. Agents Chemother.* 43 (3), 598–602. doi: 10.1128/AAC.43.3.598
- Verra, F., Mangano, V. D., and Modiano, D. (2009). Genetics of Susceptibility to *Plasmodium Falciparum*: From Classical Malaria Resistance Genes Towards Genome-Wide Association Studies. *Parasite Immunol.* 31 (5), 234–253. doi: 10.1111/j.1365-3024.2009.01106.x
- Wang, A., Huen, S. C., Luan, H. H., Baker, K., Rinder, H., Booth, C. J., et al. (2018). Glucose Metabolism Mediates Disease Tolerance in Cerebral Malaria. *Proc. Natl. Acad. Sci.* 115 (43), 11042. doi: 10.1073/pnas.1806376115
- Watson, J. A., Leopold, S. J., Simpson, J. A., Day, N. P., Dondorp, A. M., and White, N. J. (2019). Collider Bias and the Apparent Protective Effect of Glucose-6-Phosphate Dehydrogenase Deficiency on Cerebral Malaria. *Elife* 8, e43154. doi: 10.7554/eLife.43154
- Wiemer, A. J., and Wiemer, D. F. (2014). Prodrugs of Phosphonates and Phosphates: Crossing the Membrane Barrier. In: *Montchamp J.L. (eds) Phosphorus Chemistry I*. Topics in Current Chemistry, vol. 360. Springer, Cham.
- Wright, R. O., Lewander, W. J., and Woolf, A. D. (1999). Methemoglobinemia: Etiology, Pharmacology, and Clinical Management. *Ann. Emerg. Med.* 34 (5), 646–656. doi: 10.1016/S0196-0644(99)70167-8
- Wright, R. O., Magnani, B., Shannon, M. W., and Woolf, A. D. (1996). N-Acetylcysteine Reduces Methemoglobin *In Vitro*. *Ann. Emerg. Med.* 28 (5), 499–503. doi: 10.1016/S0196-0644(96)70112-9
- Xia, J., and Wishart, D. S. (2010). MetPA: A Web-Based Metabolomics Tool for Pathway Analysis and Visualization. *Bioinformatics* 26 (18), 2342–2344. doi: 10.1093/bioinformatics/btq418
- Zhou, G., and Xia, J. (2018). OmicsNet: A Web-Based Tool for Creation and Visual Analysis of Biological Networks in 3D Space. *Nucleic Acids Res.* 46 (W1), W514–W522. doi: 10.1093/nar/gky510
- Zilberter, Y., Gubkina, O., and Ivanov, A. I. (2015). A Unique Array of Neuroprotective Effects of Pyruvate in Neuropathology. *Front. Neurosci.* 9, 17. doi: 10.3389/fnins.2015.00017

Conflict of Interest: The authors declare that the research was conducted in the absence of any commercial or financial relationships that could be construed as a potential conflict of interest.

Publisher's Note: All claims expressed in this article are solely those of the authors and do not necessarily represent those of their affiliated organizations, or those of the publisher, the editors and the reviewers. Any product that may be evaluated in this article, or claim that may be made by its manufacturer, is not guaranteed or endorsed by the publisher.

Copyright © 2021 Jezewski, Lin, Reisz, Culp-Hill, Barekatin, Yan, D'Alessandro, Muller and Odom John. This is an open-access article distributed under the terms of the Creative Commons Attribution License (CC BY). The use, distribution or reproduction in other forums is permitted, provided the original author(s) and the copyright owner(s) are credited and that the original publication in this journal is cited, in accordance with accepted academic practice. No use, distribution or reproduction is permitted which does not comply with these terms.



Interaction With the Extracellular Matrix Triggers Calcium Signaling in *Trypanosoma cruzi* Prior to Cell Invasion

Nubia Carolina Manchola Varón¹, Guilherme Rodrigo R. M. dos Santos², Walter Colli¹ and Maria Julia M. Alves^{1*}

¹ Laboratory of Biochemistry of Parasites, Department of Biochemistry, Institute of Chemistry, University of São Paulo, São Paulo, Brazil, ² Department of Clinical Pathology, State University of Campinas, Campinas, São Paulo, Brazil

OPEN ACCESS

Edited by:

Martin M. Edreira,
Universidad de Buenos Aires,
Argentina

Reviewed by:

Moisés Santillán,
Centro de Investigaciones y Estudios
Avanzados, Instituto Politécnico
Nacional de México (CINVESTAV),
Mexico

Marcel I. Ramirez,
Carlos Chagas Institute (ICC), Brazil

*Correspondence:

Maria Julia M. Alves
mjmalves@iq.usp.br

Specialty section:

This article was submitted to
Parasite and Host,
a section of the journal
Frontiers in Cellular
and Infection Microbiology

Received: 27 June 2021

Accepted: 23 August 2021

Published: 04 October 2021

Citation:

Manchola NCV, dos Santos GRRM,
Colli W and Alves MJM (2021)
Interaction With the Extracellular Matrix
Triggers Calcium Signaling in
Trypanosoma cruzi
Prior to Cell Invasion.
Front. Cell. Infect. Microbiol. 11:731372.
doi: 10.3389/fcimb.2021.731372

Trypanosoma cruzi, the etiological agent of Chagas disease in humans, infects a wide variety of vertebrates. Trypomastigotes, the parasite infective forms, invade mammalian cells by a still poorly understood mechanism. Adhesion of tissue culture- derived trypomastigotes to the extracellular matrix (ECM) prior to cell invasion has been shown to be a relevant part of the process. Changes in phosphorylation, S-nitrosylation, and nitration levels of proteins, in the late phase of the interaction (2 h), leading to the reprogramming of both trypomastigotes metabolism and the DNA binding profile of modified histones, were described by our group. Here, the involvement of calcium signaling at a very early phase of parasite interaction with ECM is described. Increments in the intracellular calcium concentrations during trypomastigotes-ECM interaction depends on the Ca^{2+} uptake from the extracellular medium, since it is inhibited by EGTA or Nifedipine, an inhibitor of the L-type voltage gated Ca^{2+} channels and sphingosine-dependent plasma membrane Ca^{2+} channel, but not by Vanadate, an inhibitor of the plasma membrane Ca^{2+} -ATPase. Furthermore, Nifedipine inhibits the invasion of host cells by tissue culture- derived trypomastigotes in a dose-dependent manner, reaching 95% inhibition at 100 μM Nifedipine. These data indicate the importance of both Ca^{2+} uptake from the medium and parasite-ECM interaction for host-cell invasion. Previous treatment of ECM with protease abolishes the Ca^{2+} uptake, further reinforcing the possibility that these events may be connected. The mitochondrion plays a relevant role in Ca^{2+} homeostasis in trypomastigotes during their interaction with ECM, as shown by the increment of the intracellular Ca^{2+} concentration in the presence of Antimycin A, in contrast to other calcium homeostasis disruptors, such as Cyclopiazonic acid for endoplasmic reticulum and Bafilomycin A for acidocalcisome. Total phosphatase activity in the parasite decreases in the presence of Nifedipine, EGTA, and Okadaic acid, implying a role of calcium in the phosphorylation level of proteins that are interacting with the ECM in tissue culture- derived trypomastigotes. In summary, we describe here the increment of Ca^{2+} at an early phase of the trypomastigotes interaction with ECM, implicating both nifedipine-sensitive Ca^{2+} channels in the influx of Ca^{2+} and the

mitochondrion as the relevant organelle in Ca^{2+} homeostasis. The data unravel a complex sequence of events prior to host cell invasion itself.

Keywords: *Trypanosoma cruzi*, calcium signaling, extracellular matrix, Chagas disease, mitochondria

INTRODUCTION

Trypanosoma cruzi, the etiological agent of Chagas disease, infects approximately 7 million people, most of them living in the American continent (World Health Organization, 2020). Replicative and infective forms are present throughout the *T. cruzi* life cycle, which alternates between insect vectors from the reduviidae family and mammalian hosts. Briefly, mammals are infected by *T. cruzi* metacyclic trypomastigotes forms present in the feces and urine of contaminated insects during a blood meal and, closing the life cycle in nature, the invertebrate vectors are infected by trypomastigotes (blood trypomastigotes) during a blood meal in contaminated mammals. Epimastigotes and amastigotes are the replicative forms of the parasite in the digestive tract of the insect and in the cytoplasm of the mammalian cells, respectively, followed by their differentiation into trypomastigotes. Additionally, amastigotes released by the rupture of cells are able to infect other mammalian cells. Congenital infection, blood transfusion, or organ transplants are other forms of *T. cruzi* transmission (World Health Organization, 2020).

T. cruzi trypomastigotes invade both phagocytic and non-phagocytic mammalian cells (Tanowitz et al., 1975) by a poorly understood complex process. *In vitro* studies have highlighted the interaction of tissue culture- derived trypomastigotes with the extracellular matrix (ECM) as an important step of the invasion process. These trypomastigotes bind to distinct ECM components, such as laminin (Giordano et al., 1999), heparan sulfate (Calvet et al., 2003), collagen (Velge et al., 1988), fibronectin (Calvet et al., 2004), thrombospondin (Ulrich et al., 2002; Johnson et al., 2012; Nde et al., 2012), galectin-3 (Da Silva et al., 2017), as well as TGF- β (Nde et al., 2012; Silva et al., 2019). Additionally, extracellular vesicles secreted by the parasite (Gonçalves et al., 1991), soluble factors, and distinct proteases (Santana et al., 1997; Scharfstein et al., 2000; Motta et al., 2012; Watanabe Costa et al., 2016) acting on the host extracellular matrix influence the invasion process. Moreover, remodeling of the ECM by *T. cruzi*, with an increment in the synthesis of collagen IV, fibronectin, and laminin (Cardenas et al., 2010; Coelho et al., 2018), was described in cardiac cells. Increase in thrombospondin-1 in the case of human colon epithelial cells (Suman et al., 2018) was associated with fibrosis, which occurs in chronic Chagas disease patients (Magalhães-Santos et al., 2004; Garzoni et al., 2008; Nájera et al., 2021). Notwithstanding, biochemical events triggered by ECM on trypomastigotes during their mutual interaction are less explored (Nde et al., 2012). Coexistence of tissue culture- derived trypomastigotes with ECM for 2 h (late phase) leads to large cellular responses, with changes in the phosphorylation (Mattos et al., 2019), S-nitrosylation (Mule et al., 2021), and nitration levels of proteins

(Magalhães et al., 2020), suggesting a pre-adaptation of the parasite to its new intracellular environment. Reprogramming of the *T. cruzi* metabolism upon incubation with the ECM, involving kinases and phosphatases, was also described (Mattos et al., 2019), as well as global changes in the binding pattern of nitrated proteins to DNA, indicating changes in the chromatin structure, possibly affecting nuclear functions (Magalhães et al., 2020). Of note, nitrated histones, with the identification of the modified residue in histone H2B (Y29) by mass spectroscopy, were identified for the first time in trypomastigotes (Magalhães et al., 2020). Although the signaling pathways were not determined, the data show that the interaction of tissue culture- derived trypomastigotes with the ECM for a 2-h period activates distinct signaling responses before the parasite reaches the intracellular milieu of the host cells. However, the early events triggered by the interaction of *T. cruzi* trypomastigotes with the ECM have not been explored yet.

Calcium signaling pathways control many diverse processes in all eukaryotic cells and, particularly, Ca^{2+} is essential for the invasion of host cells by *T. cruzi* trypomastigotes, even though differences between metacyclic and tissue culture-derived trypomastigotes in the invasion process were described (Moreno et al., 1994; Yakubu et al., 1994; Ruiz et al., 1998). Although the mechanism is not fully understood, increment in the intracellular Ca^{2+} concentration in trypomastigotes, as well as in host cells, occurs at early stages of the invasion process (Tardieux et al., 1994; Moreno and Docampo, 2003; Chiurillo et al., 2019). The increment appears to be necessary in processes such as the fusion of the plasma membrane with the lysosome during invasion (Burleigh and Andrews, 1998). Acidocalcisomes, which are important Ca^{2+} stores in trypanosomatids, were implicated in this Ca^{2+} increment, since the inositol 1,4,5-triphosphate receptor (IP3R) localizes to the acidocalcisomes (Lander et al., 2016) and ablation of the IP3R gene inhibits host cells invasion by trypomastigotes (Chiurillo et al., 2020). In addition to acidocalcisomes, the single mitochondrion of *T. cruzi*, the endoplasmic reticulum, and the plasma membrane are involved in Ca^{2+} homeostasis and signaling (Lu et al., 1998; Lander et al., 2018), with different Ca^{2+} transporters implicated (Ramakrishnan et al., 2018). L-type voltage gated Ca^{2+} channels (VGCCs) (Prole and Taylor, 2011) and Ca^{2+} ATPase (PMCA) (Docampo and Huang, 2015) are responsible for Ca^{2+} uptake and extrusion, respectively, in the plasma membrane. Recently, a sphingosine-dependent Ca^{2+} channel and voltage independent was described for the Ca^{2+} uptake in the plasma membrane of *T. cruzi* (Rodríguez-Duran et al., 2019) and *Leishmania* (Benaim et al., 2013). Although this channel resembles the human L-type VGCCs, it differs in its activation by sphingosine and can be explored as a target for drug development (Ramakrishnan et al., 2018; Benaim et al., 2020). Considering the main Ca^{2+} storage

organelles, a calcium uniporter complex (MCUC) and a $\text{Ca}^{2+}/\text{H}^{+}$ exchanger for Ca^{2+} uptake and Ca^{2+} release, respectively, are present in the inner mitochondrial membrane; a Ca^{2+} -ATPase for Ca^{2+} uptake, in addition to the mentioned IP3R for calcium efflux is present in acidocalcisomes. Although a sarcoplasmic-endoplasmic reticulum-type Ca^{2+} ATPase (SERCA) for the Ca^{2+} uptake was described, no Ca^{2+} release mechanism was identified, since the IP3 receptor is absent in the endoplasmic reticulum (Chiurillo et al., 2020).

As pointed out above, we identified relevant changes in several metabolic pathways of *T. cruzi* trypomastigotes after a 2-h interaction with the extracellular matrix. Modifications in the phosphorylation, nitration, and S-nitrosylation levels, reprogramming of metabolism, as well as alterations in the chromatin structure, possibly affecting nuclear functions, strongly suggest a broad effect of parasite adhesion to the ECM, a step that precedes the invasion itself. Here, an increment in the Ca^{2+} concentrations at an early phase of the tissue culture-derived trypomastigotes interaction with the ECM is described, implicating nifedipine-sensitive Ca^{2+} channels present at the plasma membrane. Additionally, inhibition of the Ca^{2+} uptake by this channel impairs the trypomastigote invasion of mammalian cells. Data also support the conclusion that the sole mitochondrion of the parasite is the major organelle in this aspect of Ca^{2+} signaling.

MATERIALS AND METHODS

Incubation of Tissue Culture-Derived Trypomastigotes With the Extracellular Matrix (ECM) (MTy)

Cultured-derived trypomastigotes from *T. cruzi* (Y strain) were obtained by the infection of epithelial rhesus monkey cells (LLC-MK₂) as described (Andrews and Colli, 1982). The parasites released on the fifth day after infection of LLC-MK₂ were collected and purified on DEAE-Cellulose chromatography as described (de Sousa, 1983; Cruz-Saavedra et al., 2017). Then, 5×10^8 parasites in 5 ml of Modified Eagle's Medium (MEM) supplemented with 2% FBS (MEM-2%FBS) were mixed with up to 100 μL (containing between 10–45 μg of protein, as quantified by Bradford assay) of commercial ECM (GeltrexTM LDEV-Free Reduced Growth Factor Basement Membrane Matrix, Invitrogen, lots 1790948, 2030111 or 2007114) and incubated at 37°C and 5% CO₂ for different periods of time (between 0–20 min) according to the experiment, as described by Mattos et al. (2019) or with ECM elements (5 μg of collagen-1, heparan sulfate, thrombospondin, laminin-111, fibronectin). After the incubation, the parasites were centrifuged at 4,000 $\times g$ for 10 min and the pellets stored at -80°C until use (MTy samples). As a control, tissue culture-derived trypomastigotes were submitted to the same experimental conditions, except for the absence of the ECM (Ty samples). ECM-protease treated was obtained by incubating 40 μg of ECM with 5 mg/mL of proteases (P0652 Sigma) for 1 h at 35°C, followed by the addition of 50 μL of protease inhibitor cocktail (P8465 Sigma). Collagen-treated

collagenase was obtained by incubating 5 mg of Collagen I with collagenase (C6885 Sigma) as described.

Immunofluorescence

Tissue culture-derived trypomastigotes (1×10^8) were incubated in MEM-2%FBS in the presence or absence of 100 μM Nifedipine (481981 CalbioChem) for 2 h at 37°C and 5% CO₂. After incubation, the parasites were washed with PBS and fixed in 2% paraformaldehyde (PFA) for 2 h, washed, and incubated with anti-Tubulin antibody (1:100) (Sigma-Aldrich Cat# T8328, RRID: AB_1844090) in PBS-0.1% BSA. After an overnight incubation at 4°C, the samples were washed three times with PBS and incubated with Alexa-Fluor anti-mouse 488 secondary antibody (1:5,000), following the instructions of the manufacturer. The images were taken on an ExiBlueTM camera (Qimaging[®]) coupled to a Nikon Eclipse E 600 optical microscope and deconvoluted using the ImageJ 1.x software as described by Schneider et al. (2012). The exposition time was the same for each sample, in order to compare the parasite morphology.

To verify the Nifedipine (Nif) effect during the infection process, tissue culture-derived trypomastigotes were incubated in the presence of different Nif concentrations (0–100 μM , freshly prepared) for 2 h in MEM-2%FBS at 37°C and 5% CO₂, as above, centrifuged, resuspended in 500 μL of MEM-2% FBS, and employed to infect LLCMK₂ cells. LLCMK₂ cells (1×10^5 cells/well in 24-well plates) were previously cultivated in MEM-10%FBS at 37°C and 5% CO₂. After 24 h, each well containing the LLCMK₂ cells was infected with 1×10^7 trypomastigotes previously incubated in the presence or absence of Nif. After 2 h, the wells were washed 4x with PBS, followed by incubation in MEM-2% FBS at 37°C and 5% CO₂ for 48 h. After an extensive wash with PBS, the cells were fixed by the addition of 2% PFA for 2 h. The wells were then washed 2x with PBS, treated with 0.01% TritonX-100 for 5 min, followed by the addition of 0.5 $\mu\text{g}/\text{mL}$ of DAPI for staining the nucleus of the cells. The images were acquired in a DMi8 Leica microscope. To determine the rate of infection, the nucleus of LLCMK₂ and parasite cells, corresponding to 400 host cells, were counted using the Fiji Image J cell counter plugin. The pictures are representative of three independent experiments.

Immunoblotting

Tissue culture-derived trypomastigotes, 1×10^8 per sample in MEM-2%FBS, were incubated (or not) with 48 μg of ECM for 0, 5, or 10 min in the presence of 1 mM EGTA, 10 nM Okadaic acid (Sigma, Cat# O9381), or 4 μM Nifedipine in the same conditions described above. After incubation, the parasites were washed twice with PBS, resuspended in 500 μL of PBS supplemented with 20 μL of protease inhibitor cocktail (Sigma, Cat# P8465) and 20 μL of phosphatase inhibitor cocktail (Sigma, Cat# P2850). The cells were disrupted by mechanical force (Sonication 3 times at 20 power) and centrifuged at 5,000 g for 10 min. Proteins were separated by the SDS-polyacrylamide gel electrophoresis (12% SDS-PAGE), followed by the immunoblotting procedures, as described by Mattos et al. (2019), using rabbit anti-phosphorylated proteins (Pan) (Thermo Fisher Scientific

Cat# 61-8300, RRID : AB_2533941), home-made mouse monoclonal anti-parafagellar rod antibody (Anti -PFR) (1:10,000), mouse monoclonal anti-Collagen TI (1:1,000) (Sigma-Aldrich Cat# C2456, RRID : AB_476836), and the corresponding HRP-conjugated secondary antibodies. Due to the presence of ECM in the experiments involving trypomastigotes incubated with ECM, samples corresponding to the parasite number (1×10^6 parasites/lane), and not to the protein content, were loaded. Densitometry of phosphorylated proteins from the immunoblottings is expressed in Arbitrary Units normalized by the parafagellar rod protein content using a home-made monoclonal antibody (Mattos et al., 2019). Three independent experiments were performed and the statistical significance calculated (1way ANOVA) $P < 0.05$.

Intracellular Free Calcium Quantification

Trypomastigote forms purified by the DEAE-Cellulose chromatography as described above were washed twice with cold buffer A (116 mM NaCl, 5.4 mM KCl, 0.8 mM MgSO_4 , 5.5 mM D-glucose, 50 mM HEPES, pH 7.2). The parasites were resuspended to a final concentration of 1×10^9 cells per mL in buffer A supplemented with 1.5% sucrose, 3 μM Fluo-4AM fluorescent dye (Sigma, Cat# F14201) and 0.02% of Pluronic F-127 and then incubated for 1 h at 37°C under constant agitation and protected from light. After incubation, the parasites were washed three times with cold buffer A. The maximum fluorescence was determined by measuring the fluorescence of 50 μL (5×10^7 parasites per measure) at λ_{ex} : 495/ λ_{em} :520 nm in the presence of 2 mM CaCl_2 in buffer A (at 37°C) after the addition of 0.03% Triton X-100, and the minimum fluorescence was determined by adding EGTA (100 mM) after 0.03% Triton X-100 [the concentration was calculated by the CaEGTA v1.3 (Bers et al., 2010) calculator from maxchelator.stanford.edu]. The presence of the dye was checked after the experiments by observation at the fluorescence microscopy. Intracellular free calcium levels $[\text{Ca}^{2+}]_i$ were determined by the following equation, where F is the AU of fluorescence and F_{min} and F_{max} correspond to the minimum and maximum F values, respectively:

$$[\text{Ca}^{2+}]_i = Kd * \left\{ \frac{(F - F_{\text{min}})}{(F_{\text{max}} - F)} \right\}, Kd: 345 \text{ nM Fluo4 AM}$$

In order to determine whether the increase of intracellular free calcium levels was due to the extracellular calcium entry or release of calcium from any organelle, measurements were performed in the presence or absence of ECM and in 2 mM CaCl_2 -containing buffer A or 1 mM EGTA-containing buffer A. According to the experiment, different amounts of ECM were employed (between 0 and 40 $\mu\text{g}/\text{mL}$). ECM aliquots were maintained at -80°C and kept at 4°C before use in the experiments. The fluorescence changes were monitored in a Hitachi 7100 fluorescence spectrophotometer.

In order to disrupt the calcium flow through the parasite plasma membrane, 1 mM Vanadate (Van) or 4 μM Nifedipine (Nif) (freshly prepared) were added. To estimate the free intracellular calcium release from the mitochondria,

acidocalcisome, and endoplasmic reticulum, 0.3 $\mu\text{g}/\text{mL}$ of Antimycin A (AA) (Sigma, Cat# A8674), 1 μM Bafilomycin A (Baf) (MedChemExpress, Cat# HY-100558), and 0.3 μM Cyclopiazonic acid (CPA) (Sigma, Cat# C1530) were added, respectively, to trypomastigotes in the presence or absence of ECM. The data represent 5, 4 or 3 independent experiments for Baf, AA and CPA, respectively and the statistical significance calculated (1way ANOVA) $P < 0.05$.

Measurement of Phosphatase Activity

Tissue culture- derived trypomastigotes (1×10^8) were incubated (or not) with 40 μg of ECM for 10 min at 37°C in the presence of 1 mM EGTA, 4 μM Nifedipine, or 10 nM Okadaic acid (O9381 Sigma) (negative control), a specific inhibitor of serine/threonine phosphatases. The samples were centrifuged, washed two times with PBS, and resuspended in 500 μL of PBS supplemented with 50 μL of protease inhibitor cocktail (P8465 Sigma). The cells were disrupted by mechanical force (Sonication 3 times at 20 power) and the protein content of the samples was quantified by the Bradford assay. All the samples were kept on ice until the phosphatase assay. The phosphatase assay was performed as previously described (Meyer-Fernandes et al., 1999). Briefly, 1 mg/mL of the total extract was added to the reaction mixture [10 mM p-nitrophenyl phosphate (PNPP) (P4744 Sigma), 50 mM Tris-HCl pH 7.2] and incubated at 30°C for different periods of time (0, 10, 20, 30, 40, 60 min). The reaction was stopped by the addition of 1 mL of 1 N NaOH and the p-nitrophenol (PNP) produced was measured at 425 nm, using the attenuation coefficient of $1.8 \times 10^4 \text{ M}^{-1}\text{cm}^{-1}$. Three independent experiments were performed and the statistical significance calculated (One-way ANOVA) $P < 0.05$.

RESULTS

Intracellular Free Calcium Concentrations Increase in Tissue Culture-Derived Trypomastigotes After Extracellular Matrix (ECM) Addition

To investigate the role of the ECM on calcium signaling in *T. cruzi*, (5×10^7 parasites per measure) Fluo4-loaded tissue culture- derived trypomastigotes (Supplementary Figure 1-Video) were first incubated with different ECM concentrations (0, 12, 24, and 40 μg) in order to establish a dose-dependent curve (Figures 1C, D). A rapid Ca^{2+} uptake was observed with a plateau reached in less than 2 min. At 2 min of incubation, the intracellular Ca^{2+} ($[\text{Ca}^{2+}]_i$) increased from 50 nM to 65 nM, in a manner dependent on the amount of the ECM (Figure 1D). The dependence on the extracellular Ca^{2+} was verified by the incubation of Fluo4-loaded trypomastigotes in a Ca^{2+} -rich medium (2 mM CaCl_2) (Figure 1A) or in a Ca^{2+} free extracellular medium (1 mM EGTA) (Figure 1B) after the addition of 12 or 40 μg of ECM. The uptake of Ca^{2+} by trypomastigotes was observed only when extracellular calcium was present (Figure 1A).

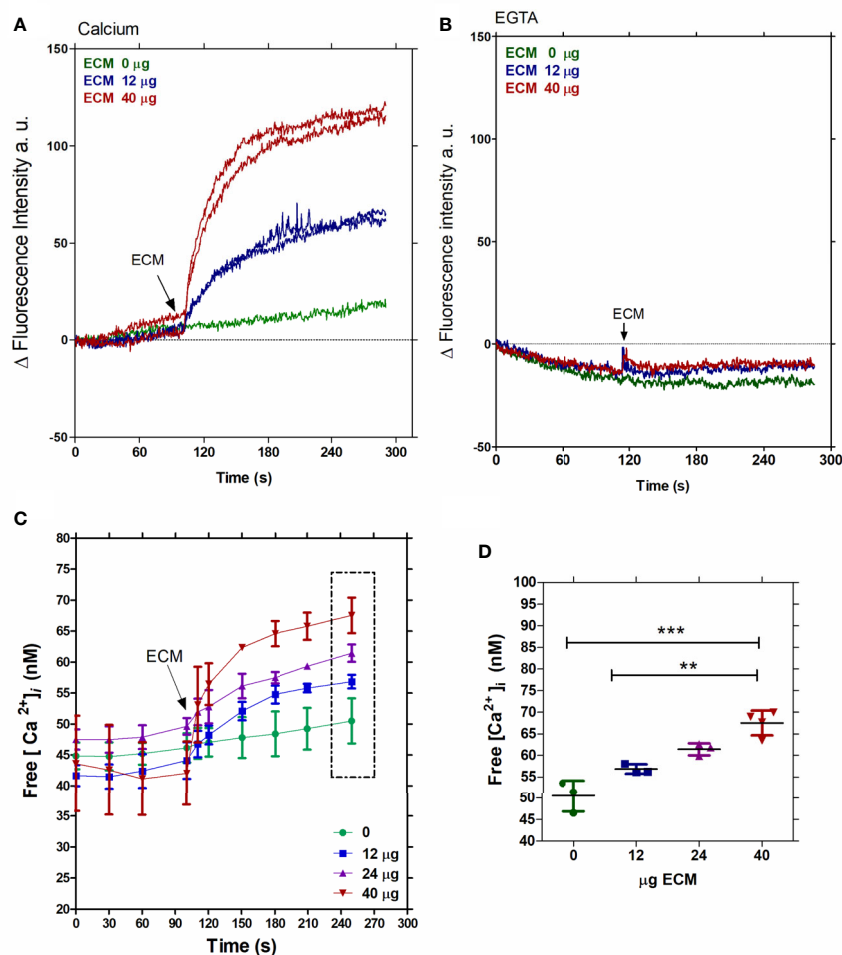


FIGURE 1 | Free intracellular calcium increases in *T. cruzi* trypomastigotes upon interaction with the ECM. Fluo-4-AM-loaded tissue culture-derived trypomastigotes were employed. **(A)** Fluorescence intensity measured in the presence of two ECM concentrations (12 or 40 μ g) and 2 mM extracellular Ca^{2+} . **(B)** Fluorescence intensity measured in the presence of two ECM concentrations (12 or 40 μ g) and 1 mM EGTA. **(C)** Increment of free intracellular $[Ca^{2+}]_i$ in response to the ECM concentrations (0, 12, 24, or 40 μ g). **(D)** Dose-dependent free intracellular $[Ca^{2+}]_i$ and ECM concentration after 2.5 min of incubation, from **Figure 1C**. Statistical significance was $P < 0.05$, Tukey test ANOVA. **Figures 1A, B** are representative of three independent experiments, using three different commercial samples of ECM. ** $P < 0.01$, *** $P < 0.001$.

Extracellular Calcium Uptake by Trypomastigotes Through Nifedipine-Sensitive Calcium Channels

To identify the plasma membrane calcium channels involved in the tissue culture-derived trypomastigotes response to the ECM, Ca^{2+} uptake was measured in the presence of Vanadate, an inhibitor of the plasma membrane Ca^{2+} ATPase, and Nifedipine, a 1,4-dihydropyridine, a well characterized inhibitor of L-type voltage gate Ca^{2+} channels (L-type VGCC) in humans, which inhibits the sphingosine-dependent plasma membrane Ca^{2+} channels described in trypanosomatids (Benaïm et al., 1991; Rodríguez-Duran et al., 2019). As shown in **Figure 2**, the addition of 4 μ M Nifedipine (Nif) totally blocked the extracellular Ca^{2+} uptake by Fluo-4-loaded trypomastigotes incubated with the ECM (**Figure 2B**), whereas 1 mM

Vanadate (Van) showed no effect (**Figure 2A**). The data indicate that the increase in the intracellular free Ca^{2+} concentration in trypomastigotes observed during the ECM stimulus occurs *via* Nifedipine – sensitive calcium channels.

The role of Nifedipine was then tested in the invasion of epithelial cultured cells by trypomastigotes, since the relevance of Ca^{2+} in the process is well established in the literature. Trypomastigotes were incubated with 0 (control), 4, 10, 50, and 100 μ M Nifedipine for 2 h and the infection level determined by counting the number of intracellular amastigotes (**Figures 3A, B**). A dose-dependent inhibition was observed, with 58% at 4 μ M and 95% at 100 μ M, the lower and the higher concentrations employed. Of note, no changes in the morphology (**Figure 3C**) nor in the motility of trypomastigotes were noticed after the treatments. The data point out the essential role of the extracellular Ca^{2+} uptake

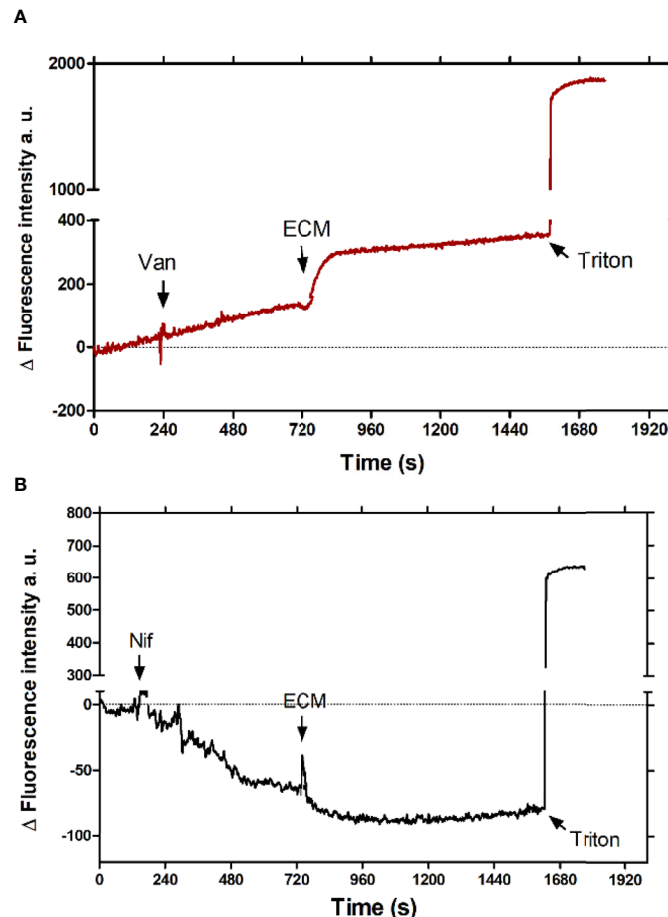


FIGURE 2 | Effect of Ca^{2+} channel inhibitors in the intracellular Ca^{2+} concentration of tissue culture-derived trypomastigotes upon interaction with the ECM. **(A)** 1 mM Vanadate (Van) (red line) or **(B)** 4 μM Nifedipine (Nif) (black line) were added to 5×10^7 Fluo-4-loaded trypomastigotes, followed by the addition of 24 μg of ECM after the signal stabilization. 0.03% Triton-X100 was added at the end of experiment to determine the maximum fluorescence value. The graph is representative of three independent experiments.

through Nifedipine-sensitive calcium channels in the trypomastigote invasion of mammalian cells.

Organelles Involved in Calcium Homeostasis During Trypomastigote-Extracellular Matrix (ECM) Interaction

Intracellular Ca^{2+} homeostasis is rapidly reestablished by the organelles that are able to release or store calcium. Acidocalcisomes, mitochondria and endoplasmic reticulum are the main intracellular stores of Ca^{2+} in trypanosomatids. Their involvement in the uptake of Ca^{2+} increase in tissue culture-derived trypomastigotes incubated with ECM can be identified by the use of inhibitory conditions specific for each organelle. PMCA, a Ca^{2+} -ATPase, similar to the plasma membrane-type Ca^{2+} -ATPase, present in acidocalcisomes, is inhibited by bafilomycin A, a specific inhibitor of vacuolar-type H^{+} -ATPases or by pH change of the organelles, e.g. by NH_4Cl ; endoplasmic reticulum has a sarcoplasmic-endoplasmic

reticulum-type Ca^{2+} -ATPase that is inhibited by cyclopiazonic acid; mitochondria have a MCU (Mitochondrial Calcium Uniporter) complex, that could be inhibited by analogues of ruthenium red and alternatively, its role can be shown by respiratory chain blockers, such as antimycin A or uncouplers of oxidative phosphorylation. In order to establish which intracellular organelles are involved in Ca^{2+} uptake, the amount of free intracellular Ca^{2+} was measured in Fluo-4-loaded tissue culture-derived trypomastigotes in the presence or absence of the ECM and specific Ca^{2+} homeostasis disruptors: (**Supplementary Figure 2**): Antimycin A (AA, 0.3 $\mu\text{g}/\text{mL}$) for mitochondria, Cyclopiazonic acid (CPA, 0.3 μM) for the endoplasmic reticulum (ER) (**Figures 4A, B**), and Bafilomycin A (Baf, 1 μM) for acidocalcisomes (**Figure 4C**). As shown in **Figure 4B**, the amount of free intracellular Ca^{2+} measured after AA treatment was higher than the sample without AA, and it is also higher than the control without the ECM (**Figure 4A**). No significant modifications were observed when CPA was added to trypomastigotes incubated or not with ECM

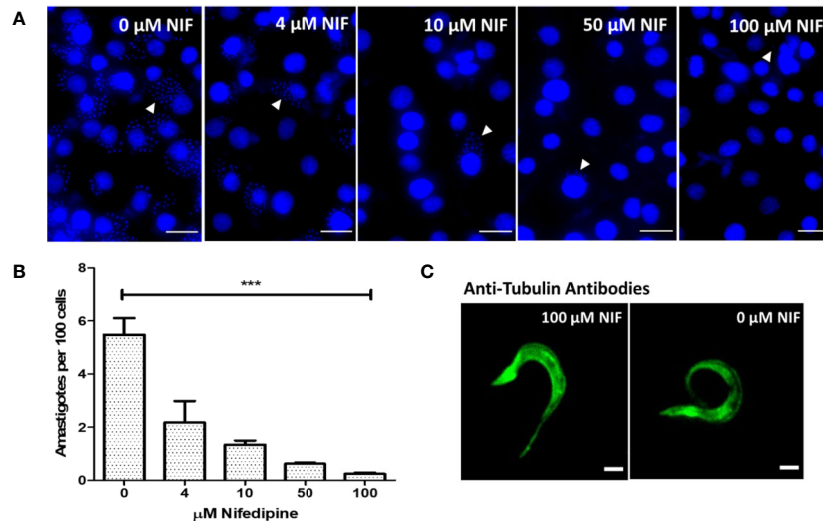


FIGURE 3 | Extracellular Ca^{2+} uptake through Nifedipine- sensitive calcium channels is essential for tissue culture-derived trypomastigotes invasion. **(A)** Epithelial cells were incubated with trypomastigotes in the presence of 0, 4, 10, 50, and 100 μM Nifedipine (Nif) for 2 h and the infection analyzed 48 h later by the presence of intracellular *T. cruzi* amastigotes. White arrows indicate the amastigotes stained kinetoplasts; white bars represent 500 μm . **(B)** Quantification of 400 host cell infection from 3A. Statistical significance when compared with (0) (One-way ANOVA) $P < 0.05$. **(C)** Trypomastigotes incubated with 0 or 100 μM Nifedipine for 2 h, fixed, and developed with anti-tubulin antibodies. White bars indicate 5 μm . *** $P < 0.001$.

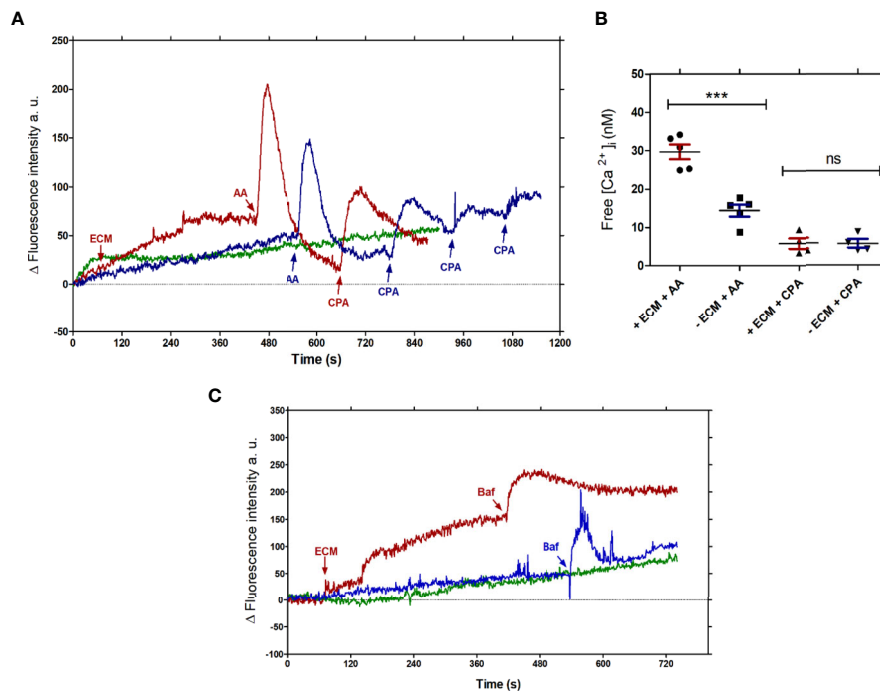


FIGURE 4 | Organelles involved in the Ca^{2+} homeostasis in *T. cruzi* trypomastigotes upon interaction with the ECM. **(A)** Measurement of the intracellular free Ca^{2+} concentration in the presence of AA (0.3 $\mu\text{g/mL}$) or CPA (0.3 μM); Trypomastigotes + ECM (MTy, red line); Trypomastigotes (Ty, Blue line); basal signal from non-stimulated 5×10^7 parasites (Green line). **(B)** Free calcium concentration measured in MTy incubated in the presence or absence of AA and CPA. The graphs are representative of five independent experiments, as shown in **Figure 4A**. The size of the peaks was estimated from the addition point to the maximum top. Statistical significance (One-way ANOVA) $p < 0.01$. **(C)** Measurement of the intracellular Ca^{2+} concentration of trypomastigotes in the presence or absence of Baf (1 μM); MTy (Red line); Ty (Blue line); basal signal from parasites not stimulated (Green line). The graph is representative of three independent experiments. MTy: 5×10^7 trypomastigotes + 24 μg of ECM. *** $P < 0.001$; ns, no significant.

(Figures 4A, B) in five independent experiments. These results show the relevance of mitochondria in the uptake of Ca^{2+} , which is dependent on the membrane potential, disrupted by the AA inhibition of complex III from the electron chain. Although acidocalcisomes contain the IP₃ receptor and are considered the main organelle involved in the calcium homeostasis (Huang and Docampo, 2020), 1 μM Bafilomycin A did not show significant differences between the sample in the presence or absence of ECM (free calcium concentration 11.17 ± 1.5 nM for Ty and 10.57 ± 0.98 nM for MTy) (Figure 4C). The data points out to the relevance of mitochondria in calcium homeostasis during the ECM-trypomastigote interaction.

Phosphoprotein Profile of Trypomastigotes Upon Extracellular Matrix (ECM) Interaction

Since phosphoproteomic analysis showed significant changes in the tissue culture-derived trypomastigotes incubated with ECM for 2 h (Mattos et al., 2019), the phosphoprotein profile was then analyzed in the early phase of the interaction by Western blot developed with anti-phospho-Ser/Thr/Tyr antibodies. To have a

clue of the downstream signaling pathways, the phosphoprotein profile was analyzed by the incubation of 1×10^8 tissue culture-derived trypomastigotes with 40 μg of ECM for 0, 5, or 10 min in the presence of 1 mM EGTA (EMTy), 10 nM Okadaic acid (OMTy), a cell permeant specific Ser/Thr phosphatase inhibitor, or 4 μM Nifedipine (NMTy). Although the analysis of phosphorylated proteins was restricted to proteins below 70 kDa due to the presence of ECM in MTy (Figure 5A, lane M), the number of phosphorylated proteins was reduced in the trypomastigotes incubated with ECM for 10 min. Okadaic acid, EGTA, or Nifedipine inhibit the dephosphorylation observed in MTy, showing the relevance of extracellular Ca^{2+} as an activator of phosphatases (Figure 5A). To confirm the results, the total p-nitro phosphatase activity was measured in cell extracts from the EMTy, NMTy, MTy, and OMTy samples from the 10-min incubation time (cf. Figure 5A). The phosphatase activity was measured for 60 min at 10-min intervals and the production of p-nitrophenol (pNP) was measured (Figures 5B, C). The presence of Nifedipine, EGTA, or Okadaic acid partially inhibited the phosphatase activity (~30%–35%), demonstrating the relevance of the Ca^{2+} uptake for the total phosphatase activity.

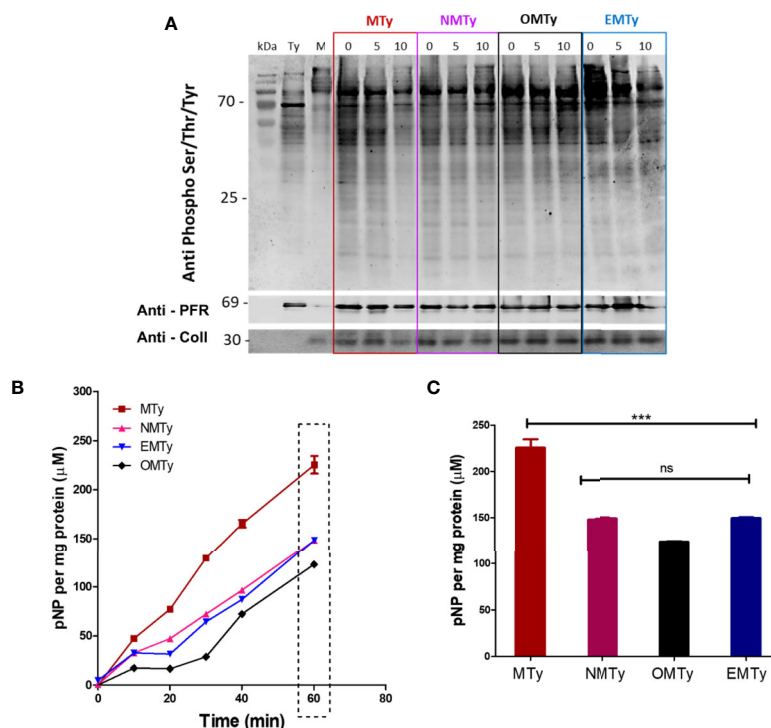


FIGURE 5 | Phosphoprotein profile (A) and p-nitrophenyl phosphatase activity (B, C) from tissue culture-derived trypomastigotes upon interaction with ECM. Ty (trypomastigotes), MTy (+40 μg of ECM), NMTy (+40 μg of ECM and 4 μM Nifedipine), OMTy (+40 μg of ECM and 10 nM Okadaic acid), EMTy (+40 μg of ECM and 1 mM EGTA). (A) Immunoblot showing the phosphorylated protein profile of the samples incubated under the described conditions for different periods of time (0, 5, or 10 min). M corresponds to the control of the ECM (0.4 μg per lane); Anti-Coll (Collagen I) antibody indicates the presence of ECM in the sample (control); Anti-PFR (Paraflagellar Rod Protein) monoclonal antibody [control for the normalization of parasites loading (1×10^6 parasites/lane)]. (B) Total p-nitro phosphatase activity of the MTy samples incubated with the drugs for 10 min. The production of pNP (p-Nitrophenol) was measured at different periods of time as indicated. The graph is representative of three independent experiments. (C) Bars representation of the square present in (B), statistical significance (One-way ANOVA) $P < 0.05$. *** $P < 0.001$; ns, no significant.

A slightly higher inhibition of enzyme activity was observed in the presence of Okadaic acid, an inhibitor of PP2A and PP1 protein phosphatases from *T. cruzi* (Szöör, 2010).

Ca²⁺ Signaling in MTy Is Dependent on the Protein Components of the Extracellular Matrix (ECM)

Since the ECM components, including Collagen I (Velge et al., 1988), are implicated in the adhesion step of trypomastigotes when invading host mammalian cells, free intracellular calcium of Fluo-4-loaded trypomastigotes was measured in the presence of Collagen I (ColI). To verify the role of this ECM protein content in Ca²⁺ signaling, trypomastigotes were incubated with ECM or protease treated-ECM. ECM was pre-treated with protease, followed by the addition of protease inhibitors (P-ECM), as described in the Materials and Methods, before incubation with Fluo-4-loaded trypomastigotes. As shown, previous protease treatment abolished the extracellular Ca²⁺ uptake (**Figure 6A**). To confirm the relevance of proteins in the process, collagen was chosen to perform a similar experiment, since collagen was previously described as an adhesion protein in the invasion process of the parasite (Velge et al., 1988), and type I collagen is abundant in the ECM employed. Intracellular Ca²⁺ measured in trypomastigotes incubated with 5 µg of type I collagen previously treated with collagenase (C-Coll) is also abolished (**Figure 6B**), confirming the role of proteins. Although the increase in calcium measured in trypomastigotes incubated with 5 µg of collagen or 40 µg of ECM is similar (**Figure 6B**), the possible role of other ECM components in calcium signaling cannot be excluded. In addition to collagen-1, 5 µg of heparan sulfate also increases the intracellular calcium concentration in tissue culture-derived trypomastigotes (**Supplementary Figure 3**).

DISCUSSION

The invasion of host mammalian cells by *T. cruzi* trypomastigotes is a complex process which requires distinct surface molecules, and the activation of multiple signaling pathways in the parasites, as well as in the host cells (De Souza et al., 2010; Caradonna and Burleigh, 2011; Maeda et al., 2012; Giorgi and de Lederkremer, 2020; Nájera et al., 2021). Molecules from the parasite surface, such as members of the gp85/Transialidase glycoproteins coded by a multigenic family, bind to the ECM components, as a first step of the invasion process (Alves and Colli, 2008; De Souza et al., 2010; Nde et al., 2012), which triggers relevant changes in phosphorylation, S-nitrosylation, and nitration levels of proteins in *T. cruzi* trypomastigotes, Y strain, which elicit a reprogramming of the parasite metabolism (Mattos et al., 2019) or modification of the DNA binding profile of nitrated histones (Magalhães et al., 2020). However, the very early signaling events triggered in tissue culture-derived trypomastigotes by the ECM interaction were not explored.

Early studies showed Ca²⁺ increment during *T. cruzi* trypomastigote and extracellular amastigote or *Leishmania* sp. *amazonensis* amastigote interactions with host cells (Misra et al., 1991; Moreno et al., 1994; Yakubu et al., 1994; Lu et al., 1998; Hashimoto et al., 2014). Here, we show that the intracellular Ca²⁺ concentration increment in culture-derived trypomastigotes triggered by the interaction with the ECM is an early event, reaching a plateau in less than 2 minutes, which occurs by the uptake of extracellular Ca²⁺, since it is abolished by EGTA (**Figure 1**). Moreover, Ca²⁺ uptake by the plasma membrane is inhibited by Nifedipine, a dihydropyridine that blocks L-type voltage channels, and, as recently described, inhibits the sphingosine dependent plasma membrane Ca²⁺ channels in *T. cruzi* (Rodriguez-Duran et al., 2019) and *Leishmania* (Benaim et al., 1991; Benaim et al., 2013; Pinto-Martinez et al., 2018).

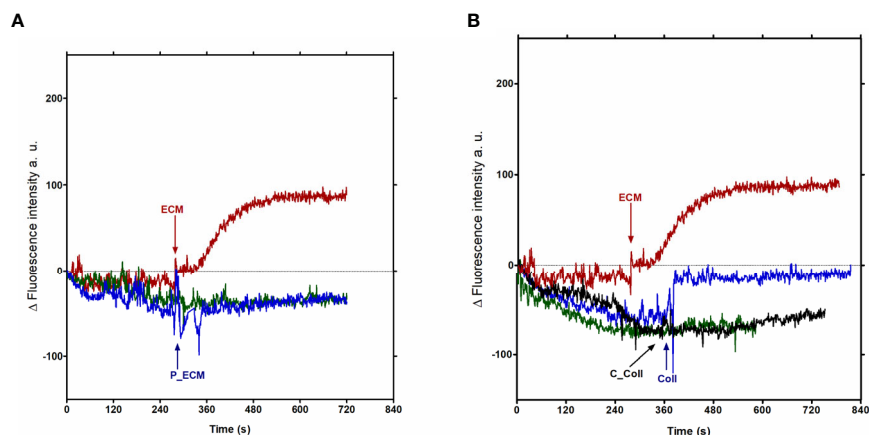


FIGURE 6 | Protein fraction of ECM is implicated in the calcium signal in trypomastigotes from *T. cruzi*. Total ECM (40 µg) and Collagen I (5 µg)-derived calcium signal. **(A)** red line: Ca²⁺ concentrations measured in the presence of ECM; blue line: ECM previously treated with protease, followed by the addition of protease inhibitor (P-ECM); green line: Ty (trypomastigotes without ECM). **(B)** red line: Ca²⁺ concentrations measured in the presence of ECM; blue line: Ca²⁺ concentrations measured in the presence of 5 µg of Collagen I; black line: Ca²⁺ concentrations measured in the presence of 5 µg of Collagen I treated with collagenase (C-Coll). The graph is representative of two independent experiments.

In addition, Nifedipine drastically inhibits the invasion of host cells by *T. cruzi* trypomastigotes, reaching more than 90% inhibition at 100 μM of the drug (**Figure 3**) without affecting the parasite morphology or motility. These data confirm the essential role of Ca^{2+} in the invasion process described in the literature (Moreno et al., 1994) and establish a role of nifedipine-sensitive calcium channels in this uptake. Moreover, the results show that Ca^{2+} signaling starts at the adhesion step of the parasite to ECM, before the invasion of the host cell itself in spite that the downstream signaling, as well as the ECM component(s) that activate the calcium channel were not thoroughly identified.

In the particular case of the tissue culture-derived trypomastigotes-ECM interaction, the protein content of the ECM seems to be an important element for the induction of Ca^{2+} increase, since it is abolished by the previous treatment of the ECM with proteases (**Figure 6A**). The same conclusion resulted from similar experiments with Collagen I and with Collagen I previously treated with collagenase (**Figure 6B**). Collagen I, abundant in ECM isolated from epithelial cells employed here (Berkholtz et al., 2006), is one of the first ECM molecules described which trypomastigotes adhere to (Velge et al., 1988). However, the involvement of other ECM molecules in Ca^{2+} influx cannot be excluded.

The intracellular destination of the Ca^{2+} taken up during our experimental conditions was investigated. Mitochondria seem to be the main intracellular organelle responsible for buffering the free Ca^{2+} during the interaction of trypomastigotes with the ECM, as suggested by the Ca^{2+} increase in the presence of Antimycin A, a potent inhibitor of the mitochondrial electron transport chain (Grimmelikhuijzen and Slater, 1973; Stoppani et al., 1980) (**Figure 4**). The increment in Ca^{2+} uptake by the mitochondrial calcium uniporter during parasite-ECM interaction may stimulate ATP production through the activation of pyruvate dehydrogenase by the calcium-sensitive pyruvate dehydrogenase phosphatase (MCU-ATP-synthase megacomplex), as described previously (Lander et al., 2018). Interestingly, the direct interaction of MCU with subunit c of the ATP Synthase in the megacomplex, coupling the ADP and P_i transport and ATP synthesis, is present in trypanosomatids, as well as in humans (Huang and Docampo, 2020), thus providing energy for the subsequent steps of the invasion process. In contrast to the mitochondria, acidocalcisomes and endoplasmic reticulum seem to not play a prominent role in regulating the calcium concentration in our experimental conditions, as suggested by the data using 1 μM Bafilomycin A, a vacuolar H^+ ATPase inhibitor specific for acidocalcisome (Docampo et al., 1995) or 0.3 μM Cyclopiazonic acid, a disruptor of calcium uptake by RE (Furuya et al., 2001) (**Figure 4**). Of note, a store operated Ca^{2+} channel (SOCE) for calcium influx in *T. equiperdum* and triggered by calcium release from ER was described for the first time in trypanosomatids (Pérez-Gordones et al., 2021) expanding the knowledge on the mechanism of calcium homeostasis in these parasites. Additionally, a membrane tension activated mechanosensitive channel has been described recently in *Trypanosoma cruzi* which, when lacking in knockout parasites, affects calcium regulation and

infectivity, among others (Dave et al., 2021). The seeming absence of acidocalcisome involvement is unexpected, since the inositol 1,4,5 triphosphate receptor (IPR3) is localized in acidocalcisomes (Lander et al., 2016), not in the ER, and ablation of the gene coding for the IP3 receptor impairs cell invasion by *T. cruzi* (Chiurillo et al., 2020). However, the proximity between the mitochondrion and acidocalcisome has been demonstrated in *T. cruzi* and *T. brucei* (Miranda et al., 2000; Ramakrishnan et al., 2018), and it has been suggested that the contact of both organelles would facilitate a calcium movement between them (Docampo et al., 2021). Possibly, the unique mitochondrion of the parasite and acidocalcisomes are both operative in regulating the binding to ECM followed by a host cell internalization of the parasite.

Cytoplasmic Ca^{2+} is important for cellular signaling as an ion regulator of many enzymes and proteins activity. The observed decrease in the phosphorylation levels of proteins could be one of the consequences of a calcium uptake from the external milieu in the case of trypomastigotes incubated with ECM, as suggested by the results obtained in the presence of Nifedipine or EGTA, where this decrease is less evident. Additionally, the total phosphatase activity decreases in the presence of Nifedipine or EGTA, almost at the same order of magnitude as Okadaic acid, an inhibitor of the protein phosphatases PP2A and PP1 in *T. cruzi* (Szöör, 2010). Although we did not explore these data further, phosphatases and calcium are associated with distinct biological functions in *T. cruzi*, including host cell invasion (Docampo and Moreno, 1986; Orrego et al., 2014) and differentiation (González et al., 2003). Moreover, decreases in the phosphorylation levels of proteins, including structural proteins, the majority of protein kinases and protein phosphatases, such as protein phosphatase PP1, seem to be a major event in the tissue culture -derived trypomastigotes incubated with the ECM for longer periods of time (2 h), as shown by the phosphoproteomic analysis and modification on enzyme activities, such as hexokinase or pyruvate kinase (Mattos et al., 2019).

In short, we show the uptake of extracellular calcium by *T. cruzi* trypomastigotes by nifedipine-sensitive calcium channel at the very early phase of its interaction with the extracellular matrix and the main role of mitochondria in calcium homeostasis during the interaction process. Calcium uptake is at least partially dependent on the protein composition of the ECM, probably triggering the activation of protein phosphatases, such as PP1 and PP2A, considering that the dephosphorylation of proteins is associated with the invasion process. However, distinct signaling pathways are expected to be triggered, since multiple molecular interactions occur between the parasite and ECM. Our studies thus deepen our understanding of the complexities of host cell invasion by *T. cruzi* trypomastigotes.

DATA AVAILABILITY STATEMENT

The raw data supporting the conclusions of this article will be made available by the authors, without undue reservation.

AUTHOR CONTRIBUTIONS

Conceptualization: MA, WC, and NM. Methodology: NM and GR. Formal analysis: MA, WC, and NM. Resources: MA, WC, NM, and GR. Original draft: NM. Writing review and editing: NM, MA, and WC. Visualization: NM and GR. Supervision: MA and WC. Funding acquisition: MA and WC. All authors contributed to the article and approved the submitted version.

FUNDING

The work was supported by grants and fellowships from Fundação de Amparo à Pesquisa do Estado de S. Paulo, FAPESP, Brazil (2014/25494-9, 2017/19854-0 to MA; 2018/03727-2 to NM; 2018/04559-6 to GR), Conselho Nacional de Desenvolvimento Científico e Tecnológico, CNPq, Brazil (304232/2014-9 to MA; 305951/2017-3 to WC; 150980/2017-5

REFERENCES

- Alves, M. J., and Colli, W. (2008). Role of the Gp85/Trans-Sialidase Superfamily of Glycoproteins in the Interaction of Trypanosoma Cruzi With Host Structures. *Subcell. Biochem.* 47, 58–69. doi: 10.1007/978-0-387-78267-6_4
- Andrews, N. W., and Colli, W. (1982). Adhesion and Interiorization of Trypanosoma Cruzi in Mammalian Cells. *J. Protozool.* 29, 264–269. doi: 10.1111/j.1550-7408.1982.tb04024.x
- Benaïm, G., García-Marchán, Y., Reyes, C., Uzcanga, G., and Figarella, K. (2013). Identification of a Sphingosine-Sensitive Ca²⁺ Channel in the Plasma Membrane of *Leishmania Mexicana*. *Biochem. Biophys. Res. Commun.* 430, 1091–1096. doi: 10.1016/j.bbrc.2012.12.033
- Benaïm, G., Losada, S., Gadelha, F. R., and Docampo, R. (1991). A Calmodulin-Activated (Ca²⁺-Mg²⁺)-ATPase is Involved in Ca²⁺ Transport by Plasma Membrane Vesicles From Trypanosoma Cruzi. *Biochem. J.* 280, 715–720. doi: 10.1042/bj2800715
- Benaïm, G., Paniz-Mondolfi, A. E., Sordillo, E. M., and Martinez-Sotillo, N. (2020). Disruption of Intracellular Calcium Homeostasis as a Therapeutic Target Against Trypanosoma Cruzi. *Front. Cell. Infect. Microbiol.* 10, 1–15. doi: 10.3389/fcimb.2020.00046
- Berkholtz, C. B., Lai, B. E., Woodruff, T. K., and Shea, L. D. (2006). Distribution of Extracellular Matrix Proteins Type I Collagen, Type IV Collagen, Fibronectin, and Laminin in Mouse Folliculogenesis. *Histochem. Cell Biol.* 126, 583–592. doi: 10.1007/s00418-006-0194-1
- Bers, D. M., Patton, C. W., and Nuccitelli, R. (2010). A Practical Guide to the Preparation of Ca²⁺ Buffers. *Methods Cell Biol.* 99, 1–26. doi: 10.1016/B978-0-12-374841-6.00001-3
- Burleigh, B. A., and Andrews, N. W. (1998). Signaling and Host Cell Invasion by Trypanosoma Cruzi. *Curr. Opin. Microbiol.* 1, 461–465. doi: 10.1016/S1369-5274(98)80066-0
- Calvet, C. M., Meuser, M., Almeida, D., Meirelles, M. N. L., and Pereira, M. C. S. (2004). Trypanosoma Cruzi-Cardiomyocyte Interaction: Role of Fibronectin in the Recognition Process and Extracellular Matrix Expression *In Vitro* and *In Vivo*. *Exp. Parasitol.* 107, 20–30. doi: 10.1016/j.exppara.2004.04.003
- Calvet, C. M., Toma, L., De Souza, F. R., De Meirelles, M. D. N. S. L., and Pereira, M. C. S. (2003). Heparan Sulfate Proteoglycans Mediate the Invasion of Cardiomyocytes by Trypanosoma cruzei. *J. Eukaryot. Microbiol.* 50, 97–103. doi: 10.1111/j.1550-7408.2003.tb00240.x
- Caradonna, K. L., and Burleigh, B. A. (2011). Mechanisms of Host Cell Invasion by Trypanosoma Cruzi. *Adv. Parasitol.* 76, 33–61. doi: 10.1016/B978-0-12-385895-5.00002-5
- Cardenas, T. C., Johnson, C. A., Pratap, S., Nde, P. N., Furtak, V., Kleshchenko, Y. Y., et al. (2010). Regulation of the Extracellular Matrix Interactome by Trypanosoma Cruzi. *Open Parasitol. J.* 4, 72–76. doi: 10.2174/1874421401004010072

to NM) and Coordenação de Aperfeiçoamento de Pessoal de Nível Superior, CAPES, Brazil. The funders had no role in study design, data collection and analysis, decision to publish, or preparation of the manuscript.

ACKNOWLEDGMENTS

The advice and laboratory support of Prof. Alicia Kowaltowski and Prof. Anibal Vercesi, and technical assistance of Célia L. Braga are greatly acknowledged.

SUPPLEMENTARY MATERIAL

The Supplementary Material for this article can be found online at: <https://www.frontiersin.org/articles/10.3389/fcimb.2021.731372/full#supplementary-material>

- Chiurillo, M. A., Lander, N., Bertolini, M. S., Vercesi, A. E., and Docampo, R. (2019). Functional Analysis and Importance for Host Cell Infection of the Ca²⁺-Conducting Subunits of the Mitochondrial Calcium Uniporter of Trypanosoma Cruzi. *Mol. Biol. Cell* 30, 1676–1690. doi: 10.1091/mbc.E19-03-0152
- Chiurillo, M. A., Lander, N., Vercesi, A. E., and Docampo, R. (2020). IP₃ Receptor-Mediated Ca²⁺ Release From Acidocalcisomes Regulates Mitochondrial Bioenergetics and Prevents Autophagy in Trypanosoma Cruzi. *Cell Calcium* 92, 1–14. doi: 10.1016/j.ceca.2020.102284
- Coelho, L. L., Pereira, I. R., Pereira, M. C. D. S., Mesquita, L., Lannes-Vieira, J., Adesse, D., et al. (2018). Trypanosoma Cruzi Activates Mouse Cardiac Fibroblasts *In Vitro* Leading to Fibroblast-Myofibroblast Transition and Increase in Expression of Extracellular Matrix Proteins. *Parasites Vectors* 11 (1), 1–11. doi: 10.1186/s13071-018-2614-1
- Cruz-Saavedra, L., Muñoz, M., León, C., Patarroyo, M. A., Arevalo, G., Pavia, P., et al. (2017). Purification of Trypanosoma Cruzi Metacyclic Trypomastigotes by Ion Exchange Chromatography in Sepharose-DEAE, A Novel Methodology for Host-Pathogen Interaction Studies. *J. Microbiol. Methods* 142, 27–32. doi: 10.1016/j.mimet.2017.08.021
- Dave, N., Cetiner, U., Arroyo, D., Fonbuena, J., Tiwari, M., Barrera, P., et al. (2021). A Novel Mechanosensitive Channel Controls Osmoregulation, Differentiation, and Infectivity in Trypanosoma Cruzi. *ELife* 10, 1–32. doi: 10.7554/ELIFE.67449
- Da Silva, A. A., Teixeira, T. L., Teixeira, S. C., Machado, F. C., dos Santos, M. A., Tomiosso, T. C., et al. (2017). Galectin-3: A Friend But Not a Foe During Trypanosoma Cruzi Experimental Infection. *Front. Cell. Infect. Microbiol.* 7, 1–9. doi: 10.3389/fcimb.2017.00463
- de Sousa, M. A. (1983). A Simple Method to Purify Biologically and Antigenically Preserved Bloodstream Trypomastigotes of Trypanosoma Cruzi Using DEAE-Cellulose Columns. *Mem. Inst. Oswaldo Cruz* 78, 317–333. doi: 10.1590/s0074-02761983000300009
- De Souza, W., De Carvalho, T. M. U., and Barrias, E. S. (2010). Review on Trypanosoma Cruzi: Host Cell Interaction. *Int. J. Cell Biol.* 2010, 1–18. doi: 10.1155/2010/295394
- Docampo, R., and Huang, G. (2015). Calcium Signaling in Trypanosomatid Parasites. *Cell Calcium* 57, 194–202. doi: 10.1016/j.ceca.2014.10.015
- Docampo, R., and Moreno, S. N. (1986). Free Radical Metabolism of Antiparasitic Agents. *Fed. Proc.* 45, 2471–2476.
- Docampo, R., Scott, D. A., Vercesi, A. E., and Moreno, S. N. J. (1995). Intracellular Ca²⁺ Storage in Acidocalcisomes of Trypanosoma Cruzi. *Biochem. J.* 310, 1005–1012. doi: 10.1042/bj3101005
- Docampo, R., Vercesi, A. E., Huang, G., Lander, N., Chiurillo, M. A., and Bertolini, M. (2021). “Mitochondrial Ca²⁺ Homeostasis in Trypanosomes,” in *International Review of Cell and Molecular Biology* (Elsevier Inc). 362, 261–289. doi: 10.1016/bs.ircmb.2021.01.002

- Furuya, T., Okura, M., Ruiz, F. A., Scott, D. A., and Docampo, R. (2001). TcSCA Complements Yeast Mutants Defective in Ca²⁺ Pumps and Encode a Ca²⁺-ATPase That Localizes to the Endoplasmic Reticulum of *Trypanosoma Cruzi*. *J. Biol. Chem.* 276, 32437–32445. doi: 10.1074/jbc.M104000200
- Garzoni, L. R., Adesse, D., Soares, M. J., Rossi, M. I. D., Borojevic, R., and de Meirelles, M. de N. L. (2008). Fibrosis and Hypertrophy Induced by *Trypanosoma Cruzi* in a Three-Dimensional Cardiomyocyte-Culture System. *J. Infect. Dis.* 197 (6), 906–915. doi: 10.1086/528373
- Giordano, R., Fouts, D. L., Tewari, D., Colli, W., Manning, J. E., and Alves, M. J. M. (1999). Cloning of a Surface Membrane Glycoprotein Specific for the Infective Form of *Trypanosoma Cruzi* Having Adhesive Properties to Laminin. *J. Biol. Chem.* 274, 3461–3468. doi: 10.1074/jbc.274.6.3461
- Giorgi, M. E., and de Lederkremer, R. M. (2020). The Glycan Structure of *T. Cruzi* Mucins Depends on the Host. Insights on the Chameleonic Galactose. *Molecules* 25, 1–19. doi: 10.3390/molecules25173913
- Gonçalves, M. F., Umezawa, E. S., Katzin, A. M., de Souza, W., Alves, M. J. M., Zingales, B., et al. (1991). *Trypanosoma Cruzi*: Shedding of Surface Antigens as Membrane Vesicles. *Exp. Parasitol.* 72, 43–53. doi: 10.1016/0014-4894(91)90119-H
- González, J., Cornejo, A., Santos, M. R. M., Cordero, E. M., Gutiérrez, B., Porcile, P., et al. (2003). A Novel Protein Phosphatase 2A (PP2A) Is Involved in the Transformation of Human Protozoan Parasite *Trypanosoma cruzi*. *Biochem. J.* 374, 647–656. doi: 10.1042/BJ20030215
- Grimmelikhuijzen, C. J. P., and Slater, E. C. (1973). Antimycin-Insensitive Mutants of *Candida Utilis*. I. Isolation and Characterization of Mutant 28. *BBA - Bioenerg.* 305, 67–79. doi: 10.1016/0005-2728(73)90232-6
- Hashimoto, M., Nara, T., Hirawake, H., Morales, J., Enomoto, M., and Mikoshiba, K. (2014). Antisense Oligonucleotides Targeting Parasite Inositol 1,4,5-Trisphosphate Receptor Inhibits Mammalian Host Cell Invasion by *Trypanosoma Cruzi*. *Sci. Rep.* 4, 1–5. doi: 10.1038/srep04231
- Huang, G., and Docampo, R. (2020). The Mitochondrial Calcium Uniporter Interacts With Subunit C of the ATP Synthase of *Trypanosoma* and Humans. *MBio*. 11 (2), 1–11. doi: 10.1128/mBio.00268-20
- Johnson, C. A., Kleshchenko, Y. Y., Ikejiani, A. O., Udoko, A. N., Cardenas, T. C., Pratap, S., et al. (2012). Thrombospondin-1 Interacts With *Trypanosoma Cruzi* Surface Calreticulin to Enhance Cellular Infection. *PLoS One* 7, 1–8. doi: 10.1371/journal.pone.0040614
- Lander, N., Chiurillo, M. A., Bertolini, M. S., Docampo, R., and Vercesi, A. E. (2018). The Mitochondrial Calcium Uniporter Complex in *Trypanosomes*. *Cell Biol. Int.* 42(6), 656–663. doi: 10.1002/cbin.10928
- Lander, N., Chiurillo, M. A., Storey, M., Vercesi, A. E., and Docampo, R. (2016). CRISPR/Cas9-Mediated Endogenous C-Terminal Tagging of *Trypanosoma Cruzi* Genes Reveals the Acidocalcisome Localization of the Inositol 1,4,5-Trisphosphate Receptor. *J. Biol. Chem.* 291, 25505–25515. doi: 10.1074/jbc.M116.749655
- Lu, H.-G., Zhong, L., de Souza, W., Benchimol, M., Moreno, S., and Docampo, R. (1998). Ca²⁺ Content and Expression of an Acidocalcisomal Calcium Pump Are Elevated in Intracellular Forms of *Trypanosoma Cruzi*. *Mol. Cell. Biol.* 18 (4), 2309–2323. doi: 10.1128/mcb.18.4.2309
- Maeda, F. Y., Cortez, C., and Yoshida, N. (2012). Cell Signaling During *Trypanosoma Cruzi* Invasion. *Front. Immunol.* 3, 1–7. doi: 10.3389/fimmu.2012.00361
- Magalhães, R. D. M., Mattos, E. C., Rozanski, A., Galante, P. A. F., Palmisano, G., Cruz, A. K., et al. (2020). Global Changes in Nitration Levels and DNA Binding Profile of *Trypanosoma Cruzi* Histones Induced by Incubation With Host Extracellular Matrix. *PLoS Negl. Trop. Dis.* 14, 1–20. doi: 10.1371/journal.pntd.0008262
- Magalhães-Santos, I. F., Souza, M. M., Costa Lima, C. S., and Andrade, S. G. (2004). Infection of *Calomys Callosus* (Rodentia Cricetidae) With Strains of Different *Trypanosoma Cruzi* Biomes: Pathogenicity, Histotropism, and Fibrosis Induction. *Mem. Inst. Oswaldo Cruz* 99, 407–413. doi: 10.1590/S0074-02762004000400011
- Mattos, E. C., Canuto, G., Manchola, N. C., Magalhães, R. D. M., Crozier, T. W. M., Lamont, D. J., et al. (2019). Reprogramming of *Trypanosoma Cruzi* Metabolism Triggered by Parasite Interaction With the Host Cell Extracellular Matrix. *PLoS Negl. Trop. Dis.* 13 (2), 1–27. doi: 10.1371/journal.pntd.0007103
- Meyer-Fernandes, J. R., Da Silva-Neto, M. A., Dos Santos Soares, M., Fernandes, E., Vercesi, A. E., and De Oliveira, M. M. (1999). Ecto-Phosphatase Activities on the Cell Surface of the Amastigote Forms of *Trypanosoma Cruzi*. *Zeitschrift Fur Naturforsch. Sect. C J. Biosci.* 54, 977–984. doi: 10.1515/znc-1999-1120
- Miranda, K., Benchimol, M., Docampo, R., and De Souza, W. (2000). The Fine Structure of Acidocalcinsomes in *Trypanosoma Cruzi*. *Parasitol. Res.* 86, 373–384. doi: 10.1007/s004360050682
- Misra, S., Naskar, K., Sarkar, D., and Ghosh, D. K. (1991). Role of Ca²⁺ Ion on Leishmania-Macrophage Attachment. *Mol. Cell. Biochem.* 102, 13–18. doi: 10.1007/BF00232154
- Moreno, S. N. J., and Docampo, R. (2003). Calcium Regulation in Protozoan Parasites. *Curr. Opin. Microbiol.* 6, 359–364. doi: 10.1016/S1369-5274(03)00091-2
- Moreno, S. N., Silva, J., Vercesi, A. E., and Docampo, R. (1994). Cytosolic-Free Calcium Elevation in *Trypanosoma Cruzi* Is Required for Cell Invasion. *J. Exp. Med.* 180, 1535–1540. doi: 10.1084/jem.180.4.1535
- Motta, F. N., Bastos, I. M. D., Faudry, E., Ebel, C., Lima, M. M., Neves, D., et al. (2012). The *Trypanosoma Cruzi* Virulence Factor Oligopeptidase B (OPBtC) Assembles Into an Active and Stable Dimer. *PLoS One* 7, 1–10. doi: 10.1371/journal.pone.0030431
- Mule, S. N., Manchola, N. C., de Oliveira, G. S., Pereira, M., Magalhães, R. D. M., Teixeira, A. A., et al. (2021). Proteome-Wide Modulation of S-Nitrosylation in *Trypanosoma Cruzi* Trypomastigotes Upon Interaction With the Host Extracellular Matrix. *J. Proteomics*. 231, 1–13. doi: 10.1016/j.jprot.2020.104020
- Nájera, C. A., Batista, M. F., Meneghelli, I., and Bahia, D. (2021). Mixed Signals – How *Trypanosoma Cruzi* Exploits Host-Cell Communication and Signaling to Establish Infection. *J. Cell Sci.* 134, 1–13. doi: 10.1242/jcs.255687
- Nde, P. N., Lima, M. F., Johnson, C. A., Pratap, S., and Villalta, F. (2012). Regulation and Use of the Extracellular Matrix by *Trypanosoma Cruzi* During Early Infection. *Front. Immunol.* 3:337, 1–10. doi: 10.3389/fimmu.2012.00337
- Orrego, P. R., Olivares, H., Cordero, E. M., Bressan, A., Cortez, M., Sagua, H., et al. (2014). A Cytoplasmic New Catalytic Subunit of Calcineurin in *Trypanosoma Cruzi* and Its Molecular and Functional Characterization. *PLoS Negl. Trop. Dis.* 8, 16. doi: 10.1371/journal.pntd.0002676
- Pérez-Gordones, M. C., Ramírez-Iglesias, J. R., Benaim, G., and Mendoza, M. (2021). A Store-Operated Ca²⁺-Entry in *Trypanosoma Equiperdum*: Physiological Evidences of Its Presence. *Mol. Biochem. Parasitol.* 244, 1–9. doi: 10.1016/j.molbiopara.2021.111394
- Pinto-Martinez, A. K., Rodriguez-Durán, J., Serrano-Martin, X., Hernandez-Rodriguez, V., and Benaim, G. (2018). Mechanism of Action of Miltefosine on *Leishmania Donovanii* Involves the Impairment of Acidocalcisome Function and the Activation of the Sphingosine-Dependent Plasma Membrane Ca²⁺ Channel. *Antimicrob. Agents Chemother.* 62, 1–10. doi: 10.1128/AAC.01614-17
- Prole, D. L., and Taylor, C. W. (2011). Identification of Intracellular and Plasma Membrane Calcium Channel Homologues in Pathogenic Parasites. *PLoS One*. 6 (10), 1–16. doi: 10.1371/journal.pone.0026218
- Ramakrishnan, S., Asady, B., and Docampo, R. (2018). Acidocalcisome-Mitochondrion Membrane Contact Sites in *Trypanosoma Brucei*. *Pathogens* 7, 1–11. doi: 10.3390/pathogens7020033
- Rodriguez-Duran, J., Pinto-Martinez, A., Castillo, C., and Benaim, G. (2019). Identification and Electrophysiological Properties of a Sphingosine-Dependent Plasma Membrane Ca²⁺ Channel in *Trypanosoma Cruzi*. *FEBS J.* 286 (19), 3909–3925. doi: 10.1111/febs.14947
- Ruiz, R. C., Favoreto, S., Dorta, M. L., Oshiro, M. E. M., Ferreira, A. T., Manque, P. M., et al. (1998). Infectivity of *Trypanosoma Cruzi* Strains Is Associated With Differential Expression of Surface Glycoproteins With Differential Ca²⁺ Signalling Activity. *Biochem. J.* 330, 505–511. doi: 10.1042/bj3300505
- Santana, J. M., Grellier, P., Schrével, J., and Teixeira, A. R. L. (1997). A *Trypanosoma Cruzi*-Secreted 80 kDa Proteinase With Specificity for Human Collagen Types I and IV. *Biochem. J.* 325, 129–137. doi: 10.1042/bj3250129
- Scharfstein, J., Schmitz, V., Morandi, V., Capella, M. M., Lima, A. P., Morrot, A., et al. (2000). Host Cell Invasion by *Trypanosoma Cruzi* Is Potentiated by Activation of Bradykinin B(2) Receptors. *J. Exp. Med.* 192, 1289–1300. doi: 10.1084/jem.192.9.1289
- Schneider, C. A., Rasband, W. S., and Eliceiri, K. W. (2012). NIH Image to ImageJ: 25 Years of Image Analysis. *Nat. Methods* 9, 671–675. doi: 10.1038/nmeth.2089
- Silva, T. A., Ferreira, L. F., de Souza Pereira, M. C., and Calvet, C. M. (2019). Differential Role of TGF-β in Extracellular Matrix Regulation During

- Trypanosoma Cruzi*-Host Cell Interaction. *Int. J. Mol. Sci.* 20, 1–21. doi: 10.3390/ijms20194836
- Stoppani, A. O. M., Docampo, R., De Boiso, J. F., and Frasch, A. C. C. (1980). Effect of Inhibitors of Electron Transport and Oxidative Phosphorylation on *Trypanosoma Cruzi* Respiration and Growth. *Mol. Biochem. Parasitol.* 2, 3–21. doi: 10.1016/0166-6851(80)90044-4
- Suman, S., Rachakonda, G., Mandape, S. N., Sakhare, S. S., Villalta, F., Pratap, S., et al. (2018). Phospho-Proteomic Analysis of Primary Human Colon Epithelial Cells During the Early *Trypanosoma Cruzi* Infection Phase. *PLoS Negl. Trop. Dis.* 12, 1–24. doi: 10.1371/journal.pntd.0006792
- Szőör, B. (2010). Trypanosomatid Protein Phosphatases. *Mol. Biochem. Parasitol.* 173, 53–63. doi: 10.1016/j.molbiopara.2010.05.017
- Tanowitz, H., Wittner, M., Kress, Y., and Bloom, B. (1975). Studies of *In Vitro* Infection by *Trypanosoma Cruzi*. I. Ultrastructural Studies on the Invasion of Macrophages and L Cells. *Am. J. Trop. Med. Hyg.* 24 (1), 25–33. doi: 10.4269/ajtmh.1975.24.25
- Tardieux, I., Nathanson, M. H., and Andrews, N. W. (1994). Role in Host Cell Invasion of *Trypanosoma Cruzi*-Induced Cytosolic-Free Ca²⁺ Transients. *J. Exp. Med.* 179, 1017–1022. doi: 10.1084/jem.179.3.1017
- Ulrich, H., Magdesian, M. H., Alves, M. J. M., and Colli, W. (2002). *In Vitro* Selection of RNA Aptamers That Bind to Cell Adhesion Receptors of *Trypanosoma Cruzi* and Inhibit Cell Invasion. *J. Biol. Chem.* 277, 20756–20762. doi: 10.1074/jbc.M111859200
- Velge, P., Ouassii, M. A., Cornette, J., Afchain, D., and Capron, A. (1988). Identification and Isolation of *Trypanosoma Cruzi* Trypomastigote Collagen-Binding Proteins: Possible Role in Cell-Parasite Interaction. *Parasitology* 97, 51–63. doi: 10.1017/s0031182000058467
- Watanabe Costa, R., da Silveira, J. F., and Bahia, D. (2016). Interactions Between *Trypanosoma Cruzi* Secreted Proteins and Host Cell Signaling Pathways. *Front. Microbiol.* 7, 1–9. doi: 10.3389/fmicb.2016.00388
- World Health Organization. (2020). *Chagas Disease (Also Known as American Trypanosomiasis)*. Available at: [https://www.who.int/news-room/fact-sheets/detail/chagas-disease-\(american-trypanosomiasis\)](https://www.who.int/news-room/fact-sheets/detail/chagas-disease-(american-trypanosomiasis)).
- Yakubu, M. A., Majumder, S., and Kierszenbaum, F. (1994). Changes in *Trypanosoma Cruzi* Infectivity by Treatments That Affect Calcium Ion Levels. *Mol. Biochem. Parasitol.* 66, 119–125. doi: 10.1016/0166-6851(94)90042-6

Conflict of Interest: The authors declare that the research was conducted in the absence of any commercial or financial relationships that could be construed as a potential conflict of interest.

Publisher's Note: All claims expressed in this article are solely those of the authors and do not necessarily represent those of their affiliated organizations, or those of the publisher, the editors and the reviewers. Any product that may be evaluated in this article, or claim that may be made by its manufacturer, is not guaranteed or endorsed by the publisher.

Copyright © 2021 Manchola Varón, dos Santos, Colli and Alves. This is an open-access article distributed under the terms of the Creative Commons Attribution License (CC BY). The use, distribution or reproduction in other forums is permitted, provided the original author(s) and the copyright owner(s) are credited and that the original publication in this journal is cited, in accordance with accepted academic practice. No use, distribution or reproduction is permitted which does not comply with these terms.



Stage-Specific Class I Nucleases of *Leishmania* Play Important Roles in Parasite Infection and Survival

Anita Leocadio Freitas-Mesquita^{1,2*} and José Roberto Meyer-Fernandes^{1,2*}

¹ Instituto de Bioquímica Médica Leopoldo De Meis, Universidade Federal do Rio de Janeiro, Rio de Janeiro, Brazil,

² Instituto Nacional de Ciência e Tecnologia em Biologia Estrutural e Bioimagem, Rio de Janeiro, Brazil

OPEN ACCESS

Edited by:

Martin M. Edreira,
Universidad de Buenos Aires
(CONICET), Argentina

Reviewed by:

Juan Miguel Burgos,
National University of General San
Martín, Argentina
Kai Zhang,
Texas Tech University, United States

*Correspondence:

José Roberto Meyer-Fernandes
meyer@bioqmed.ufrj.br
Anita Leocadio Freitas-Mesquita
anitaleocadio2@gmail.com

Specialty section:

This article was submitted to
Parasite and Host,
a section of the journal
Frontiers in Cellular and
Infection Microbiology

Received: 02 September 2021

Accepted: 29 September 2021

Published: 15 October 2021

Citation:

Freitas-Mesquita AL
and Meyer-Fernandes JR (2021)
Stage-Specific Class I Nucleases of
Leishmania Play Important Roles in
Parasite Infection and Survival.
Front. Cell. Infect. Microbiol. 11:769933.
doi: 10.3389/fcimb.2021.769933

Protozoans of the genus *Leishmania* are the causative agents of an important neglected tropical disease referred to as leishmaniasis. During their lifecycle, the parasites can colonize the alimentary tract of the sand fly vector and the parasitophorous vacuole of the mammalian host, differentiating into distinct stages. Motile promastigotes are found in the sand fly vector and are transmitted to the mammalian host during the insect blood meal. Once in the vertebrate host, the parasites differentiate into amastigotes and multiply inside macrophages. To successfully establish infection in mammalian hosts, *Leishmania* parasites exhibit various strategies to impair the microbicidal power of the host immune system. In this context, stage-specific class I nucleases play different and important roles related to parasite growth, survival and development. Promastigotes express 3'-nucleotidase/nuclease (3'-NT/NU), an ectoenzyme that can promote parasite escape from neutrophil extracellular traps (NET)-mediated death through extracellular DNA hydrolysis and increase *Leishmania*-macrophage interactions due to extracellular adenosine generation. Amastigotes express secreted nuclease activity during the course of human infection that may be involved in the purine salvage pathway and can mobilize extracellular nucleic acids available far from the parasite. Another nuclease expressed in amastigotes (P4/LmC1N) is located in the endoplasmic reticulum of the parasite and may be involved in mRNA stability and DNA repair. Homologs of this class I nuclease can induce protection against infection by eliciting a T helper 1-like immune response. These immunogenic properties render these nucleases good targets for the development of vaccines against leishmaniasis, mainly because amastigotes are the form responsible for the development and progression of the disease. The present review aims to present and discuss the roles played by different class I nucleases during the *Leishmania* lifecycle, especially regarding the establishment of mammalian host infection.

Keywords: class I nucleases, *Leishmania* lifecycle, *Leishmania* spp., parasite infection, parasite survival

INTRODUCTION

Leishmania spp. are trypanosomatid parasites that infect humans and other mammalian hosts, causing one of the most significant of neglected tropical diseases (Chang, 1983). Leishmaniasis affects more than 350 million people worldwide and is the major insect-borne disease in developing countries (Vannier-Santos et al., 2002). The manifestations of the disease include cutaneous,

mucocutaneous, diffuse cutaneous, and visceral leishmaniasis, which is the most severe form of the disease. These different manifestations are related to the complex interaction between the infecting species and the host immune response (Pace, 2014).

During their lifecycle, the parasites alternate between the promastigote form that resides in the alimentary tract of the sandfly vector and the amastigote form that is found inside the parasitophorous vacuoles of mammalian host mononuclear phagocytes. Promastigotes are transmitted from the sand fly vector to the mammalian host during blood meal consumption (Vannier-Santos et al., 2002). Since their inoculation, parasites face diverse hostile microenvironments and present various strategies to impair the microbicidal power of the host immune system and survive and proliferate during the course of infection (Podinovskaia and Descoteaux, 2015). In this context, the current review aims to present and discuss the roles played by different class I nucleases during the *Leishmania* lifecycle, especially regarding the establishment of mammalian host infection.

Class I nucleases hydrolyze nucleic acids with RNA as their main substrate and present nucleotidase activity that can hydrolyze the phosphate group at the 3' position of 3'-monophosphorylated nucleotides. Several members of the class I nuclease family have been identified in plants, protozoa and fungi (Wilson, 1982; Desai and Shankar, 2003). The P1 nuclease of *Penicillium citrinum*, which is considered one of the archetypes of class I nucleases, has been studied for its three-dimensional structure in more detail. Crystallographic assays have revealed the presence of three coordinated Zn^{2+} ions that delimit the active site of the enzyme. The proposed mechanism for catalysis involves a nucleophilic attack of Zn^{2+} activated by a water molecule (Volbeda et al., 1991; Romier et al., 1998). The sequential alignment of class I nuclease family members revealed the existence of five highly conserved regions, four of which have one or more histidine residues and are likely to be involved in the binding of Zn^{2+} ions (Yamaguchi et al., 2000).

Throughout this review, we provide an overview of the major biochemical properties of the class I nucleases identified in several *Leishmania* species, as well as their differential expression throughout the parasite lifecycle. We also discuss the physiological roles that have been attributed to these enzymes, highlighting their potential uses in leishmaniasis chemotherapy and prophylaxis.

PROMASTIGOTE STAGE-SPECIFIC CLASS I NUCLEASE

3'-NT/NU

To successfully establish infection in the mammalian host, *Leishmania* parasites must impair the microbicidal repertoire of neutrophils and macrophages. One of the strategies for neutrophil-mediated killing is the release of a lattice composed of DNA associated with histones and granular and cytoplasmic proteins named neutrophil extracellular traps (NETs). NETs can ensnare and kill microorganisms, preventing parasitic infection (Brinkmann et al., 2004; Guimarães-Costa et al., 2012). For

several microorganisms, the expression of secreted or membrane-bound nucleases has been reported as a strategy to escape the toxic effects promoted by NETs (Sumbly et al., 2005; Berends et al., 2010; Seper et al., 2013; Thammavongsa et al., 2013; Afonso et al., 2021). The bifunctional enzyme 3'-nucleotidase/nuclease (3'-NT/NU), a unique class I nuclease present in several *Leishmania* species, has been considered an important factor for parasite escape from NET-mediated death through the hydrolysis of extracellular DNA (Guimarães-Costa et al., 2014; Freitas-Mesquita et al., 2019).

3'-NT/NU was first described in *Leishmania donovani* parasites (Gottlieb and Dwyer, 1983). Acid phosphatase, 5'-nucleotidase, and 3'-nucleotidase activities were observed in the surface membrane fraction isolated from *L. donovani* promastigotes. Based on biochemical properties, primarily differential sensitivity to inhibitors, these activities were shown to correspond to different enzymes (Gottlieb and Dwyer, 1983). Posterior studies performed with several *Leishmania* species have shown that 3'-NT/NU presents stage-specific expression. While procyclic and metacyclic promastigotes express the enzyme, no expression is observed in amastigotes (Sopwith et al., 2002; Lakhal-Naouar et al., 2008).

Due to similarities in biochemical parameters and structure, the enzyme 3'-NT/NU was classified as a member of the class I nuclease family (Neubert and Gottlieb, 1990). Sequence analyses of the gene encoding 3'-NT/NU in *L. donovani* (Debrabant et al., 1995; Debrabant et al., 2000), *Leishmania mexicana* (Sopwith et al., 2002), *Leishmania major* (Lakhal-Naouar et al., 2008), and *Leishmania amazonensis* (Paletta-Silva et al., 2011) have confirmed the presence of the five highly conserved regions associated with the class I nuclease family. 3'-NT/NU is a unique class I nuclease characterized as a cell surface membrane-anchored protein (Debrabant et al., 1995). In accordance with its previously observed ectoactivity, analysis of functional domains has shown the presence of an N-terminal signal peptide that targets the enzyme to the endoplasmic reticulum and a C-terminal transmembrane domain that anchors the enzyme to the parasite surface (Debrabant et al., 2000; Yamaguchi et al., 2000).

In terms of biochemical analyses, the 3'-nucleotidase activity of 3'-NT/NU has been vastly studied, with reports in several species, including *L. donovani* (Gottlieb and Dwyer, 1983), *L. mexicana* (Hassan and Coombs, 1987), *L. major* (Lakhal-Naouar et al., 2008), *Leishmania chagasi* (Vieira et al., 2011), and *L. amazonensis* (Paletta-Silva et al., 2011). However, few studies regarding the nuclease activity of 3'-NT/NU, which is referred to as ecto-nuclease activity, are available. The first study to perform full biochemical characterization of ectonuclease activity in *Leishmania* parasites was recently carried out with *L. amazonensis* (Freitas-Mesquita et al., 2019). The biochemical parameters were determined by evaluating the hydrolysis of extracellular nucleic acids using the purified recombinant enzyme and living promastigotes. This activity was shown to be more efficient at alkaline pH values, as previously observed for the ecto-3'-nucleotidase activities of *L. donovani* (Gottlieb and Dwyer, 1983), *L. mexicana* (Hassan and Coombs, 1987), and

L. amazonensis (Paletta-Silva et al., 2011). RNA, DNA, and different polyribonucleotides were efficiently hydrolyzed by *L. amazonensis*, which showed a preference for RNA, Poly-U, and Poly-A, which is consistent with the substrate specificity previously determined in *L. donovani* (Campbell et al., 1991).

Trypanosomatids do not express the enzymes responsible for *de novo* synthesis of purines; therefore, they are strictly dependent on host sources. As nucleotides and nucleic acids cannot be transported across the plasma membrane, their sequential hydrolysis to nucleosides constitute an important step in the purine acquisition process (Hammond and Gutteridge, 1984; Gottlieb, 1989). Through its nucleotidase activity, 3'-NT/NU can generate extracellular nucleosides through dephosphorylation of 3'-monophosphorylated nucleotides. Moreover, hydrolysis of extracellular nucleic acids generates 5'-monophosphorylated nucleotides that can be converted to nucleosides by the action of ecto 5'-nucleotidase, another ectoenzyme present in the plasma membranes of several trypanosomatids (Gottlieb, 1989), as summarized in **Figure 1A**.

Studies with *L. donovani* and *L. amazonensis* have shown that the expression and activity of 3'-NT/NU are stimulated when parasites face purine deprivation during growth, corroborating their involvement in the purine salvage pathway (Gottlieb, 1985; Freitas-Mesquita et al., 2019). The starvation of inorganic phosphate (P_i), which is one of the products of the reactions catalyzed by 3'-NT/NU, can also positively modulate ecto-3'-nucleotidase activity, as observed in *L. donovani* (Sacci et al., 1990) and *L. chagasi* (Vieira et al., 2011).

The role of 3'-NT/NU in the significant generation of extracellular adenosine, which is promoted by 3'-AMP hydrolysis or even by the sequential hydrolysis of nucleic acids to nucleosides, is also important from an immunological perspective. Adenosine can interact with purinergic receptors, triggering the release of anti-inflammatory cytokines and impairing the production of proinflammatory cytokines, thus favoring the establishment of parasite infection, as shown in **Figure 1A** (Paletta-Silva and Meyer-Fernandes, 2012; Freitas-Mesquita and Meyer-Fernandes, 2014; Freitas-Mesquita and Meyer-Fernandes, 2017).

Parasite and macrophage *in vitro* interaction assays have shown that the addition of 3'-AMP to the coculture medium promotes an increase in association indices, as observed in *L. chagasi* and *L. amazonensis*. The positive modulation promoted by 3'-AMP was equivalent to that observed with the same concentration of adenosine (Paletta-Silva et al., 2011; Vieira et al., 2011). Moreover, when 3'-AMP was added together with 3'-NT/NU inhibitors, such as tetrathiomolybdate (TTM) and guanosine 5'-monophosphate (5'-GMP), the stimulatory effect was completely reverted (Paletta-Silva et al., 2011; Freitas-Mesquita et al., 2016). Taken together, these results confirm that the modulation exerted by 3'-AMP is related to its conversion to adenosine by the action of 3'-NT/NU.

Although ectonuclease activity may indirectly contribute to adenosine generation, its major biological role seems to be related to parasite escape from NETosis (**Figure 1A**). An increase in the survival rate upon interaction with neutrophils

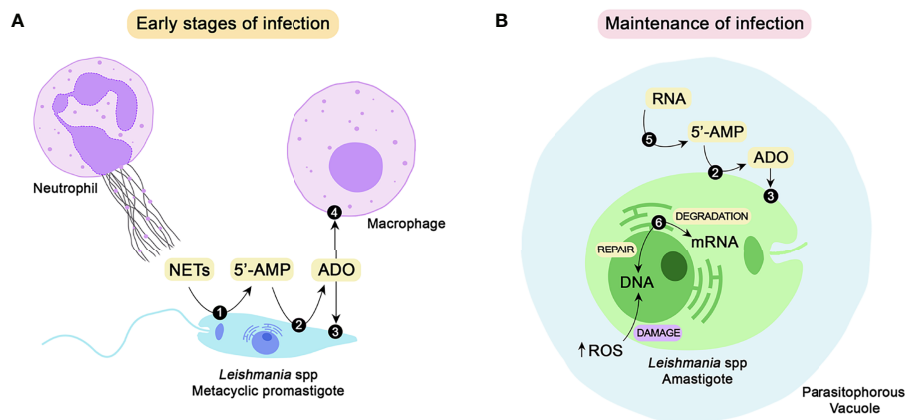


FIGURE 1 | Class I nucleases of *Leishmania* spp. and their possible roles during the establishment and maintenance of parasite infection. To successfully establish infection in the mammalian host, *Leishmania* promastigotes must impair the microbicidal repertoire of neutrophils and macrophages. One of the strategies for neutrophil-mediated killing is the release of NETs. The parasite can escape from the traps by DNA hydrolysis performed by 3'-NT/NU (1), a membrane-bound class I nuclease. Hydrolysis of extracellular nucleic acids generates 5'-monophosphorylated nucleotides, including 5'-AMP, that can be converted to adenosine by the action of ecto 5'-nucleotidase (2). Adenosine can be taken up by parasites through nucleoside transporters (3) to supply the purine salvage pathway or bind to purinergic receptors (4) of host macrophages, thus favoring parasite infection (**A**). To maintain the infective process, the parasites must differentiate into amastigotes, which can survive and proliferate inside parasitophorous vacuoles. Amastigotes express a secreted nuclease (5) that may mobilize extracellular nucleic acids located around the parasite and convert them to nucleotides, thus contributing to the purine salvage pathway. Another class I nuclease selectively expressed by amastigotes is P4/LmC1N nuclease (6). Located at the endoplasmic reticulum, this nuclease is probably involved in gene expression through mRNA degradation. Due to its endonuclease activity, this enzyme may also promote DNA repair, subverting the eventual damage caused by the oxidative burst (**B**). NETs, neutrophil extracellular traps; 5'-AMP, adenosine-5'-monophosphate; ADO, adenosine; RNA, ribonucleic acid; DNA, deoxyribonucleic acid; ROS, reactive oxygen species.

was correlated with deprivation of P_i and purines during the growth of *L. infantum* (Guimarães-Costa et al., 2014) and *L. amazonensis* (Freitas-Mesquita et al., 2019), respectively. As previously reported, 3'-NT/NU activity is sensitive to P_i and purine contents in culture medium and is increased when parasites are starved of these nutrients (Gottlieb, 1985; Sacci et al., 1990; Vieira et al., 2011). Furthermore, pretreatment of *L. infantum* parasites with TTM and 5'GMP, two 3'-NT/NU inhibitors, resulted in a decrease in NET degradation (Guimarães-Costa et al., 2014). These correlations strongly suggested the participation of 3'-NU/NU in NET hydrolysis, which was confirmed by the results obtained with the purified recombinant protein. The addition of r3'-NT/NU increased parasite survival after coculture with neutrophils and after incubation with NET-enriched supernatant. The effect promoted by r3'-NT/NU was similar to that obtained by DNase, which is known to be able to destroy NETs (Freitas-Mesquita et al., 2019).

AMASTIGOTE STAGE-SPECIFIC CLASS I NUCLEASES

P4/LmC1N

Several different drugs are available for the treatment of leishmaniasis, but pentavalent antimony-containing compounds remain to be used as the standard treatment, mainly in Latin America (Herwaldt and Berman, 1992; Berman, 1997; Ashutosh et al., 2007). However, an increase in therapeutic failure has been noted in the past few years due to the emergence of resistant parasites (Croft and Olliaro, 2011). In this context, the development of a vaccine against leishmaniasis is an extremely important aspect for the control of this disease, which affects millions of people worldwide. Although no effective vaccines against human leishmaniasis are currently available, hundreds of potential candidates are being studied (Singh and Sundar, 2012), including a class I nuclease selectively expressed by amastigotes of different *Leishmania* species (Kar et al., 2000; Campbell et al., 2003; Fakhraee et al., 2016).

Previous studies have shown that inoculation of living promastigotes is effective for preventing Old World cutaneous leishmaniasis (CL) (Greenblatt, 1980; Modabber, 1995). However, vaccination with virulent parasites is currently considered ethically unacceptable due to adverse reactions in susceptible individuals (Stober et al., 2006). First-generation vaccines have shown low efficacy since they are based on the use of killed parasites that do not mimic natural infection and are less immunogenic (Dunning, 2009; Fakhraee et al., 2016). On the other hand, second-generation vaccines induce protection using parasite antigens that may be obtained from native fractions purified from parasites (Rachamim and Jaffe, 1993; Borja-Cabrera et al., 2009; Moreno et al., 2014) or from recombinant bacteria or viruses carrying *Leishmania* antigen genes (De Oliveira et al., 2000; Smooker et al., 2004; Palatnik-de-Sousa et al., 2008; Miura et al., 2015). As amastigotes represent the parasite stage responsible for the pathology associated with leishmaniasis,

amastigote-specific antigens are of particular interest for the development of an efficient vaccine (Kar et al., 2000; Farajnia et al., 2004). One of the first studies to investigate stage-specific purified antigens reported that three antigens selectively expressed amastigotes (P2, P4, and P8) to confer partial to complete protection against infection with *Leishmania pifanoi* and *L. amazonensis* in BALB/c mice (Soong et al., 1995).

To obtain more information on this potential prophylactic target, the gene encoding the P4 antigen of *L. pifanoi* was cloned and sequenced (Kar et al., 2000). Comparative analyses using DNA-derived protein sequences have revealed significant levels of identity with the 3'-NT/NU of *L. donovani* (33.7%) and the P1 zinc-dependent nuclease of *Penicillium citrinum* (20.8%), suggesting that the P4 antigen possesses nuclease activity (Kar et al., 2000). This biological property was further confirmed by biochemical assays. Using different substrates to measure the enzymatic activity of affinity-purified *L. pifanoi* P4, the protein was observed to display endo- and exonuclease activity and can hydrolyze single-stranded DNA and RNA. 3'-monophosphorylated nucleotides are also substrates for P4 nuclease, revealing the presence of phosphomonoesterase activity (Kar et al., 2000).

Despite the level of homology and the similarities in substrate specificity, P4 nuclease differs from 3'-NT/NU in several aspects (Gottlieb and Dwyer, 1981; Gottlieb and Dwyer, 1983; Debrabant et al., 1995; Kar et al., 2000). While 3'-NT/NU is an external surface membrane protein, P4 nuclease appears to have a perinuclear location. Immunofluorescence analyses showed that P4 protein colocalizes with a binding protein (BiP), a marker of the endoplasmic reticulum (Bangs et al., 1996). Notably, nuclease activities associated with the endoplasmic reticulum are involved in mRNA stability (Bandyopadhyay et al., 1990; Ross, 1996). In this context, P4 nuclease can be speculated to play a role in gene regulation and expression. Due to its endonuclease activity, the P4 protein may also be involved in nucleotide excision and repair. This property may be crucial for parasite survival in the mammalian host once inside the phagolysosome of a macrophage. *Leishmania* parasites are constantly subjected to the oxidative burst that promotes DNA damage (Kar et al., 2000). These possible biological roles are schematized in **Figure 1B**.

In addition to localization, the most remarkable difference between 3'-NT/NU and P4 nuclease is their differential expression during the parasite lifecycle. The expression of 3'-NT/NU and P4 nuclease is virtually restricted to the promastigote and amastigote stages, respectively. Northern blot analyses using RNA purified from *L. pifanoi* and *L. amazonensis* have confirmed previous reports that P4 protein is exclusively expressed by amastigotes (Soong et al., 1995; Kar et al., 2000).

Southern blot analyses have shown that homologs of the P4 gene are present in other *Leishmania* species, including *L. amazonensis*, *L. braziliensis*, *L. major* and *L. donovani* (Kar et al., 2000). A novel class I nuclease was posteriorly identified in *L. major* (LmaC1N), presenting high similarity (87%) to the P4 nuclease of *L. pifanoi* (Farajnia et al., 2004). The gene encoding LmaC1N was cloned using primers specific for conserved regions of class I nucleases of trypanosomatids, and deduced sequence analyses confirmed the existence of all five

conserved regions (Farajnia et al., 2004). Similar to P4 nuclease and in contrast to 3'-NT/NU, LmaC1N was selectively expressed in amastigotes rather than promastigotes, as observed by RT-PCR and Western blotting assays (Farajnia et al., 2004).

Posteriorly, a homolog of P4 nuclease was identified in *L. infantum*, the causative agent of visceral leishmaniasis. The P4 nuclease gene was cloned, sequenced, and heterologously expressed for further characterization (Farajnia et al., 2011). Comparative sequence analyses have shown high homology to the P4 nucleases of *L. donovani*, *L. major* and *L. pifanoi*. The alignment results confirmed the existence of the five conserved domains of class I nucleases (Farajnia et al., 2011). Western blot analyses have shown that the P4 nuclease of *L. infantum* is expressed in both promastigotes and amastigotes. However, in accordance with previous studies involving this enzyme, its expression is significantly higher in amastigote parasites (Farajnia et al., 2011).

The high conservation among several *Leishmania* species, as well as the extensive expression found in the amastigote stage, renders P4 nuclease an excellent target for the development of a pan-*Leishmania* vaccine (Kar et al., 2000; Coler and Reed, 2005; Farajnia et al., 2011; Fakhraee et al., 2016). The first observations in this area showed that intraperitoneal injections of P4 antigen administered with *Corynebacterium parvum* as an adjuvant provided significant protection to BALB/c mice challenged with *L. pifanoi* promastigotes (Soong et al., 1995). The immunized mice developed smaller or no lesions, showing a significant parasite burden reduction after two weeks of infection. An increase in the levels of interferon gamma (IFN- γ) production was observed when immunized mice were stimulated with parasite antigens, suggesting that the resistance induced by P4 antigen is associated with a T helper 1 (Th1) cell-mediated immune response (Soong et al., 1995). Posteriorly, CD4⁺ T cells of P4-vaccinated mice were observed to produce not only IFN- γ but also macrophage migration inhibitory factor (MIF) and tumor necrosis factor/lymphotoxin (TNF/LT), leading to intracellular parasite destruction *in vitro* (Kar 2005).

A few years later, a DNA-based vaccine was tested using the *L. amazonensis* gene encoding the P4 nuclease associated with adjuvant constructs encoding murine interleukin-12 (IL-12) and *L. amazonensis* heat-shock protein 70 (HSP70) (Campbell et al., 2003). Both IL-12 and HSP70 have been reported to elicit Th1-type responses (Mattner et al., 1996; Wang et al., 2002). P4/IL-12-immunized BALB/c mice developed potent immune protection against *L. amazonensis* but remained susceptible to *L. major* infection. On the other hand, the P4/HSP70 vaccine only delayed the emergence of lesions in *L. amazonensis*-infected mice but was highly efficient against *L. major*, leading to a self-healing phenotype in infected mice (Campbell et al., 2003). To develop a DNA vaccine that promotes cross-protection against different *Leishmania* species, determining the optimal combination of several parasite genes and an appropriate adjuvant is crucial. Based on these results, P4 and HSP70 appear to be promising candidates for the development of a DNA-based vaccine for both New and Old World *Leishmania* species (Campbell et al., 2003).

Other studies in this field were performed based on LmaC1N protein, the P4 nuclease homolog from *L. major*. To evaluate LmaC1N as a potential human vaccine candidate, cellular

immune responses to recombinant LmaC1N (rLmaC1N) were examined in individuals who had recovered from Old World cutaneous leishmaniasis (Farajnia et al., 2005). In addition to being recognized in 90% of the individuals tested, rLmaC1N was shown to elicit strong Th1-like responses characterized by high levels of IFN- γ , low levels of IL-10, and minimal IL-5 production (Farajnia et al., 2005). Later, the first report using animal models showed that the use of liposome-polycation-DNA (LPD) as an immunoadjuvant renders rLmaC1N an appropriate candidate for developing a suitable vaccine against leishmaniasis (Fakhraee et al., 2016). BALB/c mice vaccinated with rLmaC1N plus LPD nanoparticles showed delayed emergence of skin lesions as well as a delay in the spread of *L. major* from the inoculation site to the spleen. The statistically significant advantageous effects observed for rLmaC1N's association with LPD nanoparticles compared to the effects obtained without coadministration of this adjuvant demonstrate the importance of selecting an efficient antigen delivery system for better protection (Fakhraee et al., 2016).

LdNuc^s

Beyond the membrane-bound 3'-NT/NU and the intracellular P4 nuclease, a secretory class I nuclease has also been identified and shown to be conserved in different geographic isolates of *L. donovani* and *L. infantum* (Joshi and Dwyer, 2007; Joshi et al., 2012). First, *L. donovani* promastigotes were observed to constitutively synthesize and release this nuclease, named LdNuc^s, into their growth medium. Then, this activity was identified in axenic amastigotes as well as *in vivo*-derived amastigotes isolated from infected hamster spleen tissue (Joshi and Dwyer, 2007). Analyses of the LdNuc^s-derived protein have confirmed the presence of the five conserved domains of class I nucleases (Joshi and Dwyer, 2007). Zymogram gels of cell lysates and culture supernatants showed marked differences between 3'-NT/NU and LdNuc^s activities. While 3'-NT/NU is ~43 kDa and insensitive to dithiothreitol (DTT) inhibition, LdNuc^s is a 35-kDa, DTT-sensitive nuclease. As previously described, 3'-NT/NU is a membrane-bound enzyme; therefore, its activity was detected only in cell lysates. On the other hand, LdNuc^s activity was detected in both cell lysates and concentrated cell-free culture supernatants (Joshi and Dwyer, 2007).

Coupled immunoprecipitation-enzymatic assays using epitope-tagged recombinant enzyme were performed to analyze other biochemical properties of LdNuc^s activity. The enzyme was capable of hydrolyzing RNA, single- and double-stranded DNA and a variety of synthetic polynucleotides. LdNuc^s appears to have a broad pH tolerance since nucleic acid hydrolysis occurred under both acidic (pH 5.0) and alkaline conditions (pH 8.5), suggesting that LdNuc^s may be completely functional within the different microenvironments faced by parasites during their lifecycle (Joshi and Dwyer, 2007).

Sera collected from infected visceral leishmaniasis patients from different geographic locations were able to recognize LdNuc^s, which clearly indicates that the enzyme is synthesized and expressed by *in vivo* amastigotes during the course of human infection (Joshi et al., 2012). The biological role played by LdNuc^s remains to be completely elucidated; however, the enzyme was postulated to participate in the purine salvage

pathway. As a secreted protein, LdNuc^s can function far away from the parasite in the mobilization of host-derived nucleic acids. Together with 3'-NT/NU and other enzymes involved in purine salvage, LdNuc^s may contribute to the availability of extracellular nucleosides and nucleobases that can be uptaken by the parasite (Joshi and Dwyer, 2007) (**Figure 1B**).

CONCLUDING REMARKS

Since the 1980s, with the first study describing the occurrence of 3'-NT/NU in *L. donovani*, several works have identified class I nucleases in different *Leishmania* species. Throughout this review, we discussed the occurrence and the major biochemical features of membrane-bound (3'-NT/NU), intracellular (P4/LmC1N), and secreted (LdNuc^s) nucleases of this pathogenic parasite. The main properties and the proposed biological functions of these class I nucleases are summarized in **Table 1**. Beyond their different localization, these enzymes were also observed to display differential expression throughout the parasite lifecycle. While 3'-NT/NU is selectively expressed in promastigotes, P4/LmC1N and LdNuc^s predominated at amastigotes (Kar et al., 2000; Sopwith et al., 2002; Farajnia et al., 2004; Joshi and Dwyer, 2007; Lakhal-Naouar et al., 2008; Farajnia et al., 2011).

Due to its ecto-localization, 3'-NT/NU can hydrolyze extracellular substrates, which is also true for LdNuc^s because it is a secreted enzyme. Because of this feature, the first biological role proposed for these nucleases was their involvement in the purine acquisition process (Sopwith et al., 2002; Joshi and Dwyer, 2007; Lakhal-Naouar et al., 2008) (**Figures 1A, B**). In addition to the nutritional viewpoint, 3'-NT/NU has also been related to the establishment of parasite infection in mammalian hosts, as represented in **Figure 1A**. By hydrolyzing extracellular nucleic acids through its ecto-nuclease activity, *Leishmania* promastigotes can escape from NETs, thus avoiding a hostile microenvironment and being able to infect macrophages (Guimarães-Costa et al., 2014; Freitas-Mesquita et al., 2019). 3'-NT/NU can provide extracellular adenosine directly by 3'-AMP hydrolysis or by converting nucleic acids to 5'-monophosphorylated nucleotides, which culminates in adenosine generation by conjugate action with ecto-5'-nucleotidase. Adenosine can interact with purinergic receptors of the host immune system, favoring *Leishmania*-macrophage interactions (Paletta-Silva et al., 2011; Vieira et al., 2011; Paletta-Silva and Meyer-Fernandes, 2012; Freitas-Mesquita and Meyer-Fernandes, 2014; Freitas-Mesquita et al., 2016).

The roles played by 3'-NT/NU are significantly relevant at the early stages of infection, which is consistent with its expression in the promastigote form of the parasite. Metacyclic promastigotes are the infective form for mammalian hosts; thus, they face the first strategies of the immune system to impair the establishment of infection. However, parasites must differentiate into amastigotes to continue the infective process, subverting the killing repertoire of macrophages. The survival and proliferation of amastigotes inside the phagolysosome vacuole determine the success of parasite infection (Pace, 2014). In this context, enzymes important for amastigote development and survival are considered potential targets for chemotherapy against leishmaniasis. LdNuc^s is conserved in different geographical isolates of *L. donovani* and *L. infantum*, is expressed by *in vivo* amastigotes during the course of human infections, and is an interesting chemotherapeutic target due to its possible role in the purine salvage pathway (Joshi and Dwyer, 2007; Joshi et al., 2012).

Another nuclease expressed in amastigotes, named P4 nuclease, was first described in *L. pifanoi* and was shown to be located in the endoplasmic reticulum of the parasite. Due to its cellular location and its endonuclease activity, P4 nuclease is probably involved in mRNA stability and nucleotide excision and repair (**Figure 1B**). Homologs of P4 nuclease were described in several *Leishmania* species, including *L. major*, which was named LmC1N. By being a protein conserved among different species, P4/LmC1N emerges as an interesting target for the development of vaccines promoting cross-protection against different manifestations of leishmaniasis (Soong et al., 1995; Farajnia et al., 2005; Fakhraee et al., 2016). Although the results obtained thus far have suggested possible cross-protection triggered by the employment of P4/LmC1N antigens, different combinations of parasite genes and appropriate adjuvants must be investigated to reach optimal conditions.

Based on all data discussed throughout this review, class I nucleases seem to play different and important roles in parasite growth, survival, and development, including the establishment and maintenance of infection in mammalian hosts. It is noteworthy that more advanced approaches in the fields of molecular biology and bioinformatics would be crucial to provide more precise information about these enzymes. The silencing or overexpression of the genes encoding these proteins would be remarkably helpful to fully comprehend their physiological roles. The availability of the genome of different *Leishmania* species allows determining the structurally and functionally conservation of the class I nucleases throughout the parasites' evolution. Additional studies are certainly required to deepen the knowledge about this important class of

TABLE 1 | Class I nucleases of *Leishmania* parasites.

Class I Nuclease	Expression during lifecycle	Localization	Potential physiological roles/applications	References
3'-NT/NU	Promastigote	Membrane-bound	Purine salvage pathway Purinergic signaling NETs hydrolysis	(Gottlieb, 1985; Debrabant et al., 1995; Lakhal-Naouar et al., 2008; Vieira et al., 2011; Guimarães-Costa et al., 2014)
P4/LmC1N	Amastigote	Perinuclear	Gene expression DNA repair Vaccine target	(Soong et al., 1995; Kar et al., 2000; Campbell et al., 2003; Farajnia et al., 2004; Fakhraee et al., 2016)
LdNuc ^s	Amastigote	Secreted	Purine salvage pathway	(Joshi and Dwyer, 2007; Joshi et al., 2012)

enzymes that has been considered a potential target for chemotherapy and prophylactics against leishmaniasis.

AUTHOR CONTRIBUTIONS

AF-M and JM-F wrote the manuscript. AF-M prepared the figure. All authors contributed to the article and approved the submitted version.

REFERENCES

- Afonso, M., Mestre, A. R., Silva, G., Almeida, A. C., Cunha, R. A., Meyer-Fernandes, J. R., et al. (2021). Candida Extracellular Nucleotide Metabolism Promotes Neutrophils Extracellular Traps Escape. *Front. Cell. Infect. Microbiol.* 11, 678568. doi: 10.3389/fcimb.2021.678568
- Ashutosh, S., Sundar, S., and Goyal, N. (2007). Molecular Mechanisms of Antimony Resistance in Leishmania. *J. Med. Microbiol.* 56 (2), 143–153. doi: 10.1099/jmm.0.46841-0
- Bandyopadhyay, R., Coutts, M., Krowczynska, A., and Brawerman, G. (1990). Nuclease Activity Associated With Mammalian mRNA in Its Native State: Possible Basis for Selectivity in mRNA Decay. *Mol. Cell. Biol.* 10 (5), 2060–2069. doi: 10.1128/mcb.10.5.2060-2069.1990
- Bangs, J. D., Brouch, E. M., Ransom, D. M., and Roggy, J. L. (1996). A Soluble Secretory Reporter System in Trypanosoma Brucei. Studies on Endoplasmic Reticulum Targeting. *J. Biol. Chem.* 271 (31), 18387–18393. doi: 10.1074/jbc.271.31.18387
- Berends, E. T. M., Horswill, A. R., Haste, N. M., Monestier, M., Nizet, V., and von Kückritz-Blickweide, M. (2010). Nuclease Expression by Staphylococcus Aureus Facilitates Escape From Neutrophil Extracellular Traps. *J. Innate Immun.* 2 (6), 576–586. doi: 10.1159/000319909
- Berman, J. D. (1997). Human Leishmaniasis: Clinical, Diagnostic, and Chemotherapeutic Developments in the Last 10 Years. *Clin. Infect. Dis.* 24 (4), 684–703. doi: 10.1093/clind/24.4.684
- Borja-Cabrera, G. P., Santos, F. B., Picillo, E., Gravino, A. E., Manna, L., and Palatnik-de-Sousa, C. B. (2009). Nucleoside Hydrolase DNA Vaccine Against Canine Visceral Leishmaniasis. *Proc. Vaccinol* 1 (1), 104–109. doi: 10.1016/j.provac.2009.07.019
- Brinkmann, V., Reichard, U., Goosmann, C., Fauler, B., Uhlemann, Y., Weiss, D. S., et al. (2004). Neutrophil Extracellular Traps Kill Bacteria. *Sci. (New York N.Y.)* 303 (5663), 1532–1535. doi: 10.1126/science.1092385
- Campbell, K., Diao, H., Ji, J., and Soong, L. (2003). DNA Immunization With the Gene Encoding P4 Nuclease of Leishmania Amazonensis Protects Mice Against Cutaneous Leishmaniasis. *Infect. Immun.* 71 (11), 6270–6278. doi: 10.1128/IAI.71.11.6270-6278.2003
- Campbell, T. A., Zlotnick, G. W., Neubert, T. A., Sacchi, J. B., and Gottlieb, M. (1991). Purification and Characterization of the 3'-Nucleotidase/Nuclease From Promastigotes of Leishmania Donovanii. *Mol. Biochem. Parasitol.* 47 (1), 109–117. doi: 10.1016/0166-6851(91)90153-w
- Chang, K. P. (1983). Cellular and Molecular Mechanisms of Intracellular Symbiosis in Leishmaniasis. *Int. Rev. Cytology. Supplement* 14, 267–305.
- Coler, R., and Reed, S. (2005). Second-Generation Vaccines Against Leishmaniasis. *Trends Parasitol* 21 (5), 244–249. doi: 10.1016/j.pt.2005.03.006
- Croft, S. L., and Olliaro, P. (2011). Leishmaniasis Chemotherapy—Challenges and Opportunities. *Clin. Microbiol. Infection* 17 (10), 1478–1483. doi: 10.1111/j.1469-0691.2011.03630.x
- Debrabant, A., Ghedin, E., and Dwyer, D. M. (2000). Dissection of the Functional Domains of the Leishmania Surface Membrane 3'-Nucleotidase/Nuclease, a Unique Member of the Class I Nuclease Family. *J. Biol. Chem.* 275 (21), 16366–16372. doi: 10.1074/jbc.M908725199
- Debrabant, A., Gottlieb, M., and Dwyer, D. M. (1995). Isolation and Characterization of the Gene Encoding the Surface Membrane 3'-Nucleotidase/Nuclease of Leishmania Donovanii. *Mol. Biochem. Parasitol.* 71 (1), 51–63. doi: 10.1016/0166-6851(95)00035-y

FUNDING

This work was supported by grants from the Brazilian agencies Conselho Nacional de Desenvolvimento Científico e Tecnológico (CNPq - Grant Number: 401134/2014–8), Coordenação de Aperfeiçoamento de Pessoal de Nível superior (CAPES - Grant Number: 0012017) and Fundação Carlos Chagas Filho de Amparo à Pesquisa do Estado do Rio de Janeiro (FAPERJ - Grant Number: e-26/201.300/2014).

- De Oliveira, M. C., Boutet, V., Fattal, E., Boquet, D., Grognet, J. M., Couvreur, P., et al. (2000). Improvement of *In Vivo* Stability of Phosphodiester Oligonucleotide Using Anionic Liposomes in Mice. *Life Sci.* 67 (13), 1625–1637. doi: 10.1016/s0024-3205(00)00745-1
- Desai, N. A., and Shankar, V. (2003). Single-Strand-Specific Nucleases. *FEMS Microbiol. Rev.* 26 (5), 457–491. doi: 10.1111/j.1574-6976.2003.tb00626.x
- Dunning, N. (2009). Leishmania Vaccines: From Leishmanization to the Era of DNA Technology. *Bioscience Horizons* 2 (1), 73–82. doi: 10.1093/biohorizons/hzp004
- Fakhraee, F., Badiie, A., Alavizadeh, S. H., Jalali, S. A., Chavoshian, O., Khamesipour, A., et al. (2016). Coadministration of L. Major Amastigote Class I Nuclease (Rlmacin) With LPD Nanoparticles Delays the Progression of Skin Lesion and the L. Major Dissemination to the Spleen in BALB/c Mice-Based Experimental Setting. *Acta Tropica* 159, 211–218. doi: 10.1016/j.actatropica.2016.04.004
- Farajnia, S., Alimohammadian, M. H., Reiner, N. E., Karimi, M., Ajdari, S., and Mahboudi, F. (2004). Molecular Characterization of a Novel Amastigote Stage Specific Class I Nuclease From Leishmania Major. *Int. J. Parasitol* 34 (8), 899–908. doi: 10.1016/j.ijpara.2004.03.005
- Farajnia, S., Mahboudi, F., Ajdari, S., Reiner, N. E., Kariminia, A., and Alimohammadian, M. H. (2005). Mononuclear Cells From Patients Recovered From Cutaneous Leishmaniasis Respond to Leishmania Major Amastigote Class I Nuclease With a Predominant Th1-Like Response. *Clin. Exp. Immunol.* 139 (3), 498–505. doi: 10.1111/j.1365-2249.2004.02702.x
- Farajnia, S., Rahbarnia, L., Maleki Zanjani, B., Alimohammadian, M. H., Abdoli Oskoei, S., Beh-Pajooh, A., et al. (2011). Molecular Cloning and Characterization of P4 Nuclease From Leishmania Infantum. *Enzyme Res.* 2011 (1), 1–6. doi: 10.4061/2011/970983
- Freitas-Mesquita, A. L., Dick, C. F., Dos-Santos, A. L. A., Nascimento, M. T. C., Rochael, N. C., Saraiva, E. M., et al. (2019). Cloning, Expression and Purification of 3'-Nucleotidase/Nuclease, an Enzyme Responsible for the Leishmania Escape From Neutrophil Extracellular Traps. *Mol. Biochem. Parasitol* 229, 6–14. doi: 10.1016/j.molbiopara.2019.02.004
- Freitas-Mesquita, A. L., Gomes, M. T., Vieira, D. P., Paes-Vieira, L., Nascimento, M. T. C., Lopes, A. H. C. S., et al. (2016). Inhibitory Effects Promoted by 5'-Nucleotides on the Ecto-3'-Nucleotidase Activity of Leishmania Amazonensis. *Exp. Parasitol* 169, 111–118. doi: 10.1016/j.exppara.2016.08.001
- Freitas-Mesquita, A. L., and Meyer-Fernandes, J. R. (2014). Ecto-Nucleotidases and Ecto-Phosphatases From Leishmania and Trypanosoma Parasites. *Sub-Cellular Biochem.* 74, 217–252. doi: 10.1007/978-94-007-7305-9_10
- Freitas-Mesquita, A. L., and Meyer-Fernandes, J. R. (2017). 3'-Nucleotidase/Nuclease in Protozoan Parasites: Molecular and Biochemical Properties and Physiological Roles. *Exp. Parasitol* 179, 1–6. doi: 10.1016/j.exppara.2017.06.001
- Gottlieb, M. (1985). Enzyme Regulation in a Trypanosomatid: Effect of Purine Starvation on Levels of 3'-Nucleotidase Activity. *Sci. (New York N.Y.)* 227 (4682), 72–74. doi: 10.1126/science.2981117
- Gottlieb, M. (1989). The Surface Membrane 3'-Nucleotidase/Nuclease of Trypanosomatid Protozoa. *Parasitol. Today (Personal Ed.)* 5 (8), 257–260. doi: 10.1016/0169-4758(89)90259-7
- Gottlieb, M., and Dwyer, D. M. (1981). Leishmania Donovanii: Surface Membrane Acid Phosphatase Activity of Promastigotes. *Exp. Parasitol.* 52 (1), 117–128. doi: 10.1016/0014-4894(81)90067-9
- Gottlieb, M., and Dwyer, D. (1983). Evidence for Distinct 5'- and 3'-Nucleotidase Activities in the Surface Membrane Fraction of Leishmania Donovanii

- Promastigotes. *Mol. Biochem. Parasitol* 7 (4), 303–317. doi: 10.1016/0166-6851(83)90013-0
- Greenblatt, C. L. (1980). The Present and Future of Vaccination for Cutaneous Leishmaniasis. *Prog. Clin. Biol. Res.* 47, 259–285.
- Guimarães-Costa, A. B., DeSouza-Vieira, T. S., Paletta-Silva, R., Freitas-Mesquita, A. L., Meyer-Fernandes, J. R., and Saraiva, E. M. (2014). 3'-Nucleotidase/Nuclease Activity Allows *Leishmania* Parasites to Escape Killing by Neutrophil Extracellular Traps. *Infection Immun.* 82 (4), 1732–1740. doi: 10.1128/IAI.01232-13
- Guimarães-Costa, A. B., Nascimento, M. T. C., Wardini, A. B., Pinto-da-Silva, L. H., and Saraiva, E. M. (2012). ETosis: A Microbicidal Mechanism Beyond Cell Death. *J. Parasitol. Res.* 2012:929743. doi: 10.1155/2012/929743
- Hammond, D. J., and Gutteridge, W. E. (1984). Purine and Pyrimidine Metabolism in the Trypanosomatidae. *Mol. Biochem. Parasitol* 13 (3), 243–261. doi: 10.1016/0166-6851(84)90117-8
- Hassan, H. F., and Coombs, G. H. (1987). Phosphomonoesterases of *Leishmania Mexicana Mexicana* and Other Flagellates. *Mol. Biochem. Parasitol* 23 (3), 285–296. doi: 10.1016/0166-6851(87)90035-1
- Herwaldt, B. L., and Berman, J. D. (1992). Recommendations for Treating Leishmaniasis With Sodium Stibogluconate (Pentostam) and Review of Pertinent Clinical Studies. *Am. J. Trop. Med. Hygiene* 46 (3), 296–306. doi: 10.4269/ajtmh.1992.46.296
- Joshi, M. B., and Dwyer, D. M. (2007). Molecular and Functional Analyses of a Novel Class I Secretory Nuclease From the Human Pathogen, *Leishmania Donovanii*. *J. Biol. Chem.* 282 (13), 10079–10095. doi: 10.1074/jbc.M610770200
- Joshi, M. B., Hernandez, Y., Owings, J. P., and Dwyer, D. M. (2012). Diverse Viscerotrophic Isolates of *Leishmania* All Express a Highly Conserved Secretory Nuclease During Human Infections. *Mol. Cell. Biochem.* 361 (1–2), 169–179. doi: 10.1007/s11010-011-1101-1
- Kar, S., Soong, L., Colmenares, M., Goldsmith-Pestana, K., and McMahon-Pratt, D. (2000). The Immunologically Protective P-4 Antigen of *Leishmania Amastigotes*. A Developmentally Regulated Single Strand-Specific Nuclease Associated With the Endoplasmic Reticulum. *J. Biol. Chem.* 275 (48), 37789–37797. doi: 10.1074/jbc.M002149200
- Lakhal-Naouar, I., Ben Achour-Chenik, Y., Boublik, Y., Meddeb, M., Aamouri, A., Fattoum, A., et al. (2008). Identification and Characterization of a New *Leishmania* Major Specific 3'nucleotidase/Nuclease Protein. *Biochem. Biophys. Res. Commun.* 375 (1), 54–58. doi: 10.1016/j.bbrc.2008.07.099
- Mattner, F., Magram, J., Ferrante, J., Launois, P., Di Padova, K., Behin, R., et al. (1996). Genetically Resistant Mice Lacking Interleukin-12 Are Susceptible to Infection With *Leishmania* Major and Mount a Polarized Th2 Cell Response. *Eur. J. Immunol.* 26 (7), 1553–1559. doi: 10.1002/eji.1830260722
- Miura, R., Kooriyama, T., Yoneda, M., Takenaka, A., Doki, M., Goto, Y., et al. (2015). Efficacy of Recombinant Canine Distemper Virus Expressing *Leishmania* Antigen Against *Leishmania* Challenge in Dogs. *PLoS Negl. Trop. Dis.* 9 (7), e0003914. doi: 10.1371/journal.pntd.0003914
- Modabber, F. (1995). Vaccines Against Leishmaniasis. *Ann. Trop. Med. Parasitol.* 89 Suppl 1, 83–88. doi: 10.1080/00034983.1995.11813017
- Moreno, J., Vouldoukis, I., Schreiber, P., Martin, V., McGahie, D., Gueguen, S., et al. (2014). Primary Vaccination With the LiESP/QA-21 Vaccine (CanilLeish) Produces a Cell-Mediated Immune Response Which Is Still Present 1 Year Later. *Veterinary Immunol. Immunopathol* 158 (3–4), 199–207. doi: 10.1016/j.vetimm.2014.01.011
- Neubert, T. A., and Gottlieb, M. (1990). An Inducible 3'-Nucleotidase/Nuclease From the Trypanosomatid *Crithidia Luciliae*. Purification and Characterization. *J. Biol. Chem.* 265 (13), 7236–7242.
- Pace, D. (2014). Leishmaniasis. *J. Infection* 69, S10–S18. doi: 10.1016/j.jinf.2014.07.016
- Palatnik-de-Sousa, C. B., Barbosa, A., de F., Oliveira, S. M., Nico, D., Bernardo, R. R., et al. (2008). FML Vaccine Against Canine Visceral Leishmaniasis: From Second-Generation to Synthetic Vaccine. *Expert Rev. Vaccines* 7 (6), 833–851. doi: 10.1586/14760584.7.6.833
- Paletta-Silva, R., and Meyer-Fernandes, J. R. (2012). Adenosine and Immune Imbalance in Visceral Leishmaniasis: The Possible Role of Ectonucleotidases. *J. Trop. Med.* 2012, 1–6. doi: 10.1155/2012/650874
- Paletta-Silva, R., Vieira, D. P., Vieira-Bernardo, R., Majerowicz, D., Gondim, K. C., Vannier-Santos, M. A., et al. (2011). *Leishmania Amazonensis*: Characterization of an Ecto-3'-Nucleotidase Activity and Its Possible Role in Virulence. *Exp. Parasitol* 129 (3), 277–283. doi: 10.1016/j.exppara.2011.07.014
- Podinovskaia, M., and Descoteaux, A. (2015). *Leishmania* and the Macrophage: A Multifaceted Interaction. *Future Microbiol.* 10 (1), 111–129. doi: 10.2217/fmb.14.103
- Rachamim, N., and Jaffe, C. L. (1993). Pure Protein From *Leishmania Donovanii* Protects Mice Against Both Cutaneous and Visceral Leishmaniasis. *J. Immunol. (Baltimore Md.: 1950)* 150 (6), 2322–2331.
- Romier, C., Dominguez, R., Lahm, A., Dahl, O., and Suck, D. (1998). Recognition of Single-Stranded DNA by Nuclease P1: High Resolution Crystal Structures of Complexes With Substrate Analogs. *Proteins* 32 (4), 414–424. doi: 10.1002/(SICI)1097-0134(19980901)32:4<414::AID-PROT2>3.0.CO;2-G
- Ross, J. (1996). Control of Messenger RNA Stability in Higher Eukaryotes. *Trends Genetics: TIG* 12 (5), 171–175. doi: 10.1016/0168-9525(96)10016-0
- Sacci, J. B., Campbell, T. A., and Gottlieb, M. (1990). *Leishmania Donovanii*: Regulated Changes in the Level of Expression of the Surface 3'-Nucleotidase/Nuclease. *Exp. Parasitol* 71 (2), 158–168. doi: 10.1016/0014-4894(90)90018-8
- Seper, A., Hosseinzadeh, A., Gorkiewicz, G., Lichtenegger, S., Roier, S., Leitner, D. R., et al. (2013). *Vibrio Cholerae* Evades Neutrophil Extracellular Traps by the Activity of Two Extracellular Nucleases. *PLoS Pathog.* 9 (9), e1003614. doi: 10.1371/journal.ppat.1003614
- Singh, B., and Sundar, S. (2012). Leishmaniasis: Vaccine Candidates and Perspectives. *Vaccine* 30 (26), 3834–3842. doi: 10.1016/j.vaccine.2012.03.068
- Smooker, P. M., Rainczuk, A., Kennedy, N., and Spithill, T. W. (2004). DNA Vaccines and Their Application Against Parasites—Promise, Limitations and Potential Solutions. *Biotechnol. Annu. Rev.* 10, 189–236. doi: 10.1016/S1387-2656(04)10007-0
- Soong, L., Duboise, S. M., Kima, P., and McMahon-Pratt, D. (1995). *Leishmania* Pifanoi Amastigote Antigens Protect Mice Against Cutaneous Leishmaniasis. *Infection Immun.* 63 (9), 3559–3566. doi: 10.1128/iai.63.9.3559-3566.1995
- Sopwith, W. F., Debrabant, A., Yamage, M., Dwyer, D. M., and Bates, P. A. (2002). Developmentally Regulated Expression of a Cell Surface Class I Nuclease in *Leishmania Mexicana*. *Int. J. Parasitol.* 32 (4), 449–459. doi: 10.1016/S0020-7519(01)00372-1
- Stober, C. B., Lange, U. G., Roberts, M. T. M., Gilmartin, B., Francis, R., Almeida, R., et al. (2006). From Genome to Vaccines for Leishmaniasis: Screening 100 Novel Vaccine Candidates Against Murine *Leishmania* Major Infection. *Vaccine* 24 (14), 2602–2616. doi: 10.1016/j.vaccine.2005.12.012
- Sumby, P., Barbican, K. D., Gardner, D. J., Whitney, A. R., Welty, D. M., Long, R. D., et al. (2005). Extracellular Deoxyribonuclease Made by Group A *Streptococcus* Assists Pathogenesis by Enhancing Evasion of the Innate Immune Response. *Proc. Natl. Acad. Sci. U. S. A.* 102 (5), 1679–1684. doi: 10.1073/pnas.0406641102
- Thammavongsa, V., Missiakas, D. M., and Schneewind, O. (2013). *Staphylococcus Aureus* Degrades Neutrophil Extracellular Traps to Promote Immune Cell Death. *Sci. (New York N.Y.)* 342 (6160), 863–866. doi: 10.1126/science.1242255
- Vannier-Santos, M., Martiny, A., and Souza, W. (2002). Cell Biology of *Leishmania* Spp.: Invading and Evading. *Curr. Pharm. Design* 8 (4), 297–318. doi: 10.2174/1381612023396230
- Vieira, D. P., Paletta-Silva, R., Saraiva, E. M., Lopes, A. H. C. S., and Meyer-Fernandes, J. R. (2011). *Leishmania Chagasi*: An Ecto-3'-Nucleotidase Activity Modulated by Inorganic Phosphate and Its Possible Involvement in Parasite-Macrophage Interaction. *Exp. Parasitol* 127 (3), 702–707. doi: 10.1016/j.exppara.2010.11.003
- Volbeda, A., Lahm, A., Sakiyama, F., and Suck, D. (1991). Crystal Structure of Penicillium Citrinum P1 Nuclease at 2.8 Å Resolution. *EMBO J.* 10 (7), 1607–1618.
- Wang, Y., Kelly, C. G., Singh, M., McGowan, E. G., Carrara, A.-S., Bergmeier, L. A., et al. (2002). Stimulation of Th1-Polarizing Cytokines, C-C Chemokines, Maturation of Dendritic Cells, and Adjuvant Function by the Peptide Binding Fragment of Heat Shock Protein 70. *J. Immunol. (Baltimore Md.: 1950)* 169 (5), 2422–2429. doi: 10.4049/jimmunol.169.5.2422
- Wilson, C. M. (1982). Plant Nucleases: Biochemistry and Development of Multiple Molecular Forms. *Isozymes* 6, 33–54.
- Yamage, M., Debrabant, A., and Dwyer, D. M. (2000). Molecular Characterization of a Hyperinducible, Surface Membrane-Anchored, Class I Nuclease of a

Trypanosomatid Parasite. *J. Biol. Chem.* 275 (46), 36369–36379. doi: 10.1074/jbc.M004036200

Conflict of Interest: The authors declare that the research was conducted in the absence of any commercial or financial relationships that could be construed as a potential conflict of interest.

Publisher's Note: All claims expressed in this article are solely those of the authors and do not necessarily represent those of their affiliated organizations, or those of the publisher, the editors and the reviewers. Any product that may be evaluated in

this article, or claim that may be made by its manufacturer, is not guaranteed or endorsed by the publisher.

Copyright © 2021 Freitas-Mesquita and Meyer-Fernandes. This is an open-access article distributed under the terms of the Creative Commons Attribution License (CC BY). The use, distribution or reproduction in other forums is permitted, provided the original author(s) and the copyright owner(s) are credited and that the original publication in this journal is cited, in accordance with accepted academic practice. No use, distribution or reproduction is permitted which does not comply with these terms.



Leishmania Parasites Differently Regulate Antioxidant Genes in Macrophages Derived From Resistant and Susceptible Mice

Haifa Bichiou^{1,2}, Sameh Rabhi¹, Cherif Ben Hamda¹, Cyrine Bouabid^{1,2}, Meriam Belghith³, David Piquemal⁴, Bernadette Trentin⁴, Imen Rabhi^{1,5} and Lamia Guizani-Tabbane^{1*}

¹ Laboratory of Medical Parasitology, Biotechnology and Biomolecules, Institut Pasteur de Tunis, Tunis-Belvedere, Tunisia,

² Faculty of Sciences of Tunis, Université de Tunis El Manar, Tunis, Tunisia, ³ Department of Immunology, Institut Pasteur de Tunis, University Tunis El-Manar, Tunis, Tunisia, ⁴ Acobiom, Grabels, France, ⁵ Higher Institute of Biotechnology at Sidi-Thabet, Biotechpole Sidi-Thabet, University of Manouba, Sidi-Thabet, Tunisia

OPEN ACCESS

Edited by:

Maria E. Francia,
Institut Pasteur de Montevideo,
Uruguay

Reviewed by:

Carlos Robello,
Universidad de la República, Uruguay
Lesly Temesvari,
Clemson University, United States

*Correspondence:

Lamia Guizani-Tabbane
lamia.guizani@pasteur.ms.tn

Specialty section:

This article was submitted to
Parasite and Host,
a section of the journal
Frontiers in Cellular and Infection
Microbiology

Received: 28 July 2021

Accepted: 20 September 2021

Published: 15 October 2021

Citation:

Bichiou H, Rabhi S,
Ben Hamda C, Bouabid C,
Belghith M, Piquemal D, Trentin B,
Rabhi I and Guizani-Tabbane L (2021)
Leishmania Parasites Differently
Regulate Antioxidant Genes in
Macrophages Derived From
Resistant and Susceptible Mice.
Front. Cell. Infect. Microbiol. 11:748738.
doi: 10.3389/fcimb.2021.748738

Macrophage–*Leishmania* interactions are central to parasite growth and disease outcome. Macrophages have developed various strategies to fight invaders, including oxidative burst. While some microorganisms seem to survive and even thrive in an oxidative environment, others are susceptible and get killed. To counter oxidative stress, macrophages switch the expressions of cytoprotective and detoxifying enzymes, which are downstream targets of the nuclear factor erythroid 2-related factor 2 (Nrf2), to enhance cell survival. We have explored the transcription of NRF2 and of its target genes and compared the effect of the parasite on their transcription in bone marrow-derived macrophages (BMdMs) from *Leishmania*-resistant and *Leishmania*-susceptible mice. While heme oxygenase 1 (HO-1) transcription is independent of the genetic background, the transcription of glutathione reductase (Gsr) and of cysteine/glutamate exchange transporter (Slc7a11), involved in glutathione accumulation, was differentially regulated in BMdMs from both mouse strains. We also show that, except for HO-1, known to favor the survival of the parasite, the transcription of the selected genes, including Gsr, CD36, and catalase (CAT), was actively repressed, if not at all time points at least at the later ones, by the parasite, especially in Balb/c BMdMs. Consistent with these results, we found that the silencing of NRF2 in this study increases the survival and multiplication of the parasite.

Keywords: *Leishmania*, macrophage, susceptibility, resistance, NRF2, antioxidants

INTRODUCTION

Leishmaniasis is a parasitic disease caused by the protozoa *Leishmania*. This disease is spread worldwide and causes different clinical manifestations ranging from cutaneous lesions healing spontaneously to visceral leishmaniasis, which is the most serious form of the disease that is fatal in the absence of treatment. *Leishmania* parasites alternate between two life stages, and the flagellated promastigotes

injected by the female sand fly transform into amastigotes when infecting host immune cells. As a main host for *Leishmania* replication, macrophages play a critical role in the outcome of the disease and in the battle between these two players: the host fighting the invaders with all available arsenal and the parasites developing various strategies to subvert the microbicidal functions of their host cells (Conceição-Silva and Morgado, 2019). Indeed, macrophages encounter *Leishmania* by employing an array of directly antimicrobial mechanisms such as the generation of reactive oxygen species (ROS) and reactive nitrogen species (RNS), which are highly destructive to *Leishmania*.

These oxidant compounds, while crucial in clearing invading pathogens, may cause oxidative damage to the host cells. Cells have developed different antioxidant defense systems to counter oxidative stress. These include the thioredoxin (Trx) and glutathione (GSH) systems, the two major thiol-dependent antioxidant mechanisms in cells, and heme oxygenase 1 (HO-1), which catalyzes the rate-limiting step of heme oxidation to biliverdin, carbon monoxide, and free ferrous iron (Tonelli et al., 2018). Most of these cytoprotective and detoxifying enzymes that enhance cell survival are downstream targets of the nuclear factor erythroid 2-related factor 2 (Nrf2).

Nrf2 is a stress-responsive transcription factor encoded by the *NFE2L2* gene in humans and is a member of the CNC ("cap 'n' collar") subfamily of basic region leucine zipper (bZIP) transcription factors (Sykietis and Bohmann, 2010). During homeostasis, Nrf2 is sequestered in the cytoplasm by Kelch-like ECH-associated protein 1 (Keap1, Nrf2 repressor protein), which drives NRF2 to ubiquitin-dependent proteasomal degradation (Baird and Yamamoto, 2020). After redox perturbation, Nrf2 is released from Keap1 and translocates into the nucleus. It then forms heterodimers with small Maf proteins and binds antioxidant response elements (AREs) regulating a broad range of expressions of antioxidant and detoxification genes (Itoh et al., 1999). The promoter of the Nrf2 gene itself contains AREs and amplifies the redox cascades via positive feedback regulation (Nguyen et al., 2003).

To clarify the contribution of the Nrf2/HO-1 axis and that of other detoxifying enzymes during *Leishmania major* infection, we explored the activation of Nrf2 and the transcription of target genes in murine macrophages from mice resistant or susceptible to *Leishmania* parasite infection.

MATERIALS AND METHODS

Ethics Statement

All mouse work was done according to the directive 86/609/EEC of the European Parliament and of the Council on the Protection of Animals Used for Scientific Purposes. Approval for mouse experiments was obtained from the Ethics Committee of Institute Pasteur of Tunis, with ethics approval no. 1204.

Parasites and Cell Culture

L. major (MHOM/TN/95/GLC94 zymodeme MON25) were maintained at 26°C in RPMI 1640 medium (Sigma, Taufkirchen, Germany) supplemented with 10% heat-inactivated fetal calf serum (Gibco, Waltham, MA, USA), penicillin (200 U/ml), streptomycin

(200 µg/ml), and glutamine (4 mM). In all assays, promastigotes in the stationary phase of growth (5–6 days) were washed in culture medium at 3,000 rpm for 10 min at 22°C, resuspended in medium again, and used for infection. Parasites are killed by a 10-min incubation at 100°C. Ds-Red promastigotes were generated as previously described (Rabhi et al., 2016). Parasites were maintained in culture in medium containing 25 µg/ml hygromycin B.

The mouse macrophage leukemia cell line Raw264.7 (ATCC, Manassas, VA, USA) was maintained in RPMI 1640 medium (Sigma) supplemented with 10% fetal bovine serum (FBS; Gibco), penicillin (200 U/ml), streptomycin (200 µg/ml), and glutamine (4 mM; SigmaG1146) at 37°C in a humidified incubator with 5% CO₂. Macrophages were cultured in 6-well plates and incubated for 12–24 h at 37°C with 5% CO₂ to adhere and then infected with *Leishmania* promastigotes at a ratio of 10:1. Macrophages interacting with *L. major* were maintained at 37°C with 5% CO₂. The infected cells were then harvested at different time points. Infections were confirmed using Giemsa staining.

Balb/c and C57BL/6 mice (Elevage Janvier, Le Genest-Saint-Isle, France) were killed and their hind legs removed for the isolation of bone marrow-derived macrophages (BMDMs). Briefly, the femurs and tibias were flushed with RPMI 1640 using a 25-gauge needle. Contaminating erythrocytes were lysed through the addition of a lysis solution. All cells were incubated in T75 culture flasks at 1.5×10^6 cells/ml in complete media added with 80 ng/ml macrophage colony-stimulating factor (M-CSF; Peprotech, Neuilly sur Seine, France) overnight for stromal cell elimination. Non-adherent, immature macrophages were transferred to fresh culture-treated Petri dishes (Nunc, Rochester, NY, USA) and grown for 7 days, with re-feeding on day 3 to induce macrophage differentiation. The purity of BMDMs was analyzed through the evaluation of the phenotypic expression of a specific macrophage subset surface marker (F4/80) by flow cytometry. Of the generated macrophages, 80%–90% were F4/80-positive.

Knockdown Macrophage Generation

Raw264.7 cells were seeded 18–20 h pre-transfection in 24-well plates at a confluency of 70%. The cells were transfected using the ESCORTTM II transfection reagent (Sigma) with the empty plasmid non-target pLKO (NT-pLKO) or one of the five different NRF2 DNAs and extracted using Maxiprep from the *NFE2L2* Mission shRNA Glycerol Stock (Sigma) according to the manufacturer's instructions.

Briefly, 2 µg of DNA was diluted and incubated for 20 min with the diluted ESCORT II reagent at room temperature to form the ESCORT II/DNA complexes. These complexes were then added to the cells growing in serum-containing culture medium and incubated at 37°C. At 24 h post-transfection, fresh growth medium was added. For selection, puromycin was added to the fresh medium 72 h post-transfection. The cells were kept in culture for 1 month with a cell medium change approximately two times a week. The cells were then cryopreserved after assessment of the silencing efficiency by Western blotting. Wild-type (WT), NT-pLKO, and si-Nrf2 cells were stimulated with 100 ng/ml lipopolysaccharide (LPS) and the intensities of the bands were compared. Cells transfected with the NRF2 clone,

which gave the higher silencing percentage, and the corresponding ones transfected with the NT-pLKO plasmids were used for subsequent experiments.

Ds-Red *Leishmania* Parasite Quantification by Flow Cytometry

We used Ds-Red-GLC94 *L. major* parasites (Rabhi et al., 2016) to infect transfected si-NRF2 and NT-pLKO cells. Seventy-two hours post-infection, the cells were immediately analyzed without fixation for the estimation of parasite multiplication by flow cytometry using a Becton Dickinson FACSCanto II flow cytometer. The analysis was fulfilled with the BD FACSDiva 6 software (Becton Dickinson, Franklin Lakes, NJ, USA).

Protein Extraction and Cell Fractionation

Cells were harvested at different time points, washed gently with ice-cold phosphate-buffered saline (PBS), scraped, and centrifuged at 1,200 rpm for 10 min. Nuclear and cytoplasmic protein extracts were prepared using a hypotonic hypertonic buffer. The pellets were resuspended in 80 μ l volume of hypotonic buffer containing 10 mM HEPES-KOH (pH 7.6), 60 mM KCl, 1 mM EDTA, 1 μ g/ml aprotinin, 1 mM orthovanadate, 1 mM dithiothreitol (DTT), and 1 mM phenylmethylsulfonyl fluoride (PMSF) for isolation of the cytoplasmic extract. After incubation on ice for 10 min, 1/30 on the volume of 10% NP40 was added for 1 min and the samples then centrifuged at 10,000 rpm for 5 min. The cytoplasmic extract was collected and stored. The nuclear pellet was resuspended in hypertonic buffer containing 10 mM HEPES-KOH (pH 7.6), 1.5 mM $MgCl_2$, 420 mM NaCl, 0.2 mM EDTA, 25% glycerol, 1 μ g/ml aprotinin, 1 mM orthovanadate, 1 mM DTT, and 1 mM PMSF. The nuclear pellets in hypotonic buffer were vortexed to homogenize the lysate, sonicated using Vibra-Cell at amplitude of 60% for three cycles of 10 s with 10-s pauses while being kept, and incubated on ice for 30 min. The lysates were then centrifuged at 14,000 rpm for 20 min to pellet any cell debris and the supernatants containing the nuclear proteins were collected into new tubes. For whole cell lysis, we used 30 μ l of lysis buffer containing 10 mM Tris-HCl (pH 7.5), 50 mM NaCl, 50 mM sodium fluoride (NaF), 2 mM EDTA, 1 mM EGTA, 2% Nonidet P-40 (NP-40), 0.75% sodium deoxycholate (DOC), 1 mM orthovanadate, 1 μ g/ml aprotinin, 1 mM PMSF, and 1 mM DTT. After 10 min incubation on ice, the extracts were centrifuged at 15,000 rpm for 20 min. All extracts were stored at $-20^{\circ}C$. The protein content of each compartment was determined using the bicinchoninic acid (BCA) protein assay (Sigma).

Western Blotting

Equal amounts of protein were separated by 10% sodium dodecyl sulfate polyacrylamide gel electrophoresis and transferred onto a 0.45- μ m polyvinylidene difluoride (PVDF) immunoblot membrane (Amersham, Amersham, UK). After membrane blocking with 5% skimmed milk in PBS with 0.01% Tween 20 (wash buffer) for 1 h at room temperature (RT), the membranes were incubated overnight at $4^{\circ}C$ with commercial primary antibodies against phospho-AKT (Cell Signaling, Danvers, MA, USA), HO-1 (Santa Cruz Biotechnology, Dallas, TX, USA), NRF2 (Santa Cruz Biotechnology), histone (Cell Signaling), β -actin

(Sigma-Aldrich, St Louis, MO, USA), and PARP (Cell Signaling). The next day, the membranes were washed three times and then incubated with horseradish peroxidase-conjugated anti-rabbit secondary antibody (1:2,000; Dako, Carpinteria, CA, USA) for another 1 h at RT. Blots were visualized with a densitometric ECL kit (Amersham) and analysis was performed using ImageJ software.

To analyze the effects of kinase inhibitors on the expressions of Nrf2 proteins, seeded raw cells in dishes were pretreated with wortmannin (200 mM) for 3 h; then, the cells were washed and infected with the *Leishmania* promastigotes for different times. The cell lysates prepared using the lysis buffer, as described above, were subjected to Western blot analysis.

RNA Extraction and qRT-PCR

Total RNA from macrophages was isolated using the TRIzol reagent (Sigma). Total RNAs from uninfected and infected macrophages were prepared using the RNeasy mini kit (Qiagen, Hilden, Germany). RNA quantity was controlled using the NanoDrop ND-1000 micro-spectrophotometer, and RNA quality and integrity (RNA integrity no. RIN.9) were monitored on the Agilent RNA Pico LabChips (Agilent Technologies, Palo Alto, CA, USA). Reverse transcriptions were performed for each sample in a final reaction volume of 20 μ l with 273 ng of total RNA using 200 U of SuperScript III enzyme (M-MLV Reverse Transcriptase, Invitrogen) and 250 ng of random primers according to the manufacturer's instructions ($25^{\circ}C$ for 10 min, $42^{\circ}C$ for 50 min, and $70^{\circ}C$ for 15 min). A negative control was included by performing reverse transcription with no template. Quantitative PCR (qPCR) experiments were carried out using EVA Green chemistry on a BioMark qPCR apparatus (Fluidigm, San Francisco, CA, USA) following the manufacturer's instructions. For each cDNA sample, specific target amplification (STA) was performed with a pool of primers targeting all selected genes (pre-amplification of 14 cycles using the TaqMan PreAmp Master Mix, Applied Biosystems, Waltham, MA, USA) and following the manufacturer's instructions. Each qPCR was performed with 1/20 STA dilution, in duplicate. Relative gene expression kinetics was created by a first normalization with four reference genes followed by a second normalization with non-infected (NI) macrophage cells. Values are expressed in fold changes ($2^{-\Delta\Delta CT}$ method) compared to NI macrophage cells.

Statistical Analysis

Data were presented as the mean and SD (standard deviation). All graphs generated and the related statistical analysis were performed using GraphPad Prism. Statistical analysis was performed using ANOVA. Significance was reached with p -values < 0.05 . P -values were shown as $*p < 0.05$, $**p < 0.01$, $***p < 0.001$, and $****p < 0.0001$.

RESULTS

Leishmania Infection Drives HO-1 Expression

We first assessed the ability of *L. major* parasites to induce the expression of HO-1. Balb/c BMDMs and/or Raw264.7 macrophages were infected with *L. major* promastigotes.

The infected cells were harvested and the expressions of HO-1 messenger RNA (mRNA) and proteins were analyzed. Our results showed that promastigotes significantly induced the transcription and the protein expression of HO-1 (**Figure 1**).

***L. major* Infection Leads to Activation of the Nrf2 Pathway**

Because the expressions of antioxidant genes are under the control of the Nrf2 transcription factor (TF), the activation of this master TF was investigated.

BMdMs from Balb/c mice or Raw264.7 cells were infected with *L. major* promastigotes for different times. The mRNA and protein were extracted for RT-PCR and Western blotting. The quantitative RT-PCR (qRT-PCR) results showed a slight but significant increase in the expression of Nrf2 mRNA, which peaked at 3 h post-infection (hpi) (**Figure 2A**). The parasite-induced expression of the NRF2 protein was detected as early as 30 min pi, and the abundance peaked between 4 and 6 hpi before declining progressively (**Figure 2B**). These data suggested an upregulation of the expression of Nrf2 by the increased transcription of the Nrf2 gene leading to increased Nrf2 protein levels in infected cells. To confirm the activation of the Nrf2 pathway, we visualized the nuclear translocation of the Nrf2 protein. Subcellular fractionation showed Nrf2 accumulation in the nucleus following infection. Nrf2 was, during the first hour post-infection, predominantly localized in the cytoplasm. At 3 hpi, the Nrf2 protein started to be exported to the nucleus, and the nuclear localization of NRF2 was observed until 12 hpi (**Figure 2C**).

PI3K/Akt and NRF2 Regulate the Expression of HO-1

To determine the upstream regulators of HO-1, macrophages were infected or pretreated with a phosphatidylinositol 3-kinase (PI3K)

inhibitor, wortmannin, and then infected by *L. major* promastigotes. Our results showed that wortmannin treatment decreased the parasite-induced phosphorylation of Akt (**Figures 3A, C**) and the expression of HO-1 protein (**Figures 3B, D**), showing that PI3K/Akt activity is required to induce HO-1 expression during *Leishmania* infection.

To investigate the antioxidant function of Nrf2, Raw264.7 si-NRF2 knockdown cells were generated. As expected, cells with disrupted Nrf2 did not express the silenced TF in response to LPS stimulation (**Figure 3E**). The effect of Nrf2 knockdown on the immunomodulatory expression of HO-1 protein was investigated with Western blot. As shown in **Figure 3F**, the silencing of Nrf2 strongly reduced the expression of HO-1 in response to *Leishmania* infection, suggesting that, in response to *Leishmania* infection, the increased expression of HO-1 is dependent on the Nrf2 TF.

Activation of NRF2 and HO-1 Transcription by *Leishmania* Parasites Is Independent of the Genetic Background

To determine whether *Leishmania* infection differentially regulates the mRNA expression of NRF2 and HO-1 in resistant and susceptible mice, Balb/c and C57Bl/6 BMdMs were infected with *L. major* promastigotes for different times. Infected cells were harvested and the expressions of antioxidant genes were analyzed using RT-PCR.

Our results showed that both Nrf2 and HO-1 mRNAs were significantly induced by the parasites in C57Bl/6 BMdMs (**Figure 4**). The transcriptional kinetics of Nrf2 is very similar in BMdMs from both mouse strains, with slightly higher expression levels in C57Bl/6 BMdMs. Regarding HO-1, the transcription peaked earlier (3 hpi), lasted longer, and was at 12 h twice as important in C57Bl/6 BMdMs. Killed parasites

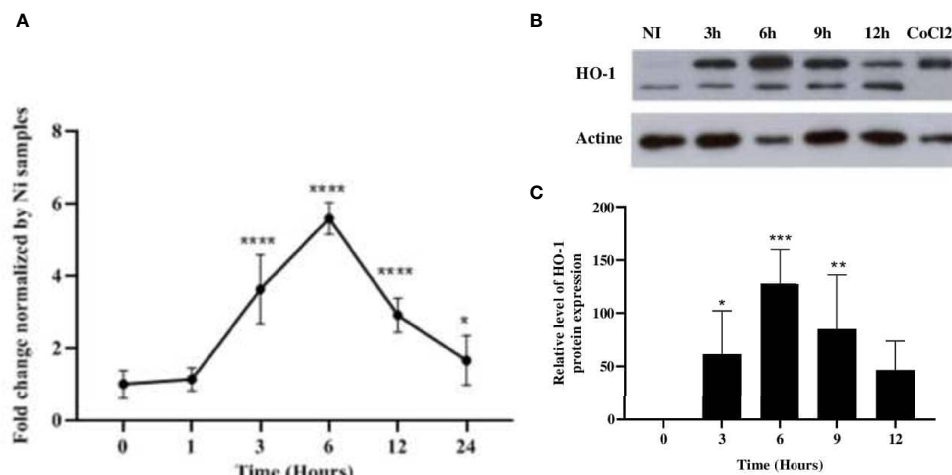


FIGURE 1 | *Leishmania major* induced the expression of HO-1 at both the mRNA and protein levels. Balb/c bone marrow-derived macrophages (BMdMs) and/or Raw264.7 cells were infected for the indicated time periods with *L. major* promastigotes. **(A)** The extracted mRNAs were used to perform RT-PCR. **(B)** The expression of heme oxygenase 1 (HO-1) was evaluated at the protein level by immunoblotting. CoCl₂ stimulation (250 ng/ml) for 3h was used as control. **(C)** Densitometric quantification of HO-1 protein levels using ImageJ. All data are expressed as the mean \pm SD from three independent experiments. Statistical significance was placed at $p < 0.05$. * $p < 0.05$, ** $p < 0.01$, *** $p < 0.001$, **** $p < 0.0001$ vs. non-stimulated cells (two-way ANOVA).

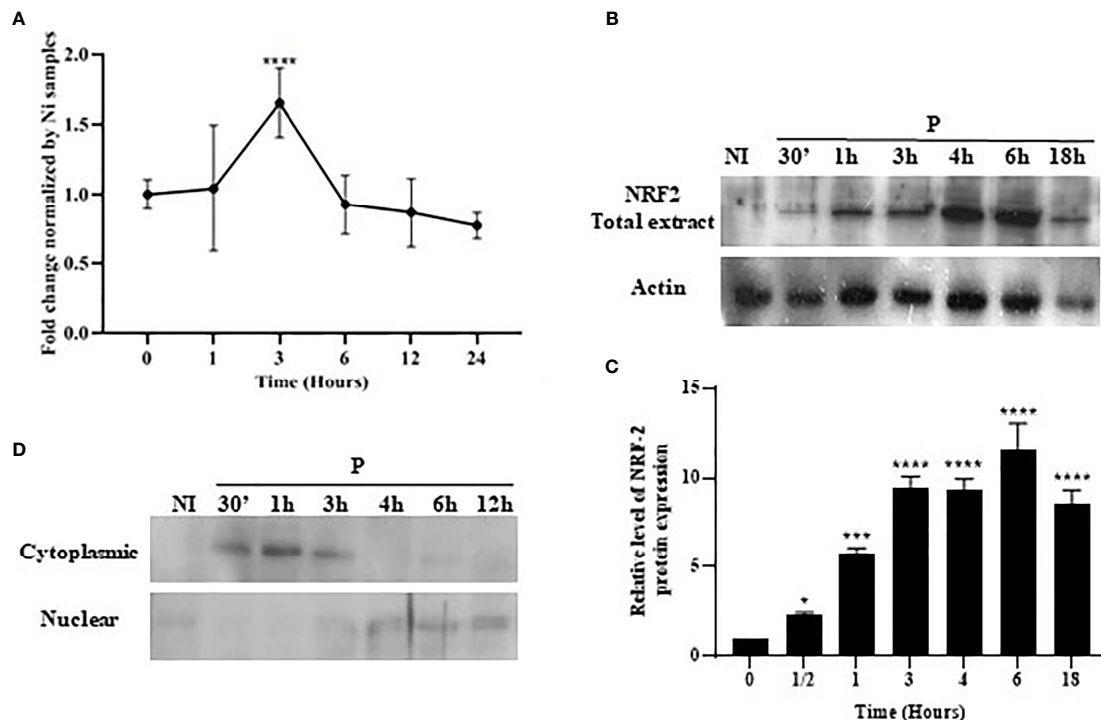


FIGURE 2 | Stimulation and nuclear accumulation of Nrf2 in response to *Leishmania major* infection. Balb/c bone marrow-derived macrophages (BMdMs) and/or Raw264.7 cells were infected for the indicated time period with *L. major* promastigotes. **(A)** The extracted mRNAs were used to perform RT-PCR. **(B)** Total Nrf2 expression was evaluated at the protein level by immunoblotting. **(C)** Densitometric quantification of the NRF2 protein levels using ImageJ. All data are expressed as the mean \pm SD from two independent experiments. * $p < 0.05$, *** $p < 0.001$, **** $p < 0.0001$ vs. non-stimulated BMdMs (two-way ANOVA). **(D)** Total protein extracts were fractionated into cytoplasmic and nuclear extracts and immunoblots performed with an anti-Nrf2 antibody. ERK1/2 and PARP were used to confirm the efficacy of cytosol and nuclear fractionation.

induced NRF2 and HO-1 to nearly the same extent as did the live parasites in BMdMs from both mouse strains.

The Impact of *Leishmania* Infection on the Expressions of Several NRF2 Antioxidant Genes

We investigated the transcription of different NRF2-regulated antioxidant genes in the infected macrophages. Our results showed that, in Balb/c BMdMs, *Leishmania* increased the transcription of the cysteine/glutamate exchange transporter (Slc7a11) regulating the cysteine influx and that of the catalytic (GCLc) and modifier (GCLm) subunits of the γ -glutamyl-cysteine ligase, the rate-limiting enzyme regulating the synthesis of glutathione (Figure 5). The parasites also increased the transcription of glutathione reductase (Gsr), CD36, and catalase (CAT). The transcription of almost all of the antioxidant genes peaked at 6 hpi, except for that of Gsr, which peaked earlier (3 hpi). Similar results were obtained in C57Bl/6 BMdMs, except for Slc7a11 and Gsr (Figure 6). Indeed, Slc7a11 mRNA was fivefold and Gsr mRNA was 20-fold higher in C57Bl/6 BMdMs. Moreover, when compared to that induced by inactivated parasites, Gsr was not only transcribed to a lesser extent but was also repressed at all time points by live parasites in Balb/c-derived macrophages. In fact, the transcription of almost

all of the selected genes was actively repressed by the live parasite; this repression was observed at all time points for Gsr, CD36, and CAT and at the later times for the other genes.

NRF2 Silencing Promotes *Leishmania* Persistence and Proliferation Inside Macrophages

Intracellular pathogens such as *Leishmania* use macrophages as a reservoir for dissemination. To test the ability of Nrf2 expression in controlling parasite load and multiplication, Ds-Red promastigotes were used to investigate the intracellular load of *Leishmania*. NT-pLKO raw cells and deficient NRF2 cells were infected with Ds-Red promastigotes for 72 h and the parasite load was analyzed by flow cytometry. Our experiments showed that Nrf2 loss in infected macrophages increased the ability of amastigotes to multiply inside the macrophages; parasite fluorescence emission is significantly more important in NRF2 knockdown cells (Figure 7).

DISCUSSION

Macrophage–*Leishmania* interaction and the response of macrophages to infection direct the outcome of the disease.

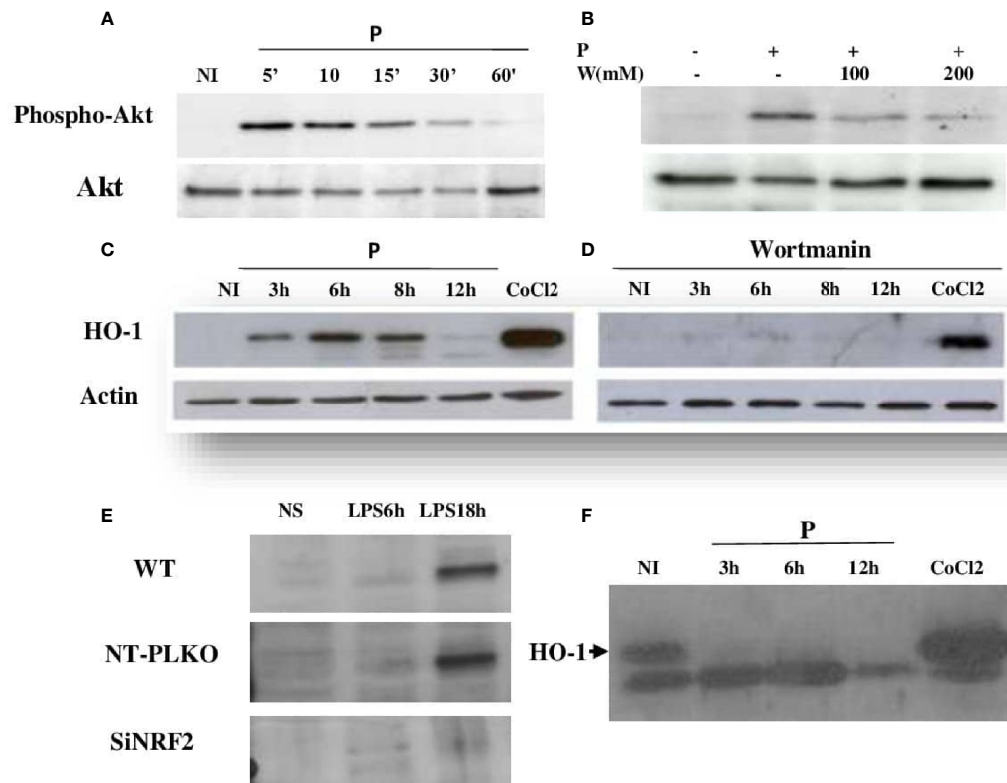


FIGURE 3 | *Leishmania major* induced HO-1 expression through PI3K/Akt and the Nrf2 transcription factor. **(A, C)** Raw264.7 cells were infected for the indicated time periods with *L. major* promastigotes and the expressions of Akt and HO-1 assessed using Western blot. CoCl₂ stimulation for 3 h (250 ng/ml) was used as the control. **(B, D)** Macrophages were pre-incubated with wortmannin (200 mM) for 3 h, followed by infection with *L. major* promastigotes for different times. Akt phosphorylation and HO-1 expression were determined by immunoblotting. **(E)** Raw264.7 cells were transfected (24 h) with either Nrf2 (Si) or control siRNA (NT-pLKO), followed by infection with lipopolysaccharide (LPS) for 18 h, lysed, and examined by Western blot for Nrf2 expression. **(F)** *NRF2*^{-/-} cells were infected for different times with *L. major* promastigotes, lysed, and examined by Western blot for HO-1 expression.

Parasite infection activates microbicidal mechanisms such as oxidative response that help protect the host against the invaders, but can be harmful for the cells. The Nrf2 signaling pathway leads to the activation of all defense genes that aim to protect the cells from the oxidative response switched to face the infection. The Nrf2 TF plays a key role in the maintenance of intracellular redox homeostasis and the regulation of inflammation. Among the antioxidative stress genes whose expressions are regulated by NRF2, HO-1, encoded by the *Hmox1* gene, has received considerable attention. HO-1 is responsible for heme detoxification and, apart from ROS neutralization, has a potent anti-inflammatory effect and plays a critical role in iron homeostasis (Vijayan et al., 2018). The inducible HO-1 isoform is induced in response to *Helicobacter pylori* infection (Gobert et al., 2014), required for protection against *Toxoplasma gondii* (Araujo et al., 2013), and critically contributes to host resistance to *Mycobacterium* infections in mice (Silva-Gomes et al., 2013). It is also activated in response to protozoan parasites, such as *Trypanosoma brucei* (Campbell et al., 2019) and *Trypanosoma cruzi* (Paiva et al., 2012). Our results indicated that *L. major* also increased the expression of HO-1 both at the mRNA and protein levels (Figure 1). This result is consistent with previous studies showing an increased expression of HO-1 in macrophages in

response to different species of *Leishmania* in either of its two forms (Pham et al., 2005; Luz et al., 2012; de Menezes et al., 2019; Saha et al., 2019).

HO-1 activation is dependent on the PI3K/Akt and Nrf2 signaling pathways. Indeed, we showed that *L. major*, as previously reported, induced the PI3K/Akt pathway (Ruhland et al., 2007) and the activation of the Nrf2 TF and its translocation to the nucleus (de Menezes et al., 2019). Wortmannin treatment and NRF2 silencing showed that these two pathways were both involved in the regulation of HO-1 expression (Figure 2).

HO-1 expression orchestrated by the activation of the Nrf2 promoter has been associated with parasite survival and persistence, as the BMdMs from *Hmox1*^{-/-} Balb/c mice presented a significantly reduced *Leishmania chagasi* parasite burden (Luz et al., 2012). In contrast, for other different pathogens including Trypanosomatidae, HO-1 seems to protect the host against the invaders. Indeed, inhibition of the activity of HO-1 increased *T. cruzi* parasitemia (Paiva et al., 2012). Similarly, the silencing of HO-1 in *H. pylori*-infected macrophages downregulated M1 polarization and favored *H. pylori* survival (Gobert et al., 2014). HO-1-deficient mice developed higher pathogen loads and were more susceptible to intravenous *Mycobacterium avium* infection, suggesting that HO-1

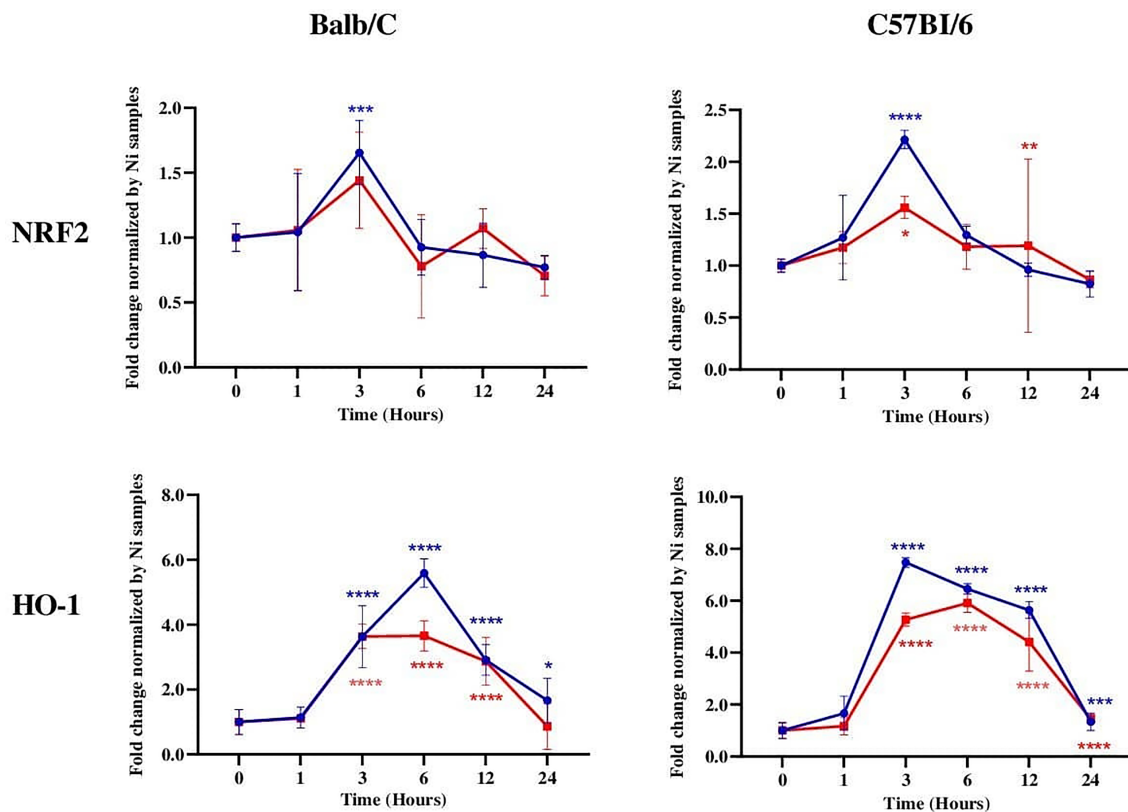


FIGURE 4 | NRF2 and HO-1 mRNAs were induced in *Leishmania*-susceptible and *Leishmania*-resistant bone marrow-derived macrophages (BMdMs). Balb/c and C57Bl/6 BMdMs were infected by live parasites (P) (blue filled circle) or heat-inactivated (Kp) (red filled square) *L. major* promastigotes for different times. RT-PCR targeting Nrf2 and HO-1 was performed. The graphs show fold change results expressed as the mean \pm SD from three independent experiments. * $p < 0.05$, ** $p < 0.01$, *** $p < 0.001$, **** $p < 0.0001$ vs. non-stimulated BMdMs (two-way ANOVA).

expression in macrophages is strictly required for protection against mycobacterial infection in mice (Silva-Gomes et al., 2013).

The host genetic background plays a key role in the development of leishmaniasis and has a strong impact on the severity and the final outcome of the disease. C57BL/6 and BALB/c mice, the prototypical Th1- and Th2-type mouse strains, are respectively resistant and susceptible to *Leishmania* parasites. The innate immune response of macrophages, different between these mouse strains, certainly affects the development of the adaptive immunity of Th1 and Th2 (Watanabe et al., 2004). We tried first to determine whether the expressions of NRF2 and HO-1 are different in these two mouse strains showing contrasting behaviors in response to *Leishmania* infection. Our results revealed that the transcriptions of NRF2 and HO-1 were not differentially regulated and were similarly induced in BMdMs issued from either Balb/c or C57Bl/6 (Figure 4). Additionally, the transcription of HO-1, which can drive the phenotypic shift to M2 macrophages (Naito et al., 2014) and favor parasite survival (Pham et al., 2005; Luz et al., 2012), peaked earlier, lasted longer, and was not repressed by the parasites in BMdMs from resistant mice. However, HO-1 has, in addition, significant anti-inflammatory effects (Vijayan et al.,

2018; Costa et al., 2020) and induces protective enzymes sequestering iron ions (Loboda et al., 2016).

Besides HO-1, GSH systems, one of the two major thiol-dependent antioxidant mechanisms in cells, are also activated by *L. major* infection. Our results also point out that initial contact with *Leishmania* was necessary and sufficient to promote the macrophage activation of the Nrf2 pathway. This pathway is therefore likely triggered by the stimulation of the receptors implicated in the recognition of the parasites, as heat-inactivated parasites also have the ability to induce the transcription of both NRF2 and its target genes.

All of the selected target genes were induced in both Balb/c and C57Bl/6 BMdMs. However, the transcriptions of the cysteine transporter (Slc7a11) and of Gsr were differentially regulated between the macrophages from the two mouse strains. Indeed, these genes were more highly transcribed in C57Bl/6 BMdMs. This increased transcription of Slc7a11, which is required to maintain the intracellular level of GSH and that of Gsr, involved in the recycling of oxidized glutathione, may result in glutathione accumulation, which has been reported to play a role in the resistance to *Leishmania* infection. Indeed, the depletion of glutathione has been shown to significantly increase the

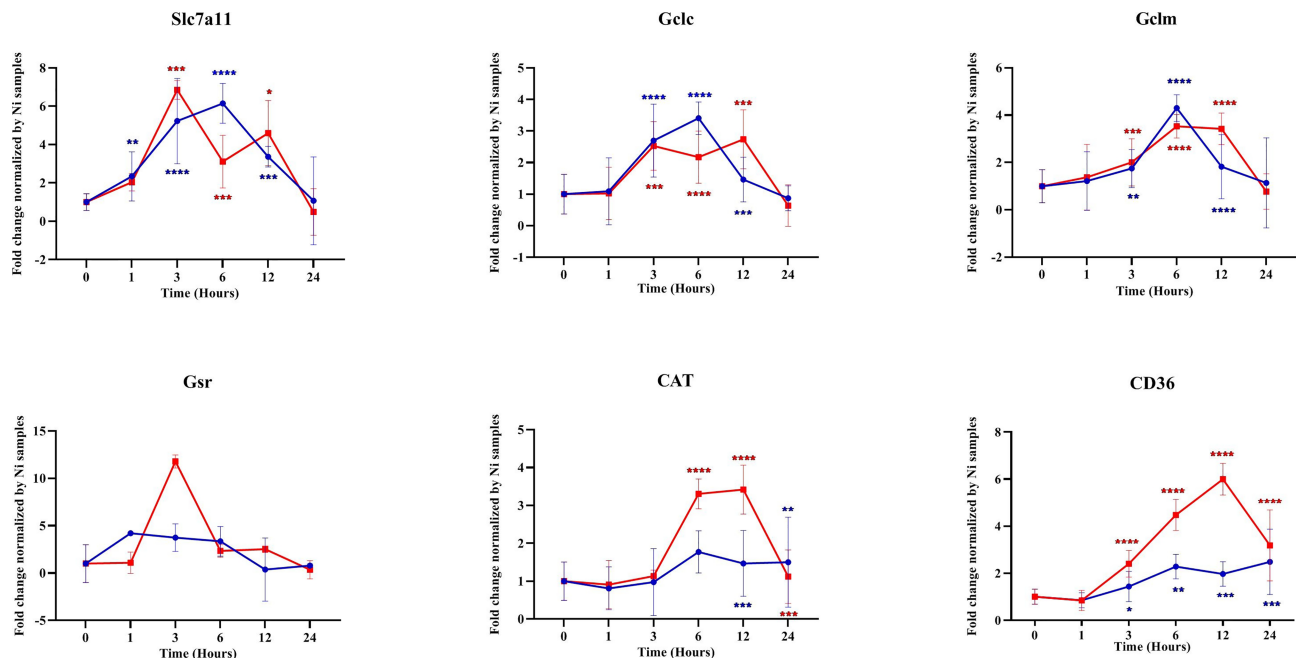


FIGURE 5 | Transcription of different antioxidant genes was repressed by parasites. Balb/c bone marrow-derived macrophages (BMdMs) were infected with live parasites (P) (blue filled circle) or heat-inactivated (Kp) (red filled square) *L. major* promastigotes for different times. RT-PCR targeting Slc7a11, GCLC, GCLM, GSR, CAT, and CD36 was performed. The graphs show fold change results expressed as the mean \pm SD from three independent experiments. * p < 0.05, ** p < 0.01, *** p < 0.001, **** p < 0.0001 vs. non-stimulated BMdMs (two-way ANOVA).

parasite load in the footpads of C57BL/6 mice infected with *L. major* (Cruz et al., 2008). Moreover, a close correlation was observed between the levels of intracellular soluble GSH and the secretion of nitrite (Buchmüller-Rouiller et al., 1995). In fact, a reduced cellular environment is important for several cellular functions, such as immune response and macrophage polarization (Fraternal et al., 2017). Thus, in contrast to HO-1, the transcription of Slc7a11 and Gsr, belonging to the glutathione system, was differentially regulated in BMdMs from resistant and susceptible mice, suggesting that glutathione may play an important role in the elimination of the parasite.

The second most striking observation is that, although the transcription of all the targeted antioxidant genes was induced by the infection and the triggering of the receptors, it was actively repressed by the parasite. This was particularly true for CD36 and CAT, a peroxide-scavenging enzyme, and for Gsr in BMdMs from susceptible mice.

CD36 represents an important part of the innate immune defense and may act as a pattern recognition receptor, in particular against bacterial pathogens (Areschoug and Gordon, 2009). CD36 is also important for host resistance to infection, and its deficiency significantly reduces mycobacteria burden (Hawkes et al., 2010), whereas its induction helps control severe malaria through parasite clearance (Olagner et al., 2011). Increased transcription of CD36 has been reported for *Leishmania infantum* (Gatto et al., 2020) and *Leishmania amazonensis* (Okuda et al., 2016). However, while CD36^{-/-} macrophages are infected but do not support *L. amazonensis* proliferation, *L. major*

amastigotes do not recruit CD36 and proliferate normally in CD36^{-/-} macrophages (Okuda et al., 2016). This is consistent with our finding that, despite their ability to induce NRF2 expression, *L. major* promastigotes actively limited CD36 transcription. In a different model, CD36 has been implicated in the regulation of ROS. Indeed, in murine vascular smooth muscle cells (VSMCs), while ROS induced the activation of the NRF2 target genes to limit oxidant stress, it also led to the generation of specific CD36 ligands, such as MP and oxLDL, allowing the scavenger receptor to phosphorylate NRF2 and, thus, to induce its exit from the nucleus and degradation (Li et al., 2010).

Thus, except for HO-1, the transcription of all the Nrf2 target genes tested was repressed, if not at all time points at least at the later ones, suggesting that these enzymes may play a role in limiting parasite survival and/or growth.

Our result showing that the silencing of the Nrf2 TF induced an increase in the parasite load is therefore in agreement with the parasite repressing the expressions of NRF2 target genes.

The role of NRF2 has also been explored, and transcriptomic and proteomic analyses highlighted the importance of Nrf2 signaling in cutaneous leishmaniasis (Vivarini et al., 2017; de Menezes et al., 2019). Indeed, the activation of NRF2 induced by *L. amazonensis* and *Leishmania braziliensis* enhanced the intracellular pathogen survival and disease progression (Vivarini et al., 2017). *L. amazonensis*-infected bone marrow macrophages exhibited increased expressions of NRF2 and antioxidant HO-1, which, together with higher levels of holotransferrin (holoTf) in parasitophorous vacuoles, contributed to the persistence of

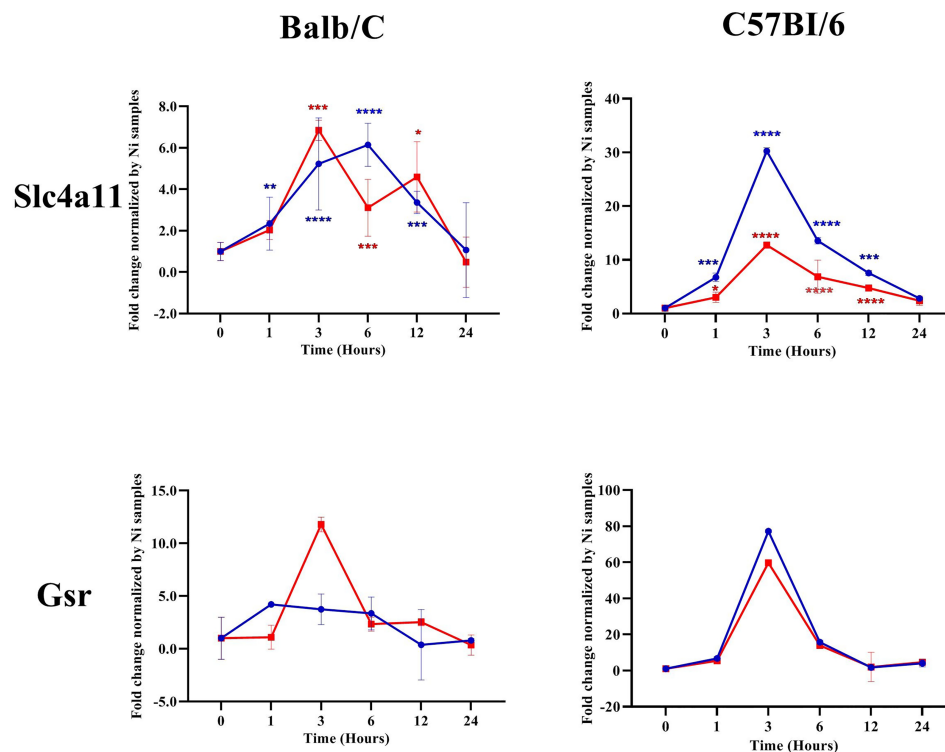


FIGURE 6 | Slc7a11 and Gsr were differentially regulated by *Leishmania* parasites in Balb/c and C57Bl/6 bone marrow-derived macrophages (BMDMs). Balb/c and C57Bl/6 BMDMs were infected by live parasites (P) (blue filled circle) or heat-inactivated (Kp) (red filled square) *L. major* promastigotes for different times. RT-PCR targeting Slc7a11 and Gsr was performed. The graphs show fold change results expressed as the mean \pm SD from three independent experiments. * $p < 0.05$, ** $p < 0.01$, *** $p < 0.001$, **** $p < 0.0001$ vs. non-stimulated BMDMs (two-way ANOVA).

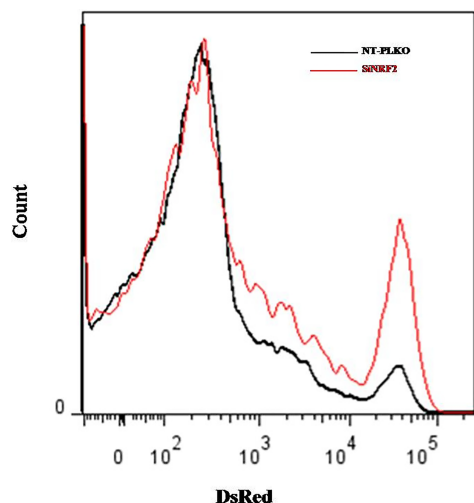


FIGURE 7 | Silencing of NRF2 promoted parasite survival. NT-pLKO or si-NRF2 Raw264.7 cells were infected with Ds-Red promastigotes. Macrophages (MΦs) parasitized with Ds-Red parasites were analyzed 72 h post-infection by flow cytometry. The percentages of Ds-Red fluorescence corresponding to the multiplication of amastigotes in parasitized MΦs were compared in NT-pLKO and si-NRF2-infected macrophages.

L. amazonensis infection (de Menezes et al., 2019). In our study, however, the silencing of NRF2 induced the persistence and multiplication of *L. major* parasites. This is in accordance with earlier results showing that treatment of *L. major*-infected BALB/c mice with *N*-acetyl-L-cysteine (NAC), a glutathione precursor and an NRF2 inducer, reduced the parasitism in their footpads (Rocha-Vieira et al., 2003).

We show in the present study that, while the master regulator of antioxidant response genes, Nrf2, is strongly induced by macrophage–*Leishmania* contact, the parasite represses the transcription of antioxidant genes and that the inactivation of the Nrf2 TF favors parasite survival and multiplication. Moreover, NRF2 target genes appear to play contrasting roles in *Leishmania*-infected macrophages, with HO-1 enabling parasite survival and enzymes of the GSH system, which are differentially regulated between BMDMs from resistant and susceptible mice, promoting parasite removal.

DATA AVAILABILITY STATEMENT

The original contributions presented in the study are included in the article/supplementary material. Further inquiries can be directed to the corresponding author.

ETHICS STATEMENT

The animal study was reviewed and approved by the Ethics Committee of Institute Pasteur of Tunis, with ethics approval no. 1204.

AUTHOR CONTRIBUTIONS

HB, SR, CH, and CB carried out the experiments. MB helped with the flow cytometry experiments. DP and BT performed the

qRT-PCR. IR supervised and contributed to the interpretation of the results. LG-T conceived and planned the experiments and wrote the manuscript. All authors contributed to the article and approved the submitted version.

FUNDING

This study was funded by the Tunisian Ministry of Higher Education.

REFERENCES

- Araujo, E. C. B., Barbosa, B. F., Coutinho, L. B., Barenco, P. V. C., Sousa, L. A., Milanezi, C. M., et al. (2013). Heme Oxygenase-1 Activity Is Involved in the Control of Toxoplasma Gondii Infection in the Lung of BALB/c and C57BL/6 and in the Small Intestine of C57BL/6 Mice. *Vet. Res.* 44, 89. doi: 10.1186/1297-9716-44-89
- Areschoug, T., and Gordon, S. (2009). Scavenger Receptors: Role in Innate Immunity and Microbial Pathogenesis. *Cell Microbiol.* 11, 1160–1169. doi: 10.1111/j.1462-5822.2009.01326.x
- Baird, L., and Yamamoto, M. (2020). The Molecular Mechanisms Regulating the KEAP1-NRF2 Pathway. *Mol. Cell Biol.* 40, e00099–e00020. doi: 10.1128/MCB.00099-20
- Buchmüller-Rouiller, Y., Corrandin, S. B., Smith, J., Schneider, P., Ransijn, A., Jongeneel, C. V., et al. (1995). Role of Glutathione in Macrophage Activation: Effect of Cellular Glutathione Depletion on Nitrite Production and Leishmanicidal Activity. *Cell Immunol.* 164, 73–80. doi: 10.1006/cimm.1995.1144
- Campbell, N. K., Williams, D. G., Fitzgerald, H. K., Barry, P. J., Cunningham, C. C., Nolan, D. P., et al. (2019). Trypanosoma Brucei Secreted Aromatic Ketoacids Activate the Nrf2/HO-1 Pathway and Suppress Pro-Inflammatory Responses in Primary Murine Glia and Macrophages. *Front. Immunol.* 10, 2137. doi: 10.3389/fimmu.2019.02137
- Conceição-Silva, F., and Morgado, F. N. (2019). Leishmania Spp-Host Interaction: There Is Always an Onset, But Is There an End? *Front. Cell Infect. Microbiol.* 9, 330. doi: 10.3389/fcimb.2019.00330
- Costa, D. L., Amaral, E. P., Andrade, B. B., and Sher, A. (2020). Modulation of Inflammation and Immune Responses by Heme Oxygenase-1: Implications for Infection With Intracellular Pathogens. *Antioxid. (Basel)* 9, E1205. doi: 10.3390/antiox9121205
- Cruz, K. K., Fonseca, S. G., Monteiro, M. C., Silva, O. S., Andrade, V. M., Cunha, F. Q., et al. (2008). The Influence of Glutathione Modulators on the Course of Leishmania Major Infection in Susceptible and Resistant Mice. *Parasit. Immunol.* 30, 171–174. doi: 10.1111/j.1365-3024.2007.01014.x
- de Menezes, J. P. B., Khouri, R., Oliveira, C. V. S., Petersen, A. L., de, O. A., de Almeida, T. F., et al. (2019). Proteomic Analysis Reveals a Predominant NFE2L2 (NRF2) Signature in Canonical Pathway and Upstream Regulator Analysis of Leishmania-Infected Macrophages. *Front. Immunol.* 10, 1362. doi: 10.3389/fimmu.2019.01362
- Fraternal, A., Brundu, S., and Magnani, M. (2017). Glutathione and Glutathione Derivatives in Immunotherapy. *Biol. Chem.* 398, 261–275. doi: 10.1515/hsz-2016-0202
- Gatto, M., Borim, P. A., Wolf, I. R., Fukuta da Cruz, T., Ferreira Mota, G. A., Marques Braz, A. M., et al. (2020). Transcriptional Analysis of THP-1 Cells Infected With Leishmania Infantum Indicates No Activation of the Inflammasome Platform. *PLoS Negl. Trop. Dis.* 14, e0007949. doi: 10.1371/journal.pntd.0007949
- Gobert, A. P., Verriere, T., Asim, M., Barry, D. P., Piazzuelo, M. B., de Sablet, T., et al. (2014). Heme Oxygenase-1 Dysregulates Macrophage Polarization and the Immune Response to Helicobacter Pylori. *J. Immunol.* 193, 3013–3022. doi: 10.4049/jimmunol.1401075
- Hawkes, M., Li, X., Crockett, M., Diassiti, A., Finney, C., Min-Oo, G., et al. (2010). CD36 Deficiency Attenuates Experimental Mycobacterial Infection. *BMC Infect. Dis.* 10, 299. doi: 10.1186/1471-2334-10-299
- Itoh, K., Ishii, T., Wakabayashi, N., and Yamamoto, M. (1999). Regulatory Mechanisms of Cellular Response to Oxidative Stress. *Free Radic. Res.* 31, 319–324. doi: 10.1080/10715769900300881
- Li, W., Febbraio, M., Reddy, S. P., Yu, D.-Y., Yamamoto, M., and Silverstein, R. L. (2010). CD36 Participates in a Signaling Pathway That Regulates ROS Formation in Murine VSMCs. *J. Clin. Invest.* 120, 3996–4006. doi: 10.1172/JCI42823
- Loboda, A., Damulewicz, M., Pyza, E., Jozkowicz, A., and Dulak, J. (2016). Role of Nrf2/HO-1 System in Development, Oxidative Stress Response and Diseases: An Evolutionarily Conserved Mechanism. *Cell Mol. Life Sci.* 73, 3221–3247. doi: 10.1007/s00018-016-2223-0
- Luz, N. F., Andrade, B. B., Feijó, D. F., Araújo-Santos, T., Carvalho, G. Q., Andrade, D., et al. (2012). Heme Oxygenase-1 Promotes the Persistence of Leishmania Chagasi Infection. *J. Immunol.* 188, 4460–4467. doi: 10.4049/jimmunol.1103072
- Naito, Y., Takagi, T., and Higashimura, Y. (2014). Heme Oxygenase-1 and Anti-Inflammatory M2 Macrophages. *Arch. Biochem. Biophys.* 564, 83–88. doi: 10.1016/j.abb.2014.09.005
- Nguyen, T., Sherratt, P. J., and Pickett, C. B. (2003). Regulatory Mechanisms Controlling Gene Expression Mediated by the Antioxidant Response Element. *Annu. Rev. Pharmacol. Toxicol.* 43, 233–260. doi: 10.1146/annurev.pharmtox.43.100901.140229
- Okuda, K., Tong, M., Dempsey, B., Moore, K. J., Gazzinelli, R. T., and Silverman, N. (2016). Leishmania Amazonensis Engages CD36 to Drive Parasitophorous Vacuole Maturation. *PLoS Pathog.* 12, e1005669. doi: 10.1371/journal.ppat.1005669
- Olagner, D., Laverne, R.-A., Meunier, E., Lefèvre, L., Dardenne, C., Aubouy, A., et al. (2011). Nrf2, a Pparγ Alternative Pathway to Promote CD36 Expression on Inflammatory Macrophages: Implication for Malaria. *PLoS Pathog.* 7, e1002254. doi: 10.1371/journal.ppat.1002254
- Paiva, C. N., Feijó, D. F., Dutra, F. F., Carneiro, V. C., Freitas, G. B., Alves, L. S., et al. (2012). Oxidative Stress Fuels Trypanosoma Cruzi Infection in Mice. *J. Clin. Invest.* 122, 2531–2542. doi: 10.1172/JCI58525
- Pham, N.-K., Mouriz, J., and Kima, P. E. (2005). Leishmania Pifanoi Amastigotes Avoid Macrophage Production of Superoxide by Inducing Heme Degradation. *Infect. Immun.* 73, 8322–8333. doi: 10.1128/IAI.73.12.8322-8333.2005
- Rabhi, S., Rabhi, I., Trentin, B., Piquemal, D., Regnault, B., Goyard, S., et al. (2016). Lipid Droplet Formation, Their Localization and Dynamics During Leishmania Major Macrophage Infection. *PLoS One* 11, e0148640. doi: 10.1371/journal.pone.0148640
- Rocha-Vieira, E., Ferreira, E., Vianna, P., De Faria, D. R., Gaze, S. T., Dutra, W. O., et al. (2003). Histopathological Outcome of Leishmania Major-Infected BALB/c Mice Is Improved by Oral Treatment With N-Acetyl-L-Cysteine. *Immunology* 108, 401–408. doi: 10.1046/j.1365-2567.2003.01582.x
- Ruhland, A., Leal, N., and Kima, P. E. (2007). Leishmania Promastigotes Activate PI3K/Akt Signalling to Confer Host Cell Resistance to Apoptosis. *Cell Microbiol.* 9, 84–96. doi: 10.1111/j.1462-5822.2006.00769.x
- Saha, S., Basu, M., Guin, S., Gupta, P., Mitterstiller, A.-M., Weiss, G., et al. (2019). Leishmania Donovanii Exploits Macrophage Heme Oxygenase-1 To Neutralize Oxidative Burst and TLR Signaling-Dependent Host Defense. *J. Immunol.* 202, 827–840. doi: 10.4049/jimmunol.1800958
- Silva-Gomes, S., Appelberg, R., Larsen, R., Soares, M. P., and Gomes, M. S. (2013). Heme Catabolism by Heme Oxygenase-1 Confers Host Resistance to

- Mycobacterium Infection. *Infect. Immun.* 81, 2536–2545. doi: 10.1128/IAI.00251-13
- Sytkiotis, G. P., and Bohmann, D. (2010). Stress-Activated Cap'n'collar Transcription Factors in Aging and Human Disease. *Sci. Signal.* 3, re3. doi: 10.1126/scisignal.3112re3
- Tonelli, C., Chio, I. I. C., and Tuveson, D. A. (2018). Transcriptional Regulation by Nrf2. *Antioxid. Redox. Signal.* 29, 1727–1745. doi: 10.1089/ars.2017.7342
- Vijayan, V., Wagener, F. A. D. T. G., and Immenschuh, S. (2018). The Macrophage Heme-Heme Oxygenase-1 System and Its Role in Inflammation. *Biochem. Pharmacol.* 153, 159–167. doi: 10.1016/j.bcp.2018.02.010
- Vivarini, A., de, C., Calejari-Silva, T. C., Saliba, A. M., Boaventura, V. S., França-Costa, J., et al. (2017). Systems Approach Reveals Nuclear Factor Erythroid 2-Related Factor 2/Protein Kinase R Crosstalk in Human Cutaneous Leishmaniasis. *Front. Immunol.* 8, 1127. doi: 10.3389/fimmu.2017.01127
- Watanabe, H., Numata, K., Ito, T., Takagi, K., and Matsukawa, A. (2004). Innate Immune Response in Th1- and Th2-Dominant Mouse Strains. *Shock* 22, 460–466. doi: 10.1097/01.shk.0000142249.08135.e9

Conflict of Interest: The authors declare that the research was conducted in the absence of any commercial or financial relationships that could be construed as a potential conflict of interest.

Publisher's Note: All claims expressed in this article are solely those of the authors and do not necessarily represent those of their affiliated organizations, or those of the publisher, the editors and the reviewers. Any product that may be evaluated in this article, or claim that may be made by its manufacturer, is not guaranteed or endorsed by the publisher.

Copyright © 2021 Bichiou, Rabhi, Ben Hamda, Bouabid, Belghith, Piquemal, Trentin, Rabhi and Guizani-Tabbane. This is an open-access article distributed under the terms of the Creative Commons Attribution License (CC BY). The use, distribution or reproduction in other forums is permitted, provided the original author(s) and the copyright owner(s) are credited and that the original publication in this journal is cited, in accordance with accepted academic practice. No use, distribution or reproduction is permitted which does not comply with these terms.



Shedding of *Trypanosoma cruzi* Surface Molecules That Regulate Host Cell Invasion Involves Phospholipase C and Increases Upon Sterol Depletion

Leonardo Loch, Thiago Souza Onofre, João Paulo Ferreira Rodrigues and Nobuko Yoshida*

Departamento de Microbiologia, Imunologia e Parasitologia, Escola Paulista de Medicina, Universidade Federal de São Paulo, São Paulo, Brazil

OPEN ACCESS

Edited by:

Martin M. Edreira,
Universidad de Buenos Aires,
Argentina

Reviewed by:

Galia Andrea Ramirez-Tolosa,
University of Chile, Chile
Noelia Lander,
University of Cincinnati, United States

*Correspondence:

Nobuko Yoshida
nyoshida@unifesp.br

Specialty section:

This article was submitted to
Parasite and Host,
a section of the journal
Frontiers in Cellular and
Infection Microbiology

Received: 02 September 2021

Accepted: 27 September 2021

Published: 19 October 2021

Citation:

Loch L, Onofre TS, Rodrigues JPF and
Yoshida N (2021) Shedding of
Trypanosoma cruzi Surface Molecules
That Regulate Host Cell Invasion
Involves Phospholipase C and
Increases Upon Sterol Depletion.
Front. Cell. Infect. Microbiol. 11:769722.
doi: 10.3389/fcimb.2021.769722

Metacyclic trypomastigote (MT) forms of *Trypanosoma cruzi* have been shown to release into medium gp82 and gp90, the stage-specific surface molecules that regulate host cell invasion, either in vesicles or in soluble form. Here, we found that during interaction of poorly invasive G strain with the host cell, gp82 and gp90 were released in vesicle-like forms, whereas no such release by highly invasive CL strain was observed. Shedding of vesicles of varying sizes by CL and G strains was visualized by scanning electron microscopy, and the protein profile of conditioned medium (CM) of the two strains was similar, but the content of gp82 and gp90 differed, with both molecules being detected in G strain as bands of high intensity in Western blotting, whereas in CL strain, they were barely detectable. Confocal images revealed a distinct distribution of gp82 and gp90 on MT surface of CL and G strains. In cell invasion assays, addition of G strain CM resulted in decreased CL strain internalization. Depletion of gp82 in G strain CM, by treatment with specific mAb-coupled magnetic beads, increased its inhibitory effect on CL strain invasion, in contrast to CM depleted in gp90. The effect of cholesterol-depleting drug methyl- β -cyclodextrin (M β CD) on gp82 and gp90 release by MTs was also examined. G strain MTs, untreated or treated with M β CD, were incubated in serum-containing medium or in nutrient-depleted PBS⁺⁺, and the CM generated under these conditions was analyzed by Western blotting. In PBS⁺⁺, gp82 and gp90 were released at lower levels by untreated MTs, as compared with M β CD-treated parasites. CM from untreated and M β CD-treated G strain, generated in PBS⁺⁺, inhibited CL strain internalization. Treatment of CL strain MTs with M β CD resulted in increased gp82 and gp90 shedding and in decreased host cell invasion. The involvement of phospholipase C (PLC) on gp82 and gp90 shedding was also investigated. The CM from G strain MTs pretreated with specific PLC inhibitor contained lower levels of gp82 and gp90, as compared with untreated parasites. Our results contribute to shed light on the mechanism by which *T. cruzi* releases surface molecules implicated in host cell invasion.

Keywords: *Trypanosoma cruzi*, metacyclic trypomastigote, surface molecule shedding, host cell invasion, gp82, gp90

INTRODUCTION

Secreted signaling molecules play essential roles in intercellular communication. As a means of communication between cells, extracellular vesicles (EVs), which are lipid bound particles containing proteins, lipids, and nucleic acids, have gained prominence and are recognized to mediate the regulation of physiological functions and to be involved in pathological processes (Yáñez-Mó et al., 2015; Zaborowski et al., 2015). Among the EV subtypes are exosomes (40–100 nm), formed from multivesicular bodies through the inward budding of the endosome membrane, and microvesicles (100–1,000 nm), released from the cell by the outward budding of the plasma membrane (Mathivanan et al., 2010; Borges et al., 2013; Zaborowski et al., 2015).

Helminths, parasitic protozoa, and bacteria produce EVs (Yáñez-Mó et al., 2015). A recent review on EVs in vector-borne trypanosomatids, *Trypanosoma cruzi*, *Trypanosoma brucei*, and *Leishmania*, has discussed their role in inducing immunomodulatory events and how they affect the parasite interaction with vertebrate and invertebrate hosts (Torrecilhas et al., 2020). As regards *T. cruzi*, the agent of Chagas disease, it was reported three decades ago that the tissue culture-derived trypomastigote (TCT) forms spontaneously shed the entire set of surface polypeptides into the culture medium, mostly as plasma membrane vesicles (Gonçalves et al., 1991). Almost two decades later, it was shown that, upon injection into mice, TCT-shed vesicles increase heart parasitism and generate an intense inflammatory response (Torrecilhas et al., 2009). From then on, an increasing number of studies about *T. cruzi* vesicles have been published, including those related to the insect stage epimastigote and metacyclic trypomastigote (MT) forms. For instance, a proteomic analysis characterized two EV populations and soluble proteins from epimastigote and MT (Bayer-Santos et al., 2013). A study with EVs derived from epimastigotes indicated that they promoted the differentiation of the replicative forms into MTs (Garcia-Silva et al., 2014). In another study, purified EVs from epimastigotes, given to two distinct triatomine insects prior to infection with epimastigotes, affected early parasite migration in the gut of *Rhodnius prolixus* but not in *Triatoma infestans* (Paranaíba et al., 2019). As regards TCT, EVs derived from different *T. cruzi* strains were shown to trigger differential innate and chronic immune responses (Nogueira et al., 2015). Quantitative and qualitative differences in TCT-shed EVs and secreted proteins from different *T. cruzi* strains, revealed by proteomic analysis, were suggested to correlate with infectivity/virulence during the host–parasite interaction (Ribeiro et al., 2018). In Toll-like-receptor 2-transfected Chinese hamster ovary (CHO) cells, an increase in the percentage of TCT-infected cells was observed upon incubation with TCT-shed EVs (Cronemberger-Andrade et al., 2020).

Studies with MTs have revealed that different strains exhibit marked differences in their ability to invade cultured mammalian cells (Yoshida, 2006). A more extensive analysis, using *T. cruzi* strains G and CL, classified as discrete typing unit TcI and TcVI, respectively (Zingales et al., 2009), has shown that the higher

efficiency of CL strain in infecting mice, by either intraperitoneal or oral route, and in invading different cell types in culture, is associated with the differential expression of MT-specific surface glycoproteins (Yoshida, 2006) and possibly with their release into medium (Clemente et al., 2016). On the basis that EVs from G strain MTs increased G strain entry into Vero cells but had no effect on invasion by Y strain (TcII), it has been suggested that only parasites of the same classification were capable of modulating the invasion process (Wyllie and Ramirez, 2017). However, this contrasts with the observation that conditioned medium (CM) from G strain, which contains vesicles of varying sizes, significantly inhibited HeLa cell invasion by MTs of either G or CL strain, whereas CM from CL strain had no effect (Clemente et al., 2016). By analyzing the CM of the two strains, as regards the content of MT-specific cell surface glycoproteins gp82 and gp90, which function as a mediator and a downregulator of host cell invasion, respectively (Yoshida, 2006), considerable amounts of these molecules were detected in G strain, as opposed to minimal levels in CL strain (Clemente et al., 2016). The basis for the differential release of gp82 and gp90 by CL and G strain is not known. Here, we analyzed how these molecules are distributed on the surface of CL and G strain MTs and investigated the factors implicated in the shedding process. Experiments were also performed to examine the involvement of gp82 and gp90 contained in G strain CM as inhibitor of host cell invasion by CL strain MTs.

MATERIALS AND METHODS

Parasites, Mammalian Cells, and Invasion Assay

T. cruzi strains G and CL were maintained alternately in mice and in liver infusion tryptose (LIT) medium containing 5% fetal bovine serum (FBS). G strain MTs were obtained in high numbers in LIT medium at the stationary growth phase. In the case of CL strain, the parasites were grown for one passage in Grace's medium (Life Technologies/Thermo Fisher Scientific) to stimulate epimastigote differentiation into MTs. Experiments were performed with MTs purified in a DEAE-cellulose column, as described (Teixeira and Yoshida, 1986). For invasion assay, human epithelial HeLa cells were incubated for 1 h with MTs in Roswell Park Memorial Institute (RPMI) medium supplemented with 10% FBS, at multiplicity of infection (MOI) = 10 (CL strain) or MOI = 20 (G strain), as previously established (Maeda et al., 2012). After fixation in Bouin solution, staining with Giemsa, and sequential dehydration in acetone, acetone:xylol, and xylol, the number of internalized parasites was quantified, by counting a total number of 250 cells.

Preparation of *Trypanosoma cruzi* Conditioned Medium and Detergent-Soluble Extract

CM was prepared by incubating MTs (5×10^8 /ml) for 30 min in RPMI medium containing 1% FBS. After centrifugation at 1,500 g

for 5 min, the supernatant was collected and filtered in a 0.20- μ m syringe filter. The pellet was reconstituted with PBS to the original volume and lysed with 0.5% nonionic detergent Igepal CA630 (USB Corporation). The supernatant, resulting from centrifugation at 14,500 *g* for 10 min, constituted the detergent-soluble MT extract. In some experiments, CM was prepared by incubating MTs in serum-free medium or in PBS⁺⁺ (phosphate-buffered saline containing per liter 140 mg of CaCl₂, 400 mg of KCl, 100 mg of MgCl₂·6H₂O, 100 mg of MgSO₄·7H₂O, and 350 mg of NaHCO₃).

Visualization of *Trypanosoma cruzi* Metacyclic Trypomastigote and Interaction With Host Cell by Confocal Microscopy

Purified parasites were fixed with 4% paraformaldehyde for 20 min, washed in PBS, and placed onto glass slides and dried. Afterwards, the parasites were incubated for 1 h with antibody directed to MT surface molecule and, following washes in PBS and incubation with the secondary antibody (Alexa Fluor-conjugated IgG), diluted 1:500 in PGN (0.15% gelatin in PBS containing 0.1% sodium azide), plus 10 μ M of 4',6'-diamino-2-phenylindole dihydrochloride (DAPI). To examine the host cell–MT interaction, HeLa cells were incubated with parasites for 30 min and then processed for immunofluorescence and confocal microscopy visualization, essentially as previously described (Rodrigues et al., 2017), using rabbit anti-human LAMP2 antibody, mAb directed to gp82 or gp90, Alexa Fluor-conjugated IgG, and DAPI. The coverslips were mounted in ProLong Gold (Invitrogen). Images were acquired in a confocal microscope (Instituto de Farmacologia e Biologia Molecular (INFAR), Universidade Federal de São Paulo), using $\times 63$ objective, processed, and analyzed using Leica LAS AF and Imaris (Bitplane) software.

Scanning Electron Microscopy

Parasites were washed with PBS, attached to coverslips pretreated with 0.05% poly-L-lysine for 30 min, and washed in water. After 5-min centrifugation at 500 *g*, the parasites were fixed for 1 h, at room temperature, with 2.5% glutaraldehyde in 0.1 M of sodium cacodylate buffer, pH 7.2. Following four washes with 0.1 M of sodium cacodylate buffer, post-fixation with 1% osmium tetroxide in the same buffer, at room temperature, and washings with cacodylate buffer, the parasites were treated for 30 min with 1% tannic acid in water. After three washes in water, 30-min impregnation with 1% osmium tetroxide, and three washes in water, the samples were subjected to a gradual dehydration in a series of ethanol solutions and dried at the critical point apparatus using CO₂. After assembly in support of the SEM sample holder (stub) using Superglue, the material was coated with gold by sputtering and observed in scanning electron microscope.

Immunoprecipitation of Gp82 or Gp90 With Magnetic Beads Crosslinked to Specific Monoclonal Antibody

Protein G magnetic beads (Pierce Crosslink Magnetic IP/Co-IP Kit, Thermo Fisher Scientific), crosslinked with anti-gp82 mAb

3F6, anti-gp90 mAb 1G7, or with mAb 2C2 directed to an amastigote surface antigen, were incubated with G strain CM for 2 h at room temperature, along with the control empty beads. After collection, the CM was checked for depletion of gp82 and gp90 by Western blotting and used for MT invasion experiments.

Antibodies and Reagents

Alexa Fluor 555-conjugated anti-mouse IgG, Alexa Fluor 488-conjugated anti-mouse IgG, and Alexa Fluor 488-conjugated anti-rabbit IgG were from Thermo Fisher Scientific. Phospholipase C (PLC) inhibitor U73122 and methyl- β -cyclodextrin (M β CD) were from Sigma/Merck.

Statistical Analysis

Student's *t*-test (GraphPad Prism software Version 6.01) was employed to evaluate significance between two groups. For multiple comparisons, we used one-way NOVA followed by Bonferroni's post-hoc test.

Ethics Statement

All procedures conformed to Brazilian National Committee on Ethics Research (CONEP) guidelines, and the study was approved by the Committee on Ethics of Animal Experimentation of Universidade Federal de São Paulo (protocol number: CEUA 9780200918).

RESULTS

During Interaction With the Host Cell, Gp82 and Gp90 Are Released at High Levels by G Strain, But Not by CL Strain

A previous study has shown that gp82 and gp90 are released into medium in considerable amounts by G strain, either in vesicles or in soluble form, whereas release by CL strain MTs is minimal (Clemente et al., 2016). Here, we performed experiments to examine the shedding of these molecules during MT interaction with the host cell. HeLa cells were incubated for 30 min with G or CL strain MTs and then processed for indirect immunofluorescence, using anti-gp82 mAb 3F6 or anti-gp90 mAb 5E7, and anti-LAMP antibody for lysosome visualization. Upon G strain interaction with cells, gp82 was detected in vesicle-like forms, around the parasite and also attached to cells, or apparently internalized, whereas no such release by CL strain was observed (**Figure 1**). Both G and CL strain MTs induced the spreading of lysosomes and accumulation at the cell edges, an event known to be stimulated by gp82 (Cortez et al., 2016), and was particularly evident in large multinucleated cells (**Figure 1**). These large cells, which represent less than 10% of the total cell population, were more susceptible to gp82-mediated CL strain invasion (**Figure S1**), possibly because they express higher levels of gp82-receptor LAMP2 on the surface (Rodrigues et al., 2019; Onofre et al., 2021). CL strain internalization was evidenced by incorporation of lysosome membrane marker into the parasitophorous vacuole (**Figure 1**). As regards gp90, its release by G strain upon interaction with HeLa cells was

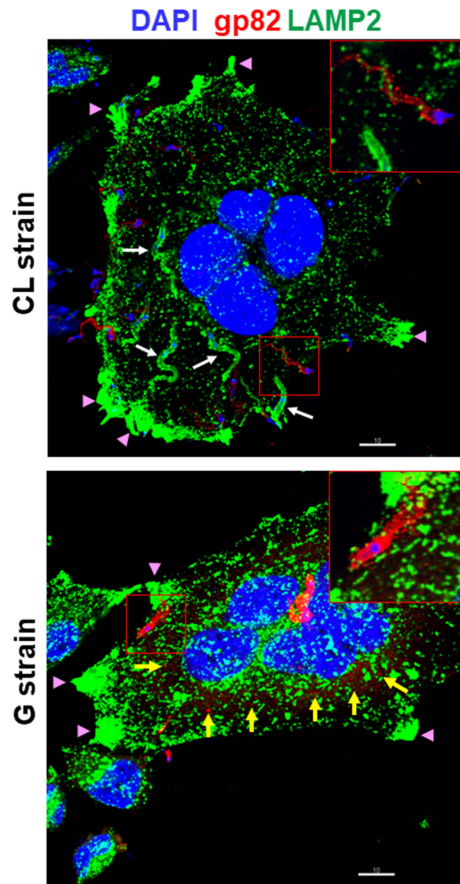


FIGURE 1 | Differential release of surface molecule gp82 by metacyclic trypomastigotes (MTs) of *Trypanosoma cruzi* strains CL and G during interaction with the host cell. HeLa cells were incubated for 30 min with MTs of CL or G strain and processed for immunofluorescence and confocal microscopy visualization of lysosomes (green), nucleus (blue), and gp82 (red). Scale bar = 10 μ m. Note the internalized CL strain MTs with lysosome membrane marker (white arrow), the gp82 released by G strain MTs (yellow arrow), and the lysosome accumulation at the cell edges (pink arrowhead). Shown on the upper right side of each panel is the magnified image from the smaller framed area.

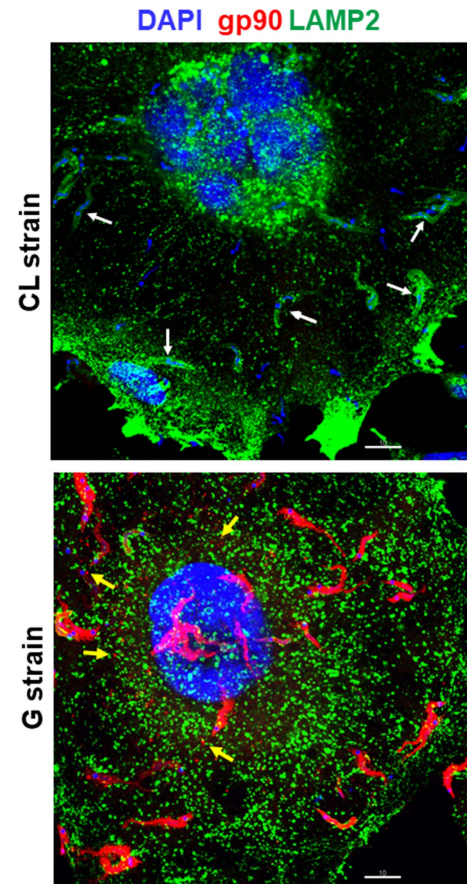


FIGURE 2 | Differential release of surface molecule gp90 by metacyclic trypomastigotes (MTs) of *Trypanosoma cruzi* strains CL and G during interaction with the host cell. HeLa cells were incubated for 30 min with MTs of CL or G strain and processed for immunofluorescence and confocal microscopy visualization of lysosomes (green), nucleus (blue), and gp90 (red). Scale bar = 10 μ m. Note the internalized CL strain MTs with lysosome membrane marker (white arrow) and the gp90 released by G strain MTs (yellow arrow).

similar to that of gp82, whereas shedding by CL strain was not detected (**Figure 2**). In contrast to CL strain, association of G strain with lysosome membrane marker was not seen, even when a high number of adherent parasites were visualized (**Figure 2**).

Vesicle Shedding and Protein Profile of Conditioned Medium Are Similar in CL and G Strains

Both CL and G strains were found to release comparable numbers of vesicles, with the difference that G strain released EVs of large size in higher amounts and EVs of smaller size in lower numbers, as compared with CL strain (Clemente et al., 2016). We visualized vesicles of varying sizes shed by CL and G strains by scanning electron microscopy (**Figure 3A**). As regards the protein content of CM, previously shown to contain large

and small vesicles, as well as soluble factors (Clemente et al., 2016), the analysis performed by using High Sensitivity Protein 250 kit and the Agilent 2100 Bioanalyzer system revealed a similar profile in CL and G strains (**Figure 3B**). In the range of 56.5–124.8 kDa, the 70.5-kDa protein was the most abundant (**Figure S3**). The major difference was observed in Western blotting of CM. Gp82 and gp90 were detected in G strain as bands of high intensity, whereas in CL strain, they were barely detectable (**Figure 3C**), compatible with the result from the immunofluorescence analysis of MT interaction with HeLa cells (**Figures 1, 2**).

CL and G Strains Differ Morphologically and in the Expression/Distribution of Gp82 and Gp90

Morphology is one of the distinctive features between CL and G strains. MTs of CL strain are slender and longer, as shown by

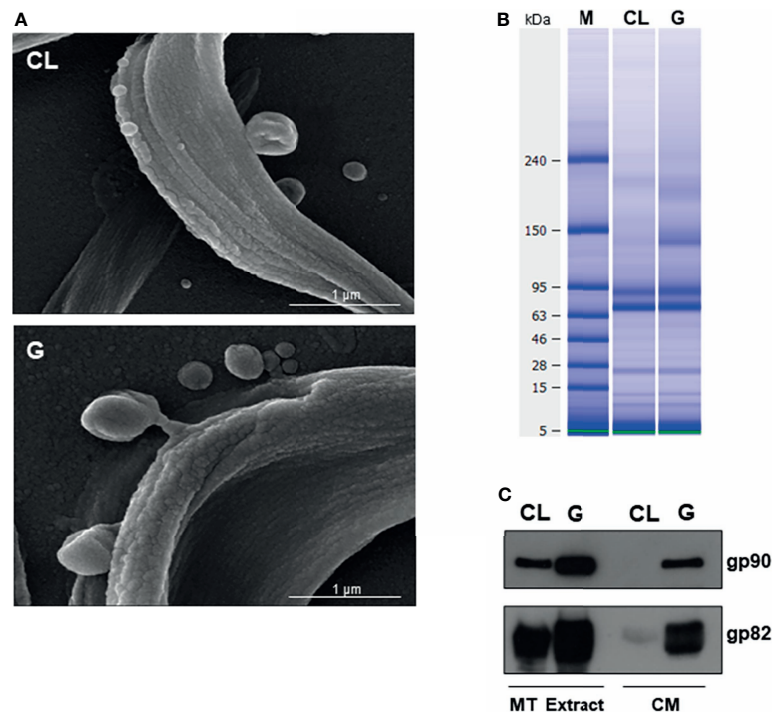


FIGURE 3 | Comparable shedding of vesicles by metacyclic trypomastigotes (MTs) of *Trypanosoma cruzi* strains CL and G and differential release of gp82 and gp90 into medium. **(A)** Parasites were washed in phosphate-buffered saline (PBS) and processed for analysis by scanning electron microscopy. Scale bar = 1 μm. **(B)** Protein profile of conditioned medium (CM) from CL and G strains, revealed by Agilent 2100 Bioanalyzer system. **(C)** Profile of gp82 and gp90 detected in Western blotting of CL and G strain CM and the respective detergent extracts.

scanning electron microscopy (Figures 4A and S3A). Such a difference in morphology between strains was evident at the population level, as shown by immunofluorescence, using anti-gp82 mAb 3F6 (Figure 4B). By calculating the area of parasites shown in Figure 4B, using ImageJ v. 1.53f51, CL strain MTs were found to be significantly larger than G strain MTs (Figure S3B). We also noted, particularly in assays of MT interaction with HeLa cells, a distinct pattern of gp82 expression in the two strains, with CL strain exhibiting a patchy gp82 distribution (Figure 1, framed area on the upper right side, and Figure 4C). To examine the relative distribution of gp82 and gp90 on MT surface, the parasites were processed for immunofluorescence analysis, using anti-gp82 mAb 3F6 and polyclonal anti-gp90 antibody generated in rabbit. Confocal images revealed a segregated distribution of gp82 and gp90 in CL strain, whereas in G strain, the two molecules appeared to be closely localized (Figure 5A). This was more evident in the magnified image of an individual parasite (Figure 5B). It is possible that the differential distribution of gp82 and gp90 on the surface of CL and G strains influences the differential shedding. Segregated localization of gp82 and gp90 in CL strain could render these molecules less amenable to shedding, whereas their release by G strain would be facilitated by the localization in a microdomain more susceptible to factors involved in shedding mechanism. Gp82 and gp90 appeared to be expressed at higher levels in G strain than in CL strain, as judged by the higher fluorescence intensity

(Figure 5A), compatible with the Western blotting profile of the MT extract (Figure 3C).

CL Strain Invasion Is Modulated by G Strain Conditioned Medium in a Manner Correlated With Gp82 and Gp90 Levels

In invasion assays, when HeLa cells were incubated with MTs for 1 h, about threefold higher number of CL strain is internalized, as compared with G strain (Figure 6A). The lower invasive capacity of G strain is correlated with the content of gp82 and gp90 at higher levels in CM (Figure 3C). It was previously shown that G strain CM can inhibit CL strain invasion (Clemente et al., 2016), but to what extent that effect was due to gp82 and/or gp90 remains to be determined. Experiments were performed to address that question. First, to confirm the inhibitory activity of G strain CM, HeLa cells were incubated for 1 h with CL strain MTs in the presence of G or CL strain CM, at 1:2 dilution, and the number of internalized parasites was quantified. CL strain internalization was significantly reduced by G strain CM, but not by CL strain CM (Figure 6B). Next, magnetic beads crosslinked to anti-gp82 mAb 3F6 or to anti-gp90 mAb 1G7 were prepared and incubated for 2 h at room temperature with G strain CM. As controls, beads crosslinked to mAb 2C2, directed to amastigote-specific surface antigen (Andrews et al., 1987), and empty beads were used. Gp82 and gp90 were considerably depleted upon incubation of CM with beads coupled to mAb 3F6 and mAb 1G7,

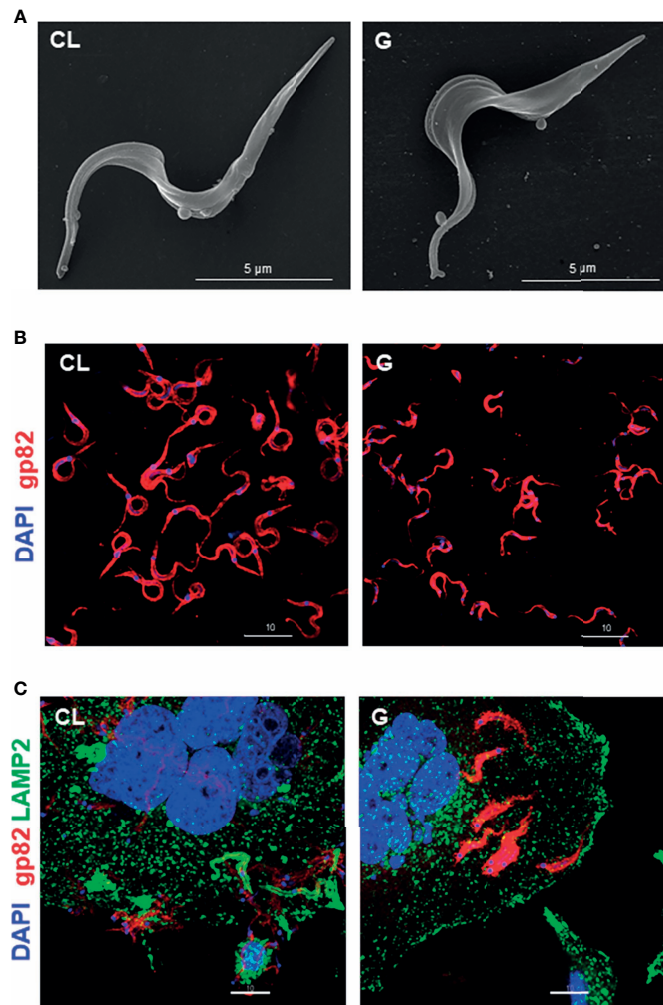


FIGURE 4 | Distinct morphology and pattern of gp82 expression in CL and G strain metacyclic trypomastigotes (MTs) upon interaction or not with HeLa cells. **(A)** Purified MTs were processed for analysis by scanning electron microscopy. Scale bar = 5 μm. **(B)** MTs were processed for immunofluorescence and confocal microscopy visualization of gp82 (red) and nucleus (blue). Scale bar = 10 μm. **(C)** MTs were incubated with HeLa cells for 30 min and processed for immunofluorescence and confocal microscopy visualization of lysosomes (green), nucleus (blue), and gp82 (red). Scale bar = 10 μm. Note a patchy distribution of gp82 on CL strain surface.

respectively, but not with empty beads or beads coupled to mAb 2C2 (**Figure 6C**). Invasion assays were then performed by incubating CL strain MTs with HeLa cells in the presence of CM prepared as above. Parasite invasion was significantly reduced in the presence of control CMs, an effect that was reversed by gp90 depletion, whereas gp82-depleted CM exhibited a higher inhibitory activity than the control CMs (**Figure 6D**). This finding indicates that gp90 is mainly involved in decreasing MT infectivity, further reinforcing its downregulatory role on host cell invasion. CM derived from G strain upon interaction with target cells was also tested. Parasites were placed onto plates, either uncoated or with adherent HeLa cells. After 30-min incubation, the medium containing parasites was collected and centrifuged. The supernatant was filtered and used for Western blotting and cell invasion assays. Western blotting analysis of CM from MTs that contacted HeLa cells

showed a modest increase in the intensity of gp82 of gp90 bands (**Figure S4A**), on the order of 10%, as quantified using GelAnalyzer 19.1 software. Cell invasion assays showed that interaction of G strain with HeLa cells did not generate CM with higher inhibitory activity towards CL strain internalization (**Figure S4B**).

Shedding of Gp82 and Gp90 Increases Upon Metacyclic Trypomastigote Treatment With Cholesterol-Depleting Drug and Decreases by Treatment With Phospholipase C Inhibitor

We examined the effect of cholesterol-depleting drug MβCD on gp82 and gp90 release by MTs. Trypanosomatids synthesize ergosterol-related sterols (Roberts et al., 2003), and treatment

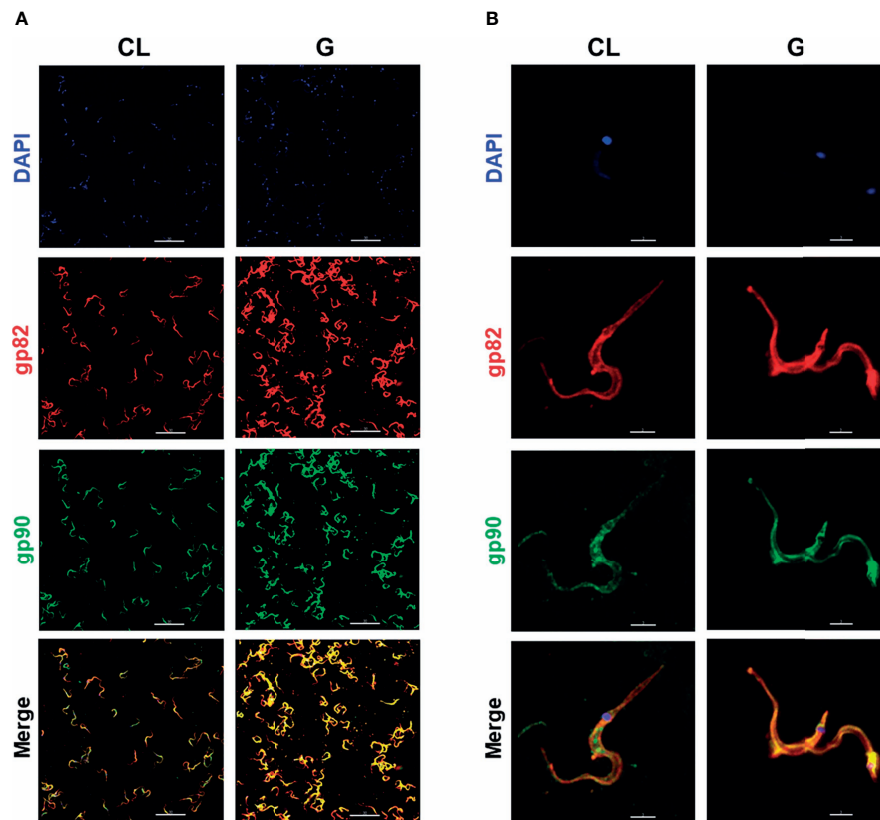


FIGURE 5 | The relative distribution of gp82 and gp90 on metacyclic trypomastigote (MT) surface of CL and G strains. **(A)** MTs were processed for immunofluorescence and confocal microscopy visualization of gp82 (red), gp90 (green), and nucleus (blue). Scale bar = 30 μ m. **(B)** Individual parasite is depicted to show the segregated distribution of gp82 and gp90 in CL strain and closer localization in G strain. Scale bar = 3 μ m.

of MTs with M β CD has been shown to efficiently deplete ergosterol (Fernandes et al., 2007). Both gp82 and gp90 are anchored to MT plasma membrane by glycosyl phosphatidylinositol (GPI) moiety (Yoshida, 2006). GPI-anchored membrane proteins are among those that are targeted to lipid rafts, which are microdomains enriched in cholesterol and sphingolipids. G strain MTs were treated with 10 mM of M β CD for 45 min in serum-free RPMI medium. After removal of the drug, the parasites were incubated for 30 min in RPMI medium containing 1% FBS (R1) or in PBS⁺⁺, which is basically PBS containing Ca²⁺ and Mg²⁺, along with the untreated controls, and the untreated CM generated under these conditions was analyzed by Western blotting. In PBS⁺⁺, gp82 and gp90 were released at low levels by untreated MTs, and at higher levels in M β CD-treated parasites (**Figure 7A**). The effect of these CMs on CL strain invasion was tested. CMs generated in PBS⁺⁺ by untreated and M β CD-treated parasites exhibited significant inhibitory activity (**Figure 7B**). We also examined the effect of M β CD on CL strain. An increase in gp82 and gp90 release was detected in CM generated in R0 by M β CD-treated parasites (**Figure 7C**). HeLa cells were then incubated for 1 h with untreated or M β CD-treated CL strain MTs in R0, and the internalized parasites were quantified. As shown in

Figure 7D, M β CD-treated parasites exhibited significantly reduced capacity to invade cells. As GPI-solubilizing PLC was found in all G strain developmental forms (de Almeida and Heise, 1993), we tested the involvement of PLC on gp82 and gp90 shedding, and G strain MTs were treated for 30 min with phosphoinositide-specific PLC inhibitor U73122 at 1 or 5 μ M. After removal of the drug, the parasites were incubated for 30 min to generate CM. Treatment of MTs with PLC inhibitor decreased the gp82 and gp90 shedding, as confirmed by measuring the intensity of the bands using GelAnalyzer 19.2 software (**Figure 7E**).

DISCUSSION

Lysosome spreading and exocytosis are critical for the process of *T. cruzi* invasion of host cells (Tardieux et al., 1992; Fernandes et al., 2011; Martins et al., 2011; Cortez et al., 2016). Studies with *T. cruzi* CL strain have shown that efficient entry of MTs into target cells is mediated by gp82, which binds to its receptor LAMP2 and triggers lysosome mobilization to the cell periphery (Cortez et al., 2016; Rodrigues et al., 2019; Onofre et al., 2021). Here, we have found that lysosome spreading is also induced by

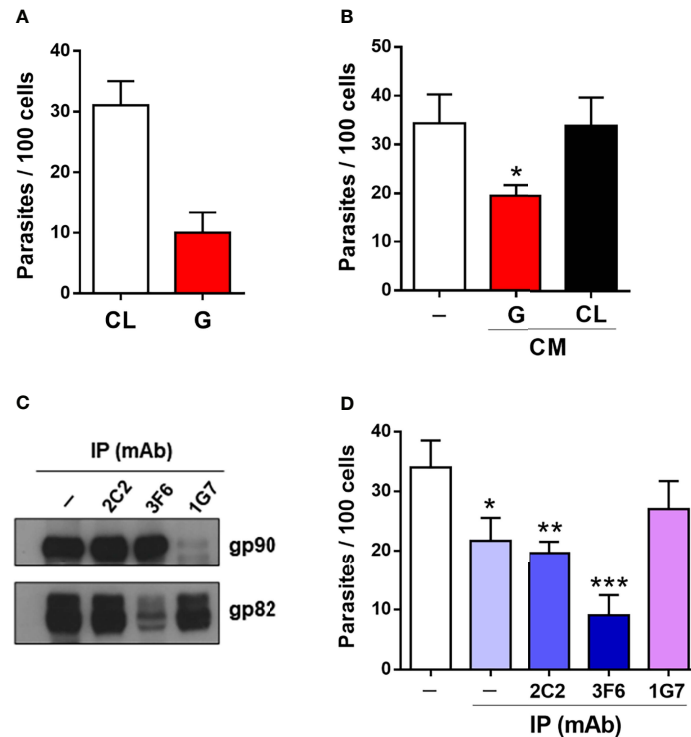
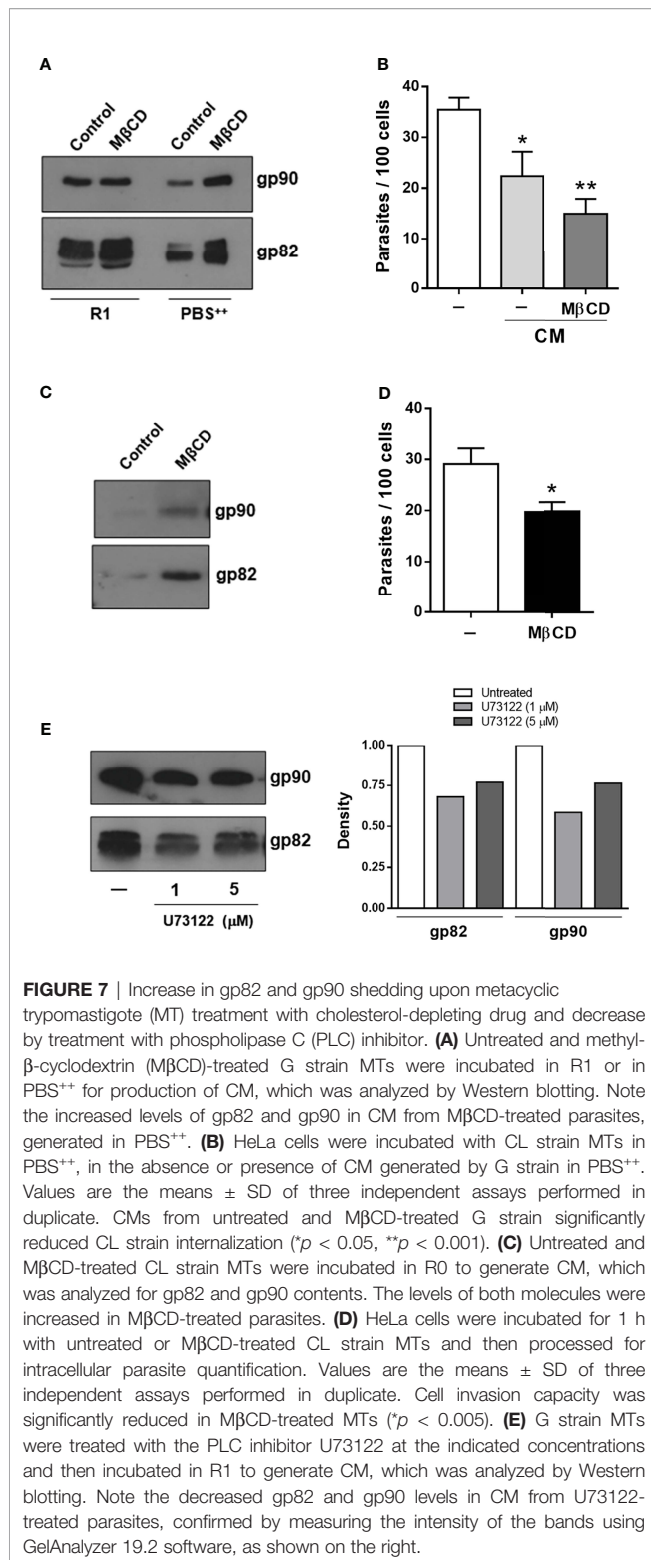


FIGURE 6 | Effect of gp82 and gp90 contained in G strain CM on host cell entry of CL strain metacyclic trypomastigotes (MTs). **(A)** HeLa cells were incubated for 1 h with CL or G strain MTs and processed for Giemsa staining and intracellular parasite quantification. Values are the means \pm SD of five independent assays performed in duplicate. **(B)** HeLa cells were incubated for 1 h with CL strain MTs in the absence or presence of CM from G or CL strain and processed for internalized parasite quantification. Values are the means \pm SD of five independent assays performed in duplicate. MT invasion was significantly inhibited by G strain CM (* $p < 0.001$), but not by CL strain CM. **(C)** Western blotting profile of gp82 and gp90 in G strain CM upon 2-h incubation with magnetic beads crosslinked to the indicated mAbs. Note the depletion of gp82 and gp90. **(D)** HeLa cells were incubated for 1 h with CL strain MTs in the absence or presence of CM shown in **(C)**, and the internalized parasites were quantified. Values are the means \pm SD of three independent assays performed in duplicate. Significant inhibition by different CMs was detected, except for the CM immunoprecipitated by mAb 1G7 (* $p < 0.05$, ** $p < 0.01$, *** $p < 0.005$).

poorly invasive G strain MTs upon interaction with the host cell, possibly as a result of recognition of shed gp82 by its receptor. Shedding of gp90, the down modulator of MT internalization (Málaga and Yoshida, 2001), was also detected. By contrast, release of gp82 and gp90 by CL strain MTs was barely detectable. Host cell invasion experiments showed the inhibitory effect of G strain CM on CL strain internalization. We examined to what extent this effect was due to gp82 and/or gp90, by depleting CM from these molecules. The inhibitory activity of CM was in the most part reversed by depletion of gp90. On the other hand, depletion of gp82 resulted in an increased inhibitory capacity of CM. From this result, we envisage the possibility that gp82 hampers gp90 interaction with the host cell, so that its absence potentiates the gp90 binding, increasing the downregulatory effect on MT invasion. The inhibitory effect of gp82-depleted CM on CL strain internalization is similar to that observed when HeLa cells were incubated with MTs in the presence of native or recombinant gp90 (Rodrigues et al., 2017).

In our search for factors that influence the release of surface molecules by MTs, the involvement of sterol was investigated. With the use of the antibiotic filipin as a probe, cholesterol was

found to be homogeneously distributed throughout *T. cruzi* epimastigote plasma membrane (Souto-Padrón and de Souza, 1983) and presumably is distributed in MTs in the same manner. It has been reported that cholesterol depletion by M β CD enhances shedding of cytokine receptor CD30 in lymphoid-derived cell lines (von Tresckow et al., 2004). By examining the effect of M β CD on gp82 and gp90 release by G strain MTs in PBS⁺⁺, we detected an increased shedding of both molecules. As compared with CM generated in PBS⁺⁺ by untreated parasites, the CM from M β CD-treated MTs contained higher gp82 and gp90 levels and, accordingly, exerted higher inhibitory activity on CL strain invasion. Treatment of CL strain MTs with M β CD resulted in increased shedding of gp82 and gp90, although not to levels comparable with G strain, and led to a decrease in the ability to invade HeLa cells. These results suggested that gp82 and gp90 are partitioned, at least partially, into lipid rafts. In G strain, gp82 and gp90 were closely localized on MT surface and were released in medium containing serum, as well as in serum-free medium. Gp82 and gp90 were more segregated in CL strain. Trans-sialidase and mucins, which are also GPI-anchored glycoproteins, were reported to be separately distributed on



TCT surface and contained in different and highly stable membrane microdomains, with sialylated mucins included in lipid-raft domains (Lantos et al., 2016). It is possible that gp82 and gp90 are differentially partitioned in membrane

microdomains of CL and G strains, and the preferential partitioning into rafts could influence their release.

Based on the observation that treatment of G strain MTs with phosphoinositide-specific PLC inhibitor resulted in decreased shedding, of gp82 and gp90, the involvement of PLC is inferred. GPI-solubilizing PLC, detected in G strain, was mostly in a soluble form in MTs and membrane-associated in TCT (de Almeida and Heise, 1993). Soluble PLC would contribute to gp82 and gp90 release by G strain. On the other hand, one possibility for the lack of shedding of these glycoproteins by CL strain is that PLC is mostly membrane associated and segregated from gp82 and gp90 molecules, thus making it unable to exert its enzyme activity. Treatment of CL and G strain MTs with PLC inhibitor was previously found to decrease host cell invasion, possibly because the intracellular Ca²⁺ mobilization required for the internalization process was blocked (Maeda et al., 2012).

Taken together, the present study has contributed to further understand the process of shedding of GPI-anchored surface molecules by *T. cruzi* and reinforced the role played by gp82 and gp90 in regulating MT invasion of host cells.

DATA AVAILABILITY STATEMENT

The raw data supporting the conclusions of this article will be made available by the authors, without undue reservation.

AUTHOR CONTRIBUTIONS

LL, TO, and NY designed the experiments. LL, TO, and JR performed the experiments. NY wrote the manuscript. All authors contributed to the article and approved the submitted version.

FUNDING

This work was supported by São Paulo Research Foundation (FAPESP) Grant 2016/15000-4 and Conselho Nacional de Desenvolvimento Científico e Tecnológico (CNPq) Grant 303825/2015-4 and in part by the Coordenação de Aperfeiçoamento de Pessoal de Nível Superior—Brazil (CAPES)—Finance Code 001.

SUPPLEMENTARY MATERIAL

The Supplementary Material for this article can be found online at: <https://www.frontiersin.org/articles/10.3389/fcimb.2021.769722/full#supplementary-material>

Supplementary Figure 1 | Higher susceptibility to MT invasion of host cells of larger size. HeLa cells were incubated for 30 min with CL strain MT and processed for immunofluorescence and confocal microscopy visualization of lysosomes (green), nucleus (blue), and gp82 (red). Scale bar = 10 μm. Note the internalized CL strain MT with lysosome membrane marker (white arrow).

Supplementary Figure 2 | Protein analysis of CM from CL and G strain MT. Parasites were incubated for 30 min in medium containing 1% FBS. After

centrifugation and filtration, the supernatant was analyzed using High Sensitivity Protein 250 kit and the Agilent 2100 Bioanalyzer system.

Supplementary Figure 3 | Difference in size between CL and G strain MT. (A)

Purified MTs were processed for analysis by scanning electron microscopy. Scale-bar = 10 μ m. (B) The size of nine MTs shown in Figure 4A was evaluated by calculating the area of each parasite, using ImageJ v. 1.53f51, and arbitrary unities were attributed to these areas. The difference between CL and G strain MT was significant (* $P < 0.05$).

REFERENCES

- Andrews, N. W., Hong, K. S., Robbins, E. S., and Nussenzweig, V. (1987). Stage-Specific Surface Antigens Expressed During the Morphogenesis of Vertebrate Forms of *Trypanosoma Cruzi*. *Exp. Parasitol.* 64, 474–484. doi: 10.1016/0014-4894(87)90062-2
- Bayer-Santos, E., Aguilar-Bonavides, C., Rodrigues, S. P., Cordero, E. M., Marques, A. F., Varela-Ramirez, A., et al. (2013). Proteomic Analysis of *Trypanosoma Cruzi* Secretome: Characterization of Two Populations of Extracellular Vesicles and Soluble Proteins. *J. Proteome Res.* 12 (2), 883–897. doi: 10.1021/pr300947g
- Borges, F. T., Reis, L. A., and Schor, N. (2013). Extracellular Vesicles: Structure, Function, and Potential Clinical Uses in Renal Diseases. *Braz. J. Med. Biol. Res.* 46, 824–830. doi: 10.1590/1414-431X20132964
- Clemente, T. M., Cortez, C., Novaes, A. D. S., and Yoshida, N. (2016). Surface Molecules Released by *Trypanosoma Cruzi* Metacyclic Forms Downregulate Host Cell Invasion. *PLoS Negl. Trop. Dis.* 10 (8), e0004883. doi: 10.1371/journal.pntd.0004883
- Cortez, C., Real, F., and Yoshida, N. (2016). Lysosome Biogenesis/Scattering Increases Host Cell Susceptibility to Invasion by *Trypanosoma Cruzi* Metacyclic Forms and Resistance to Tissue Culture Trypomastigotes. *Cell. Microbiol.* 18, 748–760. doi: 10.1111/cmi.12548
- Cronemberger-Andrade, A., Xander, P., Soares, R. P., Pessoa, N. L., Campos, M. A., Ellis, C. C., et al. (2020). *Trypanosoma Cruzi*-Infected Human Macrophages Shed Proinflammatory Extracellular Vesicles That Enhance Host-Cell Invasion via Toll-Like Receptor 2. *Front. Cell. Infect. Microbiol.* 10. doi: 10.3389/fcimb.2020.00099
- de Almeida, M. L., and Heise, N. (1993). Proteins Anchored via Glycosylphosphatidylinositol and Solubilizing Phospholipases in *Trypanosoma Cruzi*. *Biol. Res.* 26, 285–312.
- Fernandes, M. C., Cortez, M., Flannery, A. R., Tam, C., Mortara, R. A., and Andrews, N. W. (2011). *Trypanosoma Cruzi* Subverts the Sphingomyelinase-Mediated Plasma Membrane Repair Pathway for Cell Invasion. *J. Exp. Med.* 208, 909–921. doi: 10.1084/jem.20102518
- Fernandes, M. C., Cortez, M., Geraldo Yoneyama, K. A., Straus, A. H., Yoshida, N., and Mortara, R. A. (2007). Novel Strategy in *Trypanosoma Cruzi* Cell Invasion: Implication of Cholesterol and Host Cell Microdomains. *Int. J. Parasitol.* 37, 1431–1441. doi: 10.1016/j.ijpara.2007.04.025
- Garcia-Silva, M. R., Cura Das Neves, R. F., Cabrera-Cabrera, F., Sanguinetti, J., Medeiros, L. C., Robello, C., et al. (2014). Extracellular Vesicles Shed by *Trypanosoma Cruzi* are Linked to Small RNA Pathways, Life Cycle Regulation, and Susceptibility to Infection of Mammalian Cells. *Parasitol. Res.* 113, 285–304. doi: 10.1007/s00436-013-3655-1
- Gonçalves, M. F., Umezawa, E. S., Katzin, A. M., de Souza, W., Alves, M. J., Zingales, B., et al. (1991). *Trypanosoma Cruzi*: Shedding of Surface Antigens as Membrane Vesicles. *Exp. Parasitol.* 72, 43–53. doi: 10.1016/0014-4894(91)90119-h
- Lantos, A. B., Carlevaro, G., Araoz, B., Ruiz Diaz, P., Camara, M., de los, M., et al. (2016). Sialic Acid Glycobiology Unveils *Trypanosoma Cruzi* Trypomastigote Membrane Physiology. *PLoS Pathog.* 12 (4), e1005559. doi: 10.1371/journal.ppat.1005559
- Maeda, F. Y., Cortez, C., Alves, R. M., and Yoshida, N. (2012). Mammalian Cell Invasion by Closely Related *Trypanosoma* Species *T. dionisi* and *T. Cruzi*. *Acta Tropica* 121, 141–147. doi: 10.1016/j.actatropica.2011.10.017
- Málaga, S., and Yoshida, N. (2001). Targeted Reduction in Expression of *Trypanosoma Cruzi* Surface Glycoprotein Gp90 Increases Parasite Infectivity. *Infect. Immun.* 69, 353–359. doi: 10.1128/IAI.69.1.353-359.2001
- Martins, R. M., Alves, R. M., Macedo, S., and Yoshida, N. (2011). Starvation and Rapamycin Differentially Regulate Host Cell Lysosome Exocytosis and Invasion by *Trypanosoma Cruzi* Metacyclic Forms. *Cell. Microbiol.* 13 (7), 943–954. doi: 10.1111/j.1462-5822.2011.01590.x
- Mathivanan, S., Ji, H., and Simpson, R. J. (2010). Exosomes: Extracellular Organelles Important in Intercellular Communication. *J. Proteomics* 73, 1907–1920. doi: 10.1016/j.jprot.2010.06.006
- Nogueira, P. M., Ribeiro, K., Silveira, A. C. O., Campos, J. H., Martins-Filho, O. A., Bela, S. R., et al. (2015). Vesicles From Different *Trypanosoma Cruzi* Strains Trigger Differential Innate and Chronic Immune Responses. *J. Extracell. Vesicles* 4:28734. doi: 10.3402/jev.v4.28734
- Onofre, T. S., Rodrigues, J. P. F., Shio, M. T., Macedo, S., Juliano, M. A., and Yoshida, N. (2021). Interaction of *Trypanosoma Cruzi* Gp82 With Host Cell LAMP2 Induces Protein Kinase C Activation and Promotes Invasion. *Front. Cell. Infect. Microbiol.* 11. doi: 10.3389/fcimb.2021.627888
- Paranaíba, L. F., Guarneri, A. A., Torrecilhas, A. C., Melo, M. N., and Soares, R. P. (2019). Extracellular Vesicles Isolated From *Trypanosoma Cruzi* Affect Early Parasite Migration in the Gut of *Rhodnius Prolixus* But Not in *Triatoma Infestans*. *Mem. Inst. Oswaldo Cruz* 114, e190217. doi: 10.1590/0074-02760190217
- Ribeiro, K. S., Vasconcellos, C. L., Soares, R. P., Mendes, M. T., Ellis, C. C., Aguilera-Flores, M., et al. (2018). Proteomic Analysis Reveals Different Composition of Extracellular Vesicles Released by Two *Trypanosoma Cruzi* Strains Associated With Their Distinct Interaction With Host Cells. *J. Extracell. Vesicles* 7 (1), 1463779. doi: 10.1080/20013078.2018.1463779
- Roberts, C. W., McLeod, R., Rice, D. W., Ginger, M., Chance, M. L., and Goad, L. J. (2003). Fatty Acid and Sterol Metabolism: Potential Antimicrobial Targets in Apicomplexan and Trypanosomatid Parasitic Protozoa. *Mol. Biochem. Parasitol.* 126 (2), 129–142. doi: 10.1016/S0166-6851(02)00280-3
- Rodrigues, J. P. F., Souza Onofre, T., Barbosa, B. C., Ferreira, É.R., Bonfim-Melo, A., and Yoshida, N. (2019). Host Cell Protein LAMP-2 is the Receptor for *Trypanosoma Cruzi* Surface Molecule Gp82 That Mediates Invasion. *Cell. Microbiol.* 21 (5), e13003. doi: 10.1111/cmi.13003
- Rodrigues, J. P. F., Takahashi Sant'ana, G. H., Juliano, M. A., and Yoshida, N. (2017). Inhibition of Host Cell Lysosome Spreading by *Trypanosoma Cruzi* Metacyclic Stage-Specific Surface Molecule Gp90 Downregulates Parasite Invasion. *Infect. Immun.* 85 (9), e00302–17. doi: 10.1128/IAI.00302-17
- Souto-Padrón, T., and de Souza, W. (1983). Freeze-Fracture Localization of Filipin-Cholesterol Complexes in the Plasma Membrane of *Trypanosoma Cruzi*. *J. Parasitol.* 69, 129–137. doi: 10.2307/3281287
- Tardieux, I., Webster, P., Ravesloot, J., Boron, W., Lunn, J. A., Heuser, J. E., et al. (1992). Lysosome Recruitment and Fusion are Early Events Required for Trypanosome Invasion of Mammalian Cells. *Cell* 71, 1117–1130. doi: 10.1016/s0092-8674(05)80061-3
- Teixeira, M. M., and Yoshida, N. (1986). Stage-Specific Surface Antigens of Metacyclic Trypomastigotes of *Trypanosoma Cruzi* Identified by Monoclonal Antibodies. *Mol. Biochem. Parasitol.* 18, 271–282. doi: 10.1016/0166-685(86)90085-x
- Torrecilhas, A. C., Soares, R. P., Schenkman, S., Fernández-Prada, C., and Olivier, M. (2020). Extracellular Vesicles in Trypanosomatids: Host Cell Communication. *Front. Cell. Infect. Microbiol.* 10:602502. doi: 10.3389/fcimb.2020.602502
- Torrecilhas, A. C., Tonelli, R. R., Pavanelli, W. R., da Silva, J. S., Schumacher, R. I., de Souza, W., et al. (2009). *Trypanosoma Cruzi*: Parasite Shed Vesicles Increase Heart Parasitism and Generate an Intense Inflammatory Response. *Microbes Infect.* 11, 29–39. doi: 10.1016/j.micinf.2008.10.003
- von Tresckow, B., Kallen, S., Strandmann, E. P., Borchmann, P., Lange, H., Engert, A., et al. (2004). Depletion of Cellular Cholesterol and Lipid Rafts Increases Shedding of CD30. *J. Immunol.* 172, 4324–4331. doi: 10.4049/JIMMUNOL.172.7.4324
- Wyllie, M. P., and Ramirez, M. I. (2017). Microvesicles Released During the Interaction Between *Trypanosoma Cruzi* TcI and TcII Strains and Host Blood

- Cells Inhibit Complement System and Increase the Infectivity of Metacyclic Forms of Host Cells in a Strain-Independent Process. *Pathog. Dis.* 75 (7), ftx077. doi: 10.1093/femspd/ftx077
- Yáñez-Mó, M., Siljander, P. R. M., Andreu, Z., Zavec, A. B., Borràs, F. E., Buzas, E. I., et al. (2015). Biological Properties of Extracellular Vesicles and Their Physiological Functions. *J. Extracell Vesicles* 4, 1–60. doi: 10.3402/jev.v4.27066
- Yoshida, N. (2006). Molecular Basis of Mammalian Cell Invasion by *Trypanosoma Cruzi*. *An Acad. Bras. Cienc.* 78, 87–111. doi: 10.1590/S0001-37652006000100010
- Zaborowski, M. P., Balaj, L., Breakefield, X. O., and Lai, C. P. (2015). Extracellular Vesicles: Composition, Biological Relevance, and Methods of Study. *Bioscience* 65, 783–797. doi: 10.1093/biosci/biv084
- Zingales, B., Andrade, S. G., Briones, M. R. S., Campbell, D. A., Chiari, E., Fernandes, O., et al. (2009). A New Consensus for *Trypanosoma Cruzi* Intraspecific Nomenclature: Second Revision Meeting Recommends TcI to TcVI. *Mem. Inst. Oswaldo Cruz* 104, 1051–1054. doi: 10.1590/50074-0276009000700021
- Conflict of Interest:** The authors declare that the research was conducted in the absence of any commercial or financial relationships that could be construed as a potential conflict of interest.
- Publisher's Note:** All claims expressed in this article are solely those of the authors and do not necessarily represent those of their affiliated organizations, or those of the publisher, the editors and the reviewers. Any product that may be evaluated in this article, or claim that may be made by its manufacturer, is not guaranteed or endorsed by the publisher.
- Copyright © 2021 Loch, Onofre, Rodrigues and Yoshida. This is an open-access article distributed under the terms of the Creative Commons Attribution License (CC BY). The use, distribution or reproduction in other forums is permitted, provided the original author(s) and the copyright owner(s) are credited and that the original publication in this journal is cited, in accordance with accepted academic practice. No use, distribution or reproduction is permitted which does not comply with these terms.



“Immunoinformatic Identification of T-Cell and B-Cell Epitopes From *Giardia lamblia* Immunogenic Proteins as Candidates to Develop Peptide-Based Vaccines Against Giardiasis”

OPEN ACCESS

Edited by:

Maria E. Francia,
Institut Pasteur de Montevideo,
Uruguay

Reviewed by:

Yi Yang,
Hunan Agricultural University, China
Jane Homan,
ioGenetics LLC, United States

*Correspondence:

Carlos Velazquez
velaz2@unison.mx
orcid.org/0000-0002-3728-7848

Specialty section:

This article was submitted to
Parasite and Host,
a section of the journal
Frontiers in Cellular and
Infection Microbiology

Received: 02 September 2021

Accepted: 08 October 2021

Published: 27 October 2021

Citation:

Garzon T, Ortega-Tirado D,
Lopez-Romero G, Alday E,
Robles-Zepeda RE,
Garibay-Escobar A and Velazquez C
(2021) “Immunoinformatic
Identification of T-Cell and B-Cell
Epitopes From *Giardia lamblia*
Immunogenic Proteins as Candidates
to Develop Peptide-Based
Vaccines Against Giardiasis”.
Front. Cell. Infect. Microbiol. 11:769446.
doi: 10.3389/fcimb.2021.769446

Thania Garzon, David Ortega-Tirado, Gloria Lopez-Romero, Efrain Alday,
Ramón Enrique Robles-Zepeda, Adriana Garibay-Escobar and Carlos Velazquez*

Department of Chemistry-Biology, University of Sonora, Hermosillo, Mexico

Giardiasis is one of the most common gastrointestinal infections worldwide, mainly in developing countries. The etiological agent is the *Giardia lamblia* parasite. Giardiasis mainly affects children and immunocompromised people, causing symptoms such as diarrhea, dehydration, abdominal cramps, nausea, and malnutrition. In order to develop an effective vaccine against giardiasis, it is necessary to understand the host-*Giardia* interactions, the immunological mechanisms involved in protection against infection, and to characterize the parasite antigens that activate the host immune system. In this study, we identify and characterize potential T-cell and B-cell epitopes of *Giardia* immunogenic proteins by immunoinformatic approaches, and we discuss the potential role of those epitopes to stimulate the host's immune system. We selected the main immunogenic and protective proteins of *Giardia* experimentally investigated. We predicted T-cell and B-cell epitopes using immunoinformatic tools (NetMHCII and BCPREDS). Variable surface proteins (VSPs), structural (giardins), metabolic, and cyst wall proteins were identified as the more relevant immunogens of *G. lamblia*. We described the protein sequences with the highest affinity to bind MHC class II molecules from mouse (I-A^k and I-A^d) and human (DRB1*03:01 and DRB1*13:01) alleles, as well as we selected promiscuous epitopes, which bind to the most common range of MHC class II molecules in human population. In addition, we identified the presence of conserved epitopes within the main protein families (giardins, VSP, CWP) of *Giardia*. To our knowledge, this is the first *in silico* study that analyze immunogenic proteins of *G. lamblia* by combining bioinformatics strategies to identify potential T-cell and B-cell epitopes, which can be potential candidates in the development of peptide-based vaccines. The bioinformatics analysis demonstrated in this

study provides a deeper understanding of the *Giardia* immunogens that bind to critical molecules of the host immune system, such as MHC class II and antibodies, as well as strategies to rational design of peptide-based vaccine against giardiasis.

Keywords: immunogenic, epitope, protection, vaccine, immunoinformatic

INTRODUCTION

Giardiasis is a highly prevalent foodborne gastrointestinal parasitic infection in developing countries, mainly affecting children and immunocompromised individuals. The clinical manifestations of giardiasis vary from asymptomatic to acute or chronic episodes characterized by severe diarrhea, accompanied with abdominal pain and intestinal lesions that lead to nutrient malabsorption syndrome and weight loss (Eckmann, 2003; Cedillo-Rivera et al., 2009; Ankarklev et al., 2010; Lujan and Svard, 2011; Lopez-Romero et al., 2015). *Giardia lamblia* is the etiological agent of giardiasis, a binucleated and flagellated protozoan that can infect humans and other mammals. *G. lamblia* has a simple life cycle, consisting of two different developmental stages defined by specific structural and biochemical features, wherein the cyst is the infective form, whereas the trophozoite is the proliferative form that colonizes the upper tract of small intestine (Lujan, 2006; Cedillo-Rivera et al., 2009; Ankarklev et al., 2010; Lopez-Romero et al., 2015).

The establishment of endoparasitic infections rely on the intricate molecular interaction between each specific stage of the life cycle of parasites and the immune responses of their hosts (Tedla et al., 2019; Smith et al., 2021). Generally, the integration of innate and adaptive immune responses defines the fate of parasitic infections, therefore immunocompetence, immunopolymorphism and immunological memory of the host are important for the resolution of parasitic infections (Lima and Lodoen, 2019; Mukherjee et al., 2019).

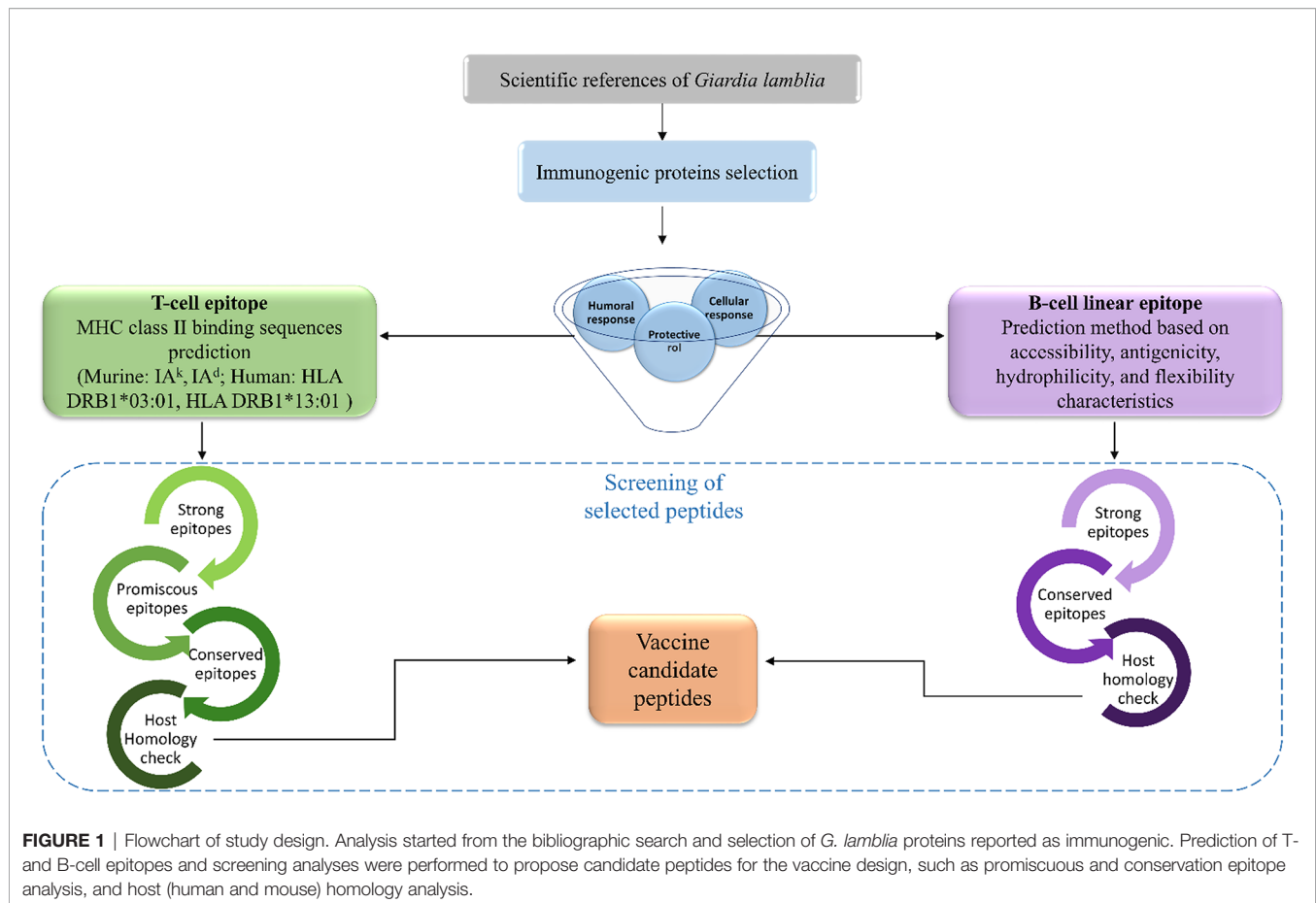
Several studies have reported the central role of the immune system in resolution of giardiasis by using different experimental approaches (Li et al., 2004; Ankarklev et al., 2010; Kamda et al., 2012; Dreesen et al., 2014; Grit et al., 2014; Lopez-Romero et al., 2015; Singer, 2016). The mechanism of pathogen clearance mainly depend on the processes mediated by adaptive effector cells, both B and T lymphocytes. Murine models of giardiasis have demonstrated that the establishment of humoral immunity could be implicated in resolution of infection (Singer and Nash, 2000; Eckmann, 2003; Velazquez et al., 2005). In addition, the role of mucosal and circulatory CD4⁺ T cells has been described as essential to collaborate with the activation of B cells and control murine giardiasis (Singer and Nash, 2000; Lujan, 2011; Singer, 2016). Interestingly, whilst CD4⁺ T cells are important effectors in giardiasis resolution, CD8⁺ T lymphocyte responses have been associated to the pathophysiological damage observed during *G. lamblia* infection, such as enterocyte ultrastructural alterations, representing a paradoxical challenge for immunotherapy against giardiasis (Scott et al., 2004; Lopez-Romero et al., 2015).

The development of effective vaccines against endoparasites is limited, partially due to the complex life-cycle of parasites and the mechanisms that have acquired to successfully overcome some immune responses, such as antigenic variation, and partially to the limitations of classical vaccine design strategies (Skwarczynski and Toth, 2016; Lima and Lodoen, 2019; Moormann et al., 2019; Autheman et al., 2021; Robleda-Castillo et al., 2021). At present, there are no approved vaccines for human use against giardiasis. However, the presence of immunogenic proteins in both, cyst and trophozoite forms of *G. lamblia* have been described by different approaches. Among the proteins of *G. lamblia* able to elicit immune responses are the variable surface proteins (VSP), heat shock proteins, lectins, cyst wall proteins (CWP) and cytoskeleton associated proteins, such as giardins and tubulins (Davids et al., 2006; Lopez-Romero et al., 2017; Quintero et al., 2017).

Nowadays, synthetic peptide-based vaccines are designed considering immunodominance, epitope structure, and adjuvants to stimulate and confer protection without the complete protein or pathogen administration (Skwarczynski and Toth, 2016; Malonis et al., 2020). Immunoinformatic analysis have been used to identify immunogenic antigens from medically important protozoa, such as *Leishmania*, *Trypanosoma*, and *Plasmodium*, which have been implemented in multi-peptide vaccines with high efficacy for the control of infection. For the malaria infection, the MosquirixTM vaccine is currently in Clinical Trial Phase III (Teh-Poot et al., 2015; Cecilio et al., 2017; Laurens, 2020; Vakili et al., 2020).

Immunoinformatic analysis allows the identification of potential B-cell and T-cell epitopes pursued for the design of new peptide-based vaccine candidates, by combining proteomics and bioinformatics strategies. Potential B-cell epitopes are considered according to their surface accessibility, flexibility and physicochemical characteristics to interact with complementarity-determining regions (CDRs) in the antibody molecule, whereas T-cell lineal peptide epitopes are predicted based on their high-affinity binding to the major histocompatibility complex (MHC) class I and II molecules (Teh-Poot et al., 2015; Goodswen et al., 2017; Robleda-Castillo et al., 2021).

The aim of this study was to identify T-cell and B-cell epitopes within the immunogenic proteins of *G. lamblia* that induce a potential protective response against giardiasis, using immunoinformatic strategies (**Figure 1**). In addition, we analyzed and discussed the potential role of those epitopes to stimulate the host's immune system, providing candidates for the development of peptide-based vaccines.



MATERIALS AND METHODS

Search and Selection of *Giardia* Immunogenic Proteins

The identification and selection of immunogenic antigens from *Giardia* was performed on the scientific platform NCBI (PubMed: <http://www.ncbi.nlm.nih.gov/pubmed/>) by filtering the results to the last 30 years, using several keywords to identify the potential articles, including: *Giardia lamblia*, immunogenic proteins, protection, immune response, vaccine, variant-surface proteins (VSPs), giardins, and cyst wall proteins (CWPs). Scientific papers were selected based on their evaluations of the humoral and cellular immune response activation by *Giardia* antigens, as well as in the *in vitro* and *in vivo* protection assays. The identified *G. lamblia* immunogens were categorized according to their functionality and location in the parasite as reported in web site Uniprot (<https://www.uniprot.org/>) and as reported in publications. The access numbers of the selected immunogens were located in GenBank and *Giardia*DB. BLASTp analysis was performed between the assemblages of each protein.

CD4+ T-Cell Epitope Prediction

For MHC-II-binding epitopes, 15-mer long epitopes for each protein were predicted using NetMHCIIpan 3.2 server ([http://](http://www.cbs.dtu.dk/services/NetMHCIIpan-3.2/)

www.cbs.dtu.dk/services/NetMHCIIpan-3.2/). We selected for T-cell epitopes prediction, the murine MHC class II molecules I-A^k and I-A^d. Those MHC molecules are expressed on the C3H/He and BALB/c mouse models, respectively, which are mouse strains frequently used in giardiasis studies (Belosevic et al., 1984; Venkatesan et al., 1997; Larocque et al., 2003; Lee et al., 2014; Serradell et al., 2019; Garzon et al., 2020). The HLA-DRB1*03:01 and HLA-DRB1*13:01 human MHC class II molecules were selected due to their probable association with susceptibility to infection (AL-Khaliq et al., 2020; El-Beshbishi et al., 2020). The proteins Hen Egg-white Lysozyme (HEL) and ovalbumin (Ova) were used as control antigens for the epitope prediction of MHC class II alleles (I-A^k and I-A^d, respectively). The predicted peptides were classified as strong and weak binders with a threshold percentile rank (% Rank) ≤ 2% and ≤ 10%, respectively. The non-binder peptides (> 10% rank) were not considered in the study. In addition, we performed a host homology analysis. We analyzed the homology of peptides with human proteins sequence (*Homo sapiens*, taxid:9606) and mouse (*Mus musculus*, taxid:10090). The immunodominant protein sequences of *Giardia* were subjected to BLASTp against non-redundant protein sequences (nr) database (Altschul et al., 1990), and complemented with Dynamic Vaxign analysis (Xiang and He, 2009; He et al., 2010). A selection of T-cell and B-cell peptide epitopes were screened in the alignments to identify homologs.

A percentage identity > 35% was set as a filter to consider homology in each epitope (Pertsemlidis and Fondon, 2001).

Prediction of Promiscuous Peptides for MHC Class II Alleles

The analyses of epitopes with promiscuous binding to a variety of MHC class II alleles permit a greater chance of the CD4⁺ T cells stimulation and allow to propose ideal epitopes for a clinically effective vaccine. The identification of T-cell epitopes with promiscuous binding to MHC class II alleles was determined with the TepiTool analysis resource from the IEDB (Paul et al., 2016) (<http://tools.iedb.org/tepitool/>). The predictions were done by using the consensus method (Wang et al., 2008; Wang et al., 2010) which employs SMM_align, NN_align, Combinatorial library, Sturniolo methods and NetMHCIIpan (Nielsen et al., 2008; Karosiene et al., 2013). A pre-selected reference panel of 26 alleles was employed and only the peptide epitopes binding at least 50% of the alleles were selected as promiscuous (Greenbaum et al., 2011). By default, Tepitool selects the epitopes with a percentile rank ≤ 20 as promiscuous. The input sequences of epitopes were those determined as the strongest binders for murine I-A^k, I-A^d alleles, HLA-DRB1*03:01 and HLA-DRB1*13:01.

B-Cell Epitope Prediction

Linear/continuous B-cell epitopes for secreted or extracellular proteins were identified using BCPred method in BCPREDS server which is based on support vector machine (SVM) that uses string kernels (<http://ailab-projects1.ist.psu.edu:8080/bcpred/predict.html>) (El-Manzalawy et al., 2008). We used the following parameters for prediction, 80% specificity and a cut-off score > 0.6. Epitopes with a length of 16-mer and 18-mer were selected for the study since most B-cell epitopes are between 15 to 25 long amino acids (Potocnakova et al., 2016), also better accuracy percentages are obtained with peptide windows of 16 amino acids in length (El-Manzalawy et al., 2008).

Epitope Conservation Analysis

To identify the percentage of conservation of the epitopes in the sequences of the proteins classified within the families, giardins, VSPs, and CWP, the FASTA sequences of proteins were selected for a multi-alignment in T-coffee (<https://www.ebi.ac.uk/Tools/msa/tcoffee/>) and Boxshade webserver (https://embnet.vital-it.ch/software/BOX_form.html). The conservancies of strong T-cell epitope and B-cell epitopes previously predicted were identified by IEDB epitope conservancy analysis tool (<http://tools.iedb.org/conservancy/>). The conservancy of epitope sequence was assigned at > 60% for giardins and CWP, and > 50% for VSPs. Every T-cell and B-cell epitopes that was filtered by the threshold, was subjected to cross-reactivity analysis (mouse and human).

RESULTS

Giardia Immunogenic Proteins Selection

To identify the *Giardia* immunogens, which have been described in the scientific literature, a screening search (last 30 years) of

articles was performed. A total of 29 research articles were selected, wherein 29 proteins with potential high immunogenicity were reported (Table 1). The selected immunogens, mainly belong to WB and GS/M-83 -H7 strains, representative of *Giardia* A and B assemblages (genetic groups), respectively. The proteins presented a homology (id%) > 78% between assemblages, unlike for VSPs, due the expressed VSPs are different between the trophozoites of assemblages A and B. (Franzén et al., 2009). Proteins were classified based on their location and function (Figure 2). Out of the 29 immunogenic proteins identified, 3 proteins correspond to cyst wall proteins (CWP 1, CWP 2, and CWP 3), 11 proteins are structural proteins located mainly in the ventral disc and cytoskeleton, such as giardins, tubulin, SALP, 21.2 protein, and GHSP-115. In addition, 5 proteins have metabolic functions in *Giardia*, such as arginine deiminase (ADI), ornithine carbamoyl transferase (OCT), fructose-bisphosphate aldolase (FBA), uridine phosphorylase (UPL), and enolase. Among the intracellular proteins, we also found the *Giardia* Trophozoite Antigens (GTA-1 and GTA-2) and the binding immunoglobulin protein (BIP). Other immunogens in the study correspond to 7 variants-specific surface proteins (VSPs). Most of the scientific papers (more than 90%) selected during the screening search performed in the present study were focused on evaluating the immunogenicity of *Giardia* proteins by analyzing the antibody-mediated immune response. Only a few have evaluated its ability to activate cellular immune responses. The immunological assays reported in those papers have been performed using human samples, and animal models susceptible to giardia infection (mice, gerbils, kittens, and puppies). Some of those articles have reported the protective capacity of certain immunogens, such as α -1 giardin, α -11 giardin, 21.2 protein, UPL-1, VSP9B10, VSP1267, VSPH7 and CWP 2 (Larocque et al., 2003; Palm et al., 2003; Serradell et al., 2018; Davids et al., 2019; Serradell et al., 2019).

T- Cell and B-Cell Epitopes From *Giardia* Immunogenic Proteins

The cellular and humoral immune responses have an important role in the clearance of giardiasis. CD4⁺ helper T lymphocytes are involved in the activation of the effector mechanisms against *Giardia*. CD4⁺ cells are activated by dendritic cells, as well as by B lymphocytes through the MHC II-peptide presentation, for this reason, we initially identified T-cell epitopes from *Giardia* immunogenic proteins. T-cell epitopes that had an affinity to the murine MHC class II I-A^k and I-A^d molecules, as well as to the human MHC class II HLA-DRB1*03:01 and HLA-DRB1*13:01 were identified. We used the NetMHCIIpan server for T-cell epitope prediction. Out of the 29 proteins that were subjected to prediction, a total of 354 strong binder peptides and 1,298 weak binder peptides were predicted (Figure 3). The subsequent analyzes were focused on strong peptides. We recorded the first 5 epitopes of each protein with the highest affinity to the MHC class II molecules I-A^k, I-A^d, HLA-DRB1 * 03: 01 and HLA-DRB1 * 13: 01 (Tables S1, S2). Then, we selected the 20 peptide epitopes with the strongest binding affinity to each MHC

TABLE 1 | Immunogenic proteins of *Giardia lamblia*.

No.	Protein	Assemblages	Id %	Location	Length (amino acids)	References
Structural proteins						
1	α -1 giardin*●	A	99%	Ventral disc	295	(Palm et al., 2003; Téllez et al., 2005; Davids et al., 2006; Feliziani et al., 2011; Jenikova et al., 2011; Feng et al., 2016; Radunovic et al., 2017; Davids et al., 2019)
		B				
2	α -2 giardin*	A	81%	Ventral disc	296	(Palm et al., 2003; Davids et al., 2006)
		B		Ventral disc	295	
3	α -7.1 giardin	A		Ventral disc	388	(Palm et al., 2003; Téllez et al., 2005)
4	α -7.3 giardin	A		Ventral disc	295	
5	α -11 giardin*●	A	91%	Ventral disc	307	(Palm et al., 2003; Davids et al., 2006; Davids et al., 2019)
		B		Ventral disc	307	
6	β -giardin*	A	100%	Cytoskeleton	272	(Palm et al., 2003; Téllez et al., 2005; Davids et al., 2006; Feliziani et al., 2011; Davids et al., 2019)
		B		Cytoskeleton	272	
7	SALP-1	A	99%	Ventral disc	255	(Palm et al., 2003)
		B		Ventral disc	255	
8	21.1 protein*●	A	95%	Ventral disc	786	(Davids et al., 2019)
		B		Ventral disc	786	
9	α -Tubulin	A	100%	Cytoskeleton	754	(Palm et al., 2003; Davids et al., 2006)
		B		Cytoskeleton	754	
10	β -Tubulin	A		Cytoskeleton	447	(Palm et al., 2003)
11	GHSP-115	A		Intracelullar	1039	
Metabolic proteins						
12	ADI*	A	89%	Intracelullar	580	(Palm et al., 2003; Téllez et al., 2005; Davids et al., 2006)
		B		Intracelullar	580	
13	OCT*	A	97%	Intracelullar	327	(Palm et al., 2003; Davids et al., 2006; Davids et al., 2019)
		B		Intracelullar	327	
14	FBA*	A	97%	Intracelullar	323	(Palm et al., 2003; Davids et al., 2006; Davids et al., 2019)
		B		Intracelullar	323	
15	UPL-1●	A	95%	Intracelullar	310	(Palm et al., 2003; Téllez et al., 2005; Davids et al., 2006; Jenikova et al., 2011)
		B*		Intracelullar	310	
16	Enolase*	A	95%	Intracelullar	445	(Palm et al., 2003; Téllez et al., 2005; Davids et al., 2006; Jenikova et al., 2011)
		B		Intracelullar	445	
Variable-specific surface proteins						
17	VSP9B10*●	A		Membrane/ Intracelullar	739	(Palm et al., 2003; Rivero et al., 2010; Cabrera-Licon et al., 2017; Serradell et al., 2018; Serradell et al., 2019)
18	VSP1267●	A		Membrane/ Intracelullar	596	
19	VSP AS8	A		Membrane/ Intracelullar	616	(Hjøllo et al., 2018)
20	TSA 417	A		Membrane	713	
21	VSPH7●	B		Membrane	557	(Stäger et al., 1997; Stäger et al., 1998; Bienz et al., 2001; Bienz et al., 2003; Serradell et al., 2018)
22	VSP5	B		Membrane/ Intracelullar	171	
23	VSP5G8	B		Membrane	607	(Quintero et al., 2017; Garzon et al., 2020)
Heat Shock Proteins						
24	BIP	A	99%	ER/ESV	662	(Lee et al., 2014; Lopez-Romero et al., 2017)
		B		ER/ESV	677	
Cyst Proteins						
25	CWP 1	A	88%	ESV	241	(Lujan et al., 1995; Abdul-Wahid & Faubert, 2008; Ma'ayeh et al., 2017)
		B*		ESV	241	

(Continued)

TABLE 1 | Continued

No.	Protein	Assemblages	Id %	Location	Length (amino acids)	References
26	CWP 2●	A	88%	Cyst	362	(Lujan et al., 1995; Larocque et al., 2003; Abdul-Wahid & Faubert, 2008; Lee et al., 2009; Feng et al., 2016; Radunovic et al., 2017)
		B		Cyst	363	
27	CWP3	A	78%	Cyst	247	(Lujan et al., 1995)
		B		Cyst	242	
Others						
28	GTA-1	A	100%	Intracellular	181	(Palm et al., 2003)
		B		Intracellular	181	
29	GTA-2	A	95%	Intracellular	225	(Palm et al., 2003; Davids et al., 2006)
		B		Intracellular	225	

Id %: percentage identity between *G. lamblia* assemblages A and B (BLAST analysis).

Giardia immunogenic proteins present in the secretome*.

Immunogenic proteins that induce protection against giardiasis ●.

class II molecule analyzed (**Tables 2, 3**). The strong binders showed a similar percentile rank to the main immunodominant epitope (48-63) of the hen egg-white lysozyme (HEL) (Nelson et al., 1992; Velazquez et al., 2002) and to the peptide (323-339) of ovalbumin (OVA) (McFarland et al., 1999) (**Table S3**). Both peptide sequences have a high affinity binding to I-A^k and I-A^d alleles, respectively. Due to the high affinity with MHC class II molecules and the capacity to activate the cellular immune response, the binding registers of HEL and OVA peptides have

been highly characterized and used as study models (McFarland et al., 1999; Bevaart et al., 2004; Dissanayake et al., 2005; Lovitch and Unanue, 2005; Landais et al., 2009; Strong and Unanue, 2011). Several sequences of giardins, UPL-1, ADI, GTA-1 and enolase showed high binding affinity for murine and human MHC II alleles (**Tables 2, 3**). Additionally, a criterion for selection of T-cell epitopes was that they should be promiscuous. Since MHC class II alleles have different binding specificities, selection of peptides that bind to several MHC

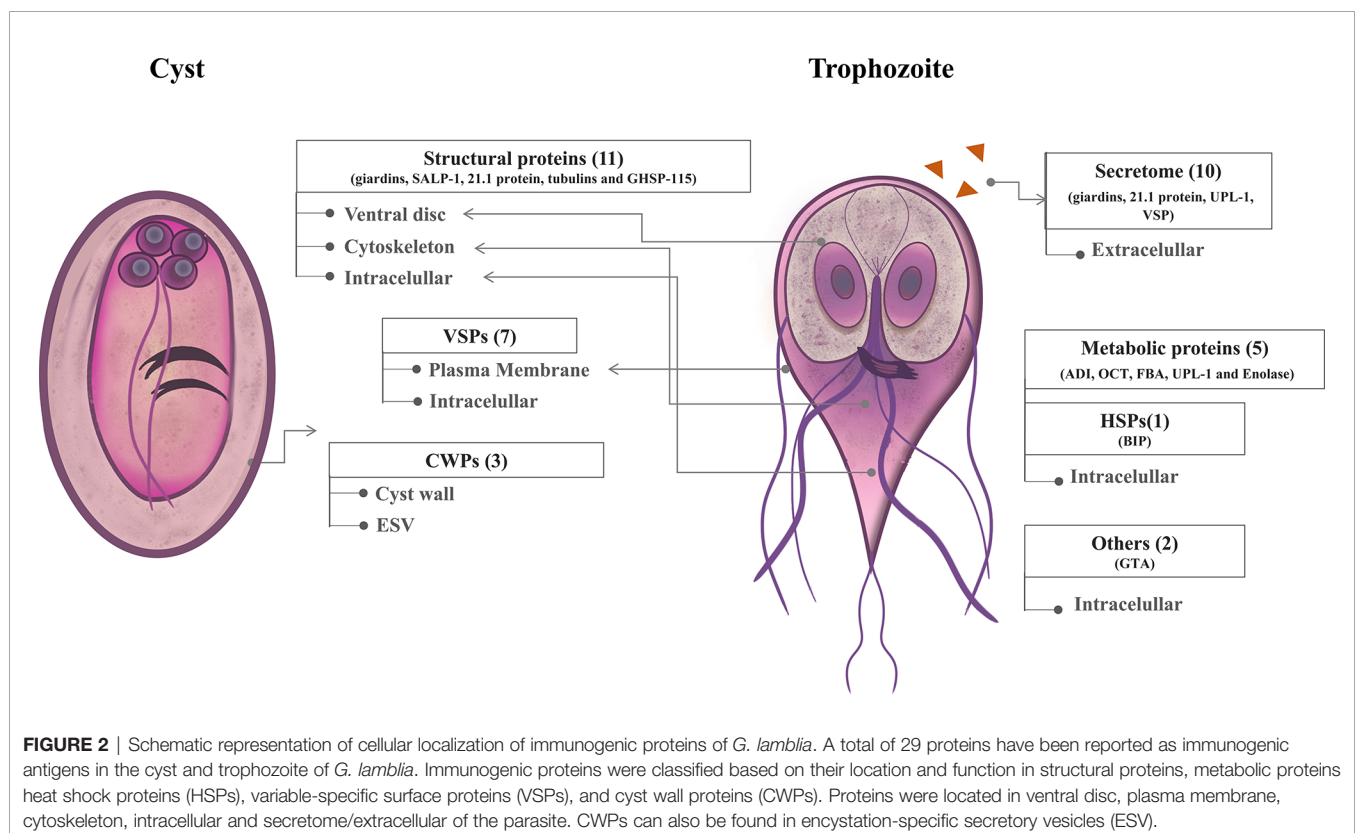


FIGURE 2 | Schematic representation of cellular localization of immunogenic proteins of *G. lamblia*. A total of 29 proteins have been reported as immunogenic antigens in the cyst and trophozoite of *G. lamblia*. Immunogenic proteins were classified based on their location and function in structural proteins, metabolic proteins heat shock proteins (HSPs), variable-specific surface proteins (VSPs), and cyst wall proteins (CWPs). Proteins were located in ventral disc, plasma membrane, cytoskeleton, intracellular and secretome/extracellular of the parasite. CWPs can also be found in encystation-specific secretory vesicles (ESV).

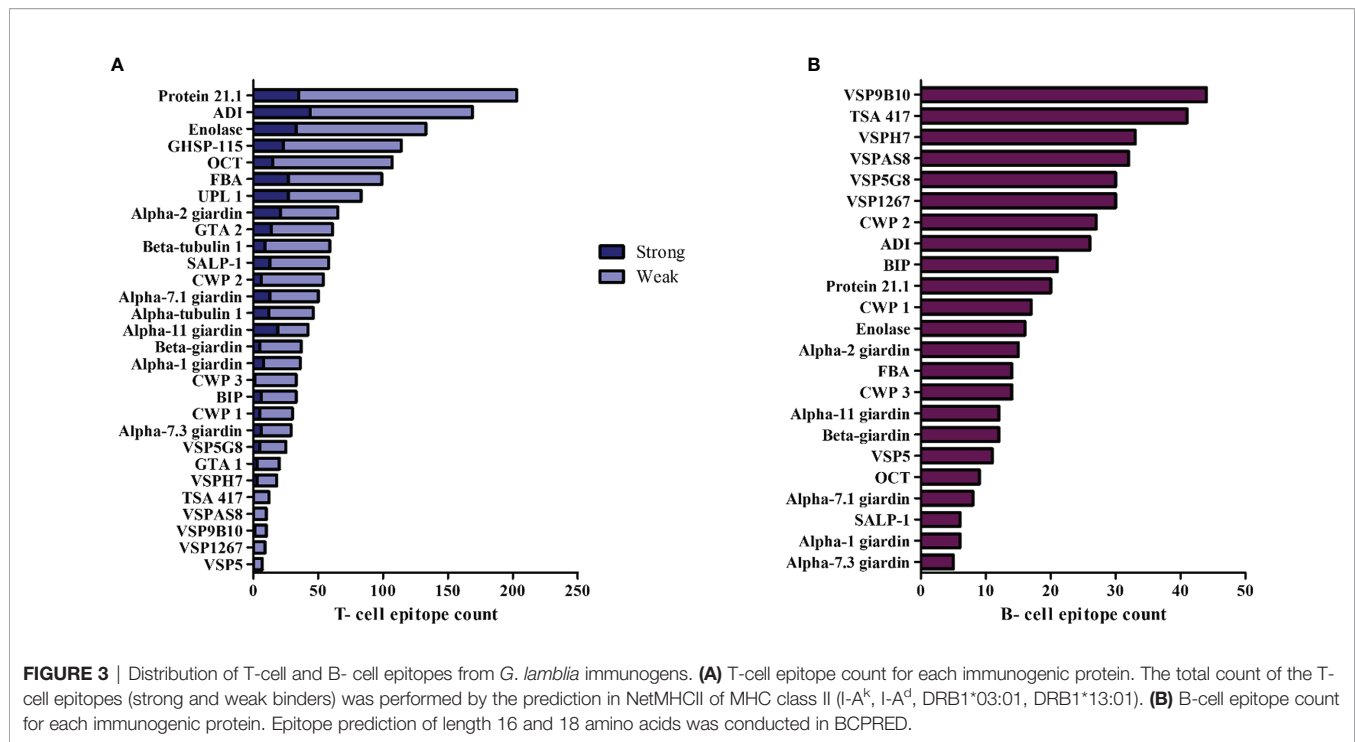


TABLE 2 | Strong binder epitopes of *G. lamblia* to murine MHC class II molecules.

MHC class II I-A ^k						MHC class II I-A ^d				
Protein/Assemblage	Position	Epitope (15 mer)	Affinity (nM)	% Rank		Protein/Assemblage	Position	Epitope (15 mer)	Affinity (nM)	% Rank
1 α -11- giardin/A,B	221	IAHYNNLAPARAVAY	3636.76	0.01		UPL 1*/B	236	AVHMSAAHIALAQRK	35.06	0.02
2 α -2- giardin/A,B	173	YISSFMAGVPPEEYK	4529.08	0.02		Enolase [#] /A,B	2	EAPSTIKAIKARMII	40.24	0.03
3 GHSP-115/A,B	354	LLNEAARALPPLSPY	4967.03	0.04		UPL 1*/A	236	AVYMSAAHIALAQRK	40.3	0.03
4 ADI*/B	381	PTIDFIKASPAYISY	5149.2	0.05		α -11- giardin/B	223	HFYNLAPARAVAYAF	40.47	0.03
5 α -11- giardin/A	224	YYNLAPARAVAYAFH	5439.79	0.09		α -7.1- giardin*/A,B	14	QHLLRGATAQAAGRA	42.4	0.04
6 α -7.1- giardin*/A,B	14	QHLLRGATAQAAGRA	5456.24	0.09		α -11- giardin/A	223	HYNNLAPARAVAYAF	43.07	0.05
7 GTA 1*/A,B	100	LELIMSLAPNHMSAI	5487.86	0.1		UPL 1/B	234	CGAVHMSAAHIALAQ	44.58	0.05
8 α -11- giardin/B	224	FYNLAPARAVAYAFY	5635.09	0.12		α -7.1- giardin/A,B	89	SAKLKMAAAKATEIK	45.63	0.06
9 UPL 1*/B	236	AVHMSAAHIALAQRK	5650.66	0.12		Enolase/A,B	1	MEAPSTIKAIKARMI	47	0.06
10 GHSP-115/A,B	516	SDELQAARAIAEAKL	5886.75	0.17		ADI*/B	381	PTIDFIKASPAYISY	52.57	0.09
11 β -tubulin 1/A,B	272	PLTSRGSQIYRALTV	5938.82	0.2		α -7.1- giardin/A,B	91	KLKMAAAKATEIKAL	57.02	0.12
12 β -giardin/A,B	135	QIAIHNDIAALRKE	6091.83	0.25		GTA-1*/A,B	100	LELIMSLAPNHMSAI	57.55	0.12
13 ADI/B	101	KYEFHPGARITPKM	6095.59	0.25		GTA-2/B	20	VVNEIRATKVMVSH	70.45	0.25
14 α -2- giardin/A,B	176	SFMAGVPPEEYKINS	6227.85	0.3		BIP/A,B	152/167	EKITKAVTVPAYFS	70.8	0.25
15 α -7.3- giardin/A,B	31	KQRAEIHAAFRATG	6319.49	0.4		ADI/B	380	QPTIDFIKASPAYIS	71.52	0.25
16 BIP/A,B	396	DEAVAWGAHVQASIL	6320.86	0.4		GHSP-115/A,B	518	ELQAARAIAEAKLAA	72.82	0.25
17 CWP 1/A,B	91	YLSNNLAGAIPEGL	6432.84	0.4		α -tubulin 1/A,B	326	KDVNAIAVIKTKRT	76.23	0.3
18 UPL 1*/A	236	AVYMSAAHIALAQRK	6437.57	0.4		ADI/B	123	YKRKVLKLSALSTRNLV	78.29	0.4
19 ADI*/B	381	PTVDFIKADPAYISY	6470.04	0.4		Enolase/A	70	LENIRKIAPALIGM	78.93	0.4
20 GTA-2/A,B	92	NASYHCAAQFQDSIR	6668.76	0.5		α -7.1- giardin/A,B	86	RNSSAKLKMAAAKAT	79.17	0.4

The 20 epitopes with the highest affinity to I-A^k and I-A^d MHC class II were selected.

Epitopes were organized according to % rank of affinity. Epitopes with conserved prediction with murine (*) and human (#) MHC class II molecules.

variants can allow the designing of vaccines to achieve a broad allelic coverage and protect against infection. We used the cut-off values of Tepitool to be binding to $\geq 50\%$ of the MHC class II alleles more frequently in the world population, we found that 26

peptides sequences were highly promiscuous epitopes (Table 4). These data were used as screening for subsequent analyzes.

B-cell linear epitopes of *Giardia* immunogens were identified by using BCPRED tool. A total of 535 B-cell epitopes were

TABLE 3 | Strong binder epitopes of *G. lamblia* to HLA class-II molecules.

HLA class-II DRB1*03:01					HLA class-II DRB1*13:01				
Protein/Assemblage	Position	Epitope (15 mer)	Affinity (nM)	% Rank	Protein/Assemblage	Position	Epitope (15 mer)	Affinity (nM)	% Rank
1 α -2- giardin/A	4	LSQIVADMKQAIDAK	24.31	0.03	Enolase [#] /A,B	2	EAPSTIKAIAKARMII	9.23	0.01
2 α -2- giardin/B	4	LSQIVADIKQAIDAK	24.48	0.03	UPL 1/A,B	47	EVKFIRRAPRLFTTI	10.39	0.02
3 α - tubulin 1/A,B	112	KEIVDLVLDVRVKLA	28.47	0.06	α - tubulin 1/A,B	329	NAAIAVIKTKRTIQF	13.02	0.09
4 ADI/A,B	88	EREVLMDQAMASLKY	29.02	0.07	UPL 1/A,B	44	PGFEVKFIRRAPRLF	14.83	0.17
5 ADI/B	495	SREIADVHKLYQKL	29.86	0.07	BIP/A,B	281/296	AKDMAVKKIAISRLRR	16.24	0.25
6 GHSP-115/A,B	847	LARLRLRLDESLPAL	30.95	0.08	FBA/A	258	SRMAMTGAIRKVFVE	16.51	0.3
7 FBA/B	249	ICKINVSDSRMAMT	31.77	0.09	FBA/B	258	SRMAMTGAIRKVFAE	16.9	0.3
8 FBA/A	249	VCKINVSDSRMAMT	32.4	0.1	GTA 1 [#] /A,B	100	LELIMSLAPNHMSAI	17.37	0.4
9 CWP 1/B	60	NNYVIALDLSDMSLT	36.35	0.15	GHSP-115/A,B	660	EVIKTLRKQLVGKAT	17.63	0.4
10 α -11- giardin/B	274	WGVMRDDISRFQSK	37.88	0.17	α -11- giardin/A	75	SARVNVKKAMKKNVN	19.64	0.5
11 FBA/A,B	251	KINVSDSRMAMTGA	39.88	0.25	α -11- giardin/B	75	SARVNVKKAMKGVN	19.76	0.5
12 BIP/A,B	416/431	HDVLLIDVPTLTGI	40.31	0.25	UPL 1/B	157	LTSIVRKHVAALSYK	20.11	0.6
13 OCT/B	18	KELMYLVDRALDMKK	41.1	0.25	ADI/B	143	EPVIHLIPGVRNTAL	21.64	0.7
14 CWP 1/A	60	NNYVIALDLSDMGLT	42.32	0.25	Enolase/A	68	QALENIRKIIAPALI	22.03	0.7
15 BIP/A,B	102/117	YKVINKDGRPFVQLS	42.34	0.25	BIP/A,B	280/295	KAKDMAVKKIAISRLR	22.05	0.7
16 α -11- giardin/A	274	WGVMRDDISRFQSK	44.39	0.3	α -11- giardin/A	77	RVNVKKAMKKNVND	22.94	0.8
17 GHSP-115/A,B	153	KAMISHDEKTAJLA	48.05	0.4	UPL 1/B	155	HDLTISIVRKHVAALS	23.41	0.9
18 α -7.3- giardin/A, B	64	LMMIVLDEIDVRCR	48.53	0.4	α -1- giardin, α -2- giardin /A,B	244	DEKRMRRITGMMVVDK	24.17	0.9
19 21.1 protein/A,B	355	NQAFKVDLNTLMSTK	49.95	0.4	Enolase/B	68	QALENIRKIITPALI	24.46	1
20 α -7.1- giardin/A, B	157	LMMIVLDEIDVRCK	50.29	0.5	α -1- giardin, α -2- giardin/ A,B	221	HFALLGMHRLAAYLI	24.69	1

The 20 epitopes with the highest affinity to HLA class-II DRB1*03:01 and DRB1*13:01 were selected.

Epitopes were organized according to % rank of affinity. Epitopes with conserved prediction with murine (*) and human (#) MHC class II molecules.

identified (**Figure 3**). The analysis showed that the VSP membrane proteins presented a higher number of B-cell epitopes than other intracellular or cytoskeletal proteins such as giardins. The B-cell epitopes with the highest score were selected, a total of 32 epitopes were identified with a score > 0.970 (**Table 5**). Some B-cell epitopes of proteins, such as β -giardin, tubulins and VSPs obtained the maximum score issued by the BCPRED algorithm. Only in certain sequences a high homology with the proteins of human and mouse were observed, as was the case with BIP. Some predicted epitope sequences present dipeptides of proline/glycine (PG) and glutamine/proline (QP or PQ) which have been identified frequently in B-cell epitopes that induce an IgA antibody response, as well as dipeptide of alanine/serine (AG), glycine/proline (GP) and tryptophan/lysine (WK) in epitopes that activate an IgG antibody response (Gupta et al., 2013).

Giardins, VSPs, and CWPs Have Conserved T-Cell and B-Cell Epitopes

Among the immunogenic proteins identified on *Giardia*, there are three families highly characterized in the parasite, giardins, VSPs, and CWPs. It was of our interest to know whether those *Giardia* protein families conserved the predicted T-cells and B-cells epitopes. A multiple alignment of those three protein families was carried out and the epitopes that had > 60% conservation for the giardins and CWPs, and > 50% conservation for the VSPs were located. Giardins present 11 T-cell and 10 B-cell conserved epitopes (**Table 6**). The T-cell epitopes 3, 7, and 9 have amino acid residues shared with the B-cell epitopes 2, 6, and 4, respectively (**Figure 4A**).

Regarding the VSPs, we identified 5 T-cell and 6 B-cell conserved epitopes (**Table 7**), which are found at the C-terminal amino acid residues. The number 1 T-cell epitope was conserved in seven proteins. In addition, the T-cell epitope 3 was the only one that overlaps with the numbers 2 and 3 of B-cell epitopes (**Figure 4B**). In the CWP family, we identified 8 and 7 T-cell and B-cell conserved epitopes, respectively (**Table 8**). Several T-cell and B-cell epitopes overlap in CWPs as T-cell epitope 1 (159-173 aa) with B-cell epitope 4 (164-181 aa) (**Figure 4C**).

DISCUSSION

Vaccine development has evolved over the years since Edward Jenner introduced the smallpox vaccine in 1796. Nowadays, in order to generate specific and safe vaccines with fewer side effects, extensive research is needed to design vaccines. In the initial phases, it is necessary to understand pathophysiology of infection, the pathogen-host relationship, as well as also to identify and characterize the immunodominant antigens that can generate immunity. Each research focused on those aspects supports the design of effective and safe vaccines for the population. At present, there is no vaccine for human giardiasis. Therefore, in this study, several T-cell and B-cell epitopes of *G. lamblia* immunogens were identified, which presented different immunogenic characteristics, some T-cell epitopes were promiscuous with strong binding affinity to MHC class II molecules, epitopes without homology to the hosts and conserved among protein families.

TABLE 4 | Promiscuous epitopes from immunogenic proteins of *G. lamblia* to MHC class II molecules.

	Epitope	Protein/Assemblage	Position	MHC II selected	Host-homol	No. Binding alleles
1	PTIDFIKASPAYISY	ADI/B	381	I-A ^K ,I-A ^d	H: No M: No	20
2	QPTIDFIKASPAYIS	ADI/B	380	I-A ^d	H: No M: No	19
3	KELMYLVDRALDMKK	OCT/B	18	HLA-DRB1*03:01	H: No M: No	18
4	IAHYYNLAPARAVAY	α -11- giardin	221	I-A ^K	H: No M: No	17
5	HFYNLAPARAVAYAF	α -11- giardin/B	223	I-A ^d	H: No M: No	16
6	HYYNLAPARAVAYAF	α -11- giardin/A	223	I-A ^d	H: No M: No	16
7	KEIVDLVLDRVRKLA	α - tubulin 1	112	HLA-DRB1*03:01	H: Yes (93%) M: Yes (93%)	16
8	YYNLAPARAVAYAFH	α -11- giardin/A	224	I-A ^K	H: No M: No	16
9	LELIMSLAPNHMSAI	GTA 1	100	I-A ^K ,I-A ^d	H: No M: No	15
10	FYNLAPARAVAYAFY	α -11- giardin/B	224	HLA-DRB1*03:01 HLA-DRB1*13:01 I-A ^K	H: No M: No	15
11	PGFEVKFIRRAPRLF	UPL 1	44	HLA-DRB1*13:01	H: No M: No	15
12	WNEIRATKVMVSH	GTA-2/B	20	I-A ^d	H: No M: No	15
13	HDVLLIDVTPLTGI	BIP	416/431	HLA-DRB1*03:01	H: 73% M: 73%	15
14	PTVDFIKADPAYISY	ADI/B	381	I-A ^K	H: No M: No	15
15	LENIRKIAPALIGM	Enolase/A	70	I-A ^d	H: Yes (53%) M: Yes (53%)	15
16	YKRKVLSSALSTRNLV	ADI/B	123	I-A ^d	H: No M: No	15
17	AVHMSAAHIALAQRK	UPL 1/B	236	I-A ^K ,I-A ^d	H: No M: No	14
18	EVKFIRRAPRLFTTI	UPL 1	47	HLA-DRB1*13:01	H: No M: No	14
19	AVYMSAAHIALAQRK	UPL 1/A	236	I-A ^K ,I-A ^d	H: No M: No	14
20	LTSIVRKHVAALSYK	UPL 1/B	157	HLA-DRB1*13:01	H: No M: No	14
21	QALENIRKIAPALI	Enolase/A	68	HLA-DRB1*13:01	H: Yes (60%) M: Yes (66%)	14
22	HFALLGMHRLAAYLI	α -1- giardin, α -2- giardin	221	HLA-DRB1*13:01	H: No M: No	14
23	EAPSTIKAIAKARMII	Enolase	2	I-A ^d	H: No M: No	13
24	NAAIAVIKTKRTIQF	α - tubulin 1	329	HLA-DRB1*13:01 HLA-DRB1*13:01	H: Yes (93%) M: Yes (93%)	13
25	QALENIRKIITPALI	Enolase/B	68	HLA-DRB1*13:01	H: Yes (53%) M: Yes (60%)	13
26	LARLRLRLDESLPAL	GHSP-115	847	HLA-DRB1*03:01	H: No M: No	12

The *G. lamblia* antigens shown in **Table 1** are molecules that have been experimentally characterized as immunogens. In addition to the physicochemical properties, other characteristics contribute to the immunogenicity of a molecule. i) Foreignness of the immunogen: there must be a degree of phylogenetic difference between the candidate molecule and the host to avoid self-reactivity (Crompton, 1974). In the present study, several amino acid regions of *G. lamblia* immunogens (tubulin, enolase, BIP, CWP and VSP) showed some degree of

homology with human and mouse molecules, ubiquitous proteins in eukaryotic cells. Although, those peptides could potentially cause an autoimmune or allergenic reaction, suggesting the necessity to do additional studies to evaluate the safety of those predicted peptides. ii) Exposure to the immune system: *Giardia* is a non-invasive parasite of the intestinal mucosa, therefore extracellular proteins play an important role in stimulating the immune system (Troeger et al., 2007; Cotton et al., 2011). The antigen location is crucial for easy recognition

TABLE 5 | Predicted B-cell immunodominant epitopes of *G. lamblia* proteins.

Protein		Position	Epitope(16 or 18 mer)	Score	Human homology	Mouse homology
1	β-giardin	238	DREKAERKEAEDKIVN	1.000	No	No
2	SALP-1	216	NRAIEEERAEFTEN AG	1.000	No	No
3	21.1 protein	24	AIPRF AG STNG AG DTG	1.000	No	No
4	α-Tubulin	438	ETLGDGEGEDMEEDDA	1.000	No	No
5	β-Tubulin	430	VDEGEFFEEEEEDFGDE	1.000	No	No
6	GHSP-115	790	SV QPTT STIVEEGGSD	1.000	No	No
7	FBA	274	PEKFDPRDYL GPGR DA	1.000	No	No
8	VSP9B10	125	AQGYFVP PG ADASHQS	1.000	No	No
9	VSP1267	543	TDGTSDDNSGNGGDST	1.000	No	No
10	VSP AS8	546	CAPP AGGS GPVTCYVTQQ	1.000	No	No
11	TSA 417	113	CTEA APGY FAPVGAAN	1.000	No	No
12	VSPH7	371	ARA APPG STPDKTNGVCT	1.000	No	No
13	VSP5	114	SCAPPTTP PGP VTCYV	1.000	Yes (37 %)	No
14	VSP5G8	505	CATCTTAASTCSTCAD	1.000	Yes (37 %)	Yes (37 %)
15	BIP	488	LNDIPPAPRG TPQ IEVTF	1.000	Yes (83 %)	Yes (83 %)
16	GTA-2	60	VPDSPPTRPSIEQLKE	1.000	No	No
17	α-11- giardin	8	PEVKAILEAKNEEEFV	0.999	No	No
18	Enolase	220	GDEGGFAPNVADPEVP	0.998	Yes (56 %)	Yes (56 %)
19	CWP 1	29	YDATDGAN WKT NNWLS	0.998	No	No
20	α-7.1- giardin	57	TYSPPRRTTARCDKGR	0.997	No	No
21	ADI	80	VLSEASPAEREVLMDQ	0.996	No	No
22	CWP 1	29	YDATDGAN WKS NNWLS	0.996	No	No
23	CWP 2	48	SYCSWTGITCDSNNNV	0.992	No	No
24	α-1- giardin	148	RVSR PG SPEDAEQRLD	0.991	No	No
25	CWP 3	25	FYDSTDGANWMPNNWL	0.987	No	No
26	OCT	243	MSYHITKEQKEARLK	0.985	No	No
27	OCT	242	WMSYHITKEQKEARLK	0.978	Yes (37 %)	No
28	α-2- giardin	235	VNCACNDKGDEKRMRR	0.977	No	No
29	α-7.3- giardin	94	TDTLLTTTPEIYARVK	0.977	No	No
30	CWP 3	25	QFYDSTDGAN WKL NNW	0.975	No	No
31	GTA-1	162	RSIIRLPCPVSDAEVEVE	0.974	No	No
32	UPL-1	48	VKFIRRAPRLFTTITG	0.971	No	No

Bold and underline letters correspond to dipeptide regions related to activation of specific-isotype antibody response.

by the immune response, which is why surface proteins have been targets for vaccine development (Serradell et al., 2016; Abdi et al., 2019; Uwase et al., 2020). *Giardia* proteins that are located in the cytoskeleton, ventral disc, membrane, and proteins of secretome (proteins with an asterisk in **Table 1**) can have greater accessibility for the immune system, activating an efficient antibody-mediated response, as well as antigen uptake and presentation by antigen-presenting cells (Kaufmann and Hess, 1999; Foged et al., 2005; Mora and Telford, 2010). iii) Chemical stability and conservation of proteins: Giardins are a large group of structural proteins that are divided into alpha, beta, and gamma, there are 21 genes for alpha-giardins that are conserved in assemblages A and B (Feliziani et al., 2011). CWP 1, CWP 2, and CWP 3 have around 60% identity in a sequence of 26 kDa, as well as conserved regions rich in leucine and cysteine (Lujan et al., 1995; Sun et al., 2003; Abdul-Wahid and Faubert, 2004). VSPs also have multiple cysteine domains, which also make them resistant to reduction by proteases (Nash et al., 1991; Papanastasiou et al., 1997). Besides, the three families of proteins mentioned above have been found expressed in the early stages of the encystation/excystation of *G. lamblia* (McCaffery et al., 1994; Hehl et al., 2000; Carranza et al., 2002; Weiland et al., 2003).

The characterization of immune responses induced by *Giardia* immunogens has mainly focused on IgA and IgG humoral response, perhaps due to the accessibility and feasibility of

in vitro immunological assays, together with the evaluation in experimental animals. Infected mice with *G. lamblia* have demonstrated the establishment of humoral immunity around the third to fifth week post-infection, which could be implicated in the resolution of infection (Singer and Nash, 2000; Eckmann, 2003; Velazquez et al., 2005). We identified 24 immunodominant B-cell epitopes from immunogenic proteins of *Giardia* by bioinformatic analysis. Several studies have demonstrated the high immunogenicity of excretory/secretory proteins of *Giardia* (Palm et al., 2003; Hanevik et al., 2011; Jiménez et al., 2014). The metabolic proteins ADI, OCT, and enolase were recognized by serum from patients with acute giardiasis (Palm et al., 2003). In other microorganisms, the immunological role of those proteins has been evaluated. Enolase has a protective role in candidiasis (Montagnoli et al., 2004). OCT activates an antibody response in *Streptococcus suis* infection, and it is involved in reducing pathogenicity factors (Wang et al., 2020). VSPs are highly expressed on the membrane of *Giardia* trophozoite and are involved in the antigenic variation of the parasite. Although the mechanisms that induce antigenic switching are unknown, it is hypothesized that anti-VSP antibodies could stimulate the VSP switching. Several studies indicate the high effectiveness of VSPs to activate an antibody-mediated response in infected humans and animals (Stäger et al., 1998; Hjøllø et al., 2018; Serradell et al., 2018), as well as the effector mechanisms of anti-VSP antibodies

TABLE 6 | Epitope conservation of giardins family.**T- cell epitope**

Predicted epitope		Protein match	Epitope sequence	Position	Identity (%)	Host-homology >35%	
						Human	Mouse
1	IAHYYNLAPARAVAY	α -11 giardin/A	IAHYYNLAPARAVAY	221-235	100	No	No
		α -11 giardin/B	IAH F YNLAPARAVAY	221-235	100	No	No
2	WGVMRDDIISRFQSK	α -11 giardin/A	WGVMRDDI L SRFQSK	274-288	93.33	No	No
		α -11 giardin/B	WGVMRDDIISRFQSK	274-288	100	No	No
3	KQRAEIHAAFRAATG	α -7.1 giardin	R QRAEIHAAFRAAT NG	124-138	80	No	No
		α -7.3 giardin	KQRAEIHAAFRAATG	31-45	100	No	No
4	LMMIVLDDEIDVRCR	α -7.1 giardin	LMMIVLDDEIDVRC K	157-171	93.33	No	No
		α -7.3 giardin	LMMIVLDDEIDVRCR	64-78	100	No	No
5	YLIDFFGTVPSEAYR	α -1 giardin	YLIDFFGTVPSEAYR	173-187	100	No	No
		α -2 giardin/B	YLIDFFGTVPSEAYR	173-187	100	No	No
6	KYAYKTYGSMKADVE	α -1 giardin	KHAYK IYGD MG TDIE	263-277	60	No	No
		α -2 giardin/A	KYAYKTYGSMKADVE	263-277	100	No	No
		α -2 giardin/B	KHAYK IYGD MG ADIE	263-277	66.67	No	No
7	DEKRMRRITGMMVVK	α -1 giardin	DEKRMRRITGMMVVK	244-258	100	No	No
		α -2 giardin/A	DEKRMRRITGMMVVK	244-258	100	No	No
		α -2 giardin/B	DEKRMRRITGMMVVK	244-258	100	No	No
8	HYGNLAKDIRATMSK	α -7.1 giardin	HYGNLAKDIRATMSK	361-375	100	No	No
		α -7.3 giardin	HYGNLAKDIR K TMSK	268-282	93.33	No	No
9	RPIAEAFKAQNGKSI	α -1 giardin	RPIAEAFKAQNGKSI	187-201	100	No	No
		α -2 giardin/B	RPIAEAFKAQNGKSI	187-201	100	No	No
10	VLIATPDERLKLAQ	α -11 giardin/A	VLIATPDERLKLAQ	97-111	100	No	No
		α -11 giardin/B	V LIATPDERLKLAQ	97-111	93.33	No	No

B- cell epitope

Predicted epitope		Protein match	Epitope sequence	Position	Identity (%)	Host-homology >35%	
						Human	Human
1	RVSRPGSPEDEAQRLD	α -1 giardin	RVSR P GSPEDEAQRLD	143-163	100	No	No
		α -2 giardin/B	RAS P GSPEDEAQRLD	143-163	93.75	No	No
2	INCACNDKGDEKMRMR	α -1 giardin	INCACNDKGDEKMRMR	235-250	100	No	No
		α -2 giardin/A	V NCACNDKGDEKMRMR	235-250	93.75	No	No
		α -2 giardin/B	INCACNDKGDEKMRMR	235-250	100	No	No
		α -1 giardin	AKAYV AS YGKELPDDIKK	39-56	100	Yes (61%)	No
3	AKAYVASYGKELPDDIKK	α -2 giardin/A	AQGYRDQ YGKELPDDIKK	39-56	72.22	No	No
		α -2 giardin/B	AQGYKDQY NKELPDDIKK	39-56	66.67	No	No
		α -1 giardin	AEAFKAQNGKSIEQAIAT	190-207	100	No	No
4	AEAFKAQNGKSIEQAIAT	α -2 giardin/B	AEAFKAQNGKSIEQAIAT	190-207	100	No	No
		α -7.1 giardin	AFCRSARNNAQGDAEALK	236-253	100	No	No
5	AFCRSARNNAQGDAEALK	α -7.3 giardin	AFCRSARN V QGDAEALK	143-160	94.44	No	No
6	AEIYAAFRAANGKTASEY	α -7.1 giardin	AEIYAAFRAANGKT AS EY	127-144	100	No	No
		α -7.3 giardin	AEI H AAFRAAT GKTT SEY	34-51	83.33	No	No
		α -7.1 giardin	ALCCCNATLHCPARGAAY	309-326	100	No	No
7	ALCCCNATLHCPARGAAY	α -7.3 giardin	ALCCCNATLHCPARGAAY	216-233	100	No	No
		α -7.1 giardin	TD ALL TTT PEV YARVK	187-202	87.50	No	No
8	TDTLLTTTPEIYARVK	α -7.3 giardin	TDTLLTTTPEIYARVK	94-109	100	No	No
		α -11 giardin/A	TFTSRWSAEERKELRT	24-39	100	No	No
9	TFTSRWSAEERKELRT	α -11 giardin/B	TFTSRWSAEERKELRT	24-39	100	No	No
		α -11 giardin/A	GKSVQEAETRYADKENA	199-216	100	Yes (38%)	No
		α -11 giardin/B	GKSVQEAET K YADKENA	199-216	100	Yes (38%)	No
10	GKSVQEAETRYADKENA	β giardin/A	FHDKMENEIVRRVDD	41-56	100	No	No
		β giardin/B	FHDKMENEIVRRVDD	41-56	100	No	No
11	FHDKMENEIVRRVDD						

Red letters correspond to amino acids residues other than the predicted epitope.

Bold and underline letters correspond to dipeptide regions related to activation of specific-isotype antibody response.

against trophozoites, such as cytotoxicity, opsonization, and neutralization (Nash and Aggarwal, 1986; Stäger et al., 1997; Rivero et al., 2010).

The clearance of *Giardia* infection requires humoral and cellular immune mechanisms. In *Giardia*, there is little

research focused on characterizing the cellular response, however, it is known that CD4+ T lymphocytes play an important role in infection. CD4-deficient mice treated with an anti-CD4 antibody could not clear the infection, as well as CD4+ T cells deficiency is related to chronic giardiasis (Heyworth et al.,

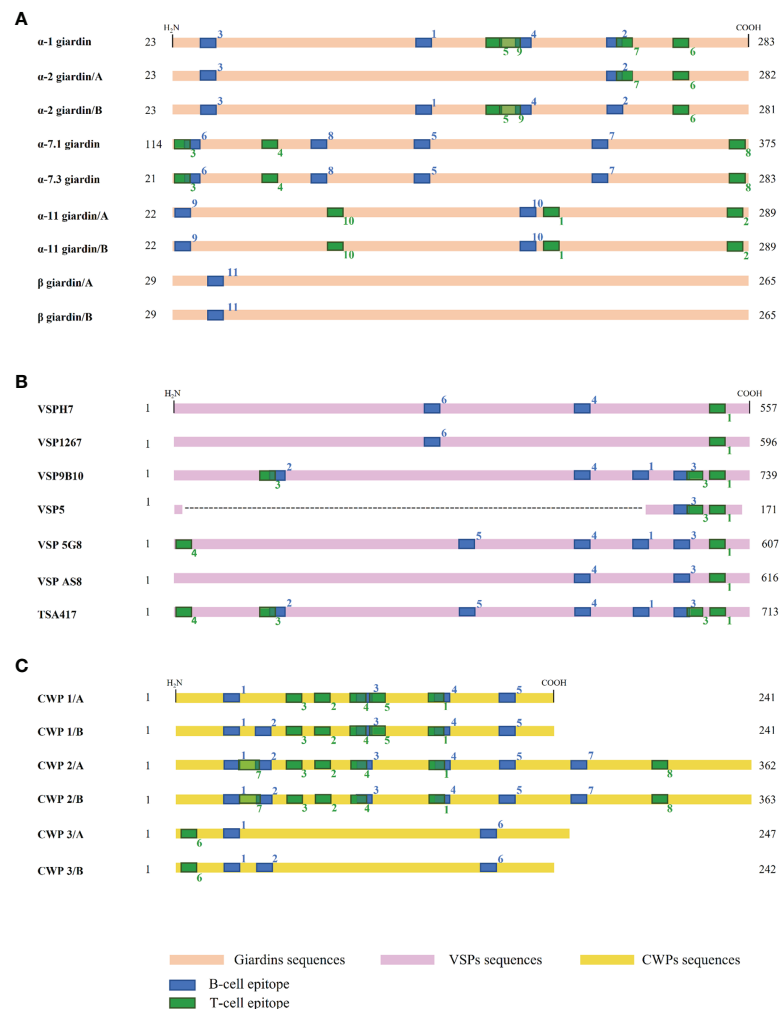


FIGURE 4 | Giardins, VSPs, and CWPs conserved T-cell and B-cell epitopes. Epitope conservation analysis with a cutoff > 60% conservancy for giardins **(A)** and VSPs **(B)**, a cutoff > 50% conservancy for CWPs **(C)**. The regions shown in green, and blue are T-cell and B-cell epitopes, respectively. Conserved epitopes shown in this figure are found in **Tables 6–8**.

1987; Singer and Nash, 2000). In this study, 26 epitopes are proposed to activate CD4+ cells due to their high affinity to several MHC class II molecules. First, four MHC class II alleles were chosen, the MHC class II I-A^k and I-A^d that are expressed in mice widely used as model for giardiasis, as well as the HLA-DRB1 * 03: 01 and HLA-DRB1 * 13: 01 alleles that are related to an increased risk of *G. lamblia* infection (AL-Khaliq et al., 2020; El-Beshbishi et al., 2020). MHC class II molecules are expressed in dendritic cells and B lymphocytes, which are chemoattracted by trophozoite-stimulated epithelial cells (Roxström-Lindquist et al., 2005). Dendritic cells pre-stimulated with *Giardia* antigens can confer IL-6-dependent protection, which has been related to B-lymphocyte growth and T-cell differentiation (Weaver et al., 2006; Kamda et al., 2012). Proinflammatory chemokines, including TNF- α , and B lymphocyte activating interleukins, such as IL-4 and IL-5 belong to the chemokine profile described in *Giardia* infection (Cotton et al., 2015; Serradell

et al., 2018). Additionally, an increase in IL-17 producing CD4+ cells from infected patients with *Giardia* (Saghaug et al., 2015). Interleukin IL-17 has been associated with IgA production and infection control (Dann et al., 2015). Although we focused the analysis on the strong epitopes classified by the NetMHCII algorithm, we did not disregard sequences with low affinity to MHC class II for future tests, due peptides with a low binding affinity can activate effective T-cell response, as the HEL 20-35 peptide (Nelson et al., 1992; Velazquez et al., 2002).

In this study, we identified conserved epitopes among giardins, VSPs, and CWPs. T-cell and B-cell epitopes overlap in some amino acid residues. Responses between B and T cells are closely linked for the development of an effective immune response. B cells as an antigen presenting cell can recognize antigens through the BCR, as well as present T-dependent antigens through the binding of peptides to MHC class II molecules. T-helper cells recognize peptide-MHC class II

TABLE 7 | Epitope conservation of VSP family.**T- cell epitope**

Predicted epitope		Protein match	Epitope sequence	Position	Identity (%)	Host- homology >35%	
						Human	Mouse
1	LSTGAIAGISVAAFV	VSP 5G8	LS S GAIAGISVAV I V	574-588	80	No	No
		VSPH7	LS S GAIAGISVAV I V	524-538	80	No	No
		VSP9B10	LS A GAIAGI A VAV I I	706-720	66.67	No	No
		VSP1267	LSTGAIAGISVAAFV	563-577	100	No	No
		VSP AS8	LSTGAIAGISVAV A	583-597	80	No	No
		VSP5	LS S GAIAGISVAV I A	147-161	73.33	Yes (46%)	No
		TSA417	LSTGAIAGISVAV I V	574-588	86.67	No	No
2	SRCNTGFVPINGQCA	VSP9B10	SRCNTGFVPINGQCA	51-65	100	Yes (40%)	No
		VSP1267	MQ CN Q GKVPING I CT	39-53	60	No	No
3	PVLCYLVRDSASVNIK	VSP 5G8	PVLCYLVRDSASVNIK	557-571	100	No	No
		VSP9B10	S VL C YL V S Q S G E NT N K	689-703	53.33	No	No
		TSA417	S VL C YL I K D S G S T N K	663-677	66.67	No	No
4	VAVILQIARAACPTG	VSP 5G8	VAVILQIARAACPTG	8-22	100	No	No
		TSA417	A IV I L Q L A R T A C T Q E	8-22	60	No	No
5	QAAQGYFVPPGADAS	VSP9B10	QAAQGYFVPPGADAS	123-137	100	No	No
		TSA417	E A A P G Y F A P V G A A N T	115-129	53.33	No	No

B- cell epitope

Predicted epitope		Protein match	Epitope sequence	Position	Identity (%)	Host- homology >35%	
						Human	Mouse
1	CATCTTAASTCSTCAD	VSP 5G8	CATCTTAA AST CSTCAD	505-520	100	Yes (37%)	Yes (37%)
		VSP9B10	CATC AGSASNC DT CTST	635-650	56.25	Yes (50%)	Yes (43%)
		TSA417	C ETCNGAATTC KACAT	608-623	56.25	Yes (50%)	Yes (50%)
2	AQGYFVPPGADASHQS	VSP9B10	AQGYFV PP GAD ASH QS	125-140	100	No	No
		TSA417	APGYF APVGA ANTEQS	117-132	56.25	No	No
3	SCAPPTTTPPGPVTCYV	VSP 5G8	SCA APSGSTGP VLCY L	547-562	56.25	No	No
		VSP9B10	NCAPPLNNKGS VLCY L	679-694	50	No	No
		VSP AS8	SCA PPAGSSGP VTCYV	545-560	75	No	No
		VSP5	SCA PPTTTPPGP VTCYV	114-129	100	Yes (37%)	No
		TSA417	NCAPPPNNKGS VLCY L	653-668	50	No	No
4	PGSTVCVTAPTGGTCT	VSP 5G8	PGSTVCVTAPTGGTCT	438-453	100	Yes (37%)	No
		VSPH7	PG NTLCTTA D AGKCTT	408-423	50	No	Yes (37%)
		VSP1267	AGRDVSVCTA TGGKCT	406-421	50	No	No
		VSP AS8	PGS SVCTA Q NK G QCQ	464-479	50	No	No
		TSA417	PG KTVCS AP N GGT CQ	543-558	68.75	No	No
5	KGATASDCTACPAGRA	VSP 5G8	KGAT ASD CTACPAGRA	329-344	100	Yes (50%)	Yes (43%)
		TSA417	SAGTASDCTE CPT GKA	433-448	62.50	Yes (43%)	Yes (37%)
6	TDCPAGTYAVSGDSGS	VSPH7	QDCPAGTYAD SNVCKP	272-287	56.25	Yes (62%)	Yes (50%)
		VSP1267	TDCPAGTYAVSGDSGS	303-318	100	Yes (50%)	Yes (57%)

Red letters correspond to amino acids residues other than the predicted epitope.

Bold and underline letters correspond to dipeptide regions related to activation of specific-isotype (IgG and IgA) antibody response.

complex and send activation signals to the B cell (Shimoda and Koni, 2007; Akkaya et al., 2019). Those pathways promote processes such as the isotype switch, affinity maturation and immunological memory, necessary in the development of protective immune responses. Does it remain to be evaluated whether these epitopes can be generated naturally? Are they resistant to antigen processing? if the antibodies generated are limited to the course of the infection or will it be a long-lived response?. In the analysis of multiple alignments between the proteins showed several semi-conserved epitopes in the three protein families (giardins, CWPs and VSPs), although we understand that changes in amino acids can reduce the binding affinity with MHC class II and immunoglobulins,

these regions can be targets for a vaccine that protects by dampening the variations that occur in the parasite throughout its life cycle.

The proteins described in this study have been proven to be immunogenic, however, only few of them have been evaluated in protection assays. Prior to consider an immunogen as a vaccine candidate, it is crucial to demonstrate its protective capacity by using experimental models. The proteins α -1 giardin, α -11 giardin, 21.2 protein, UPL-1, VSP9B10, VSP1267, VSPH7 and CWP 2 have shown to induce a protective immune response against infection by *G. lamblia* (Table 1) when administered orally or intraperitoneally. Mice and Mongolian gerbils were commonly used as animal models in protection assays, although

TABLE 8 | Epitope conservation of CWP family.

T-cell epitopes							
Predicted epitope		Protein match	Epitope sequence	Position	Identity (%)	Host- homology >35%	
						Human	Mouse
1	LKELHLDNCNQLTGDV	CWP 1/A	LKELHLDNCNQL SG TV	159-173	86.67	Yes (60%)	Yes (53%)
		CWP 1/B	LKELHLDNCNQLTGDV	159-173	100	Yes (60%)	Yes (60%)
		CWP 2/A	LKELHLDNCN EL TGDV	159-173	93.33	Yes (53%)	Yes (40%)
		CWP 2/B	LKELHLDNCN EL TGDV	159-173	93.33	Yes (53%)	Yes (40%)
2	YLSNNSLAGAIP EGL	CWP 1/A	YLSNNSLAGAIP EGL	91-105	100	Yes (53%)	Yes (53%)
		CWP 1/B	YLS SN TLTG DI PEGL	91-105	73.33	Yes (46%)	Yes (40%)
		CWP 2/A	YL NN DLAG PI TDL	91-105	66.67	Yes (46%)	Yes (46%)
		CWP 2/B	YL NN DLAG PI TDL	91-105	73.33	Yes (40%)	Yes (46%)
3	DLSDSL TGAIPENI	CWP 1/A	DLSDM GL TG T IPENI	67-81	86.67	Yes (46%)	Yes (46%)
		CWP 1/B	DLSDSL TGAIPENI	67-81	100	No	Yes (46%)
		CWP 2/A	DLSDM GL TG AL P ADI	67-81	73.33	Yes	No
		CWP 2/B	DLSDM GL TG AI P TDI	67-81	80	No	No
4	LTNLQYLQINKAGLT	CWP 1/A	LTNLQYLC VNS AGLT	108-122	86.67	No	Yes (46%)
		CWP 1/B	LTNLQYLQINKAGLT	108-122	100	Yes (40%)	Yes (40%)
		CWP 2/A	LT SM QYLQINNAGLT	108-122	80	Yes (53%)	Yes (46%)
		CWP 2/B	LT SM QYLQINNAGLT	108-122	80	No	Yes (46%)
5	IPECICDLTHMMFWY	CWP 1/A	IPEC MC DL I HLMFWY	125-139	80	No	No
		CWP 1/B	IPEC MC DL V HLMFWY	125-139	80	No	No
		CWP 2/A	IPECICDLTHMMFWY	125-139	100	No	No
		CWP 2/B	IPECICDLTHMMFWY	125-139	100	No	No
6	IEIGYGLADAQHDAL	CWP 3/A	LEV GYGL VDM QYDAL	8-22	66.67	No	No
		CWP 3/B	IEIGYGLADAQHDAL	9-23	100	No	No
7	WKSNNWLAADVSYCS	CWP 2/A	WKSNNWL TP DVSYCS	37-51	86.67	No	No
		CWP 2/B	WKSNNWLAADVSYCS	37-51	100	No	No
8	GNASRSAVARPTARA	CWP 2/A	GNASRSAVARPTARA	321-335	100	No	No
		CWP 2/B	GS ASRS TT S RPTARA	321-335	73.33	No	No
B- cell epitope							
Predicted epitope		Proteins match	Epitope sequence	Position	Identity (%)	Host- homology >35%	
						Human	Mouse
1	YDATDGANWKTNNWLS	CWP 1/A	YDATDGAN WK TNNWLS	29-44	100.	No	No
		CWP 1/B	YDATDGAN WKS NNWLS	29-44	93.75	No	No
		CWP 2/A	YDAL D GAN WKS NNWL T	29-44	81.25	No	No
		CWP 2/B	YDAL D GAN WKS NNWL A	29-44	81.25	No	No
		CWP 3/A	YD ST DGANW MP NNWL Q	26-41	75	No	No
		CWP 3/B	YD ST DGAN WK LNNWL Q	27-42	81.25	No	No
2	SYCSWTGITCDSNNNV	CWP 1/B	S I C TWTG V TC D AS NNY	47-62	62.50	No	No
		CWP 2/A	SYCSWTGITCDSNNNV	48-63	100	No	No
		CWP 2/B	SYCSWTGITCDSNNNV	48-63	100	No	No
		CWP 3/B	D Y C E W TG V S C D D NNNV	45-60	68.75	No	No
3	LQINNAGLTGDIPECI	CWP 1/A	LQI VNS GLTGDIPEC M	114-129	81.25	No	Yes (40%)
		CWP 1/B	LQIN K AGLTG S IPEC M	114-129	81.25	Yes (37%)	Yes (37%)
		CWP 2/A	LQINNAGLTGDIPECI	114-129	100	Yes (43%)	Yes (37%)
		CWP 2/B	LQINNAGLTGDIPECI	114-129	100	Yes (50%)	Yes (37%)
4	LDCNQLTGDVPVGLMTLP	CWP 1/A	LDCNQL SG TVPVGLMTLP	164-181	88.89	Yes (61%)	Yes (44%)
		CWP 1/B	LDCNQLTGDVPVGLMTLP	164-181	100	Yes (61%)	Yes (44%)
		CWP 2/A	LDCN EL TGDVP AD L F DLP	164-181	72.22	Yes (44%)	No
		CWP 2/B	LDCN EL TGDVP AD L F DLP	164-181	72.22	Yes (44%)	No
5	TTDCDYCTALPPTNCPTT	CWP 1/A	DV D C EN CG T L P P T N C AQC	210-227	50	Yes 38%)	Yes (39%)
		CWP 1/B	DV D C D DC GT L P P T N C PQC	210-227	61.11	No	No
		CWP 2/A	TTDCDYCTAL P P T N C P T T	211-228	100	No	No
		CWP 2/B	TTDCDYCTAL P P T N C P ET	211-228	94.44	No	No
6	ACGSNHCNNCVEKTTC	CWP 3/A	ACG EN H C ST CV K KTTC	205-220	75	No	No
		CWP 3/B	ACGSNHCNNCVEKTTC	206-221	100	No	No
7	CNARSASNC GAKSNMHN	CWP 2/A	CNARS AS NCGAKAKSNMHN	252-269	100	No	No
		CWP 2/B	CNARS AS NCGAKAKSNMHN	252-269	100	No	No

Red letters correspond to amino acids residues other than the predicted epitope.

Bold and underline letters correspond to dipeptide regions related to activation of specific-isotype (IgG and IgA) antibody response.

other *Giardia*-susceptible animals, such as cats and dogs have also been used (Serradell et al., 2016). Currently, there is no human or dog effective vaccine against *G. lamblia*. In 1999, Fort Dodge Animal Health developed a vaccine based on killed disrupted trophozoites (*GiardiaVax*), which attenuated giardiasis symptoms, produced antibodies, and reduced the shedding cysts to 30% and 5% in vaccinated kitten and puppies respectively (Olson et al., 2000). *GiardiaVax* was also tested on *Meriones unguiculatus*, showing protection in 33% of the mice at the third day post-infection, the rest of the vaccinated group cleared the infection at seventh day (Jiménez-Cardoso et al., 2002). However, other studies differ in the vaccine efficacy. It was reported that the *Giardia* parasite persisted by week 28 in vaccinated cats with three doses of *Giardiavax* (Stein et al., 2003), as well as in dogs, no differences were found in the elimination of cysts between the control and vaccinated group (Anderson et al., 2004). First-generation vaccines, such as the whole pathogen vaccine are characterized by generating no or low cell-mediated response and can also generate adverse effects such as hypersensitivity (Jiskoot et al., 2019). In recent years, protection strategies for clinically relevant pathogens have been focused on the peptide- and epitope-based vaccines (Table S4). Initially, *in silico* analysis facilitate the identification of T- and B-cell epitopes, and which can significantly reduce time and cost of research. Peptide-based vaccines can generate an effective and targeted immune response if the proper adjuvants and delivery system are considered. In gastrointestinal infections such as giardiasis several mucosal adjuvants can be used, such as choleric toxin, which increase the permeability of the intestinal epithelium promoting the antigen-uptake by immune cells (Rhee et al., 2012).

Validation strategies for the effectiveness of a peptide-based vaccine can be completed with additional *in silico* and experimental assays. In several viral pathogens, IFN- γ response activation is evaluated, due to the importance of this cytokine in effector mechanisms. Additionally, 3-D modeling and molecular docking are performed for the multi-epitopes vaccine constructs. All subunit- and epitope-based vaccines shown in Table S4 have high protection efficacy in their respective diseases, as well as induced specific humoral and cellular responses. The advances in vaccines design of parasites show methodological strategies for the antigens characterization that can be implemented in *Giardia* studies. Likewise, *Giardia* shares some characteristics with other protozoa. *Giardia* presents antigenic variation, characteristic of the differential expression of variable surface proteins (VSP). *Plasmodium* and *Trypanosoma* are other parasites that express variable surface antigens (Borst and Ulbert, 2001; Kyes et al., 2007). Heat shock proteins are highly conserved molecules, in *Leishmania* which have been described as immunomodulatory proteins as well as have been used as components of vaccines (Lopez-Romero et al., 2017). Although there is little research on the immunological characterization of *Giardia* HSPs, studies have described the BIP protein as an immunogenic protein (Lee et al., 2014). We believe that more studies are needed to analyze the similarities among immunogenic antigens of *Giardia* and other pathogens, as well as the immune responses that may activate.

Our study is restricted by limiting immunoinformatic analyses to *G. lamblia* immunogenic proteins. At present, proteins are the molecules most characterized at the immunological level, however, different types of antigens may contribute to elicit immune responses during *G. lamblia* infection. Trophozoites of *G. lamblia* are able to activate innate immune responses, such as the complement system through the lectin pathway, after the recognition of surface N-acetylglucosamine (GlcNAc) by mannose-binding lectin (MBL). Interestingly, specific surface glycoconjugate antigens, glycosylphosphatidylinositol (GPI) and lipophosphoglycan (LPG) have been described as important inducers of immune responses during parasitic infection with *Trypanosoma* spp, *Leishmania* spp, *Plasmodium falciparum*, *Cryptosporidium* y *Entamoeba histolytica* (Ropert and Gazzinelli, 2000; Priest et al., 2003; Wong-Baeza et al., 2010). Based on this information, it is necessary to address future analyses at the molecular basis under the immune responses elicited by GlcNAc and other glycoconjugate antigens present in trophozoites and cysts of *G. lamblia*, in addition, the immunogenic role of post-translational modifications, such as glycosylation in VSPs, should be fully analyzed.

The present study describes a global approach to the identification of immunodominant and protective antigens of *Giardia*, being the first study to determine potential T-cell and B-cell immunogenic epitopes predicted by immunoinformatic tools as candidates for a vaccine against *Giardia* infection. For effective vaccine development against *Giardia*, it is necessary to consider several factors: i) the inclusion of conserved and variable protein sequences from the most common *Giardia* assemblages in humans (A and B); ii) the activation of the immune mechanisms of innate and adaptive response, considering the relationship between the parasite, gut mucosal immune system, microbiota, and the tolerogenic environment.; iii) the use of proper adjuvants; iv) administration routes to guarantee an immune response in mucosa. For future studies, *in vitro* and *in vivo* assays are required to verify the effectiveness and protective role of T-cell and B-cell epitopes in giardiasis. These results obtained in the present study suggest that experimental administration of a multi-epitope vaccine constructed on basis of immunoinformatic approach could provide an effective prophylactic strategy against *Giardia*.

DATA AVAILABILITY STATEMENT

The original contributions presented in the study are included in the article/Supplementary Material. Further inquiries can be directed to the corresponding author.

AUTHOR CONTRIBUTIONS

TG performed and is involved in immunoinformatic analyses, wrote the manuscript, and prepared all figures. GL-R and

DO-T performed *in silico* assays and analyzed the data. EA contributed to the writing and editing of the manuscript. AG-E contributed to the writing and editing of the manuscript. RR-Z contributed to the library searches and assembling relevant literature. CV designed and supervised the project, revised the manuscript, and was responsible for the funding. All authors contributed to the article and approved the submitted version.

FUNDING

National Council for Science and Technology of Mexico (CONACyT, CB2017-2018 A1-S-21831).

REFERENCES

- Abdi, R. D., Dunlap, J. R., Gillespie, B. E., Ensermu, D. B., Almeida, R. A., and Dego, O. K. (2019). Comparison of Staphylococcus Aureus Surface Protein Extraction Methods and Immunogenicity. *Heliyon* 5 (10), e02528. doi: 10.1016/j.heliyon.2019.e02528
- Abdul-Wahid, A., and Faubert, G. M. (2004). Similarity in Cyst Wall Protein (CWP) Trafficking Between Encysting Giardia Duodenalis Trophozoites and CWP-Expressing Human Embryonic Kidney-293 Cells. *Biochem. Biophys. Res. Commun.* 324 (3), 1069–1080. doi: 10.1016/j.bbrc.2004.09.167
- Abdul-Wahid, A., and Faubert, G. (2008). Characterization of the Local Immune Response to Cyst Antigens During the Acute and Elimination Phases of Primary Murine Giardiasis. *Int. J. Parasitol.* 38 (6), 691–703. doi: 10.1016/j.ijpara.2007.10.004
- Akkaya, M., Kwak, K., and Pierce, S. K. (2019). B Cell Memory: Building Two Walls of Protection Against Pathogens. *Nat. Rev. Immunol.* 20, 4, 229–238. doi: 10.1038/s41577-019-0244-2
- AL-Khaliq, I. M. A., Ghabban, M. M., and Karimau, K. A. A. L. H. (2020). Influence of Human Leukocyte Antigen HLA-Drb1 on Susceptibility To Giardia Lamblia Infection of Iraqi Patients. *Biochem. Cell. Arch.* 20 (2), 5513–5516.
- Altschul, S. F., Gish, W., Miller, W., Myers, E. W., and Lipman, D. J. (1990). Basic Local Alignment Search Tool. *J. Mol. Biol.* 215 (3), 403–410. doi: 10.1016/S0022-2836(05)80360-2
- Anderson, K. A., Brooks, A. S., Morrison, A. L., Reid-Smith, R. J., Martin, S. W., Benn, D. M., et al. (2004). Impact of Giardia Vaccination on Asymptomatic Giardia Infections in Dogs at a Research Facility. *Can. Vet. J.* 45 (11), 924–930.
- Ankarklev, J., Jerlström-Hultqvist, J., Ringqvist, E., Troell, K., and Svärd, S. G. (2010). Behind the Smile: Cell Biology and Disease Mechanisms of Giardia Species. *Nat. Rev. Microbiol.* 8 (6), 413–422. doi: 10.1038/nrmicro2317
- Autheman, D., Crosnier, C., Clare, S., Goulding, D. A., Brandt, C., Harcourt, K., et al. (2021). An Invariant Trypanosoma Vivax Vaccine Antigen Induces Protective Immunity. *Nature* 595, 96–100. doi: 10.1038/s41586-021-03597-x
- Bae, S. S., Kim, J., Kim, T. S., Yong, T. S., and Park, S. J. (2009). Giardia Lamblia: Immunogenicity and Intracellular Distribution of GHSP-115, a Member of the Giardia Head-Stalk Family of Proteins. *Exp. Parasitol.* 122 (1), 11–16. doi: 10.1016/j.exppara.2009.01.005
- Belosevic, M., Faubert, G. M., Skamene, E., and MacLean, J. D. (1984). Susceptibility and Resistance of Inbred Mice to Giardia Muris. *Infect. Immun.* 44 (2), 282–286. doi: 10.1128/iai.44.2.282-286.1984
- Bevaart, L., Van Ojik, H. H., Sun, A. W., Sulahian, T. H., Leusen, J. H. W., Weiner, G. J., et al. (2004). CpG Oligodeoxynucleotides Enhance FcγR-Mediated Cross Presentation by Dendritic Cells. *Int. Immunol.* 16 (8), 1091–1098. doi: 10.1093/intimm/dxh110
- Bienz, M., Dai, W. J., Welle, M., Gottstein, B., and Müller, N. (2003). Interleukin-6-Deficient Mice Are Highly Susceptible to Giardia Lamblia Infection But Exhibit Normal Intestinal Immunoglobulin A Responses Against the Parasite. *Infect. Immun.* 71 (3), 1569–1573. doi: 10.1128/IAI.71.3.1569-1573.2003

ACKNOWLEDGMENTS

The authors TG and DO-T would like to express their gratitude to CONACyT for the scholarship granted, also EA express his gratitude for postdoctoral fellowship, Estancias Posdoctorales por México, 2020, CONACyT. In addition, we appreciate the support by Lucila Rascon, laboratory technical assistant.

SUPPLEMENTARY MATERIAL

The Supplementary Material for this article can be found online at: <https://www.frontiersin.org/articles/10.3389/fcimb.2021.769446/full#supplementary-material>

- Bienz, M., Wittwer, P., Zimmermann, V., and Müller, N. (2001). Molecular Characterisation of a Predominant Antigenic Region of Giardia Lamblia Variant Surface Protein H7. *Int. J. Parasitol.* 31 (8), 827–832. doi: 10.1016/S0020-7519(01)00182-5
- Borst, P., and Ulbert, S. (2001). Control of VSG Gene Expression Sites. *Mol. Biochem. Parasitol.* 114, 17–27. doi: 10.1016/S0166-6851(01)00243-2
- Cabrera-Licona, A., Solano-González, E., Fonseca-Liñán, R., Bazán-Tejeda, M. L., Argüello-García, R., Bermúdez-Cruz, R. M., et al. (2017). Expression and Secretion of the Giardia Duodenalis Variant Surface Protein 9B10A by Transfected Trophozoites Causes Damage to Epithelial Cell Monolayers Mediated by Protease Activity. *Exp. Parasitol.* 179, 49–64. doi: 10.1016/j.exppara.2017.06.006
- Carranza, P. G., Feltes, G., Ropolo, A., Quintana, S. M. C., Touz, M. C., and Luján, H. D. (2002). Simultaneous Expression of Different Variant-Specific Surface Proteins in Single Giardia Lamblia Trophozoites During Encystation. *Infect. Immun.* 70 (9), 5265–5268. doi: 10.1128/IAI.70.9.5265-5268.2002
- Cecilio, P., Pérez-Cabezas, B., Fernández, L., Moreno, J., Carrillo, E., Requena, J. M., et al. (2017). Pre-Clinical Antigenicity Studies of an Innovative Multivalent Vaccine for Human Visceral Leishmaniasis. *PloS Negl. Trop. Dis.* 11 (11), e0005951. doi: 10.1371/journal.pntd.0005951
- Cedillo-Rivera, R., Leal, Y. A., Yépez-Mulia, L., Gómez-Delgado, A., Ortega-Pierres, G., Tapia-Conyer, R., et al. (2009). Seroepidemiology of Giardiasis in Mexico. *Am. J. Trop. Med. Hyg.* 80 (1), 6–10. doi: 10.4269/ajtmh.2009.80.6
- Cotton, J., Amat, C., and Buret, A. (2015). Disruptions of Host Immunity and Inflammation by Giardia Duodenalis: Potential Consequences for Co-Infections in the Gastro-Intestinal Tract. *Pathogens* 4 (4), 764–792. doi: 10.3390/pathogens4040764
- Cotton, J. A., Beatty, J. K., and Buret, A. G. (2011). Host Parasite Interactions and Pathophysiology in Giardia Infections. *Int. J. Parasitol.* 41 (9), 925–933. doi: 10.1016/j.ijpara.2011.05.002
- Crumpton, M. J. (1974). "CHAPTER 1 - Protein Antigens: The Molecular Bases of Antigenicity and Immunogenicity,". *The antigens*. Academic Press, p. 1–78. doi: 10.1016/B978-0-12-635502-4.50008-4.
- Dann, S. M., Manthey, C. F., Le, C., Miyamoto, Y., Gima, L., Abraham, A., et al. (2015). IL-17A Promotes Protective IgA Responses and Expression of Other Potential Effectors Against the Lumen-Dwelling Enteric Parasite Giardia. *Exp. Parasitol.* 156, 68–78. doi: 10.1016/j.exppara.2015.06.003
- Davids, B. J., Liu, C. M., Hanson, E. M., Le, C. H. Y., Ang, J., Hanevik, K., et al. (2019). Identification of Conserved Candidate Vaccine Antigens in the Surface Proteome of Giardia Lamblia. *Infect. Immun.* 87 (6), 1–14. doi: 10.1128/IAI.00219-19
- Davids, B. J., Palm, J. E. D., Housley, M. P., Smith, J. R., Andersen, Y. S., Martin, M. G., et al. (2006). Polymeric Immunoglobulin Receptor in Intestinal Immune Defense Against the Lumen-Dwelling Protozoan Parasite Giardia. *J. Immunol.* 177 (9), 6281–6290. doi: 10.4049/jimmunol.177.9.6281
- Dissanayake, S. K., Tuera, N., and Ostrand-Rosenberg, S. (2005). Presentation of Endogenously Synthesized MHC Class II-Restricted Epitopes by MHC Class II Cancer Vaccines Is Independent of Transporter Associated With Ag

- Processing and the Proteasome. *J. Immunol.* 174 (4), 1811–1819. doi: 10.4049/jimmunol.174.4.1811
- Dreesen, L., De Bosscher, K., Grit, G., Staels, B., Lubberts, E., Bauge, E., et al. (2014). Giardia Muris Infection in Mice Is Associated With a Protective Interleukin 17a Response and Induction of Peroxisome Proliferator-Activated Receptor Alpha. *Infect. Immun.* 82 (8), 3333–3340. doi: 10.1128/IAI.01536-14
- Eckmann, L. (2003). Mucosal Defences Against Giardia. *Parasite Immunol.* 25, 259–270. doi: 10.1046/j.1365-3024.2003.00634.x
- El-Beshbishi, S., Elblihi, A., Atia, R., Megahed, A., and Auf, F. (2020). Human Leukocyte Antigen Class-II DRB1 Alleles and Giardia Lamblia Infection in Children: A Case-Control Study. *Asian Pac. J. Trop. Med.* 13 (2), 56–61. doi: 10.4103/1995-7645.275413
- El-Manzalawy, Y., Dobbs, D., and Honavar, V. (2008). Predicting Linear B-Cell Epitopes Using String Kernels. *J. Mol. Recognit.* 21 (4), 243–255. doi: 10.1002/jmr.893
- Feliziani, C., Merino, M. C., Rivero, M. R., Hellman, U., Pistoiresi-Palencia, M. C., and Rápalo, A. S. (2011). Immunodominant Proteins α -1 Giardin and β -Giardin Are Expressed in Both Assemblages A and B of Giardia Lamblia. *BMC Microbiol.* 11 (1), 233. doi: 10.1186/1471-2180-11-233
- Feng, X. M., Zheng, W. Y., Zhang, H. M., Shi, W. Y., Li, Y., Cui, B. J., et al. (2016). Vaccination With Bivalent DNA Vaccine of A1-Giardin and Cwp2 Delivered by Attenuated Salmonella Typhimurium Reduces Trophozoites and Cysts in the Feces of Mice Infected With Giardia Lamblia. *PloS One* 11 (6), 1–16. doi: 10.1371/journal.pone.0157872
- Foged, C., Brodin, B., Frokjaer, S., and Sundblad, A. (2005). Particle Size and Surface Charge Affect Particle Uptake by Human Dendritic Cells in an *In vitro* Model. *Int. J. Pharm.* 298 (2), 315–322. doi: 10.1016/j.ijpharm.2005.03.035
- Franzén, O., Jerlström-Hultqvist, J., Castro, E., Sherwood, E., Ankarklev, J., Reiner, D. S., et al. (2009). Draft Genome Sequencing of Giardia Intestinalis Assemblage B Isolate GS: Is Human Giardiasis Caused by Two Different Species? *PloS Pathog.* 5 (8), e1000560. doi: 10.1371/journal.ppat.1000560
- Garzon, T., Valencia, L., Dominguez, V., Rascon, L., Quintero, J., Garibay-Escobar, A., et al. (2020). Differential Antibody Responses to Giardia Lamblia Strain Variants Expressing Dissimilar Levels of an Immunogenic Protein. *Parasite Immunol.* 42 (10), 1–11. doi: 10.1111/pim.12767
- Goodswen, S. J., Kennedy, P. J., and Ellis, J. T. (2017). On the Application of Reverse Vaccinology to Parasitic Diseases: A Perspective on Feature Selection and Ranking of Vaccine Candidates. *Int. J. Parasitol.* 47 (12), 779–790. doi: 10.1016/j.ijpara.2017.08.004
- Greenbaum, J., Sidney, J., Chung, J., Brander, C., Peters, B., and Sette, A. (2011). Functional Classification of Class II Human Leukocyte Antigen (HLA) Molecules Reveals Seven Different Supertypes and a Surprising Degree of Repertoire Sharing Across Supertypes. *Immunogenetics* 63 (6), 325–335. doi: 10.1007/s00251-011-0513-0
- Grit, G. H., Van Coppenolle, S., Devriendt, B., Geurden, T., Dreesen, L., Hope, J., et al. (2014). Evaluation of Cellular and Humoral Systemic Immune Response Against Giardia Duodenalis Infection in Cattle. *Vet. Parasitol.* 202 (3–4), 145–155. doi: 10.1016/j.vetpar.2014.03.012
- Gupta, S., Ansari, H. R., Gautam, A., and Raghava, G. P. S. (2013). Identification of B-Cell Epitopes in an Antigen for Inducing Specific Class of Antibodies. *Biol. Direct* 8 (1), 1–15. doi: 10.1186/1745-6150-8-27
- Hanevik, K., Kristoffersen, E., Svard, S., Bruserud, O., Ringqvist, E., Sørnes, S., et al. (2011). Human Cellular Immune Response Against Giardia Lamblia 5 Years After Acute Giardiasis. *J. Infect. Dis.* 204 (11), 1779–1786. doi: 10.1093/infdis/jir639
- Hehl, A. B., Marti, M., and Köhler, P. (2000). Stage-Specific Expression and Targeting of Cyst Wall Protein-Green Fluorescent Protein Chimeras in Giardia. *Mol. Biol. Cell* 11 (5), 1789–1800. doi: 10.1091/mbc.11.5.1789
- He, Y., Xiang, Z., and Mobley, H. L. T. (2010). Vaxign: The First Web-Based Vaccine Design Program for Reverse Vaccinology and Applications for Vaccine Development. *J. Biomed. Biotechnol.* 2010, 15. doi: 10.1155/2010/297505
- Heyworth, M. F., Carlson, J. R., and Ermak, T. H. (1987). Clearance of Giardia Muris Infection Requires Helper/Inducer T Lymphocytes. *J. Exp. Med.* 165 (6), 1743–1748. doi: 10.1084/jem.165.6.1743
- Hjøllo, T., Bratland, E., Steinsland, H., Radunovic, M., Langeland, N., and Hanevik, K. (2018). Longitudinal Cohort Study of Serum Antibody Responses Towards Giardia Lamblia Variant-Specific Surface Proteins in a Non-Endemic Area. *Exp. Parasitol.* 191 (May), 66–72. doi: 10.1016/j.exppara.2018.06.005
- Jenikova, G., Hruz, P., Andersson, M. K., Tejman-Yarden, N., Ferreira, P. C. D., Andersen, Y. S., et al. (2011). A1-Giardin Based Live Heterologous Vaccine Protects Against Giardia Lamblia Infection in a Murine Model. *Vaccine* 29 (51), 9529–9537. doi: 10.1016/j.vaccine.2011.09.126
- Jiménez-Cardoso, E., Eligio-García, L., and Cortés-Campos, A. (2002). Evaluación De La Capacidad Immunogénica De La Vacuna Giardia-Vax, Utilizando Un Modelo Experimental De Giardiasis En Geros (Meriones Unguiculatus). *Vet. Mex.* 33 (1), 49–54. doi: 10.21753/vmoa.33.001.60
- Jiménez, J. C., Fontaine, J., Creusy, C., Fleurisse, L., Grzych, J. M., Capron, M., et al. (2014). Antibody and Cytokine Responses to Giardia Excretory/Secretory Proteins in Giardia Intestinalis-Infected BALB/c Mice. *Parasitol. Res.* 113 (7), 2709–2718. doi: 10.1007/s00436-014-3927-4
- Jiskoot, W., Kersten, G. F. A., Mastrobattista, E., and Slütter, B. (2019). “Chapter 22-Vaccines,” in *Pharmaceutical Biotechnology: Fundamentals and Applications*. Eds. D. J. A. Crommelin, R. D. Sindelar and B. Meibohm, Springer. 281–304.
- Kamda, J. D., Nash, T. E., and Singer, S. M. (2012). Giardia Duodenalis: Dendritic Cell Defects in IL-6 Deficient Mice Contribute to Susceptibility to Intestinal Infection. *Exp. Parasitol.* 130 (3), 288–291. doi: 10.1016/j.exppara.2012.01.003
- Karosiene, E., Rasmussen, M., Blicher, T., Lund, O., Buus, S., and Nielsen, M. (2013). NetMHCIIpan-3.0, a Common Pan-Specific MHC Class II Prediction Method Including All Three Human MHC Class II Isotypes, HLA-DR, HLA-DP and HLA-DQ. *Immunogenetics* 65 (10), 711–724. doi: 10.1007/s00251-013-0720-y
- Kaufmann, S. H. E., and Hess, J. (1999). Impact of Intracellular Location of and Antigen Display by Intracellular Bacteria: Implications for Vaccine Development. *Immunol. Lett.* 65 (1–2), 81–84. doi: 10.1016/S0165-2478(98)00128-X
- Kyes, S. A., Kraemer, S. M., and Smith, J. D. (2007). Antigenic Variation in Plasmodium Falciparum: Gene Organization and Regulation of the Var Multigene Family. *Eukaryot. Cell* 6, 1511–1520. doi: 10.1128/EC.00173-07
- Landais, E., Romagnoli, P. A., Corper, A. L., Shires, J., Altman, J. D., Wilson, I. A., et al. (2009). New Design of MHC Class II Tetramers to Accommodate Fundamental Principles of Antigen Presentation. *J. Immunol.* 183 (12), 7949–7957. doi: 10.4049/jimmunol.0902493
- Larocque, R., Nakagaki, K., Lee, P., Abdul-Wahid, A., and Faubert, G. M. (2003). Oral Immunization of BALB/c Mice With Giardia Duodenalis Recombinant Cyst Wall Protein Inhibits Shedding of Cysts. *Infect. Immun.* 71 (10), 5662–5669. doi: 10.1128/IAI.71.10.5662-5669.2003
- Laurens, M. B. (2020). RTS,S/AS01 Vaccine (Mosquirix™): An Overview. *Hum. Vaccin. Immunother.* 16 (3), 480–489. doi: 10.1080/21645515.2019.1669415
- Lee, P., Abdul-Wahid, A., and Faubert, G. M. (2009). Comparison of the Local Immune Response Against Giardia Lamblia Cyst Wall Protein 2 Induced by Recombinant Lactococcus Lactis and Streptococcus Gordonii. *Microbes Infect.* 11 (1), 20–28. doi: 10.1016/j.micinf.2008.10.002
- Lee, H. Y., Kim, J., Noh, H. J., Kim, H. P., and Park, S. J. (2014). Giardia Lamblia Binding Immunoglobulin Protein Triggers Maturation of Dendritic Cells via Activation of TLR4-MyD88-P38 and ERK1/2 MAPKs. *Parasite Immunol.* 36 (12), 627–646. doi: 10.1111/pim.12119
- Lima, T. S., and Lodoen, M. B. (2019). Mechanisms of Human Innate Immune Evasion by Toxoplasma Gondii. *Front. Cell. Infect. Microbiol.* 9 (MAR), 1–8. doi: 10.3389/fcimb.2019.00103
- Li, E., Zhou, P., Petrin, Z., and Singer, S. M. (2004). Mast Cell-Dependent Control of Giardia Lamblia Infections in Mice. *Infect. Immun.* 72 (11), 6642–6649. doi: 10.1128/IAI.72.11.6642-6649.2004
- Lopez-Romero, G., Garzon, T., Rascon, R., Valdez, A., Quintero, J., Arvizu-Flores, A. A., et al. (2017). Characterization of BIP Protein of G. Lamblia as a Potential Immunogen in a Mouse Infection Model. *Immunobiology* 222 (8–9), 884–891. doi: 10.1016/j.imbio.2017.05.008
- Lopez-Romero, G., Quintero, J., Astiazarán-García, H., and Velazquez, C. (2015). Host Defences Against Giardia Lamblia. *Parasite Immunol.* 37 (8), 394–406. doi: 10.1111/pim.12210
- Lovitch, S. B., and Unanue, E. R. (2005). Conformational Isomers of a Peptide-Class II Major Histocompatibility Complex. *Immunol. Rev.* 207, 293–313. doi: 10.1111/j.0105-2896.2005.00298.x
- Lujan, H. D. (2006). Giardia and Giardiasis | Giardia Y Giardiasis. *Medicina* 66 (1), 70–74.

- Lujan, H. D. (2011). Mechanisms of Adaptation in the Intestinal Parasite *Giardia* *Lamb*lia. *Essays Biochem.* 51 (1), 177–191. doi: 10.1042/bse0510177
- Lujan, H. D., Mowatt, M. R., Conrad, J. T., Bowers, B., and Nash, T. E. (1995). Identification of a Novel *Giardia* *Lamb*lia Cyst Wall Protein With Leucine-Rich Repeats: Implications for Secretory Granule Formation and Protein Assembly Into the Cyst Wall. *J. Biol. Chem.* 270 (49), 29307–29313. doi: 10.1074/jbc.270.49.29307
- Lujan, H. D., and Svard, S. (2011). *Giardia* A Model Organism. Wien: Springer, vol. 2011, 31–402.
- Ma'ayeh, S. Y., Liu, J., Peirasmaki, D., Hörnaeus, K., Lind, S. B., Grabherr, M., et al. (2017). Characterization of the *Giardia* *Intestinalis* Secretome During Interaction With Human Intestinal Epithelial Cells: The Impact on Host Cells. *PLoS Negl. Trop. Dis.* 11 (12), e0006120. doi: 10.1371/journal.pntd.0006120
- Malonis, R. J., Lai, J. R., and Vergnolle, O. (2020). Peptide-Based Vaccines: Current Progress and Future Challenges. *Chem. Rev.* 120 (6), 3210–3229. doi: 10.1021/acs.chemrev.9b00472
- McCaffery, J. M., Faubert, G. M., and Gillin, F. D. (1994). *Giardia* *Lamb*lia: Traffic of a Trophozoite Variant Surface Protein and a Major Cyst Wall Epitope During Growth, Encystation, and Antigenic Switching. *Exp. Parasitol.* 79 (3), 236–249. doi: 10.1006/expr.1994.1087
- McFarland, B. J., Sant, A. J., Lybrand, T. P., and Beeson, C. (1999). Ovalbumin (323–339) Peptide Binds to the Major Histocompatibility Complex Class II I-A (d) Protein Using Two Functionally Distinct Registers. *Biochemistry* 38 (50), 16663–16670. doi: 10.1021/bi991393l
- Montagnoli, C., Sandini, S., Bacci, A., Romani, L., and La Valle, R. (2004). Immunogenicity and Protective Effect of Recombinant Enolase of *Candida Albicans* in a Murine Model of Systemic Candidiasis. *Med. Mycol.* 42 (4), 319–324. doi: 10.1080/13693780310001644653
- Moormann, A. M., Nixon, C. E., and Forconi, C. S. (2019). Immune Effector Mechanisms in Malaria: An Update Focusing on Human Immunity. *Parasite Immunol.* 41 (8), 1–14. doi: 10.1111/pim.12628
- Mora, M., and Telford, J. L. (2010). Genome-Based Approaches to Vaccine Development. *J. Mol. Med.* 88 (2), 143–147. doi: 10.1007/s00109-009-0574-9
- Mukherjee, S., Huda, S., and Sinha Babu, S. P. (2019). Toll-Like Receptor Polymorphism in Host Immune Response to Infectious Diseases: A Review. *Scand. J. Immunol.* 90 (1), 1–18. doi: 10.1111/sji.12771
- Nash, T. E., and Aggarwal, A. (1986). Cytotoxicity of Monoclonal Antibodies to a Subset of *Giardia* Isolates. *J. Immunol.* 136 (7), 2628 LP–2632.
- Nash, T. E., Merritt, J. W., and Conrad, J. T. (1991). Isolate and Epitope Variability in Susceptibility of *Giardia* *Lamb*lia to Intestinal Proteases. *Infect. Immun.* 59 (4), 1334–1340. doi: 10.1128/iai.59.4.1334-1340.1991
- Nelson, C. A., Roof, R. W., McCourt, D. W., and Unanue, E. R. (1992). Identification of the Naturally Processed Form of Hen Egg White Lysozyme Bound to the Murine Major Histocompatibility Complex Class II Molecule I-Ak. *Proc. Natl. Acad. Sci. USA* 89 (16), 7380–7383. doi: 10.1073/pnas.89.16.7380
- Nielsen, M., Lundegaard, C., Blicher, T., Peters, B., Sette, A., Justesen, S., et al. (2008). Quantitative Predictions of Peptide Binding to Any HLA-DR Molecule of Known Sequence: NetMHCIIpan. *PLoS Comput. Biol.* 4 (7), 1–10. doi: 10.1371/journal.pcbi.1000107
- Olson, M. E., Ceri, H., and Morck, D. W. (2000). *Giardia* Vaccination. *Parasitol. Today* 16 (5), 213–217. doi: 10.1016/S0169-4758(99)01623-3
- Palm, J. E. D., Weiland, M. E.-L., Griffiths, W. J., Ljungström, I., and Svärd, S. G. (2003). Identification of Immunoreactive Proteins During Acute Human Giardiasis. *J. Infect. Dis.* 187 (12), 1849–1859. doi: 10.1086/375356
- Papanastasiou, P., Bruderer, T., Li, Y., Bommeli, C., and Köhler, P. (1997). Primary Structure and Biochemical Properties of a Variant-Specific Surface Protein of *Giardia* 1Note: The Nucleotide Sequence Information Reported in This Paper Has Been Submitted to the EMBL Data Library With the Accession No. Z83743.1. *Mol. Biochem. Parasitol.* 86 (1), 13–27. doi: 10.1016/S0166-6851(97)02836-3
- Paul, S., Sidney, J., Sette, A., and Peters, B. (2016). TepiTool: A Pipeline for Computational Prediction of T Cell Epitope Candidates. *Curr. Protoc. Immunol.* 114, 18.19.1–18.19.24. doi: 10.1002/cpim.12
- Pertsemliadis, A., and Fondon, J. W. (2001). Having a BLAST With Bioinformatics (and Avoiding BLASTphemy). *Genome Biol.* 2 (10), reviews2002.1. doi: 10.1186/gb-2001-2-10-reviews2002
- Potocnakova, L., Bhide, M., and Borszekova Pulzova, L. (2016). An Introduction to B-Cell Epitope Mapping and *In Silico* Epitope Prediction. *J. Immunol. Res.* 2016, 11. doi: 10.1155/2016/6760830
- Priest, J. W., Mehlert, A., Arrowood, M. J., Riggs, M. W., and Ferguson, M. A. J. (2003). Characterization of a Low Molecular Weight Glycolipid Antigen From *Cryptosporidium Parvum*. *J. Biol. Chem.* 278 (52), 52212–52222. doi: 10.1074/jbc.M306835200
- Quintero, J., Valdez, A., Samaniego, B., Lopez-Romero, G., Astiazaran-Garcia, H., Rascon, L., et al. (2017). Isolation and Partial Characterization of an Immunogenic Antigen of *Giardia* *Lamb*lia. *Parasitol. Int.* 66 (3), 324–330. doi: 10.1016/j.parint.2017.01.007
- Radunovic, M., Klotz, C., Saghaug, C. S., Brattbakk, H. R., Aebischer, T., Langeland, N., et al. (2017). Genetic Variation in Potential *Giardia* Vaccine Candidates Cyst Wall Protein 2 and A1-Giardin. *Parasitol. Res.* 116 (8), 2151–2158. doi: 10.1007/s00436-017-5516-9
- Reiner, D. S., and Gillin, F. D. (1991). Human Secretory and Serum Antibodies Recognize Environmentally Induced Antigens of *Giardia* *Lamb*lia. *Infect. Immun.* 60 (2), 637–643. doi: 10.1128/iai.60.2.637-643.1992
- Rhee, J. H., Lee, S. E., and Kim, S. Y. (2012). Mucosal Vaccine Adjuvants Update. *Clin. Exp. Vaccine Res.* 1 (1), 50–63. doi: 10.7774/cevr.2012.1.1.50
- Rivero, F. D., Saura, A., Prucca, C. G., Carranza, P. G., Torri, A., and Lujan, H. D. (2010). Disruption of Antigenic Variation Is Crucial for Effective Parasite Vaccine. *Nat. Med.* 16 (5), 551–557. doi: 10.1038/nm.2141
- Robledo-Castillo, R., Ros-Lucas, A., Martinez-Peinado, N., and Alonso-Padilla, J. (2021). An Overview of Current Uses and Future Opportunities for Computer-Assisted Design of Vaccines for Neglected Tropical Diseases. *Adv. Appl. Bioinform. Chem.* 14, 25–47. doi: 10.2147/AABC.S258759
- Roport, C., and Gazzinelli, R. T. (2000). Signaling of Immune System Cells by Glycosylphosphatidylinositol (GPI) Anchor and Related Structures Derived From Parasitic Protozoa. *Curr. Opin. Microbiol.* 3 (4), 395–403. doi: 10.1016/S1369-5274(00)00111-9
- Roxström-Lindquist, K., Ringqvist, E., Palm, D., and Svärd, S. (2005). *Giardia* *Lamb*lia-Induced Changes in Gene Expression in Differentiated Caco-2 Human Intestinal Epithelial Cells. *Infect. Immun.* 73 (12), 8204–8208. doi: 10.1128/IAI.73.12.8204-8208.2005
- Saghaug, C. S., Sörnes, S., Peirasmaki, D., Svärd, S., Langeland, N., and Hanevik, K. (2015). Human Memory CD4+ T Cell Immune Responses Against *Giardia* *Lamb*lia. *Clin. Vaccine Immunol.* 23 (1), 11–18. doi: 10.1128/CVI.00419-15
- Scott, K. G. E., Yu, L. C. H., and Buret, A. G. (2004). Role of CD8+ and CD4+ T Lymphocytes in Jejunal Mucosal Injury During Murine Giardiasis. *Infect. Immun.* 72 (6), 3536–3542. doi: 10.1128/IAI.72.6.3536-3542.2004
- Serradell, M. C., Gargantini, P. R., Saura, A., Oms, S. R., Rupil, L. L., Berod, L., et al. (2018). Cytokines, Antibodies, and Histopathological Profiles During *Giardia* Infection and Variant-Specific Surface Protein-Based Vaccination. *Infect. Immun.* 86 (6), e00773–e00717. doi: 10.1128/IAI.00773-17
- Serradell, M. C., Rupil, L. L., Martino, R. A., Prucca, C. G., Carranza, P. G., Saura, A., et al. (2019). Efficient Oral Vaccination by Bioengineering Virus-Like Particles With Protozoan Surface Proteins. *Nat. Commun.* 10 (1), 361. doi: 10.1038/s41467-018-08265-9
- Serradell, M. C., Saura, A., Rupil, L. L., Gargantini, P. R., Faya, M. I., Furlan, P. J., et al. (2016). Vaccination of Domestic Animals With a Novel Oral Vaccine Prevents *Giardia* Infections, Alleviates Signs of Giardiasis and Reduces Transmission to Humans. *NPJ Vaccines* 1, 16018. doi: 10.1038/npjvaccines.2016.18
- Shimoda, M., and Koni, P. A. (2007). MHC-Restricted B-Cell Antigen Presentation in Memory B-Cell Maintenance and Differentiation. *Crit. Rev. Immunol.* 27 (1), 47–60. doi: 10.1615/CritRevImmunol.v27.i1.40
- Singer, S. M. (2016). Control of Giardiasis by Interleukin-17 in Humans and Mice - Are the Questions All Answered? *Clin. Vaccine Immunol.* 23 (1), 2–5. doi: 10.1128/CVI.00648-15
- Singer, S. M., and Nash, T. E. (2000). T-Cell-Dependent Control of Acute *Giardia* *Lamb*lia Infections in Mice. *Infect. Immun.* 68 (1), 170–175. doi: 10.1128/IAI.68.1.170-175.2000
- Skwarczynski, M., and Toth, I. (2016). Peptide-Based Synthetic Vaccines. *Chem. Sci.* 7 (2), 842–854. doi: 10.1039/C5SC03892H
- Smith, N. C., Sinden, R. E., and Ramakrishnan, C. (2021). Editorial: Get Over the Gut: Apicomplexan Parasite Interaction, Survival and Stage Progression in

- Vertebrate and Invertebrate Digestive Tracts 11, 680555. doi: 10.3389/fcimb.2021.680555
- Stäger, S., Felleisen, R., Gottstein, B., and Müller, N. (1997). Giardia Lamblia Variant Surface Protein H7 Stimulates a Heterogeneous Repertoire of Antibodies Displaying Differential Cytological Effects on the Parasite. *Mol. Biochem. Parasitol.* 85 (1), 113–124. doi: 10.1016/S0166-6851(96)02818-6
- Stäger, S., Gottstein, B., Sager, H., Jungi, T. W., and Müller, N. (1998). Influence of Antibodies in Mother's Milk on Antigenic Variation of Giardia Lamblia in the Murine Mother-Offspring Model of Infection. *Infect. Immun.* 66 (4), 1287–1292. doi: 10.1128/IAI.66.4.1287-1292.1998
- Stein, J. E., Radecki, S. V., and Lappin, M. R. (2003). Efficacy of Giardia Vaccination in the Treatment of Giardiasis in Cats. *J. Am. Vet. Med. Assoc.* 222 (11), 1548–1551. doi: 10.2460/javma.2003.222.1548
- Strong, B. S.I., and Unanue, E. R. (2011). Presentation of Type B Peptide-MHC Complexes From Hen Egg White Lysozyme by TLR Ligands and Type I IFNs Independent of H2-DM Regulation. *J. Immunol. (Baltimore Md.: 1950)* 187 (5), 2193–2201. doi: 10.4049/jimmunol.1100152
- Sun, C. H. J., McCaffery, M., Reiner, D. S., and Gillin, F. D. (2003). Mining the Giardia Lamblia Genome for New Cyst Wall Proteins. *J. Biol. Chem.* 278 (24), 21701–21708. doi: 10.1074/jbc.M302023200
- Tedla, M. G., Every, A. L., and Scheerlinck, J. P. Y. (2019). Investigating Immune Responses to Parasites Using Transgenesis. *Parasit. Vectors* 12 (1), 1–14. doi: 10.1186/s13071-019-3550-4
- Teh-Poot, C., Tzec-Arjona, E., Martínez-Vega, P., Jesus Ramirez-Sierra, M., Rosado-Vallado, M., and Dumonteil, E. (2015). From Genome Screening to Creation of Vaccine Against Trypanosoma Cruzi by Use of Immunoinformatics. *J. Infect. Dis.* 211 (2), 258–266. doi: 10.1093/infdis/jiu418
- Téllez, A., Palm, D., Weiland, M., Alemán, J., Winięcka-Krusnell, J., Linder, E., et al. (2005). Secretory Antibodies Against Giardia Intestinalis in Lactating Nicaraguan Women. *Parasite Immunol.* 27 (5), 163–169. doi: 10.1111/j.1365-3024.2005.00758.x
- Troeger, H., Joerg Epple, H., Schneider, T., Wahnschaffe, U., Ullrich, R., Burchard, G. D., et al. (2007). Effect of Chronic Giardia Lamblia Infection on Epithelial Transport and Barrier Function in Human Duodenum. *Gut* 56 (3), 328–335. doi: 10.1136/gut.2006.100198
- Uwase, J., Chu, R., Kassegne, K., Lei, Y., Shen, F., Fu, H., et al. (2020). Immunogenicity Analysis of Conserved Fragments in Plasmodium Ovale Species Merozoite Surface Protein 4. *Malaria J.* 19 (1), 1–11. doi: 10.1186/s12936-020-03207-7
- Vakili, B., Nezafat, N., Zare, B., Erfani, N., Akbari, M., Ghasemi, Y., et al. (2020). A New Multi-Epitope Peptide Vaccine Induces Immune Responses and Protection Against Leishmania Infantum in BALB/c Mice. *Med. Microbiol. Immunol.* 209 (1), 69–79. doi: 10.1007/s00430-019-00640-7
- Velazquez, C., Beltran, M., Ontiveros, N., Rascon, L., Figueroa, D. C., Granados, A. J., et al. (2005). Giardia Lamblia Infection Induces Different Secretory and Systemic Antibody Responses in Mice. *Parasite Immunol.* 27 (9), 351–356. doi: 10.1111/j.1365-3024.2005.00793.x
- Velazquez, C., Vidavsky, I., Der Van Drift, K., Gross, M. L., and Unanue, E. R. (2002). Chemical Identification of a Low Abundance Lysozyme Peptide Family Bound to I-A K Histocompatibility Molecules. *J. Biol. Chem.* 277 (45), 42514–42522. doi: 10.1074/jbc.M202316200
- Venkatesan, P., Finch, R. G., and Wakelin, D. (1997). A Comparison of Mucosal Inflammatory Responses to Giardia Muris in Resistant B10 and Susceptible BALB/c Mice. *Parasite Immunol.* 19 (3), 137–143. doi: 10.1046/j.1365-3024.1997.d01-189.x
- Wang, P., Sidney, J., Dow, C., Mothé, B., Sette, A., and Peters, B. (2008). A Systematic Assessment of MHC Class II Peptide Binding Predictions and Evaluation of a Consensus Approach. *PLoS Comput. Biol.* 4 (4), e1000048. doi: 10.1371/journal.pcbi.1000048
- Wang, P., Sidney, J., Kim, Y., Sette, A., Lund, O., Nielsen, M., et al. (2010). Peptide Binding Predictions for HLA DR, DP and DQ Molecules. *BMC Bioinformatics* 11 (1), 568. doi: 10.1186/1471-2105-11-568
- Wang, Y., Yi, L., Sun, L. Y., Liu, Y. C., Wen, W. Y., Li, X. K., et al. (2020). Identification and Characterization of a Streptococcus Suis Immunogenic Ornithine Carbamoyltransferase Involved in Bacterial Adherence. *J. Microbiol. Immunol. Infect.* 53 (2), 234–239. doi: 10.1016/j.jmii.2018.05.004
- Weaver, C. T., Harrington, L. E., Mangan, P. R., Gavioli, M., and Murphy, K. M. (2006). Th17: An Effector CD4 T Cell Lineage With Regulatory T Cell Ties. *Immunity* 24 (6), 677–688. doi: 10.1016/j.immuni.2006.06.002
- Weiland, M. E.L., Palm, J.E.D., Griffiths, W. J., McCaffery, J.M., and Svård, S. G. (2003). Characterisation of Alpha-1 Gardin: An Immunodominant Giardia Lamblia Annexin With Glycosaminoglycan-Binding Activity. *Int. J. Parasitol.* 33 (12), 1341–1351. doi: 10.1016/S0020-7519(03)00201-7
- Wong-Baeza, I., Alcántara-Hernández, M., Mancilla-Herrera, I., Ramírez-Saldivar, I., Arriaga-Pizano, L., Ferat-Osorio, E., et al. (2010). The Role of Lipopeptidophosphoglycan in the Immune Response to Entamoeba Histolytica. *J. Biomed. Biotechnol.* 2010, 254521. doi: 10.1155/2010/254521
- Xiang, Z., and He, Y. (2009). Vaxign: A Web-Based Vaccine Target Design Program for Reverse Vaccinology. *Proc. Vaccinol.* 1 (1), 23–29. doi: 10.1016/j.provac.2009.07.005

Conflict of Interest: The authors declare that the research was conducted in the absence of any commercial or financial relationships that could be construed as a potential conflict of interest.

Publisher's Note: All claims expressed in this article are solely those of the authors and do not necessarily represent those of their affiliated organizations, or those of the publisher, the editors and the reviewers. Any product that may be evaluated in this article, or claim that may be made by its manufacturer, is not guaranteed or endorsed by the publisher.

Copyright © 2021 Garzon, Ortega-Tirado, Lopez-Romero, Alday, Robles-Zepeda, Garibay-Escobar and Velazquez. This is an open-access article distributed under the terms of the Creative Commons Attribution License (CC BY). The use, distribution or reproduction in other forums is permitted, provided the original author(s) and the copyright owner(s) are credited and that the original publication in this journal is cited, in accordance with accepted academic practice. No use, distribution or reproduction is permitted which does not comply with these terms.



EhVps23: A Component of ESCRT-I That Participates in Vesicular Trafficking and Phagocytosis of *Entamoeba histolytica*

OPEN ACCESS

Edited by:

Natalia de Miguel,
CONICET Instituto Tecnológico de
Chascomús (INTECH), Argentina

Reviewed by:

Serge Ankri,
Technion Israel Institute of
Technology, Israel
Lesly Temesvari,
Clemson University, United States

*Correspondence:

Esther Orozco
esther@cinvestav.mx

Specialty section:

This article was submitted to
Parasite and Host,
a section of the journal
Frontiers in Cellular and
Infection Microbiology

Received: 04 September 2021

Accepted: 12 October 2021

Published: 29 October 2021

Citation:

Galindo A, Javier-Reyna R,
García-Rivera G, Bañuelos C,
Montaño S, Ortega-Lopez J,
Chávez-Munguía B, Salazar-Villatoro L
and Orozco E (2021) EhVps23:
A Component of ESCRT-I
That Participates in Vesicular
Trafficking and Phagocytosis of
Entamoeba histolytica.
Front. Cell. Infect. Microbiol. 11:770759.
doi: 10.3389/fcimb.2021.770759

Ausencio Galindo¹, Rosario Javier-Reyna¹, Guillermina García-Rivera¹, Cecilia Bañuelos²,
Sarita Montaño³, Jaime Ortega-Lopez⁴, Bibiana Chávez-Munguía¹,
Lizbeth Salazar-Villatoro¹ and Esther Orozco^{1*}

¹ Departamento de Infectómica y Patogénesis Molecular, Centro de Investigación y de Estudios Avanzados del IPN, Ciudad de México, México, ² Programa Transdisciplinario en Desarrollo Científico y Tecnológico para la Sociedad, Centro de Investigación y de Estudios Avanzados del IPN, Ciudad de México, México, ³ Laboratorio de Bioinformática y Simulación Molecular, Facultad de Ciencias Químico-Biológicas, Universidad Autónoma de Sinaloa, Sinaloa, México, ⁴ Departamento de Biotecnología y Bioingeniería, Centro de Investigación y de Estudios Avanzados del IPN, Ciudad de México, México

The endosomal sorting complex required for transport (ESCRT) is formed by ESCRT-0, ESCRT-I, ESCRT-II, ESCRT-III complexes, and accessory proteins. It conducts vesicular trafficking in eukaryotes through the formation of vesicles and membrane fission and fusion events. The trophozoites of *Entamoeba histolytica*, the protozoan responsible for human amoebiasis, presents an active membrane movement in basal state that increases during phagocytosis and tissue invasion. ESCRT-III complex has a pivotal role during these events, but ESCRT-0, ESCRT-I and ESCRT-II have been poorly studied. Here, we unveiled the *E. histolytica* ESCRT-I complex and its implication in vesicular trafficking and phagocytosis, as well as the molecular relationships with other phagocytosis-involved molecules. We found a gene encoding for a putative EhVps23 protein with the ubiquitin-binding and Vps23 core domains. In basal state, it was in the plasma membrane, cytoplasmic vesicles and multivesicular bodies, whereas during phagocytosis it was extensively ubiquitinated and detected in phagosomes and connected vesicles. Docking analysis, immunoprecipitation assays and microscopy studies evidenced its interaction with EhUbiquitin, EhADH, EhVps32 proteins, and the lysobisphosphatidic acid phospholipid. The knocking down of the *EhVps23* gene resulted in lower rates of phagocytosis. Our results disclosed the concert of finely regulated molecules and vesicular structures participating in vesicular trafficking-related events with a pivotal role of EhVps23.

Keywords: vesicular trafficking, *Entamoeba histolytica*, ESCRT, phagocytosis, EhVps23

INTRODUCTION

The plasma and internal membranes of the trophozoites of *Entamoeba histolytica*, the protozoan responsible of human amoebiasis, (WHO, 1997), are constantly producing invaginations, forming vesicles that fuse and split, and generating endosomes, multivesicular bodies (MVBs), tubes and pseudopodia; events necessary to capture, ingest and digest the prey, as well as for the selection of proteins that will be recycled or secreted. The incessant internal movements and the avid phagocytosis of the parasite are linked to its ability to invade tissues. Several molecules have been already identified as involved in these tasks (Bolaños et al., 2016; Castellanos-Castro et al., 2016a), but the molecular events underlying them are not well understood.

The endosomal sorting complex required for transport (ESCRT), formed by the ESCRT-0, ESCRT-I, ESCRT-II, ESCRT-III complexes, and accessory proteins, is one of the main players in vesicle trafficking. Proteins that conform these complexes differ in sequence along organisms through the evolutionary scale (Leung et al., 2008), but conserve their functional domains that allow them to participate in cell division, endocytosis, virus budding and other functions (Calistri et al., 2021). In *E. histolytica*, ESCRT machinery is involved in phagocytosis (Lopez-Reyes et al., 2010; Avalos-Padilla et al., 2015; Avalos-Padilla et al., 2018), a virulence landmark of the parasite (García-Rivera et al., 1999). Thus, this protozoan is an excellent model to study the ESCRT machinery and its role in events involving vesicular trafficking, such as phagocytosis and tissue invasion (Alfred and Vaccari, 2016; Liu et al., 2019; Vietri et al., 2020).

At least 15 out of 20 ESCRT genes detected in *E. histolytica* are transcribed (Lopez-Reyes et al., 2010), and four of them, and the *Ehadh* gene, whose product is an associated protein of the ESCRT machinery (Bañuelos et al., 2012), appeared down- or up-regulated during phagocytosis. EhADH, an ALIX family protein involved in adhesion, interacts with EhVps32, a member of ESCRT-III, during MVBs formation (Bañuelos et al., 2012). In yeast, the Bro1 protein, an EhADH orthologue, forms a bridge between ESCRT-I and ESCRT-III complexes (Strack et al., 2003; Nikko and André, 2007).

The assembly sequence of *E. histolytica* ESCRT-III proteins on the endosomal membrane is essential for intraluminal vesicles (ILVs) formation (Avalos-Padilla et al., 2018). The active EhVps20 binds first to membranes and interacts with the active EhVps32, causing invaginations. EhVps32 recruits EhVps24 that allows the detachment of nascent vesicles inside the MVBs, whereas EhVps2 modulates the ILVs size (Avalos-Padilla et al., 2018). Then, the EhVps4-ATPase disrupts the complex to start a new assembly round (Lopez-Reyes et al., 2010). Here, we analyzed the ESCRT-I complex, particularly the EhVps23 protein, whose orthologue, TSG101, has been linked to malignant transformation in mammalian cells. In trophozoites in the basal state, EhVps23, was found in the cytoplasm, in MVBs and in the inner plasma membrane, but immediately after sensing the presence of RBCs, it moves to the attachment area of the prey. During this process, EhVps23 interacts with the

EhADH, EhVps32 proteins, and the lysobisphosphatidic acid (LBPA). The knock-down of the *EhVps23* gene resulted in a lower rate of phagocytosis, strengthening the role of EhVps23 in the virulence of the parasite.

MATERIALS AND METHODS

Identification of EhVps23 and Phylogenetic Trees Construction

H. sapiens (TGS101) and *S. cerevisiae* Vps23 proteins sequences (access numbers: Q99816 and P25604, respectively), retrieved from the Uniprot database (<https://www.uniprot.org>) were used as query to search an *E. histolytica* Vps23 protein (EhVps23) in the AmoebaDB database (<https://amoebadb.org/amoeba/app>). Structural domains of the candidates were identified using the SMART genomics server (<http://smart.embl-heidelberg.de/>) and the motif tool of KEGG (<https://www.genome.jp/kegg/>). The predicted amino acid sequences of the putative EhVps23 (C4M9S4) were aligned with orthologous sequences. Data were submitted to phylogenetic analysis by UPGMA using the MEGA 5.05 software (Tamura et al., 2011). Bootstrapping was performed for 1000 replicates.

3D Structure Modeling

To obtain the EhVps23 3D model, we used the crystal structure of the Vps23 protein from *S. cerevisiae* (3R3Q:A) as a template on the I-TASSER server (<https://zhanglab.dcm.med.umich.edu/I-TASSER/>) (Roy et al., 2010). After selecting the most energetically stable model, we evaluated their quality by the RAMPAGE server (<http://mordred.bioc.cam.ac.uk/~rapper/rampage.php>). The amino acid sequences of HsTSG101 were analyzed using the RaptorX server (<http://raptorx.uchicago.edu/>) to obtain the HsTSG101 3D structures (Källberg et al., 2012). The structures were visualized using the UCSF Chimera software. Similarities between the UEV and Vps23 core domains of both proteins was analyzed using the RaptorX Structure Alignment tool.

E. histolytica Cultures

E. histolytica trophozoites, strain HM1:IMSS, were axenically grown at 37°C in TYI-S-33 medium (Diamond et al., 1978) and harvested at logarithmic growth phase. To perform the experiments, the culture flasks were chilled at 4°C and trophozoites were collected by centrifugation. All experiments were performed at least three times by duplicate.

Antibodies

As primary antibodies we used: mouse monoclonal α -histidine (α -His; Roche), mouse monoclonal α -BtUb (α -Ub; SantaCruz), rabbit α -EhADH (α -EhADH18) (Díaz-Hernández et al., 2021), mouse α -EhVps32 (α -EhVps32) (Avalos-Padilla et al., 2015), mouse α -LBPA (α -LBPA; Echelon Bioscience) and mouse monoclonal α -human actin (α -actin) (kindly given by Dr. Manuel Hernández, Cell Biology Department, CINVESTAV IPN). Secondary antibodies were: HRP-labelled α -rabbit,

mouse and rat IgGs (Zymed) for western blot. FITC-labelled α -rabbit and α -mouse IgGs and TRITC-labelled α -rat IgGs (Life Technologies) for immunofluorescence. For immunoelectron microscopy experiments, we used α -rat IgG, conjugated with 10 nm gold particles and α -mouse IgG, conjugated with 20 nm gold particles (TED Pella Inc).

PCR Assays

Total RNA was isolated from trophozoites using TRIzol reagent (Invitrogen), according to manufacturer's recommendations. Complementary DNA (cDNA) was synthesized using oligo dT primers and the Superscript II reverse transcriptase (Invitrogen). PCR amplifications were carried out using Q5[®] High-Fidelity DNA Polymerase (Biolabs) with 20 ng of cDNA as templates, and specific primers. Products were separated by electrophoresis in 1% agarose gels, and stained with ethidium bromide. As controls for PCR amplifications, instead of DNA, nuclease-free water was used.

Plasmid Constructs

The *EhVps23*_{1123-1485 bp} or *EhVps23*_{1-341 pb} sequences were PCR-amplified using cDNA as template and specific primers: for *EhVps23*_{1123-1485 bp}: sense 5'-GGGGTACCATGGAAGAGTCTG AAGAAATACCTCATG-3', antisense 5'-CCGGATCCCTTATT CAGTTATGCAATACTTTGCATGAA-3'; for *EhVps23*_{1-341 pb} 5'-GGGAGCTCATGCAACCTATAAACAATGAAAAGAA TATTAAC-3' and the antisense 5'-CCGGTACCAACTTTCCT AATAACACCATTTCATCTAC-3. Underlined sequences correspond to the enzyme restriction sites added to the primers. Fragments were cloned in pColdI for producing a recombinant protein tagged with 6X His, and in pL4440 for silencing experiments, generating the *pColdIEhVps23*_{1123-1485 pb} and *pL4440EhVps23*_{1-341 pb}, plasmids, respectively. The quality of the constructs were verified by restriction enzyme analyses and automatic DNA sequencing.

Expression and Purification of Recombinant His-EhVps23 Protein

E. coli BL21 (DE3) bacteria were transformed with the *pColdIEhVps23*_{1123-1485 bp} plasmid to produce the His-tagged EhVps23_{375-494 aa} recombinant protein (rEhVps23). Protein expression was induced by 0.4 mM isopropyl beta-D-thiogalactopyranoside (IPTG) in the LB medium for 16 h at 16°C. After lysis, the rEhVps23 protein was recovered from the inclusion bodies, using the solubilization buffer containing 20 mM Tris-HCL pH 7.5; 8 M Urea, 0.5 M NaCl, 1 mM β -mercaptoethanol and 5 mM imidazole. rEhVps23 protein was purified through chromatography in Ni-Sepharose 6 columns (GE Healthcare in the NGC Q Chromatographic System, Bio-Rad) (de la Cruz et al., 2019). Identity and integrity of the purified rEhVps32 protein was verified by 10% SDS-PAGE and western blot assays.

Generation of Polyclonal Antibodies Against EhVps23

150 μ g of purified rEhVps23 protein were emulsified in Titer-Max Gold adjuvant (1:1) (Sigma) and subcutaneously and

intramuscularly inoculated in Wistar rats (Avalos-Padilla et al., 2015). One more dose without Titer-Max was injected after 4 weeks. Pre-immune sera were obtained before immunizations.

Western Blot Assays

Total extracts from trophozoites (prepared in the presence of 100 mM PHMB, 2.7 mM E64 and inhibitors cocktail) and bacterial lysates (prepared in the presence of 100 mM PMSF), were separated by SDS-PAGE gels, transferred onto PVDF or nitrocellulose membranes, and probed with rat α -EhVps23 (1:500), mouse α -His (1:500), mouse α -Ub (1:100), rabbit α -EhADH18, (1:500), mouse α -EhVps32 (1:500) or mouse or α -human actin (1:3,500) antibodies. Membranes were incubated with the species-specific horseradish peroxidase (HRP)-labelled secondary antibodies (1:10,000), and developed with the ECL Prime detection reagent (GE-Healthcare). Pre-immune serum was used as a control and competition experiments were performed using the recombinant protein to assure the proper identification of EhVps32 in trophozoites lysates.

Phagocytosis Assays

For phagocytosis assays the trophozoites were incubated for 0, 2, 5, 15, and 30 min with RBCs (1:25) at 37°C. At different times, trophozoites were prepared for immunofluorescence (García-Rivera et al., 1982) and observed through the laser confocal microscope. Other preparations were stained by Novikoff technique (Novikoff et al., 1972) and ingested erythrocytes were counted in 100 trophozoites through the light microscope (Axiolab, Zeiss). For pulse-chase experiments, incubation with RBCs was carried out for 2 min at 37°C. Then, preparations were incubated with TYI-water (2:1) for 5 min at 37°C to remove the adhered and non-ingested erythrocytes, cell mixtures were again incubated at 37°C for different times and samples were treated for immunofluorescence and observed through the Carl Zeiss LMS 700 laser confocal microscope.

Immunofluorescence Assays

Trophozoites (grown on coverslips) were fixed with 4% paraformaldehyde at 37°C for 1 h, permeabilized with 0.2% Triton X-100 and blocked with 10% fetal bovine serum in PBS. Preparations were incubated at 4°C overnight (ON) with α -EhADH18 (1:50), or α -EhVps32 (1:50), α -LBPA (1:30), or α -EhVps23 (1:50) or α -Ub (1:15) antibodies, followed by incubation for 30 min at 37°C with TRITC-labelled α -rat IgG for α -EhVps23, FITC-labelled α -rabbit IgG for α -EhADH18 and α -EhVps32, or FITC-labeled α -mouse IgG for α -LBPA and α -Ub (1:100). Preparations were preserved using Vectashield antifade reagent (Vector) and then, 0.5 μ m laser sections were examined through the confocal microscope and processed with ZEN 2009 Light Edition Software (Zeiss). To evaluate the co-localization between molecules, Pearson coefficients were obtained from at least 25 confocal images using the ImageJ 1.45v software and the JACoP plugin.

Immunoelectron Microscopy

Samples were prepared for TEM as described (Bolaños et al., 2016). Briefly, trophozoites were fixed with 4%

paraformaldehyde and 0.5% glutaraldehyde in PBS for 1 h at room temperature. Samples were embedded in LR White resin (London Resin Co) and polymerized under UV at 4°C for 48 h to obtain thin sections (60 nm) that were mounted on Formvar-covered nickel grids followed by ON incubation with α -EhVps23 (1:30) and α -LBPA (1:10). The thin sections were incubated ON with secondary antibodies (1:50) conjugated to 10-nm (for α -EhVps23) or 20-nm (for α -LBPA) gold particles, contrasted with uranyl acetate and lead citrate and observed through a Joel JEM-1011 transmission electron microscope.

Protein-Protein Docking

The 3D predicted and refined structures of EhADH and EhVps32 proteins were used for docking experiments (Montaño et al., 2017) whereas the 3D structure of EhVps23 protein was generated in this work. The snapshots were obtained using the clustering analysis in the last 50 ns of the MDS with the Carma software (Koukos and Glykos, 2013). The protein-protein docking analysis were done employing different conformers with the Cluspro server (Comeau et al., 2004a; Comeau et al., 2004b; Kozakov et al., 2013). The conformers with the highest cluster members and the lowest energy, calculated in FireDock (Mashiach et al., 2008), were taken for analysis on the PDZSum server (Laskowski et al., 1997). Visualization of 3D structures was performed by VMD (Humphrey et al., 1996). To obtain the binding site between EhVps23 and EhUbiquitin, the crystal structure of EhUbiquitin (PDB:4GSW: B) and Vps23 3D structure from yeast were structurally aligned to get the coordinates of the binding site between the EhVps23 with the EhUbiquitin.

Protein-Ligand Docking

The LBPA structure was obtained and optimized as reported (Castellanos-Castro et al., 2016b). Molecular docking was performed using Autodock4 (Morris et al., 2009), Autodock Vina (Trott and Olson, 2009) and AutoDock Tools 1.5.7, and performed using a grid box of 80 Å and a grid space of 0.375 Å. Then, polar hydrogen atoms and Kollman charges (Singh and Kollman, 1984) were localized in EhVps23. For scoring sampling, the Lamarckian Genetic Algorithm using an initial randomized population of 100 individuals and a maximum number of energy evaluations of 1×10^7 runs were performed. The predicted lowest energy binding position was considered for the analysis.

Immunoprecipitation Assays

Trophozoites were lysed in the presence of 10 mM Tris-HCl, 50 mM NaCl, and proteases inhibitors, by cycles of freeze-thawing in liquid nitrogen and vortexing. Immunoprecipitation assays were performed using 200 μ l of protein G-agarose (Invitrogen) and α -EhVps23 antibody. Immunoprecipitated proteins were analyzed by western blot assays using α -EhVps23, α -EhADH18 α -EhVps32, and α -Ub, as described above.

Ehvps23 Gene Silencing Based on dsRNA

To knock-down the *Ehvps23* gene we used bacterial double-stranded RNA (dsRNA) and parasite soaking experiments (Solis

et al., 2009). Briefly, the competent RNase III-deficient *E. coli* strain HT115 (rnc14:DTn10) was transformed with the *pL4440Ehvps23₁₋₃₄₁ pb*. Bacteria were grown at 37°C in LB or 2YT broth for dsRNA expression, in the presence of ampicillin (100 mg/ml) and tetracycline (10 mg/ml), using 2 mM (IPTG) for induction, ON at 37°C. Then, the bacterial pellet was mixed with 1 M ammonium acetate and 10 mM EDTA, incubated with phenol:chloroform:isoamyl alcohol (25: 24:1) and centrifuged. The supernatant was mixed with isopropanol, centrifuged, and the nucleic acid pellet was washed with 70% ethanol. DNase I (Invitrogen) and RNase A (Ambion) were added to eliminate ssRNA and dsDNA molecules; *Ehvps23*-dsRNA was washed again with isopropanol and ethanol, analyzed by agarose gel electrophoresis and concentration was determined by spectrophotometry. Purified *Ehvps23*-dsRNA (5 μ g/ml) were added to the trophozoites (3.0×10^4) growing in TYI-S-33 complete medium and incubated at 37°C for 72 hr. Cells growing in standard conditions (without dsRNA, or with an unrelated dsRNA) were used as controls.

Statistical Analyses

Values for all experiments were expressed as the mean and standard error of at least three independent assays, carried out by duplicate. Statistical analyses were performed using the GraphPad Prism v5.01 software by a paired Student's t test. * $p < 0.05$; ** $p < 0.01$, and *** $p < 0.001$.

Ethics Statement

CINVESTAV fulfills the standard of the Mexican Official Norm (NOM-062-ZOO-1999) "Technical Specifications for the Care and Use of Laboratory Animals", based on the Guide for the Care and Use of Laboratory Animals ("The Guide," 2011, NRC, USA with the Federal Register Number BOO.02.03.02.01.908), awarded by the National Service for Agrifood Health, Safety and Quality (SENASICA). This organization verifies the state of compliance of such NOM in Mexico and belongs to the Ministry of Agriculture and Rural Development. The Institutional Committee for Animal Care and Use (IACUC/Ethics committee) from CINVESTAV, the regulatory office for research protocols approval involving the use of laboratory animals, reviewed, and approved all animal experiments (Protocol Number 0505-12, CICUAL 001).

RESULTS

EhVps23 Has Functional Domains With Similarities to Putative Orthologues

In humans and yeast, ESCRT-I is an elongated heterotetrameric complex (1:1:1:1) that interacts by one side with the HRS/STAM (ESCRT-0), and by the other with the Vps36 protein (ESCRT-II). It is formed by TSG101 (named Vps23 in yeast), Vps28, Vps37, and UBAP1 (MVB12 in yeast) proteins (**Figure 1A**). Vps23 from *Saccharomyces cerevisiae* and *Homo sapiens* orthologues have been already crystallized and their role in vital cellular functions has been studied (Kostelansky et al., 2007; Im et al., 2010;

Ren and Hurley, 2011; Flower et al., 2020). In *E. histolytica*, the ESCRT-III proteins have been studied, but little is known on the other complexes of the ESCRT machinery. Using as templates the Vps23 core and the UEV (referred to the ubiquitin E2 variant domain found in TSG101 protein and in many other ubiquitin-binding proteins) domains of the *S. cerevisiae* Vps23 protein, we uncovered two contigs in the *E. histolytica* genome with intronless open reading frames, predicting 494 and 283 amino acid sequences (Figure 1B), but the smaller one (Leung et al., 2008), lacks the Vps23 core domain, that is the Vps23 proteins signature, thus, it was not considered for this work. Additionally, we did not detect consensus sequences with domains described for Vps28, Vps37, and MVB12 (Kostelansky et al., 2006; Kostelansky et al., 2007). Lopez-Reyes (Lopez-Reyes et al., 2010) found a Vps37D protein, but its tertiary structure lacks the alpha helices necessary for the EhVps23 functions (Kostelansky et al., 2007). However, given the variation of the ESCRT proteins of *E. histolytica*, compared with their orthologues (Lopez-Reyes et al., 2010; Avalos-Padilla et al., 2018) (Figures S1, S2), the existence of other ESCRT-I members cannot be discarded.

The phylogenetic analysis showed two genes in *E. dispar*, one in *E. invadens* and two in *E. moshkovskii* grouped in a clade close to *Trypanosoma cruzi* and *T. brucei*, in which *E. histolytica* is between *E. dispar* and *E. moshkovskii* (Figure 1C).

The Main Domains of EhVps23 3D Structure Overlap With TSG101

The 3D structure of EhVps23 was obtained from the I-TASSER server. It was selected according to its C-score and the best Ramachandran plot values after MDS during 70 ns in a soluble environment (Figures 2A–D). The Ramachandran plot (<https://zlab.umassmed.edu/bu/rama/>) (Hooft et al., 1997) showed 76.2%

amino acids in the favored regions, 97.3% in the allowed regions, and 2.6% in the outlier ones (see Figure S-3), suggesting that the refinement of torsion angles of certain amino acids through MDS, occurred. RMSD calculations indicated that EhVps23 reached the equilibrium after 50 ns (Figure 2A), and Rg data revealed that EhVps23 is an extended protein that compacts through the dynamics (Figure 2B). The RMSF values showed a peak of fluctuation in a disordered region from Q200 to P334 amino acids, formed by random coils. Another fluctuation peak was located at the carboxy-terminus from N358 to E494 amino acids, where an α -helix is formed (Figure 2C). Thus, these analysis showed that EhVps23 has the 3D structure described for its orthologues (Kostelansky et al., 2007; Im et al., 2010; Ren and Hurley, 2011; Flower et al., 2020) with fourteen alpha helices and six beta-sheets (Figure 2D).

The UEV (Figures 2F, G) and Vps23 core (Figures 2I, J) domains of EhVps23 (Figure 2D) and human TSG101 (Figure 2E) exhibited 82% (RMSD: 2.44) and 90% (RMSD: 0.84) structural identity, respectively (Figures 2H–K). Besides, the carboxy terminus (Vps23 core domain) of EhVps23 presents the alpha helices described as responsible for the ESCRT-I heterotetramer formation, suggesting that these structures could contact amoebic proteins that we did not identify here. The analysis of the 3D structures strongly suggests that EhVps23 is indeed an orthologue of yeast Vps23 and human TSG101 proteins.

In Trophozoites in Basal State, EhVps23 Is Localized in Vesicles

To study the location and follow the movement of EhVps23 in the trophozoites, we produced specific antibodies against the carboxy terminus of the protein. A fragment containing 1123 to 1485 bp of the gene, absent in the truncated contig (Figure 3A), was used to

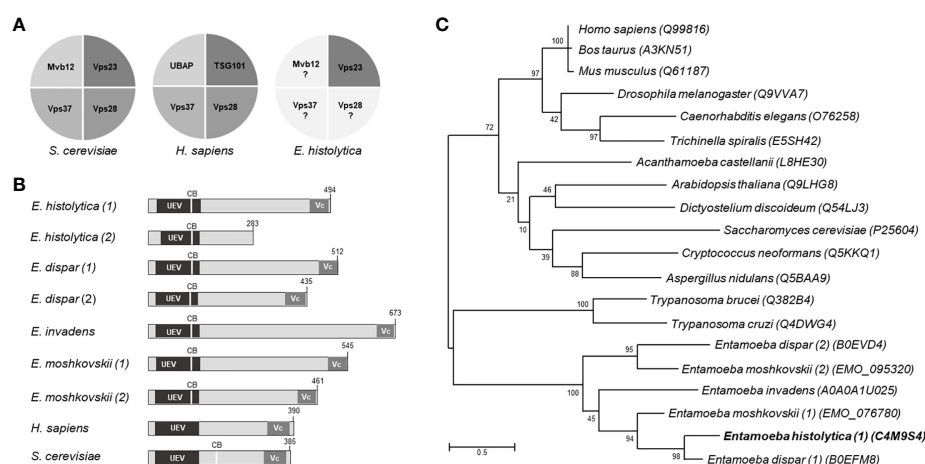


FIGURE 1 | Structural domains and phylogenetic trees of Vps23 proteins. **(A)** Proteins that form the ESCRT-I complex in *Saccharomyces cerevisiae*, *Homo sapiens* and *Entamoeba histolytica*. **(B)** Schematic comparison of the Vps23 domains of *Entamoeba* spp., *H. sapiens* and *S. cerevisiae*. UEV, ubiquitin binding domain; Vc, Vps23 core domain; CB, Clathrin box. Numbers at the right correspond to the number of amino acids forming the proteins. **(C)** Phylogenetic tree indicating the position of *E. histolytica* Vps23 (EhVps23) protein among different species. Numbers on horizontal lines indicate the confidence percentages of the tree topology from bootstrap analysis of 1,000 replicates.

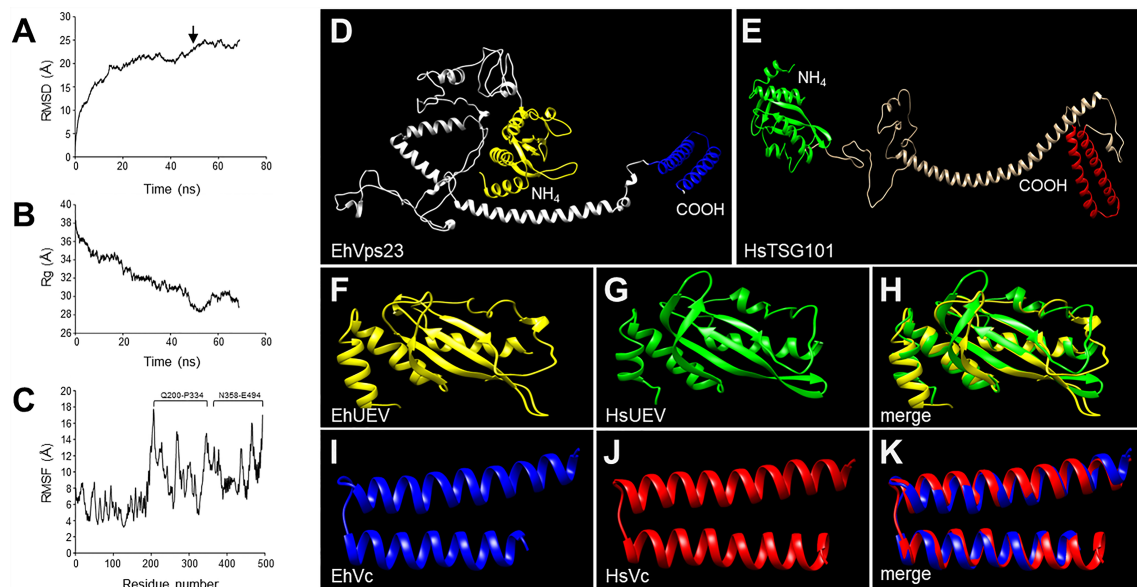


FIGURE 2 | MDS of EhVps23 and its predicted 3D model. **(A)** RMSD: Root mean square deviation. Arrow: signals the ns of protein stability. **(B)** Rg: Radius of gyration. **(C)** RMSF, Root mean square fluctuation. Brackets: The most flexible regions. **(D)** Prediction of the EhVps23 tertiary structure. **(E)** HsTSG101 tertiary structure. **(F)** UEV domain of the EhVps23 protein [21 to 140 amino acids]. **(G)** UEV domain of HsTSG101 [17 to 141 amino acids]. **(H)** Overlapping of EhVps23 and HsTSG101 UEV domains. **(I)** Vps23 core (Vc) domain of EhVps23 [436 to 492 amino acids] **(J)** Vps23 core of HsTSG101 [322 to 381 amino acids]. **(K)** Overlapping of EhVps23 and HsTSG101 Vc domains.

obtain the recombinant EhVps23₃₇₅₋₄₉₄ aa polypeptide (rEhVps23) in *Escherichia coli*, labelled with a histidine tag (His-tag). The polypeptide was injected into rats to generate antibodies. In western blot assays, antibodies recognized a 15 kDa band (**Figure 3B**). The rat α -EhVps23₃₇₅₋₄₉₄ aa antibodies (α -EhVps23) (**Figure 3B**) reacted with the rEhVps23 polypeptide in bacteria and revealed a 54 kDa band in trophozoites lysates (**Figure 3B**), the molecular weight deduced from the amino acids sequence. Through the confocal microscope, these antibodies detected EhVps23 clustered, probably in vesicles (**Figure 3C**).

Under the Erythrocyte's Stimulus, EhVps23 Moves to the Adherence Spots and Surrounds the Ingested RBCs

To explore the fate of EhVps23 under the stimulus of phagocytosis, the protein was tracked using the α -EhVps23 and TRITC-labelled anti-rat secondary antibodies (**Figure 3D**). Confocal images of trophozoites in contact with red blood cells (RBCs) revealed the displacement of EhVps23 at the site of contact with the target cell. At 2 and 5 min, the label was localized in the adhered and ingested RBCs (**Figure 3D**, 2 and 5 min). In other experiments, the cell mixture was incubated at 37°C for 2 min, and adhered and non-ingested RBCs were removed by mild osmotic shock to avoid the noise of new ingested cells, and trophozoites were again incubated at 37°C. In these experiments, at 5 min (2 + 5), the antibodies detected larger vesicles in the cytoplasm and around the ingested erythrocytes. At 2 + 30 and 2 + 60 min, some of the protein appeared in cytoplasm vesicles not in contact with the ingested

RBCs, whereas another part of the label remained surrounding the RBCs (**Figure 3D**). Elongated and round vesicles were observed close to or inside of large phagosomes and MVBs (**Figures 3D, E**). Magnification of the images revealed chains of relatively ordered vesicles of different sizes, as if they were forming specific cellular structures. Many of them, seem to be emerging from or fusing to other vesicles, however other type of experiments are needed to prove this (**Figure 3E**). In synthesis, the analysis of many confocal images revealed that, after the RBCs stimulus, EhVps23 moves from the cytoplasm to the adherence site at the plasma membrane, then, after ingestion, it borders the erythrocytes-containing phagosomes and MVBs; later, it appears close to or inside of vesicles, giving a panoramic of the movement of EhVps23 during the active vesicular trafficking and phagocytosis of trophozoites.

Transmission Electron Microscopy Disclosed EhVps23 Located in MVBs, Plasma Membrane and Endosomes

To obtain further data on the moving of EhVps23, we performed transmission electron microscopy (TEM) analysis using the α -EhVps23 and gold-labeled secondary antibodies. TEM images revealed the protein on the plasma membrane and in the extracellular space, close to several vesicles of about 0.6–0.9 μ m, suggesting that EhVps23 could be secreted (**Figures 4A, B**) and inside MVBs and ILVs (**Figures 4C–E**), like the ones discovered in *Dictyostelium discoideum* treated with the drug U1866A (cationic sterol) that impairs fusion of endosomes with lysosomes, which causes the accumulation of membranous structures (Marchetti et al., 2004),

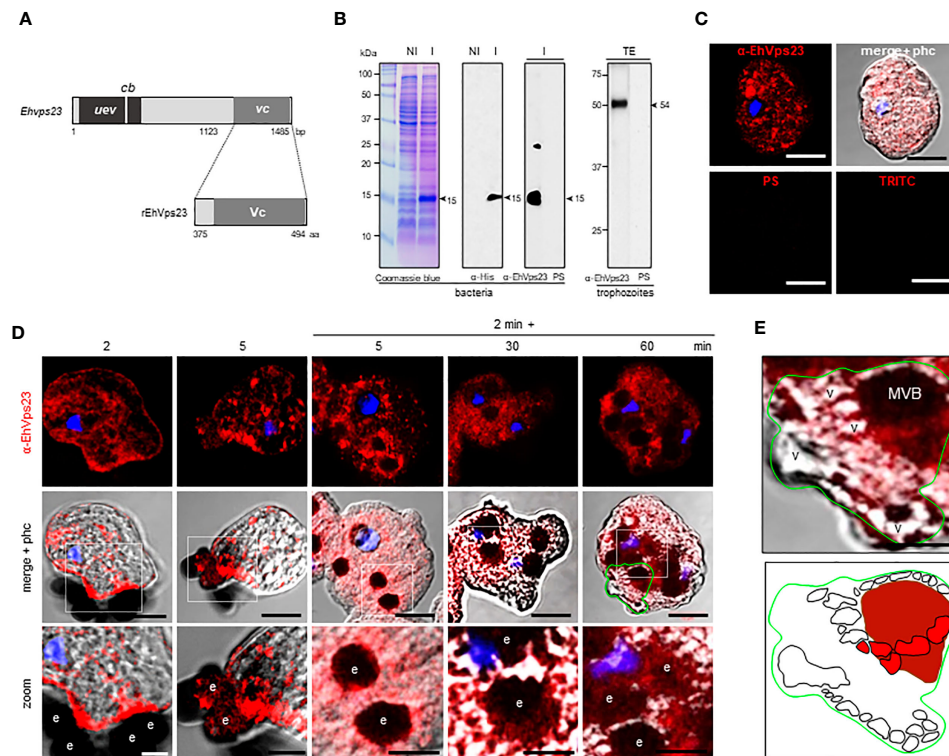


FIGURE 3 | Localization of EhVps23 in the trophozoites. **(A)** Schematic representation of the *EhVps23* gene and the fragment cloned to express the rEhVps23 polypeptide (375 to 494 amino acids) used to generate the rat α -EhVps23 antibodies. **(B)** Coomassie blue-stained gels (10% PAGE-SDS) containing protein extracts of non-induced (NI) and induced (I) bacteria. At right: western blot assays of induced bacteria proteins (I) or total extracts (TE) of trophozoites developed with α -His tag or α -EhVps23 antibodies. PS; pre-immune serum. Numbers at left: molecular weight standards. **(C)** Confocal images of trophozoites in basal conditions incubated with the α -EhVps23 antibodies and TRITC-labelled α -rat secondary antibodies, or with PS or only with the secondary antibody (TRITC). **(D)** Confocal microscopy images were obtained from trophozoites incubated with RBCs for 2 and 5 min at 37°C; or with trophozoites incubated for 2 min at 37°C with the RBCs, the adhered and not ingested RBCs were removed by osmotic shock and preparations were incubated again at 37°C for 5, 30 and 60 min (2 min + 5, 30 and 60 min). Lower panel: Zoom of regions marked by white squares. **(E)** Magnification of MVBs surrounded by multiple vesicular structures. Lower panel: Schematic depiction of **(E)**. v, vesicles; MVBs, multivesicular bodies. Scale bar = 10 μ m.

and in *E. histolytica* overexpressing EhADH (Bañuelos et al., 2012). These vesicles appeared surrounded by other labelled vesicles (Figures 4D, E), like those observed through the confocal microscope. The different numbers and sizes of the vesicles could suggest a distinct maturation state of MVBs. Around some MVBs and vesicles, there were labelled networks (Figure 4B, E). Scarce label was detected free in the cytoplasm (Figures 4A–F), and it did not appear in controls treated with secondary antibodies (Figure 4G).

After 15 min contact with RBCs, TEM images showed convoluted membranous structures penetrating the phagosomes and ingested RBCs, and the protein was detected there (Figures 4H, J). Tubular structures appeared very close each other (Figures 4I, J). This and the white convoluted arrangements inside the RBCs suggest that some vesicles could be transporting different molecules including lytic enzymes, (necessary for digestion of the cargo) from one vesicle to another and that possibly their content are shed on the RBCs-containing phagosomes. The digested hemoglobin could account for the form and size of the arrangements observed in MVBs or phagosomes with ingested RBCs. Like in basal conditions, the labelled phagosomes were

surrounded by other labelled vesicles (Figure 4J). By their appearance and their expansion inside ingested RBCs, lytic enzymes and lipids could be transported there.

EhVps23 Associates to Ubiquitin During Phagocytosis

According to Dupré et al., a yeast protein complex, containing the Vps23 protein, or its mammalian counterpart, TSG101, contains ubiquitin receptors (Dupré et al., 2001). *E. histolytica* possesses the ubiquitination machinery (Bosch and Siderovski, 2013), this, and the predicted ubiquitin domain in EhVps23 and its movement during phagocytosis (Figure 5A), suggested that EhVps23 could be also ubiquitinated or be in contact with ubiquitinated proteins. Thus, we used a commercial antibody against ubiquitin to explore this. In basal conditions, the α -ubiquitin antibodies detected ubiquitin in the cytoplasm of trophozoites, but reduced co-localization with EhVps23 was observed (Figure 5A). However, after 2 + 5 min of phagocytosis, an extensive co-localization of both proteins emerged, and after 2 + 60 min, when EhVps23 was returned to its basal state, both proteins were observed again

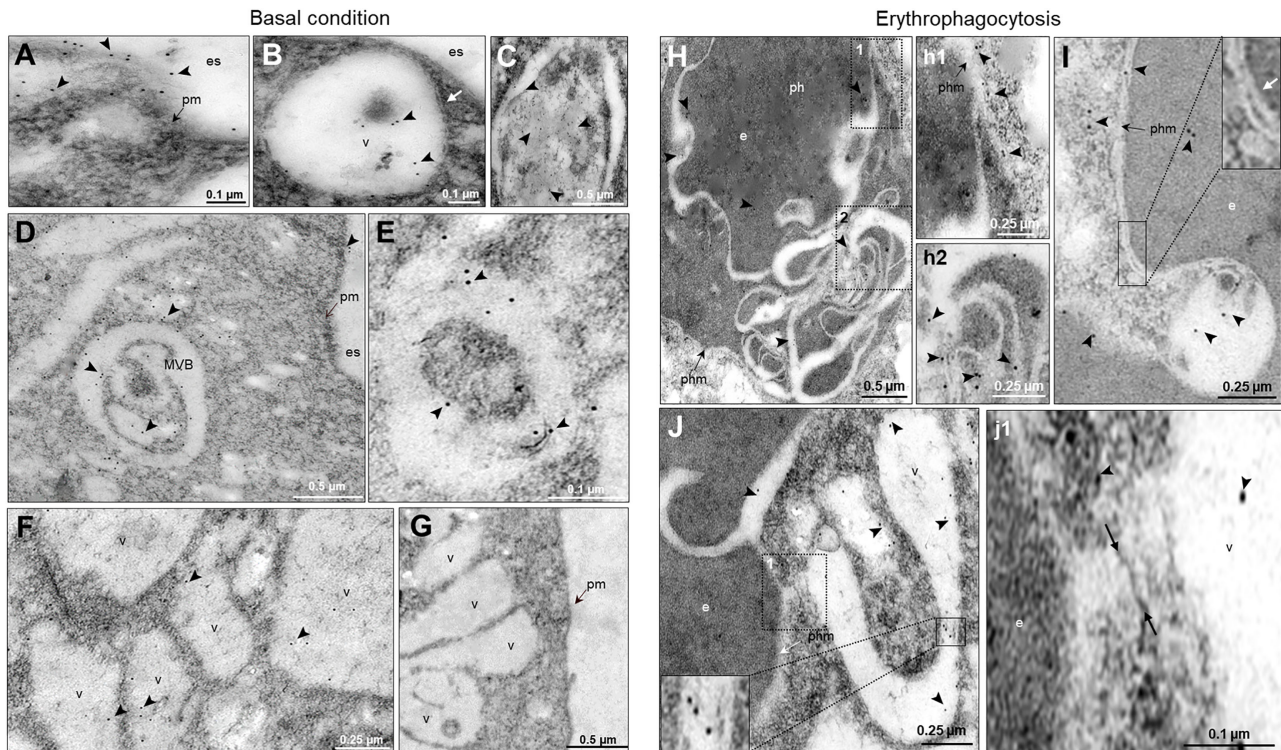


FIGURE 4 | Location by TEM of the EhVps23 protein in trophozoites in basal conditions and during erythrophagocytosis. In basal condition: **(A)** Thin sections of trophozoites incubated with α -EhVps23 and α -rat secondary antibodies coupled to 10 nm colloidal gold particles. **(B)** Vesicles (v) close to the plasma membrane (pm) and in the extracellular space (es) containing labelled EhVps23. White arrows in B: ripples of the vesicular membrane. **(C–E)** Multivesicular bodies (MVB) and vesicles (v) labelled with EhVps23. **(F)** EhVps23 in vesicles (v). **(G)** Control trophozoites using only secondary antibodies. During erythrophagocytosis: **(H)** Thin section showing phagosome (ph) with an erythrocyte (e) exhibiting convoluted membranous structures with labelled EhVps23, phm: phagosome membrane. (h1) and (h2): Magnification of the black squared areas in H **(I)** Vesicle apparently entering the erythrocyte (e) inside a phagosome, where the two membranes can be observed together (inset). The white arrow is signaling the vesicle and phagosome membrane (phm). **(J)** Tubular and round vesicles containing EhVps23. **(j1)** Magnification of the discontinuous black square. Arrowheads: labelled EhVps23, white arrows mark the join between two vesicles. es, extracellular space; pm, plasma membrane; v, vesicles; phm, phagosome membrane; e, erythrocytes.

separated (**Figures 5A, B**), suggesting that ubiquitination could activate EhVps23 to carry out its tasks during phagocytosis, which is supported by the fact that K50, K67, K100, K370, K403, K435, K436 and K445 amino acids are susceptible to ubiquitination. However, the presence of the UEV domain also makes probable that EhVps23 is interacting in a non-covalent way with ubiquitinated proteins, and that this interaction allows EhVps23 to perform its functions during erythrophagocytosis. Both events could be happening. After a certain time, ubiquitin and EhVps23 appeared again separated in the cell. In western blot assays, the α -ubiquitin commercial antibody recognized several bands (**Figure 5C**) corresponding to EhUbiquitin-conjugated proteins. The 10 and 15 kDa bands detected by the antibody exhibited the molecular weight deduced by the amino acids forming the *E. histolytica* ubiquitin (Wostmann et al., 1992; Arya et al., 2012).

EhVps23 Co-Localizes With EhADH, EhVps32, and LBPA

EhADH participates along the process of phagocytosis (García-Rivera et al., 1999). Associated with the EhCP112 cysteine protease,

it forms the EhCPADH complex involved in the adherence to and destruction of target cells (García-Rivera et al., 1999). After the EhCPADH complex contacts the prey, it surrounds the ingested RBCs and penetrates the phagosomes, interacting with ESCRT-III proteins during ILVs formation (Avalos-Padilla et al., 2018). EhADH also binds to cholesterol and to the EhNCP1 and EhNCP2 proteins, responsible for cholesterol transport (Bolaños et al., 2016), and to the LBPA phospholipid (Castellanos-Castro et al., 2016a), acting as a scaffold molecule, performing distinct cellular functions. We explore here the relationship of EhVps23 with EhADH, EhVps32 and LBPA, three molecules involved in phagocytosis.

In basal conditions, EhADH and EhVps23 co-localized in regions close to the inner plasma membrane, as well as in small vesicles (**Figures 6A, B**). After the trophozoites sense the RBCs, both proteins move to the phagocytic cups (**Figure 6A**). At longer times, interaction persisted in the plasma membrane. Interestingly, we distinguished EhVps23 forming bunches of vesicles close to the membrane and in some labelled spots outside the cell with EhADH (**Figure 6A**, 30 min). A recent proteomic study describes the presence of EhVps23 protein in secretion products (Sharma et al.,

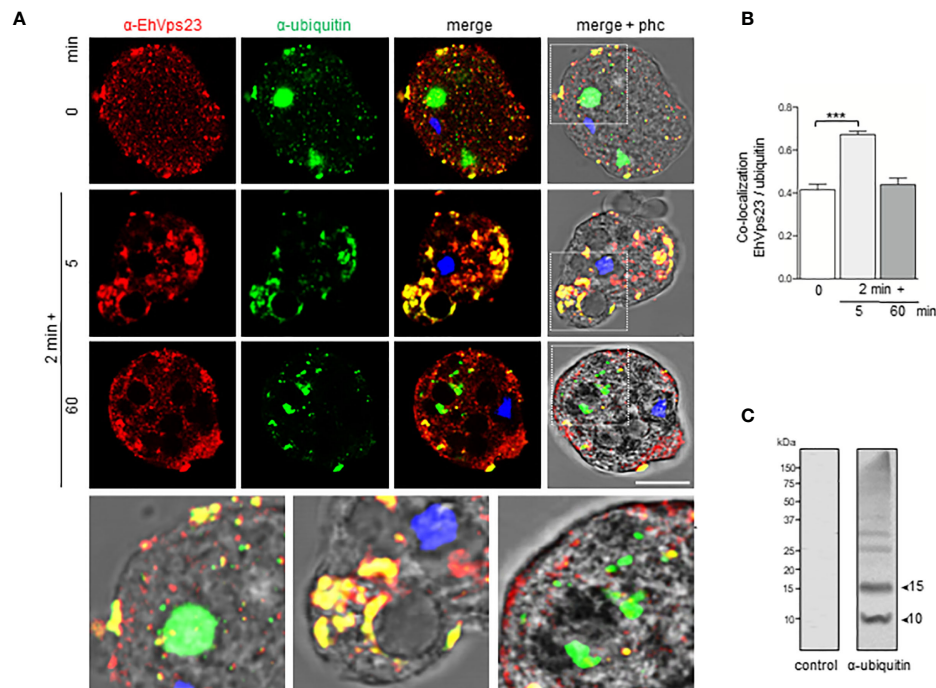


FIGURE 5 | Co-localization of EhVps23 and EhUbiquitin in trophozoites. Trophozoites were incubated for 2 min at 37°C with RBCs, non-ingested RBCs were lysed and preparation incubated again for different times. **(A)** Trophozoite in basal conditions (0 time) and during distinct times of phagocytosis, treated with α-EhVps23 (red), α-ubiquitin (green) antibodies, and DAPI (blue). Lower panel: Magnification of the regions marked with white squares in merge+phc. phc: phase contrast. Scale bar = 10 μm. **(B)** Pearson's coefficient for EhVps23 and ubiquitin co-localization (***) $P < 0.001$. **(C)** Western blot analysis of trophozoites lysates in basal condition, developed with the α-ubiquitin antibodies and control. Numbers at left: molecular weight standards.

2020). The proximity and the cellular movement of these two proteins during phagocytosis support their involvement in vesicular traffick and phagocytosis. In contrast, we detected a minor interaction between EhVps23 and EhVps32 (Figures 6C, D). Interestingly, both proteins were distinguished inside MVBs, indicating a specific function of EhVps23 that could act as a carrier of molecules that are directed to these structures.

LBPA associates to EhADH and it is a marker of late endosomes (Castellanos-Castro et al., 2016a). We investigated whether this phospholipid interacts with EhVps23 in the convoluted membranous structures observed through TEM (see Figure 4). In basal conditions, LBPA was found in vesicles in the cytoplasm and as discrete spots in the plasma membrane. Interestingly, 5 min after the RBCs stimulus was given; both molecules were visualized around the ingested RBCs and MVBs, although we also observed many clumps of LBPA without any interaction with EhVps23 (Figures 7A, B). Inside large phagosomes, networks of strands stained by the α-LBPA antibody appeared close to EhVps23 covering big areas of the phagosomes, and its ramifications reached the plasma membrane and the extracellular space (Figure 7A, 30 min). By TEM experiments, we also investigated whether LBPA was present in the convoluted membranous structures, co-localizing with EhVps23, using gold labeled antibodies of different sizes. TEM images showed both molecules together in the membranous structures (Figure 7C a-d), in vacuoles,

and around phagosomes (Figure 7C). These results together give a panoramic of the complex process of phagocytosis, from the prey's capture up to its digestion, and evidence distinct molecules and structures participating in these functions, as other authors have also shown (García-Rivera et al., 1999; Petri et al., 2002; Perdomo et al., 2016; Javier-Reyna et al., 2019). They also evidenced the role of EhADH, ESCRT proteins and LBPA in phagocytosis.

Molecular Docking and Immunoprecipitation Assays Confirm EhVps23 Binding to EhUbiquitin, EhADH, LBPA and EhVps32

We delve into the study of EhVps23 putative interactions with EhUbiquitin, EhADH, EhVps32 and LBPA by docking analysis and immunoprecipitation assays. First, we aligned the homologous crystal structure of the complex Vps23-ubiquitin (from *S. cerevisiae*) (1UZX), with the EhUbiquitin crystal (4GSW) (Teo et al., 2004; Bosch and Siderovski, 2013). Then, we used the coordinates from this analysis to carry out a second alignment with the EhVps23 3D model obtained here. The structural alignment presented an RMSD of 1.577 (Figure S4), whereas the interaction site between EhVps23 and EhUbiquitin matched with the binding site reported by the crystal structure of *S. cerevisiae* Vps23 interacting with *Bos taurus* ubiquitin (Teo et al., 2004). In docking analysis, the binding site between EhUbiquitin and the

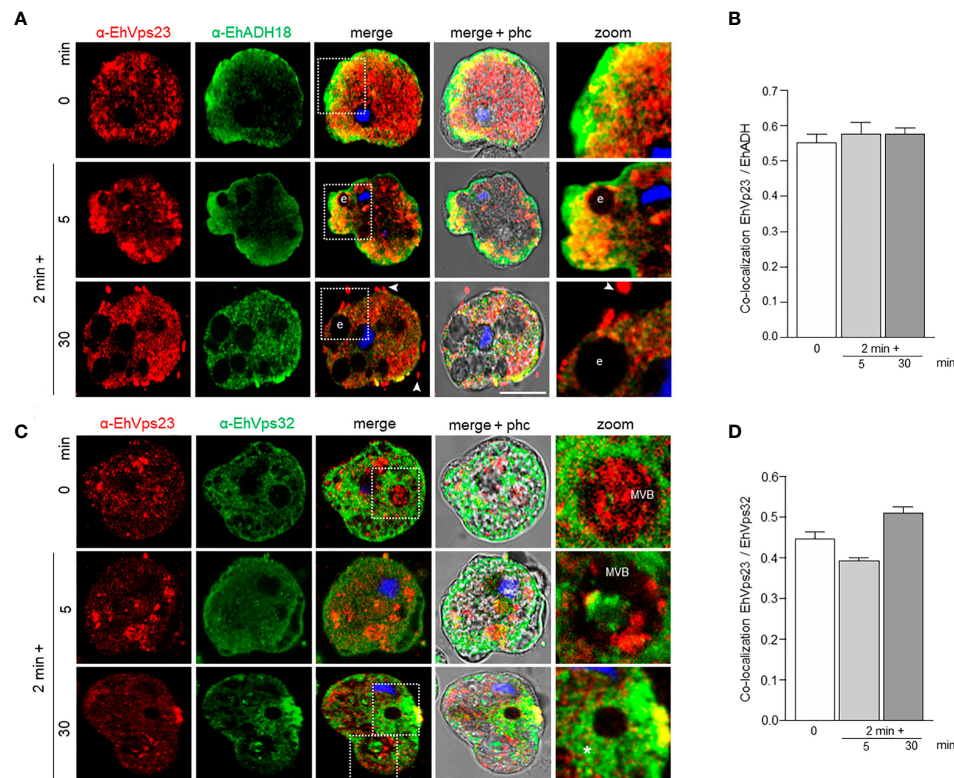


FIGURE 6 | Co-localization of EhVps23 and EhADH or EhVps32 in trophozoites. Trophozoites were incubated for 2 min at 37°C with RBCs, and after lysis of non-ingested RBCs, incubated again for 5 and 30 min. **(A)** Confocal images of trophozoites treated with α -EhVps23 (red), α -EhADH18 (green) antibodies and DAPI (blue). **(B)** Pearson's coefficient for EhVps23 and EhADH co-localization. **(C)** Confocal images of trophozoites treated with α -EhVps23 (red), α -EhVps32 (green) antibodies and DAPI (blue). **(D)** Pearson's coefficient for EhVps23 and EhVps32 co-localization. Zoom: Magnification of regions marked by squares in merged images. Arrowheads: EhVps23 in the extracellular space. Asterisks: networks labelled by the α -EhVps32 antibody. e, erythrocytes; MVB, multivesicular bodies; phc, phase contrast. Scale bar = 10 μ m.

EhVps23 UEV domain appeared conserved (**Figure 8A**). The residues from EhVps23 binding to EhUbiquitin were: T44, S45, R46, I47, I91, H101, E106, N107, G108 and V109, while the residues from EhUbiquitin were: L11, I47, F48, A49, G50, K51, Q65, K66, E67, S68, T69, H71, V73 and R75 (**Figure 8A**).

Docking analysis also predicted that EhVps23 interacts with EhADH, EhVps32 and LBPA. The global free energy of EhVps23-EhADH interaction was calculated in -186.14 kcal/mol, given by two salt bridges and thirteen hydrogen bonds. The EhVps23 residues that interacted with EhADH were N64, R66, E96, E106, Q144, T149 and N339 located mainly in the UEV domain; meanwhile, in EhADH were R172, D219, K222, I227, T228, F231, Q278, K270, N309 and N310, located in the Bro1 domain (**Figure 8A**). The EhVps23-EhVps32 interaction showed a global free energy of -155.13 kcal/mol. The binding site was formed by four salt bridges and fifteen hydrogen bonds. The residues from EhVps23 interacting with EhVps32 were L62, K99, N132, R136, Y137, P138, R141, Q142, N145, H147, T149 and S175 located mainly in the UEV domain. The residues from EhVps32 were T105, K106, D112, D121, N127, C131, L137, G138, E139, D140, L141, Q142, I144, D145, E148, and E150, located in the Snf7 domain (**Figure 8A**).

EhVps23 bound to LBPA with an energy of -9.3 kcal/mol. The residues from EhVps23 interacting with LBPA were M1, Q2, I4, E7, K8, N11, E25, P323, G324, D326, L329, A330, N331 and E386, located in amino terminus and between UEV and Vps23 core domains (**Figure 8A**).

These interactions were experimentally tested by immunoprecipitation assays using α -EhVps23 antibodies and total extracts of trophozoites. EhUbiquitin, EhADH and EhVps32 appeared in the immunoprecipitates. As a negative control we used a preimmune serum (**Figure 8B**). These results evidenced the direct or indirect association of EhVps23 with these molecules involved in the phagocytosis process.

The Knock-Down of the *EhVps23* Gene Diminishes the Rate of Phagocytosis and Migration of Trophozoites

To obtain additional data on the function of EhVps23, we knocked-down the gene using dsRNA (Solis et al., 2009). Western blot assays using silenced trophozoites (*EhVps23*-KD), evidenced that EhVps23 is expressed between 35 to 40% less in the knocked down trophozoites than in the control (**Figures 9A, B**). The immunofluorescence assays

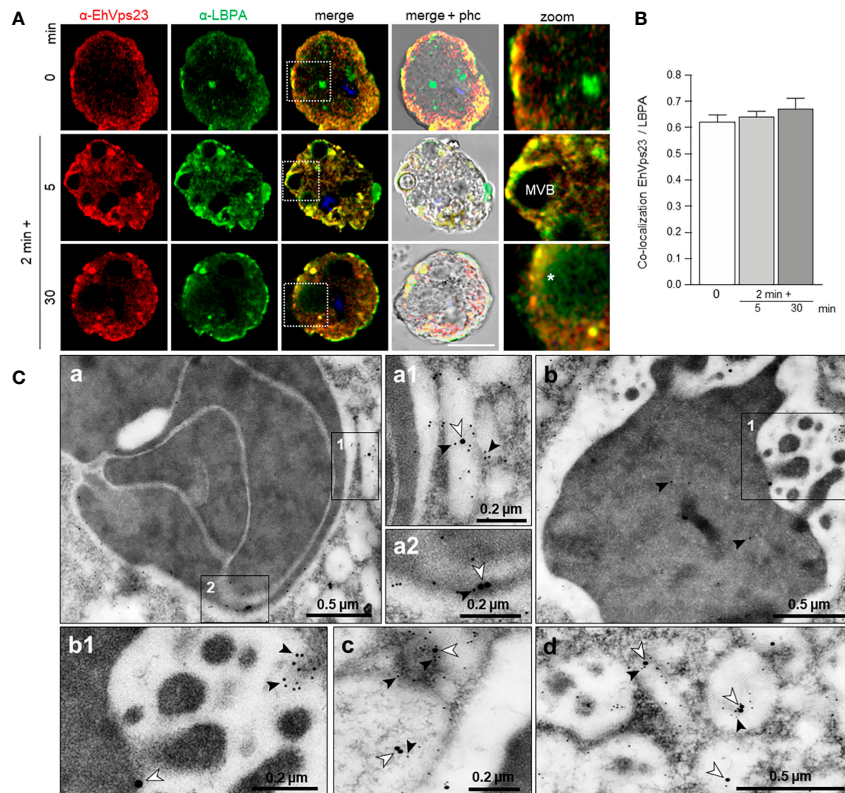


FIGURE 7 | Co-localization of EhVps23 and LBPA in trophozoites. Trophozoites were incubated for 2 min at 37°C with RBCs and after removing the non-ingested RBCs, preparations were re-incubated for 5 and 30 min, and processed for immunofluorescence. **(A)** Confocal images of trophozoites treated with α -EhVps23 (red) and α -LBPA (green) antibodies, and DAPI (blue). Zoom: Magnification of regions marked by squares in merged images. Asterisks: network labeled with the α -LBPA antibody. MVB, multivesicular bodies; phc, phase contrast. Scale bar = 10 μ m. **(B)** Pearson's coefficient for EhVps23 and LBPA co-localization. **(C)** TEM localization of EhVps23 and LBPA in trophozoites after erythrophagocytosis. (a): Thin sections of trophozoites incubated with α -EhVps23 and α -LBPA antibodies followed by incubation with gold-labelled secondary antibodies of 10 and 20-nm, respectively. (a1) and (a2): Magnification of the areas in black squares in (a). (b) Degraded RBC inside a phagosome labelled with EhVps23 and LBPA. (b1) Magnification of the black squared area in (b). (c) and (d): in vesicles of different sizes and shapes marked with EhVps23 and LBPA. White arrowheads point out LBPA label, and black arrowheads EhVps23.

corroborated these results (**Figures 9C, D**). The rate of growth of the *EhVps23*-KD trophozoites was retarded, but after five days of incubation at 37°C, cultures reached the same number of cells that the control did at four days (**Figure 9E**). These results are inconcordance with results obtained in other systems (Leung et al., 2008).

Next we evaluated the role of EhVps23 in the rate of phagocytosis using the silenced trophozoites. Interestingly, at 15 min, the rate of phagocytosis of the *EhVps23*-KD trophozoites was like the controls, but at 30 min, the *EhVps23*-KD cells phagocytosed half of the RBCs than the control cells (**Figures 9F, G**). These results strengthen the assumption that the EhVps23 protein is involved in the phagocytosis of trophozoites, probably due to its active participation in vesicular trafficking.

DISCUSSION

We have studied the ESCRT-I complex here, particularly the participation of its EhVps23 protein, the only one that we have

detected in phagocytosis and vesicular trafficking in *E. histolytica*. Although drugs are available to combat this parasite, it continues causing 100 million infections and 100 thousand deaths each year (Mortimer and Chadee, 2010). The relevance of this work relies in the following facts: i) It provides new evidence on the concerted participation of several molecules with EhVps23 in vesicular trafficking and phagocytosis of this parasite (**Figure 10A**). ii) Phagocytosis is a pivotal event in the aggressive mechanism of *E. histolytica* trophozoites during tissue invasion; the knowledge of proteins involved in this function will give clues to combat this parasitosis. iii) Vesicular trafficking is crucial during phagocytosis and tissue invasion, thus, a better knowledge of the molecules involved these events, will help to uncover molecular mechanisms that are performed during these functions. iv) The ESCRT machinery has been poorly investigated in protozoan parasites (Leung et al., 2008; Lopez-Reyes et al., 2010; Lumb et al., 2011; Bañuelos et al., 2012; Ali et al., 2014; Avalos-Padilla et al., 2015; Avalos-Padilla et al., 2018; Iriarte et al., 2018; Saha et al., 2018; Moyano et al., 2019). Furthermore, protozoa and plants, exhibit remarkable differences with other eukaryotes, hence, this research can provide novel data to

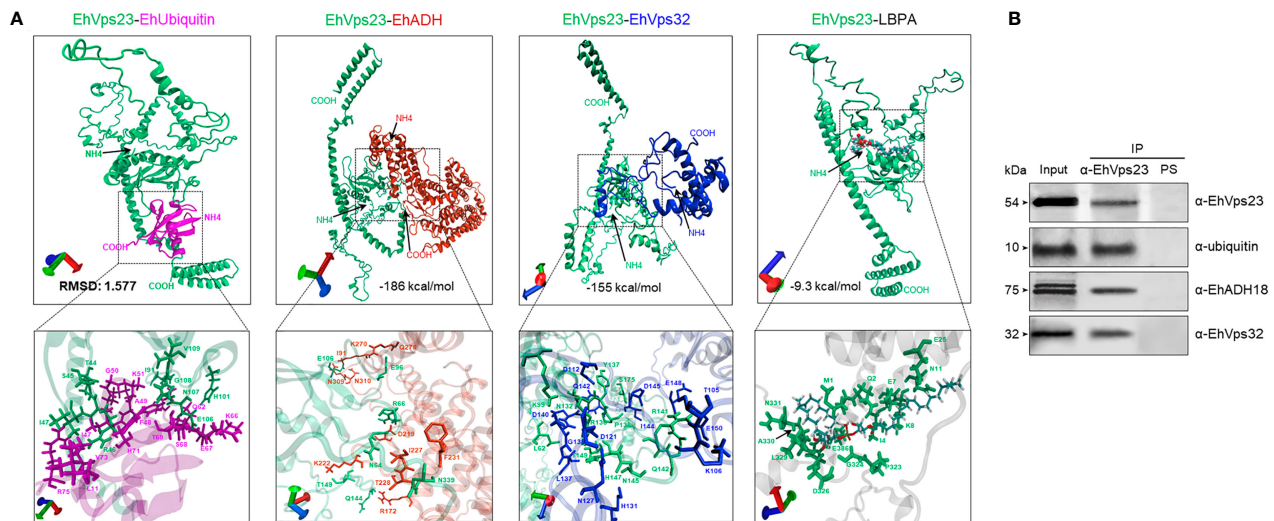


FIGURE 8 | Molecular docking of EhVps23 with EhUbiquitin, EhADH, EhVps32 and LBPA and immunoprecipitation assays. **(A)** Three-dimensional conformation of proteins and association of the EhVps23 (green)/Eh-Ubiquitin (pink), EhVp23 (green)/EhADH (red), EhVps23 (green)/EhVps32 (blue) and EhVps23 (green)/LBPA. Lower panels: magnification of the residues that allow the interaction between the pairs of molecules. **(B)** Immunoprecipitation. HM1-trophozoites in basal conditions were lysed and immunoprecipitated using the α -EhVps23 antibody or pre-immune sera (PS). Immunoprecipitated proteins were analyzed by western blot using α -EhVps23, α -EhADH18, α -ubiquitin, and α -EhVps32 antibodies. Numbers at left: proteins molecular weight.

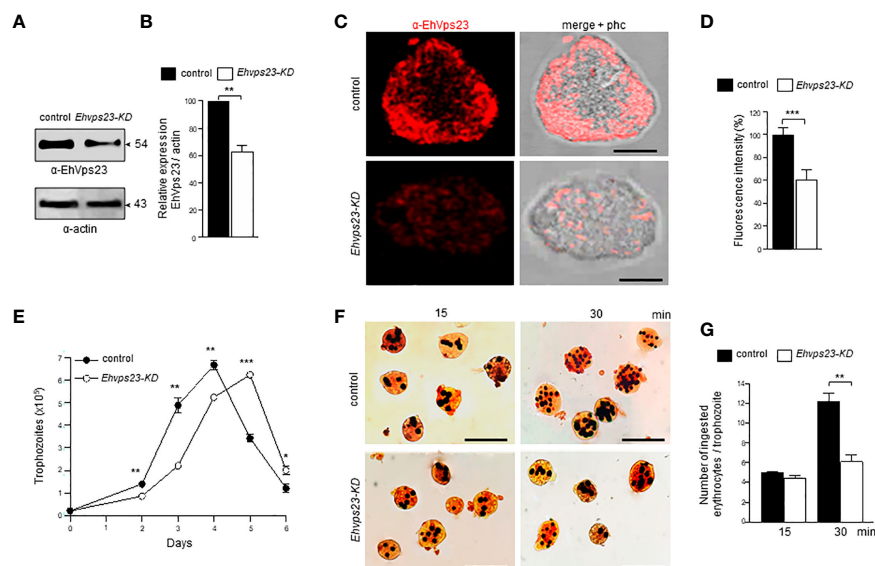


FIGURE 9 | Silencing of the *Ehvps23* gene in *E. histolytica*. The *Ehvps23* gene was knocked down using the *pL4440Ehvps23*₁₋₃₄₁ pb plasmid as described in materials and methods. **(A)** Western blot using lysates of non-silenced (control) and silenced (*Ehvps23*-KD) trophozoites in basal conditions, using the α -EhVps23 and the α -actin antibodies. **(B)** Densitometric analysis of bands showed in **(A)**, normalized against the actin protein bands. **(C)** Representative image of confocal microscopy of non-silenced and *Ehvps23*-KD trophozoites under basal condition using the α -EhVps23 antibody, and a TRITC-secondary antibody. Scale bar = 10 μ m. **(D)** Fluorescence intensity measured by pixels. **(E)** Growth curve of *Ehvps23*-KD. **(F)** Novikoff staining of trophozoites after erythrophagocytosis. **(G)** Quantification of ingested erythrocytes by the trophozoites. Data represent the mean and standard error of the erythrocytes number counted inside of 100 trophozoites. * $P < 0.05$, ** $P < 0.01$, *** $P < 0.001$.

understand the evolutionary process of the ESCRT machinery. Thus, the Vps23 protein was also found in other *Entamoeba* species, that appeared grouped in a single clade, remarking the common origin of the protein in these amoebae species (**Figure 1C**). v) By their function as the core of vesicular trafficking and their divergence with mammalian cells, the ESCRT proteins are good targets for developing vaccines and therapeutic methods against pathogens. In fact, the role of the ESCRT proteins in virulence has been already reported for *Cryptococcus neoformans* (Hu et al., 2013) and *Candida albicans* (Dawson et al., 2020), among others.

We only found EhVps23 as a member of ESCRT-I and we did not find the canonical proteins forming the ESCRT-0. However, these findings did not discard the presence of orthologues with high divergence in the parasite. Instead, other molecules could perform the tasks carried out by ESCRT-0, such as Tom1 and others can interact with EhVps23 to form the ESCRT-I complex, however, we do not know this. In *Arabidopsis* and *D. discoideum* (Blanc et al., 2009; Mosesso et al., 2019), Tom1 recognizes ubiquitinated cargo and gathers the proteins that will be conducted through ESCRT-I to the MVBs. In fact, Tom1 is present in *E. histolytica* (Herman et al., 2011) and its functions are currently under study in our laboratory.

Confocal and TEM observations evidenced that in trophozoites in basal state, EhVps23 is in vesicles (**Figure 4**), like in *T. brucei* (Leung et al., 2008; Silverman et al., 2013). During phagocytosis, it moves to the site of contact of trophozoites with RBCs, interacting with other molecules that may be acting as receptors for the target cell. Then, the prey and these molecules are internalized and transported through endosomes to phagosomes and MVBs where ILVs are formed (**Figures 3, 4**). From there, proteins may be conducted for recycling, degradation, or secretion (**Figures 10A, B**). EhVps23 is present along the event with the participation of membranous structures, which appeared under the microscope as round and elongated vesicles that connect to each other and were marked by α -EhVps23 and α -LBPA antibodies. This active vesicular trafficking involved the participation of

EhVps23, EhADH and LBPA and digested hemoglobin appeared in erythrocytes-containing phagosomes.

Our work give evidence of a significant number of molecules involved in phagocytosis, that interact with EhVps23 along the vesicular traffick and phagocytosis. Immunofluorescence and immunoprecipitation as well as molecular docking analysis predicted that EhVps23 binds to EhUbiquitin, EhADH and EhVps32 through the UEV domain (**Figure 10A**). The binding to ubiquitin could be due to the direct ubiquitination of EhVps23, because the protein has lysines capable of receiving this modification. But it is also possible that the UVE domain of EhVps23 allows it to interact with ubiquitinated proteins, or both speculations could be true. The interaction seems to be similar to those reported for the binding of ScVps23-BtUb (Teo et al., 2004) and HsTSG101-PTAP-containing proteins (Im et al., 2010). On the other hand, the interaction between LBPA and EhVps23 was predicted to be carried out through amino acids located between the UEV and Vps23 core domains. This is the first report on binding of EhVps23 to LBPA (Urbé et al., 2000; Raiborg et al., 2001).

In conclusion: i) Our work give a panoramic of the complex interactions among distinct molecules, including proteins and LBPA, during the vesicular trafficking and phagocytosis of *E. histolytica*. ii) The EhVps23 protein, the only member of the ESCRT-I complex detected here, is a pivotal molecule in both functions in trophozoites: two indispensable functions for the parasite survival and virulence expression. iii) There is an intimate relationship among EhADH, EhVps32, EhVps23, EhUbiquitin and LBPA to perform phagocytosis, together with other molecular mechanisms and proteins involved in these functions, including the calcium binding proteins (Babuta et al., 2020; Kumar et al., 2020), Rab proteins (Javier-Reyna et al., 2019; Verma et al., 2020), as well as the Gal/GalNac (Petri et al., 2002), KERP1 protein (Perdomo et al., 2016), the cytoskeleton (Rath and Gourinath, 2020) and some others. iv) The distinct strategies and experiments performed here, evidenced the presence of abundant vesicular structures, tubules, and networks that arise, interact, and disappear during phagocytosis. Thus, the primitive

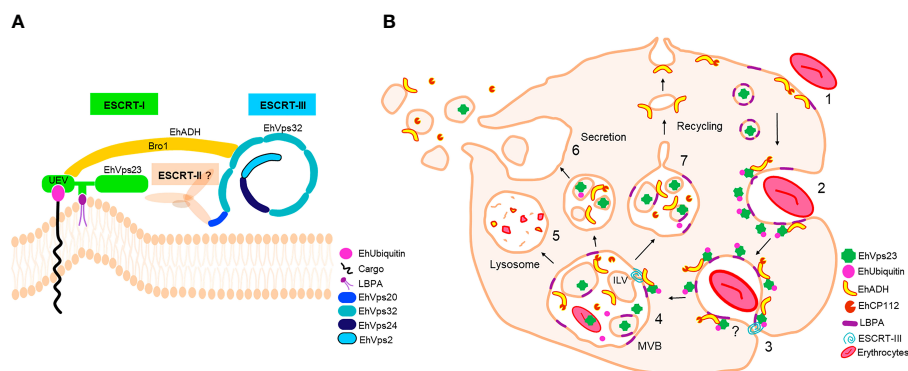


FIGURE 10 | ESCRT machinery of *E. histolytica* and EhVps23 participation. **(A)** ESCRT machinery identified in *E. histolytica*. EhVps23 member of ESCRT-I complex interacts with LBPA, during cell membranes binding. The UEV domain of EhVps23 interacts with ubiquitinated proteins and EhADH. EhADH recruits to EhVps32 (ESCRT-III complex). EhVps20, EhVps32, EhVps24 and EhVps2 (ESCRT-II) polymerize generating helical structures to generate ILVs. **(B)** EhVps23 in phagocytosis. (1) Attachment to human erythrocytes to the trophozoites. (2) Phagocytic cup formation with the presence of EhVps23. (3) EhVps23 surrounds the nascent phagosome. (4) MVBs formation is triggered by the action of ESCRT-III polymers and EhVps23. (5) MVBs fuse to lysosomes or (6) to the cytoplasmic membrane to expel the ILVs content. (7) Pathways that direct proteins to the plasma membrane through recycling vesicles.

protozoan *E. histolytica* is an excellent model to study vesicular trafficking, as well as the role of the ESCRT complex and its proteins; and by their differences with other organisms, it is also a suitable model for evolutionary studies to understand the nature, and phylogenetic relationships among the ESCRT machinery in other species.

DATA AVAILABILITY STATEMENT

Most contributions are included in the article. Other raw data supporting this research will be made available by the authors, without undue reservation. Further inquiries can be directed to the corresponding author.

AUTHOR CONTRIBUTIONS

AG, research, methodology, writing. RJ-R, research, methodology, supervision, and writing. GG-R, research

methodology and supervision. CB, supervision and writing. SM, JO-L, BC-M, and LS-V, methodology. EO, supervision, writing, and research. All authors contributed to the article and approved the submitted version.

FUNDING

This work was supported by the National Council for Science and Technology (Conacyt) of Mexico (grant A1-S8380 for EO), and RJR received a Conacyt Postdoctoral Fellowship.

SUPPLEMENTARY MATERIAL

The Supplementary Material for this article can be found online at: <https://www.frontiersin.org/articles/10.3389/fcimb.2021.770759/full#supplementary-material>

REFERENCES

- Alfred, V., and Vaccari, T. (2016). When Membranes Need an ESCRT: Endosomal Sorting and Membrane Remodelling in Health and Disease. *Swiss Med. Wkly* 146, 1–14. doi: 10.4414/SMW.2016.14347
- Ali, M., Leung, K. F., and Field, M. C. (2014). The Ancient Small GTPase Rab21 Functions in Intermediate Endocytic Steps in Trypanosomes. *Eukaryot Cell* 13, 304–319. doi: 10.1128/EC.00269-13
- Arya, S., Sharma, G., Gupta, P., and Tiwari, S. (2012). In Silico Analysis of Ubiquitin/Ubiqutin-Like Modifiers and Their Conjugating Enzymes in Entamoeba Species. *Parasitol. Res.* 111, 37–51. doi: 10.1007/s00436-011-2799-0
- Avalos-Padilla, Y., Betanzos, A., Javier-Reyna, R., García-Rivera, G., Chávez-Munguía, B., Lagunes-Guillén, A., et al. (2015). EhVps32 Is a Vacuole-Associated Protein Involved in Pinocytosis and Phagocytosis of Entamoeba Histolytica. *PLoS Pathog.* 11, 1–24. doi: 10.1371/journal.ppat.1005079
- Avalos-Padilla, Y., Knorr, R. L., Javier-Reyna, R., García-Rivera, G., Lipowsky, R., Dimova, R., et al. (2018). The Conserved ESCRT-III Machinery Participates in the Phagocytosis of Entamoeba Histolytica. *Front. Cell. Infect. Microbiol.* 8, 53. doi: 10.3389/fcimb.2018.00053
- Babuta, M., Bhattacharya, S., and Bhattacharya, A. (2020). Entamoeba Histolytica and Pathogenesis: A Calcium Connection. *PLoS Pathog.* 16, 1–11. doi: 10.1371/journal.ppat.1008214
- Bañuelos, C., García-Rivera, G., López-Reyes, I., Mendoza, L., González-Robles, A., Herranz, S., et al. (2012). EhADH112 Is a Bro1 Domain-Containing Protein Involved in the Entamoeba Histolytica Multivesicular Bodies Pathway. *J. Biomed. Biotechnol.* 2012, 1–15. doi: 10.1155/2012/657942
- Blanc, C., Charette, S. J., Mattei, S., Aubry, L., Smith, E. W., Cosson, P., et al. (2009). Dictyostelium Tom1 Participates to an Ancestral ESCRT-0 Complex. *Traffic* 10, 161–171. doi: 10.1111/j.1600-0854.2008.00855.x
- Bolaños, J., Betanzos, A., Javier-Reyna, R., García-Rivera, G., Huerta, M., Pais-Morales, J., et al. (2016). EhNPC1 and EhNPC2 Proteins Participate in Trafficking of Exogenous Cholesterol in Entamoeba Histolytica Trophozoites: Relevance for Phagocytosis. *PLoS Pathog.* 12, 1–29. doi: 10.1371/journal.ppat.1006089
- Bosch, D. E., and Siderovski, D. P. (2013). Structural Determinants of Ubiquitin Conjugation in Entamoeba Histolytica. *J. Biol. Chem.* 288, 2290–2302. doi: 10.1074/jbc.M112.417337
- Calistri, A., Reale, A., Palù, G., and Parolin, C. (2021). Why Cells and Viruses Cannot Survive Without an ESCRT. *Cells* 10, 1–31. doi: 10.3390/cells10030483
- Castellanos-Castro, S., Cerda-García-Rojas, C. M., Javier-Reyna, R., Pais-Morales, J., Chávez-Munguía, B., and Orozco, E. (2016a). Identification of the Phospholipid Lysobisphosphatidic Acid in the Protozoan Entamoeba Histolytica: An Active Molecule in Endocytosis. *Biochem. Biophys. Rep.* 5, 224–236. doi: 10.1016/j.bbrep.2015.12.010
- Castellanos-Castro, S., Montaña, S., and Orozco, E. (2016b). Data on Docking and Dynamics Simulation of Entamoeba Histolytica EhADH (an ALIX Protein) and Lysobisphosphatidic Acid. *Data Br.* 7, 457–459. doi: 10.1016/j.dib.2016.02.067
- Comeau, S. R., Gatchell, D. W., Vajda, S., and Camacho, C. J. (2004a). ClusPro: A Fully Automated Algorithm for Protein-Protein Docking. *Nucleic Acids Res.* 32, 96–99. doi: 10.1093/nar/gkh354
- Comeau, S. R., Gatchell, D. W., Vajda, S., and Camacho, C. J. (2004b). ClusPro: An Automated Docking and Discrimination Method for the Prediction of Protein Complexes. *Bioinformatics* 20, 45–50. doi: 10.1093/bioinformatics/btg371
- Dawson, C. S., Garcia-Ceron, D., Rajapaksha, H., Faou, P., Bleackley, M. R., and Anderson, M. A. (2020). Protein Markers for Candida Albicans EVs Include Claudin-Like Sur7 Family Proteins. *J. Extracell. Vesicles* 9, 1–20. doi: 10.1080/20013078.2020.1750810
- de la Cruz, J. J., Villanueva-Lizama, L., Dzúl-Huchim, V., Ramírez-Sierra, M. J., Martínez-Vega, P., Rosado-Vallado, M., et al. (2019). Production of Recombinant TSA-1 and Evaluation of its Potential for the Immunotherapeutic Control of Trypanosoma Cruzi Infection in Mice. *Hum. Vaccines Immunother.* 15, 210–219. doi: 10.1080/21645515.2018.1520581
- Diamond, L. S., Harlow, D. R., and Cunnick, C. C. (1978). A New Medium for the Axenic Cultivation of Entamoeba Histolytica and Other Entamoeba. *Trans. R. Soc. Trop. Med. Hyg.* 72, 431–432. doi: 10.1016/0035-9203(78)90144-X
- Díaz-Hernández, M., Javier-Reyna, R., Sotto-Ortega, I., García-Rivera, G., Montaña, S., Betanzos, A., et al. (2021). Protein Sumoylation is Crucial for Phagocytosis in Entamoeba Histolytica Trophozoites. *Int. J. Mol. Sci.* 22, 1–24. doi: 10.3390/ijms22115709
- Dupré, S., Volland, C., and Haguenaue-Tsapis, R. (2001). Membrane Transport: Ubiquitylation in Endosomal Sorting. *Curr. Biol.* 11, R932–R934. doi: 10.1016/S0960-9822(01)00558-9
- Flower, T. G., Takahashi, Y., Hudait, A., Rose, K., Tjahjono, N., Pak, A. J., et al. (2020). A Helical Assembly of Human ESCRT-I Scaffolds Reverse-Topology Membrane Scission. *Nat. Struct. Mol. Biol.* 27, 570–580. doi: 10.1038/s41594-020-0426-4
- García-Rivera, G., Rodríguez, M. A., Ocádiz, R., Martínez-López, M. C., Arroyo, R., González-Robles, A., et al. (1999). Entamoeba Histolytica: A Novel Cysteine Protease and an Adhesin Form the 112 kDa Surface Protein. *Mol. Microbiol.* 33, 556–568. doi: 10.1046/j.1365-2958.2000.00911.x
- García-Rivera, G., Sánchez, T., Orozco, E., and Guarneros, G. (1982). Isolation of Clones of E. Histolytica Deficient in Adhesion to Human Erythrocytes. *Arch. Invest. Med. (Mex)* 13 (Suppl3), 129–136.
- Herman, E. K., Walker, G., van der Giezen, M., and Dacks, J. B. (2011). Multivesicular Bodies in the Enigmatic Amoeboflagellate Breviata

- Anathema and the Evolution of ESCRT. *J. Cell Sci.* 124, 613–621. doi: 10.1242/jcs.078436
- Hoof, R. W. W., Sander, C., and Vriend, G. (1997). Objectively Judging the Quality of a Protein Structure From a Ramachandran Plot. *Bioinformatics* 13, 425–430. doi: 10.1093/bioinformatics/13.4.425
- Hu, G., Caza, M., Cadieux, B., Chan, V., Liu, V., and Kronstad, J. (2013). Cryptococcus Neoformans Requires the ESCRT Protein Vps23 for Iron Acquisition From Heme, for Capsule Formation, and for Virulence. *Infect. Immun.* 81, 292–302. doi: 10.1128/IAI.01037-12
- Humphrey, W., Dalke, A., and Schulten, K. (1996). VMD: Visual Molecular Dynamics. *J. Mol. Graph* 14, 33–38. doi: 10.1016/j.carbon.2017.07.012
- Im, Y. J., Kuo, L., Ren, X., Burgos, P. V., Zhao, X. Z., Liu, F., et al. (2010). Crystallographic and Functional Analysis of the ESCRT-I/HIV-1 Gag PTAP Interaction. *Structure* 18, 1536–1547. doi: 10.1016/j.str.2010.08.010
- Iriarte, L. S., Midlej, V., Frontera, L. S., Moros Duarte, D., Barbeito, C. G., de Souza, W., et al. (2018). TfVPS32 Regulates Cell Division in the Parasite *Trichomonas Foetus*. *J. Eukaryot Microbiol.* 65, 28–37. doi: 10.1111/jeu.12424
- Javier-Reyna, R., Montañó, S., García-Rivera, G., Rodríguez, M. A., González-Robles, A., and Orozco, E. (2019). EhRabB Mobilises the EhCPADH Complex Through the Actin Cytoskeleton During Phagocytosis of Entamoeba Histolytica. *Cell. Microbiol.* 21, 1–18. doi: 10.1111/cmi.13071
- Källberg, M., Wang, H., Wang, S., Peng, J., Wang, Z., Lu, H., et al. (2012). Template-Based Protein Structure Modeling Using the RaptorX Web Server. *Nat. Protoc.* 7, 1511–1522. doi: 10.1038/nprot.2012.085
- Kostelansky, M. S., Schluter, C., Tam, Y. Y. C., Lee, S., Ghirlando, R., Beach, B., et al. (2007). Molecular Architecture and Functional Model of the Complete Yeast ESCRT-I Heterotetramer. *Cell* 129, 485–498. doi: 10.1021/nn2045246.Multifunctional
- Kostelansky, M. S., Sun, J., Lee, S., Kim, J., Ghirlando, R., Hierro, A., et al. (2006). Structural and Functional Organization of the ESCRT-I Trafficking Complex. *Cell* 125, 113–126. doi: 10.1016/j.cell.2006.01.049
- Koukos, P. I., and Glykos, N. M. (2013). Grcarna: A Fully Automated Task-Oriented Interface for the Analysis of Molecular Dynamics Trajectories. *J. Comput. Chem.* 34, 2310–2312. doi: 10.1002/jcc.23381
- Kozakov, D., Beglov, D., Bohnuud, T., Mottarella, S. E., Xia, B., Hall, D. R., et al. (2013). How Good is Automated Protein Docking? *Proteins* 81, 2159–2166. doi: 10.1002/prot.24403.How
- Kumar, S., Mishra, S., and Gourinath, S. (2020). Structural and Functional Diversity of Entamoeba Histolytica Calcium-Binding Proteins. *Biophys. Rev.* 12, 1331–1341. doi: 10.1007/s12551-020-00766-6
- Laskowski, R. A., Hutchinson, E. G., Michie, A. D., Wallace, A. C., Jones, M. L., and Thornton, J. M. (1997). PDBsum: A Web-Based Database of Summaries and Analyses of All PDB Structures. *Trends Biochem. Sci.* 22, 488–490. doi: 10.1016/S0968-0004(97)01140-7
- Leung, K. F., Dacks, J. B., and Field, M. C. (2008). Evolution of the Multivesicular Body ESCRT Machinery: Retention Across the Eukaryotic Lineage. *Traffic* 9, 1698–1716. doi: 10.1111/j.1600-0854.2008.00797.x
- Liu, Z., Tian, Z., Cao, K., Zhang, B., Wen, Q., Zhou, X., et al. (2019). TSG101 Promotes the Proliferation, Migration and Invasion of Hepatocellular Carcinoma Cells by Regulating the PEG10. *J. Cell. Mol. Med.* 23, 70–82. doi: 10.1111/jcmm.13878
- Lopez-Reyes, I., García-Rivera, G., Bañuelos, C., Herranz, S., Vincent, O., Lopez-Camarillo, C., et al. (2010). Detection of the Endosomal Sorting Complex Required for Transport in Entamoeba Histolytica and Characterization of the EhVps4 Protein. *J. Biomed. Biotechnol.* 2010, 1–15. doi: 10.1155/2010/890674
- Lumb, J. H., Leung, K. F., DuBois, K. N., and Field, M. C. (2011). Rab28 Function in Trypanosomes: Interactions With Retromer and ESCRT Pathways. *J. Cell Sci.* 124, 3771–3783. doi: 10.1242/jcs.079178
- Marchetti, A., Mercanti, V., Cornillon, S., Alibaud, L., Charette, S. J., and Cosson, P. (2004). Formation of Multivesicular Endosomes in Dictyostelium. *J. Cell Sci.* 117, 6053–6059. doi: 10.1242/jcs.01524
- Mashiach, E., Schneidman-Duhovny, D., Andrusier, N., Nussinov, R., and Wolfson, H. J. (2008). FireDock: A Web Server for Fast Interaction Refinement in Molecular Docking. *Nucleic Acids Res.* 36, 229–232. doi: 10.1093/nar/gkn186
- Montañó, S., Orozco, E., Correa-Basurto, J., Bello, M., Chávez-Munguía, B., and Betanzos, A. (2017). Heterodimerization of the Entamoeba Histolytica EhCPADH Virulence Complex Through Molecular Dynamics and Protein–Protein Docking. *J. Biomol. Struct. Dyn* 35, 486–503. doi: 10.1080/07391102.2016.1151831
- Morris, G. M., Ruth, H., Lindstrom, W., Sanner, M. F., Belew, R. K., Goodsell, D. S., et al. (2009). Software News and Updates AutoDock4 and AutoDockTools4: Automated Docking With Selective Receptor Flexibility. *J. Comput. Chem.* 30, 2785–2791. doi: 10.1002/jcc.21256
- Mortimer, L., and Chadee, K. (2010). The Immunopathogenesis of Entamoeba Histolytica. *Exp. Parasitol.* 126, 366–380. doi: 10.1016/j.exppara.2010.03.005
- Mosesso, N., Nagel, M. K., and Isono, E. (2019). Ubiquitin Recognition in Endocytic Trafficking - With or Without ESCRT-0. *J. Cell Sci.* 132, 1–10. doi: 10.1242/jcs.232868
- Moyano, S., Musso, J., Feliziani, C., Zamponi, N., Frontera, L. S., Ropolo, A. S., et al. (2019). Exosome Biogenesis in the Protozoa Parasite Giardia Lamblia: A Model of Reduced Interorganellar Crosstalk. *Cells* 8, 1–19. doi: 10.3390/cells8121600
- Nikko, E., and André, B. (2007). Split-Ubiquitin Two-Hybrid Assay to Analyze Protein-Protein Interactions at the Endosome: Application to Saccharomyces Cerevisiae Bro1 Interacting With ESCRT Complexes, the Doa4 Ubiquitin Hydrolase, and the Rsp5 Ubiquitin Ligase. *Eukaryot Cell* 6, 1266–1277. doi: 10.1128/EC.00024-07
- Novikoff, A. B., Novikoff, P. M., Davis, C., and Quintana, N. (1972). Studies on Microperoxisomes II. A Cytochemical Method for Light and Electron Microscopy. *J. Histochem. Cytochem.* 20, 1006–1023. doi: 10.1177/20.12.1006
- Perdomo, D., Manich, M., Syan, S., Olivo-Marin, J. C., Dufour, A. C., and Guillén, N. (2016). Intracellular Traffic of the Lysine and Glutamic Acid Rich Protein KERP1 Reveals Features of Endomembrane Organization in Entamoeba Histolytica. *Cell. Microbiol.* 18, 1134–1152. doi: 10.1111/cmi.12576
- Petri, W. A., Haque, R., and Mann, B. J. (2002). The Bittersweet Interface of Parasite and Host: Lectin-Carbohydrate Interactions During Human Invasion by the Parasite Entamoeba Histolytica. *Annu. Rev. Microbiol.* 56, 39–64. doi: 10.1146/annurev.micro.56.012302.160959
- Raiborg, C., Bremnes, B., Mehlum, A., Gillooly, D. J., D'Arrigo, A., Stang, E., et al. (2001). FYVE and Coiled-Coil Domains Determine the Specific Localisation of Hrs to Early Endosomes. *J. Cell Sci.* 114, 2255–2263. doi: 10.1242/jcs.114.12.2255
- Rath, P. P., and Gourinath, S. (2020). The Actin Cytoskeleton Orchestra in Entamoeba Histolytica. *Proteins Struct. Funct. Bioinforma* 88, 1361–1375. doi: 10.1002/prot.25955
- Ren, X., and Hurlay, J. H. (2011). Structural Basis for Endosomal Recruitment of ESCRT-I by ESCRT-0 in Yeast. *EMBO J.* 30, 2130–2139. doi: 10.1038/emboj.2011.122
- Roy, A., Kucukural, A., and Zhang, Y. (2010). I-TASSER: A Unified Platform for Automated Protein Structure and Function Prediction. *Nat. Protoc.* 5, 725–738. doi: 10.1038/nprot.2010.5
- Saha, N., Dutta, S., Datta, S. P., and Sarkar, S. (2018). The Minimal ESCRT Machinery of Giardia Lamblia has Altered Inter-Subunit Interactions Within the ESCRT-II and ESCRT-III Complexes. *Eur. J. Cell Biol.* 97, 44–62. doi: 10.1016/j.ejcb.2017.11.004
- Sharma, M., Morgado, P., Zhang, H., Ehrenkaufer, G., Manna, D., and Singh, U. (2020). Characterization of Extracellular Vesicles From Entamoeba Histolytica Identifies Roles in Intercellular Communication That Regulates Parasite Growth and Development. *Infect. Immun.* 88, 1–17. doi: 10.1128/IAI.00349-20
- Silverman, J. S., Muratore, K. A., and Bangs, J. D. (2013). Characterization of the Late Endosomal ESCRT Machinery in Trypanosoma Brucei. *Traffic* 14, 1078–1090. doi: 10.1111/tra.12094
- Singh, U. C., and Kollman, P. A. (1984). An Approach to Computing Electrostatic Charges for Molecules. *J. Comput. Chem.* 5, 129–145. doi: 10.1002/jcc.540050204
- Solis, C. F., Santi-Rocca, J., Perdomo, D., Weber, C., and Guillén, N. (2009). Use of Bacterially Expressed Dsrna to Downregulate Entamoeba Histolytica Gene Expression. *PLoS One* 4, 1–11. doi: 10.1371/journal.pone.0008424
- Strack, B., Calistri, A., Craig, S., Popova, E., and Göttlinger, H. G. (2003). AIP1/ALIX Is a Binding Partner for HIV-1 P6 and EIAV P9 Functioning in Virus Budding. *Cell* 114, 689–699. doi: 10.1016/S0092-8674(03)00653-6
- Tamura, K., Peterson, D., Peterson, N., Stecher, G., Nei, M., and Kumar, S. (2011). MEGA5: Molecular Evolutionary Genetics Analysis Using Maximum Likelihood, Evolutionary Distance, and Maximum Parsimony Methods. *Mol. Biol. Evol.* 28, 2731–2739. doi: 10.1093/molbev/msr121
- Teo, H., Vepintsev, D. B., and Williams, R. L. (2004). Structural Insights Into Endosomal Sorting Complex Required for Transport (ESCRT-I) Recognition

- of Ubiquitinated Proteins. *J. Biol. Chem.* 279, 28689–28696. doi: 10.1074/jbc.M400023200
- Trott, O., and Olson, A. J. (2009). AutoDock Vina: Improving the Speed and Accuracy of Docking With a New Scoring Function, Efficient Optimization, and Multithreading. *J. Comput. Chem.* 31, NA–NA. doi: 10.1002/jcc.21334
- Urbé, S., Mills, I. G., Stenmark, H., Kitamura, N., and Clague, M. J. (2000). Endosomal Localization and Receptor Dynamics Determine Tyrosine Phosphorylation of Hepatocyte Growth Factor-Regulated Tyrosine Kinase Substrate. *Mol. Cell. Biol.* 20, 7685–7692. doi: 10.1128/mcb.20.20.7685-7692.2000
- Verma, K., Srivastava, V. K., and Datta, S. (2020). Rab GTPases Take Centre Stage in Understanding Entamoeba Histolytica Biology. *Small GTPases* 11, 320–333. doi: 10.1080/21541248.2018.1528840
- Vietri, M., Radulovic, M., and Stenmark, H. (2020). The Many Functions of ESCRTs. *Nat. Rev. Mol. Cell Biol.* 21, 25–42. doi: 10.1038/s41580-019-0177-4
- World Health Organization (1997). Amoebiasis = Amibiase. Weekly Epidemiological Record = Relevé épidémiologique hebdomadaire. 72 (14), 97–99. Available at: <https://apps.who.int/iris/handle/10665/230092>.
- Wostmann, C., Tannich, E., and Bakker-Grunwald, T. (1992). Ubiquitin of Entamoeba Histolytica Deviates in Six Amino Acid Residues From the Consensus of All Other Known Ubiquitins. *Fed Eur. Biochem. Soc* 308, 54–58. doi: 10.4324/9781003066026-7
- Conflict of Interest:** The authors declare that the research was conducted in the absence of any commercial or financial relationships that could be construed as a potential conflict of interest.
- Publisher's Note:** All claims expressed in this article are solely those of the authors and do not necessarily represent those of their affiliated organizations, or those of the publisher, the editors and the reviewers. Any product that may be evaluated in this article, or claim that may be made by its manufacturer, is not guaranteed or endorsed by the publisher.

Copyright © 2021 Galindo, Javier-Reyna, García-Rivera, Bañuelos, Montaña, Ortega-Lopez, Chávez-Munguía, Salazar-Villatoro and Orozco. This is an open-access article distributed under the terms of the Creative Commons Attribution License (CC BY). The use, distribution or reproduction in other forums is permitted, provided the original author(s) and the copyright owner(s) are credited and that the original publication in this journal is cited, in accordance with accepted academic practice. No use, distribution or reproduction is permitted which does not comply with these terms.



E-NTPDases: Possible Roles on Host-Parasite Interactions and Therapeutic Opportunities

Lisvane Paes-Vieira^{1*}, André Luiz Gomes-Vieira² and José Roberto Meyer-Fernandes^{1,3*}

¹ Laboratório de Bioquímica Celular, Instituto de Bioquímica Médica Leopoldo de Meis, Centro de Ciências da Saúde, Universidade Federal do Rio de Janeiro, Rio de Janeiro, Brazil, ² Departamento de Bioquímica, Instituto de Química, Universidade Federal Rural do Rio de Janeiro, Seropédica, Brazil, ³ Instituto Nacional de Ciência e Tecnologia em Biologia Estrutural e Bioimagem, Rio de Janeiro, Brazil

OPEN ACCESS

Edited by:

Martin M. Edreira,
Universidad de Buenos Aires,
Argentina

Reviewed by:

Jean Sévigny,
Laval University, Canada
Natasa Mitrovic,
University of Belgrade, Serbia

*Correspondence:

José Roberto Meyer-Fernandes
meyer@bioqmed.ufrj.br
Lisvane Paes-Vieira
lisvane@bioqmed.ufrj.br

Specialty section:

This article was submitted to
Parasite and Host,
a section of the journal
Frontiers in Cellular and
Infection Microbiology

Received: 02 September 2021

Accepted: 25 October 2021

Published: 09 November 2021

Citation:

Paes-Vieira L, Gomes-Vieira AL and
Meyer-Fernandes JR (2021)
E-NTPDases: Possible Roles
on Host-Parasite Interactions and
Therapeutic Opportunities.
Front. Cell. Infect. Microbiol. 11:769922.
doi: 10.3389/fcimb.2021.769922

Belonging to the GDA1/CD39 protein superfamily, nucleoside triphosphate diphosphohydrolases (NTPDases) catalyze the hydrolysis of ATP and ADP to the monophosphate form (AMP) and inorganic phosphate (Pi). Several NTPDase isoforms have been described in different cells, from pathogenic organisms to animals and plants. Biochemical characterization of nucleotidases/NTPDases has revealed the existence of isoforms with different specificities regarding divalent cations (such as calcium and magnesium) and substrates. In mammals, NTPDases have been implicated in the regulation of thrombosis and inflammation. In parasites, such as *Trichomonas vaginalis*, *Trypanosoma* spp., *Leishmania* spp., *Schistosoma* spp. and *Toxoplasma gondii*, NTPDases were found on the surface of the cell, and important processes like growth, infectivity, and virulence seem to depend on their activity. For instance, experimental evidence has indicated that parasite NTPDases can regulate the levels of ATP and Adenosine (Ado) of the host cell, leading to the modulation of the host immune response. In this work, we provide a comprehensive review showing the involvement of the nucleotidases/NTPDases in parasites infectivity and virulence, and how inhibition of NTPDases contributes to parasite clearance and the development of new antiparasitic drugs.

Keywords: Ecto-nucleotidases, E-NTPDases, purinergic signaling, parasite infection, antiparasitic drugs

INTRODUCTION

There are four important subfamilies of ecto-nucleotidases with different substrate specificities (nucleotide hydrolysis): (i) the ecto-nucleoside triphosphate diphosphohydrolases (E-NTPDases), (ii) the ecto-5'-nucleotidases (5'-NT), (iii) the ecto-nucleotidase pyrophosphatase/phosphodiesterases (NPPs), and (iv) alkaline phosphatases (Aps) (Barros et al., 2000; Meyer-Fernandes et al., 2000; de Souza Leite et al., 2007; Paletta-Silva and Meyer-Fernandes, 2012; Zimmermann et al., 2012).

The ecto-nucleoside triphosphate diphosphohydrolases are ecto-nucleotidases that hydrolyze different tri- and diphosphate nucleosides to their monophosphate counterpart (Zimmermann et al., 2012; Zimmermann, 2021a). The E-NTPDase activity is dependent on the presence of divalent cations, such as calcium and magnesium (Handa and Guidotti, 1996; Robson et al., 2006).

Eight members of the E-NTPDase family were identified in mammals. The isoforms 1 (known as CD39), 2, 3, and 8 are typical E-NTPDases, located on the cell surface. The isoforms 4 and 7 were found in the Golgi apparatus and intracellular membrane compartment, respectively. After heterologous expression, the isoforms 5 and 6 were found only in the supernatant, suggesting that they could be secreted forms (Robson et al., 2006; Zimmermann et al., 2012).

All these enzymes conserve five “apyrase conserved regions”, known as ACR1 to ACR5 (Robson et al., 2006; Zimmermann et al., 2012). They are usually located on the cell membrane with the catalytic site oriented to the extracellular milieu. Some of them are also bound to the organelle membrane, with the catalytic site oriented to the lumen of the organelle (Bernardes et al., 2000; Meyer-Fernandes, 2002; Sansom et al., 2008). The E-NTPDases are proteins characterized by having a high degree of glycosylation. Not only are there different numbers of N-glycosylation sites but also the placement of the sites relative to the apyrase conserved regions is different as well. For example, four out of seven glycosylation sites in NTPDase 3 are near the ACR regions, whereas NTPDase 4 and 5 have no glycosylation sites approximate to ACR regions (Zhong et al., 2017).

In parasites, nucleotidases/E-NTPDases seem to be involved in crucial processes, such as virulence, infectivity, purine salvage pathways, and parasite adhesion on the host cell (Sansom, 2012; Figueiredo et al., 2016; Paes-Vieira et al., 2018; Silva-Gomes et al., 2020). During parasite infection, the host cell releases ATP as a danger signal, leading to the augmentation of the extracellular ATP level (Trautmann, 2009). For instance, during *Leishmania* spp. infection, the parasite interacts with Toll-like receptors (TLR) present in the surface of the host cell, inducing the release of ATP to the extracellular milieu *via* pannexin-1 channels. The extracellular ATP can be now metabolized by parasite E-NTPDase and 5'-NT, increasing the extracellular Adenosine (Ado) level (Chaves et al., 2021). Such sequential hydrolysis of extracellular ATP to adenosine was demonstrated in different parasite species, indicating that not only E-NTPDases but also ecto-5'-nucleotidases could be present in protozoa parasites, including *Leishmania* spp., *Trypanosoma* spp., *Trichomonas vaginalis*, *Tritrichomonas foetus*, *Toxoplasma gondii*, and *Schistosoma* spp. (Berrêdo-Pinho et al., 2001; Meyer-Fernandes, 2002; Sansom, 2012; Pimentel et al., 2016; Paes-Vieira et al., 2018).

Many studies have suggested the involvement of parasite E-NTPDases in host immune defense suppression since their activity would lead to the reduction of ATP and ADP levels. According to these studies, parasite E-NTPDases (CD39 gene family) hydrolyze extracellular ATP to ADP and AMP, which is, in sequence, hydrolyzed by the parasite ecto-5'-nucleotidases (CD73 gene family). The hydrolysis of AMP by parasite ecto-5'-nucleotidases increases the levels of adenosine, leading to the reduction of the host inflammatory response (Fredholm et al., 2007; Sansom et al., 2008; Arora and Rai, 2019).

Parasite E-NTPDases and 5'NTs have received special attention because they are cell-surfaced enzymes whose activity can modulate the host purinergic signaling, a signal transduction pathway mediated by purine nucleotides and nucleosides, such as ATP

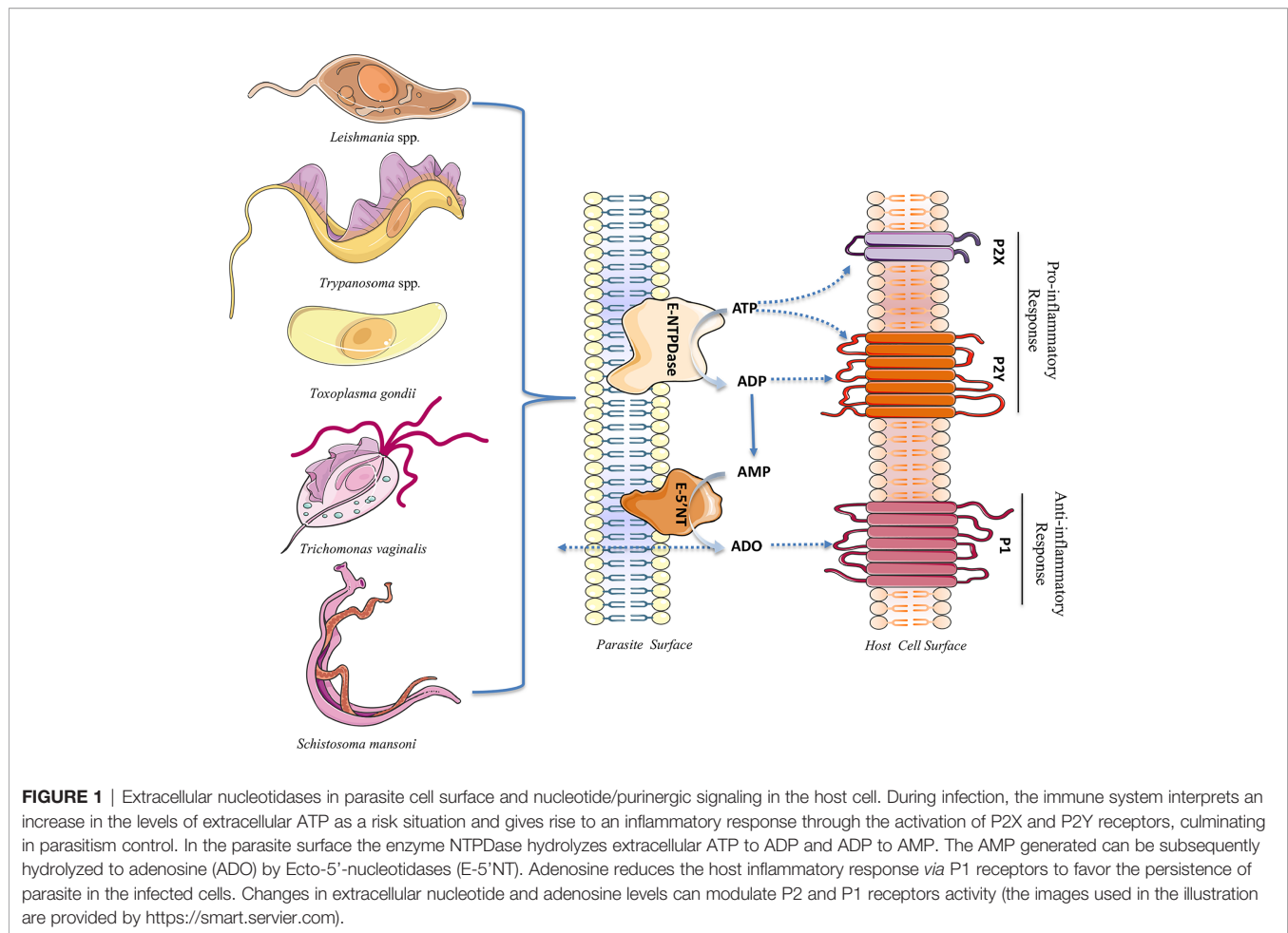
and adenosine, which bind and activate specific surface proteins called purinergic receptors (Figueiredo et al., 2016; Zimmermann 2021b). In host cells, two families of purinergic receptors, P1 and P2, mediate purinergic signaling. The P1 receptors are metabotropic G protein-coupled receptors, encompass four subtypes, called A₁, A_{2A}, A_{2B}, and A₃; all of them use adenosine as ligand. The P2 receptors are responsive to tri- and diphosphonucleotides (ATP, ADP, UTP and UDP) and are divided into P2X and P2Y subtypes. The P2X receptor is also called ionotropic and functions as non-selective cation ion channel. Meanwhile, P2Y receptor is coupled to G protein. The family of P2Y receptors can modulate many cellular processes related to inflammatory and immune responses, such as cell differentiation, adhesion, migration, phagocytosis, and secretion in the host cell (such as macrophages, monocytes, neutrophils, and dendritic cells) (Coutinho-Silva and Savio, 2021; Klaver and Thurnher, 2021). The most well-studied of the P2X receptors is the P2X₇ subtype. It has been shown that the interaction between ATP and the P2X₇ receptor leads to an inflammatory response by the host immune system. Such inflammatory response triggered by extracellular ATP activates macrophage and dendritic cells, leading to an increase of IL-12 and TNF- α , reactive oxygen species (ROS), and nitric oxide (NO) production, culminating in intracellular pathogen elimination (Savio and Coutinho-Silva, 2019; Chaves et al., 2021; Coutinho-Silva and Savio, 2021).

Acting on P1 receptors of the host cell, extracellular adenosine, generated by parasite E-NTPDases and 5'-NTs, increases the intracellular level of cAMP in the host cell, leading to the modulation of the inflammatory response (Figueiredo et al., 2017). In summary, adenosine leads to the suppression of inflammatory cytokines by macrophages and dendritic cells and the production of antimicrobial substances by macrophages and neutrophils. In addition, adenosine increases the level of IL-10, an important regulatory cytokine (Wilson et al., 2009; Figueiredo et al., 2016; Haskó et al., 2018; Antonioli et al., 2019). Thus, the dual effect of both ATP and adenosine on the host immune response seems to depend on different factors such as ATP and adenosine concentration, time of exposure, and conditions of the host cell. Thus, the balance between these two molecules (ATP and adenosine) is crucial for the proper immune response (Zhao et al., 2017). **Figure 1** summarizes the role/effect of parasite ectonucleotidases on the nucleotide/purinergic signaling of the host cell.

In this review article, we discuss the role of nucleotidases/E-NTPDases in parasite infectivity and virulence and show the potential of these enzymes as antiparasitic drug targets. In this sense, we also provide an overview of the latest studies concerning the development of nucleotidase/E-NTPDase inhibitors and their effect on parasite physiology.

DEVELOPMENT OF E-NTPDASES INHIBITORS

Ecto-nucleotidases have been implicated in different pathological conditions. The interplay of ecto-nucleotidases with the nucleotide and adenosine receptor systems has received special attention.



P1 and P2 receptor activity can be controlled by changes in the extracellular levels of both adenosine and nucleotide (Kukulski et al., 2011). Thus, the search for strong and subtype-specific ecto-nucleotidase inhibitors is important not only for developing potential therapeutics but also for developing proper molecular tools for studying the role of ecto-nucleotidases in parasite-host interaction. However, the development of such inhibitors is an obstacle to overcome since they must be E-NTPDase-specific, not affecting other types of ecto-nucleotidases or nucleotide receptors (Zimmermann, 2021a; Zimmermann, 2021b).

While several non-selective chemical compounds have been used to inhibit E-NTPDases activity, strong and specific inhibitors are rare, most of them are nucleotide analogs (Zimmermann 2021a; Zimmermann, 2021b). The most well-known CD39 inhibitors include an impermeant inhibitor, DIDS (4,4'-diisothiocyanostilbene-2,2'-disulfonic acid) (Meyer-Fernandes et al., 1997; Bernardes et al., 2000), sodium azide (NaN₃), suramin (Bisaggio et al., 2003; Fonseca et al., 2006), chelators (EDTA and EGTA) (Iqbal and Shah, 2018), ARL67156 (6-N, N-diethyl-D-b,g-dibromomethylene ATP) (Lévesque et al., 2007), 8-BuS-ATP derivatives (8-thiobutyladenosine 50-triphosphate) (Gendron et al., 2000; Lecka et al., 2013) and BG0136 (1-naphthol-3, 6-disulfonic acid) (Gendron et al.,

2002). Such inhibitors can increase ATP and ADP levels, causing the augmentation of purinergic signaling. However, inhibitors like suramin bind to P2 receptors and antagonize their effects (Munkonda et al., 2007). Since these chemicals are not CD39-specific, their use has been shown to be limited (Battastini et al., 2021). Other classes have been reported as inhibitors of E-NTPDases, such as polyoxometalates (POMs) (Lee et al., 2015; Schachter et al., 2015; Jeffrey et al., 2020), thiadiazolopyrimidones (Afzal et al., 2020), Schiff bases of tryptamine (Kanwal et al., 2019), quinoline (Hayat et al., 2019; Murtaza et al., 2021) and anthraquinone derivatives (Al-Rashida and Iqbal, 2014; Baqi et al., 2020), sulfopolysaccharides (Lopez et al., 2021) and carboxamide derivatives (Afzal et al., 2021). Moreover, specific antibodies have also been used as inhibitors of NTPDases (Munkonda et al., 2009; Pelletier et al., 2017).

Since E-NTPDases have been implicated in different processes of parasite physiology, such as differentiation, nutrition, invasion, survival in the host cell, and modulation of the host immune response to establish infection, these enzymes have been seen as promising targets for drug development (Paes-Vieira et al., 2018). In this sense, many works have shown the effects of several compounds on parasite E-NTPDases (Knowles, 2011; Pimentel et al., 2016; de Carvalho et al., 2019; da Silva et al., 2021).

***Leishmania* spp.**

The genus *Leishmania* encompasses at least 20 different species of protozoa parasites, which can cause a tropical disease called leishmaniasis. An estimated 0.7-1 million new cases of leishmaniasis per year are reported from nearly 100 endemic countries (Burza et al., 2018). Leishmaniasis is characterized by three different clinical manifestations, which are determined by the *Leishmania* species. Self-healing lesions in the infectious site characterize the cutaneous leishmaniasis (CL). In the mucocutaneous leishmaniasis (ML), besides cutaneous lesions, mucosal damage may occur, leading to disseminated or diffuse CL. In visceral leishmaniasis (VL), parasites migrate to the liver, spleen, and bone marrow, causing a more severe condition that can be fatal (Pace, 2014).

In *Leishmania* species (*L. amazonensis*, *L. mexicana*, *L. tropica*, *L. braziliensis*, *L. donovani*, *L. infantum*, *L. major*), two genes encoding putative NTPDases (LNTPDase 1 and LNTPDase 2) have been found in genome databases (Sansom, 2012; Paes-Vieira et al., 2018). In different *Leishmania* species, LNTPDase and ecto-5'-nucleotidase activities have been implicated with virulence and infectivity (Berrêdo-Pinho et al., 2001; Pinheiro et al., 2006; de Almeida Marques-da-Silva et al., 2008; Souza et al., 2011; Leite et al., 2012; Maia et al., 2013).

In *L. amazonensis*, LaNTPDase activity is differentially regulated among promastigote, amastigotes, and metacyclic promastigote forms. The authors showed that LaNTPDase activity is lower in promastigotes, and significantly higher in metacyclic promastigote forms (Paes-Vieira et al., 2021). Moreover, overexpression of *ntpd1* and *ntpd2* led to a reduced lesion in mice transfected with such overexpressing-*L. amazonensis*, compared to control. It was suggested that *L. amazonensis* overexpressing *ntpd1* and *ntpd2* leads to the augmentation of extracellular adenosine levels, modulating the host immune response and promoting pathogen clearance (Paes-Vieira et al., 2021). A mutant of *L. major* lacking the Golgi NTPDase 1 exhibited a delayed capacity to induce lesions in susceptible mice by promastigote forms. On the other hand, parasites not expressing the secreted LmNTPDase 2 did not show alterations in *L. major* virulence (Sansom et al., 2014).

Interaction and infection of macrophage with *L. amazonensis* and *L. infantum* pretreated with anti-NTPDase antibodies were significantly reduced, suggesting that parasite E-NTPDases could be involved in host cell interaction and invasion (Pinheiro et al., 2006; Vasconcellos et al., 2014; Peres et al., 2018). In addition, the involvement of ecto-ATPases in the invasion process of macrophage by *L. amazonensis* was investigated in the works of Moreira et al. (2009) and Ennes-Vidal et al. (2011). The authors pretreated promastigote forms with an ecto-ATPase inhibitor known as CrATP (chromium (III) adenosine 5-triphosphate) and observed a decrement in the adhesion and endocytic indices. Polyclonal antibodies against a conserved B domain from the potato apyrase polypeptide (r-potDomain B) and synthetic peptides designed from the B domain (LbB1LJ and LbB2LJ) were able to reduce parasite NTPDase 1 activity in different species of *Leishmania* (Porcino et al., 2012; Detoni et al., 2013; Maia et al., 2013).

These studies could contribute to the development of specific NTPDase inhibitors.

In *L. amazonensis*, extracellular adenosine (produced by sequential dephosphorylation of ATP by LaNTPDases and ecto-5'-nucleotidase) binds to P1 receptors (A_{2A} and A_{2B}) on macrophage membrane (Csóka et al., 2008; Figueiredo et al., 2012; Figueiredo et al., 2016). Because of the interaction between adenosine and P1 receptors, activated macrophages reduce IL-12 and TNF- α cytokines levels, leading to the decrement of nitric oxide (NO^{*}) production and the establishment of parasites in the host cell. Thus, the increase of adenosine levels during *Leishmania* infection seems to contribute to the host-parasite interaction, increasing the parasitism and delaying the lesion remission (Olivier et al., 2005; Gomes et al., 2015; Vijayamahantesh et al., 2017). Interestingly, when the adenosine receptor is blocked or ablated, or even when adenosine is removed by enzymatic activity, during the infection, the host-parasite interaction is significantly reduced (Figueiredo et al., 2017).

The incubation of *L. amazonensis* (original strain) with DIDS (4,4'-diisothiocyanatostilbene 2,2'-disulfonic acid), a well-known LaNTPDase inhibitor, prevents the reduction of NO^{*} by activated macrophages (J774), decreasing the parasite survival (Gomes et al., 2015). Moreover, the production of IL-12 and TNF- α by macrophages infected with DIDS-treated *L. amazonensis* was significantly higher than that observed for macrophages infected with untreated parasites. Such results suggest that the inhibition of the LaNTPDase activity by DIDS reduced *L. amazonensis* capacity to down-modulate the release of inflammatory cytokines, which are essential for NO^{*} production by inducible Nitric Oxide Synthase (iNOS) (Gomes et al., 2015). The results obtained by Gomes et al. (2015) reinforce the role of LaNTPDase in modulating the host immune system, which is crucial for the success of *L. amazonensis* infection.

Gomes et al. (2015) showed that the blockage of receptors A_{2B} in J774 macrophages led to the increase of NO^{*} production and the reduction of parasite survival in stimulated macrophages. The authors also showed that the blockage of A_{2B} receptors led to the increase of TNF- α and IL-12 production in macrophages infected with *L. amazonensis*, indicating the importance of adenosine production to the macrophages' modulation. Interestingly, using the adenosine analog known as NECA (5'-(N-Ethylcarbox- amido) adenosine-NECA) during the infection of macrophages with the avirulent clone 1IIId, the authors observed an increase in the ability of the avirulent clone to survive within macrophages. Moreover, the treatment with NECA was able to reduce the levels of TNF- α , IL-12, and NO^{*} in macrophages, showing that the interaction between adenosine and A_{2B} receptors is essential for the host immune system modulation since the treatment with NECA was able to recover the capacity of the 1IIId clone to survive in stimulated macrophages. Thus, Gomes et al. (2015) described a mechanism that correlates LaNTPDase/nucleotidase activity and the capacity of the parasite to down-modulate the host immune system. Specifically, the augmentation of adenosine levels at the

beginning of infection seems to compromise the macrophage activation, leading to the blockage of cytokines on the host cell (Gomes et al., 2015).

Working with *L. amazonensis* promastigotes resistant to vinblastine (a cell division blocker), Giarola et al. (2014) observed an increase in the ecto-ATPase activity and a more severe disease scenario. The authors also found a two-fold higher ecto-ATPase protein expression in vinblastine-resistant promastigotes than in control cells. The data obtained by Giarola et al. (2014) show that there seems to be a positive correlation between higher ecto-ATPase activity and greater infectivity/disease severity.

Trypanosoma spp.

Parasites from the genus *Trypanosoma* (Trypanosomatida, Kinetoplastea) are flagellated protozoa that cause a wide range of diseases in both humans and animals. Such parasites are transmitted between hosts by insect vectors (Hutchinson and Stevens, 2018). Among the numerous parasite species belonging to the genus *Trypanosoma*, some of them have medical (*T. cruzi*, which cause Chagas disease in the Americas and *T. brucei rhodesiense* and *T. brucei gambiense* that cause sleeping sickness in human African) and veterinarian (*T. evansi*, *T. vivax*, *T. brucei*, *T. copemani*, *T. equiperdum*) importance (Büscher et al., 2017).

Trypanosoma cruzi is the etiological agent of American trypanosomiasis or Chagas disease. The disease is endemic in the southern USA and 21 countries across Latin America, with ~7 million people infected and 70 million at risk (Moretti et al., 2020). *Trypanosoma evansi* is the etiologic agent of surra, a disease that occurs in several animal species, such as equids, leading to significant losses in global production since it can be fatal when is late diagnosed (Desquesnes et al., 2013).

In *T. cruzi*, only one gene coding for TcNTPDase is present in its genome, named TcNTPDase 1 (Fietto et al., 2004; da Silva et al., 2021). The TcNTPDase 1 coding sequence has been cloned and expressed in the bacterial system. Biochemical characterization showed that TcNTPDase 1 is an Apyrase/CD39/E-NTPDase family member. Moreover, TcNTPDase1 activity on *T. cruzi* membrane has also been demonstrated (Bisaggio et al., 2003; Fietto et al., 2004; Meyer-Fernandes et al., 2004; Santos et al., 2009; Giarola et al., 2013; Mariotini-Moura et al., 2014; da Silva et al., 2021).

Recently, Silva-Gomes et al. (2020) engineered *T. cruzi* parasites overexpressing the TcNTPDase 1 gene and observed higher infectivity rates when compared to the control cell line. On the other hand, when TcNTPDase 1 gene was silenced, the infectivity rates decreased significantly. These data are in agreement with the idea that TcNTPDase 1 could be involved in *T. cruzi* infectivity (Silva-Gomes et al., 2020).

In vitro studies showed that *T. cruzi* adhesion and internalization into macrophages were significantly compromised when parasites were treated with DIDS and Suramin, a treatment that also inhibited the ecto-ATPase activity. On the other hand, the augmentation of ecto-ATPase activity was accompanied by the increase of parasite adhesion to macrophages (Bisaggio et al., 2003).

Experiments using recombinant TcNTPDase 1 (acting as a competitor) or anti-TcNTPDase 1 polyclonal antibodies (acting as blockers) evidenced the involvement of TcNTPDase 1 in parasite-host interaction and cell adhesion (Mariotini-Moura et al., 2014).

Santos et al. (2009) also showed the importance of *T. cruzi* NTPDase 1 in infectivity and virulence. *T. cruzi* treated with E-NTPDase partial inhibitors (ARL67156, Gadolinium, and Suramin), and TcNTPDase 1 antibody markedly reduced trypomastigotes infectivity. The authors observed lower levels of parasitemia when TcNTPDase-inhibited trypomastigotes were used to infect mice, which increased the host survival (Santos et al., 2009).

Studies have shown that suramin is a potent inhibitor of *T. cruzi* E-NTPDase, and *in vivo* experiments suggest that this drug can negatively affect the purinergic signaling of host cells infected with *T. cruzi* (Bisaggio et al., 2003; Santos et al., 2009). Novaes et al. (2018) studied the effect of suramin in the chemotherapy of murine model of Chagas disease. *T. cruzi*-infected mice submitted to Suramin-based chemotherapy showed increased reactive tissue damage, inflammation, and parasitism. In addition, Suramin-based treatment aggravated myocarditis cases and increased the mortality rates (Novaes et al., 2018). This unexpected result could be explained by the fact that Santos et al. (2009) used Suramin only in the parasites, before infection, while Novaes et al. (2018) used Suramin in the host cells. In addition, it is worth mentioning that Suramin is a P2 antagonist in mammalian cells (Lambrecht et al., 2002). Thus, the apparent disagreement between the works of Santos et al. (2009) and Novaes et al. (2018) seems due to the absence of specificity of Suramin, acting on both P2 receptors and *T. cruzi* E-NTPDase. These results reinforce the importance of working with specific E-NTPDase inhibitors, whose absence has become an obstacle to be overcome (da Silva et al., 2021).

The enzyme adenosine deaminase (ADA) is responsible for regulating the extracellular adenosine concentration, converting adenosine to inosine (Franco et al., 1997). do Carmo et al., (2017) performed an experimental combined treatment of Chagas disease using both deoxyconformycin (a potent ADA inhibitor) and 3'-deoxyadenosine (adenosine analogue). According to the authors, the results observed in the experiments, which include reduced parasitemia and cardiac inflammatory infiltrates, are due to the modulation of seric NTPDase and ADA activities (do Carmo et al., 2017). Similar results were observed when mice were infected with *T. evansi* (Dalla Rosa et al., 2013; Dalla Rosa et al., 2015) and *T. brucei* (Rottenberg et al., 2005).

Fracasso et al. (2021) investigated the effects of benznidazole (BNZ, currently used in the treatment of Chagas Disease), and resveratrol (RSV, a natural polyphenol with antioxidant and neuroprotector activities) alone and in combination during acute *T. cruzi* infection in the mouse cerebral cortex. The treatment with RSV in the infected group reduced NTPDase and 5'-NT activity and diminished ATP, ADP, and AMP hydrolysis compared to the non-treated group. The combination of RSV + BNZ decreased AMP hydrolysis in infected animals compared to the non-treated group, exerting an anti-inflammatory effect. Treatment with BNZ and RSV alone or associated reduced adenosine (ADO) levels and converted

inosine by E-ADA (adenosine deaminase extracellular). These results suggested a suitable immunosuppressive effect of RSV during acute *T. cruzi* infection. Thus, the authors concluded that resveratrol could act as a neuroprotective molecule, probably preventing inflammatory changes caused by infection by *T. cruzi*, even though the mice experienced high levels of parasitemia (Fracasso et al., 2021).

The pre-treatment with curcumin in rats infected with *T. evansi* decreased parasitemia and mortality (Wolkmer et al., 2013; Wolkmer et al., 2019), maintained the NTPDase activity reduced and enhanced ADA activity on the surface of lymphocytes. These results suggest that curcumin treatment can improve immunomodulatory response mediated by ecto-nucleotidases, favoring the response against the parasite (Wolkmer et al., 2019).

Taking together, these studies show that purinergic signaling carries out a pivotal function in the immune and inflammatory responses in the course of parasite infections.

Trichomonas vaginalis

The flagellated protozoan *Trichomonas vaginalis* infects the human urogenital tract causing trichomoniasis, a sexually transmitted disease. In women, such infection can lead to cervical cancers, infertility, pelvic inflammatory disease, and pregnancy complications (Mielczarek and Blaszkowska, 2016).

Five putative NTPDase genes (*TvNTPDase1–5*) were found in the *T. vaginalis* genome database (Frasson et al., 2016). Regarding substrate specificity, *T. vaginalis* NTPDase activity was able to hydrolyze both purine and pyrimidine nucleosides, 5-di- and 5-triphosphate (de Aguiar Matos et al., 2001; Frasson et al., 2012). In addition, *TvNTPDases* localization and activity have been shown on *T. vaginalis* surface (de Jesus et al., 2002; Tasca et al., 2004), as well as on *T. fetus* surface (Jesus et al., 2002). The presence of such enzymes on the cell surface is important for parasite viability when exposed to extracellular nucleotides. Cell surfaced-localized *TvNTPDases* play an important role concerning the maintenance of extracellular adenosine levels and the purine salvage pathway in the parasite (de Jesus et al., 2002; Jesus et al., 2002; Ferla and Tasca, 2021).

The effect of the compounds metronidazole (MTZ) and tinidazole (TNZ) on *T. vaginalis* NTPDase and 5'NT activities was investigated (Tasca et al., 2003). In this study, two strains were used, one long-term-grown isolate and one fresh clinical isolate. The hydrolysis of ATP and ADP was found to be 5- to 7-fold higher in the fresh clinical isolate than in the long-term-grown strain. In fresh clinical isolate, the compound TNZ inhibited the ATP hydrolysis by 33%. On the other hand, the same enzyme activity was induced by MTZ in long-term grown strain. When both isolates were treated with MTZ for 2 h, the ATP and ADP hydrolysis was significantly inhibited, while only fresh clinical isolate had the ATP and ADP hydrolysis inhibited by treatment with TNZ. The 5'NT activity was not changed by TNZ or MTZ treatment. Taken together, these data indicate that the parasite modulates the extracellular ATP and ADP levels when submitted to the treatment with TNZ and MTZ as a protection mechanism to survive in unfavorable conditions (Tasca et al., 2003; Ferla and Tasca, 2021).

The ecto-NTPDase activity of the *T. vaginalis* was inhibited by the plant alkaloids lycorine and candimine (Giordani et al., 2010; Petró-Silveira et al., 2020). Recent studies demonstrated that the effect of lycorine involves the inhibition of *T. vaginalis* NTPDase, generating extracellular ATP accumulation and stimulating ROS release by neutrophils. According to Petró-Silveira et al. (2020), lycorine could make *T. vaginalis* more susceptible to the host immune system, leading to parasite elimination. Moreover, during *T. vaginalis* infection, NO production by neutrophils, via A_{2A} receptors activation, seems to be dependent on both the ecto-5'-nucleotidase activity and the adenosine levels (Frasson et al., 2012). In addition, the levels of ROS and IL-8 were decreased by Adenosine in neutrophils infected with *T. vaginalis*, probably due to the activation of A1 adenosine receptors (Frasson et al., 2017). Thus, *TvNTPDase* and 5'NT activities carry out an important role in adenosine production, triggering an efficient purinergic-signaling cascade, which allows the parasite to escape the host immune response (Petró-Silveira et al., 2020). In addition, the treatment of trophozoites of *T. vaginalis* freshly isolated with hormones, especially steroids, also inhibited *TvNTPDase* activity, and this inhibition seems to be associated with the decreased gene expression of the *TvNTPDases* (Rückert et al., 2009; Rückert et al., 2010).

Toxoplasma gondii

The intracellular protozoan *Toxoplasma gondii* infects mammals and other animals, causing a disease known as toxoplasmosis, which can be severe to the fetus, when infection takes place during pregnancy, and to immunocompromised individuals (Montoya and Liesenfeld, 2004).

Both isoforms, *TgNTPDase 1* and *TgNTPDase 2* are expressed in virulent strains, while in avirulent strains only the *TgNTPDase 2* isoform is expressed. These isoforms have different enzymatic specificity. *TgNTPDase 1* hydrolyzes nucleoside triphosphate, and *TgNTPDase 2* hydrolyzes diphosphate substrates. However, both forms of *TgNTPDase* are activated by dithiothreitol (Asai et al., 1995; Nakaar et al., 1998).

The *T. gondii* NTPDases have become a target in drug development. Parasites expressing an antisense *TgNTPDase*-RNA showed reduced *TgNTPDase* expression and activity. In addition, parasites expressing the antisense *TgNTPDase*-RNA showed a lower ability to proliferate, suggesting that *TgNTPDases* could be involved in *T. gondii* replication (Nakaar et al., 1999). This conclusion was supported by studies with monoclonal antibodies against NTPDase 2 of *T. gondii* that inhibited *TgNTPDase* activity and decreased *T. gondii* tachyzoites replication (Tan et al., 2010).

The treatment of mice infected with *T. gondii* with Diphenyl diselenide (PhSe)₂ reduced histological inflammatory markers, ROS levels, and ADA activity in the spleen, besides reversing splenomegaly. In addition, *TgNTPDase* and 5'NT activity were increased in the spleen, stimulating the hydrolysis of ATP and the enhancement of adenosine production in the tissue. These results indicate that purinergic signaling could be involved in the pathogenesis of *T. gondii* infection (Doleski et al., 2017a; Doleski et al., 2017b).

Bottari et al. (2020) demonstrated that mice treated with resveratrol during chronic infection by *T. gondii* increased

NTPDase and reduced ADA activities. The adenosine signalization by regulating A_1 and A_{2A} receptors expression promoted anti-inflammatory and neuroprotector mechanisms during *T. gondii* infection (Bottari et al., 2020).

Schistosoma spp.

The genus *Schistosoma* holds helminth parasites responsible for causing a human disease known as Schistosomiasis, which causes liver, intestinal, lung, and chronic pelvic inflammations (Colley and Secor, 2014).

In *Schistosoma mansoni* two NTPDase isoforms (*SmATPDases* 1 and 2) were detected and partially purified. It was shown that *S. mansoni* NTPDase activity can be found throughout the parasite life cycle, besides the involvement in the worm metabolism and the host-parasite interaction (Vasconcelos et al., 1993; Vasconcelos et al., 1996; DeMarco et al., 2003; Da'dara et al., 2014). *SmATPDase* 1 is located on the surface and *SmATPDase* 2 is in the tegument and secreted by eggs and adult worms (Faria-Pinto et al., 2004; Fietto et al., 2004; Levano-Garcia et al., 2007). Both isoforms showed immune cross-reactivity with antipotato apyrase antibodies (Faria-Pinto et al., 2008; Faria-Pinto et al., 2010). Macrophages incubated with antibodies against the ATPDase isoforms of *S. mansoni* showed reduced NTPDase 1 activity, and the parasite proliferation was inhibited (Marconato et al., 2017).

Schistosoma eggs found in the host tissues trigger an inflammatory response known as granulomatous, characterized by the presence of granulomas in the infected tissues (Farah et al., 2000). Gusmão et al. (2021) showed that immunization of C57BL/6 mice with potato apyrase was ineffective in triggering a protective immune response against *Schistosoma* infection. Differently, immunization using potato apyrase decreased the granulomatous response, accompanied by an enhancement of multinucleated giant cells. In this sense, immunotherapies developed from potato apyrase-immunization to avoid granuloma development seems to be a potential prophylaxis strategy (Gusmão et al., 2021).

Recently, studies have demonstrated that some flavonoids and chalcones (natural plant metabolites), such as licoflavone B and cardamonin display antiparasitic activities against adult worms of *S. mansoni* (de Carvalho et al., 2015; de Castro et al., 2015; Souza et al., 2017). The effects of licoflavone B and cardamonin on the *S. mansoni* NTPDase activity were investigated. In addition, a molecular docking approach was also used to study the mode of action of such compounds on *S. mansoni* ATPDase 1 (de Castro et al., 2015; de Carvalho et al., 2015). de Castro et al. (2015) showed that ATP-diphosphohydrolase activity was inhibited by about 82% by cardamonin (40 μ M), with an IC_{50} of 23.54 μ M, while ADPase activity was unchanged. In addition, interactions between cardamonin and *SmATPDase* 1 seem to be done especially through hydrogen and hydrophobic bonds, as revealed by molecular docking studies (de Castro et al., 2015). Regarding licoflavone B, a concentration of 40 μ M was able to abolish 84% of the ATP-diphosphohydrolase activity, with an IC_{50} of 23.78 μ M. Different from cardamonin that did not show *SmADPase* activity inhibition, licoflavone B in a concentration of 40 μ M

inhibited 56% of the *SmADPase* activity. The interaction between licoflavone B and *SmATPDase* 1 seems to involve nine dock positions at the Nucleotide-Binding Site of the enzyme (de Carvalho et al., 2015; de Carvalho et al., 2019).

The schistosomicidal effect of two synthetic chalcones (*E*-4'-hydroxychalcone and *E*-2'-hydroxy-4-methoxychalcone) was studied by Pereira et al. (2018). The authors showed that both compounds can inhibit *S. mansoni* ATP-diphosphohydrolase activity, besides causing a decrease in parasite load in mice. Martins et al. (2000) evaluated the inhibitory effect of sesquiterpene lactones on *S. mansoni* ATP-diphosphohydrolase. The authors showed that the compounds thapsigargin and thapsigarginin inhibited 70% and 57% of the enzyme's activity, respectively.

CONCLUDING REMARKS

Many studies have described the involvement of E-NTPDase activity in parasite nutrition, differentiation, invasion, survival in the host cell, modulation of the host immune response, and establishment of infection. Since E-NTPDases have been implicated in important events for different parasite species, such enzymes have been considered as ideal drug targets for many therapeutic applications, including parasitic diseases. In addition, ecto-nucleotidase activity associated with the purinergic signaling seems to be crucial to parasite-host interaction, besides contributing to adenine acquisition *via* the purine salvage pathway.

In this context, this review emphasizes the importance of ecto-nucleotidases in parasite physiology and pathogenesis. Moreover, we highlight the importance of such enzymes as drug target candidates to the development of new antiparasitic compounds, including those able to inhibit specifically the different ecto-nucleotidases isoforms.

Although many compounds have been assayed against ecto-nucleotidases from different parasites to inhibit the enzyme activity, the low specificity of these molecules represents an obstacle to be eliminated, still requiring huge efforts in the search for new selective and effective ecto-nucleotidase inhibitors.

AUTHOR CONTRIBUTIONS

LP-V, AG-V, and JM-F designed the study and wrote the paper. LP-V, AG-V, and JM-F edited and reviewed the final version of the manuscript. All authors contributed equally to the article and approved the submitted version.

FUNDING

This work was supported by grants from the Brazilian funding agencies Conselho Nacional de Desenvolvimento Científico e Tecnológico (CNPq - Grant Number: 401134/2014-8), Coordenação de Aperfeiçoamento de Pessoal de Nível superior (CAPES - Grant Number: 0012017), Fundação Carlos Chagas Filho de Amparo à Pesquisa do Estado do Rio de Janeiro (FAPERJ - Grant Number: e-26/201.300/2014) to JM-F.

REFERENCES

- Afzal, S., Al-Rashida, M., Hameed, A., Pelletier, J., Sévigny, J., and Iqbal, J. (2021). Synthesis, *In-Vitro* Evaluation and Molecular Docking Studies of Oxindolin Phenylhydrazine Carboxamides as Potent and Selective Inhibitors of Ectonucleoside Triphosphate Diphosphohydrolase (NTPDase). *Bioorg. Chem.* 112, 104957. doi: 10.1016/j.bioorg.2021.104957
- Afzal, S., Zaib, S., Jafari, B., Langer, P., Lecka, J., Sévigny, J., et al. (2020). Highly Potent and Selective Ectonucleoside Triphosphate Diphosphohydrolase (ENTPDase1, 2, 3 and 8) Inhibitors Having 2-Substituted-7-Trifluoromethyl-Thiadiazolopyrimidone. *Med. Chem.* 16 (5), 689–702. doi: 10.2174/1573406415666190614095821
- Al-Rashida, M., and Iqbal, J. (2014). Therapeutic Potentials of Ecto-Nucleoside Triphosphate Diphosphohydrolase, Ecto-Nucleotide Pyrophosphatase/Phosphodiesterase, Ecto-5'-Nucleotidase, and Alkaline Phosphatase Inhibitors. *Med. Res. Rev.* 34 (4), 703–743. doi: 10.1002/med.21302
- Antonoli, L., Fornai, M., Blandizzi, C., Pacher, P., and Haskó, G. (2019). Adenosine Signaling and the Immune System: When a Lot Could be Too Much. *Immunol. Lett.* 205, 9–15. doi: 10.1016/j.imlet.2018.04.006
- Arora, K., and Rai, A. K. (2019). Dependence of *Leishmania* Parasite on Host Derived ATP: An Overview of Extracellular Nucleotide Metabolism in Parasite. *J. Parasitol. Dis.* 43 (1), 1–13. doi: 10.1007/s12639-018-1061-4
- Asai, T., Miura, S., Sibley, L. D., Okabayashi, H., and Takeuchi, T. (1995). Biochemical and Molecular Characterization of Nucleoside Triphosphate Hydrolase Isozymes From the Parasitic Protozoan *Toxoplasma Gondii*. *J. Biol. Chem.* 270 (19), 11391–11397. doi: 10.1074/jbc.270.19.11391
- Baqi, Y., Rashed, M., Schäkel, L., Malik, E. M., Pelletier, J., Sévigny, J., et al. (2020). Development of Anthraquinone Derivatives as Ectonucleoside Triphosphate Diphosphohydrolase (NTPDase) Inhibitors With Selectivity for NTPDase2 and Ntpdase3. *Front. Pharmacol.* 11, 1282. doi: 10.3389/fphar.2020.01282
- Barros, F. S., De Menezes, L. F., Pinheiro, A. A., Silva, E. F., Lopes, A. H., De Souza, W., et al. (2000). Ectonucleotide Diphosphohydrolase Activities in *Entamoeba Histolytica*. *Arch. Biochem. Biophys.* 375, 304–314. doi: 10.1006/abbi.1999.1592
- Battastini, A. M. O., Figueiró, F., Leal, D. B. R., Doleski, P. H., and Schetinger, M. R. C. (2021). CD39 and CD73 as Promising Therapeutic Targets: What Could Be the Limitations? *Front. Pharmacol.* 12, 633603. doi: 10.3389/fphar.2021.633603
- Bernardes, C. F., Meyer-Fernandes, J. R., Saad-Nehme, J., Vannier-Santos, M. A., Peres-Sampaio, C. E., and Vercesi, A. E. (2000). Effects of 4,4'-Diisothiocyanatostilbene-2,2'-Disulfonic Acid on *Trypanosoma Cruzi* Proliferation and Ca²⁺ Homeostasis. *Int. J. Biochem. Cell Biol.* 32, 519–527. doi: 10.1016/S1357-2725(00)00002-9
- Berrêdo-Pinho, M., Peres-Sampaio, C. E., Chrispim, P. P., Belmont-Firpo, R., Lemos, A. P., Martiny, A., et al. (2001). A Mg-Dependent Ecto-ATPase in *Leishmania Amazonensis* and its Possible Role in Adenosine Acquisition and Virulence. *Arch. Biochem. Biophys.* 391 (1), 16–24. doi: 10.1006/abbi.2001.2384
- Bisaggio, D. F., Peres-Sampaio, C. E., Meyer-Fernandes, J. R., and Souto-Padron, T. (2003). Ecto-ATPase Activity on the Surface of *Trypanosoma Cruzi* and its Possible Role in the Parasite-Host Cell Interaction. *Parasitology Res.* 91 (4), 273–282. doi: 10.1007/s00436-003-0965-8
- Bottari, N. B., Reichert, K. P., Fracasso, M., Dutra, A., Assmann, C. E., Ulrich, H., et al. (2020). Neuroprotective Role of Resveratrol Mediated by Purinergic Signalling in Cerebral Cortex of Mice Infected by *Toxoplasma Gondii*. *Parasitol. Res.* 119 (9), 2897–2905. doi: 10.1007/s00436-020-06795-0
- Burza, S., Croft, S. L., and Boelaert, M. (2018). Leishmaniasis. *Lancet (London England)* 392 (10151), 951–970. doi: 10.1016/S0140-6736(18)31204-2
- Büscher, P., Cecchi, G., Jamonneau, V., and Priotto, G. (2017). Human African Trypanosomiasis. *Lancet (London England)* 390 (10110), 2397–2409. doi: 10.1016/S0140-6736(17)31510-6
- Chaves, M. M., Savio, L., and Coutinho-Silva, R. (2021). Purinergic Signaling: A New Front-Line Determinant of Resistance and Susceptibility in Leishmaniasis. *Biomed. J.* S2319-4170(21)00069-X. doi: 10.1016/j.bj.2021.06.003
- Colley, D. G., and Secor, W. E. (2014). Immunology of Human Schistosomiasis. *Parasite Immunol.* 36 (8), 347–357. doi: 10.1111/pim.12087
- Coutinho-Silva, R., and Savio, L. (2021). Purinergic Signalling in Host Innate Immune Defence Against Intracellular Pathogens. *Biochem. Pharmacol.* 187, 114405. doi: 10.1016/j.bcp.2021.114405
- Csóka, B., Himer, L., Selmecezy, Z., Vizi, E. S., Pacher, P., Ledent, C., et al. (2008). Adenosine A2A Receptor Activation Inhibits T Helper 1 and T Helper 2 Cell Development and Effector Function. *FASEB J.* 22 (10), 3491–3499. doi: 10.1096/fj.08-107458
- Da'dara, A. A., Bhardwaj, R., and Skelly, P. J. (2014). Schistosome Apyrase SmATPDase1, But Not SmATPDase2, Hydrolyses Exogenous ATP and ADP. *Purinergic Signal.* 10 (4), 573–580. doi: 10.1007/s11302-014-9416-5
- Dalla Rosa, L., da Silva, A. S., Gressler, L. T., Oliveira, C. B., Dambrós, M. G., Miletto, L. C., et al. (2013). Cordycepin (3'-Deoxyadenosine) Pentostatin (Deoxycoformycin) Combination Treatment of Mice Experimentally Infected With *Trypanosoma Evansi*. *Parasitology* 140 (5), 663–671. doi: 10.1017/S0031182012001990
- Dalla Rosa, L., Da Silva, A. S., Oliveira, C. B., Gressler, L. T., Arnold, C. B., Baldissera, M. D., et al. (2015). Dose Finding of 3'-deoxyadenosine and Deoxycoformycin for the Treatment of *Trypanosoma Evansi* Infection: An Effective and Nontoxic Dose. *Microb. Pathog.* 85, m21–m28. doi: 10.1016/j.micpath.2015.05.005
- da Silva, W., da Rocha Torres, N., de Melo Agripino, J., da Silva, V., de Souza, A., Ribeiro, I. C., et al. (2021). ENTDPases From Pathogenic Trypanosomatids and Purinergic Signaling: Shedding Light Towards Biotechnological Applications. *Curr. Topics Med. Chem.* 21 (3), 213–226. doi: 10.2174/1568026620666201005125146
- de Aguiar Matos, J. A., Borges, F. P., Tasca, T., Bogo, M. R., De Carli, G. A., da Graça Fauth, M., et al. (2001). Characterization of an ATP Diphosphohydrolase (Apyrase, EC 3.6.1.5) Activity in *Trichomonas Vaginalis*. *Int. J. Parasitol.* 31 (8), 770–775. doi: 10.1016/s0020-7519(01)00191-6
- de Almeida Marques-da-Silva, E., de Oliveira, J. C., Figueiredo, A. B., de Souza Lima Júnior, D., Carneiro, C. M., Rangel Fietto, J. L., et al. (2008). Extracellular Nucleotide Metabolism in *Leishmania*: Influence of Adenosine in the Establishment of Infection. *Microbes Infect.* 10 (8), 850–857. doi: 10.1016/j.micinf.2008.04.016
- de Carvalho, L., Alves, I. J., Junqueira, L. R., Silva, L. M., Riani, L. R., de Faria Pinto, P., et al. (2019). ATP-Diphosphohydrolases in Parasites: Localization, Functions and Recent Developments in Drug Discovery. *Curr. Protein Pept. Sci.* 20 (9), 873–884. doi: 10.2174/1389203720666190704152827
- de Carvalho, L. S. A., Geraldo, R. B., De Moraes, J., Silva Pinto, P. L., De Faria Pinto, P., Pereira, O. D. S., et al. (2015). Schistosomicidal Activity and Docking of *Schistosoma Mansoni* ATPDase 1 With Licoflavone B Isolated From *Glycyrrhiza Inflata* (Fabaceae). *Exp. Parasitol.* 159, 207–214. doi: 10.1016/j.exppara.2015.09.015
- de Castro, C. C., Costa, P. S., Laktin, G. T., de Carvalho, P. H., Geraldo, R. B., de Moraes, J., et al. (2015). Cardamonin, a Schistosomicidal Chalcone From Piper Aduncum L. (Piperaceae) That Inhibits *Schistosoma Mansoni* ATP Diphosphohydrolase. *Phytomedicine* 22 (10), 921–928. doi: 10.1016/j.phymed.2015.06.009
- de Jesus, J. B., de Sá Pinheiro, A. A., Lopes, A. H., and Meyer-Fernandes, J. R. (2002). An Ectonucleotide ATP-Diphosphohydrolase Activity in *Trichomonas Vaginalis* Stimulated by Galactose and its Possible Role in Virulence. *Z. Naturforsch.* C, 57, 890–896. doi: 10.1515/znc-2002-9-1022
- DeMarco, R., Kowaltowski, A. T., Mortara, R. A., and Verjovski-Almeida, S. (2003). Molecular Characterization and Immunolocalization of *Schistosoma Mansoni* ATP-Diphosphohydrolase. *Biochem. Biophys. Res. Commun.* 307 (4), 831–838. doi: 10.1016/S0006-291X(03)01268-3
- de Souza Leite, M., Thomaz, R., Fonseca, F. V., Panizzutti, R., Vercesi, A. E., and Meyer-Fernandes, J. R. (2007). *Trypanosoma Brucei Brucei*: Biochemical Characterization of Ecto-Nucleoside Triphosphate Diphosphohydrolase Activities. *Exp. Parasitol.* 115 (4), 315–323. doi: 10.1016/j.exppara.2006.09.002
- Desquesnes, M., Dargantes, A., Lai, D. H., Lun, Z. R., Holzmüller, P., and Jittapalpong, S. (2013). *Trypanosoma Evansi* and Surra: A Review and Perspectives on Transmission, Epidemiology and Control, Impact, and Zoonotic Aspects. *BioMed. Res. Int.* 2013, 321237. doi: 10.1155/2013/321237
- Detoni, M. L., Fessel, M. R., Maia, A. C., Porcino, G. N., Quellis, L. R., Faria-Pinto, P., et al. (2013). An Antigenic Domain of the *Leishmania Amazonensis* Nucleoside Triphosphate Diphosphohydrolase (NTPDase 1) Is Associated With Disease Progression in Susceptible Infected Mice. *Parasitol. Res.* 112 (8), 2773–2782. doi: 10.1007/s00436-013-3445-9
- do Carmo, G. M., Doleski, P. H., de Sá, M. F., Grando, T. H., Azevedo, M. I., Manzoni, A. G., et al. (2017). Treatment With 3'-Deoxyadenosine and Deoxycoformycin in Mice Infected by *Trypanosoma Cruzi* and Its Side Effect

- on Purinergic Enzymes. *Microb. Pathog.* 113, 51–56. doi: 10.1016/j.micpath.2017.10.030
- Doleski, P. H., Leal, D., Machado, V. S., Bottari, N. B., Manzoni, A. G., Casali, E. A., et al. (2017b). Diphenyl Diselenide Modulates Nucleotidases, Reducing Inflammatory Responses in the Liver of *Toxoplasma Gondii*-Infected Mice. *Purinergic Signal.* 13 (4), 489–496. doi: 10.1007/s11302-017-9575-2
- Doleski, P. H., Ten Caten, M. V., Passos, D. F., Castilhos, L. G., Leal, D., Machado, V. S., et al. (2017a). Toxoplasmosis Treatment With Diphenyl Diselenide in Infected Mice Modulates the Activity of Purinergic Enzymes and Reduces Inflammation in Spleen. *Exp. Parasitol.* 181, 7–13. doi: 10.1016/j.exppara.2017.07.001
- Ennes-Vidal, V., Castro, R. O., Britto, C., Barrabin, H., D'Avila-Levy, C. M., and Moreira, O. C. (2011). CrATP Interferes in the Promastigote-Macrophage Interaction in *Leishmania Amazonensis* Infection. *Parasitology* 138 (8), 960–968. doi: 10.1017/S0031182011000710
- Farah, I. O., Nyindo, M., King, C. L., and Hau, J. (2000). Hepatic Granulomatous Response to *Schistosoma Mansoni* Eggs in BALB/c Mice and Olive Baboons (*Papio Cynocephalus Anubis*). *J. Comp. Pathol.* 123 (1), 7–14. doi: 10.1053/jcpa.1999.0378
- Faria-Pinto, P., Meirelles, M. N., Lenzi, H. L., Mota, E. M., Penido, M. L., Coelho, P. M., et al. (2004). ATP Diphosphohydrolase From *Schistosoma Mansoni* Egg: Characterization and Immunocytochemical Localization of a New Antigen. *Parasitology* 129, 51–57. doi: 10.1017/s0031182004005244
- Faria-Pinto, P., Montesano, M. A., Jacinto, A. A., Santos, R. S., Bordin, F. H., Ferreira, A. P., et al. (2010). Antibody Reactivity Against Potato Apyrase, a Protein That Shares Epitopes With *Schistosoma Mansoni* ATP Diphosphohydrolase Isoforms, in Acute and Chronically Infected Mice, After Chemotherapy and Reinfection. *Memorias do Inst Oswaldo Cruz* 105 (4), 374–379. doi: 10.1590/s0074-02762010000400005
- Faria-Pinto, P., Rezende-Soares, F. A., Molica, A. M., Montesano, M. A., Marques, M. J., Rocha, M. O., et al. (2008). Mapping of the Conserved Antigenic Domains Shared Between Potato Apyrase and Parasite ATP Diphosphohydrolases: Potential Application in Human Parasitic Diseases. *Parasitology* 135 (8), 943–953. doi: 10.1017/S0031182008004538
- Ferla, M., and Tasca, T. (2021). The Role of Purinergic Signaling in *Trichomonas Vaginalis* Infection. *Curr. Topics Medicinal Chem.* 21 (3), 181–192. doi: 10.2174/1568026620999200904122212
- Fietto, J. L., DeMarco, R., Nascimento, I. P., Castro, I. M., Carvalho, T. M., de Souza, W., et al. (2004). Characterization and Immunolocalization of an NTP Diphosphohydrolase of *Trypanosoma Cruzi*. *Biochem. Biophys. Res. Commun.* 316, 454–460. doi: 10.1016/j.bbrc.2004.02.07
- Figueiredo, A. B., Serafim, T. D., Marques-da-Silva, E. A., Meyer-Fernandes, J. R., and Afonso, L. C. C. (2012). *Leishmania Amazonensis* Impairs DC Function by Inhibiting CD40 Expression via A_{2B} Adenosine Receptor Activation. *Eur. J. Immunol.* 42, 1203–1215. doi: 10.1002/eji.201141926
- Figueiredo, A. B., Souza-Testasica, M. C., and Afonso, L. C. C. (2016). Purinergic Signaling and Infection by *Leishmania*: A New Approach to Evasion of the Immune Response. *Biomed. J.* 39 (4), 244–250. doi: 10.1016/j.bj.2016.08.004
- Figueiredo, A. B., Souza-Testasica, M. C., Mineo, T. W. P., and Afonso, L. C. C. (2017). *Leishmania Amazonensis*-Induced cAMP Triggered by Adenosine A_{2B} Receptor Is Important to Inhibit Dendritic Cell Activation and Evade Immune Response in Infected Mice. *Front. Immunol.* 8, 849. doi: 10.3389/fimmu.2017.00849
- Fonseca, F. V., Fonseca de Souza, A. L., Mariano, A. C., Entringer, P. F., Gondim, K. C., and Meyer-Fernandes, J. R. (2006). *Trypanosoma Rangeli*: Characterization of a Mg-Dependent Ecto ATP-Diphosphohydrolase Activity. *Exp. Parasitology* 112 (2), 76–84. doi: 10.1016/j.exppara.2005.09.005
- Fracasso, M., Reichert, K., Bottari, N. B., da Silva, A. D., Schetinger, M., Monteiro, S. G., et al. (2021). Involvement of Ectonucleotidases and Purinergic Receptor Expression During Acute Chagas Disease in the Cortex of Mice Treated With Resveratrol and Benznidazole. *Purinergic Signal.* 17 (3), 493–502. doi: 10.1007/s11302-021-09803-9
- Franco, R., Casadó, V., Ciruela, F., Saura, C., Mallol, J., Canela, E. I., et al. (1997). Cell Surface Adenosine Deaminase: Much More Than an Ecto-enzyme. *Prog. Neurobiol.* 52 (4), 283–294. doi: 10.1016/s0301-0082(97)00013-0
- Frasson, A. P., De Carli, G. A., Bonan, C. D., and Tasca, T. (2012). Involvement of Purinergic Signaling on Nitric Oxide Production by Neutrophils Stimulated With *Trichomonas Vaginalis*. *Purinergic Signal.* 8 (1), 1–9. doi: 10.1007/s11302-011-9254-7
- Frasson, A. P., Dos Santos, O., Meirelles, L. C., Macedo, A. J., and Tasca, T. (2016). Five Putative Nucleoside Triphosphate Diphosphohydrolase Genes Are Expressed in *Trichomonas Vaginalis*. *FEMS Microbiol. Lett.* 363 (2), fnv221. doi: 10.1093/femsle/fnv221
- Frasson, A. P., Menezes, C. B., Goelzer, G. K., Gnoatto, S. C. B., Garcia, S. C., and Tasca, T. (2017). Adenosine Reduces Reactive Oxygen Species and Interleukin-8 Production by *Trichomonas Vaginalis*-Stimulated Neutrophils. *Purinergic Signal.* 13 (4), 569–577. doi: 10.1007/s11302-017-9584-1
- Fredholm, B. B., Chern, Y., Franco, R., and Sitkovsky, M. (2007). Aspects of the General Biology of Adenosine A_{2A} Signaling. *Prog. Neurobiol.* 83, 263–276. doi: 10.1016/j.pneurobio.2007.07.005
- Gendron, F. P., Benrezzak, O., Krugh, B. W., Kong, Q., Weisman, G. A., and Beaudoin, A. R. (2002). Purine Signaling and Potential New Therapeutic Approach: Possible Outcomes of NTPDase Inhibition. *Curr. Drug Targets* 3 (3), 229–245. doi: 10.2174/1389450023347713
- Gendron, F. P., Halbfinger, E., Fischer, B., Duval, M., D'Orléans-Juste, P., and Beaudoin, A. R. (2000). Novel Inhibitors of Nucleoside Triphosphate Diphosphohydrolases: Chemical Synthesis and Biochemical and Pharmacological Characterizations. *J. Med. Chem.* 43 (11), 2239–2247. doi: 10.1021/jm000020b
- Giarola, N. L., de Almeida-Amaral, E. E., Collopy-Júnior, I., Fonseca-de-Souza, A. L., Majerowicz, D., Paes, L. S., et al. (2013). *Trypanosoma Cruzi*: Effects of Heat Shock on Ecto-ATPase Activity. *Exp. Parasitol.* 133 (4), 434–441. doi: 10.1016/j.exppara.2012.12.014
- Giarola, N. L., Silveira, T. S., Inacio, J. D., Vieira, L. P., Almeida-Amaral, E. E., and Meyer-Fernandes, J. R. (2014). *Leishmania Amazonensis*: Increase in Ecto-ATPase Activity and Parasite Burden of Vinblastine-Resistant Protozoa. *Exp. Parasitol.* 146, 25–33. doi: 10.1016/j.exppara.2014.08.013
- Giordani, R. B., Weizenmann, M., Rosemberg, D. B., De Carli, G. A., Bogo, M. R., Zuanazzi, J. A., et al. (2010). *Trichomonas Vaginalis* Nucleoside Triphosphate Diphosphohydrolase and Ecto-5'-Nucleotidase Activities are Inhibited by Lycorine and Candimime. *Parasitol. Int.* 59 (2), 226–231. doi: 10.1016/j.parint.2010.02.004
- Gomes, R. S., de Carvalho, L. C., de Souza Vasconcellos, R., Fietto, J. L., and Afonso, L. C. (2015). E-NTPDase (Ecto-Nucleoside Triphosphate Diphosphohydrolase) of *Leishmania Amazonensis* Inhibits Macrophage Activation. *Microbes Infect.* 17 (4), 295–303. doi: 10.1016/j.micinf.2014.12.009
- Gusmão, M., Júnior, S. M., Marconato, D. G., Emidio, N. B., Farani, P., Gollner, Á. M., et al. (2021). Potato Apyrase Reduces Granulomatous Area and Increases Presence of Multinucleated Giant Cells in Murine Schistosomiasis. *Parasitology Int.* 83, 102317. doi: 10.1016/j.parint.2021.102317
- Handa, M., and Guidotti, G. (1996). Purification and Cloning of a Soluble ATP-Diphosphohydrolase (Apyrase) From Potato Tubers (*Solanum Tuberosum*). *Biochem. Biophys. Res. Commun.* 218 (3), 916–923. doi: 10.1006/bbrc.1996.0162
- Haskó, G., Antonioli, L., and Cronstein, B. N. (2018). Adenosine Metabolism, Immunity and Joint Health. *Biochem. Pharmacol.* 151, 307–313. doi: 10.1016/j.bcp.2018.02.002
- Hayat, K., Afzal, S., Saeed, A., Murtaza, A., Ur Rahman, S., Khan, K. M., et al. (2019). Investigation of New Quinoline Derivatives as Promising Inhibitors of NTPDases: Synthesis, SAR Analysis and Molecular Docking Studies. *Bioorg. Chem.* 87, 218–226. doi: 10.1016/j.bioorg.2019.03.019
- Hutchinson, R., and Stevens, J. R. (2018). Barcoding in Trypanosomes. *Parasitology* 145 (5), 563–573. doi: 10.1017/S0031182017002049
- Iqbal, J., and Shah, S. (2018). Molecular Dynamic Simulations Reveal Structural Insights Into Substrate and Inhibitor Binding Modes and Functionality of Ecto-Nucleoside Triphosphate Diphosphohydrolases. *Sci. Rep.* 8 (1), 2581. doi: 10.1038/s41598-018-20971-4
- Jeffrey, J. L., Lawson, K. V., and Powers, J. P. (2020). Targeting Metabolism of Extracellular Nucleotides via Inhibition of Ectonucleotidases CD73 and CD39. *J. Med. Chem.* 63 (22), 13444–13465. doi: 10.1021/acs.jmedchem.0c01044
- Jesus, J. B., Lopes, A. H., and Meyer-Fernandes, J. R. (2002). Characterization of an Ecto-ATPase of *Trichomonas Foetus*. *Vet. Parasitol.* 103, 29–42. doi: 10.1016/s0304-4017(01)00576-3
- Kanwal, M., Mohammed Khan, K., Salar, U., Afzal, S., Wadood, A., Taha, M., et al. (2019). Schiff Bases of Tryptamine as Potent Inhibitors of Nucleoside Triphosphate Diphosphohydrolases (NTPDases): Structure-Activity Relationship. *Bioorg. Chem.* 82, 253–266. doi: 10.1016/j.bioorg.2018.10.046
- Klaver, D., and Thurnher, M. (2021). Control of Macrophage Inflammation by P2Y Purinergic Receptors. *Cells* 10 (5), 1098. doi: 10.3390/cells10051098

- Knowles, A. F. (2011). The GDA1_CD39 Superfamily: NTPDases With Diverse Functions. *Purinergic Signal.* 7 (1), 21–45. doi: 10.1007/s11302-010-9214-7
- Kukulski, F., Lévesque, S. A., and Sévigny, J. (2011). Impact of Ecto-enzymes on P2 and P1 Receptor Signaling. *Adv. Pharmacol.* 61, 263–299. doi: 10.1016/B978-0-12-385526-8.00009-6
- Lambrecht, G., Braun, K., Damer, M., Ganso, M., Hildebrandt, C., Ullmann, H., et al. (2002). Structure-Activity Relationships of Suramin and Pyridoxal-5'-Phosphate Derivatives as P2 Receptor Antagonists. *Curr. Pharm. Design* 8 (26), 2371–2399. doi: 10.2174/1381612023392973
- Lecka, J., Gillerman, I., Fausther, M., Salem, M., Munkonda, M. N., Brosseau, J. P., et al. (2013). 8-BuS-ATP Derivatives as Specific NTPDase1 Inhibitors. *Br. J. Pharmacol.* 169 (1), 179–196. doi: 10.1111/bph.12135
- Lee, S. Y., Fiene, A., Li, W., Hanck, T., Brylev, K. A., Fedorov, V. E., et al. (2015). Polyoxometalates–Potent and Selective Ecto-Nucleotidase Inhibitors. *Biochem. Pharmacol.* 93 (2), 171–181. doi: 10.1016/j.bcp.2014.11.002
- Leite, P. M., Gomes, R. S., Figueiredo, A. B., Serafim, T. D., Tafuri, W. L., de Souza, C. C., et al. (2012). Ecto-Nucleotidase Activities of Promastigotes From *Leishmania (Viannia) Braziliensis* Relates to Parasite Infectivity and Disease Clinical Outcome. *PLoS Neglected Trop. Dis.* 6 (10), e1850. doi: 10.1371/journal.pntd.0001850
- Levano-García, J., Mortara, R. A., Verjovski-Almeida, S., and DeMarco, R. (2007). Characterization of *Schistosoma Mansoni* ATPDase2 Gene, a Novel Apyrase Family Member. *Biochem. Biophys. Res. Commun.* 352 (2), 384–389. doi: 10.1016/j.bbrc.2006.11.023
- Lévesque, S. A., Lavoie, E. G., Lecka, J., Bigonnesse, F., and Sévigny, J. (2007). Specificity of the Ecto-ATPase Inhibitor ARL 67156 on Human and Mouse Ectonucleotidases. *Br. J. Pharmacol.* 152 (1), 141–150. doi: 10.1038/sj.bjp.070736
- Lopez, V., Schäkel, L., Schuh, H., Schmidt, M. S., Mirza, S., Renn, C., et al. (2021). Sulfated Polysaccharides From Macroalgae Are Potent Dual Inhibitors of Human ATP-Hydrolyzing Ectonucleotidases NPP1 and CD39. *Marine Drugs* 19 (2), 51. doi: 10.3390/md19020051
- Maia, A. C., Porcino, G. N., Detoni, M., Emidio, N. B., Marconato, D. G., Faria-Pinto, P., et al. (2013). An Antigenic Domain Within a Catalytically Active *Leishmania Infantum* Nucleoside Triphosphate Diphosphohydrolase (NTPDase 1) is a Target of Inhibitory Antibodies. *Parasitol. Int.* 62 (1), 44–52. doi: 10.1016/j.parint.2012.09.004
- Marconato, D. G., Gusmão, M., Melo, J., Castro, J., Macedo, G. C., Vasconcelos, E. G., et al. (2017). Antischistosome Antibodies Change NTPDase 1 Activity From Macrophages. *Parasite Immunol.* 39 (11), e12487. doi: 10.1111/pim.12487
- Mariotini-Moura, C., Silva e Bastos, M., de Castro, F. F., Trindade, M. L., Vasconcellos, R., Neves-do-Valle, M. A., et al. (2014). *Trypanosoma Cruzi* Nucleoside Triphosphate Diphosphohydrolase 1 (TcNTPDase-1) Biochemical Characterization, Immunolocalization and Possible Role in Host Cell Adhesion. *Acta Tropica* 130, 140–147. doi: 10.1016/j.actatropica.2013.11.008
- Martins, S. M., Torres, C. R., and Ferreira, S. T. (2000). Inhibition of the Ecto-ATPDiphosphohydrolase of *Schistosoma Mansoni* by Thapsigargin. *Biosci Rep.* 20 (5), 369–381. doi: 10.1023/a:1010330017583
- Meyer-Fernandes, J. R. (2002). Ecto-ATPases in Protozoa Parasites: Looking for a Function. *Parasitol. Int.* 51 (3), 299–303. doi: 10.1016/s1383-5769(02)00017-x
- Meyer-Fernandes, J. R., Dutra, P. M., Rodrigues, C. O., Saad-Nehme, J., and Lopes, A. H. (1997). Mg-Dependent Ecto-ATPase Activity in *Leishmania Tropica*. *Arch. Biochem. Biophys.* 341 (1), 40–46. doi: 10.1006/abbi.1997.9933
- Meyer-Fernandes, J. R., Lanz-Mendoza, H., Gondim, K. C., Willott, E., and Wells, M. A. (2000). Ectonucleotide Diphosphohydrolase Activities in Hemocytes of Larval *Manduca Sexta*. *Arch. Biochem. Biophys.* 382 (1), 152–159. doi: 10.1006/abbi.2000.1980
- Meyer-Fernandes, J. R., Saad-Nehme, J., Peres-Sampaio, C. E., Belmont-Firpo, R., Bisaggio, D. F., Do Couto, L. C., et al. (2004). A Mg-Dependent Ecto-ATPase Is Increased in the Infective Stages of *Trypanosoma Cruzi*. *Parasitol. Res.* 93 (1), 567–576. doi: 10.1007/s00436-003-1066-4
- Mielczarek, E., and Blaszkowska, J. (2016). *Trichomonas Vaginalis*: Pathogenicity and Potential Role in Human Reproductive Failure. *Infection* 44 (4), 447–458. doi: 10.1007/s15010-015-0860-0
- Montoya, J. G., and Liesenfeld, O. (2004). Toxoplasmosis. *Lancet (London England)* 363 (9425), 1965–1976. doi: 10.1016/S0140-6736(04)16412-X
- Moreira, O. C., Rios, P. F., Esteves, F. F., Meyer-Fernandes, J. R., and Barrabin, H. (2009). CrATP as a New Inhibitor of Ectoatpases of Trypanosomatids. *Parasitology* 136, 35–44. doi: 10.1017/S0031182008005118
- Moretti, N. S., Mortara, R. A., and Schenkman, S. (2020). *Trypanosoma Cruzi*. *Trends Parasitol.* 36 (4), 404–405. doi: 10.1016/j.pt.2019.10.002
- Munkonda, M. N., Kauffenstein, G., Kukulski, F., Lévesque, S. A., Legendre, C., Pelletier, J., et al. (2007). Inhibition of Human and Mouse Plasma Membrane Bound NTPDases by P2 Receptor Antagonists. *Biochem. Pharmacol.* 74 (10), 1524–1534. doi: 10.1016/j.bcp.2007.07.033
- Munkonda, M. N., Pelletier, J., Ivanenkov, V. V., Fausther, M., Tremblay, A., Künzli, B., et al. (2009). Characterization of a Monoclonal Antibody as the First Specific Inhibitor of Human NTP Diphosphohydrolase-3: Partial Characterization of the Inhibitory Epitope and Potential Applications. *FEBS J.* 276 (2), 479–496. doi: 10.1111/j.1742-4658.2008.06797.x
- Murtaza, A., Afzal, S., Zaman, G., Saeed, A., Pelletier, J., Sévigny, J., et al. (2021). Divergent Synthesis and Elaboration of Structure Activity Relationship for Quinoline Derivatives as Highly Selective NTPDase Inhibitor. *Bioorg Chem.* 115, 105240. doi: 10.1016/j.bioorg.2021.105240
- Nakaar, V., Beckers, C. J., Polotsky, V., and Joiner, K. A. (1998). Basis for Substrate Specificity of the *Toxoplasma Gondii* Nucleoside Triphosphate Hydrolase. *Mol. Biochem. Parasitol.* 97 (1–2), 209–220. doi: 10.1016/S0166-6851(98)00153-4
- Nakaar, V., Samuel, B. U., Ngo, E. O., and Joiner, K. A. (1999). Targeted Reduction of Nucleoside Triphosphate Hydrolase by Antisense RNA Inhibits *Toxoplasma Gondii* Proliferation. *J. Biol. Chem.* 274 (8), 5083–5087. doi: 10.1074/jbc.274.8.5083
- Novaes, R. D., Santos, E. C., Cupertino, M. C., Bastos, D., Mendonça, A., Marques-da-Silva, E. A., et al. (2018). Purinergic Antagonist Suramin Aggravates Myocarditis and Increases Mortality by Enhancing Parasitism, Inflammation, and Reactive Tissue Damage in *Trypanosoma Cruzi*-Infected Mice. *Oxid. Med. Cell. Longev.* 2018, 7385639. doi: 10.1155/2018/7385639
- Olivier, M., Gregory, D. J., and Forget, G. (2005). Subversion Mechanisms by Which *Leishmania* Parasites can Escape the Host Immune Response: A Signaling Point of View. *Clin. Microbiol. Rev.* 18, 293–305. doi: 10.1128/CMR.18.2.293-305.2005
- Pace, D. (2014). Leishmaniasis. *J. Infect.* 69 (Suppl 1), S10–S18. doi: 10.1016/j.jinf.2014.07.016
- Paes-Vieira, L., Gomes-Vieira, A., and Meyer-Fernandes, J. R. (2018). NTPDase Activities: Possible Roles on *Leishmania Spp* Infectivity and Virulence. *Cell Biol. Int.* 42, 670–682. doi: 10.1002/cbin.10944
- Paes-Vieira, L., Rocco-Machado, N., Freitas-Mesquita, A. L., Dos Santos Emiliano, Y. S., Gomes-Vieira, A. L., de Almeida-Amaral, E. E., et al. (2021). Differential Regulation of E-NTPDases During *Leishmania Amazonensis* Lifecycle and Effect of Their Overexpression on Parasite Infectivity and Virulence. *Parasitol. Int.* 85, 102423. doi: 10.1016/j.parint.2021.102423
- Paletta-Silva, R., and Meyer-Fernandes, J. R. (2012). Adenosine and Immune Imbalance in Visceral Leishmaniasis: The Possible Role of Ectonucleotidases. *J. Trop. Med.* 2012:650874. doi: 10.1155/2012/650874
- Pelletier, J., Agonsanou, H., Delvalle, N., Fausther, M., Salem, M., Gulbransen, B., et al. (2017). Generation and Characterization of Polyclonal and Monoclonal Antibodies to Human NTPDase2 Including a Blocking Antibody. *Purinergic Signal.* 13 (3), 293–304. doi: 10.1007/s11302-017-9561-8
- Pereira, V., Junior, I., da Silveira, L. S., Geraldo, R. B., de F. Pinto, P., Teixeira, F. S., et al. (2018). *In Vitro* and *In Vivo* Antischistosomal Activities of Chalcones. *Chem. Biodivers* 15 (12), e1800398. doi: 10.1002/cbdv.201800398
- Peres, N. T. A., Cunha, L. C. S., Barbosa, M. L. A., Santos, M. B., Oliveira, F. A., de Jesus, A. M. R., et al. (2018). Infection of Human Macrophages by *Leishmania Infantum* Is Influenced by Ecto-Nucleotidases. *Front. Immunol.* 8, 1954. doi: 10.3389/fimmu.2017.01954
- Petró-Silveira, B., Rigo, G. V., da Silva Trentin, D., Macedo, A. J., Sauer, E., de Oliveira Alves, E., et al. (2020). *Trichomonas Vaginalis* NTPDase Inhibited by Lycorine Modulates the Parasite-Neutrophil Interaction. *Parasitol. Res.* 119 (8), 2587–2595. doi: 10.1007/s00436-020-06739-8
- Pimentel, F. G., Bastos, M. S., Santos, R. F., Mariotini-Moura, C., Bressan, G. C., Silva-Junior, A., et al. (2016). The *Leishmania*-Macrophage Interactions: Role of E-NTPDases and Purinergic Signaling. *Macrophage* 3, 1143–1155. doi: 10.14800/Macrophage.1143
- Pinheiro, C. M., Martins-Duarte, E. S., Ferraro, R. B., Fonseca de Souza, A. L., Gomes, M. T., Lopes, A. H., et al. (2006). *Leishmania Amazonensis*: Biological and Biochemical Characterization of Ecto-Nucleoside Triphosphate Diphosphohydrolase Activities. *Exp. Parasitol.* 114 (1), 16–25. doi: 10.1016/j.exppara.2006.02.007

- Porcino, G. N., Carvalho-Campos, C., Maia, A. C., Detoni, M. L., Faria-Pinto, P., Coimbra, E. S., et al. (2012). *Leishmania (Viannia) Braziliensis* Nucleoside Triphosphate Diphosphohydrolase (NTPDase 1): Localization and *In Vitro* Inhibition of Promastigotes Growth by Polyclonal Antibodies. *Exp. Parasitol.* 132 (2), 293–299. doi: 10.1016/j.exppara.2012.08.009
- Robson, S. C., Sévigny, J., and Zimmermann, H. (2006). The E-NTPDase Family of Ectonucleotidases: Structure Function Relationships and Pathophysiological Significance. *Purinergic Signal.* 2 (2), 409–430. doi: 10.1007/s11302-006-9003-5
- Rottenberg, M. E., Masocha, W., Ferella, M., Petitto-Assis, F., Goto, H., Kristensson, K., et al. (2005). Treatment of African Trypanosomiasis With Cordycepin and Adenosine Deaminase Inhibitors in a Mouse Model. *J. Infect. Dis.* 192 (9), 1658–1665. doi: 10.1086/496896
- Rückert, C., Stuepp, C., Gottardi, B., Rosa, J., Cisolotto, J., Borges, F. P., et al. (2009). Steroid Hormones Alter AMP Hydrolysis in Intact Trophozoites of *Trichomonas Vaginalis*. *Parasitol. Res.* 105 (6), 1701–1706. doi: 10.1007/s00436-009-1618-3
- Rückert, C., Stuepp, C., Gottardi, B., Rosa, J., Cisolotto, J., Borges, F. P., et al. (2010). *Trichomonas Vaginalis*: Dehydroepiandrosterone Sulfate and 17 β -Estradiol Alter NTPDase Activity and Gene Expression. *Exp. Parasitol.* 125 (3), 187–195. doi: 10.1016/j.exppara.2010.01.029
- Sansom, F. M. (2012). The Role of the NTPDase Enzyme Family in Parasites: What do We Know, and Where to From Here? *Parasitology* 139, 963–980. doi: 10.1017/S003118201200025X
- Sansom, F. M., Ralton, J. E., Sernee, M. F., Cohen, A. M., Hooker, D. J., Hartland, E. L., et al. (2014). Golgi-Located NTPDase1 of *Leishmania Major* is Required for Lipophosphoglycan Elongation and Normal Lesion Development Whereas Secreted NTPDase2 Is Dispensable for Virulence. *PLoS Negl. Trop. Dis.* 8, e3402. doi: 10.1371/journal.pntd.0003402
- Sansom, F. M., Robson, S. C., and Hartland, E. L. (2008). Possible Effects of Microbial Ecto-Nucleoside Triphosphate Diphosphohydrolases on Host-Pathogen Interactions. *Microbiol. Mol. Biol. Rev.* 72 (4), 765–781. doi: 10.1128/MMBR.00013-08
- Santos, R. F., Pôssa, M. A., Bastos, M. S., Guedes, P. M., Almeida, M. R., Demarco, R., et al. (2009). Influence of Ecto-Nucleoside Triphosphate Diphosphohydrolase Activity on Trypanosoma Cruzi Infectivity and Virulence. *PLoS Negl. Trop. Dis.* 3 (3), e387. doi: 10.1371/journal.pntd.0000387
- Savio, L., and Coutinho-Silva, R. (2019). Immunomodulatory Effects of P2X7 Receptor in Intracellular Parasite Infections. *Curr. Opin. Pharmacol.* 47, 53–58. doi: 10.1016/j.coph.2019.02.005
- Schachter, J., Delgado, K. V., Barreto-de-Souza, V., Bou-Habib, D. C., Persechini, P. M., and Meyer-Fernandes, J. R. (2015). Inhibition of Ecto-ATPase Activities Impair HIV-1 Infection of Macrophages. *Immunobiology* 220 (5), 589–596. doi: 10.1016/j.imbio.2014.12.004
- Silva-Gomes, N. L., Rampazzo, R. C. P., Moreira, C. M. N., Porcino, G. N., Bezerra dos Santos, C. M., Krieger, M. A., et al. (2020). Knocking Down TcNTPDase-1 Gene Reduces *In Vitro* Infectivity of *Trypanosoma Cruzi*. *Front. Microbiol.* 11, 434. doi: 10.3389/fmicb.2020.00434
- Souza, R. L., Gonçalves, U. O., Badoco, F. R., de Souza Galvão, L., Santos, R., de Carvalho, P., et al. (2017). Licochalcone A Induces Morphological and Biochemical Alterations in Schistosoma Mansoni Adult Worms. *Biomed. Pharmacother.* 96, 64–71. doi: 10.1016/j.biopha.2017.09.128
- Souza, V. L., Veras, P. S., Welby-Borges, M., Silva, T. M., Leite, B. R., Ferraro, R. B., et al. (2011). Immune and Inflammatory Responses to *Leishmania Amazonensis* Isolated From Different Clinical Forms of Human Leishmaniasis in CBA Mice. *Memorias do Inst Oswaldo Cruz* 106 (1), 23–31. doi: 10.1590/s0074-02762011000100004
- Tan, F., Hu, X., Pan, C. W., Ding, J. Q., and Chen, X. G. (2010). Monoclonal Antibodies Against Nucleoside Triphosphate Hydrolase-II can Reduce the Replication of *Toxoplasma Gondii*. *Parasitol. Int.* 59 (2), 141–146. doi: 10.1016/j.parint.2009.12.007
- Tasca, T., Bonan, C. D., De Carli, G. A., and Sarkis, J. J. (2004). *Trichomonas Vaginalis*: Cytochemical Localization of a NTPDase1 and an Ecto-5'-Nucleotidase and Effects of Adenine Nucleotides on Cellular Viability. *Parasitol. Res.* 93 (4), 300–303. doi: 10.1007/s00436-004-1126-4
- Tasca, T., Borges, F. P., Bonan, C. D., De Carli, G. A., Battastini, A. M., and Sarkis, J. J. (2003). Effects of Metronidazole and Tinidazole on NTPDase1 and Ecto-5'-Nucleotidase From Intact Cells of *Trichomonas Vaginalis*. *FEMS Microbiol. Lett.* 226 (2), 379–384. doi: 10.1016/S0378-1097(03)00637-2
- Trautmann, A. (2009). Extracellular ATP in the Immune System: More Than Just a "Danger Signal. *Sci. Signaling* 2 (56), pe6. doi: 10.1126/scisignal.256pe6
- Vasconcellos, R., Mariotini-Moura, C., Gomes, R. S., Serafim, T. D., Firmino, R., Silva E Bastos, M., et al. (2014). *Leishmania Infantum* Ecto-Nucleoside Triphosphate Diphosphohydrolase-2 is an Apyrase Involved in Macrophage Infection and Expressed in Infected Dogs. *PLoS Negl. Trop. Dis.* 8 (11), e3309. doi: 10.1371/journal.pntd.0003309
- Vasconcelos, E. G., Ferreira, S. T., Carvalho, T. M., Souza, W., Kettlun, A. M., Mancilla, M., et al. (1996). Partial Purification and Immunohistochemical Localization of ATP Diphosphohydrolase From *Schistosoma Mansoni*. Immunological Cross-Reactivities With Potato Apyrase and Toxoplasma Gondii Nucleoside Triphosphate Hydrolase. *J. Biol. Chem.* 271 (36), 22139–22145. doi: 10.1074/jbc.271.36.22139
- Vasconcelos, E. G., Nascimento, P. S., Meirelles, M. N., Verjovski-Almeida, S., and Ferreira, S. T. (1993). Characterization and Localization of an ATP-Diphosphohydrolase on the External Surface of the Tegument of *Schistosoma Mansoni*. *Mol. Biochem. Parasitol.* 58 (2), 205–214. doi: 10.1016/0166-6851(93)90042-v
- Vijayamahantesh, A., Dikhit, M. R., Mishra, A., Singh, A. K., Das, V. N., et al. (2017). Adenosine Generated by Ectonucleotidases Modulates the Host Immune System During Visceral Leishmaniasis. *Cytokine* 91, 170–179. doi: 10.1016/j.cyto.2017.01.001
- Wilson, J. M., Ross, W. G., Agbai, O. N., Frazier, R., Figler, R. A., Rieger, J., et al. (2009). The A_{2B} Adenosine Receptor Impairs the Maturation and Immunogenicity of Dendritic Cells. *J. Immunol. (Baltimore Md.: 1950)* 182 (8), 4616–4623. doi: 10.4049/jimmunol.0801279
- Wolkmer, P., Pereira, A. B., da Silva, C. B., Paim, F. C., Palma, H. E., Bueno, A., et al. (2019). Curcumin Pre-Treatments Modulate the Activities of Adenine Nucleotide and Nucleoside Degradation Enzymes in Lymphocyte of Rats Infected With *Trypanosoma Evansi*. *Parasitol. Int.* 73, 101948. doi: 10.1016/j.parint.2019.101948
- Wolkmer, P., Silva, C. B., Paim, F. C., Duarte, M. M., Castro, V., Palma, H. E., et al. (2013). Pre-Treatment With Curcumin Modulates Acetylcholinesterase Activity and Proinflammatory Cytokines in Rats Infected With *Trypanosoma Evansi*. *Parasitol. Int.* 62 (2), 144–149. doi: 10.1016/j.parint.2012.11.004
- Zhao, H., Bo, C., Kang, Y., and Li, H. (2017). What Else can CD39 Tell Us? *Front. Immunol.* 8, 72. doi: 10.3389/fimmu.2017.0072
- Zhong, A. H., Gordon Jiang, Z., Cummings, R. D., and Robson, S. C. (2017). Various N-Glycoforms Differentially Upregulate E-NTPDase Activity of the NTPDase3/CD39L3 Ecto-Enzymatic Domain. *Purinergic Signal.* 13 (4), 601–609. doi: 10.1007/s11302-017-9587-y
- Zimmermann, H. (2021a). Ectonucleoside Triphosphate Diphosphohydrolases and Ecto-5'-Nucleotidase in Purinergic Signaling How the Field Developed and Where We are Now. *Purinergic Signal.* 17, 117–125. doi: 10.1007/s11302-020-09755-6
- Zimmermann, H. (2021b). History of Ectonucleotidases and Their Role in Purinergic Signaling. *Biochem. Pharmacol.* 187, 114322. doi: 10.1016/j.bcp.2020.114322
- Zimmermann, H., Zebisch, M., and Strater, N. (2012). Cellular Function and Molecular Structure of Ecto-Nucleotidases. *Purinergic Signal.* 8, 437–502. doi: 10.1007/s11302-012-9309-4

Conflict of Interest: The authors declare that the research was conducted in the absence of any commercial or financial relationships that could be construed as a potential conflict of interest.

Publisher's Note: All claims expressed in this article are solely those of the authors and do not necessarily represent those of their affiliated organizations, or those of the publisher, the editors and the reviewers. Any product that may be evaluated in this article, or claim that may be made by its manufacturer, is not guaranteed or endorsed by the publisher.

Copyright © 2021 Paes-Vieira, Gomes-Vieira and Meyer-Fernandes. This is an open-access article distributed under the terms of the Creative Commons Attribution License (CC BY). The use, distribution or reproduction in other forums is permitted, provided the original author(s) and the copyright owner(s) are credited and that the original publication in this journal is cited, in accordance with accepted academic practice. No use, distribution or reproduction is permitted which does not comply with these terms.



Trypanosoma cruzi Induces B Cells That Regulate the CD4⁺ T Cell Response

OPEN ACCESS

Edited by:

Martin M. Edreira,
Universidad de Buenos Aires
(CONICET), Argentina

Reviewed by:

Carolina Verónica Poncini,
Consejo Nacional de Investigaciones
Científicas y Técnicas (CONICET),
Argentina

Celio Geraldo Freire-de-Lima,
Federal University of Rio de Janeiro,
Brazil

Jorge Gonzalez,
University of Antofagasta, Chile

*Correspondence:

Juan Mucci
jmucci@unsam.edu.ar

[†]These authors share last authorship

Specialty section:

This article was submitted to
Parasite and Host,
a section of the journal
Frontiers in Cellular and
Infection Microbiology

Received: 04 October 2021

Accepted: 06 December 2021

Published: 05 January 2022

Citation:

Somoza M, Bertelli A,
Pratto CA, Verdun RE,
Campetella O and Mucci J
(2022) Trypanosoma cruzi
Induces B Cells That Regulate
the CD4⁺ T Cell Response.
Front. Cell. Infect. Microbiol. 11:789373.
doi: 10.3389/fcimb.2021.789373

Martín Somoza¹, Adriano Bertelli¹, Cecilia A. Pratto¹, Ramiro E. Verdun²,
Oscar Campetella^{1†} and Juan Mucci^{1*†}

¹ Instituto de Investigaciones Biotecnológicas, Universidad Nacional de San Martín-CONICET, Buenos Aires, Argentina,

² Sylvester Comprehensive Cancer Center and Division of Hematology, Department of Medicine, University of Miami Miller School of Medicine, Miami, FL, United States

Trypanosoma cruzi infection induces a polyclonal B cell proliferative response characterized by maturation to plasma cells, excessive generation of germinal centers, and secretion of parasite-unrelated antibodies. Although traditionally reduced to the humoral response, several infectious and non-infectious models revealed that B lymphocytes could regulate and play crucial roles in cellular responses. Here, we analyze the trypomastigote-induced effect on B cells, their effects on CD4⁺ T cells, and their correlation with *in vivo* findings. The trypomastigotes were able to induce the proliferation and the production of IL-10 or IL-6 of naïve B cells in co-culture experiments. Also, we found that IL-10-producing B220^o cells were elicited *in vivo*. We also found up-regulated expression of FasL and PD-L1, proteins involved in apoptosis induction and inhibition of TCR signaling, and of BAFF and APRIL mRNAs, two B-cell growth factors. Interestingly, it was observed that IL-21, which plays a critical role in regulatory B cell differentiation, was significantly increased in B220⁺/IL-21⁺ in *in vivo* infections. This is striking since the secretion of IL-21 is associated with T helper follicular cells. Furthermore, trypomastigote-stimulated B-cell conditioned medium dramatically reduced the proliferation and increased the apoptotic rate on CD3/CD28 activated CD4⁺ T cells, suggesting the development of effective regulatory B cells. In this condition, CD4⁺ T cells showed a marked decrease in proliferation and viability with marginal IL-2 or IFN γ secretion, which is counterproductive with an efficient immune response against *T. cruzi*. Altogether, our results show that B lymphocytes stimulated with trypomastigotes adopt a particular phenotype that exerts a strong regulation of this T cell compartment by inducing apoptosis, arresting cell division, and affecting the developing of a proinflammatory response.

Keywords: B cell proliferation, Chagas disease, IL-21, regulatory B cells, T CD4⁺ cells

INTRODUCTION

B cells are the main effectors of the humoral immunity, which is mediated by their activation and secretion of different classes of immunoglobulins against the original antigen (Nutt et al., 2015). However, these cells exhibit other antibody-independent functions such as their performance as antigen-presenting-cell (APC) or cytokine secretion that modulate the entire immune response (Shen and Fillatreau, 2015; Getahun and Cambier, 2019).

The immune response associated with survival against infection by *Trypanosoma cruzi*, the agent of Chagas disease, infection relies on the generation of a CD4⁺ T helper 1 (Th1) profile and a strong CD8⁺ T response that is, however, unable to resolve the infection (Tarleton et al., 2000; Kumar and Tarleton, 2001). Although the T cell response is the one that carries out the effector action, several other cell types such as macrophages and dendritic cells are also involved and have been well studied (Acevedo et al., 2018). On the other hand, beyond the particular parasite-induced proliferative effects that have been observed, our knowledge on the effect of *T. cruzi* infection on B cells is still unclear. *T. cruzi* induces polyclonal lymphocytes proliferation and unspecific hypergammaglobulinemia during the early stage of the acute phase of the infection with an antigen-specific delayed response (Ortiz-Ortiz et al., 1980; Minoprio et al., 1988; Rottenberg et al., 1993; el Bouhdidi et al., 1994; Bermejo et al., 2011). This unspecific antibody response is characterized by their maturation as plasma cells and the secretion of parasite-unrelated antibodies, a response that is maintained all along the infectious process (D'Imperio Lima et al., 1986; Minoprio et al., 1988; Bermejo et al., 2011). This pathogenic manifestation is known as polyclonal expansion and is histologically characterized by an excessive generation of germinal centers (typical and atypical) accompanied by extensive generation of extra-follicular B cell response (Montes et al., 2007; Bermejo et al., 2011). Particularly, different cell extracts or antigen preparations from either epimastigotes (the insect replicative stage) or trypomastigotes (the mammal infective stage) induce a T cell-independent B cell proliferative response and even several components of the parasite are related to this effect, although just a few are molecularly identified such as *trans*-sialidase, malate or glutamate dehydrogenase and proline racemase (Montes et al., 1999; Reina-San-Martín et al., 2000; Montes et al., 2002; Gao et al., 2002; Montes et al., 2006). In contrast, studies with live trypomastigotes are scarce.

In several models, both infectious and non-infectious, the importance of B cells in the development of the T cell response has been addressed and it has been shown that B lymphocytes can act as regulators of the T response and play an important role in the effector activities of the cellular response (Candando et al., 2014; Gorosito Serrán et al., 2015; Lykken et al., 2015; Catalán et al., 2021). There is indirect evidence of the regulatory role of B cells in the development of the immune response against *T. cruzi*. Although there are some discrepancies, most of the evidence supports the idea that both, partial (Xid mouse) and absolute (μ MT mouse) deficiencies in B cells generate important outcomes in the development of the infection, generally associated with a stronger inflammatory response presenting higher levels of IFN γ , IL-6, IL-18 and TNF α in serum (Minoprio et al., 1993; Cardillo et al., 2007; Gorosito Serrán et al., 2017; da Rocha et al., 2019). In the μ MT

mouse absolute depletion model, Gorosito Serrán et al. demonstrate that the increased of infected animals mortality was associated with an unconventional CD4⁺ T cell exacerbated response leading to an uncontrolled immune response and increased inflammation (Gorosito Serrán et al., 2017). Furthermore, it was reported that B cells help to develop the CD8⁺ response in mice infected with *T. cruzi* (Fiocca Vernengo et al., 2020). These results lead us to infer that B cells undoubtedly play a regulatory role in the overall immune response against the parasite. However, little is known about the mechanisms associated with this ability, and there is almost no direct cellular evidence that mechanistically interprets and supports these findings.

In this work, we analyze the effects of live trypomastigotes on B cells and, in turn, their regulation of the T cell compartment. In search for clues that could provide evidence, we followed the proliferative response of B cells induced by trypomastigotes, and we then analyzed their effects on T cells and their correlation with the *in vivo* findings.

MATERIALS AND METHODS

Mice

The protocol of this study was approved by the Committee on the Ethics of Animal Experiments of the Universidad Nacional de San Martín (UNSAM), following the recommendations of the Guide for the Care and Use of Laboratory Animals of the National Institutes of Health. C57BL/6J mice were obtained from The Jackson Laboratory and bred in our facilities. Male mice (60 to 90 days old) were used in all experiments.

Parasites and Infections

CL Brener parasites were obtained from infected Vero cell culture supernatants. For trypomastigotes purification, supernatants were centrifuged at high speed and incubated for 4h at 37°C and 5% CO₂, allowing motile parasites to swim towards the top of the suspension. Then, the trypomastigote-enriched upper layer was removed carefully.

For mice infections, RA trypomastigotes were obtained from infected mice whole blood and 50 parasites were injected by intraperitoneal route (i.p.). Animals were euthanized at day +14.

T and B Naïve Cell Purification

Mouse splenocytes were obtained as described previously (Díaz et al., 2015). For CD4⁺ T cell purification, MojoSort Mouse CD4 Naïve Cell Untouched Isolation kit was used, following the manufacturer's instructions (Biolegend). Cell purity (>90%) was checked by flow cytometry. For CD43⁺ naïve B cell purification, Dynabeads Mouse CD43 (Untouched B Cells) was used, following the manufacturer's instructions (Thermo Fisher Scientific). Cell purity (>95%) was checked by flow cytometry.

Cell Cultures

Purified naïve cells were plated at 1.5x10⁶/ml in the presence of 1x10⁶/ml trypomastigotes for 3-5 days depending upon the experiment. Stimulation with 5 μ g/ml anti-CD40 (1C10 clone) was used. For T cell stimulation assays, purified naïve T cells

were plated at 1×10^6 /ml in CD3 ($1 \mu\text{g}/\text{ml}$) and CD28 ($2 \mu\text{g}/\text{ml}$) pre-coated plates and incubated for 3 days. In B-T co culture experiments, cells were plated at a 1:1 ratio.

ELISAs

For cytokine secretion assays, cell culture supernatants were collected at corresponding time points, depending on the experiment. The cytokine concentrations in culture supernatants were assayed by ELISA using paired antibodies (Biolegend). For IgG assays, plates were first coated with anti-total mouse Ig's and then incubated with anti-IgG specific antibody, both from Sigma.

Standard curves were performed in the case of cytokines. For total IgG, OD values were normalized to the control condition.

Briefly, plates were coated with the corresponding antibody in Phosphate Buffer (pH 9) ON at 4°C . Blocking was performed using TBS-BSA 1% solution for 1h at RT. Samples were then incubated for 1h at RT. Detection biotinylated antibodies were incubated in TBS-BSA 0.1% solution for 1h at RT. Streptavidin-HRP conjugate (Biolegend) was added for 30' at RT in the dark. Washing steps were performed with TBS-Tween 20 0.05% three times each. Colorimetric reaction was performed with TMB (Sigma) and hydrogen peroxide in 10mM Citrate Buffer (pH 5.5). Finally, reaction was halted with Sulfuric Acid 0.2M and absorbance at 450nm was measured in Filtermax F5 (Molecular Devices).

RNA Isolation and RT-qPCR

Cells were pelleted and lysed in TRIzol solution (Thermo Fisher Scientific). mRNA was obtained following manufacturer's instructions and treated with RQ1 DNase (Promega) to eliminate possible genomic DNA contamination. RNA was quantified with NanoDrop spectrophotometer ND-1000 (Thermo). Then, RNA was retro-transcribed to cDNA with M-MLV reverse transcriptase (Promega) using Oligo dT primers (Integrated DNA Technologies), according to manufacturer's recommendations.

For qPCR, Kapa SYBR[®] Fast qPCR kit (Kapa Biosystems) was used and reactions were followed in Gene Amp 7500 Sequence Detection System (Applied Biosystems).

Polymerase chain reaction was performed using the following primer pairs: BAFF Fwd: 5'-AAGACCGTTTCTCCAGTCCTTT-3', Rv: 5'-CATGTGTACCCCAAGGCAAA-3'; APRIL Fwd: 5'-CTCTTGCCACCTCACTTCTG-3', Rv: 5'-GGAGATGAGGCTGGCATGA-3'. As housekeeping control genes: Ubiquitin C Fwd: 5'-GCCAGTGTTACCAACAAGA-3', Rv: 5'-CCCATCACACCAAGAACA-3'; GAPDH Fwd: 5'-CATCACTGCCACCCAGAAGACTG-3', Rv: 5'-ATGCCAGTGAGCTTCCCGTTTCAG-3'. Samples were analyzed by triplicate. Analysis of data was performed with LinReg software.

Flow Cytometry Analysis

Cell suspensions were incubated in PBS-azide plus anti-FcR monoclonal antibody (CD16/32; Clone 93) for 30 min on ice. Then, anti-CD80 (Clone 16-10AI), anti-CD86 (Clone PO3), anti-MHC-II (Clone M5/114.15.2), anti-CD11c (Clone N418), or anti-CD11b (Clone M1/70) mAb, anti-B220 (Clone RA3-6B2), anti-CD1d (Clone 1B1), anti-CD5 (Clone 53-7.3), anti-CD21 (Clone Bu32), anti-CD23 (Clone B3B4), anti-FasL (Clone

MFL3), anti-PDL1 (MIHS), anti-Syndecan-1 (Clone 281-2), anti-IL-6 (MP5-20F3), anti-IL-10 (JES5-16E3), anti-IL-21 (mhalx21) conjugated to distinct fluorochromes, were added in the recommended concentrations. After 1h, cells were washed, fixed with 1% *p*-formaldehyde in PBS, and analyzed by flow cytometry. All antibodies and their isotype controls were from Biolegend.

For B10 detection, splenocytes were harvested and cultured for 48h in the presence of anti-CD40 (1C10 clone) with PMA (50 ng/ml) and Ionomycin (500 ng/ml) (Sigma) for 6h and Monensin plus Brefeldin A (Biolegend) for 4h before staining. For intracellular staining, BD Cytofix/Cytoperm[™] Fixation/Permeabilization Solution Kit (Becton Dickinson) was used, following the manufacturer's instructions. Cells were analyzed in a CyFlow space (Partec, Germany) or FACSAriaII (Becton Dickinson) cytometers.

Proliferation Dye Staining

Cell suspensions were stained with CFSE following the manufacturer's instructions (Thermo Fisher Scientific). Briefly, cell suspensions were cultured in $5 \mu\text{M}$ dye solution in PBS for 15min at 37°C . The reaction was halted adding 2% cold FBS and washed.

Apoptosis Assays

Annexin V Apoptosis Detection Kit was used, following the manufacturer's instructions (Thermo Fisher Scientific). Briefly, cells were incubated in a calcium-enriched buffer, which allows binding of Annexin-V to exposed phosphatidylserine in apoptotic cell membranes. Before the flow cytometer run, cells were incubated in a propidium iodide solution to check the membrane integrity.

Statistical Analysis

Analysis of variance (ANOVA) with Bonferroni's correction or Student's *t* test were used for statistical analysis.

RESULTS

T. cruzi Trypomastigotes Induce Proliferation and Activation of B Cells

It has been observed *in vivo* that unspecific B cells proliferate during *T. cruzi* infection, which could be considered to occur in a T-dependent and/or in a T-independent manner (D'Imperio Lima et al., 1985; Minoprio et al., 1987). To study this phenomenon, highly purified naïve B cells (Supplementary Figure 1) stained with CFSE were cocultured with *T. cruzi* trypomastigotes during 72h (Figure 1A). As shown in Figure 1B, live trypomastigotes induced a drastic increase in the proliferation of B cells *in vitro* in a dose dependent manner. Then, to analyze the possible influence of T-cells, a CD40 agonist antibody was added because the CD40-CD40L interaction is crucial to stimulate and maintain of B cell response (Cyster and Allen, 2019). We found that the B cell proliferation was strikingly

enhanced when the agonist anti-CD40 antibody was added to the culture to mimic the presence of CD40L (**Figure 1B**). These findings support that T cells signaling plays a significant role in this process and that both T-independent and T-dependent activation are involved. In fact, in addition to an unrelated IgM response a strong collection of IgG antibodies is known to also occur.

Then, we wanted to determine the activation state of proliferating B cells exposed to trypomastigotes for 72h by determining the expression levels of the major histocompatibility complex (MHC) and costimulatory molecules. Analysis of these cell activation markers in these cultures indicated that trypomastigotes induced an activated state determined by the expression of MHC-II, CD80, and CD86 on the B cells surface (**Figure 1C**). The presence of these molecules ensures the interaction between the B cell and T cells allowing the development of their immune synapse. The immune synapse is a cornerstone in communication between the

cells involved, improving the delivery efficiency of secreted factors, and allowing the interaction of surface molecules, resulting in the regulation of the immune response.

Then, we sought to analyze the cytokine content of the supernatants coming from B cells/trypomastigotes co-cultures. We detected increased concentrations of IL-6 and IL-10 (**Figure 2A**), which are known to be associated with the regulation of the immune system (Couper et al., 2008; Jones and Jenkins, 2018). This increment was even more pronounced when an agonist anti-CD40 antibody was included to mimic the interaction with the corresponding T cells. No significant differences were detected for IL-2, IL-4, IL-17, or IFN γ (not shown) in these conditions. Intracellular staining analysis revealed the secretion of IL-10 and IL-6 only in B220⁺ cells (**Figure 2A**), showing that these cytokines were secreted from B cells and not from any other possible population of minor contaminant cells.

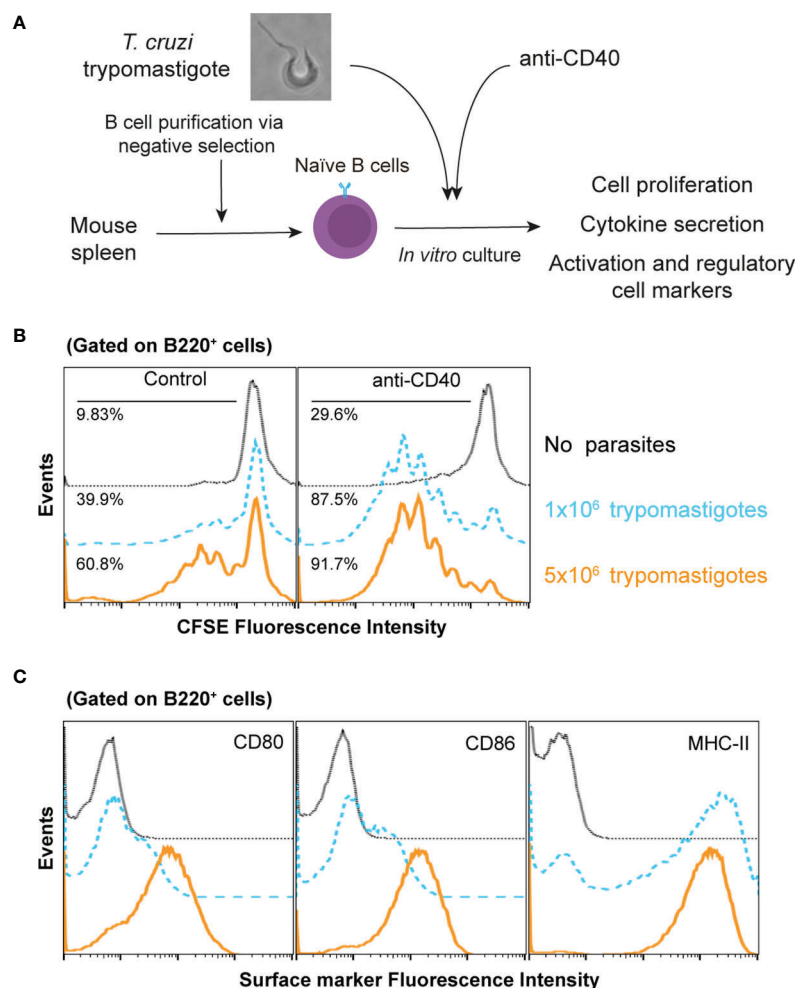


FIGURE 1 | *T. cruzi* trypomastigotes induce naïve B cell proliferation and activation. **(A)** Schematic experimental representation **(B)** CFSE-stained naïve B cells were cultured in several conditions. Dotted lines: untreated B cells; dashed lines 1x10⁶ trypomastigotes/ml; solid lines 5x10⁶ trypomastigotes/ml. **(C)** CD80, CD86 and MHCII surface expression by naïve B cells after culture with 1x10⁶ trypomastigotes/ml, as determined by flow cytometry. Dotted lines: isotypes control; dashed lines untreated B cells; solid lines cells cocultured with trypomastigotes.

We then tested whether the proliferation induced by trypomastigotes was mediated by IL-6 and IL-10, which are also involved in the activation and proliferation of B cells (Tosato et al., 1988; Rousset et al., 1992; Kopf et al., 1994; Burdin et al., 1997). Surprisingly, when the association of these cytokines with autocrine B cell proliferation was tested by adding neutralizing monoclonal antibodies to block cytokine/receptor interactions, we found that they were not involved in the process (**Supplementary Figure 2**). As described above, during *T. cruzi* infection an unrelated IgM and IgG antibodies response is known to be elicited (D'Imperio Lima et al., 1986; Minoprio et al., 1988; Bermejo et al., 2011). Regarding that, we evaluated the IgG spontaneous secretion in these conditions. We found that in B lymphocytes stimulated with trypomastigotes and cultured with neutralizing antibodies to IL-6 or IL-10, IgG secretion decreased (**Figure 2B**), suggesting that these cytokines could be involved in the unspecific secretion of immunoglobulins.

Since we have found regulatory cytokines in the supernatants of our co-cultures, we determined the expression of well-known regulatory ligands on the surface of B cells. We found that *T. cruzi* trypomastigotes positively regulate the expression of FasL and PD-L1, which are involved in inducing apoptosis of target cells and inhibiting TCR signaling, respectively. The parasite *per se* could induce the expression of both regulatory molecules. However, only when the anti-CD40 antibody was included in the co-culture, an enhancement in FasL expression was observed. This enhancement of PD-L1 levels was not detected in the previous conditions (**Figure 2C**). Finally, we wondered if the expression of these two molecules is enhanced in B cells in our *in vivo* mouse infection model. Mice were infected with 50 trypomastigotes (RA strain), and on day 15 post-infection the percentages of B220⁺/PD-L1⁺ and B220⁺/FasL⁺ were evaluated. As shown in **Figure 2D**, we found that both populations were expanded significantly in the infected mice, six times for PD-L1 and twice for FasL. This results are in concordance with previous reports in mice and human (Zuñiga et al., 2002; Girard et al., 2021). The presence of these molecules on the surface of B cells allows them to elicit various regulatory mechanisms in addition to those mediated by cytokines.

Next, we searched whether *T. cruzi* trypomastigotes can increase BAFF and APRIL transcripts, two well-known B cell growth factors involved in the B cell survival and/or differentiation (Hsu et al., 2002; Mackay et al., 2003). Consistent with the promotion of cell division, we found that both mRNAs were upregulated measured by qPCR only in the presence of anti-CD40 antibody (**Figure 3A**). This finding is relevant since it was previously described that these factors are mainly secreted by macrophages and dendritic cells and T cells (Mackay et al., 2003; Ng et al., 2005), but the absence of accessory cells in these cultures suggests that trypomastigotes act directly on B cells for their induction.

Several reports emphasize the relevance of IL-21 in the induction of IL-10 secreting regulatory B cells (Tedder, 2015), although it is also associated to proliferation/apoptosis, plasma cell differentiation or immunoglobulin production (Spolski and

Leonard, 2014). Generally, the IL-21 secretion is associated mainly, although not exclusively, with the CD4⁺ follicular (Tfh) and CD4⁺ Th17 cells (Lüthje et al., 2012; Spolski and Leonard, 2014). Given the function attributed to this cytokine, we sought to determine whether B cells could be effectively secreting IL-21 in the context of *T. cruzi* infection.

Based on the described above, we performed *in vivo* assays to validate this hypothesis in the mouse model. After 2 weeks of infection with 50 trypomastigotes of *T. cruzi* (RA strain), we detected an increase in IL-21 producing B220⁺ cells (**Figure 3B**). We found two different populations, one B220^{lo} and the other B220^{high} that secreted IL-21 during the acute stage of the infection. This finding is noteworthy as IL-21 expression has only been reported in Hodgkin's lymphoma (B-cell-related lineage) but not in physiologically regulated or untransformed B cells (Scheeren et al., 2008).

Collectively, we have observed here that trypomastigotes can activate and induce proliferation and a regulatory phenotype in naïve B cells, secreting cytokines involved in immune regulation and the induction of regulatory ligands on the cell surface.

Trypomastigote-Stimulated B Cells Exert CD4⁺ T Cell Regulation

To test whether this B cells regulatory phenotype exerts functional activity on CD4⁺ T cells, the conditioned medium from trypomastigote-stimulated B cells was assayed on purified naïve CD4⁺ T cells pre-treated with antibodies anti-CD3 and CD28 (**Figure 4A**). As indicated by CFSE staining, the proliferation of CD4⁺ T cells was drastically dampened in these conditions (**Figure 4B**).

We then analyzed the supernatant cytokine content and determined that the secretion of IL-2, the main proliferative cytokine for CD4⁺ T cells clonal expansion, was significantly reduced (**Figure 4B**). Next, we analyzed whether the induced T helper profile was altered by measure of the released cytokine to the medium. Also we measured the IFN γ secretion, typically associated with Th1 profile, and we found a drastically reduction (**Figure 4C**). Note that the conditioned media from trypomastigotes cultured alone did not have any effect on CD4⁺ T cells, and that the regulation is only exerted when B cells interact with parasites (**Figure 4C**). Therefore, the conditioned media of the B cells stimulated with trypomastigotes exerted a strong regulation of the CD4⁺ T cells response because their cell division was inhibited, and the elicited cytokine secretion was altered.

Considering into account the observed upregulation of the regulatory ligands, the ability of B cells stimulated with trypomastigotes to induce apoptosis in CD4⁺ T cells was also tested. As expected, T cells cultured in the presence of parasites pre-stimulated B cells showed a significant increase in the apoptotic population (Annexin-V⁺/IP⁺ population) (**Figure 4D**), which correlates with the augmented number of hypodiploid TCD4⁺ cells when stimulated with B cells (**Supplementary Figure 3**). This result might constitute a regulatory mechanism to avoid the immune response against the parasite.

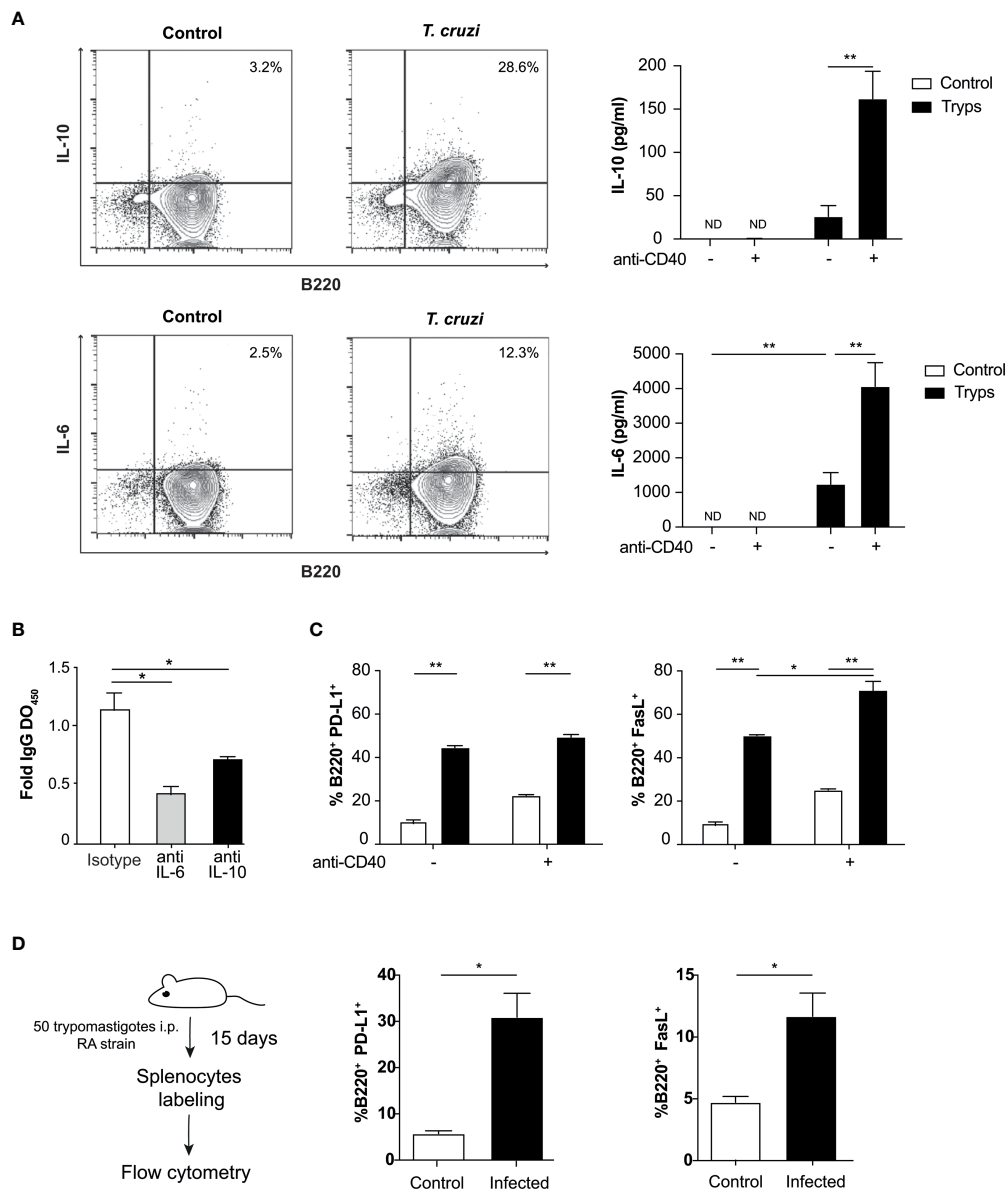


FIGURE 2 | B cells secrete cytokines and express surface regulatory ligands after stimulation with *T. cruzi* trypomastigotes. **(A)** Detection of B cell derived cytokines by flow cytometry and ELISA upon parasite stimulation. Supernatants from naïve B cells cocultured with trypomastigotes and treated or not with anti-CD40 were tested by ELISA for IL-10 (top panel) and IL-6 (bottom panel). The presence of an agonist anti-CD40 antibody induced ILs even strongly. Control (unfilled bars): unstimulated B cells, trypomastigotes (filled histograms): cells stimulated by the addition of 1×10^6 trypomastigotes/ml. $^{**}p < 0.001$. ND: not detected **(B)** B cells were cultured in presence of IL-6 or IL-10 blocking antibodies or an isotype control and total IgG OD were determined by ELISA. $^{*}p < 0.05$ **(C)** B cells were cultured with 1×10^6 trypomastigotes/ml and the anti-CD40 antibody and surface expression of PD-L1 and Fas-L regulatory proteins were then tested by cytometry. Control (unfilled bars): unstimulated B cells, trypomastigotes (filled bars): cells stimulated by the addition of trypomastigotes. Two-way ANOVA with Bonferroni's correction was used, $^{*}p < 0.05$, $^{**}p < 0.001$. **(D)** Surface expression of PD-L1 and FasL in splenocytes from naïve or *T. cruzi* infected mice evaluated by cytometry. Student's t test was used, $^{*}p < 0.05$.

Different IL-10 Producing B Cell Subsets Are Present in *T. cruzi*-Infected Mice

From the results described above, it can be concluded that trypomastigotes can induce functional regulatory abilities on B cells. The relevance of these findings was verified under *in vivo* conditions. Spleens from mice after two weeks of infection were

collected and tested for the actual presence of IL-10-producing B cells (Figure 5A). A discrete population of regulatory IL-10-producing B cells was identified, thus providing further support to the previous observations (Figure 5B). Then, we analyzed the phenotype of IL-10-producing B cells by using three different panels of surface markers that consider their ontogeny and

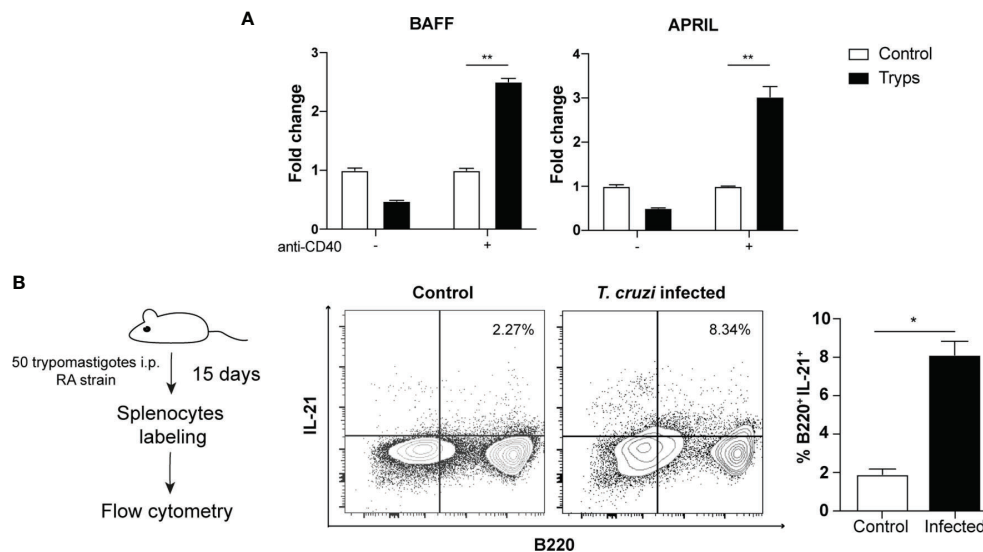


FIGURE 3 | Trypomastigotes induce the expression of B cell growth and differentiation factors. **(A)** The mRNAs of BAFF and APRIL were quantified by qPCR after coculture of naïve B cells with trypomastigotes, in the presence or not of an agonist anti-CD40 antibody. Tryps (filled bars): cells stimulated by the addition of 1×10^6 trypomastigotes/ml. Two-way ANOVA with Bonferroni's correction was used, $^{**}p < 0.001$. **(B)** Cytoplasmic expression of IL-21 in B220⁺/CD4⁻ cells harvested from naïve or infected mice. Student's *t* test was used, $^{*}p < 0.05$.

functional characteristics. The phenotype of these IL-10-producing B cells, a hallmark cytokine, was associated with a higher proportion of germinal center (Fas⁺/GL-7⁺), naïve or newly formed T1 B cells (NF-B, with a CD21⁻/CD23⁻ phenotype) and CD5⁺ regulatory B cell phenotypes (CD1d⁺/CD5⁺) (Figure 5C). Surprisingly, IL-10-producing B cells showed low expression of B220, an event characteristic of plasmablasts. Thus, confirming the results obtained in the *in vitro* model.

Therefore, *T. cruzi* trypomastigotes induced regulatory populations of B cells *in vitro* able to dampen the T cell response. In this model, we found that trypomastigote-stimulated B cells secrete and enhance the production of regulatory cytokines and membrane ligands such as IL-6, IL-10, PD-L1 and FasL. Moreover, IL-10, FasL and PD-L1 were also detected in the course of *T. cruzi* infection. Furthermore, in this model, we detected the presence of IL-21-producing B cells which is a cytokine associated with the development of B regulatory cells.

DISCUSSION

Within the physiology of infection by *T. cruzi*, the relevance of B cells was circumscribed to the production of antibodies. Despite the humoral response as a whole is not sufficient to effectively eliminate the parasite (Acevedo et al., 2018), relevant antibodies are induced during the infection such as lytic antibodies directed against anti- α -gal epitopes, neutralizing the activity of *trans*-sialidase and TcDAF (Tambourgi et al., 1993; Almeida et al., 1994; Buschiazzi et al., 2012). On the other hand, there are defined parasite factors such as *trans*-sialidase, proline-racemase and glutamate dehydrogenase that can, directly or indirectly,

induce cytokine secretion and proliferation in B cells (Reina-San-Martín et al., 2000; Gao et al., 2002; Montes et al., 2006).

Although B cell ability to secrete cytokines and to act as an antigen-presenting cell is well known, it was historically considered as a secondary role. During the last years, it demonstrated that B cells turned out to be more than producers of immunoglobulins. Effector B cells are capable of secreting IL-2, IL-4, IL-6, IL-12, IL-13, IL-15, GM-CSF, and IFN γ , important cytokines in regulating the assembly and functionality of the immune system (Lund, 2008; Shen and Fillatreau, 2015). Furthermore, it was demonstrated that in *T. cruzi* infection, B cells are able to produce IL-17 *via* the action of *trans*-sialidase (Bermejo et al., 2013). In models of autoimmune diseases, chronic inflammatory processes and cancer, there are multiple reports of regulatory B cells (Gorosito Serrán et al., 2015; Sarvaria et al., 2017). Regulatory B cells (Breg) are a heterogeneous population that produces IL-10, IL-35 and/or TGF β capable of inhibiting the Th1, Th17 and CD8⁺ responses, as well as the secretion of pro-inflammatory cytokines such as IFN γ or TNF α by macrophages or dendritic cells (Catalán et al., 2021). Furthermore, they could favor the development of regulatory T cells that, in turn, might impede the resolution of the pathology (Burdin et al., 1997; Candando et al., 2014; Lykken et al., 2015; Rosser and Mauri, 2015; Catalán et al., 2021). Other molecules have been associated in the generation of Breg such as APRIL and Blimp-1 (Fehres et al., 2019; Wang et al., 2019). In Figure 3, we showed that in our model we could detect the up-regulation of APRIL transcript.

So far, multiple populations of Breg have been identified according to their surface markers and the cytokines they release. The reported B populations that can express IL-10 are T2-MZP (CD21⁺/CD23⁺), classical B10 (CD5⁺/CD1d⁺), MZ (CD21⁺/

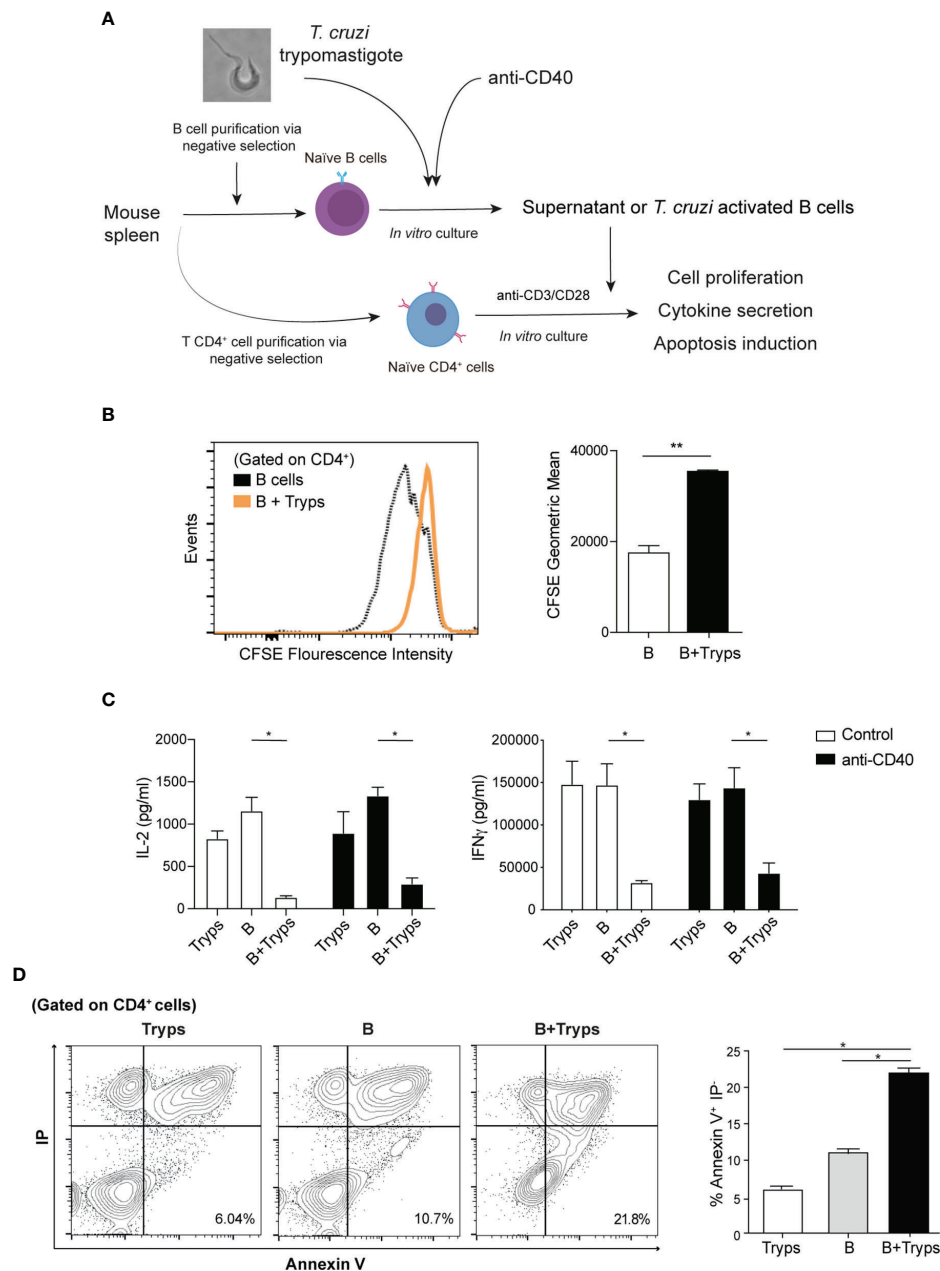


FIGURE 4 | Supernatants from trypomastigote-stimulated B cells halted CD4⁺ T cells proliferation and altered the induced cytokine profile. **(A)** Schematic experimental representation. **(B)** CFSE proliferation labeling of CD4⁺ T cells after addition of conditioned media from B cell cultures. B cells; supernatants from B cells alone, B+Tryps: B cells plus trypomastigotes cocultures. Student's *t* test was used, ***p* < 0.001. **(C)** Cytokine ELISA from CD3/CD28 stimulated CD4⁺ T cells in the presence of conditions media from diverse conditions. Tryps: supernatants from trypomastigotes alone, B: supernatants from B cells alone, B+Tryps: supernatants from B cells plus trypomastigotes cocultures. Two-way ANOVA with Bonferroni's correction was used, ***p* < 0.001. **(D)** CD4⁺ T cells stained by both propidium iodide and Annexin-V detected by flow cytometry. Tryps: CD4⁺ T cells cultured in the presence of conditioned media from trypomastigotes; B: CD4⁺ T cells cultured in the presence of conditioned media from unstimulated B cells; B+Tryps: CD4⁺ T cells cultured in the presence of conditioned media from B cells plus trypomastigotes. Student's *t* test was used, ***p* < 0.001.

CD23^{lo/-}), plasma cells and plasmablasts (CD138⁺) (Rosser and Mauri, 2015). At present, the induction mechanism of these cells has not been fully elucidated and there is no known specific transcription factor that regulates this cell differentiation which might reflect the plasticity of these cells. However, some required

pathways have been described. In an inflammatory context (IL-1 β , IL-2, IL-6 and IFN α , among others) there are at least two known pathways that are involved in the generation of these cells, the B receptor-dependent (BCR) and the Toll-like receptors dependent. In the first one, it would appear that signaling

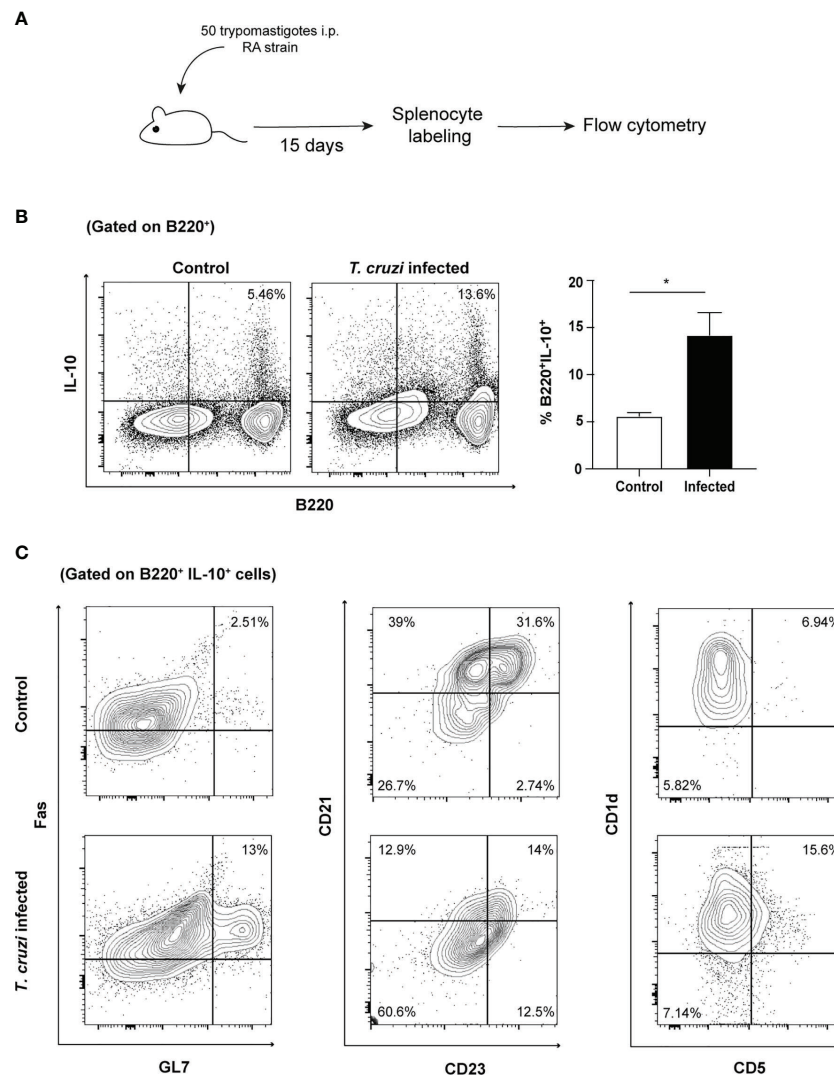


FIGURE 5 | IL-10-producing B cells are expanded during *in vivo* *T. cruzi* infection and present several phenotypes. **(A)** Schematic experimental representation. **(B)** Cytoplasmic IL-10 presence in splenocytes from naïve or infected mice (B220/IL-10 cells, 15 days post-infection). **(C)** Phenotypic analysis of IL-10 producing B cells.

through the BCR is critical. In this pathway, the Bregs would be antigen-specific and when presenting the antigen in the context of MHC-II to the lymphocyte T CD4⁺ they would be stimulated by it *via* CD40/CD40L and IL-21. In the second route, it was possible to determine that the TLR2/4/9 receptors are involved and their signaling *via* MyD88 plus IL-21 would induce the secretion of IL-10 by B cells (Yoshizaki et al., 2012; Horikawa et al., 2013; Lykken et al., 2015; Okada et al., 2018).

The presence of Breg cells and their regulatory activity on the T cell response have recently been described in the course of infectious diseases caused by pathogens of the genera *Plasmodium*, *Listeria*, *Leishmania*, and *Schistosoma* (Horikawa et al., 2013; Gorosito Serrán et al., 2015; Silva-Barrios et al., 2017). Within the parasitic infections, the B populations capable of developing this regulatory profile differ in each case and in several of them they were little studied. For example, in *Leishmania donovani* a CD19⁺/CD21⁺/

CD23^{lo} (marginal zone phenotype) secreting IL-10 population was identified, while in the related *Leishmania major*, the identified population was CD19⁺/CD1d⁺/CD5^{lo} (B10 phenotype) (Ronet et al., 2010). On the other hand, in *Plasmodium* they are described as IL-10 secreting B220⁺ and in *Schistosoma* as IL-10 and TGF- β secreting CD19⁺/CD1d⁺ cells (Liu et al., 2013; Van Der Vlugt et al., 2014).

In *T. cruzi* infection, previous works with B cell-depleted Xid or μ MT mice provided evidence supporting that B cells can regulate the T cell response (Minoprio et al., 1993; Gorosito Serrán et al., 2017; Fiocca Vernengo et al., 2020). However, the mechanisms and cell populations involved in the T CD4⁺ modulation process are still not understood.

In this study, we demonstrated that the infectious form of the parasite directly stimulated B cells that can regulate T CD4⁺ cells, impairing their proliferation and inducing an apoptotic process.

Notably, we determined that trypomastigotes directly induced naïve B cell proliferation accompanied by secretion of IL-6 and IL-10. These molecules are involved in B activation and cell proliferation. Although here we have shown that they are not involved in B cell division, both regulated the immunoglobulin secretion. There are several reports that support the induction of IL-6 and IL-10 *via* TLR4 (Greenhill et al., 2011; Sanin et al., 2015). It has also been reported that *T. cruzi* GIPLs are able to stimulate TLR4 (DosReis et al., 2002). Since B cells express TLR4 (Ma et al., 2015), the mechanism of induction of these cytokines might be explained in this way. Also, we detected the presence of APRIL and BAFF transcripts which are classically expressed by myeloid accessory cells, representing a hypothetic autocrine mechanism induced directly by trypomastigotes on B cells in the context of CD40 stimulation. Even these growth factors are canonically secreted by another cell source rather than B cells, evidence has emerged of its expression by B cells themselves both *in vitro* and *in vivo* (Mackay et al., 2003; Ng et al., 2005; Chu et al., 2007). Several reports state that toll-like receptors (TLRs) signaling could stimulate BAFF and APRIL expression in B cells and other antigen presenting cells (APCs) (Chu et al., 2007; Sakai and Akkoyunlu, 2017). In this line, pathogen-associated molecular patterns (PAMPs) from trypomastigotes have been identified, including GPI anchored mucins, membrane GIPL, DNA CpGs and parasite RNA (Rodrigues et al., 2012). Since B cells express variety and quantity of TLRs (Ma et al., 2015), the expression of BAFF and APRIL might be associated with their presence.

Bermejo et al. (2011) have reported that, in the context of *T. cruzi* infection, BAFF levels are elevated and it is related to polyclonal B cell response and antibody titers. Moreover, in another report of the same workgroup they observed that the *T. cruzi* antigen glutamate dehydrogenase induced B cells proliferation mediated by BAFF produced by CD11b⁺ cells. The authors hypothesized that these cells were macrophages but exist the possibility that they could be also CD11b⁺ expressing B cells (Montes et al., 2006).

In humans, circulating regulatory B10 results altered during the chronic stage and is associated with improved cardiac function in the indeterminate stage of Chagas disease (Passos et al., 2019; Girard et al., 2021). Also, since we observed a regulatory phenotype on parasite-stimulated B cells we tested for the presence of IL-21, a cytokine related to regulatory B10 cell generation (Horikawa et al., 2013). Surprisingly, given that IL-21 is paradigmatically mainly produced by CD4⁺ cells, we have found IL-21 expression in B cells during the experimental infection. This finding is noteworthy as IL-21 expression has previously been reported only in Hodgkin's lymphoma (B-cell-related lineage) (Scheeren et al., 2008). It has been proved that IL-6 is able to induce the production of IL-21 in CD4⁺ cells (Dienz et al., 2009). It is also known that B cells are responsive to IL-6 and constitute a growth and differentiation factor. In our model, we showed that this cytokine is involved in IgG secretion (**Figure 2B**). Furthermore, NFAT, a downstream signaling molecule shared in the TCR and BCR cascade, has been shown to be involved in IL-21 secretion (Antony et al., 2004). Therefore, the combination of IL-6 and BCR signals in B cells could be

plausible stimuli to induce IL-21 in these cells. Overall, the expression of B cell growth factors such as BAFF and APRIL plus IL-21 by B cells could represent a mechanism of *T. cruzi* to generate B-cell subsets that regulate the immune response against the pathogen.

We also showed that *T. cruzi* stimulated B cells damped T cell proliferation, the typically Th1-like cytokine secretion, and increased the apoptotic rate (Annexin V⁺/PI⁺) of CD4⁺ activated T cells. Moreover, recent evidence from Gorosito-Serran et al. (2015) described that the absence of B cells results in an uncontrolled CD4⁺ inflammatory response. These results suggest that *T. cruzi* trypomastigotes are able to manipulate B cells to restrain the CD4⁺ T cell activation inhibiting cell proliferation and increasing apoptosis induction.

The stimulation of CD40 on B cells was necessary for most of the described features or the enhancement of B regulatory cells generation in this model. This opens two hypotheses about the CD40L source *in vivo* during *T. cruzi* infection: the first, according to the paradigm, is that CD4⁺ cells present in lymphoid tissues are the natural CD40L source. Upon stimulation with CD40L from these cells, regulatory B cells are generated and constitute a restraint of the immune response against the parasite, contributing to the prevention of pathogen clearance from the host. The other possibility is that CD40L stimuli proceed from another source, like platelets. It is well-known that in the course of an acute infection with *T. cruzi*, platelet blood count decreases dramatically generating thrombocytopenia (de Titto and Araujo, 1988). In a previous work from our laboratory, we demonstrated that *trans*-sialidase from the parasite alters platelet surface glycan profile and induces their removal from circulation, promoting the marked platelet count fall (Tribulatti et al., 2005). In addition to this phenomenon, platelet activation results in its own disassembling into smaller fragments (vesiculation) and can also cause thrombocytopenia (Heemskerk et al., 2002; Taus et al., 2019). During platelet activation, they release several components, including CD40L. Some reports claim that platelet-derived CD40L might represent a relevant source of the circulating form, which is crucial for the proper development of the B response (André et al., 2002; Viallard et al., 2002; Sprague et al., 2008; Aloui et al., 2014). Moreover, the injection of small molecules that mimic the functional trimeric CD40L can control parasitemia and mortality (Fournel et al., 2005; Habib et al., 2007). Further research needed to be performed to clarify these issues.

In the context of *T. cruzi* infection we have found that IL-10 production by B cells is elicited by different subpopulations. Surprisingly, we detected that follicular phenotype B cells (Fas⁺/GL7⁺) express IL-10 upon *T. cruzi* infection. A recent report of *Leishmania amazonensis* infection also concludes that B2 follicular cells are relevant on IL-10 production, indicating that both pathogens might share common mechanisms relying on their phylogenetic similarity (Firmino-Cruz et al., 2018). Also, we observed that newly formed B cells (NF-B) constitute an important source of IL-10 in *T. cruzi* infection (**Figure 5**). It has been reported that NF-B are significant IL-10 producers in healthy individuals and expand in several viral (HIV, HCV) and bacterial infections, thus, they might represent a new

regulating subset in parasitic infections, as Chagas disease (Giltiay et al., 2019). In addition, we observed the appearance of CD5⁺/CD1d IL-10⁺ B cells after infection according to several previous reports in different infectious processes, (Gorosito Serrán et al., 2015). This former phenotype is associated with the classical regulatory B cell subset, which shares molecular markers with B1 cells.

According to our *in vitro* results, the proliferation of purified murine B cells is induced by trypomastigotes *per se*, but a significant fraction of cells does not divide. However, upon CD40 stimulation the fraction of undivided cells was reduced. This fact reflects itself the heterogeneity of natural B subsets, each needing a different nature and combination of stimuli including TLR, BCR and CD40 among others. Moreover, it is well-known that *T. cruzi* induces a massive expansion of the B cell compartment, reflected in the characteristic splenomegaly, and a consequent polyclonal response. According to these facts, it seems reasonable that the expression of IL-10 by B cells is not confined to a unique subset but comes from different phenotypes with different ontogenesis.

All the evidence described here suggests that *T. cruzi* trypomastigotes are able to modulate the fate of B cells. In this condition, the stimulated B cells secrete various cytokines and immunoglobulins and module the response of T CD4⁺ cells by altering cytokine secretion, arresting cell division, and apoptosis induction. Our results add strong evidence of the central relevance of B cells during the pathogenesis of Chagas disease beyond the antibodies production.

DATA AVAILABILITY STATEMENT

The original contributions presented in the study are included in the article/**Supplementary Material**. Further inquiries can be directed to the corresponding author.

ETHICS STATEMENT

The animal study was reviewed and approved by Committee on the Ethics of Animal Experiments of the Universidad Nacional de San Martín (UNSAM).

REFERENCES

- Acevedo, G. R., Girard, M. C., and Gómez, K. A. (2018). The Unsolved Jigsaw Puzzle of the Immune Response in Chagas Disease. *Front. Immunol.* 9, 1–23. doi: 10.3389/fimmu.2018.01929
- Almeida, I. C., Ferguson, M. A. J., Schenkman, S., and Travassos, L. R. (1994). Lytic Anti-Alpha-Galactosyl Antibodies From Patients With Chronic Chagas' Disease Recognize Novel O-Linked Oligosaccharides on Mucin-Like Glycosyl-Phosphatidylinositol-Anchored Glycoproteins of *Trypanosoma Cruzi*. *Biochem. J.* 304 (Pt 3), 793–802.
- Aloui, C., Prigent, A., Sut, C., Tariket, S., Hamzeh-Cognasse, H., Pozzetto, B., et al. (2014). The Signaling Role of CD40 Ligand in Platelet Biology and in Platelet Component Transfusion. *Int. J. Mol. Sci.* 15, 22342–22364. doi: 10.3390/ijms151222342

AUTHOR CONTRIBUTIONS

MS, RV, OC, and JM were responsible for the study design and/or funding acquisition. MS, AB, CAP, and JM performing the experiments. MS, OC, and JM were responsible for results analysis. Project supervision was performed by OC and JM. MS, OC, and JM were responsible for writing the original manuscript draft. All authors contributed to the article and approved the submitted version.

FUNDING

This work was funded by grants from the Agencia Nacional de Promoción de la Investigación, el Desarrollo Tecnológico y la Innovación (ANPCyT), Argentina and from the National Institutes of Health, USA (grant R01AI104531 to OC). RV is supported by R01GM121595 from the National Institute of General Medical Sciences (NIH/NIGMS), 1R01CA233945 and from the National Cancer Institute of the National Institutes of Health (NIH/NCI) and the National Cancer Institute of the National Institutes of Health under Award Number P30CA240139. The funders had no role in the design of studies, data collection, and analysis, or in the decision to publish or the preparation of the manuscript.

ACKNOWLEDGMENTS

MS, AB, and CP are fellows and JM, and OC are researchers from the CONICET. We are in debt with Dr. Adriana Gruppi for helpful advice and Dr. Juan P. Fededa for providing anti-PD-L1 antibody. We thank Liliana Sferco and Agustina Chidichimo for culturing parasites. We also thank Fabio Fraga and Marisa Sarmenti for animal care.

SUPPLEMENTARY MATERIAL

The Supplementary Material for this article can be found online at: <https://www.frontiersin.org/articles/10.3389/fcimb.2021.789373/full#supplementary-material>

- André, P., Nannizzi-Alaimo, L., Prasad, S. K., and Phillips, D. R. (2002). Platelet-Derived CD40L: The Switch-Hitting Player of Cardiovascular Disease. *Circulation* 106, 896–899. doi: 10.1161/01.CIR.0000028962.04520.01
- Antony, P., Petro, J. B., Carlesso, G., Shinnars, N. P., Lowe, J., and Khan, W. N. (2004). B-Cell Antigen Receptor Activates Transcription Factors NFAT (Nuclear Factor of Activated T-Cells) and NF-κB (Nuclear Factor κB) via a Mechanism That Involves Diacylglycerol. *Biochem. Soc. Trans.* 32, 113–115. doi: 10.1042/BST0320113
- Bermejo, D. A., Amezcua Vesely, M. C., Khan, M., Acosta-Rodríguez, E. V., Montes, C. L., Toellner, K. M., et al. (2011). *Trypanosoma Cruzi* Infection Induces a Massive Extrafollicular and Follicular Splenic B-Cell Response Which is a High Source of non-Parasite-Specific Antibodies. *Immunology* 132, 123–133. doi: 10.1111/j.1365-2567.2010.03347.x

- Bermejo, D. A., Jackson, S. W., Gorosito-Serran, M., Acosta-Rodriguez, E. V., Amezcuza Vesely, M. C., Sather, B. D., et al. (2013). *Trypanosoma Cruzi* Trans-Sialidase Initiates a Program Independent of the Transcription Factors Ror γ t and AhR That Leads to IL-17 Production by Activated B Cells. *Nat. Immunol.* 14, 514–522. doi: 10.1038/ni.2569
- Burdin, N., Rousset, F., and Banchereau, J. (1997). B-Cell-Derived IL-10: Production and Function. *Methods A Companion to Methods Enzymol.* 11, 98–111. doi: 10.1006/meth.1996.0393
- Buschiazio, A., Muia, R., Larrieux, N., Pitcovsky, T., Mucci, J., and Campetella, O. (2012). *Trypanosoma Cruzi* Trans-Sialidase in Complex With a Neutralizing Antibody: Structure/function Studies Towards the Rational Design of Inhibitors. *PLoS Pathog.* 8. doi: 10.1371/journal.ppat.1002474
- Candiano, K. M., Lykken, J. M., and Tedder, T. F. (2014). B10 Cell Regulation of Health and Disease. *Immunol. Rev.* 259, 259–272. doi: 10.1111/imr.12176
- Cardillo, F., Postol, E., Nihei, J., Aroeira, L. S., Nomizo, A., and Mengel, J. (2007). B Cells Modulate T Cells So as to Favour T Helper Type 1 and CD8⁺ T-Cell Responses in the Acute Phase of *Trypanosoma Cruzi* Infection. *Immunology* 122, 584–595. doi: 10.1111/j.1365-2567.2007.02677.x
- Catalán, D., Mansilla, M. A., Ferrier, A., Soto, L., Oleinika, K., Aguillón, J. C., et al. (2021). Immunosuppressive Mechanisms of Regulatory B Cells. *Front. Immunol.* 12:1–30. doi: 10.3389/fimmu.2021.611795
- Chu, V. T., Enghard, P., Riemekasten, G., and Berek, C. (2007). *In Vitro* and *In Vivo* Activation Induces BAFF and APRIL Expression in B Cells. *J. Immunol.* 179, 5947–5957. doi: 10.4049/jimmunol.179.9.5947
- Couper, K. N., Blount, D. G., and Riley, E. M. (2008). IL-10: The Master Regulator of Immunity to Infection. *J. Immunol.* 180, 5771–5777. doi: 10.4049/jimmunol.180.9.5771
- Cyster, J. G., and Allen, C. D. C. (2019). B Cell Responses: Cell Interaction Dynamics and Decisions. *Cell* 177, 524–540. doi: 10.1016/j.cell.2019.03.016
- da Rocha, R. F. D. B., LaRocque-De-Freitas, I. F., Arcanjo, A. F., Logullo, J., Nunes, M. P., Freire-De-Lima, C. G., et al. (2019). B-1 Cells may Drive Macrophages Susceptibility to *Trypanosoma Cruzi* Infection. *Front. Microbiol.* 10, 1–10. doi: 10.3389/fmicb.2019.01598
- de Titto, E. H., and Araujo, F. G. (1988). Serum Neuraminidase Activity and Hematological Alterations in Acute Human Chagas' Disease. *Clin. Immunol. Immunopathol.* 46, 157–161. doi: 10.1016/0090-1229(88)90016-5
- Díaz, P. R., Mucci, J., Meira, M. A., Bogliotti, Y., Musikant, D., Leguizamón, M. S., et al. (2015). *Trypanosoma Cruzi* Trans-Sialidase Prevents Elicitation of Th1 Cell Response via Interleukin 10 and Downregulates Th1 Effector Cells. *Infect. Immun.* 83, 2099–2108. doi: 10.1128/IAI.00031-15
- Dienz, O., Eaton, S. M., Bond, J. P., Neveu, W., Moquin, D., Noubade, R., et al. (2009). The Induction of Antibody Production by IL-6 is Indirectly Mediated by IL-21 Produced by CD4⁺ T Cells. *J. Exp. Med.* 206, 69–78. doi: 10.1084/jem.20081571
- D'Imperio Lima, M. R., Eisen, H., Minoprio, P., Joskowicz, M., and Coutinho, A. (1986). Persistence of Polyclonal B Cell Activation With Undetectable Parasitemia in Late Stages of Experimental Chagas' Disease. *J. Immunol.* 137, 353–356.
- D'Imperio Lima, M. R., Joskowicz, M., Coutinho, A., Kipnis, T., and Eisen, H. (1985). Very Large and Isotypically Atypical Polyclonal Plaque-Forming Cell Responses in Mice Infected With *Trypanosoma Cruzi*. *Eur. J. Immunol.* 15, 201–203. doi: 10.1002/eji.1830150219
- DosReis, G. A., Peçanha, L. M. T., Bellio, M., Previato, J. O., and Mendonça-Previato, L. (2002). Glycosylated Phospholipids From *Trypanosoma Cruzi* Transmit Signals to the Cells of the Host Immune System Through Both Ceramide and Glycan Chains. *Microbes Infect.* 4, 1007–1013. doi: 10.1016/S1286-4579(02)01616-7
- el Bouhdidi, A., Truys, C., Rivera, M. T., Bazin, H., and Carlier, Y. (1994). *Trypanosoma Cruzi* Infection in Mice Induces a Polyisotypic Hypergammaglobulinaemia and Parasite-Specific Response Involving High IgG2a Concentrations and Highly Avid IgG1 Antibodies. *Parasite Immunol.* 16, 69–76. doi: 10.1111/j.1365-3024.1994.tb00325.x
- Fehres, C. M., Van Uden, N. O., Yermenko, N. G., Fernandez, L., Salinas, G. F., Van Duivenvoorde, L. M., et al. (2019). April Induces a Novel Subset of IgA⁺ Regulatory B Cells That Suppress Inflammation via Expression of IL-10 and PD-L1. *Front. Immunol.* 10:1368. doi: 10.3389/fimmu.2019.01368
- Fiocca Vernengo, F., Beccaria, C. G., Araujo Furlan, C. L., Tosello Boari, J., Almada, L., Gorosito Serrán, M., et al. (2020). CD8⁺ T Cell Immunity Is Compromised by Anti-CD20 Treatment and Rescued by Interleukin-17a. *MBio* 11. doi: 10.1128/mBio.00447-20
- Firmino-Cruz, L., Ramos, T. D., da Fonseca-Martins, A. M., Maciel-Oliveira, D., Oliveira-Silva, G., Pratti, J. E. S., et al. (2018). Immunomodulating Role of IL-10-Producing B Cells in Leishmania Amazonensis Infection. *Cell. Immunol.* 334, 20–30. doi: 10.1016/j.cellimm.2018.08.014
- Fournel, S., Wieckowski, S., Sun, W., Trouche, N., Dumortier, H., Bianco, A., et al. (2005). C3-Symmetric Peptide Scaffolds are Functional Mimetics of Trimeric CD40L. *Nat. Chem. Biol.* 1, 377–382. doi: 10.1038/nchembio746
- Gao, W., Wortis, H. H., and Pereira, M. A. (2002). The *Trypanosoma Cruzi* Trans-Sialidase is a T Cell-Independent B Cell Mitogen and an Inducer of non-Specific Ig Secretion. *Int. Immunol.* 14, 299–308. doi: 10.1093/intimm/14.3.299
- Getahun, A., and Cambier, J. C. (2019). Non-Antibody-Secreting Functions of B Cells and Their Contribution to Autoimmune Disease. *Annu. Rev. Cell Dev. Biol.* 35, 337–356. doi: 10.1146/annurev-cellbio-100617-062518
- Giltiay, N. V., Giordano, D., and Clark, E. A. (2019). The Plasticity of Newly Formed B Cells. *J. Immunol.* 203, 3095–3104. doi: 10.4049/jimmunol.1900928
- Girard, M. C., Ossowski, M. S., Muñoz-Calderón, A., Fernández, M., Hernández-Vásquez, Y., Chadi, R., et al. (2021). *Trypanosoma Cruzi* Induces Regulatory B Cell Alterations in Patients With Chronic Chagas Disease. *Front. Cell. Infect. Microbiol.* 11, 1–15. doi: 10.3389/fcimb.2021.723549
- Gorosito Serrán, M., Fiocca Vernengo, F., Beccaria, C. G., Acosta-Rodriguez, E. V., Montes, C. L., and Gruppi, A. (2015). The Regulatory Role of B Cells in Autoimmunity, Infections and Cancer: Perspectives Beyond IL10 Production. *FEBS Lett.* 589, 3362–3369. doi: 10.1016/j.febslet.2015.08.048
- Gorosito Serrán, M., Tosello Boari, J., Fiocca Vernengo, F., Beccaria, C. G., Ramello, M. C., Bermejo, D. A., et al. (2017). Unconventional Pro-Inflammatory CD4⁺ T Cell Response in B Cell-Deficient Mice Infected With *Trypanosoma Cruzi*. *Front. Immunol.* 8, 1548. doi: 10.3389/fimmu.2017.01548
- Greenhill, C. J., Rose-John, S., Lissila, R., Ferlin, W., Ernst, M., Hertzog, P. J., et al. (2011). IL-6 Trans-Signaling Modulates TLR4-Dependent Inflammatory Responses via STAT3. *J. Immunol.* 186, 1199–1208. doi: 10.4049/jimmunol.1002971
- Habib, M., Rivas, M. N., Chamekh, M., Wieckowski, S., Sun, W., Bianco, A., et al. (2007). Cutting Edge: Small Molecule CD40 Ligand Mimetics Promote Control of Parasitemia and Enhance T Cells Producing IFN- γ During Experimental *Trypanosoma Cruzi* Infection. *J. Immunol.* 178, 6700–6704. doi: 10.4049/jimmunol.178.11.6700
- Heemskerk, J. W. M., Bevers, E. M., and Lindhout, T. (2002). Platelet Activation and Blood Coagulation. *Thromb. Haemost.* 88, 186–193. doi: 10.1055/s-0037-1613209
- Horikawa, M., Weimer, E. T., DiLillo, D. J., Venturi, G. M., Spolski, R., Leonard, W. J., et al. (2013). Regulatory B Cell (B10 Cell) Expansion During Listeria Infection Governs Innate and Cellular Immune Responses in Mice. *J. Immunol.* 190, 1158–1168. doi: 10.4049/jimmunol.1201427
- Hsu, B. L., Harless, S. M., Lindsley, R. C., Hilbert, D. M., and Cancro, M. P. (2002). Cutting Edge: BlyS Enables Survival of Transitional and Mature B Cells Through Distinct Mediators. *J. Immunol.* 168, 5993–5996. doi: 10.4049/jimmunol.168.12.5993
- Jones, S. A., and Jenkins, B. J. (2018). Recent Insights Into Targeting the IL-6 Cytokine Family in Inflammatory Diseases and Cancer. *Nat. Rev. Immunol.* 130. doi: 10.1038/s41577-018-0066-7
- Kopf, M., Baumann, H., Freer, G., Freudenberg, M., Lamers, M., Kishimoto, T., et al. (1994). Impaired Immune and Acute-Phase Responses in Interleukin-6-Deficient Mice. *Nature* 368, 339–342. doi: 10.1038/368339a0
- Kumar, S., and Tarleton, R. L. (2001). Antigen-Specific Th1 But Not Th2 Cells Provide Protection From Lethal *Trypanosoma Cruzi* Infection in Mice. *J. Immunol.* 166, 4596–4603. doi: 10.4049/jimmunol.166.7.4596
- Liu, Y., Chen, Y., Li, Z., Han, Y., Sun, Y., Wang, Q., et al. (2013). Role of IL-10-Producing Regulatory B Cells in Control of Cerebral Malaria in *Plasmodium Berghei* Infected Mice. *Eur. J. Immunol.* 43, 2907–2918. doi: 10.1002/eji.201343512
- Lund, F. E. (2008). Cytokine-Producing B Lymphocytes - Key Regulators of Immunity. *Curr. Opin. Immunol.* 20, 332–338. doi: 10.1016/j.coi.2008.03.003
- Lüthje, K., Kallies, A., Shimohakamada, Y., Belz, G. T., Light, A., Tarlinton, D. M., et al. (2012). The Development and Fate of Follicular Helper T Cells Defined by an IL-21 Reporter Mouse. *Nat. Immunol.* 13, 491–498. doi: 10.1038/ni.2261

- Lykken, J. M., Candando, K. M., and Tedder, T. F. (2015). Regulatory B10 Cell Development and Function. *Int. Immunol.* 27, 471–477. doi: 10.1093/intimm/dxv046
- Mackay, F. S., Schneider, P., Rennert, P., and Browning, J. (2003). BAFF and APRIL: A Tutorial on B Cell Survival. *Annu. Rev. Immunol.* 21, 231–264. doi: 10.1146/annurev.immunol.21.120601.141152
- Ma, K., Li, J., Fang, Y., and Lu, L. (2015). Roles of B Cell-Intrinsic TLR Signals in Systemic Lupus Erythematosus. *Int. J. Mol. Sci.* 16, 13084–13105. doi: 10.3390/ijms160613084
- Minoprio, P., Burlen, O., Pereira, P., Guilbert, B., Andrade, L., Hontebeyrie-Joskowicz, M., et al. (1988). Most B Cells in Acute *Trypanosoma Cruzi* Infection Lack Parasite Specificity. *Scand. J. Immunol.* 28, 553–561. doi: 10.1111/j.1365-3083.1988.tb01487.x
- Minoprio, P., Eisen, H., Joskowicz, M., Pereira, P., and Coutinho, A. (1987). Suppression of Polyclonal Antibody Production in *Trypanosoma Cruzi*-Infected Mice by Treatment With Anti-L3T4 Antibodies. *J. Immunol.* 139, 545–54550.
- Minoprio, P., el Cheikh, M. C., Murphy, E., Hontebeyrie-Joskowicz, M., Coffman, R., Coutinho, A., et al. (1993). Xid-Associated Resistance to Experimental Chagas' Disease is IFN-Gamma Dependent. *J. Immunol.* 151, 4200–4208.
- Montes, C. L., Acosta-Rodríguez, E. V., Merino, M. C., Bermejo, D. A., and Gruppi, A. (2007). Polyclonal B Cell Activation in Infections: Infectious Agents' Devilry or Defense Mechanism of the Host? *J. Leukoc. Biol.* 82, 1027–1032. doi: 10.1189/jlb.0407214
- Montes, C. L., Acosta-Rodríguez, E. V., Mucci, J., Zuñiga, E., Campetella, O., and Gruppi, A. (2006). A *Trypanosoma Cruzi* Antigen Signals CD11b⁺ Cells to Secrete Cytokines That Promote Polyclonal B Cell Proliferation and Differentiation Into Antibody-Secreting Cells. *Eur. J. Immunol.* 36, 1474–1485. doi: 10.1002/eji.200535537
- Montes, C. L., Zuñiga, E., Minoprio, P., Vottero-Cima, E., and Gruppi, A. (1999). A *Trypanosoma Cruzi* Alkaline Antigen Induces Polyclonal B-Cell Activation of Normal Murine Spleen Cells by T-Cell-Independent, BCR-Directed Stimulation. *Scand. J. Immunol.* 50, 159–166. doi: 10.1046/j.1365-3083.1999.00577.x
- Montes, C. L., Zuñiga, E. I., Vazquez, J., Arce, C., and Gruppi, A. (2002). *Trypanosoma Cruzi* Mitochondrial Malate Dehydrogenase Triggers Polyclonal B-Cell Activation. *Clin. Exp. Immunol.* 127, 27–36. doi: 10.1046/j.1365-2249.2002.01746.x
- Ng, L. G., Mackay, C. R., and Mackay, F. (2005). The BAFF/APRIL System: Life Beyond B Lymphocytes. *Mol. Immunol.* 42, 763–772. doi: 10.1016/j.molimm.2004.06.041
- Nutt, S. L., Hodgkin, P. D., Tarlinton, D. M., and Corcoran, L. M. (2015). The Generation of Antibody-Secreting Plasma Cells. *Nat. Rev. Immunol.* 15, 160–171. doi: 10.1038/nri3795
- Okada, Y., Ochi, H., Fujii, C., Hashi, Y., Hamatani, M., Ashida, S., et al. (2018). Signaling via Toll-Like Receptor 4 and CD40 in B Cells Plays a Regulatory Role in the Pathogenesis of Multiple Sclerosis Through Interleukin-10 Production. *J. Autoimmun.* 88, 103–113. doi: 10.1016/j.jaut.2017.10.011
- Ortiz-Ortiz, L., Parks, D. E., Rodriguez, M., and Weigle, W. O. (1980). Polyclonal B Lymphocyte Activation During *Trypanosoma Cruzi* Infection. *J. Immunol.* 124, 121–126.
- Passos, L. S. A., Magalhães, L. M. D., Soares, R. P., Marques, A. F., Alves, M. L. R., Giunchetti, R. C., et al. (2019). Activation of Human CD11b⁺ B1 B-Cells by *Trypanosoma Cruzi*-Derived Proteins is Associated With Protective Immune Response in Human Chagas Disease. *Front. Immunol.* 10, 1–14. doi: 10.3389/fimmu.2018.03015
- Reina-San-Martín, B., Degraeve, W., Rougeot, C., Cosson, A., Chamond, N., Cordeiro-da-Silva, A., et al. (2000). A B-Cell Mitogen From a Pathogenic Trypanosome is a Eukaryotic Proline Racemase. *Nat. Med.* 6, 890–897. doi: 10.1038/78651
- Rodrigues, M. M., Oliveira, A. C., and Bellio, M. (2012). The Immune Response to *Trypanosoma Cruzi*: Role of Toll-Like Receptors and Perspectives for Vaccine Development. *J. Parasitol. Res.* 2012. doi: 10.1155/2012/507874
- Ronet, C., Torre, Y. H.-L., Revaz-Breton, M., Mastelic, B., Tacchini-Cottier, F., Louis, J., et al. (2010). Regulatory B Cells Shape the Development of Th2 Immune Responses in BALB/c Mice Infected With *Leishmania Major* Through IL-10 Production. *J. Immunol.* 184, 886–894. doi: 10.4049/jimmunol.0901114
- Rosser, E. C., and Mauri, C. (2015). Regulatory B Cells: Origin, Phenotype, and Function. *Immunity* 42, 607–612. doi: 10.1016/j.immuni.2015.04.005
- Rottenberg, M. E., Bakhtiet, M., Olsson, T., Kristensson, K., Mak, T., Wigzell, H., et al. (1993). Differential Susceptibilities of Mice Genomically Deleted of CD4 and CD8 to Infections With *Trypanosoma Cruzi* or *Trypanosoma Brucei*. *Infect. Immun.* 61, 5129–5133. doi: 10.1128/iai.61.12.5129-5133.1993
- Rousset, F., Garcia, E., Defrance, T., Peronne, C., Vezzio, N., Hsu, D. H., et al. (1992). Interleukin 10 is a Potent Growth and Differentiation Factor for Activated Human B Lymphocytes. *Proc. Natl. Acad. Sci. U. S. A.* 89, 1890–1893. doi: 10.1073/pnas.89.5.1890
- Sakai, J., and Akkoyunlu, M. (2017). The Role of BAFF System Molecules in Host Response to Pathogens. *Clin. Microbiol. Rev.* 30, 991–1014. doi: 10.1128/CMR.00046-17
- Sanin, D. E., Prendergast, C. T., and Mountford, A. P. (2015). IL-10 Production in Macrophages Is Regulated by a TLR-Driven CREB-Mediated Mechanism That Is Linked to Genes Involved in Cell Metabolism. *J. Immunol.* 195, 1218–1232. doi: 10.4049/jimmunol.1500146
- Sarvaria, A., Madrigal, J. A., and Saudemont, A. (2017). B Cell Regulation in Cancer and Anti-Tumor Immunity. *Cell. Mol. Immunol.* 14, 662–674. doi: 10.1038/cmi.2017.35
- Scheeren, F. A., Diehl, S. A., Smit, L. A., Beaumont, T., Naspetti, M., Bende, R. J., et al. (2008). IL-21 is Expressed in Hodgkin Lymphoma and Activates STAT5: Evidence That Activated STAT5 is Required for Hodgkin Lymphomagenesis. *Blood* 111, 4706–4715. doi: 10.1182/blood-2007-08-105643
- Shen, P., and Fillatreau, S. (2015). Antibody-Independent Functions of B Cells: A Focus on Cytokines. *Nat. Rev. Immunol.* 15, 441–451. doi: 10.1038/nri3857
- Silva-Barrios, S., Charpentier, T., and Stäger, S. (2017). The Deadly Dance of B Cells With *Trypanosomatids*. *Trends Parasitol.* 1–17. doi: 10.1016/j.pt.2017.10.001
- Spolski, R., and Leonard, W. J. (2014). Interleukin-21: A Double-Edged Sword With Therapeutic Potential. *Nat. Rev. Drug Discov.* 13, 379–395. doi: 10.1038/nrd4296
- Sprague, D. L., Elzey, B. D., Crist, S. A., Waldschmidt, T. J., Jensen, R. J., and Ratliff, T. L. (2008). Platelet-Mediated Modulation of Adaptive Immunity: Unique Delivery of CD154 Signal by Platelet-Derived Membrane Vesicles. *Blood* 111, 5028–5036. doi: 10.1182/blood-2007-06-097410
- Tambourgi, D. V., Kipnis, T. L., Da Silva, W. D., Joiner, K. A., Sher, A., Heath, S., et al. (1993). A Partial cDNA Clone of Trypomastigote Decay-Accelerating Factor (T-DAF), a Developmentally Regulated Complement Inhibitor of *Trypanosoma Cruzi*, has Genetic and Functional Similarities to the Human Complement Inhibitor DAF. *Infect. Immun.* 61, 3656–3663. doi: 10.1128/iai.61.9.3656-3663.1993
- Tarleton, R. L., Grusby, M. J., and Zhang, L. (2000). Increased Susceptibility of Stat4-Deficient and Enhanced Resistance in Stat6-Deficient Mice to Infection With *Trypanosoma Cruzi*. *J. Immunol.* 165, 1520–1525. doi: 10.4049/jimmunol.165.3.1520
- Taus, F., Meneguzzi, A., Castelli, M., and Minuz, P. (2019). Platelet-Derived Extracellular Vesicles as Target of Antiplatelet Agents. What is the Evidence? *Front. Pharmacol.* 10:1–12. doi: 10.3389/fphar.2019.01256
- Tedder, T. F. (2015). B10 Cells: A Functionally Defined Regulatory B Cell Subset. *J. Immunol.* 194, 1395–1401. doi: 10.4049/jimmunol.1401329
- Tosato, G., Seamon, K. B., Goldman, N. D., Sehgal, P. B., May, L. T., Washington, G. C., et al. (1988). Monocyte-Derived Human B-Cell Growth Factor Identified as Interferon- β 2 (BSF-2, IL-6). *Science* (80-.) 239, 502–504. doi: 10.1126/science.2829354
- Tribulatti, M. V., Mucci, J., Van Rooijen, N., Leguizamón, M. S., and Campetella, O. (2005). The Trans-Sialidase From *Trypanosoma Cruzi* Induces Thrombocytopenia During Acute Chagas' Disease by Reducing the Platelet Sialic Acid Contents. *Infect. Immun.* 73, 201–207. doi: 10.1128/IAI.73.1.201-207.2005
- Van Der Vlugt, L. E. P. M., Zinsou, J. F., Ozir-Fazalikhah, A., Kremsner, P. G., Yazdanbakhsh, M., Adegnik, A. A., et al. (2014). Interleukin 10 (IL-10)-Producing CD1d^{hi} Regulatory B Cells From *Schistosoma Haematobium*-Infected Individuals Induce IL-10-Positive T Cells and Suppress Effector T-Cell Cytokines. *J. Infect. Dis.* 210, 1207–1216. doi: 10.1093/infdis/jiu257
- Viallard, J. F., Solanilla, A., Gauthier, B., Contin, C., Déchanet, J., Grosset, C., et al. (2002). Increased Soluble and Platelet-Associated CD40 Ligand in Essential

- Thrombocythemia and Reactive Thrombocytosis. *Blood* 99, 2612–2614. doi: 10.1182/blood.V99.7.2612
- Wang, Y. H., Tsai, D. Y., Ko, Y. A., Yang, T. T., Lin, I. Y., Hung, K. H., et al. (2019). Blimp-1 Contributes to the Development and Function of Regulatory B Cells. *Front. Immunol.* 10:1909. doi: 10.3389/fimmu.2019.01909
- Yoshizaki, A., Miyagaki, T., Dillillo, D. J., Matsushita, T., Horikawa, M., Kountikov, E. I., et al. (2012). Regulatory B Cells Control T-Cell Autoimmunity Through IL-21-Dependent Cognate Interactions. *Nature* 491, 264–268. doi: 10.1038/nature11501
- Zuñiga, E., Motran, C. C., Montes, C. L., Yagita, H., and Gruppi, A. (2002). *Trypanosoma Cruzi* Infection Selectively Renders Parasite-Specific IgG + B Lymphocytes Susceptible to Fas/Fas Ligand-Mediated Fratricide. *J. Immunol.* 168, 3965–3973. doi: 10.4049/jimmunol.168.8.3965

Author Disclaimer: This content is solely the responsibility of the authors and does not necessarily represent the official views of the National Institutes of Health.

Conflict of Interest: The authors declare that the research was conducted in the absence of any commercial or financial relationships that could be construed as a potential conflict of interest.

Publisher's Note: All claims expressed in this article are solely those of the authors and do not necessarily represent those of their affiliated organizations, or those of the publisher, the editors and the reviewers. Any product that may be evaluated in this article, or claim that may be made by its manufacturer, is not guaranteed or endorsed by the publisher.

Copyright © 2022 Somoza, Bertelli, Pratto, Verdun, Campetella and Mucci. This is an open-access article distributed under the terms of the Creative Commons Attribution License (CC BY). The use, distribution or reproduction in other forums is permitted, provided the original author(s) and the copyright owner(s) are credited and that the original publication in this journal is cited, in accordance with accepted academic practice. No use, distribution or reproduction is permitted which does not comply with these terms.



Biological and Molecular Effects of *Trypanosoma cruzi* Residence in a LAMP-Deficient Intracellular Environment

Anny Caroline Silva Oliveira^{1,2}, Luisa Rezende¹, Vladimir Gorshkov², Marcella Nunes Melo-Braga³, Thiago Verano-Braga⁴, Wesley Fernandes-Braga³, Jorge Luís de Melo Guadalupe¹, Gustavo Batista de Menezes¹, Frank Kjeldsen², Héli da Monteiro de Andrade⁵ and Luciana de Oliveira Andrade^{1*}

OPEN ACCESS

Edited by:

Martin M. Edreira,
Universidad de Buenos Aires
(CONICET), Argentina

Reviewed by:

Norma Andrews,
University of Maryland, College Park,
United States
Patricia Silvia Romano,
Dr. Mario H. Burgos Institute of
Histology and Embryology (IHEM)
(CONICET), Argentina

*Correspondence:

Luciana de Oliveira Andrade
lucianaandrade@ufmg.br

Specialty section:

This article was submitted to
Parasite and Host,
a section of the journal
Frontiers in Cellular and
Infection Microbiology

Received: 02 October 2021

Accepted: 06 December 2022

Published: 06 January 2022

Citation:

Oliveira ACS, Rezende L,
Gorshkov V, Melo-Braga MN,
Verano-Braga T, Fernandes-Braga W,
Guadalupe JLM, de Menezes GB,
Kjeldsen F, de Andrade HM and
Andrade LdO (2022) Biological and
Molecular Effects of *Trypanosoma*
cruzi Residence in a LAMP-Deficient
Intracellular Environment.
Front. Cell. Infect. Microbiol. 11:788482.
doi: 10.3389/fcimb.2021.788482

¹ Department of Morphology, Biological Sciences Institute—ICB, Federal University of Minas Gerais (UFMG), Belo Horizonte, Brazil, ² Protein Research Group, Department of Biochemistry and Molecular Biology, University of Southern Denmark, Odense, Denmark, ³ Department of Biochemistry and Immunology, Biological Sciences Institute—ICB, Federal University of Minas Gerais (UFMG), Belo Horizonte, Minas Gerais, Brazil, ⁴ Hypertension Lab/Functional Proteomics Group, Department of Physiology and Biophysics, Biological Sciences Institute—ICB, Federal University of Minas Gerais (UFMG), Belo Horizonte, Brazil, ⁵ Laboratory of Leishmanioses, Department of Parasitology, Biological Sciences Institute—ICB, Federal University of Minas Gerais (UFMG), Belo Horizonte, Brazil

Trypanosoma cruzi invades non-professional phagocytic cells by subverting their membrane repair process, which is dependent on membrane injury and cell signaling, intracellular calcium increase, and lysosome recruitment. Cells lacking lysosome-associated membrane proteins 1 and 2 (LAMP1 and LAMP2) are less permissive to parasite invasion but more prone to parasite intracellular multiplication. Several passages through a different intracellular environment can significantly change *T. cruzi*'s gene expression profile. Here, we evaluated whether one single passage through LAMP-deficient (KO) or wild-type (WT) fibroblasts, thus different intracellular environments, could influence *T. cruzi* Y strain trypomastigotes' ability to invade L6 myoblasts and WT fibroblasts host cells. Parasites released from LAMP2 KO cells (TcY-L2^{-/-}) showed higher invasion, calcium signaling, and membrane injury rates, for the assays in L6 myoblasts, when compared to those released from WT (TcY-WT) or LAMP1/2 KO cells (TcY-L1/2^{-/-}). On the other hand, TcY-L1/2^{-/-} showed higher invasion, calcium signaling, and cell membrane injury rates, for the assays in WT fibroblasts, compared to TcY-WT and TcY-L1/2^{-/-}. Albeit TcY-WT presented an intermediary invasion and calcium signaling rates, compared to the others, in WT fibroblasts, they induced lower levels of injury, which reinforces that signals mediated by surface membrane protein interactions also have a significant contribution to trigger host cell calcium signals. These results clearly show that parasites released from WT or LAMP KO cells are distinct from each other. Additionally, these parasites' ability to invade the cell may be distinct depending on which cell type they interact with. Since these alterations most likely would reflect differences among parasite

surface molecules, we also evaluated their proteome. We identified few protein complexes, membrane, and secreted proteins regulated in our dataset. Among those are some members of MASP, mucins, trans-sialidases, and gp63 proteins family, which are known to play an important role during parasite infection and could correlate to TcY-WT, TcY-L1/2^{-/-}, and TcY-L2^{-/-} biological behavior.

Keywords: *Trypanosoma cruzi*, Chagas disease, LAMP proteins, parasite invasion, intracellular environment, proteomic analysis, TMT (tandem mass tags)

INTRODUCTION

Trypanosoma cruzi is an important human pathogen that causes the American trypanosomiasis or Chagas disease—a tropical neglected disease estimated to affect about 6–7 million people worldwide (WHO, 2021). *T. cruzi*'s infective trypomastigote forms invade non-professional phagocytic cells through a process dependent on parasite interaction with host cells and activation of calcium signaling pathways that lead to parasite internalization (Andrade and Andrews, 2005; de Souza et al., 2010; Fernandes and Andrews, 2012). For this invasion process, *T. cruzi* subverts plasma membrane repair mechanism through promoting small wounds at the host cell plasma membrane and by engaging host cell surface receptors. Both events trigger signaling pathways, which lead to intracellular calcium increase in the host cell (Burleigh and Woolsey, 2002) and promote lysosomal recruitment and fusion at the parasite contact site (Tardieux et al., 1992), triggering a compensatory endocytosis process that leads to parasite internalization into the host cell (Tam et al., 2010; Fernandes et al., 2011; Fernandes and Andrews, 2012). Other lysosomes fuse to this newly formed parasitophorous vacuole (Fernandes et al., 2011) guaranteeing parasite's retention in the host cell cytoplasm (Andrade and Andrews, 2004).

In the last decade, our group has shown that cells deficient in two lysosomal membrane glycoproteins, both rich in sialic acid and known as lysosome-associated membrane protein (LAMP), LAMP-1 and LAMP-2 (Kornfeld and Mellman, 1989), are less permissive to *T. cruzi* invasion but more prone to parasite intracellular development (Albertti et al., 2010). We have also shown that LAMP-2 absence alone is sufficient for the decreased parasite invasion rate observed in LAMP-1/2-deficient cells (LAMP1/2^{-/-}) (Couto et al., 2017). The latter is due to the compromised ability of cells deficient in LAMP-2 in performing plasma membrane repair (Couto et al., 2017). Even though lysosomal exocytosis is normal in these cells, the compensatory endocytosis triggered by these exocytic events is compromised and therefore also parasite internalization (Couto et al., 2017). LAMP-2 proteins were shown to participate in the endosomal/lysosomal cholesterol export (Schneede et al., 2011). Therefore, LAMP-2 deficiency leads to accumulation of cholesterol in endo-/lysosomal compartments and, consequently, lower levels of cholesterol content in their plasma membrane (Schneede et al., 2011; Couto et al., 2017). This, in turn, leads to less caveolin at the cell surface, interfering with the compensatory endocytosis process, imperative for the

membrane repair process and parasite internalization (Couto et al., 2017). Aside from cholesterol accumulation in endo-/lysosomal compartments, cells lacking LAMP-2 or both LAMPs also accumulated autophagic vacuoles in their cytoplasm at different degrees (Eskelinen et al., 2004), therefore creating a different intracellular environment.

Changes in the intracellular environment have been previously shown to interfere with parasite gene expression profile. Dos Santos et al. (2012) showed that trypomastigotes derived from distinct cell types presented a differential expression profile of the MASP surface protein family (dos Santos et al., 2012). For this study, they used *T. cruzi* CL Brener trypomastigote forms obtained after 17 weekly maintenance passages in L6 myoblasts or LLC-MK2 epithelial cells. This differential profile of MASP expression is also reflected in differences in parasite invasion ability (dos Santos et al., 2012). As mentioned before, cells lacking LAMP-2 protein present higher cholesterol content in their cytoplasm. In addition, in these cells, *T. cruzi* intracellular multiplication rates are higher when compared to the rates observed for control cells. Thus, in the present work, we evaluated whether one passage through wild-type (WT) and LAMP-deficient fibroblasts, thus different intracellular environments, could also induce differences in parasite biological and biochemical parameters, such as protein expression profile, consequently influencing parasite invasion. For this, *T. cruzi* Y strain trypomastigotes obtained from LLC-MK2 epithelial cells were used to infect WT, LAMP1/2^{-/-}, and LAMP2^{-/-} cells, from which cultures recovered trypomastigotes were evaluated concerning their ability to adhere, invade, trigger intracellular calcium signaling, and induce membrane injury in L6 myoblasts and wild-type fibroblasts. In addition, through a proteomic approach, we also evaluated the newly released trypomastigotes' membrane and regulated subproteomes and their correlations to the parasites' biological characteristics and behavior.

MATERIAL AND METHODS

Trypanosoma cruzi and Cell Cultures

Mouse fibroblasts cell lines, derived from WT, LAMP-1/2^{-/-}, or LAMP-2^{-/-} knockout C57BL/6J mice, were obtained from a collection of cell lines from Dr. Paul Saftig's laboratory (Biochemisches Institut/Christian-Albrechts-Universität Kiel, Germany), which were previously generated by spontaneous immortalization of primary fibroblasts in culture around passages 10–20 (Eskelinen et al., 2004). The cells were maintained in high-glucose Dulbecco's modified Eagle's

medium (DMEM) (Thermo Fischer Scientific) supplemented with 10% fetal bovine serum (FBS), 1% penicillin/streptomycin (100 U/ml and 100 µg/ml, respectively) and 1% glutamine (DMEM 10%).

Tissue culture trypomastigotes from the *T. cruzi* Y strain were obtained and purified from the supernatant of infected LLC-MK2 monolayers, as described previously (Andrews et al., 1987), and used to infect wild-type or LAMP-deficient fibroblasts.

Trypanosoma cruzi Invasion Assays

For invasion assays, 5×10^4 cells (WT fibroblasts or L6 murine myoblasts) in high-glucose DMEM 10% were plated per well on a 24-well plate, containing 13-mm round glass coverslips. Cells were plated 24 h before the experiment and incubated at 37°C and 5% CO₂. Cells were then exposed to *T. cruzi* Y strain trypomastigotes obtained from wild-type (TcY-WT), LAMP-2-deficient (TcY-L2^{-/-}), or LAMP-1- and LAMP-2-deficient (TcY-L1/2^{-/-}) fibroblasts for 40 min at 37°C at a multiplicity of infection (MOI) of 50. After parasite exposure, the monolayers were washed four times with phosphate-buffered saline containing Ca²⁺ and Mg²⁺ (PBS^{+/+}), in order to remove the non-internalized parasites, and fixed in 4% paraformaldehyde overnight. After fixation, cells were processed for immunofluorescence.

Immunofluorescence and Quantification of Parasite Invasion

After fixation, coverslips with attached cells were washed three times in PBS, incubated for 20 min with PBS containing 2% bovine serum albumin (BSA) and processed for an inside/outside immunofluorescence invasion assay as described previously (Andrews et al., 1987). Briefly, extracellular parasites were immunostained with rabbit anti-*T. cruzi* polyclonal antibodies in a 1:500 dilution in PBS/BSA for 1 h at room temperature (RT) and washed and labeled with Alexa Fluor-546 conjugated anti-rabbit IgG antibody (Thermo Fischer Scientific) in a proportion of 1:500 in PBS/BSA for 45 min. After that, the DNA of host cells and parasites was stained for 1 min with DAPI (4',6-diamidino-2-phenylindole, dihydrochloride, Sigma), 0.1 µM in PBS, mounted, and examined on a ZEISS Axio Vert.A1 microscope.

Trypanosoma cruzi Adhesion Assays

The assays followed the protocol previously described by Schenkman, Diaz, and Nussenzweig (1991) (Schenkman et al., 1991). Briefly, WT fibroblasts or L6 myoblasts were plated in each well of a 24-well plate, containing 13-mm round glass coverslips, 24 h before the experiment and incubated at 37°C and 5% CO₂. Cells were then washed with Hank's balanced salt solution (HBSS, Sigma), pre-fixed with 2% glutaraldehyde in PBS^{+/+} for 5 min at 4°C and incubated for 24 h in 0.16M pH 8.3 ethanolamine solution. Before parasite exposure, cells were washed two times with DMEM containing 0.2% BSA. Cells were exposed to TcY-WT, TcY-L2^{-/-}, and TcY-L1/2^{-/-} trypomastigotes at 37°C and 5% CO₂ for 40 min at an MOI of 50. After exposure, cells were washed with PBS, fixed with 4% paraformaldehyde (PFA), and stained using rapid panotic staining. Attached parasites were counted using a microscope.

Host Cell Membrane Injury Assays

WT fibroblasts or L6 myoblasts were cultured in a 24-well plate (5×10^4 cells/well) at 37°C in 5% CO₂ in DMEM 10%. After 24 h, cell monolayers were exposed to DMEM 10% containing PI (10 µg/ml) in the presence or absence of TcY-WT, TcY-L2^{-/-}, or TcY-L1/2^{-/-} trypomastigotes for 30 min at 37°C at an MOI of 100. Alternatively, cells were exposed to parasites for 40 min, washed three times with PBS^{+/+}, and then exposed to PI staining for another 40 min. All cells were washed twice with PBS^{+/+}, trypsinized, and analyzed by flow cytometry (FACS Scan; Becton Dickinson). The data were analyzed using FlowJo v10.1 software (Tree Star, Inc.).

Calcium Signaling Assays

For the calcium signaling assays, 2.5×10^4 cells (WT fibroblasts or L6 myoblasts) in high-glucose DMEM 10% were plated in each well of four-well confocal glass-bottom dishes and, 24 h later, incubated with a fluorescent calcium probe [5 µM Fluo-4/AM (Thermo Fisher), 0.01% pluronic acid and 2.0 mM probenecid (Sigma), for 50 min at 37°C (Luo et al., 2011)]. Afterwards, cells were exposed to the following conditions: (1) culture medium; (2) ionomycin (5 µM); and (3) TcY-WT, TcY-L2^{-/-}, or TcY-L1/2^{-/-} trypomastigotes at an MOI of 100. Cells were analyzed in a Nikon C2 Plus confocal microscope using the time lapsing resource and photographed for 600 s without intervals. The changes observed for the intracellular calcium concentration were expressed as the probe intensity fluorescence fold change accordingly with the equation (F/F_0) , F being the maximum fluorescence intensity observed and F₀ the basal fluorescence observed for the point 0 (Pinto et al., 2013; Oliveira et al., 2015).

Gelatin Zymography Assays

To evaluate proteolytic activity in TcY-WT, TcY-L1/2^{-/-}, and TcY-L2^{-/-} trypomastigotes, cellular extracts were prepared using 5×10^8 trypomastigotes (70% pure regarding amastigote forms contamination) in lysis buffer [5 mM Tris-HCl pH 8.0, 10% glycerol, 1 mM EDTA (Sigma), 1 mM DTT (Promega), 10 mM cOmplete Mini EDTA-free protease inhibitors (Roche)] and protein concentration quantified by Bradford's method (Bradford, 1976). Gelatin zymography assays were performed as previously described (Leber and Balkwill, 1997) with few adaptations. Briefly, 12.5 µg of total protein were mixed with loading buffer without reducing agents and electrophoresed through a 12% polyacrylamide gel copolymerized with gelatin (Sigma) at a final concentration of 1 mg/ml. Gels were soaked in renaturing buffer [50 mM Tris-HCl, pH 7.5; 2.5% Triton X-100 (Sigma)] for 30 min at (RT), followed by one wash for 30 min at (RT) in development buffer (50 mM Tris-HCl, 200 mM NaCl, 5 mM CaCl₂, pH 7.5) and incubated for 24 h in development buffer at 37°C. Gels were stained with R-250 Coomassie brilliant blue (Sigma). Gelatinolytic activities were detected as pale bands against the dark blue background. Band intensities were quantified using ImageJ software and expressed as the pixels fold change regarding TcY-WT pixels read mean. The molecular weight standard was purchased from BioRad Prestained SDS-PAGE Standards, Broad Range.

Enzymatic Kinetics Assays

To evaluate the cysteine and serine proteolytic activities in TcY-WT, TcY-L1/2^{-/-}, and TcY-L2^{-/-} trypanomastigotes, cellular extracts were prepared as described above and 5 µg of total protein extract mixed with 50 µM N-acetyl-Tyr-Val-Ala-Asp-7-amido-4-trifluoromethylcoumarin (Ac-YVAD-AFC #A9965, Sigma-Aldrich) caspase-like or 13 µM N-succinyl-Leu-Leu-Val-Tyr 7-Amido-4-Methylcoumarin (Suc-LLVY-AMC, #S6510—Sigma-Aldrich) chymotrypsin-like fluorogenic substrates. The reactions were performed in buffer containing 50 mM Tris-HCl, pH 8.0, 10 mM MgCl₂, and 1 mM DTT, in the presence or absence of 20 µM MG-132 (#M7449, Sigma-Aldrich) inhibitor, and incubated at 37°C from 0 to 120 min with readings every 20 min. The readings were performed in the Synergy 2 Multi-detection Microplate (BioTek Instruments, Inc.) with excitation wavelength of 380/20 and emission wavelengths of 508/20 or 440/40 for Ac-YVAD-AFC or Suc-LLVY-AMC substrates, respectively.

Membrane Proteins Fraction and Sample Preparation for MS/MS Analysis

To obtain the membrane proteins fraction, about 1×10^8 trypanomastigotes forms released from wild-type or LAMP-deficient fibroblasts, presenting about 70%–80% purity regarding amastigote forms contamination, were centrifuged during 10 min at 2,200g at 4°C and washed two times with PBS (pH 7.2). Samples were resuspended in 0.1M sodium carbonate lysis buffer (pH 11.5) supplemented with protease inhibitor cocktail (Protease Inhibitor Mix, GE Healthcare, USA), submitted to two ultrasonic pulses during 20 s on ice and incubated for 1 h on ice before ultracentrifugation at 150,000g for 90 min at 4°C (Sorvall Ultra Pro 80 Ultracentrifuge). Pellets were washed one time with 500 mM triethylammonium bicarbonate (TEAB) and one time with 50 mM TEAB.

Samples were suspended in 6M urea, 2M thiourea, and 50 mM TEAB buffer and reduced with 10 mM dithiothreitol (DTT) at (RT) for 1 h. After reduction, free thiols were alkylated with 20 mM iodoacetamide (IAA) in the dark for 1 h (RT). Samples were digested for 3 h (RT) in 1:100 ratio with Lys-C. Afterwards, samples were diluted eightfold with 50 mM TEAB (pH 8.0) and proteins digested with 1:100 ratio trypsin (Promega, Madison, WI) for overnight at 37°C. The reaction was quenched by adding formic acid (FA; 1% final concentration, Sigma-Aldrich, St. Louis, MO) followed by centrifugation at 14,000g for 10 min.

Peptide TMT Labeling

The dried and digested peptides were resuspended in 100 mM HEPES (pH 8.5) with about 10 µg of peptide, as determined using a Qubit Protein Assay Kit (Thermo Fisher), from each sample used for TMT labeling. Six tags (tags 126, 127N, 128N, 129N, 130N, and 131N) from a TMT 11-plex kit (Thermo Fisher) were used to label the samples from each biological replicate. Aliquots (0.8 mg) of each reagent in 41 µl of anhydrous acetonitrile were incubated with peptide samples for 2 h at RT. The reaction was quenched by the addition of 8 µl of 5% hydroxylamine followed by incubation for 15 min at R. For each biological replicate, equal amounts of the six TMT-labeled

samples were mixed, and the TMT-labeled peptides were purified on an Oasis HLB 10 mg cartridge (Waters Corporation), which had been wetted with 100% acetonitrile and equilibrated twice with 0.1% aqueous trifluoroacetic acid (TFA). Adsorbed peptides were washed with 2 ml 0.1% TFA twice, eluted in 300 µl of 30% acetonitrile and 300 µl of 60% acetonitrile, and dried using a SpeedVac evaporator. Afterwards, the dried TMT-labeled peptides were resuspended in 2% acetonitrile in 10 mM ammonium formate (pH 9.3) for high-pH reverse phase chromatography.

High-pH Reverse Phase Chromatography

TMT-labeled peptides were injected onto an C18 Acquity UPLC MClass CSH 1.7 µm, 300 µm × 100 mm (Waters), using a Dionex Ultimate 3000 HPLC system. Buffer A was composed of 2% acetonitrile in 10 mM ammonium formate (pH 9.3) and buffer B of 80% acetonitrile in 10 mM ammonium formate (pH 9.3). Columns were run at 5 µl/min at 30°C, starting at 2% buffer B, and rising to 40% B over the course of a 27-min linear gradient. Buffer B was increased to 50% for 4 min; to 70% for 4 min; to 95% for 10 min, followed by a drop back to 2% B for 1 min, which was maintained until the end of the run at 71 min. Fractions were collected from the 4th to the 44th min with 180 s per fraction, producing 30 fractions. Fractions were concatenated into 10 samples, for example, the 1st, 11th, and 21st fractions were pooled in the same well of a 96-well plate. The 11 samples (10 samples plus the flow through—peptides eluted in the beginning of the starting conditions of high pH separation) were dried using a SpeedVac evaporator and solubilized in 0.1% FA.

LC-MS/MS and Data Analysis

Samples were analyzed by an EASY-nano LC system (Proxeon Biosystems, Odense, Denmark) coupled online to an Q Exactive HF—Orbitrap mass spectrometer (QE-HF) (Thermo Scientific, Waltham, USA). Peptides from each fraction (2 µg each) were loaded onto a 18-cm fused silica column with integrated emitter (75 µm inner diameter) packed in-house with reverse phase resin ReproSil-Pur C18-AQ 3 µm (Dr. Maisch GmbH, Germany) and eluted using a gradient from 97% phase A (0.1% FA) to 28% phase B (0.1% FA, 95% acetonitrile) for 64 min, for all 11 fractions, 28–45% phase B for 10 min, 45–100% phase B for 3 min, and 100% phase B for 8 min in a total of 86 min at 250 nl/min. After each run, the column was washed with phase B and re-equilibrated with phase A. Mass spectra were acquired in positive ion mode applying data-dependent acquisition. Each MS scan in the Orbitrap (mass range of *m/z* of 350–1,500 and resolution 120,000 at *m/z* 200) was followed by MS/MS of the 20 most intense ions (Top 20). Fragmentation was performed by higher energy collisional dissociation (HCD), and selected ions were dynamically excluded for 20 s. Raw data were viewed in Xcalibur v.4.2 (Thermo Scientific, Waltham, USA). Data processing was performed using Proteome Discoverer v.2.4 (Thermo Scientific, Waltham, USA), by searching raw files with SequestHT algorithm against a *T. cruzi* Y strain database (release 47, downloaded in May 2020), containing the proteins of the parasite found in the newly sequenced *T. cruzi* Y strain

(Callejas-Hernandez et al., 2018). Common contaminant proteins were also added to the database, and all contaminant proteins identified were filtered and removed from the result lists. The searches were performed with the following parameters: MS accuracy, 10 ppm; MS/MS accuracy, 0.02 Da; trypsin digestion with up to two missed cleavage allowed, carbamidomethyl modification of cysteine and peptide N-terminus TMT-6plex modification as fixed modifications and oxidized methionine and lysine modification by TMT-6plex as variable modifications. Number of proteins, protein groups, and number of peptides were filtered for false discovery rate (FDR) <1%, peptides with rank 1 and proteins with at least 2 peptides using Proteome Discoverer. ProteinCenter software (Thermo Scientific, Waltham, USA) was used to generate FASTA formatted files of groups of proteins of interest. Proteins were considered as regulated when their log₂ fold change was higher than the mean plus two times the standard deviation or lower than the mean minus two times the standard deviation and their coefficient of variation lower than 40%. Transmembrane domain predictions were performed using TMHMM v.2.0 (<https://services.healthtech.dtu.dk/service.php?TMHMM-2.0>) (Sonnhammer et al., 1998; Krogh et al., 2001), and glycosylphosphatidylinositol (GPI) prediction was performed using the web tools GPI-SOM (<http://gpi.unibe.ch/>) and big-PI Predictor (https://mendel.imp.ac.at/gpi/gpi_server.html) (Eisenhaber et al., 1998; Sunyaev et al., 1999; Eisenhaber et al., 1999; Eisenhaber et al., 2000). DeepLoc (<http://www.cbs.dtu.dk/services/DeepLoc/index.php>) (Almagro Armenteros et al., 2017) was used to predict the proteins subcellular localization. SignalP v.5.0 (<https://services.healthtech.dtu.dk/service.php?SignalP-5.0>) (Almagro Armenteros et al., 2019) was used to predict proteins secreted by classical ER/Golgi pathway, and SecretomeP v.2.0 (<http://www.cbs.dtu.dk/services/SecretomeP/>) (Bendtsen et al., 2005) was used to predict non-classical protein secretion. Overrepresented categories were investigated through Gene Ontology (GO) enrichment analysis using TriTrypDB (<http://tritrypdb.org/tritrypdb/>), and redundant GO terms generated were summarized in clusters by REVIGO tool (<http://revigo.irb.hr/>) (Supek et al., 2011).

Repository Data

The mass spectrometry proteomics data have been deposited to the ProteomeXchange Consortium (Deutsch et al., 2020) via the PRIDE (Perez-Riverol et al., 2019) partner repository with the dataset identifier PXD028897.

Statistical Methods

Quantitative data were expressed as mean ± standard deviation (SD) of three independent experiments unless otherwise indicated. Statistical analysis was carried out using GraphPad Prism 7.0 software via one-way ANOVA followed by Fisher's least significant difference (LSD) test or by controlling the false discovery rate (FDR) using the original procedure of Benjamini and Hochberg for multiple comparisons. Means were considered significantly different when $p < 0.05$.

RESULTS

The Residence in a LAMP-Deficient Intracellular Environment Modifies *T. cruzi* Invasion Profile

T. cruzi multiplication is increased in a LAMP-deficient environment (LAMP1/2^{-/-} or LAMP2^{-/-} fibroblasts) (Albertti et al., 2010), which suggests that differences in the intracellular environment can modify parasite biological behavior inside the host cell. In order to evaluate whether this LAMP-deficient environment may also influence the biological behavior of parasites released from these cells, *T. cruzi* Y strain trypomastigotes collected from a single infection cycle in WT (TcY-WT), LAMP1/2^{-/-} (TcY-L1/2^{-/-}) or LAMP2^{-/-} (TcY-L2^{-/-}) fibroblasts were evaluated concerning their ability to invade L6 myoblasts and WT fibroblasts. For this, these cells were exposed to TcY-WT, TcY-L1/2^{-/-}, and TcY-L2^{-/-} infective trypomastigote forms at an MOI of 50 for 40 min.

For L6 myoblasts, TcY-L2^{-/-} parasites presented the highest invasion rates, as evidenced by the number of intracellular parasites per 100 cells, when compared to TcY-WT and TcY-L1/2^{-/-} parasites, which did not show statistically significant differences between them (Figure 1A). On the other hand, for WT fibroblasts, TcY-L2^{-/-} parasites presented the lowest invasion rates, when compared to the other parasites, TcY-L1/2^{-/-} and TcY-WT (Figure 1B). Additionally, for these fibroblasts, TcY-WT invasion rate was higher than that observed for TcY-L2^{-/-} parasites, which were the less infective ones. As expected, for both host cells, the number of parasites per infected cell was about one, for all tested groups.

T. cruzi Adhesion Profile Is Also Affected by Residence in a LAMP-Deficient Intracellular Environment, but Does Not Correlate With Parasite Invasion Rate

T. cruzi adhesion to the host cell has been considered as the initial step for the invasion process (Andrews and Colli, 1982; Piras et al., 1982; Piras et al., 1983), since this proximity could aid the interaction between the parasite and host cell surface proteins, which is responsible for triggering the necessary signaling pathways that lead to parasite internalization (Fernandes and Andrews, 2012). To investigate whether the differences found in the parasite invasion rates were related to their ability in adhering to these cells, we exposed pre-fixed L6 myoblasts or WT fibroblasts to TcY-WT, TcY-L1/2^{-/-}, and TcY-L2^{-/-} trypomastigotes at an MOI of 50, for 40 min, and analyzed parasites that remained attached to the cell surface after several washes.

The adhesion assay in L6 myoblasts, revealed that TcY-L1/2^{-/-} trypomastigotes presented the highest adhesion rates when compared to TcY-WT and TcY-L2^{-/-} parasites (Figure 1C). TcY-WT parasites showed an intermediate adhesion rate compared to TcY-L2^{-/-} parasites, which in turn showed the lowest adhesion rates (Figure 1C). For WT fibroblasts, TcY-L1/2^{-/-} trypomastigotes presented the lowest adhesion rates when compared to TcY-WT and TcY-L2^{-/-} parasites (Figure 1D).

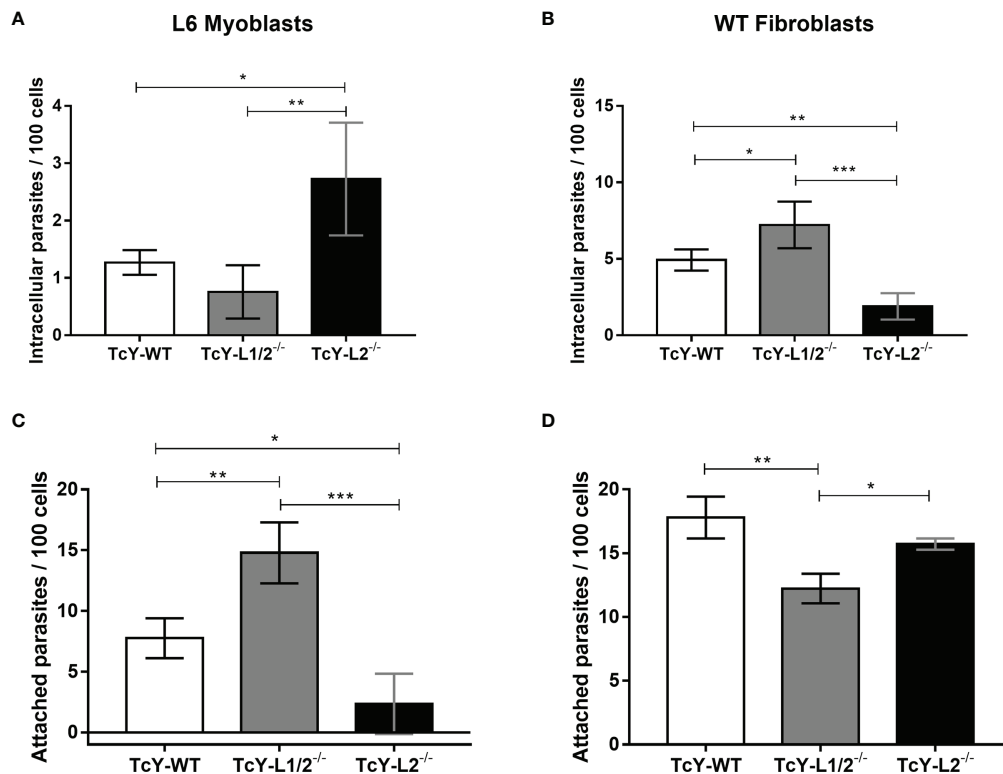


FIGURE 1 | Parasite invasion and adhesion rates are altered by passage through WT or LAMP deficient fibroblasts but do not correlate to each other. Invasion assays (**A**, **B**). L6 myoblasts (**A**) or WT fibroblasts (**B**) were exposed to TcY-WT, TcY-L1/2^{-/-}, and TcY-L2^{-/-} trypomastigotes for 40 min at an MOI of 50. Cells were fixed with 4% PFA and labeled with *T. cruzi* antibody and DAPI. Adhesion assays (**C**, **D**). L6 myoblasts (**C**) or WT fibroblasts (**D**) were fixed with 2% glutaraldehyde prior to incubation with TcY-WT, TcY-L1/2^{-/-}, and TcY-L2^{-/-} trypomastigotes for 40 min at MOI of 50. Cells were fixed with 4% PFA and stained with rapid panoptic staining. Asterisks represent statistical significance between groups (**p* < 0.05, ***p* < 0.01, ****p* < 0.001, *****p* < 0.0001, One-way ANOVA, Fisher's LSD).

There was no statistically significant difference between TcY-L2^{-/-} and TcY-WT parasites. Despite the differences found in the adhesion rates among the studied parasites in the two studied cell types, these results revealed that adhesion and invasion rates did not necessarily correlate with each other.

***T. cruzi* Biological Characteristics Correlates to its Invasion Profile Reinforcing the Modulatory Role of Residing in a LAMP-Deficient Intracellular Environment**

As mentioned before, *T. cruzi* invasion into host cells is dependent on the parasite's ability to trigger host cell intracellular calcium signaling and subverting the host cell plasma membrane repair mechanism. *T. cruzi* is able to initiate this calcium signaling by both causing microlesions in the host cell plasma membrane or inducing calcium signaling events through engagement of host cell surface receptors (Fernandes and Andrews, 2012). The increase in intracellular calcium concentration leads to lysosomal exocytosis and compensatory endocytosis events, culminating in parasite internalization (Tardieux et al., 1994). Since calcium ions play a crucial role in *T. cruzi* invasion, we decided to investigate whether the changes observed for the invasion rates could correlate to

parasite ability in triggering calcium signals. For that, L6 myoblasts or WT fibroblasts were loaded with the fluorescent calcium-binding probe Fluo4-AM and exposed to TcY-WT, TcY-L1/2^{-/-}, and TcY-L2^{-/-} infective trypomastigote forms at an MOI of 100, while recording the fluorescence increase in real time by confocal microscopy. For L6 myoblasts, calcium signaling induced by TcY-L2^{-/-} was significantly higher than the signaling induced by TcY-WT or TcY-L1/2^{-/-} parasites, while those two did not present statistically significant differences between them (Figure 2A, Supplementary Figure S1). On the other hand, for WT fibroblasts, calcium signaling induced by TcY-L2^{-/-} parasites was significantly lower than the signaling induced by the other two parasites, TcY-WT and TcY-L1/2^{-/-}, being the highest calcium signals induced by TcY-L1/2^{-/-} parasites (Figure 2B, Supplementary Figure S2). For both host cell types, myoblasts and fibroblasts, the calcium signals induced by the different parasites directly correlated with their invasion rates, meaning the higher the calcium signaling triggered by the parasite, the higher the cell invasion efficiency. These results reinforce the important role played by calcium signaling events during the *T. cruzi* invasion process.

To investigate further the differences in the calcium signaling triggered by the distinct parasites in the different cell types, we

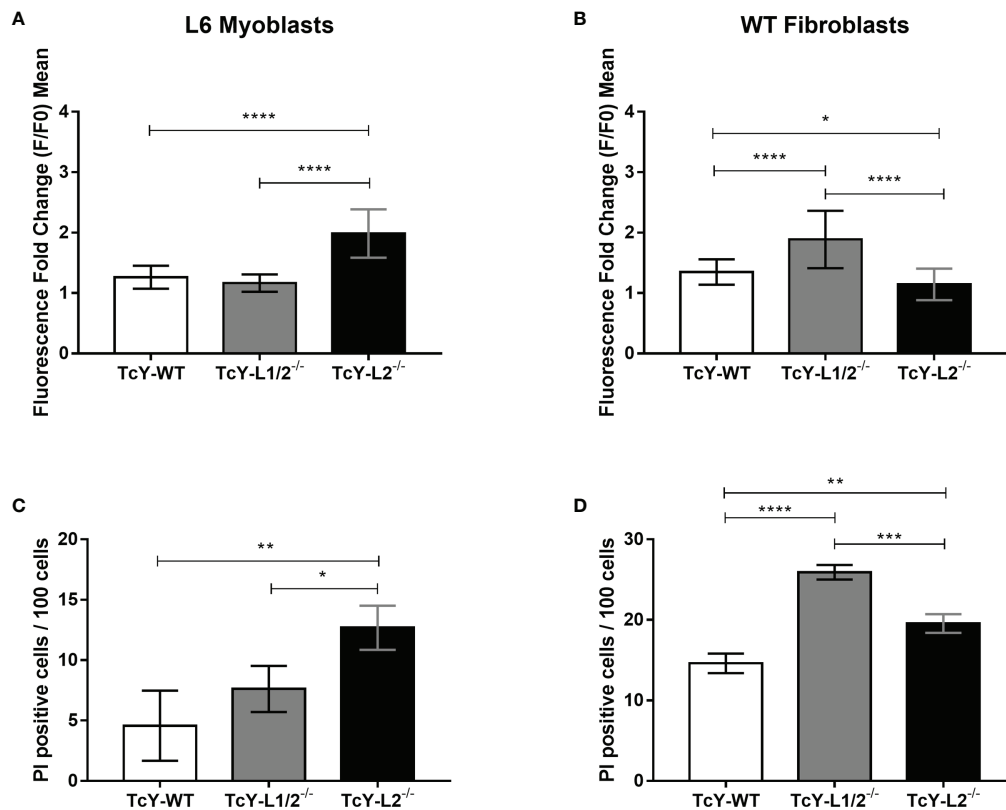


FIGURE 2 | Parasites derived from WT or LAMP deficient cells differ in their ability in triggering host calcium signaling events, and these differences correlate, in part, with their ability to inducing microinjuries in the host cell plasma membrane. L6 myoblasts or WT fibroblasts were exposed to TcY-WT, TcY-L1/2^{-/-}, and TcY-L2^{-/-} trypomastigotes as described in *Materials and methods*. Calcium signaling assays in L6 myoblasts (**A**) and WT fibroblasts (**B**); the cells were also exposed to ionomycin as positive control and culture medium as negative control. Membrane injury assays in L6 myoblasts (**C**) and WT fibroblasts (**D**). Asterisks represent statistical difference between groups (*p < 0.05, **p < 0.01, ***p < 0.001, ****p < 0.0001, one-way ANOVA, Fisher's LSD).

evaluated whether the calcium-signaling events were generated by micro-injuries at the host cell plasma membrane or triggered by activation of host cell surface receptors. To investigate the calcium signaling induced by plasma membrane injuries, we exposed L6 myoblasts or WT fibroblasts to TcY-WT, TcY-L1/2^{-/-}, and TcY-L2^{-/-} trypomastigotes at an MOI of 100 in the presence of propidium iodide (PI) for 30 min. PI is a red-fluorescent nuclear and chromosome counterstain, not permeant to live cells. Therefore, PI staining indicates membrane permeabilization by injury. For L6 myoblasts, TcY-L2^{-/-} parasites induced injury to a higher number of cells when compared to TcY-WT and TcY-L1/2^{-/-} parasites, corroborating their invasion profile and suggesting that for these parasites, calcium signals are triggered through injuries at the host cell membrane (Figure 2C). No statistically significant differences were observed between the number of PI positive cells for TcY-WT and TcY-L1/2^{-/-} parasites, indicating that these parasites likely induce similar levels of injury to L6 myoblasts (Figure 2C, Supplementary Figure S3). Again, these results corroborate with the invasion profile observed for these parasites. Alternatively, cells were incubated with parasites in the absence of PI, washed, and then incubated with PI. As expected, no statistically significant differences were observed among PI

staining of cells incubated with PI post *T. cruzi* infection, for all parasites, and the negative control (cells incubated with PI only, without being previously exposed to the parasite) (Supplementary Figure S4). For WT fibroblasts, TcY-L1/2^{-/-} parasites induced injury to a higher number of cells when compared to TcY-WT and TcY-L2^{-/-} parasites, corroborating their invasion profile in these cells (Figure 2D and Supplementary Figure S5). TcY-WT parasites induced injury to the lowest number of cells, when compared to the others, even though calcium signaling triggered by these parasites in WT fibroblasts was higher than that observed for TcY-L2^{-/-} parasites (Figures 2B, D).

T. cruzi Proteome Is Influenced by the Residence in a LAMP-Deficient Intracellular Environment

Once parasites released from the distinct cell types presented different biological behaviors, we decided to investigate whether changes in these parasites' surface membrane protein profiles could account for the biological phenotypes obtained. For this, we performed quantitative mass spectrometry-based proteomic analysis to identify and quantify the membrane-enriched protein

preparation from TcY-WT, TcY-L1/2^{-/-}, and TcY-L2^{-/-} trypomastigotes. *T. cruzi* Y strain trypomastigotes were cultured in the wild-type or LAMP-deficient fibroblasts, collected, lysed, and then ultra-centrifuged to separate the membrane-enriched protein fraction. Extracted proteins were digested, reduced, and alkylated, and the tryptic peptides were labeled with TMT 6-plex (Thermo Fisher), analyzed by mass spectrometry-based proteomics, and submitted to bioinformatics tools to perform functional analyses. For protein identification from the peptide sequences, we used the Y strain annotated proteins from TriTrypDB website (released on April 23, 2020 and downloaded on May 2020) (Callejas-Hernandez et al., 2018).

We identified 3,806 proteins with high confidence level and containing at least one unique peptide in all three samples (**Supplementary Table S1**). A principal component analysis was performed to evaluate the biological replicates similarity, using the normalized quantitative abundance values (**Supplementary Figure S6**). This analysis showed an acceptable level of similarity between replicates within the same group. A total of 1,365 proteins were annotated as uncharacterized or hypothetical proteins, corresponding to about 36% of the identified proteins in our data set. The high percentage of uncharacterized proteins is not surprising, since for the *T. cruzi* Y strain genome, 56.94% of the proteins correspond to hypothetical proteins of unknown function (Callejas-Hernandez et al., 2018). Because of this, we performed a GO analysis with Fisher exact test filtering for FDR <0.05, using the GO enrichment analysis tool on the TriTrypDB in order to verify if our samples were in fact enriched in membrane terms. Regarding the GO cellular component level, the analysis showed that our data set presented an enrichment in many terms related to membrane, such as intrinsic component of membrane, integral component of membrane, and endomembrane system (**Supplementary Figure S7**). Even though the most enriched term is cytoplasm, the QuickGO definition of this term comprises the contents of a cell excluding the plasma membrane and nucleus, but including other subcellular structures (<https://www.ebi.ac.uk/QuickGO/GTerm?id=GO:0005737>). Therefore, many organelle membrane proteins present in our data set fell into this GO cytoplasm term.

We then compared the proteomes of TcY-L1/2^{-/-} and TcY-L2^{-/-} trypomastigotes' membrane-enriched proteins preparation to that from TcY-WT trypomastigotes. We considered as regulated proteins, all members that presented a log2 fold change higher than the mean plus 2 times the standard deviation or lower than the mean minus 2 times the standard deviation and coefficient of variation lower than 40%—referred from here as the regulated subproteome. We found 75 and 90 proteins in the TcY-L1/2^{-/-} and TcY-L2^{-/-} regulated subproteomes, respectively (**Supplementary Table S2**) that matched these criteria. From these proteins, either a considerable percentage, in both regulated subproteomes, had predicted transmembrane domains or to be classically or non-classically secreted (**Table 1**). Additionally, important *T. cruzi* virulence factors, such as members of trans-sialidase superfamily, and other surface proteins families, such as MASP and surface protease gp63 (Goncalves et al., 1991; Trocoli Torrecilhas et al.,

2009; Bayer-Santos et al., 2013), were found to be differentially regulated in these parasites (**Table 2**).

In the TcY-L1/2^{-/-} regulated subproteome, 51 proteins were upregulated and 24 were downregulated, and in the TcY-L2^{-/-} regulated subproteome, 55 proteins were upregulated and 35 were down regulated, when compared to TcY-WT proteome. There were only four upregulated proteins, three of them being hypothetical proteins, and nine downregulated proteins shared between TcY-L1/2^{-/-} and TcY-L2^{-/-} regulated subproteomes (**Figure 3**).

For further understanding the possible role of these differentially regulated proteins in the biological behavior observed for TcY-L1/2^{-/-} and TcY-L2^{-/-}, we classified and grouped them in distinct biological processes, based on their gene ontology, using the enrichment test available on TriTrypDB with Fisher exact test filtering for FDR <0.05. Regarding the TcYL1/2^{-/-} regulated subproteome regulated subproteome, there was no enriched biological processes (BP) from the up regulated proteins and we found 15 BP enriched from the down regulated. We removed the redundant terms from them using the REVIGO tool (<http://revigo.irb.hr/>), and after summarizing the terms, we found eight BP downregulated (protein folding, cellular ketone metabolic process, quinone biosynthetic process, pentose-phosphate shunt, glyceraldehyde-3-phosphate metabolic process, microtubule-based movement, cellular process, movement of cell or subcellular component) in comparison to TcY-WT proteome (**Figure 4A** and **Supplementary Table S3**). Six proteins were relevant for two or more downregulated BP in the TcY-L1/2^{-/-} regulated subproteome: 6-phosphogluconate dehydrogenase, decarboxylating, putative (TcYC6_0069460), ubiquinone biosynthesis protein COQ7-like, putative (TcYC6_0110760), kinesin-13 3, putative (TcYC6_0081520), kinesin, putative (TcYC6_0110780), T-complex protein 1, delta subunit, putative (TcYC6_0023210), and chaperonin/T-complex protein 1 gamma subunit, putative (TcYC6_0030620). We next performed a GO biological process enrichment analysis using the membrane-associated proteins that presented transmembrane domains and/or were assigned as membrane by the DeepLoc analysis (referred from here as membrane subproteome). From this analysis, we did not find any enriched BP either from the up- or the downregulated proteins list. However, for the upregulated membrane subproteome, we found the sphingolipid metabolism (ec00600:PK:KEGG) pathway enriched, using the Metabolic Pathway Enrichment analysis tool on TriTrypDB with KEGG as pathway source and filtering FDR <0.05.

For TcY-L2^{-/-} regulated subproteome, there was no enriched BP from the downregulated proteins, and we found 25 BP enriched from the upregulated. After summarizing the terms with the REVIGO tool, we found five BP upregulated (proteolysis involved in cellular protein catabolic process, catabolic process, proteolysis, cellular protein-containing complex assembly, mitochondrion organization) in comparison to TcY-WT proteome (**Figure 4B** and **Supplementary Table S3**). Six proteins were present in two or more upregulated BP: proteasome alpha 1 subunit, putative (TcYC6_0071370), proteasome alpha 2 subunit, putative (TcYC6_0023180), proteasome beta 3 subunit,

TABLE 1 | Number of proteins from the regulated subproteome with predicted transmembrane domains, GPI-anchor, classically and non-classically secreted, and enzymes.

Subproteome	Total regulated	TM Domains*	GPI anchored*	SignalP*	SecretomeP*	Enzymes**
TcY-L1/2 ^{-/-}	75	27 (36.0%)	8 (10.7%)	7 (9.3%)	19 (25.3%)	20 (26.7%)
↑ UP	51	26 (51.0%)	8 (15.7%)	6 (11.8%)	13 (25.5%)	12 (23.5%)
↓ DOWN	24	1 (4.2%)	0 (0.0%)	1 (4.2%)	4 (16.7%)	6 (25.0%)
TcY-L2 ^{-/-}	90	34 (37.8%)	8 (8.9%)	16 (17.8%)	11 (12.2%)	23 (25.6%)
↑ UP	55	31 (56.4%)	7 (12.7%)	12 (21.8%)	5 (9.1%)	18 (32.7%)
↓ DOWN	35	3 (8.6%)	1 (2.9%)	4 (11.4%)	5 (14.3%)	5 (14.3%)

*Absolute numbers and percentages of regulated protein groups with predicted transmembrane (TM) domains or GPI-anchored, ER/Golgi signal peptide (SignalP), or non-classically secreted (SecretomeP) related to the total number of regulated proteins identified in each subproteome compared to TcY-WT proteome.

**Absolute numbers and percentages of enzymes in each subproteome related to the total number of regulated proteins compared to TcY-WT proteome.

putative (TcYC6_0044600), proteasome beta 6 subunit, putative (TcYC6_0041700), proteasome beta 7 subunit, putative (TcYC6_0091650), and putative mitochondrial chaperone BCS1 (TcYC6_0123290). Using the Metabolic Pathway Enrichment analysis tool on TriTrypDB with KEGG as pathway source and filtering FDR <0.05, we found two upregulated pathways [arginine and proline metabolism (ec00330:PK:KEGG), and Diterpenoid biosynthesis (ec00904:PK:KEGG)] and one downregulated pathway [ether lipid metabolism (ec00565:PK:KEGG)]. The GO biological process enrichment analysis of TcY-L2^{-/-} membrane subproteome revealed one upregulated BP, the vacuolar proton-transporting V-type ATPase complex assembly. We did not find any enriched pathways for this membrane subproteome.

In order to establish a better understanding of the LAMP-deficient cells-derived parasites, we compared the TcY-L1/2^{-/-} and TcY-L2^{-/-} proteomes. These parasites were the most different regarding their invasion characteristics. In fact, the proteomic analysis revealed a higher number of differentially regulated proteins between them, 136 proteins—55 downregulated and 81 upregulated (using the same previously described criteria) (Supplementary Table S2). From these proteins, a considerable

part is predicted to have transmembrane domains or to be classically or non-classically secreted (Table 3). Interestingly, we also found a higher number of membrane surface proteins regulated between TcY-L1/2^{-/-} and TcY-L2^{-/-} trypanosomes (Table 4).

The GO BP enrichment analysis from these differentially regulated proteins between TcY-L1/2^{-/-} and TcY-L2^{-/-} trypanosomes showed 13 BPs from the down regulated proteins list and no BP from the upregulated protein list. After summarizing the terms using the REVIGO tool, three downregulated BP remained (proteolysis involved in cellular protein catabolic process, catabolic process, and proteolysis) (Figure 4C and Supplementary Table S3). Five proteasome proteins were present in all three BPs: proteasome alpha 1 subunit, putative (TcYC6_0071370), proteasome alpha 2 subunit, putative (TcYC6_0023180), proteasome alpha 7 subunit, putative (TcYC6_0044220), proteasome beta 3 subunit, putative (TcYC6_0044600), and proteasome beta 7 subunit, putative (TcYC6_0091650). The metallo-peptidase, Clan MF, Family M17, putative (TcYC6_0033380), cytoskeleton-associated protein CAP5.5, putative (TcYC6_0107360), and surface protease GP63, putative (TcYC6_0169090) proteins also contributed to the proteolysis enrichment.

TABLE 2 | Important surface membrane proteins regulated in TcY-L1/2^{-/-} and TcY-L2^{-/-} trypanosomes compared to TcY-WT trypanosomes.

TriTryp ID	Protein description	log2 FC TcY-L1/2 ^{-/-} /TcY-WT	log2 FC TcY-L2 ^{-/-} /TcY-WT
TcYC6_0114230	membrane protein, putative	NDR	1.04
TcYC6_0162290	Mucin-associated surface protein (MASP), subgroup S002	NDR	0.88
TcYC6_0158360	Mucin-associated surface protein (MASP), subgroup S017	0.88	NDR
TcYC6_0161780	Mucin-associated surface protein (MASP), subgroup S061	NDR	-1.66
TcYC6_0160330	Mucin-associated surface protein (MASP), subgroup S097	0.31	NDR
TcYC6_0124770	Surface membrane protein	NDR	1.08
TcYC6_0169700	Surface protease GP63, putative	NDR	1.32
TcYC6_0169840	Surface protease GP63, putative	0.29	NDR
TcYC6_0016150	Transmembrane protein	NDR	-0.98
TcYC6_0128720	Trans-sialidase, Group II, putative	0.8	NDR
TcYC6_0131410	Trans-sialidase, Group II, putative	0.36	NDR
TcYC6_0131440	Trans-sialidase, Group II, putative	NDR	0.87
TcYC6_0130520	Trans-sialidase, Group V, putative	0.69	NDR
TcYC6_0129770	Trans-sialidase, Group VI, putative	0.32	NDR
TcYC6_0128910	Trans-sialidase, putative	0.78	NDR
TcYC6_0130010	Trans-sialidase, putative	NDR	0.9

NDR, not differentially regulated; red, upregulated; blue, downregulated

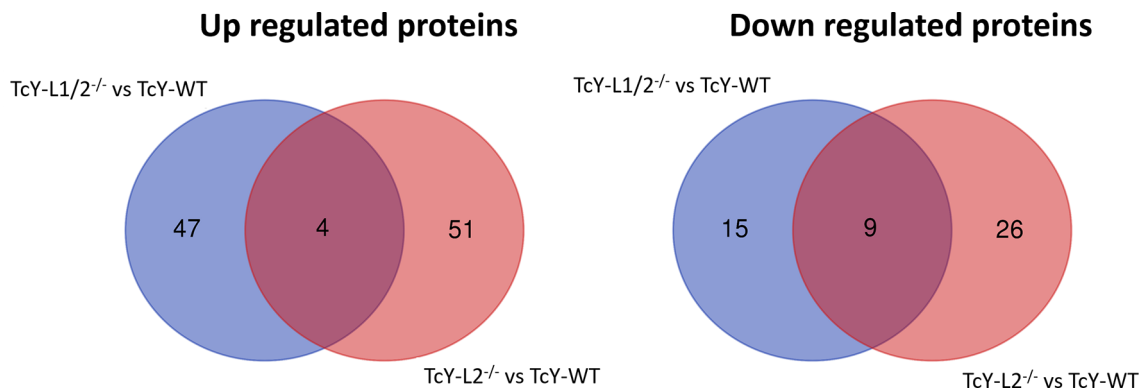


FIGURE 3 | TcY-WT, TcY-L1/2^{-/-}, and TcY-L2^{-/-} trypomastigotes present differentially regulated proteins among them. Venn diagrams showing the exclusively regulated and the shared proteins in TcY-L1/2^{-/-} and TcY-L2^{-/-} regulated subproteomes in comparison to TcY-WT proteome. This figure was prepared using the Draw Venn Diagram webtool (<http://bioinformatics.psb.ugent.be/webtools/Venn/>).

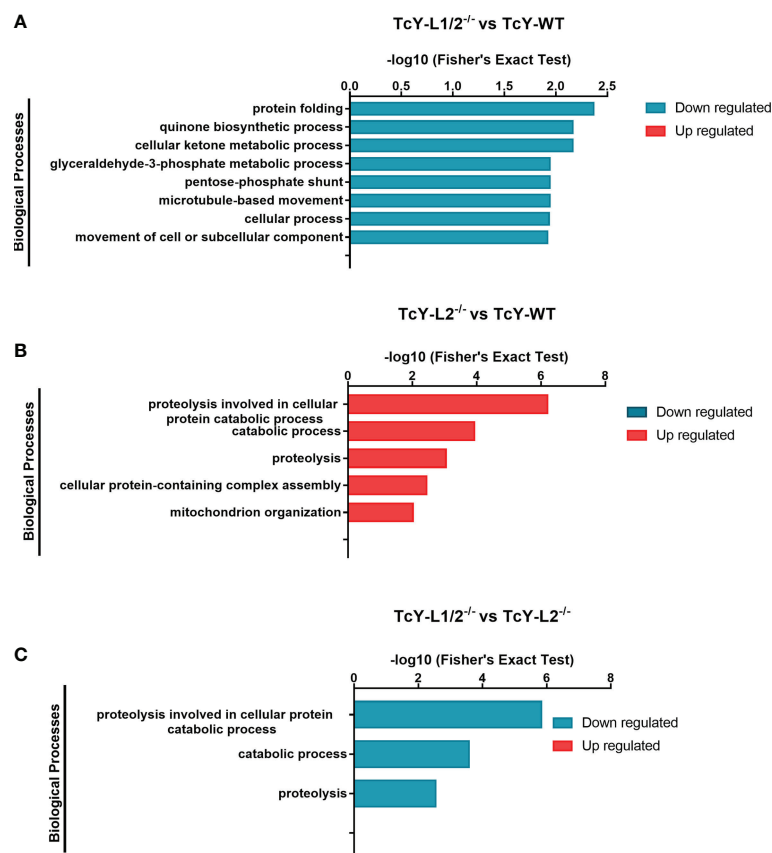


FIGURE 4 | Gene ontology enrichment analysis of biological processes terms in TcY-L1/2^{-/-} or TcY-L2^{-/-}-regulated subproteomes. The graph shows the different biological processes up- or downregulated, based on the differentially expressed proteins of TcY-L1/2^{-/-} (A) or TcY-L2^{-/-} (B) compared to TcY-WT proteome and on the differentially expressed proteins of TcY-L1/2^{-/-} (C) compared to TcY-L2^{-/-} proteome.

TABLE 3 | Number of proteins from the regulated subproteome with predicted transmembrane domains, GPI-anchor, classically and non-classically secreted, and enzymes.

Subproteome	Total regulated	TM Domains*	GPI anchored*	SignalP*	SecretomeP*	Enzymes**
TcY-L1/2 ^{-/-} vs TcY-L2 ^{-/-}	136	34 (25.0%)	10 (7.4%)	18 (13.2%)	28 (20.6%)	39 (28.7%)
↑ UP	81	10 (12.3%)	2 (2.5%)	6 (7.4%)	17 (21.0%)	17 (21.0%)
↓ DOWN	55	24 (43.6%)	8 (14.5%)	12 (21.8%)	11 (20.0%)	22 (40.0%)

*Absolute numbers and percentages of regulated protein groups with predicted transmembrane (TM) domains or GPI-anchored, ER/Golgi signal peptide (SignalP), or non-classically secreted (SecretomeP) related to the total number of regulated proteins identified in each subproteome compared to TcY-WT proteome.

**Absolute numbers and percentages of enzymes in each subproteome related to the total number of regulated proteins compared to TcY-WT proteome.

Residence in a LAMP-2-Deficient Intracellular Environment Increases *T. cruzi* Proteolytic Activity

Since many proteolysis-related terms were enriched in the TcY-L2^{-/-} regulated subproteome compared to TcY-WT and TcY-L1/2^{-/-} proteomes, we decided to further investigate the parasites' proteolytic activity. For that, we evaluated the parasites' proteolytic activity through gelatin zymography assays. The results showed a higher gelatinolytic activity for TcY-L2^{-/-} trypomastigotes compared to TcY-WT and TcY-L1/2^{-/-} (Figure 5), thus corroborating the proteomic analysis.

In order to investigate deeper the higher proteolytic profile observed for TcY-L2^{-/-} trypomastigotes, we decided to test the protein extracts for serine proteases and cysteine proteases activity. Enzyme activity assays were performed using Ac-YVAD-AFC caspase-like and Suc-LLVY-AMC chymotrypsin-like fluorogenic substrates, for cysteine and serine proteases, respectively. For caspase-like activity, TcY-L1/2^{-/-} and TcY-L2^{-/-} protein extracts showed slightly higher activities than TcY-WT protein extract (Figures 6A, C). For all protein extracts, the inhibitor MG-132 decreased caspase-like activity in 2.23 ± 0.055 , 1.98 ± 0.25 , and 1.94 ± 0.34 times for TcY-WT, TcY-L1/2^{-/-}, and TcY-L2^{-/-}, respectively (Figures 6A, C). For chymotrypsin-like activity, TcY-L2^{-/-} protein extract showed the highest activity,

while TcY-L1/2^{-/-} presented the lowest (Figures 6B, D). Here again, for all protein extracts, the inhibitor MG-132 considerably decreased their activities in 12.12 ± 1.53 , 8.91 ± 0.48 , and 15.73 ± 0.53 times for TcY-WT, TcY-L1/2^{-/-}, and TcY-L2^{-/-} respectively. For Suc-LLVY-AMC substrate, the kinetic activity also showed a similar profile to the one revealed by the zymography assays.

DISCUSSION

In previous studies carried out by our group, we showed that the alteration of a single protein in the host cell—LAMP (a lysosomal protein)—changed the biological behavior of two distinct *T. cruzi* strains, Y and CL, belonging to TcI and TcVI lineages, respectively (Albertti et al., 2010). It was shown that parasites from both strains increased their intracellular growth in LAMP-deficient cells (LAMP1/2^{-/-}), releasing a significantly higher number of trypomastigote forms at the end of a single intracellular cycle, when compared to infections on wild-type (WT) cells (Albertti et al., 2010). Lysosomes are relevant host-cell organelles that affect *T. cruzi* invasion success, since they are recruited to the parasite entry site, not only donating membrane for the formation of the parasitophorous vacuole (Tardieux et al., 1992) but also are crucial for parasite's permanence in the cell (Andrade and Andrews, 2004). Therefore, the present study

TABLE 4 | Important surface membrane proteins regulated in TcY-L1/2^{-/-} trypomastigotes compared to TcY-L2^{-/-} trypomastigotes.

TriTryp ID	Protein description	log2 FC TcY-L1/2 ^{-/-} /TcY-L2 ^{-/-}
TcYC6_0154080	mucin TcMUCII, putative	-1.46
TcYC6_0150670	mucin TcMUCII, putative	-0.98
TcYC6_0154140	mucin TcMUCII, putative	0.38
TcYC6_0158360	Mucin-associated surface protein (MASP), subgroup S017	0.71
TcYC6_0164190	Mucin-associated surface protein (MASP), subgroup S054	-0.98
TcYC6_0161500	Mucin-associated surface protein (MASP), subgroup S074	-1.47
TcYC6_0124770	Surface membrane protein	-1.09
TcYC6_0169090	Surface protease GP63, putative	-1.11
TcYC6_0077110	Surface protein ToIT, putative	-1.5
TcYC6_0078130	Surface protein ToIT, putative	-1.46
TcYC6_0078140	Surface protein ToIT, putative	-1.44
TcYC6_0141330	Trans-sialidase (pseudogene), putative	0.34
TcYC6_0130150	Trans-sialidase, Group II, putative	-1.18
TcYC6_0131910	Trans-sialidase, Group II, putative	-1.01
TcYC6_0132210	Trans-sialidase, Group II, putative	-1.01
TcYC6_0128720	Trans-sialidase, Group II, putative	0.88
TcYC6_0130010	Trans-sialidase, putative	-0.93
TcYC6_0128910	Trans-sialidase, putative	0.76

Red, upregulated; blue or purplish, downregulated.

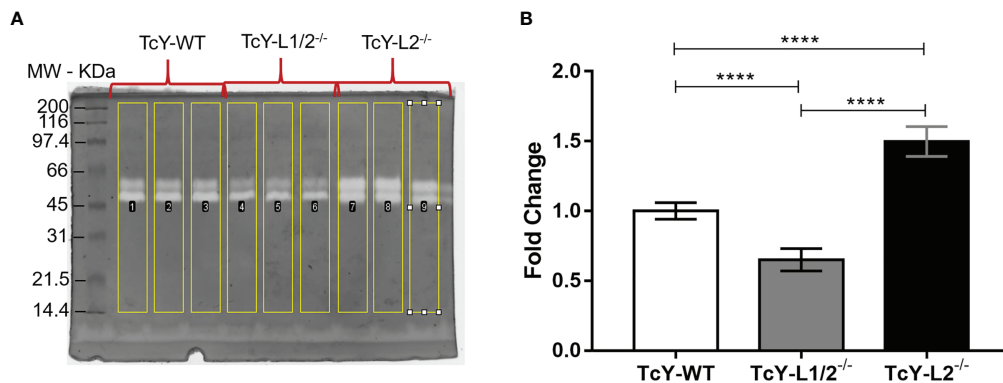


FIGURE 5 | Increased proteolytic activity of TcY-L2^{-/-} assessed by gelatin zymography assays. **(A)** Representative SDS-PAGE gel showing the negative bands from gelatinolytic activity. **(B)** Quantification obtained from gels using ImageJ software—TcY-WT values were used as a normalizer for all groups. Asterisks represent statistical difference between groups (****p < 0.0001, one-way ANOVA, Fisher's LSD).

aimed to understand whether the parasites released from the different intracellular environments, therefore from the LAMP-deficient or WT cells, exhibited different biological behavior among them. For this, we evaluated four characteristics related to the parasite's entry process into the host cell: the invasion and adhesion rates, the calcium signal profile induced by these parasites, and their ability to induce host cell membrane

micro-injuries. These parameters were evaluated in two different host cell lines: L6 myoblasts and WT fibroblasts.

Our results first revealed that only one passage through a LAMP-deficient environment was able to modify the parasite's invasion rate. To the best of our knowledge, this is the first time that it is shown that one single passage through different intracellular environments may induce such significant changes

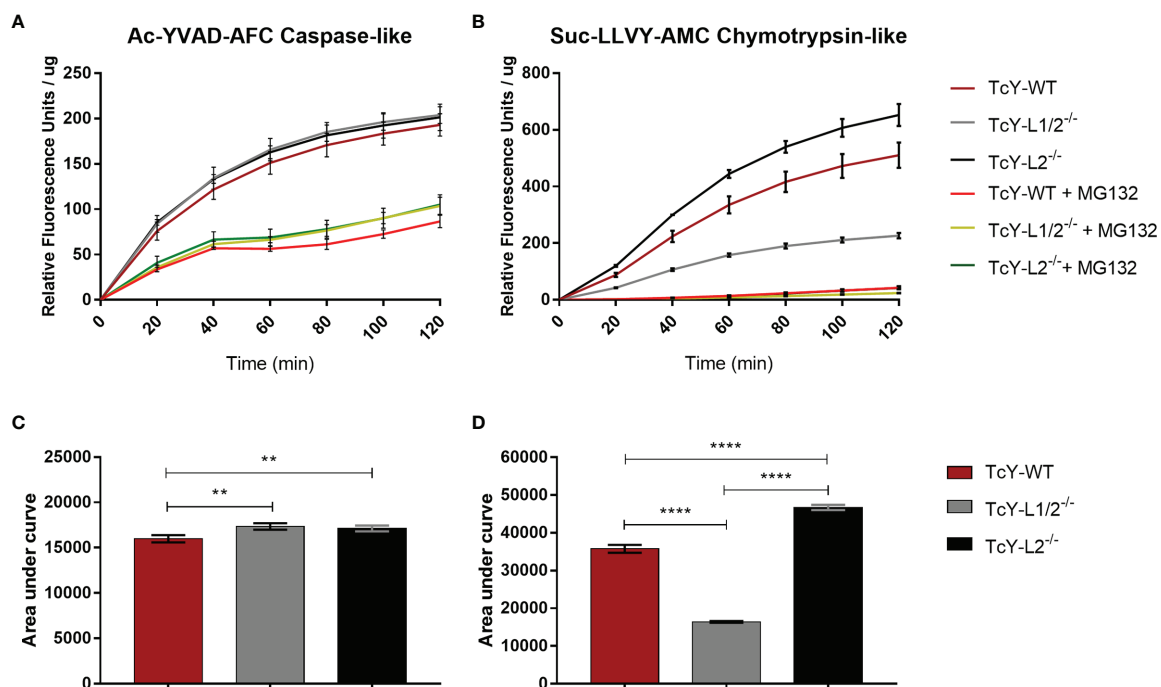


FIGURE 6 | Cysteine protease and serine protease enzymatic activity kinetics. Cysteine **(A)** or serine **(B)** activity in TcY-WT, TcY-L1/2^{-/-}, or TcY-L2^{-/-} trypanomastigotes protein extracts were assayed using a fluorescence method with caspase substrate Ac-YVAD-AFC for caspase-like cysteine enzyme activity or chymotrypsin substrate Suc-LLVY-AMC for chymotrypsin-like serine enzyme activity. The data are mean ± SD for the kinetic curves **(A, B)** (**p < 0.01, ****p < 0.0001, one-way ANOVA, Fisher's LSD).

in the parasite behavior. As mentioned before, in the work from Dos Santos et al. (2012), changes in the MASP expression profile or invasion rates were studied upon several passages through different cell types (dos Santos et al., 2012). Additionally, we showed that the absence of only LAMP-2 or both LAMP proteins affect the parasite differently. Although *LAMP2*^{-/-} and *LAMP1/2*^{-/-} cells have similar lysosomal distribution and enzyme activity, it has been shown that the latter present an increased number of autophagic vacuoles, both before or after starvation, in relation to *LAMP2*^{-/-} or WT cells (Eskelinen et al., 2004; Eskelinen, 2006). Additionally, the level of cholesterol accumulation in endo-/lysosomal compartments is distinct for *LAMP2*^{-/-} and *LAMP1/2*^{-/-} cells (Tanaka et al., 2000; Eskelinen et al., 2002; Eskelinen et al., 2004). In *LAMP1/2*^{-/-} cells, due to this disturbed cholesterol traffic, there was also a decrease in amount of lipid droplets (Eskelinen et al., 2004). Apparently, the lack of both LAMPs implicates in an exacerbated phenotype. In fact, LAMP-2-deficient mice complete its embryonic development, although 50% die shortly after they are born (between 20 and 40 postnatal day), while the deficiency in both LAMP-1 and 2 is embryonic lethal with prenatal death between embryonic days 14.5 and 16.5. The above-mentioned indicates that the intracellular environment and cellular behavior are not similar between *LAMP2*^{-/-} and *LAMP1/2*^{-/-} cells. These changes may likely signal differently to intracellular *T. cruzi*. Autophagosomes have been shown to participate in *T. cruzi* infection in host cells (Romano et al., 2009). In this study, Romano et al. (2009) showed that the induction of autophagy favors parasite invasion and that an increasing number of internalized parasites colocalize with LC3, an autophagosome marker, with time of infection (Romano et al., 2009). Whether the percentage of parasites colocalizing with autophagosome markers or even the time length of association of these markers varies among WT, *LAMP2*^{-/-}, and *LAMP1/2*^{-/-} cells is not known, but if so, they may account for at least part of the distinct behavior observed for the parasites release from *LAMP2*^{-/-} and *LAMP1/2*^{-/-} cells. We also showed that the cell type that the parasite is interacting with affected the invasion rate. For example, we observed that the TcY-L1/2^{-/-} trypomastigotes were the most infective in WT fibroblasts but the least infective in L6 myoblasts. On the other hand, TcY-L2^{-/-} trypomastigotes were the least infective in WT fibroblasts, but the most infective in L6 myoblasts. In fact, differences in *T. cruzi*'s ability to invade different cell types has been shown previously (Andrade et al., 2010; Maeda et al., 2016). This has to do with the fact that although parasite invasion is always dependent on calcium signaling, lysosome recruitment, and fusion, the pathways involved in eliciting these signals may vary a lot among different parasite strains and the host cell type (Burleigh and Woolsey, 2002; Barrias et al., 2013; Ferri and Edreira, 2021).

The recruitment and fusion of lysosomes, crucial steps for the invasion process, occur at the parasite adhesion site (Tardieux et al., 1992; Tardieux et al., 1994), and the existence of a correlation between cell adhesion and invasion rates by *T. cruzi* has been reported (Piras et al., 1982; Andrews and Colli, 1982; Piras et al., 1983). Therefore, we also investigated whether the adhesion profiles of TcY-WT, TcY-L1/2^{-/-}, or TcY-L2^{-/-} trypomastigotes differed from each other.

Indeed, the adhesion profiles not only varied among the different parasites but also between the two cell types for the same parasite population. Data obtained here, from both invasion and adhesion rates, demonstrate that developing in an intracellular environment absent in LAMP proteins most likely induces changes in the expression of trypomastigote surface proteins. It also reinforces data from the literature demonstrating that changes in the *T. cruzi*'s trypomastigotes expression profile alters parasite tropism for specific cells (Andrade et al., 1999; Macedo et al., 2004; dos Santos et al., 2012). Nonetheless, contrary to expected, no correlation between adhesion and invasion was observed. In fact, we observed an inverse relation for some cell types, since less adherent parasites had the highest invasion rates. Again, to the best of our knowledge, this is the first time that an opposite relation between adhesion and invasion rates are shown for *T. cruzi*. These data also support the idea that proteins involved in adhesion may differ from those required for signaling and triggering the cell invasion process, the latter being probably the main factor in the host cell infection process. Therefore, a high adhesion with a low cell signaling would be ineffective to increase invasion.

Based on the above-mentioned, we investigated whether differences in the invasion rates among TcY-WT, TcY-L1/2^{-/-}, or TcY-L2^{-/-} would correlate with these parasites' ability to trigger host intracellular calcium signaling. As mentioned previously, calcium signaling, either induced *via* surface receptors stimulus and intracellular calcium stock mobilization or *via* extracellular calcium influx triggered by microinjuries, is a crucial step to *T. cruzi* invasion success (Fernandes and Andrews, 2012). Indeed, a direct correlation between the amount of calcium signaling and invasion rates was observed, corroborating the data observed for cell invasion. To understand further the contribution of calcium triggered *via* host surface receptor engagement and parasite induced host membrane microinjuries, we also performed a membrane injury assay. For most studied parasites and cell types tested, calcium signaling correlated with parasites' ability to induce host cell membrane microinjuries, showing that this pathway is relevant for parasite host cell entry. However, for TcY-WT and TcY-L2^{-/-} in WT fibroblasts, this correlation was not observed. TcY-WT showed significantly higher invasion rates and calcium signals in WT fibroblasts when compared to TcY-L2^{-/-} trypomastigotes, although lower levels of host cell membrane microinjury when compared to TcY-L2^{-/-}. Thus, calcium from the extracellular milieu would not be enough to account for the results obtained, meaning that calcium from intracellular stocks, released from the ER *via* host cell surface protein signaling, triggered by the parasite, was likely to contribute. These results reinforce that both calcium signaling *via* microinjury and *via* host cell membrane receptors are relevant to *T. cruzi*'s invasion process. Additionally, these results reinforce that, without the ability of parasites in successfully triggering calcium signaling events in the host cell, adhesion alone is not enough for inducing parasite invasion. In fact, proteins involved in *T. cruzi* adhesion (members of trans-sialidase or MASPs families for example) to host cells are usually not the ones shown to induce calcium signaling (calcium agonist generated by oligopeptidase B from the parasite or

bradykinin obtained from the activity of cruzipain from the parasite) (Burleigh and Woolsey, 2002; Alves and Colli, 2007).

All observed biological alterations for all three parasites groups indicated differences in their surface proteins expression profile. Based on our data, we hypothesize that the intracellular environment can induce changes in the parasite during its development, including surface molecules. To analyze possible differences in the protein surface profiles among the three studied parasites, we performed a quantitative mass-spectrometry-based proteomic analysis in a membrane-enriched protein preparation.

The data obtained from this approach confirmed that the intracellular environment is indeed able to modulate *T. cruzi*'s protein abundance. In comparison to TcY-WT trypomastigotes, TcY-L1/2^{-/-} and TcY-L2^{-/-} regulated subproteomes only share 13 regulated proteins (four upregulated and nine downregulated—**Figure 4**), which confirms that only one cycle of infection in a different intracellular environment can induce changes in the parasite surface. Additionally, we observed that a considerable percentage of proteins had predicted transmembrane domains or to be classically or non-classically secreted (**Tables 1, 3**). These percentages are similar to previously published data from tissue-culture-derived trypomastigotes and axenic amastigotes cell surface proteomes (Queiroz et al., 2014) and *T. cruzi*'s secretome (Bayer-Santos et al., 2013).

From the comparison between the TcY-L1/2^{-/-} or TcY-L2^{-/-} and the TcY-WT proteome (**Table 2**) and between the TcY-L1/2^{-/-} and the TcY-L2^{-/-} proteome (**Table 4**), several glycosylphosphatidylinositol (GPI)-anchored proteins, such as trans-sialidases, mucins, MASP members, and gp63 proteins, were found regulated. It is very well known in the literature that GPI-anchored proteins widely coat *T. cruzi*'s plasma membrane and are involved in several aspects of host-parasite interactions, such as adhesion to and invasion of host cells, evasion from the host immune system, and pathogenesis (McConville and Ferguson, 1993; Ferguson, 1999; McConville and Menon, 2000; Buscaglia et al., 2006; Gazzinelli and Denkers, 2006). Mucin and trans-sialidase protein families are very relevant to *T. cruzi*'s invasion process (McConville and Menon, 2000). The latter protein family can bind to host cell receptors and transfer sialic-acid residues from host glycoconjugates to the major surface glycoproteins of *T. cruzi*—the mucin family, which has been shown to be important for parasite host cell invasion (Buscaglia et al., 2006). Antibodies raised against synthetic glycopeptides that mimic the parasite mucin glycoproteins remarkably affected *T. cruzi* Y strain metacyclic trypomastigotes invasion in LLC-MK2 cells after incubation (Campo et al., 2014). Another work showed that purified GPI mucins from *T. cruzi* modulated trypomastigote invasion during interaction with LLC-MK2 cells (Soares et al., 2012). A transcriptomic analysis of a virulent (CL Brener) and a non-virulent (CL-14) strain from *T. cruzi* revealed different patterns of expression for the gene families that encode surface proteins such as trans-sialidases, mucins and MASPs (Belew et al., 2017). This comparative analysis indicated that the non-virulent phenotype of the CL-14 strain could be due, in part, to a reduced or delayed expression of genes encoding these surface proteins (Belew et al., 2017). Thus, the fact that these proteins have been shown to be differentially present in TcY-WT, TcY-L1/2^{-/-} and TcY-L2^{-/-}

parasites may correlate with our biological findings, particularly with the invasion rates.

One remarkable difference observed in the protein extract from TcY-L2^{-/-} trypomastigotes was its higher levels of proteolytic activity when compared to TcY-WT and TcY-L1/2^{-/-} trypomastigotes. In fact, the GO analysis showed an enrichment in proteolysis terms for TcY-L2^{-/-} regulated subproteome, when compared to both TcY-WT and TcY-L1/2^{-/-} proteomes. Besides proteasome proteins, three other *T. cruzi* proteases were responsible for this GO enrichment: metallo-peptidase, Clan MF, Family M17, putative (TcYC6_0033380), cytoskeleton-associated protein CAP5.5, putative (TcYC6_0107360) and surface protease GP63, and putative (TcYC6_0169090). The metallo-peptidase, Clan MF, Family M17 belongs to the leucyl aminopeptidase family (EC 3.4.11.1; LAPs) and is a metalloaminopeptidase that catalyzes the removal of N-terminal amino acid residues, preferentially leucine, from proteins and peptides. This peptidase was shown to be expressed in all *T. cruzi* forms and does not present gelatinolytic activity (Cadavid-Restrepo et al., 2011). The cytoskeleton-associated protein CAP5.5 is a calpain-like protein that was first reported in *T. brucei* and presents post-translational modifications, such as myristoylation and palmytoylation, indicating an association to plasma membrane (Hertz-Fowler et al., 2001). In *T. cruzi*, the cytoskeleton-associated protein CAP5.5 was identified in both membrane and myristoylation proteomic studies (Giese et al., 2008; Kulkarni et al., 2009), and it was also present in the secretome of metacyclic trypomastigotes (Bayer-Santos et al., 2013). However, Giese et al. (2008) detected no proteolytic activity in gelatin zymography assays, which was consistent with other calpain-like proteins and suggesting that this protein could have a role in signal transduction (Giese et al., 2008). The surface protease gp63 is a very well-known protease from *T. cruzi* important for host cell infection (Kulkarni et al., 2009) and presents metalloprotease activity (Cuevas et al., 2003). In our gelatin zymography assays, we observed gelatinolytic activity that could be related to the presence of gp63, since the negative bands presented a size between 45 and 66 kDa (Rebello et al., 2019).

Other differences found upon the proteomic analysis were related to specific metabolic pathways. The pathway enrichment analysis also revealed three pathways enriched for TcY-L2^{-/-} trypomastigotes in comparison to the TcY-WT trypomastigotes (**Supplementary Table 3**), one from the down regulated proteins list (ether lipid metabolism) and two from the up regulated proteins list (arginine and proline metabolism and, diterpenoid biosynthesis). The ether lipid synthesis has not been fully studied yet and many related proteins are still to be characterized in *T. cruzi* (Booth and Smith, 2020). The amino acid proline has been demonstrated to be involved in several essential aspects of *T. cruzi*'s life cycle, such as differentiation of epimastigotes into metacyclic trypomastigotes and among intracellular stages, host cell invasion, and survival to thermal and nutritional stress (Tonelli et al., 2004; Martins et al., 2009; Paes et al., 2013). Tonelli et al. (2004) observed that under L-proline supplementation, CHO-K1-infected cell cultures released a higher number of trypomastigotes to the extracellular milieu from the fifth to the ninth day post-infection (Tonelli et al., 2004), although the authors did not measure

the intracellular parasite multiplication. Based on their data, the previous data from our group (Albertti et al., 2010), and the above-mentioned pathway enrichment analysis, we are prone to believe that perhaps trypomastigotes derived from LAMP-2-deficient fibroblasts possess a more active proline metabolism, which, in turn, could also explain their higher multiplication rate previously observed by our group (Albertti et al., 2010). Experimental data are still needed to prove this hypothesis. Additionally, Martins et al. (2009) have observed a recovery of gp82-mediated invasion capacity promoted by L-proline treatment of starved *T. cruzi*'s Y strain metacyclic trypomastigotes after 54 h in starvation media (Martins et al., 2009). The authors also observed that L-proline increased *T. cruzi*'s CL strain parasites' ability to traverse a gastric mucin layer toward target epithelial cells in the stomach mucosa, which is an essential requirement for subsequent cell invasions (Martins et al., 2009).

We also found that the sphingolipid metabolism pathway is enriched in the TcY-L1/2^{-/-} membrane subproteome from the upregulated proteins (**Supplementary Table S3**), therefore, indicating that this pathway was likely enriched in TcY-L1/2^{-/-} trypomastigotes in comparison to the TcY-WT trypomastigotes. We did not find upregulated proteins that would relate directly to the sphingolipid metabolism pathway (Booth and Smith, 2020). However, *T. cruzi* synthesizes the inositolphosphorylceramide as its primary phosphosphingolipid, which is also an attached lipid of GPI anchors (McConville and Ferguson, 1993; Lester and Dickson, 1993; Bertello et al., 1995; Uhrig et al., 1996; Figueiredo et al., 2005). Indeed, the proteins addressed to this pathway by the enrichment analysis, the UDP-Gal or UDP-GlcNAc-dependent glycosyltransferase (TcYC6_0105630) and five trans-sialidase members (TcYC6_0128720, TcYC6_0128910, TcYC6_0129770, TcYC6_0130520, and TcYC6_0131410), would relate better to the GPI-anchor pathway. N-Acetylglucosamine (GlcNAc) is transferred onto the acyl/alkyl-PI by glycosyltransferase complexes, and trans-sialidases are GPI-anchored proteins (Heise et al., 1996; Prevato et al., 2004). Both the glycosylation process and the production of glycosylated proteins are known as important for mediating cellular recognition, host cell adhesion and invasion, and immune evasion by the parasite (Acosta-Serrano et al., 2001; Alves and Colli, 2007; Giorgi and de Lederkremer, 2011). Interestingly, TcY-L1/2^{-/-} trypomastigotes have the highest invasion rates in WT fibroblasts when compared to TcY-WT and TcY-L2^{-/-}.

The present work provides evidence that the intracellular environment can modulate *T. cruzi*'s biological behavior through inducing changes on its surface molecules. The results described here led us to think that this intracellular modulation could be part of *T. cruzi*'s adaptability and ability to infect different cell types. In turn, the surface molecules modulation could contribute to *T. cruzi*'s tropism to host specific tissues and perhaps to immune system evasion as well. Evidence to this hypothesis needs still to be addressed.

DATA AVAILABILITY STATEMENT

The datasets presented in this study can be found in online repositories. The names of the repository/repositories and

accession number(s) can be found below. The mass spectrometry proteomics data have been deposited to the ProteomeXchange Consortium *via* the PRIDE (WHO, 2021) partner repository with the dataset identifier PXD028897.

AUTHOR CONTRIBUTIONS

Conceptualization: LA and HA. Data curation: LA and HA. Formal analysis: AO. Funding acquisition: LA. Investigation: AO, LR, JG, and WB. Methodology: LA, AO, HA, MB, VG, FK, and LR. Project administration: LA. Resources: LA, HA, TB, GM, and FK. Supervision: LA, HA, VG, and FK. Validation: AO. Visualization: AO. Writing—original draft: AO. Writing—review and editing: LA, AO, HA, MB, VG, FK, and LR.

FUNDING

Below are the funding resources for the development of this research: Conselho Nacional de Desenvolvimento Científico e Tecnológico (CNPq) (MCTIC/CNPq No 28/2018—Universal 429635/2018-4) Fundação de Amparo à Pesquisa do Estado de Minas Gerais (FAPEMIG—APQ-02974-17), Coordenação de Aperfeiçoamento de Pessoal de Nível Superior (CAPES / PROEX). None of the fundings received allow for publication fees, the resources being destined only to the acquisition of reagents for the development of the methodological assays.

ACKNOWLEDGMENTS

We are especially grateful to Dr. Paul Saftig and Dr. Renato Mortara for providing the LAMP1/2 and LAMP2 knockout cells that have been used in this work, and the Laboratório de Equipamentos Multiusuários for the use of the Synergy2 and Jamil Silvano de Oliveira from Laboratório de Biologia Estrutural for technical assistance with the ultracentrifuge—Department of Biochemistry and Immunology, ICB/UFMG. We are grateful to the Laboratório de Citometria from the Centro de Laboratórios Multiusuários (CELAM-ICB) and to Daniela Silva dos Reis for technical assistance. We are also grateful to the funding agencies: Conselho Nacional de Desenvolvimento Científico e Tecnológico—CNPq (MCTIC/CNPq No. 28/2018—Universal 429635/2018-4), Fundação de Amparo à Pesquisa do Estado de Minas Gerais (FAPEMIG—APQ-02974-17) and Coordenação de Aperfeiçoamento de Pessoal de Nível Superior (CAPES fellowship).

SUPPLEMENTARY MATERIAL

The Supplementary Material for this article can be found online at: <https://www.frontiersin.org/articles/10.3389/fcimb.2021.788482/full#supplementary-material>

REFERENCES

- Acosta-Serrano, A., Almeida, I. C., Freitas-Junior, L. H., Yoshida, N., and Schenkman, S. (2001). The Mucin-Like Glycoprotein Super-Family of Trypanosoma Cruzi: Structure and Biological Roles. *Mol. Biochem. Parasitol.* 114 (2), 143–150. doi: 10.1016/S0166-6851(01)00245-6
- Albertti, L. A. G., Macedo, A. M., Chiari, E., Andrews, N. W., and Andrade, L. O. (2010). Role of Host Lysosomal Associated Membrane Protein (LAMP) in Trypanosoma Cruzi Invasion and Intracellular Development. *Microbes Infection* 12 (10), 784–789. doi: 10.1016/j.micinf.2010.05.015
- Almagro Armenteros, J. J., Sønderby, C. K., Sønderby, S. K., Nielsen, H., and Winther, O. (2017). DeepLoc: Prediction of Protein Subcellular Localization Using Deep Learning. *Bioinformatics* 33 (21), 3387–3395. doi: 10.1093/bioinformatics/btx431
- Almagro Armenteros, J. J., Tsirigos, K. D., Sønderby, C. K., Petersen, T. N., Winther, O., Brunak, S., et al. (2019). SignalP 5.0 Improves Signal Peptide Predictions Using Deep Neural Networks. *Nat. Biotechnol.* 37 (4), 420–423. doi: 10.1038/s41587-019-0036-z
- Alves, M. J., and Colli, W. (2007). Trypanosoma Cruzi: Adhesion to the Host Cell and Intracellular Survival. *IUBMB Life* 59 (4-5), 274–279. doi: 10.1080/15216540701200084
- Andrade, L., and Andrews, N. (2004). Lysosomal Fusion Is Essential for the Retention of Trypanosoma Cruzi Inside Host Cells. *J. Exp. Med.* 200 (9), 1135–1143. doi: 10.1084/jem.20041408
- Andrade, L., and Andrews, N. (2005). The Trypanosoma Cruzi-Host-Cell Interplay: Location, Invasion, Retention. *Nat. Rev. Microbiol.* 3 (10), 819–823. doi: 10.1038/nrmicro1249
- Andrade, L., Machado, C. R. S., Chiari, E., Pena, S. D. J., and Macedo, A. M. (1999). Differential Tissue Distribution of Diverse Clones of Trypanosoma Cruzi in Infected Mice. *Mol. Biochem. Parasitol.* 100 (2), 163–172. doi: 10.1016/S0166-6851(99)90035-X
- Andrade, L. O., Galvão, L. M., Meirelles M de, N. S., Chiari, E., Pena, S. D., Macedo, A. M., et al. (2010). Differential Tissue Tropism of Trypanosoma Cruzi Strains: An In Vitro Study. *Mem. Inst. Oswaldo Cruz* 105 (6), 834–837. doi: 10.1590/S0074-02762010000600018
- Andrews, N. W., and Colli, W. (1982). Adhesion and Interiorization of Trypanosoma Cruzi in Mammalian Cells. *J. Protozool.* 29 (2), 264–269. doi: 10.1111/j.1550-7408.1982.tb04024.x
- Andrews, N. W., ES, R., and Nussenzweig, V. (1987). Stage-Specific Surface Antigens Expressed During the Morphogenesis of Vertebrate Forms of Trypanosoma Cruzi. *Exp. Parasitol.* 64, 474–484. doi: 10.1016/0014-4894(87)90062-2
- Barrias, E. S., de Carvalho, T. M., and De Souza, W. (2013). Trypanosoma Cruzi: Entry Into Mammalian Host Cells and Parasitophorous Vacuole Formation. *Front. Immunol.* 4, 186. doi: 10.3389/fimmu.2013.00186
- Bayer-Santos, E., Aguilar-Bonavides, C., Rodrigues, S. P., Cordero, E. M., Marques, A. F., Varela-Ramirez, A., et al. (2013). Proteomic Analysis of Trypanosoma Cruzi Secretome: Characterization of Two Populations of Extracellular Vesicles and Soluble Proteins. *J. Proteome Res.* 12 (2), 883–897. doi: 10.1021/pr300947g
- Belew, A. T., Junqueira, C., Rodrigues-Luiz, G. F., Valente, B. M., Oliveira, A. E. R., Polidoro, R. B., et al. (2017). Comparative Transcriptome Profiling of Virulent and Non-Virulent Trypanosoma Cruzi Underlines the Role of Surface Proteins During Infection. *PLoS Pathog.* 13 (12), e1006767. doi: 10.1371/journal.ppat.1006767
- Bendtsen, J. D., Kiemer, L., Fausbøll, A., and Brunak, S. (2005). Non-Classical Protein Secretion in Bacteria. *BMC Microbiol.* 5, 58. doi: 10.1186/1471-2180-5-58
- Bertello, L. E., Gonçalves, M. F., Colli, W., and de Lederkremer, R. M. (1995). Structural Analysis of Inositol Phospholipids From Trypanosoma Cruzi Epimastigote Forms. *Biochem. J.* 310 (Pt 1), 255–261. doi: 10.1042/bj3100255
- Booth, L. A., and Smith, T. K. (2020). Lipid Metabolism in Trypanosoma Cruzi: A Review. *Mol. Biochem. Parasitol.* 240, 111324. doi: 10.1016/j.molbiopara.2020.111324
- Bradford, M. M. (1976). A Rapid and Sensitive Method for the Quantitation of Microgram Quantities of Protein Utilizing the Principle of Protein-Dye Binding. *Anal. Biochem.* 72, 248–254. doi: 10.1016/0003-2697(76)90527-3
- Burleigh, B. A., and Woolsey, A. M. (2002). Cell Signalling and Trypanosoma Cruzi Invasion. *Cell Microbiol.* 4 (11), 701–711. doi: 10.1046/j.1462-5822.2002.00226.x
- Buscaglia, C. A., Campo, V. A., Frasc, A. C. C., and Di Noia, J. M. (2006). Trypanosoma Cruzi Surface Mucins: Host-Dependent Coat Diversity. *Nat. Rev. Microbiol.* 4 (3), 229–236. doi: 10.1038/nrmicro1351
- Cadavid-Restrepo, G., Gastardelo, T. S., Faudry, E., de Almeida, H., Bastos, I. M., Negreiros, R. S., et al. (2011). The Major Leucyl Aminopeptidase of Trypanosoma Cruzi (LAP^{Tc}) Assembles Into a Homohexamer and Belongs to the M17 Family of Metallopeptidases. *BMC Biochem.* 12, 46. doi: 10.1186/1471-2091-12-46
- Callejas-Hernandez, F., Rastrojo, A., Poveda, C., Gironès, N., and Fresno, M. (2018). Genomic Assemblies of Newly Sequenced Trypanosoma Cruzi Strains Reveal New Genomic Expansion and Greater Complexity. *Sci. Rep.* 8 (1), 14631.
- Campo, V. L., Riul, T. B., Carvalho, I., and Baruffi, M.-D. (2014). Antibodies Against Mucin-Based Glycopeptides Affect Trypanosoma Cruzi Cell Invasion and Tumor Cell Viability. *Chembiochem* 15 (10), 1495–1507. doi: 10.1002/cbic.201400069
- Couto, N. F., Pedersane, D., Rezende, L., Dias, P. P., Corbani, T. L., Bentini, L. C., et al. (2017). LAMP-2 Absence Interferes With Plasma Membrane Repair and Decreases T. Cruzi Host Cell Invasion. *PLoS Negl. Trop. Dis.* 11 (6), e0005657.
- Cuevas, I. C., Cazzulo, J. J., and Sanchez, D. O. (2003). Gp63 Homologues in Trypanosoma Cruzi: Surface Antigens With Metalloprotease Activity and a Possible Role in Host Cell Infection. *Infect. Immun.* 71 (10), 5739–5749. doi: 10.1128/IAI.71.10.5739-5749.2003
- de Souza, W., de Carvalho, T. M., and Barrias, E. S. (2010). Review on Trypanosoma Cruzi: Host Cell Interaction. *Int. J. Cell Biol.* 2010, 1–18.
- Deutsch, E. W., Bandeira, N., Sharma, V., Perez-Riverol, Y., Carver, J. J., Kundu, D. J., et al. (2020). The ProteomeXchange Consortium in 2020: Enabling 'Big Data' Approaches in Proteomics. *Nucleic Acids Res.* 48 (D1), D1145–D1152.
- dos Santos, S. L., Freitas, L. M., Lobo, F. P., Rodrigues-Luiz, G. F., Mendes TA de, O., Oliveira, A. C. S., et al. (2012). The MASP Family of Trypanosoma Cruzi: Changes in Gene Expression and Antigenic Profile During the Acute Phase of Experimental Infection. *PLoS Neglected Trop. Dis.* 6 (8), e1779. doi: 10.1371/journal.pntd.0001779
- Eisenhaber, B., Bork, P., and Eisenhaber, F. (1998). Sequence Properties of GPI-Anchored Proteins Near the Omega-Site: Constraints for the Polypeptide Binding Site of the Putative Transamidase. *Protein Eng.* 11 (12), 1155–1161. doi: 10.1093/protein/11.12.1155
- Eisenhaber, B., Bork, P., and Eisenhaber, F. (1999). Prediction of Potential GPI-Modification Sites in Preprotein Sequences. *J. Mol. Biol.* 292 (3), 741–758. doi: 10.1006/jmbi.1999.3069
- Eisenhaber, B., Bork, P., Yuan, Y., Löffler, G., and Eisenhaber, F. (2000). Automated Annotation of GPI Anchor Sites: Case Study C. Elegans. *Trends Biochem. Sci.* 25 (7), 340–341. doi: 10.1016/S0968-0004(00)01601-7
- Eskelinen, E. L. (2006). Roles of LAMP-1 and LAMP-2 in Lysosome Biogenesis and Autophagy. *Mol. Aspects Med.* 27 (5-6), 495–502. doi: 10.1016/j.mam.2006.08.005
- Eskelinen, E. L., Illert, A. L., Tanaka, Y., Schwarzmann, G., Blanz, J., von Figura, K., et al. (2002). Role of LAMP-2 in Lysosome Biogenesis and Autophagy. *Mol. Biol. Cell* 13 (9), 3355–3368. doi: 10.1091/mbc.e02-02-0114
- Eskelinen, E. L., Schmidt, C. K., Neu, S., Willenborg, M., Fuertes, G., Salvador, N., et al. (2004). Disturbed Cholesterol Traffic But Normal Proteolytic Function in LAMP-1/LAMP-2 Double-Deficient Fibroblasts. *Mol. Biol. Cell* 15 (7), 3132–3145. doi: 10.1091/mbc.e04-02-0103
- Ferguson, M. A. (1999). The Structure, Biosynthesis and Functions of Glycosylphosphatidylinositol Anchors, and the Contributions of Trypanosome Research. *J. Cell Sci.* 112 (Pt 17), 2799–2809. doi: 10.1242/jcs.112.17.2799
- Fernandes, M. C., and Andrews, N. W. (2012). Host Cell Invasion by Trypanosoma Cruzi: A Unique Strategy That Promotes Persistence. *FEMS Microbiol. Rev.* 36 (3), 734–747. doi: 10.1111/j.1574-6976.2012.00333.x
- Fernandes, M. C., Cortez, M., Flannery, A. R., Tam, C., Mortara, R. A., and Andrews, N. W. (2011). Trypanosoma Cruzi Subverts the Sphingomyelinase-Mediated Plasma Membrane Repair Pathway for Cell Invasion. *J. Exp. Med.* 208 (5), 909–921. doi: 10.1084/jem.20102518
- Ferri, G., and Edreira, M. M. (2021). All Roads Lead to Cytosol: Trypanosoma Cruzi Multi-Strategic Approach to Invasion. *Front. Cell Infect. Microbiol.* 11, 634793. doi: 10.3389/fcimb.2021.634793

- Figueiredo, J. M., Dias, W. B., Mendonça-Previano, L., Previano, J. O., and Heise, N. (2005). Characterization of the Inositol Phosphorylceramide Synthase Activity From *Trypanosoma Cruzi*. *Biochem. J.* 387 (Pt 2), 519–529. doi: 10.1042/BJ20041842
- Gazzinelli, R. T., and Denkers, E. Y. (2006). Protozoan Encounters With Toll-Like Receptor Signalling Pathways: Implications for Host Parasitism. *Nat. Rev. Immunol.* 6 (12), 895–906. doi: 10.1038/nri1978
- Giese, V., Dallagiovanna, B., Marchini, F. K., Pavoni, D. P., Krieger, M. A., and Goldenberg, S. (2008). *Trypanosoma Cruzi*: A Stage-Specific Calpain-Like Protein Is Induced After Various Kinds of Stress. *Mem. Inst. Oswaldo Cruz* 103 (6), 598–601. doi: 10.1590/S0074-02762008000600015
- Giorgi, M. E., and de Lederkremer, R. M. (2011). Trans-Sialidase and Mucins of *Trypanosoma Cruzi*: An Important Interplay for the Parasite. *Carbohydr. Res.* 346 (12), 1389–1393. doi: 10.1016/j.carres.2011.04.006
- Goncalves, M. F., Umezawa, E. S., Katzin, A. M., de Souza, W., Alves, M. J. M., Zingales, B., et al. (1991). *Trypanosoma Cruzi*: Shedding of Surface Antigens as Membrane Vesicles. *Exp. Parasitol.* 72 (1), 43–53. doi: 10.1016/0014-4894(91)90119-H
- Heise, N., Raper, J., Buxbaum, L. U., Peranovich, T. M. S., and de Almeida, M. L. C. (1996). Identification of Complete Precursors for the Glycosylphosphatidylinositol Protein Anchors of *Trypanosoma Cruzi*. *J. Biol. Chem.* 271 (28), 16877–16887. doi: 10.1074/jbc.271.28.16877
- Hertz-Fowler, C., Ersfeld, K., and Gull, K. (2001). CAP5.5, a Life-Cycle-Regulated, Cytoskeleton-Associated Protein Is a Member of a Novel Family of Calpain-Related Proteins in *Trypanosoma Brucei*. *Mol. Biochem. Parasitol.* 116 (1), 25–34.
- Kornfeld, S., and Mellman, I. (1989). The Biogenesis of Lysosomes. *Annu. Rev. Cell. Biol.* 5, 483–525. doi: 10.1146/annurev.cb.05.110189.002411
- Krogh, A., Larsson, B., von Heijne, G., and Sonnhammer, E. L. (2001). Predicting Transmembrane Protein Topology With a Hidden Markov Model: Application to Complete Genomes. *J. Mol. Biol.* 305 (3), 567–580. doi: 10.1006/jmbi.2000.4315
- Kulkarni, M. M., Olson, C. L., Engman, D. M., and McGwire, B. S. (2009). *Trypanosoma Cruzi* GP63 Proteins Undergo Stage-Specific Differential Posttranslational Modification and Are Important for Host Cell Infection. *Infect. Immun.* 77 (5), 2193–2200. doi: 10.1128/IAI.01542-08
- Leber, T. M., and Balkwill, F. R. (1997). Zymography: A Single-Step Staining Method for Quantitation of Proteolytic Activity on Substrate Gels. *Anal. Biochem.* 249 (1), 24–28. doi: 10.1006/abio.1997.2170
- Lester, R. L., and Dickson, R. C. (1993). Sphingolipids With Inositolphosphate-Containing Head Groups. *Adv. Lipid Res.* 26, 253–274.
- Luo, J., Zhu, Y., Zhu, M. X., and Hu, H. (2011). Cell-Based Calcium Assay for Medium to High Throughput Screening of TRP Channel Functions Using FlexStation 3. *J. Vis. Exp.* 54, 3149. doi: 10.3791/3149
- Macedo, A. M., Machado, C. R., Oliveira, R. P., and Pena, S. D. J. (2004). *Trypanosoma Cruzi*: Genetic Structure of Populations and Relevance of Genetic Variability to the Pathogenesis of Chagas Disease. *Mem. Inst. Oswaldo Cruz* 99 (1), 1–12. doi: 10.1590/S0074-02762004000100001
- Maeda, F. Y., Clemente, T. M., Macedo, S., Cortez, C., and Yoshida, N. (2016). Host Cell Invasion and Oral Infection by *Trypanosoma Cruzi* Strains of Genetic Groups TcI and TcIV From Chagasic Patients. *Parasit. Vectors* 9, 189. doi: 10.1186/s13071-016-1455-z
- Martins, R. M., Covarrubias, C., Rojas, R. G., Silber, A. M., and Yoshida, N. (2009). Use of L-Proline and ATP Production by *Trypanosoma Cruzi* Metacyclic Forms as Requirements for Host Cell Invasion. *Infect. Immun.* 77 (7), 3023–3032. doi: 10.1128/IAI.00138-09
- McConville, M. J., and Ferguson, M. A. (1993). The Structure, Biosynthesis and Function of Glycosylated Phosphatidylinositols in the Parasitic Protozoa and Higher Eukaryotes. *Biochem. J.* 294 (Pt 2), 305–324. doi: 10.1042/bj2940305
- McConville, M. J., and Menon, A. K. (2000). Recent Developments in the Cell Biology and Biochemistry of Glycosylphosphatidylinositol Lipids (Review). *Mol. Membr. Biol.* 17 (1), 1–16. doi: 10.1080/096876800294443
- Oliveira, A. G., Andrade, V. A., Guimarães, E. S., Florentino, R. M., Sousa, P. A., Marques, P. E., et al. (2015). Calcium Signalling From the Type I Inositol 1,4,5-Trisphosphate Receptor Is Required at Early Phase of Liver Regeneration. *Liver Int.* 35 (4), 1162–1171. doi: 10.1111/liv.12587
- Paes, L. S., Suárez Mantilla, B., Zimbres, F. M., Pral, E. M. F., Diogo de Melo, P., Tahara, E. B., et al. (2013). Proline Dehydrogenase Regulates Redox State and Respiratory Metabolism in *Trypanosoma Cruzi*. *PLoS One* 8 (7), e69419. doi: 10.1371/journal.pone.0069419
- Perez-Riverol, Y., Csordas, A., Bai, J., Bernal-Llinares, M., Hewapathirana, S., Kundu, D. J., et al. (2019). The PRIDE Database and Related Tools and Resources in 2019: Improving Support for Quantification Data. *Nucleic Acids Res.* 47 (D1), D442–D450. doi: 10.1093/nar/gky1106
- Pinto, M. C., Cota, B. B., Rodrigues, M. A., Leite, M. F., and de Souza-Fagundes, E. M. (2013). The Cytotoxic and Proapoptotic Activities of Hypnophillin Are Associated With Calcium Signaling in UACC-62 Cells. *J. Biochem. Mol. Toxicol.* 27 (11), 479–485. doi: 10.1002/jbt.21507
- Piras, M. M., Piras, R., and Henriquez, D. (1982). Changes in Morphology and Infectivity of Cell Culture-Derived Trypomastigotes of *Trypanosoma Cruzi*. *Mol. Biochem. Parasitol.* 6, 67–81. doi: 10.1016/0166-6851(82)90066-4
- Piras, R., Piras, M. M., and Henriquez, D. (1983). *Trypanosoma Cruzi*-Fibroblastic Cell Interactions Necessary for Cellular Invasion. *Ciba Found Symp.* 99, 31–51. doi: 10.1002/9780470720806.ch3
- Previano, J. O., Wait, R., Jones, C., DosReis, G. A., Todeschini, A. R., Heise, N., et al. (2004). Glycoinositolphospholipid From *Trypanosoma Cruzi*: Structure, Biosynthesis and Immunobiology. *Adv. Parasitol.* 56, 1–41.
- Queiroz, R. M., Charneau, S., Bastos, I. M. D., Santana, J. M., Sousa, M. V., Roepstorff, P., et al. (2014). Cell Surface Proteome Analysis of Human-Hosted *Trypanosoma Cruzi* Life Stages. *J. Proteome Res.* 13 (8), 3530–3541. doi: 10.1021/pr401120y
- Rebello, K. M., Uehara, L. A., Ennes-Vidal, V., Garcia-Gomes, A. S., Britto, C., Azambuja, P., et al. (2019). Participation of *Trypanosoma Cruzi* Gp63 Molecules on the Interaction With *Rhodnius Prolixus*. *Parasitology* 146 (8), 1075–1082. doi: 10.1017/S0031182019000441
- Romano, P. S., Arboit, M. A., Vázquez, C. L., and Colombo, M. I. (2009). The Autophagic Pathway Is a Key Component in the Lysosomal Dependent Entry of *Trypanosoma Cruzi* Into the Host Cell. *Autophagy* 5 (1), 6–18. doi: 10.4161/auto.5.1.7160
- Schenkman, S., Robbins, E. S., and Nussenzweig, V. (1991). Attachment of *Trypanosoma Cruzi* To Mammalian Cells Requires Parasite Energy, and Invasion can be Independent of the Target Cell Cytoskeleton. *Infect. Immun.* 59, 645–654. doi: 10.1128/iai.59.2.645-654.1991
- Schneede, A., Schmidt, C. K., Hölttä-Vuori, M., Heeren, J., Willenborg, M., Blanz, J., et al. (2011). Role for LAMP-2 in Endosomal Cholesterol Transport. *J. Cell Mol. Med.* 15 (2), 280–295. doi: 10.1111/j.1582-4934.2009.00973.x
- Soares, R. P., Torrecilhas, A. C., Assis, R. R., Rocha, M. N., Moura e Castro, F. A., Freitas, G. F., et al. (2012). Intraspecies Variation in *Trypanosoma Cruzi* GPI-Mucins: Biological Activities and Differential Expression of Alpha-Galactosyl Residues. *Am. J. Trop. Med. Hyg.* 87 (1), 87–96. doi: 10.4269/ajtmh.2012.12-0015
- Sonnhammer, E. L., von Heijne, G., and Krogh, A. (1998). A Hidden Markov Model for Predicting Transmembrane Helices in Protein Sequences. *Proc. Int. Conf. Intell. Syst. Mol. Biol.* 6, 175–182.
- Sunyaev, S. R., Eisenhaber, F., Rodchenkov, I. V., Eisenhaber, B., Tumanyan, V. G., and Kuznetsov, E. N. (1999). PSIC: Profile Extraction From Sequence Alignments With Position-Specific Counts of Independent Observations. *Protein Eng.* 12 (5), 387–394. doi: 10.1093/protein/12.5.387
- Supek, F., Bošnjak, M., Škunca, N., and Šmuc, T. (2011). REVIGO Summarizes and Visualizes Long Lists of Gene Ontology Terms. *PLoS One* 6 (7), e21800. doi: 10.1371/journal.pone.0021800
- Tam, C., Idone, V., Devlin, C., Fernandes, M. C., Flannery, A., He, X., et al. (2010). Exocytosis of Acid Sphingomyelinase by Wounded Cells Promotes Endocytosis and Plasma Membrane Repair. *J. Cell Biol.* 189 (6), 1027–1038. doi: 10.1083/jcb.201003053
- Tanaka, Y., Guhde, G., Suter, A., Eskelinen, E. L., Hartmann, D., Lüllmann-Rauch, R., et al. (2000). Accumulation of Autophagic Vacuoles and Cardiomyopathy in LAMP-2-Deficient Mice. *Nature* 406 (6798), 902–906. doi: 10.1038/35022595
- Tardieux, I., Webster, P., Ravesloot, J., Boron, W., Lunn, J. A., Heuser, J. E., et al. (1992). Lysosome Recruitment and Fusion Are Early Events Required for *Trypanosome* Invasion of Mammalian Cells. *Cell* 71 (7), 1117–1130. doi: 10.1016/S0092-8674(05)80061-3
- Tardieux, I., Nathanson, M. H., and Andrews, N. W. (1994). Role in Host Cell Invasion of *Trypanosoma Cruzi*-Induced Cytosolic-Free Ca²⁺ Transients. *J. Exp. Med.* 179 (3), 1017–1022. doi: 10.1084/jem.179.3.1017
- Tonelli, R. R., Silber, A. M., Almeida-de-Faria, M., Hirata, I. Y., Colli, W., and Alves, M. J. M. (2004). L-Proline Is Essential for the Intracellular Differentiation of *Trypanosoma Cruzi*. *Cell Microbiol.* 6 (8), 733–741. doi: 10.1111/j.1462-5822.2004.00397.x
- Trocoli Torrecilhas, A. C., Tonelli, R. R., Pavanelli, W. R., da Silva, J. S., Schumacher, R. I., de Souza, W., et al. (2009). *Trypanosoma Cruzi*: Parasite

- Shed Vesicles Increase Heart Parasitism and Generate an Intense Inflammatory Response. *Microbes Infect.* 11 (1), 29–39. doi: 10.1016/j.micinf.2008.10.003
- Uhrig, M. L., Couto, A. S., Colli, W., and de Lederkremer, R. M. (1996). Characterization of Inositolphospholipids in *Trypanosoma Cruzi* Trypomastigote Forms. *Biochim. Biophys. Acta* 1300 (3), 233–239. doi: 10.1016/0005-2760(96)00021-5
- WHO. (2021). *Chagas Disease (American Trypanosomiasis)*. Available from: [https://www.who.int/en/news-room/fact-sheets/detail/chagas-disease-\(americantrypanosomiasis\)](https://www.who.int/en/news-room/fact-sheets/detail/chagas-disease-(americantrypanosomiasis))

Conflict of Interest: The authors declare that the research was conducted in the absence of any commercial or financial relationships that could be construed as a potential conflict of interest.

Publisher's Note: All claims expressed in this article are solely those of the authors and do not necessarily represent those of their affiliated organizations, or those of the publisher, the editors and the reviewers. Any product that may be evaluated in this article, or claim that may be made by its manufacturer, is not guaranteed or endorsed by the publisher.

Copyright © 2022 Oliveira, Rezende, Gorshkov, Melo-Braga, Verano-Braga, Fernandes-Braga, Guadalupe, de Menezes, Kjeldsen, de Andrade and Andrade. This is an open-access article distributed under the terms of the Creative Commons Attribution License (CC BY). The use, distribution or reproduction in other forums is permitted, provided the original author(s) and the copyright owner(s) are credited and that the original publication in this journal is cited, in accordance with accepted academic practice. No use, distribution or reproduction is permitted which does not comply with these terms.



TNF-TNFR1 Signaling Enhances the Protection Against *Neospora caninum* Infection

Flávia Batista Ferreira França, Murilo Vieira Silva, Mariana Ferreira Silva, Eliézer Lucas Pires Ramos, Vanessa dos Santos Miranda, Caroline Martins Mota, Fernanda Maria Santiago, José Roberto Mineo and Tiago Wilson Patriarca Mineo *

Laboratory of Immunoparasitology "Dr. Mário Endsfeldz Camargo", Department of Immunology, Institute of Biomedical Sciences, Federal University of Uberlândia, Uberlândia, Brazil

OPEN ACCESS

Edited by:

Natalia de Miguel,
CONICET Instituto Tecnológico de
Chascomús (INTECH), Argentina

Reviewed by:

Valeria Analía Sander,
CONICET Institute of Biotechnological
Research (IIB-INTECH), Argentina
Alexandra Correia,
Universidade do Porto, Portugal

*Correspondence:

Tiago Wilson Patriarca Mineo
tiago.mineo@ufu.br

Specialty section:

This article was submitted to
Parasite and Host,
a section of the journal
Frontiers in Cellular and
Infection Microbiology

Received: 04 October 2021

Accepted: 15 December 2021

Published: 07 January 2022

Citation:

Ferreira França FB, Silva MV,
Silva MF, Ramos ELP, Miranda VdS,
Mota CM, Santiago FM, Mineo JR
and Mineo TWP (2022) TNF-TNFR1
Signaling Enhances the Protection
Against *Neospora caninum* Infection.
Front. Cell. Infect. Microbiol. 11:789398.
doi: 10.3389/fcimb.2021.789398

Neospora caninum is a protozoan associated with abortions in ruminants and neuromuscular disease in dogs. Classically, the immune response against apicomplexan parasites is characterized by the production of proinflammatory cytokines, such as IL-12, IFN- γ and TNF. TNF is mainly produced during the acute phases of the infections and binds to TNF receptor 1 (CD120a, p55, TNFR1) activating a variety of cells, hence playing an important role in the induction of the inflammatory process against diverse pathogens. Thus, in this study, we aimed to evaluate the role of TNF in cellular and humoral immune responses during *N. caninum* infection. For this purpose, we used a mouse model of infection based on wildtype (WT) and genetically deficient C57BL/6 mice in TNFR1 (*Tnfr1*^{-/-}). We observed that *Tnfr1*^{-/-} mice presented higher mortality associated with inflammatory lesions and increased parasite burden in the brain after the infection with *N. caninum* tachyzoites. Moreover, *Tnfr1*^{-/-} mice showed a reduction in nitric oxide (NO) levels *in vivo*. We also observed that *Tnfr1*^{-/-} mice showed enhanced serum concentration of antigen-specific IgG2 subclass, while IgG1 production was significantly reduced compared to WT mice, suggesting that TNFR1 is required for regular IgG subclass production and antigen recognition. Based on our results, we conclude that the TNF-TNFR1 complex is crucial for mediating host resistance during the infection by *N. caninum*.

Keywords: neosporosis, TNF, chronic phase, effector molecules, antibodies

INTRODUCTION

Neosporosis is an infectious disease caused by the parasite *Neospora caninum* which was first described as the causative of neurological disorders in dogs (Bjerkas et al., 1984). Formally classified in 1988, *N. caninum* is an obligatory intracellular parasite that belongs to Apicomplexa phylum (Dubey et al., 1988), a group composed by a range of parasites with great importance in human and veterinary medicine (Cowper et al., 2012). *N. caninum* is closely related to *Toxoplasma gondii*, presenting similar morphological characteristics (Dubey et al., 2007).

N. caninum has been reported to infect varied species of animals, including dogs, cattle, sheep, goat, among others. This infection occurs mainly through ingestion of food and/or water contaminated with oocysts eliminated in feces of canids, which are its definitive hosts (Almeria et al., 2017). Furthermore, the transplacental transmission is also considered an important transmission route, especially in cattle (Marugan-Hernandez, 2017), causing abortions and generating significant economic impacts in dairy and beef production (Dubey and Schares, 2011; Reichel et al., 2014; Mansilla et al., 2015).

The host immune response required to control *N. caninum* infection is based on the production of Th1-skewed inflammatory mediators. Moreover, the efficiency of Th1 adaptive responses against *N. caninum* is linked to the proper activation of innate immune cells, through parasite recognition by pattern recognition receptors (PRRs) such as Toll-Like Receptors (TLRs). Once activated, these receptors will signal through adapter molecules, as MyD88 or TRIF, which leads to production of inflammatory mediators as tumor necrosis factor (TNF) (Fereig and Nishikawa, 2020).

TNF is a cytokine that was originally described due to its antitumor properties (Carswell et al., 1975). Nowadays, it is known to be induced in response to injuries and infections, being produced mainly by macrophages, neutrophils, lymphocytes and other immune cells (Brietzke and Kapczynski, 2008; Davignon et al., 2018). Its function is linked to a variety of biological activities, including inflammation, cellular proliferation, differentiation, apoptosis and necroptosis (Aggarwal et al., 2012). Two distinct types of receptors – TNF receptor 1 (TNFR1) and TNF receptor 2 (TNFR2), may mediate TNF action (Wajant et al., 2003; Wajant and Siegmund, 2019). Its recognition by TNFR1 leads to the majority of its known biological activities, and is initiated by the activation of the transcription factor Nuclear Factor kappa-light-chain-enhancer of activated B cells (NF- κ B) and mitogen-activated protein kinases (MAPK) (Chen and Goeddel, 2002; Wajant and Scheurich, 2011; Brenner et al., 2015).

Previous studies showed that this cytokine plays an important role in infections caused by protozoan parasites as *Toxoplasma*, *Leishmania* and *Trypanosoma* (Derouich-Guergour et al., 2001). For *N. caninum*, however, little is known about its role during the infection. It has been previously shown to reduce/inhibit parasite growth in primary tissue culture that used brain cells (Yamane et al., 2000; Jesus et al., 2013). In that sense, due to the lack of information regarding this key cytokine in the context of the infection, we aimed to evaluate the role of TNF in the regulation of cellular and humoral immune responses against *N. caninum*, using genetically deficient mice in its main receptor - TNF receptor I (TNFR1) - as a model.

MATERIALS AND METHODS

Animals

Wild type C57BL/6 mice (WT, C57BL/6J, JAX 000664) and genetically deficient mice in TNF receptor superfamily member

1a (*Tnfr1*^{-/-}, C57BL/6J-*Tnfrsf1a*^{tm1lhx}/J, JAX 003242, (Peschon et al., 1998), were bred and maintained under specific pathogen-free conditions at the institutional animal facility (REBIR/UFU), in an environment with controlled temperature (22-25°C), food and water *ad libitum* and light/dark cycles of 12h each. For the experiments described below, we used 6-8 weeks old female mice, housed in groups of up to 5 mice/cage. *Tnfr1*^{-/-} mice were chosen due to the primordial role of the receptor in TNF signaling, rendering mice susceptible to other intracellular pathogens, although protecting against septic shock.

Parasites and Antigen Preparation

Tachyzoites of the *N. caninum* isolate 1 (Nc-1) were maintained in monolayers of HeLa cells (CCL-2, ATCC, USA) at 37°C with 5% CO₂ in RPMI 1640 medium supplemented with glutamine (2mM) and antibiotics/antimycotics (Thermo Scientific, USA). After cell lysis, the parasite suspensions were obtained as described previously (Davoli-Ferreira et al., 2016). The supernatant containing the parasite suspension was collected and centrifuged at 800 × g for 10 minutes at 4°C, and the pellet was resuspended in RPMI 1640. Tachyzoites were counted in a Neubauer chamber and used immediately for infection of mice or macrophages. The remainder of the parasites were washed twice (800 × g for 10 minutes at 4°C) with PBS and the final pellet was stored at -20°C for subsequent preparation of antigens.

N. caninum antigen lysate (NLA) was prepared according to the methods described previously (Mota et al., 2016). Parasite suspensions were diluted in PBS and treated with protease inhibitors (Complete Mini, Roche, Germany) and submitted to rapid freezing and thawing cycles, followed by sonication on ice. Parasite lysates were centrifuged (10,000×g, 30 min, 4°C), the resulting supernatant was collected and the protein concentration quantified using the Bradford method (Bradford, 1976). NLA aliquots were stored at -20°C until its use in ELISA procedures.

Experimental Infections

Groups of WT and *Tnfr1*^{-/-} mice (*n* = 10/group) were infected intraperitoneally (i.p.) with 1×10⁷ *N. caninum* tachyzoites for survival assays. For the analysis of acute and chronic phases of the infection, WT and *Tnfr1*^{-/-} mice (*n* = 5/group) were infected with 1×10⁶ tachyzoites. All experiments were performed at least twice, in an independent manner, for confirmation purposes, and all sampled mice were analyzed individually. The acute phase experiments (7 days post-infection, dpi) were analyzed by the quantification of cytokines, parasite burden, histological alterations and nitric oxide production. During the chronic phase of the infection (30 dpi), parasite burden and histological changes were analyzed solely in brain tissues. For the quantification of specific IgG antibodies produced during the infection, serum of WT and *Tnfr1*^{-/-} mice were collected at 0, 7, 14, 21 and 28 dpi.

Determination of Parasite Burden

The parasite burden was determined in WT and *Tnfr1*^{-/-} mice infected with 1 × 10⁶ tachyzoites. With that intent, tissue fragments

and peritoneal cells were submitted to a real-time quantitative polymerase chain reaction (qPCR) using SYBR green detection system (Promega Co, USA), as previously described (Ribeiro et al., 2009), using primer pairs designed for the Nc5 sequence of *N. caninum*: Forward: 5'-GCTGAACACCGTATGTCGTAAA-3'; Reverse: 5'-AGAGGAATGCCACATAGAAGC- 3'. Genomic DNA was extracted from 20 mg of each analyzed tissue, or 1×10^6 of peritoneal cells, using a commercial kit (Genomic DNA Kit, Promega), according to the manufacturer's instructions. DNA concentrations were quantified by spectrophotometer (260/280 ratio; Nanodrop Lite, Thermo Scientific) and adjusted to 40 ng/ μ L with sterile DNase free water. The reaction to determine parasite loads was performed in a Real-time PCR thermal cycler (StepOne Plus, Thermo Scientific, USA) and parasite counts were calculated by interpolation from a standard curve with known amounts of DNA extracted from *N. caninum* tachyzoites that were included in each analysis.

Histological Analysis

Samples of livers, lungs, and brains of WT and *Tnfr1*^{-/-} mice were collected and fixed in 10% buffered formalin at room temperature for 24 hours, and storage in alcohol 70% until the paraffin inclusion process. After inclusion, the organs were sliced (5 μ m thick) and deposited on microscopic slides, subsequently stained with hematoxylin and eosin for evaluation of inflammatory infiltrates and tissue damage (Mineo et al., 2009). The sections were photographed using an automated microscope (FSX100, Olympus, Japan).

Cytokine Quantification

The production of the cytokines IL-12p40 and IFN- γ were measured in peritoneal fluids, sera, as well as liver and lung homogenates, using commercial ELISA kits, according to the protocols recommended by the manufacturer (BD Biosciences, USA). Tissue homogenates were prepared by grinding (IKA, Germany) 100 mg of freshly collected tissue in PBS supplemented with protease inhibitor cocktail (Complete Mini, Roche), followed by a centrifugation for supernatant removal and storage at -80°C until use (along with serum and peritoneal fluid samples). Optical density (OD) was read at 450 nm in a plate reader (M2e SpectraMax, Molecular Devices, USA). The concentration of each cytokine was determined by a standard curve with known concentrations of the cytokines expressed in pg/mL. Detection limits: IFN- γ = 4.1 pg/mL and IL-12p40 = 15.16 pg/mL. In addition, IFN- γ levels were also measured in serum samples using Cytometric Bead Array (CBA, BD Biosciences), read in a flow cytometer (FACSCanto II, BD Biosciences). IFN- γ CBA Detection limit: 0.5 pg/mL. IL-12 concentrations were measured in serum samples by ELISA method, as previously described.

Quantification of Nitric Oxide

Nitric oxide (NO) production in peritoneal fluids of WT and *Tnfr1*^{-/-} mice infected by *N. caninum* was determined through

the reduction of nitrate and measurement of nitrite concentration by a commercial kit, according to the manufacturer's instructions (R&D Systems Inc., USA). The assay was read at 540 nm (wavelength correction at 690 nm), and the concentration was estimated by a standard curve with lower detection limit at 0.78 μ mol/L.

Quantification of Specific IgG Antibodies

Serum levels of antigen specific IgG and its subclasses (IgG1 and IgG2) were measured in individual serum samples of infected WT and *Tnfr1*^{-/-} mice by ELISA, as previously described (Mineo et al., 2010). Briefly, high-affinity microplates (Corning-Costar, USA) were coated with NLA (10 μ g/mL) and incubated for 18 hours at 4°C. The reaction was blocked with 5% skim milk for total IgG and 1% bovine serum albumin (BSA) for IgG1 and IgG2a. Serum samples were diluted 1:25 and incubated for 1h (total IgG) and 2h (IgG1 and IgG2a) at 37°C. Peroxidase-labeled goat anti-mouse IgG (1:1000; Sigma-Aldrich Cat# A3673) or biotin-labeled goat anti-mouse IgG1 (1:4000; Caltag Lab/Invitrogen Cat# M32115) and anti-mouse IgG2a (1:2000; Caltag Lab/Invitrogen Cat # M32315) antibodies were added and incubated for 1h at 37°C. For detection of IgG1 and IgG2a, plates were further incubated with streptavidin-peroxidase (1:1000; Sigma-Aldrich), for 30 minutes at room temperature. Between each step, plates were washed with PBS plus 0.05% Tween 20 (PBS-T). The reaction was developed with 2,2-azino-bis-3-ethyl-benzthiazoline sulfonic acid (ABTS; KPL, USA) and the optical density (OD) determined at 405 nm in a plate reader (M2e SpectraMax, Molecular Devices).

For the immunoblots, we followed a previously published protocol (Ribeiro et al., 2009). Briefly, after NLA was submitted to electrophoresis in a 12% polyacrylamide gel under non-reducing conditions and transferred to nitrocellulose membranes, the reaction was blocked with 5% skim milk in PBS-T, incubated with individual mouse sera from each group, diluted 1:50, and then with peroxidase-goat anti-mouse IgG (diluted 1:1000) or biotin-labeled goat anti-mouse IgG1 (1:4000) and anti-mouse IgG2a (1:2000) antibodies. For the subclasses, an additional step with streptavidin-peroxidase (1:1000) was performed before the reaction was developed by adding 0.03% H₂O² and 3,3'-diaminobenzidine tetrahydrochloride (DAB; Sigma). The apparent molecular masses of antigenic bands were determined in relation to a standard molecular weight curve.

Statistical Analysis

Statistical analyses were carried out using GraphPad Prism 9 software (GraphPad Software Inc., USA). Differences between groups were analyzed using Two-way ANOVA, with the respective Bonferroni post-tests, T-test, and Mann Whitney test, when appropriated. Survival rates were compared using Kaplan-Meier survival analysis, through a log-rank Mantel-Cox test. Values for $p < 0.05$ were considered significant.

RESULTS

TNFR1 Contributes to Mice Survival During *N. caninum* Infection

To evaluate the importance of receptor 1 of TNF in the resistance of mice during the infection by *N. caninum*, WT and *Tnfr1*^{-/-} mice were infected with a lethal dose of *N. caninum* for 50% of the animals (DL50, 1x10⁷ tachyzoites), and were monitored for 30 days for survival (Figure 1). We observed that mice of both experimental groups presented clinical signs around a week after the infection. However, *Tnfr1*^{-/-} mice were less resistant to the infectious dose compared to WT, since 100% of the animals in this group had to be euthanized until the 20th day of infection, while – as expected – 50% of the WT mice survived ($P < 0.05$).

TNFR1 Affects Cerebral Parasite Load and Inflammation

In order to evaluate whether the parasite burden profile was altered in the absence of TNFR1, we determined the amount of parasite genomic DNA in tissues of both groups infected with a sublethal dose of *N. caninum* tachyzoites (1x10⁶ parasites/mice). No significant difference was observed in parasite burden of peritoneal cells (Figure 2A), lungs (Figure 2B) and livers (Figure 2C) of *Tnfr1*^{-/-} mice in relation to WT controls during the acute phase (7 days after infection). On the other hand, during the chronic phase (30 days after infection), quantification of the parasite burden in the brain showed increased quantities of *N. caninum* genomic DNA in *Tnfr1*^{-/-} mice, if compared to the WT counterparts ($P < 0.05$, Figure 2D).

We next analyzed whether TNF receptor 1 had a role in tissue inflammation during the infection with *N. caninum*.

Inflammatory infiltrates were observed in all tissue sections obtained from both groups of mice (WT and *Tnfr1*^{-/-}). No clear differences were noted in liver and lung samples of both groups analyzed during the acute phase of infection (7 dpi). While sparse inflammatory foci were observed in liver sections (Figure 3A), a cellular infiltration in the pulmonary septum led to a marked loss of alveolar spaces in the lungs of both groups (Figure 3B). On the other hand, the absence of TNFR1 lead to an extensive inflammation in the brains of infected mice, with focal and diffuse infiltration of mononuclear cells throughout the parenchyma after 30 days of infection (Figure 3C), clearly compromising tissue integrity.

NO Production Is Mediated by TNFR1 in Response to *N. caninum* Infection

Based on the previous observations, we then went on to analyze whether the presence of TNF receptor 1 would modulate the production of key immune mediators. *In vivo*, we found an intriguing increment of IL-12 and IFN- γ levels in bodily fluids and lung homogenates of *Tnfr1*^{-/-} mice during the first week of infection. IL-12p40 levels were significantly higher in the peritoneal exudates and serum samples of *Tnfr1*^{-/-} mice compared to WT controls seven days post-infection ($P < 0.05$, Figure 4A). In the same manner, IFN- γ production was also upregulated in the peritoneal fluid, serum and lung homogenates of *Tnfr1*^{-/-} mice at the same time point ($P < 0.05$, Figure 4B). No differences in the concentration of IL-12 and IFN- γ were detected in liver homogenates of both mouse lines, even between naïve and infected mice, which denotes a probable non-specific detection of the cytokines in that tissue. In order to explain these apparently contradictory results, we sought to determine

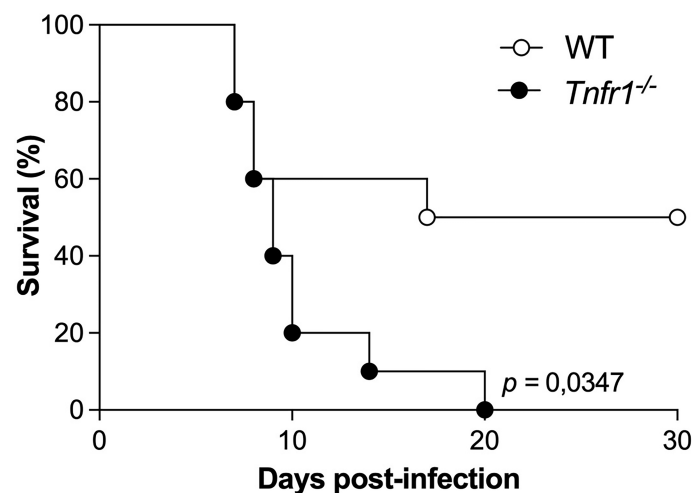


FIGURE 1 | TNF is crucial for the survival of mice against *Neospora caninum*. Groups of WT and *Tnfr1*^{-/-} mice were infected with 1x10⁷ Nc-1 tachyzoites and survival was observed for 30 days. Differences between groups were compared using Kaplan Meier survival analysis, through the log-rank (Mantel-Cox) test. Statistically significant differences ($p < 0.05$). Two independent experiments were performed with similar results, and the graphs represent the biological replicates ($n = 10$ mice/group) of one of those individual experiments.

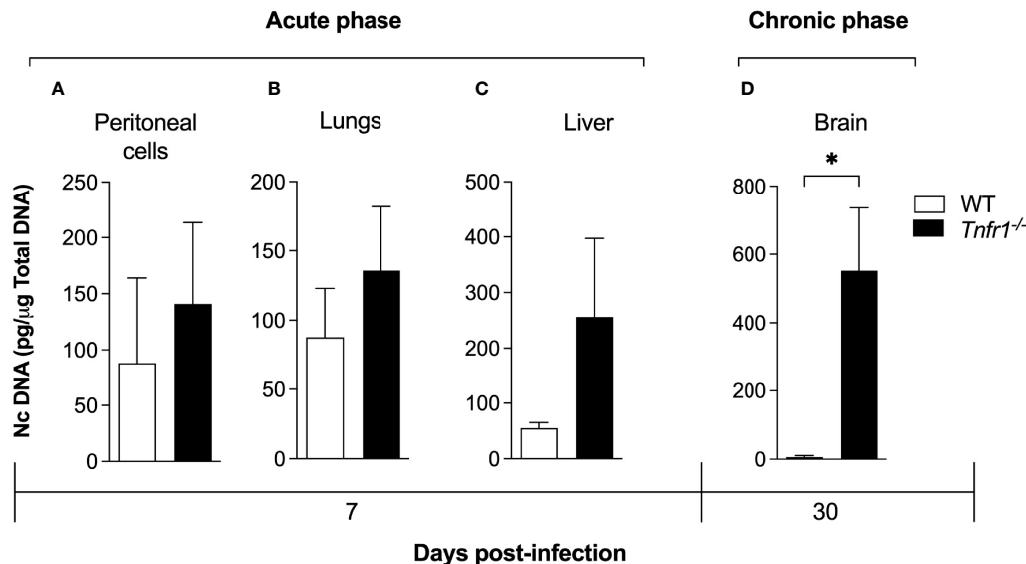


FIGURE 2 | TNF is required to control the parasite burden during the chronic phase of infection. WT and *Tnfr1*^{-/-} mice (n = 5 mice/group) infected with 1×10⁶ Nc-1 tachyzoites were evaluated for parasite burden by qPCR. Peritoneal exudates (A), lungs (B), liver (C) and brains (D) were evaluated for the number of copies of the genomic sequence NC5. Two independent experiments were performed with similar results, and the graphs represent the biological replicates (n = 5 mice/group) of one of those individual experiments. Results are expressed as mean ± standard error of the mean (SEM). Data were analyzed using the Mann Whitney test.

*Statistically significant differences (p < 0.05).

whether the absence of TNF receptor 1 would impact the production of effector molecules known to be crucial for parasite killing. We analyzed the production of nitric oxide (NO) in the peritoneal fluids of WT and genetically deficient mice. Interestingly, the concentration of NO was significantly reduced in *Tnfr1*^{-/-} mice if compared to WT controls ($P < 0.05$, **Figure 4C**), suggesting that signaling through TNFR1 is necessary to induce the production of proper amounts of effector molecules in response to *N. caninum*.

TNFR1 Alters the Balance of IgG Subclasses Raised Against *N. caninum*

We also aimed to elucidate the role of TNFR1 in the specific humoral immune response generated against *N. caninum*. With that intent, the concentration of *Neospora*-specific IgG and subclasses (IgG1 and IgG2) produced were measured weekly in the sera of infected WT and *Tnfr1*^{-/-} mice against *N. caninum* soluble antigens. While no statistical differences were observed in the production of antigen-specific total IgG during the infection (**Figure 5A**), *Tnfr1*^{-/-} mice produced significantly less antigen specific-IgG1 ($P < 0.05$, **Figure 5B**) and higher concentration of IgG2 ($P < 0.05$, **Figure 5C**) when compared to WT mice.

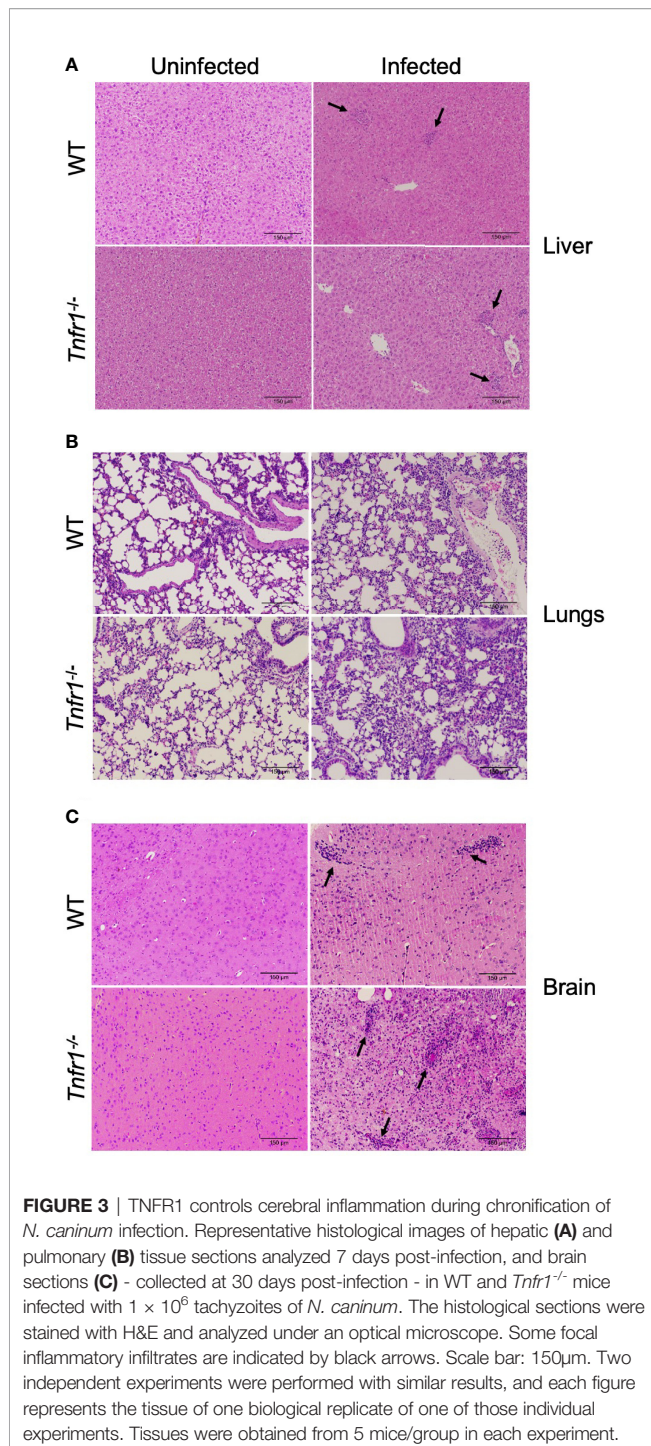
With the intention of verifying if antigen recognition was also altered by the absence of TNFR1, we ran western blots of the parasite's soluble antigens against sera obtained from infected mice and checked for IgG reactivity. As expected, total IgG from WT mice recognized increasing numbers of parasite antigens as the infection progressed (**Figure 6A**), and this

could also be observed for IgG1 and (**Figure 6B**) IgG2a (**Figure 6C**) subclasses. That same phenotype was not observed in *Tnfr1*^{-/-} mice, which did not sustain a continuous increment in recognition of the soluble antigens by total IgG (**Figure 6A**). This was probably due to the failure of specific-IgG1 production and recognition of the antigens (**Figure 6B**), as IgG2 seemed to sustain a minimal recognition pattern of the antigens throughout the observed period, although recognizing less antigens at the latest time point (**Figure 6C**).

DISCUSSION

Neospora caninum has been associated with abortions in cattle and neuromuscular diseases in dogs, with a significant economic impact in countries that produce meat and dairy products (Reichel et al., 2014). Thus, to elucidate functions of immune modulators/activators is crucial for the development of prophylactic and therapeutic measures against neosporosis (Hemphill et al., 2016).

TNFR1 is the main receptor of TNF cytokine and is associated with the regulation of the inflammatory response, prevention of tissue damage, once it regulates the action of antigen presenting cells, and maintenance of tissue homeostasis (Zakharova and Ziegler, 2005; Hao et al., 2012; Wajant and Siegmund, 2019). Given the relevance of other pro-inflammatory cytokines in the immune response against *N. caninum*, we investigated here the role of TNF pathway in this infection.



The importance of TNF in the resistance against other intracellular protozoa is well described (El-Sayed et al., 2016). For the closely related *T. gondii*, *Tnfr1/r2*^{-/-} and *Tnfr1*^{-/-} mice were highly susceptible to the infection, whereas *Tnfr2*^{-/-} animals are resistant (Deckert-Schluter et al., 1998; Yap et al., 1998). In our study, infected *Tnfr1*^{-/-} mice presented 100% of mortality during the course of infection, with high parasite burden and

intense inflammatory infiltrates in the brain (30 d.p.i), indicating that this pathway contributes to host protection during infection latency. Also in agreement with what was found for *T. gondii*, previous studies demonstrated that *Tnfr2*^{-/-} mice were resistant during the acute phase of infection by *N. caninum*, although mortality was described later on, during the chronic phase of infection (Ritter et al., 2002). The authors also described similar cerebral tissue damage amongst the groups, which is a clear difference from our results. In corroboration, the absence of intact TNF signaling did not alter the phenotype induced by the acute phase of the infection, with similar parasite burden and inflammatory status of livers and lungs of both groups of mice. Similar observations were previously recorded for lungs and brains of mice genetically deficient in the cytokine itself (*Tnf*^{-/-}) during the acute phase of the infection - no significant differences in parasite burden if compared to WT mice (Correia et al., 2015).

Cytokines as IL-12 and IFN- γ are important for the control of intracellular parasite replication and host resistance during the acute phase of the infection against *N. caninum* (Khan et al., 1997). As observed in this study, the absence of TNFR1 did not impair the production of these key cytokines. In fact, these cytokines were not only produced but also upregulated during the infection in peritoneum, serum, and lungs, probably in a compensatory mechanism related to the lack of effector molecules, as NO. TNF is a key component for the induction of these cellular effectors, due to the activation of STAT1 and NF- κ B, in a positive feedback loop (Ohmori et al., 1997; Blaser et al., 2016). Also, the synergy and mutual dependence between TNF and IFN- γ to induce those crucial factors has also been intensively demonstrated (Nacy et al., 1991; Liew, 1993; Schäffer et al., 2006; Karki et al., 2021). In an infection model with *Citrobacter rodentium*, severe tissue damage and increased expression of IL-12p40 and IFN- γ in *Tnfr1*^{-/-} mice was also observed (Gonçalves et al., 2001). On the other hand, WT and *Tnfr1*^{-/-} mice showed similar production of IFN- γ during *T. gondii* infection, although *Tnfr1*^{-/-} mice were highly susceptible to the infection (Deckert-Schluter et al., 1998). Partial IFN- γ signaling due to the lack of receptor 1 (IFN- γ R1) had in TNF a compensatory mechanism to induce killing of *T. gondii*, while the same strategy would not be sufficient to kill *Salmonella typhimurium* (Janssen et al., 2002). In that sense, in a scenario where one of these key cytokines is missing, it's likely that the lack of effector molecules will prompt parasite growth, and the increment in antigen availability will attract more inflammatory cells, in a recurrent phenomena that may lead the animals to death.

As speculated above, we wondered if TNF controlled *N. caninum* replication through the induction of effector molecules in the tested system. Previous work by our group demonstrated that nitric oxide is a key molecule for direct control of *N. caninum*, since deficient mice in iNOS presented uncontrolled parasite replication and extensive inflammatory lesions (Barros et al., 2019). Thus, as expected, the production of NO in *Tnfr1*^{-/-} mice during *N. caninum* infection was diminished, indicating that both pathways are linked. Some

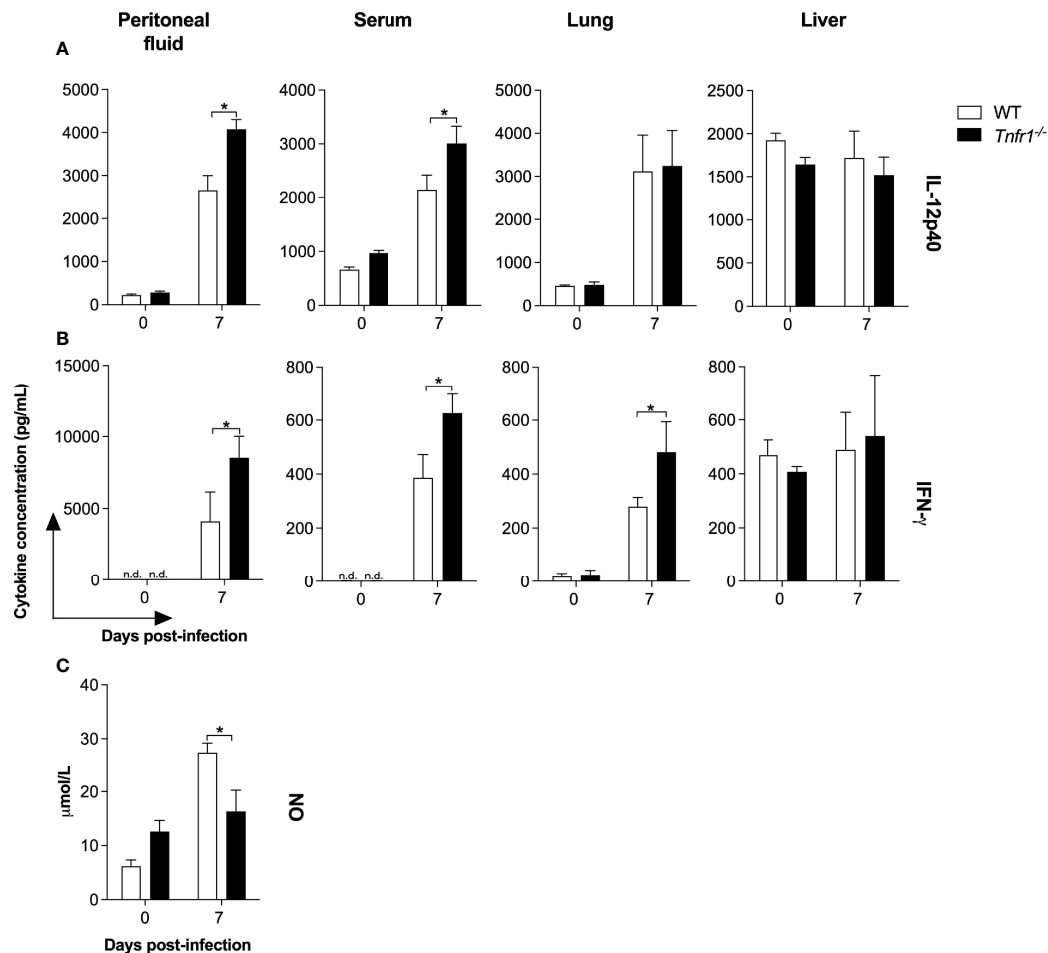


FIGURE 4 | While TNFR1 does not downmodulate the production of key Th1 cytokines during the infection, it is essential for the production of proper levels of nitric oxide (NO). Groups of WT and *Tnfr1*^{-/-} mice were evaluated for IL-12p40 (A) and IFN-γ (B) production 7 days after the infection with 1×10^6 Nc-1 tachyzoites in the peritoneal fluids, serum samples, lung and liver homogenates. NO concentration was evaluated 7 days after infection in peritoneal fluids (C). Values are expressed as mean \pm standard error of the mean (SEM). Data were analyzed using the Two-way ANOVA test, followed by Bonferroni post-test. Differences were considered statistically significant (*) when $p < 0.05$. For the *in vivo* assays, two independent experiments were performed with similar results, and the graphs represent the biological replicates ($n = 5$ mice/group) of one of those individual experiments.

studies also showed more susceptibility to *T. gondii* infection in *Tnfr1*^{-/-} or *Tnfr1*^{-/-} mice due to the absence of NO, which contributed to an increased parasite burden (Gazzinelli et al., 1993; Deckert-Schluter et al., 1998; Schluter et al., 2003). It is important to note that a study with murine microglial cells infected with *T. gondii* showed that TNF and NO production are crucial to control the infection even in the absence of IL-12 and IFN-γ (Pimenta et al., 2018).

The cytokine milieu induced by activated cells contribute to isotype changes of antibodies, where the profile of antibodies produced is directly related to the immune response triggered by the pathogen (Innes, 2007). Indeed, in *N. caninum* infection, the production of specific immunoglobulin is important to inhibit the invasion of tachyzoites in host cells and to control parasite replication (Aguado-Martinez et al., 2017). Our study showed

that the absence of TNFR1 stimulated an exacerbated Th1 response, followed by a humoral response skewed towards IgG2a-specific antibodies. IFN-γ is a hallmark of Th1-type cellular responses against *N. caninum* (Mineo et al., 2010) and plays an important role in IgG class switch with predominant IgG2a isotype, inhibiting the expression of the other subclasses (Snapper and Paul, 1987; Long et al., 1998; Rojo-Montejo et al., 2009), specially IgG1 – an IgG subclass biased towards the Th2 phenotype (Stevens et al., 1988). IL-12 is a key cytokine in that context, committing CD4+ T cells to the Th1 phenotype (Germann et al., 1993). Overall, antigen specific IgG1 antibodies were not only less concentrated in the serum of *Tnfr1*^{-/-} mice, but also did not recognize the major antigenic bands present in parasite's soluble extract, denoting a probable loss of function that should be properly investigated. Also,

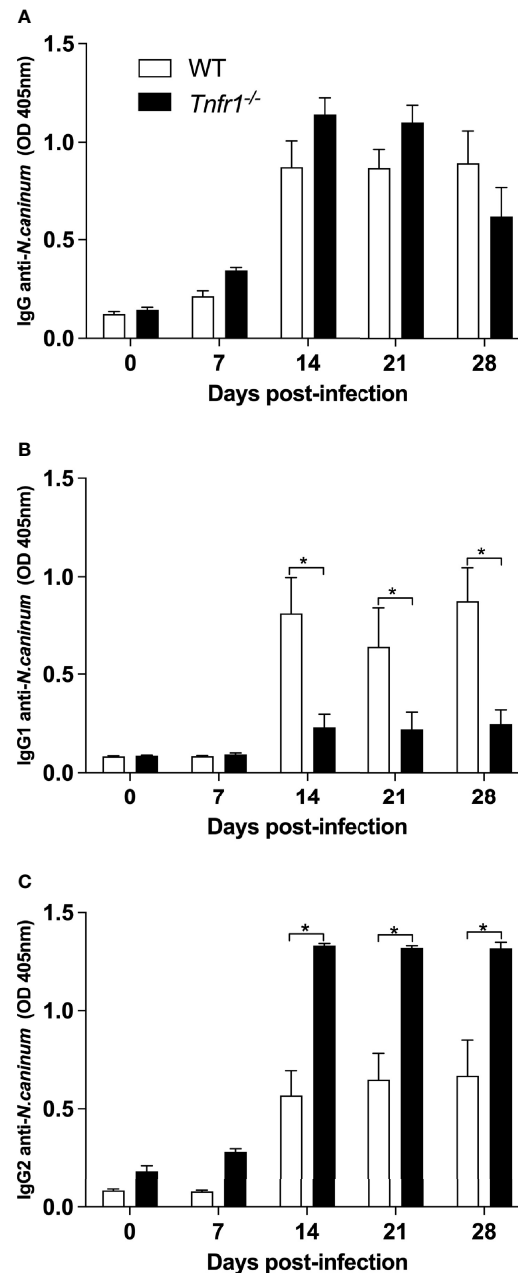


FIGURE 5 | TNFR1 controls the production of IgG subclasses against soluble antigens. WT and *Tnfr1*^{-/-} mice were infected intraperitoneally with 1×10^6 Nc-1 tachyzoites and sampled weekly for serum samples until 28 days of infection. Levels of IgG **(A)**, IgG1 **(B)** and IgG2a **(C)** were determined by ELISA and values are indicated as optical density (OD) at 405nm, being expressed as mean \pm standard error of the mean (SEM). Data were analyzed using the Two-way ANOVA test followed by Bonferroni post-test. Differences were considered statistically significant (*) when $p < 0.05$. Two independent experiments were performed with similar results, and the graphs represent the biological replicates ($n = 5$ mice/group) of one of those individual experiments.

detection of antigen-specific total IgG showed signs of early decay in *Tnfr1*^{-/-} mice by ELISA and WB. Although we are not able to point out the specific reason for the phenomenon, it is probably related to the fundamental role of TNF signaling in B cell biology and its proper responses to antigens (Figgett et al., 2014).

Taken together, our results indicated that TNF - TNF receptor 1 signaling is crucial for an appropriated response against *N. caninum* infection, especially during chronification of the infection in the central nervous system. Since this pathway was shown to regulate the concentration of effector molecules and antibodies during the infection, future projects could

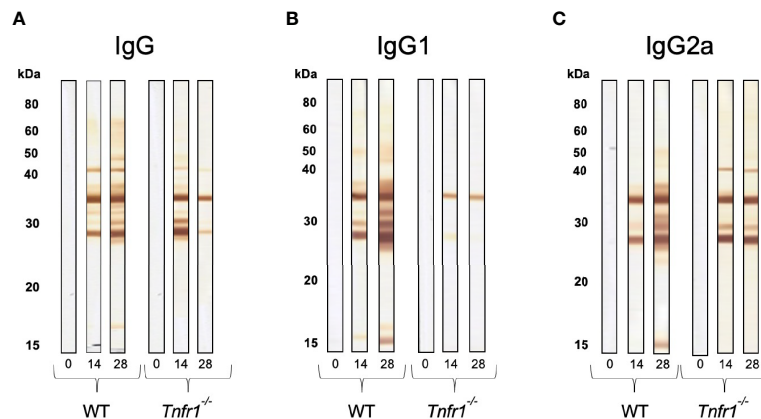


FIGURE 6 | Immunoblots show the lack of proper antigen recognition in the absence of TNFR1. Individual serum samples of WT and *Tnfr1*^{-/-} mice, obtained at 0, 14 and 28 days after the infection by *Neospora caninum*, were submitted to immunoblots for the determination of the pattern of recognition by specific IgG (A), IgG1 (B) and IgG2a (C) antibodies against the parasite's soluble antigen. We have displayed immunoblots that are representative of the reactivity obtained by an individual mouse/group/antibody, and that had similar results in two independent experiments with 5 mice/group each.

evaluate the use of TNF as an immune modulator, aiming to reduce tissue inflammation and cerebral parasite burden in models of clinical neosporosis.

DATA AVAILABILITY STATEMENT

The original contributions presented in the study are included in the article/supplementary material. Further inquiries can be directed to the corresponding author.

ETHICS STATEMENT

All experiments were previously approved by the ethics committee in animal experimentation (Comite de Ética na Utilização de Animais da Universidade Federal de Uberlândia - CEUA/UFU) under protocol 109/16. All procedures were carried out in accordance with the recommendations in the International Guiding Principles for Biomedical Research Involving Animals (https://olaw.nih.gov/sites/default/files/Guiding_Principles_2012.pdf), of the International Council for Laboratory Animal Science (ICLAS), countersigned by the Conselho Nacional de Controle de Experimentação Animal (CONCEA; Brazilian National Consul for the Control of Animal Experimentation). The institutional animal facility (Rede de Biotérios de Roedores—REBIR/UFU) is accredited by the National's Commissions in Animal Experimentation

(CONCEA, CIAEP:01.0105.2014) and Biosecurity (CTNBio, CQB 163/02).

AUTHOR CONTRIBUTIONS

Designed experiments, FF, FS, JM, and TM. Performed the experiments, FF, MVS, MFS, ER, VM, CM, and FS. Analyzed data and wrote the paper, FF and TM. Supplied reagents, JM and TM. All authors contributed to the article and approved the submitted version.

FUNDING

This work was supported by Brazilian funding agencies (CNPq - 313761/2020-5; FAPEMIG - CVZ-PPM-00547-17, CVZ-APQ-01313-14, RED-00313-16; CAPES-PrInt - AUXPE 2694/2018 - 88881.311510/2018-01). Funding sources had no involvement in study design, collection, analysis and interpretation of data, in writing the manuscript or in the decision to submit it for publication.

ACKNOWLEDGMENTS

The authors thanks Ana Cláudia Arantes Marquez Pajuaba, Marley Dantas Barbosa and Zilda Mendonça da Silva Rodrigues for their technical assistance.

REFERENCES

- Aggarwal, B. B., Gupta, S. C., and Kim, J. H. (2012). Historical Perspectives on Tumor Necrosis Factor and its Superfamily: 25 Years Later, A Golden Journey. *Blood* 119, 651–665. doi: 10.1182/blood-2011-04-325225
- Aguado-Martinez, A., Basto, A. P., Leita, A., and Hemphill, A. (2017). *Neospora Caninum* in Non-Pregnant and Pregnant Mouse Models: Cross-Talk Between Infection and Immunity. *Int. J. Parasitol.* 47, 723–735. doi: 10.1016/j.ijpara.2017.09.001
- Almeria, S., Serrano-Perez, B., and Lopez-Gatius, F. (2017). Immune Response in Bovine Neosporosis: Protection or Contribution to the Pathogenesis of Abortion. *Microb. Pathog.* 109, 177–182. doi: 10.1016/j.micpath.2017.05.042
- Barros, P. D. S. C., Mota, C. M., dos Santos Miranda, V., Ferreira, F. B., Ramos, E. L. P., Santana, S. S., et al. (2019). Inducible Nitric Oxide Synthase Is Required for Parasite Restriction and Inflammatory Modulation During *Neospora Caninum* Infection. *Vet. Parasitol.* 276, 108990. doi: 10.1016/j.vetpar.2019.108990

- Bjerkas, I., Mohn, S. F., and Presthus, J. (1984). Unidentified Cyst-Forming Sporozoan Causing Encephalomyelitis and Myositis in Dogs. *Z. Parasitenkd.* 70, 271–274. doi: 10.1007/BF00942230
- Blaser, H., Dostert, C., Mak, T. W., and Brenner, D. (2016). TNF and ROS Crosstalk in Inflammation. *Trends Cell Biol.* 26, 249–261. doi: 10.1016/j.tcb.2015.12.002
- Bradford, M. M. (1976). A Rapid and Sensitive Method for the Quantitation of Microgram Quantities of Protein Utilizing the Principle of Protein-Dye Binding. *Anal. Biochem.* 72, 248–254. doi: 10.1016/0003-2697(76)90527-3
- Brenner, D., Blaser, H., and Mak, T. W. (2015). Regulation of Tumour Necrosis Factor Signalling: Live or Let Die. *Nat. Rev. Immunol.* 15, 362–374. doi: 10.1038/nri3834
- Brietzke, E., and Kapczinski, F. (2008). TNF-Alpha as a Molecular Target in Bipolar Disorder. *Prog. Neuropsychopharmacol. Biol. Psychiatry* 32, 1355–1361. doi: 10.1016/j.pnpbp.2008.01.006
- Carswell, E. A., Old, L. J., Kassel, R. L., Green, S., Fiore, N., and Williamson, B. (1975). An Endotoxin-Induced Serum Factor That Causes Necrosis of Tumors. *Proc. Natl. Acad. Sci. U. S. A.* 72, 3666–3670. doi: 10.1073/pnas.72.9.3666
- Chen, G., and Goeddel, D. V. (2002). TNF-R1 Signaling: A Beautiful Pathway. *Science* 296, 1634–1635. doi: 10.1126/science.1071924
- Correia, A., Ferreirinha, P., Botelho, S., Belinha, A., Leitão, C., Caramalho, Í., et al. (2015). Predominant Role of Interferon- γ in the Host Protective Effect of CD8⁺ T Cells Against *Neospora Caninum* Infection. *Sci. Rep.* 5, 14913. doi: 10.1038/srep14913
- Cowper, B., Matthews, S., and Tomley, F. (2012). The Molecular Basis for the Distinct Host and Tissue Tropisms of Coccidian Parasites. *Mol. Biochem. Parasitol.* 186, 1–10. doi: 10.1016/j.molbiopara.2012.08.007
- Davignon, J. L., Rauwel, B., Degboe, Y., Constantin, A., Boyer, J. F., Kruglov, A., et al. (2018). Modulation of T-Cell Responses by Anti-Tumor Necrosis Factor Treatments in Rheumatoid Arthritis: A Review. *Arthritis Res. Ther.* 20, 229. doi: 10.1186/s13075-018-1725-6
- Davoli-Ferreira, M., Fonseca, D. M., Mota, C. M., Dias, M. S., Lima-Junior, D. S., da Silva, M. V., et al. (2016). Nucleotide-Binding Oligomerization Domain-Containing Protein 2 Prompts Potent Inflammatory Stimuli During *Neospora Caninum* Infection. *Sci. Rep.* 6, 29289. doi: 10.1038/srep29289
- Deckert-Schluter, M., Bluethmann, H., Rang, A., Hof, H., and Schluter, D. (1998). Crucial Role of TNF Receptor Type 1 (P55), But Not of TNF Receptor Type 2 (P75), in Murine Toxoplasmosis. *J. Immunol.* 160, 3427–3436.
- Derouich-Guergour, D., Brenier-Pinchart, M. P., Ambroise-Thomas, P., and Pelloux, H. (2001). Tumour Necrosis Factor Alpha Receptors: Role in the Physiopathology of Protozoan Parasite Infections. *Int. J. Parasitol.* 31, 763–769. doi: 10.1016/S0020-7519(01)00194-1
- Dubey, J. P., Carpenter, J. L., Speer, C. A., Topper, M. J., and Uggla, A. (1988). Newly Recognized Fatal Protozoan Disease of Dogs. *J. Am. Vet. Med. Assoc.* 192, 1269–1285.
- Dubey, J. P., and Schares, G. (2011). Neosporosis in Animals—the Last Five Years. *Vet. Parasitol.* 180, 90–108. doi: 10.1016/j.vetpar.2011.05.031
- Dubey, J. P., Schares, G., and Ortega-Mora, L. M. (2007). Epidemiology and Control of Neosporosis and *Neospora Caninum*. *Clin. Microbiol. Rev.* 20, 323–367. doi: 10.1128/CMR.00031-06
- El-Sayed, N. M., Ismail, K. A., Badawy, A. F., and Elhasanein, K. F. (2016). *In Vivo* Effect of Anti-TNF Agent (Etanercept) in Reactivation of Latent Toxoplasmosis. *J. Parasitol. Dis.* 40, 1459–1465. doi: 10.1007/s12639-015-0712-y
- Fereig, R. M., and Nishikawa, Y. (2020). From Signaling Pathways to Distinct Immune Responses: Key Factors for Establishing or Combating *Neospora Caninum* Infection in Different Susceptible Hosts. *Pathogens* 9, 384. doi: 10.3390/pathogens9050384
- Figgett, W. A., Vincent, F. B., Saulep-Easton, D., and Mackay, F. (2014). Roles of Ligands From the TNF Superfamily in B Cell Development, Function, and Regulation. *Semin. Immunol.* 26, 191–202. doi: 10.1016/j.smim.2014.06.001
- Gazzinelli, R. T., Eltoum, I., Wynn, T., and Sher, A. (1993). Acute Cerebral Toxoplasmosis Is Induced by *In Vivo* Neutralization of TNF-Alpha and Correlates With the Down-Regulated Expression of Inducible Nitric Oxide Synthase and Other Markers of Macrophage Activation. *J. Immunol.* 151, 3672–3681.
- Germann, T., Gately, M. K., Schoenhaut, D. S., Lohoff, M., Mattner, F., Fischer, S., et al. (1993). Interleukin-12/T Cell Stimulating Factor, a Cytokine With Multiple Effects on T Helper Type 1 (Th1) But Not on Th2 Cells. *Eur. J. Immunol.* 23, 1762–1770. doi: 10.1002/eji.1830230805
- Gonçalves, N. S., Ghaem-Maghani, M., Monteleone, G., Frankel, G., Dougan, G., Lewis, D. J., et al. (2001). Critical Role for Tumor Necrosis Factor Alpha in Controlling the Number of Luminal Pathogenic Bacteria and Immunopathology in Infectious Colitis. *Infect. Immun.* 69, 6651–6659. doi: 10.1128/IAI.69.11.6651-6659.2001
- Hao, N. B., Lu, M. H., Fan, Y. H., Cao, Y. L., Zhang, Z. R., and Yang, S. M. (2012). Macrophages in Tumor Microenvironments and the Progression of Tumors. *Clin. Dev. Immunol.* 2012, 948098. doi: 10.1155/2012/948098
- Hemphill, A., Aguado-Martinez, A., and Muller, J. (2016). Approaches for the Vaccination and Treatment of *Neospora Caninum* Infections in Mice and Ruminant Models. *Parasitology* 143, 245–259. doi: 10.1017/S0031182015001596
- Innes, E. A. (2007). The Host-Parasite Relationship in Pregnant Cattle Infected With *Neospora caninum*. *Parasitology* 134, 1903–1910. doi: 10.1017/S0031182007000194
- Janssen, R., Van Wengen, A., Verhard, E., De Boer, T., Zomerdijs, T., Ottenhoff, T. H., et al. (2002). Divergent Role for TNF- α in IFN- γ -Induced Killing of *Toxoplasma Gondii* and *Salmonella Typhimurium* Contributes to Selective Susceptibility of Patients With Partial IFN- γ Receptor 1 Deficiency. *J. Immunol.* 169, 3900–3907. doi: 10.4049/jimmunol.169.7.3900
- Jesus, E. E., Pinheiro, A. M., Santos, A. B., Freire, S. M., Tardy, M. B., El-Bacha, R. S., et al. (2013). Effects of IFN-Gamma, TNF-Alpha, IL-10 and TGF-Beta on *Neospora Caninum* Infection in Rat Glial Cells. *Exp. Parasitol.* 133, 269–274. doi: 10.1016/j.exppara.2012.11.016
- Karki, R., Sharma, B. R., Tuladhar, S., Williams, E. P., Zalduendo, L., Samir, P., et al. (2021). Synergism of TNF- α and IFN- γ Triggers Inflammatory Cell Death, Tissue Damage, and Mortality in SARS-CoV-2 Infection and Cytokine Shock Syndromes. *Cell* 184, 149–168. doi: 10.1016/j.cell.2020.11.025
- Khan, I. A., Schwartzman, J. D., Fonseca, S., and Kasper, L. H. (1997). *Neospora Caninum*: Role for Immune Cytokines in Host Immunity. *Exp. Parasitol.* 85, 24–34. doi: 10.1006/expr.1996.4110
- Liew, F. Y. (1993). The Role of Nitric Oxide in Parasitic Diseases. *Ann. Trop. Med. Parasitol.* 87 (6), 637–642. doi: 10.1080/00034983.1993.11812822
- Long, M. T., Baszler, T. V., and Mathison, B. A. (1998). Comparison of Intracerebral Parasite Load, Lesion Development, and Systemic Cytokines in Mouse Strains Infected With *Neospora Caninum*. *J. Parasitol.* 84, 316–320. doi: 10.2307/3284489
- Mansilla, F. C., Moore, D. P., Quintana, M. E., Cardoso, N., Hecker, Y. P., Gual, I., et al. (2015). Safety and Immunogenicity of a Soluble Native *Neospora Caninum* Tachyzoite-Extract Vaccine Formulated With a Soy Lecithin/Beta-Glucan Adjuvant in Pregnant Cattle. *Vet. Immunol. Immunopathol.* 165, 75–80. doi: 10.1016/j.vetimm.2015.03.007
- Marugan-Hernandez, V. (2017). *Neospora Caninum* and Bovine Neosporosis: Current Vaccine Research. *J. Comp. Pathol.* 157, 193–200. doi: 10.1016/j.jcpa.2017.08.001
- Mineo, T. W., Benevides, L., Silva, N. M., and Silva, J. S. (2009). Myeloid Differentiation Factor 88 Is Required for Resistance to *Neospora Caninum* Infection. *Vet. Res.* 40, 32. doi: 10.1051/vetres/2009015
- Mineo, T. W., Oliveira, C. J., Gutierrez, F. R., and Silva, J. S. (2010). Recognition by Toll-Like Receptor 2 Induces Antigen-Presenting Cell Activation and Th1 Programming During Infection by *Neospora Caninum*. *Immunol. Cell Biol.* 88, 825–833. doi: 10.1038/icb.2010.52
- Mota, C. M., Oliveira, A. C., Davoli-Ferreira, M., Silva, M. V., Santiago, F. M., Nadipuram, S. M., et al. (2016). *Neospora Caninum* Activates P38 MAPK as an Evasion Mechanism Against Innate Immunity. *Front. Microbiol.* 7, 1456. doi: 10.3389/fmicb.2016.01456
- Nacy, C. A., Meierovics, A. I., Belosevic, M., and Green, S. J. (1991). Tumor Necrosis Factor-Alpha: Central Regulatory Cytokine in the Induction of Macrophage Antimicrobial Activities. *Pathobiology* 59, 182–184. doi: 10.1159/000163640
- Ohmori, Y., Schreiber, R. D., and Hamilton, T. A. (1997). Synergy Between Interferon- γ and Tumor Necrosis Factor- α in Transcriptional Activation Is Mediated by Cooperation Between Signal Transducer and Activator of Transcription 1 and Nuclear Factor κ B. *Biol. Chem.* 272, 14899–14907. doi: 10.1074/jbc.272.23.14899
- Peschon, J. J., Torrance, D. S., Stocking, K. L., Glaccum, M. B., Otten, C., Willis, C. R., et al. (1998). TNF Receptor-Deficient Mice Reveal Divergent Roles for P55 and P75 in Several Models of Inflammation. *J. Immunol.* 160, 943–952.

- Pimenta, T. S., Chaves, N. F., Rodrigues, A. P. D., Diniz, C. W. P., DaMatta, R. A., and Diniz Junior, J. A. P. (2018). Granulocyte Macrophage Colony-Stimulating Factor Alone Reduces *Toxoplasma Gondii* Replication in Microglial Culture by Superoxide and Nitric Oxide, Without IFN-Gamma Production: A Preliminary Report. *Microbes Infect.* 20, 385–390. doi: 10.1016/j.micinf.2018.05.006
- Reichel, M. P., McAllister, M. M., Pomroy, W. E., Campero, C., Ortega-Mora, L. M., and Ellis, J. T. (2014). Control Options for *Neospora Caninum*—Is There Anything New or Are We Going Backwards? *Parasitology* 141, 1455–1470. doi: 10.1017/S0031182014000158
- Ribeiro, D. P., Freitas, M. M., Cardoso, M. R., Pajuaba, A. C., Silva, N. M., Mineo, T. W., et al. (2009). CpG-ODN Combined With *Neospora Caninum* Lysate, But Not With Excreted-Secreted Antigen, Enhances Protection Against Infection in Mice. *Vaccine* 27, 2570–2579. doi: 10.1016/j.vaccine.2009.02.028
- Ritter, D. M., Kerlin, R., Sibert, G., and Brake, D. (2002). Immune Factors Influencing the Course of Infection With *Neospora Caninum* in the Murine Host. *J. Parasitol.* 88, 271–280. doi: 10.1645/0022-3395(2002)088[0271:IFITCO]2.0.CO;2
- Rojo-Montejo, S., Collantes-Fernandez, E., Blanco-Murcia, J., Rodriguez-Bertos, A., Risco-Castillo, V., and Ortega-Mora, L. M. (2009). Experimental Infection With a Low Virulence Isolate of *Neospora Caninum* at 70 Days Gestation in Cattle did Not Result in Foetopathy. *Vet. Res.* 40, 49. doi: 10.1051/vetres/2009032
- Schäffer, M., Bongartz, M., Hoffmann, W., and Viebahn, R. (2006). Regulation of Nitric Oxide Synthesis in Wounds by IFN- γ Depends on TNF- α . *J. Invest. Surg.* 19, 371–379. doi: 10.1080/08941930600985710
- Schluter, D., Kwok, L. Y., Lutjen, S., Soltek, S., Hoffmann, S., Korner, H., et al. (2003). Both Lymphotoxin-Alpha and TNF Are Crucial for Control of *Toxoplasma Gondii* in the Central Nervous System. *J. Immunol.* 170, 6172–6182. doi: 10.4049/jimmunol.170.12.6172
- Snapper, C. M., and Paul, W. E. (1987). Interferon-Gamma and B Cell Stimulatory Factor-1 Reciprocally Regulate Ig Isotype Production. *Science* 236, 944–947. doi: 10.1126/science.3107127
- Stevens, T. L., Bossie, A., Sanders, V. M., Fernandez-Botran, R., Coffman, R. L., Mosmann, T. R., et al. (1988). Regulation of Antibody Isotype Secretion by Subsets of Antigen-Specific Helper T Cells. *Nature* 334, 255–258. doi: 10.1038/334255a0
- Wajant, H., Pfizenmaier, K., and Scheurich, P. (2003). Tumor Necrosis Factor Signaling. *Cell Death Differ.* 10, 45–65. doi: 10.1038/sj.cdd.4401189
- Wajant, H., and Scheurich, P. (2011). TNFR1-Induced Activation of the Classical NF-kappaB Pathway. *FEBS J.* 278, 862–876. doi: 10.1111/j.1742-4658.2011.08015.x
- Wajant, H., and Siegmund, D. (2019). TNFR1 and TNFR2 in the Control of the Life and Death Balance of Macrophages. *Front. Cell Dev. Biol.* 7, 91. doi: 10.3389/fcell.2019.00091
- Yamane, I., Kitani, H., Kokuho, T., Shibahara, T., Haritani, M., Hamaoka, T., et al. (2000). The Inhibitory Effect of Interferon Gamma and Tumor Necrosis Factor Alpha on Intracellular Multiplication of *Neospora Caninum* in Primary Bovine Brain Cells. *J. Vet. Med. Sci.* 62, 347–351. doi: 10.1292/jvms.62.347
- Yap, G. S., Scharton-Kersten, T., Charest, H., and Sher, A. (1998). Decreased Resistance of TNF Receptor P55- and P75-Deficient Mice to Chronic Toxoplasmosis Despite Normal Activation of Inducible Nitric Oxide Synthase *In Vivo*. *J. Immunol.* 160, 1340–1345.
- Zakharova, M., and Ziegler, H. K. (2005). Paradoxical Anti-Inflammatory Actions of TNF-Alpha: Inhibition of IL-12 and IL-23 via TNF Receptor 1 in Macrophages and Dendritic Cells. *J. Immunol.* 175, 5024–5033. doi: 10.4049/jimmunol.175.8.5024

Conflict of Interest: The authors declare that the research was conducted in the absence of any commercial or financial relationships that could be construed as a potential conflict of interest.

Publisher's Note: All claims expressed in this article are solely those of the authors and do not necessarily represent those of their affiliated organizations, or those of the publisher, the editors and the reviewers. Any product that may be evaluated in this article, or claim that may be made by its manufacturer, is not guaranteed or endorsed by the publisher.

Copyright © 2022 Ferreira França, Silva, Silva, Ramos, Miranda, Mota, Santiago, Mineo and Mineo. This is an open-access article distributed under the terms of the Creative Commons Attribution License (CC BY). The use, distribution or reproduction in other forums is permitted, provided the original author(s) and the copyright owner(s) are credited and that the original publication in this journal is cited, in accordance with accepted academic practice. No use, distribution or reproduction is permitted which does not comply with these terms.



An Iron Transporter Is Involved in Iron Homeostasis, Energy Metabolism, Oxidative Stress, and Metacyclogenesis in *Trypanosoma cruzi*

OPEN ACCESS

Edited by:

Maria E. Francia,
Institut Pasteur de Montevideo,
Uruguay

Reviewed by:

Veronica Jimenez,
California State University, Fullerton,
United States
Noelia Lander,
University of Cincinnati, United States

*Correspondence:

Claudia F. Dick
cfdick@bioqmed.ufrj.br

Specialty section:

This article was submitted to
Parasite and Host,
a section of the journal
Frontiers in Cellular and
Infection Microbiology

Received: 04 October 2021

Accepted: 06 December 2021

Published: 10 January 2022

Citation:

Dick CF, Rocco-Machado N,
Dos-Santos ALA, Carvalho-Kelly LF,
Alcantara CL, Cunha-E-Silva NL,
Meyer-Fernandes JR and Vieyra A
(2022) An Iron Transporter Is
Involved in Iron Homeostasis,
Energy Metabolism, Oxidative
Stress, and Metacyclogenesis in
Trypanosoma cruzi.
Front. Cell. Infect. Microbiol. 11:789401.
doi: 10.3389/fcimb.2021.789401

Claudia F. Dick^{1,2,3*}, Nathália Rocco-Machado^{1,3}, André L. A. Dos-Santos^{1,3},
Luiz F. Carvalho-Kelly^{1,3}, Carolina L. Alcantara^{2,3}, Narcisa L. Cunha-E-Silva^{2,3},
José R. Meyer-Fernandes^{1,3} and Adalberto Vieyra^{2,3,4}

¹ Leopoldo de Meis Institute of Medical Biochemistry, Federal University of Rio de Janeiro, Rio de Janeiro, Brazil, ² Carlos Chagas Filho Institute of Biophysics, Federal University of Rio de Janeiro, Rio de Janeiro, Brazil, ³ National Center of Structural Biology and Bioimaging (CENABIO), Federal University of Rio de Janeiro, Rio de Janeiro, Brazil, ⁴ Graduate Program in Translational Biomedicine/BIOTRANS, Unigranrio University, Duque de Caxias, Brazil

The parasite *Trypanosoma cruzi* causes Chagas' disease; both heme and ionic Fe are required for its optimal growth, differentiation, and invasion. Fe is an essential cofactor in many metabolic pathways. Fe is also harmful due to catalyzing the formation of reactive O₂ species; for this reason, all living systems develop mechanisms to control the uptake, metabolism, and storage of Fe. However, there is limited information available on Fe uptake by *T. cruzi*. Here, we identified a putative 39-kDa Fe transporter in *T. cruzi* genome, TcIT, homologous to the Fe transporter in *Leishmania amazonensis* and *Arabidopsis thaliana*. Epimastigotes grown in Fe-depleted medium have increased TcIT transcription compared with controls grown in regular medium. Intracellular Fe concentration in cells maintained in Fe-depleted medium is lower than in controls, and there is a lower O₂ consumption. Epimastigotes overexpressing TcIT, which was encountered in the parasite plasma membrane, have high intracellular Fe content, high O₂ consumption—especially in phosphorylating conditions, high intracellular ATP, very high H₂O₂ production, and stimulated transition to trypomastigotes. The investigation of the mechanisms of Fe transport at the cellular and molecular levels will assist in elucidating Fe metabolism in *T. cruzi* and the involvement of its transport in the differentiation from epimastigotes to trypomastigotes, virulence, and maintenance/progression of the infection.

Keywords: iron transporter, *Trypanosoma cruzi*, reactive O₂ species production, parasite O₂ consumption, parasite proliferation, parasite differentiation, maintenance of *T. cruzi* infection

1 INTRODUCTION

Trypanosoma cruzi, the etiological agent of Chagas' disease, has a complex life cycle, alternating between an intermediate invertebrate host and a definitive mammalian host (de Souza, 1984). *Trypanosoma cruzi* has a high requirement for iron (Fe) for proliferation, *in vitro* and *in vivo*, mobilizing heme and non-heme iron (Lalonde and Holbein, 1984). *Trypanosoma cruzi* can hijack Fe-proteins from a mammalian host. The addition of deferoxamine, an Fe chelator, or transferrin-free serum can inhibit the proliferation of amastigote cells in culture, an indication that Fe is an obligatory nutrient (Lima and Villalta, 1990). This form of the parasite presents receptors for human transferrin, which bind exogenous transferrin. Transferrin bound to amastigote cells is not removed by acid treatment, indicating a possible internalization and utilization of this transferrin (Lima and Villalta, 1990). In epimastigotes, transferrin uptake occurs through the cytostome, a specialized structure composed of a membrane invagination in the anterior region, close to the flagellar pocket (Porto-Carreiro et al., 2000), an early observation showing that Fe-carrying molecules are important for the parasite in its different morphological stages and, therefore, for the establishment, maintenance, and evolution of the infection in the vertebrate host. Heme is also utilized as an Fe source for *T. cruzi*; it can stimulate *T. cruzi* proliferation in culture in a dose-dependent manner (Lara et al., 2007). Moreover, heme/porphyrin translocates in epimastigote forms of *T. cruzi*, possibly mediated by an ABC transporter protein (Cupello et al., 2011). However, the limiting step for the utilization of heme by pathogenic trypanosomatids is the initial heminic ring hydrolysis for Fe liberation (Taylor and Kelly, 2010), since there is no heme oxidase gene in the *T. cruzi* genome (El-Sayed et al., 2005).

Before direct Fe incorporation by cells, Fe^{3+} (the predominant redox form in nature) has to be reduced to Fe^{2+} , catalyzed by an Fe-reductase (Sedláček et al., 2009). In this way, the identification of an Fe-reductase activity in *Leishmania chagasi* (Wilson et al., 2002), *Leishmania amazonensis* (Flannery et al., 2011), and more recently, *T. cruzi* (Dick et al., 2020) is strongly indicative of a Fe^{2+} transport mechanism in trypanosomatids. Due to the Fe low redox potential ($E^\circ = -0.04$ V for the reaction $\text{Fe}^{3+} + 3\text{e}^- \rightarrow \text{Fe}$), it becomes a suitable element for redox catalysis reactions (Atkins and de Paula, 2006), where it can act as an electron donor and receptor. The ability to pass readily through oxidation/reduction cycles leads to the inherent toxicity of Fe, since it catalyzes the formation of reactive O_2 species (ROS) as hydroxyl radical (OH^\bullet), which provides a high redox potential ($E^\circ = +2.33$ V for the reaction $\text{OH}^\bullet + \text{e}^- + \text{H}^+ \rightarrow \text{H}_2\text{O}$) (Krumova and Cosa, 2016), *via* the Fenton reaction.

Regarding Fe metabolism in *T. cruzi*, there is strong evidence that it is important in the catalysis by antioxidant defenses (Paiva et al., 2012). Superoxide dismutase isoforms (SODs) are metalloproteins that can dismutate O_2^- in H_2O_2 and O_2 . Metallic ions are present in the catalytic center from SODs, e.g., Cu-Zn-SOD in eukaryotes (Tainer et al., 1983) and Mn-SOD in bacteria, such as *Escherichia coli* (Geslin et al., 2001), whereas

trypanosomatids exclusively have Fe-SOD, with Fe as the cofactor (Wilkinson et al., 2006). However, there is little information regarding Fe uptake in *T. cruzi* (Sutak et al., 2008) and its role in i) the differentiation process that is required for the infection of the vertebrate host and ii) the stimulus of oxidative stress within the parasite, which favors this differentiation process.

We have identified a sequence putatively annotated as the Zn/Fe transporter. *In-silico* analysis demonstrated its homology to the Fe transporters described in *L. amazonensis* (Huynh et al., 2006) and *Arabidopsis thaliana* (Vert et al., 2002). It is the first identification of an Fe transporter (TcIT) homologous to LIT1 possibly responsible for Fe uptake in *T. cruzi*, working coupled to the Fe-reductase TcFR recently described in our laboratory (Dick et al., 2020). We hypothesize that this transporter may be important in the maintenance and progression of *T. cruzi* infection.

2 MATERIALS AND METHODS

Epimastigote Growth and Metacyclogenesis

Epimastigotes of *T. cruzi* (Dm28c strain) were maintained at 28°C in stationary phase by using brain heart infusion (BHI) medium supplemented with 10% FBS, 30 μM hemin, and 1% penicillin-streptomycin cocktail (regular medium, RM). Iron-depleted medium (IDM) was prepared using BHI medium without hemin and supplemented with 10% iron-free FBS, following the protocol described in Dick et al. (2020). The viability of the parasites was assayed by evaluating the mitochondrial transmembrane potential. When this potential is generated and maintained, the 3-(4,5-dimethylthiazol)-2,5-diphenyltetrazolium (MTT) bromide (Sigma-Aldrich, Saint Louis, MO, USA) is converted to insoluble formazan. The concentration of formazan was spectrophotometrically determined at 570 nm after its solubilization with Triton X-100.

For the assay of epimastigote proliferation, the parasites were inoculated (10^6 cells/ml) on the 6th day of culture into the BHI medium (RM or IDM, with or without G418). Cell proliferation was assessed every day by counting the number of cells in a hemocytometer. Metacyclogenesis was induced as described in Contreras et al. (1985) and Koeller et al. (2014). Briefly, epimastigotes in transition from logarithmic to stationary phase were adjusted to 5×10^8 parasites/ml in triatomine artificial urine (TAU) medium [190 mM NaCl, 17 mM KCl, 2 mM MgCl_2 , 2 mM CaCl_2 , 0.035% (w/v) NaHCO_3 , and 8 mM phosphate buffer at pH 6.0]. After 2 h at 28°C, the cultures were diluted 100-fold in 10 ml TAU medium supplemented with 10 mM L-proline, 50 mM glutamic acid, 2 mM aspartic acid and 10 mM glucose (TAU3AAG), and 500 $\mu\text{g/ml}$ G418 (Sigma-Aldrich) and transferred to T25 flasks—lying at an angle of 45° to increase the area in contact with O_2 —and maintained at 28°C to promote metacyclogenesis. After 3–5 days, the parasites were quantified by hemocytometry, and the percentage of metacyclic trypomastigotes was estimated by their morphology after Giemsa staining.

The percentage of trypomastigotes was also quantified by cytometry as previously described (Bayer-Santos et al., 2013). Briefly, live parasites (4×10^7) were incubated for 30 min on ice with the monoclonal antibody 1G7 against GP90, diluted in 1% bovine serum albumin in phosphate-buffered saline (BSA/PBS). Later, the cells were washed in PBS and were fixed with 4% paraformaldehyde (PFA) in PBS for 15 min. Then, after washings in PBS, the parasites were incubated with Alexa Fluor 488-conjugated anti-mouse IgG diluted in 1% BSA/PBS for 1 h at room temperature. Subsequently, after two more washes, fluorescence was determined on a FACSCalibur II cytometer (Becton Dickinson, Franklin Lakes, NJ, USA), and data analysis was performed using the CellQuest software (Becton Dickinson).

In-Silico Analysis

From the *in-silico* analysis of the genome of the Dm28c strain of *T. cruzi* (available through the TriTryp database under the accession no. TCDM_06386) (Grisard et al., 2014), we found a homolog (TcIT) to the Fe transporter of *L. major* (available from the TriTryp database under the accession no. LmjF.31.3070-LIT). The model of TcIT was constructed using the protein structure prediction PHYRE (www.sbg.bio.ic.ac.uk/phyre/) (Kelley and Sternberg, 2009), which is based on the model of the SERCA ATPase and visualized with the standard molecular viewer PyMOL 2002 (PyMOL Molecular Graphics System, DeLano Scientific, San Carlos, CA, USA; <http://pymol.sourceforge.net/>). Phylogenetic analysis used the MEGA 7 software. The evolutionary history was inferred using the neighbor-joining method (Saitou and Nei, 1987). Amino-acid multiple sequence alignments were obtained by using Clustal W and Clustal X software version 2.0 (<http://www.ebi.ac.uk/Tools/msa/clustalw2>).

Cloning and Overexpression of TcIT in *Trypanosoma cruzi*

The full-length TcIT coding region was amplified from Dm28c gDNA, by using designated primers FTcIT (5'-GGATCCATGAACAACGTTGAGTCAAGTGACGCG-CACCT) introducing the *Bam*HI restriction site at the 5'-end and RTcITHA (5'-AAGCTTTTAAGCGTAATCTGGAACATCGTATGGGTACGCCCACTTCCCAAGGAGCGTCATAA), with the addition of *Hind*III restriction site with the hemagglutinin (HA) epitope tag at the 3'-end, thus generating the TcIT-HA insert. The amplicon was subcloned into pCR2.1-TOPO vector (Thermo Fisher Scientific, Waltham, MA, USA), released by digestion with *Bam*HI and *Hind*III (sites underlined above), and ligated into similarly digested expression vector pTEX (Kelly et al., 1992). The shuttle vector pTEX-TcIT-HA, which replicates in *E. coli* and *T. cruzi*, was used as the vehicle for the expression of TcIT-HA in *T. cruzi*. Cell electroporation was performed with an Amaxa Nucleofector II device with human T-cell buffer (Lonza, Basel, Switzerland). A total of 5×10^7 epimastigotes were transfected with pTEX-TcIT-HA or empty pTEX (pTEX-Ø) vectors (10 µg DNA). After electroporation, the cells were cultured for 48 h in standard medium and 500 µg/ml G418 (Sigma-Aldrich) was added. Non-DNA control cells died after 3 to 4 weeks. Cultures

were 5-fold diluted with fresh G418-containing medium after 5–10 days. Stable resistant cells were obtained ~30 days after transfection, indicating resistance to G418.

Intracellular Iron Concentration Determination

The concentration of intracellular Fe accumulated under different conditions and by different strains (wild type and mutants obtained as described above) was determined by a colorimetric assay based on the use of ferrozine. Suspensions containing 10^8 parasites were collected from different cultures and washed three times with PBS pretreated with 5 g/100 ml Chelex resin (Sigma-Aldrich). The cells were lysed with 100 µl 50 mM NaOH, followed by the addition of 100 µl 10 mM HCl; the release of ionic Fe bound to intracellular structures was achieved by adding 100 µl of a mixture of 1.4 M HCl and 4.5% (w/v) KMnO_4 (1:1) to the cell lysate, followed by incubation at 60°C for 2 h. Then, 30 µl Fe detection reagent (6.5 mM ferrozine, 6.5 mM neocuproine, 2.5 M ammonium acetate, and 1 M ascorbic acid) was added. After 30 min of incubation at room temperature, the absorbance of the sample was recorded at 550 nm. The concentration of Fe was determined using a standard curve with known FeCl_3 concentrations (0–75 µM) (Mittra et al., 2013).

Membrane Fraction Preparation

Mutant epimastigotes (5×10^9 cells) in late log phase of growth were harvested by centrifugation and washed three times in cold PBS. The plasma membrane fraction/PM was obtained as previously reported (Gottlieb and Dwyer, 1983; Pinheiro et al., 2006; Dick et al., 2020), with slight modifications. The washed organisms, overexpressing pTEX-TcIT or pTEX-Ø, were resuspended in Tris-EDTA buffer (10 mM Tris-HCl at pH 8.0, 125 mM sucrose, 3 mM MgCl_2 , 2 mM EDTA, and 1 mM phenylmethanesulfonyl fluoride) and maintained on ice for 30 min. The parasites were mixed with glass beads (1:4) and disrupted by abrasion for 10 min on an ice bath. After grinding, glass beads, unbroken cells, and large cell debris were removed by centrifugation at $1,000 \times g$ for 15 min at 4°C. The supernatant (total homogenate/HG) was centrifuged at $200,000 \times g$ for 1 h. The resulting pellet (total membranes/TM) was resuspended in 50 mM Tris-HCl (pH 8.0) and subsequently applied to a continuous density gradient of 18% Percoll in 0.25 M sucrose and 12 mM Tris-HCl (pH 7.4), to obtain the PM-enriched fraction. After centrifugation at $40,000 \times g$ for 1 h, the bands were removed by aspiration, analyzed for 5'-nucleotidase activity [the marker of PM in epimastigote forms of *T. cruzi* (Zingales et al., 1979) and Fe-reductase activity, and the two fractions (TM and PM) were kept at -80°C, along with aliquots of HG, for further assays. Protein concentration was determined by the Lowry method (Lowry et al., 1951), using BSA as standard. **Supplementary Figure S1** depicts the assays of 5'-nucleotidase and Fe-reductase activities, demonstrating i) the enrichment of the PM fraction with both enzymes and ii) that these activities were barely detectable in the supernatant recovered after centrifugation of HG at $200,000 \times g$ for 1 h (the cytosolic fraction/C).

Western Blotting and Immunolocalization

For Western blotting detection, the proteins of the fractions obtained as described above (30 µg/lane) were separated by 12% SDS-PAGE and transferred to nitrocellulose membranes (Merck Millipore, Burlington, MA, USA), which were blocked with 5% milk in PBS plus 0.1% (w/v) Tween 20, probed overnight at 4°C with the primary rabbit anti-HA antibody (1:1,000, Sigma-Aldrich), and detected using an HRP-conjugated anti-rabbit IgG secondary antibody (1:10,000, Santa Cruz Biotechnology, Dallas, TX, USA). Ponceau red was used as loading control.

Immunofluorescence was assayed as previously described, with minor modifications (Dick et al., 2020). The mutant *T. cruzi* epimastigotes (10^7 cells, pTEX-TcIT or pTEX-Ø) were washed three times in 0.5 ml PBS and the suspension was fixed with 500 µl formaldehyde 4% (w/v) in PBS for 1 h at room temperature. The samples were washed twice with 0.5 ml PBS, suspended in 40 µl PBS, and settled on poly-L-lysine-coated coverslips for 15 min. The coverslips were incubated in 0.4% (w/v) saponin in PGN [PBS at pH 7.2, supplemented with 0.2% (w/v) gelatin and 0.1% (w/v) NaN_3] for 15 min to allow parasite permeabilization. The samples were incubated with anti-HA antibody raised in rabbit (1:1,000, Sigma-Aldrich) and mouse anti-TcSMP (surface membrane proteins) antibody (1:100), prepared and used as described by Martins et al. (2015) in PGN with 0.1% saponin, and incubated overnight at 4°C. After washing with PGN, the samples were incubated with anti-rabbit FITC conjugated (1:100, Sigma-Aldrich) and anti-mouse Alexa 594 (1:1,000, Sigma-Aldrich) in PGN for 1 h at room temperature. Coverslips were washed in PBS and incubated with 0.1 µg/ml 4',6-diamino-2-phenylindole (DAPI, Sigma-Aldrich) for 30 min. After washing, coverslips were mounted on slides in Miowol (Antifade) reagent. Images were taken with a Leica TCS-SPE confocal microscope and processed with Leica confocal software.

Transmission Electron Microscopy

Cells were fixed by using 2.5% (v/v) glutaraldehyde in 0.1 M cacodylate buffer (pH 7.2) for 1 h at room temperature and post-fixed using an osmium-thiocarbohydrazide-osmium (OTO) protocol (Willingham and Rutherford, 1984). Briefly, the cells were incubated in a post-fixative solution [1% (v/v) OsO_4 , 0.8% (v/v) potassium ferrocyanide, and 5 mM CaCl_2 in 0.1 M cacodylate buffer (pH 7.2)] for 40 min, washed twice in water, and then incubated in a solution of 1% (w/v) thiocarbohydrazide (TCH, Sigma-Aldrich) in water for 5 min. After three washes in water, the cells were incubated again in the post-fixative solution for 3 min. Samples were dehydrated in an acetone series and embedded in epoxy resin. Ultrathin sections (70 nm) were stained post-embedding with 5% (w/v) uranyl acetate and lead citrate and observed by using a Tecnai Spirit electron microscope (FEI Co., Hillsboro, OR, USA) operating at 120 kV.

Real-Time PCR

Total *T. cruzi* RNA was extracted using a Direct-zol RNA MiniPrep Kit (Zymo Research, Orange, CA, USA) from epimastigotes maintained at RM or IDM for 6 days, or mutants pTEX-TcIT or pTEX-Ø (as indicated in the figure legends). Total RNA was subjected to reverse transcription using the High-Capacity cDNA reverse transcription kit (Thermo Fisher Scientific, Waltham, MA,

USA). For RT-PCR, 100 ng/µl cDNA per well was used (15 µl total volume), along with 5 µM primer mix and 7 µl PowerUp SYBR green master mix (Thermo Fisher Scientific). The primers 5'-TCTGGTCGC-TTCTCTTCTCG and 5'-TAAAGA-CTC CGGCACACAGT were used to amplify a 152-bp fragment of the *TcIT* gene. The primers 5'-AGCGCGCTCTAAGACTTACA and 5'-TG-GAGCTGCGGTTGTCATT that amplify the glyceraldehyde-3-phosphate dehydrogenase (GAPDH) constitutive gene were used to provide an endogenous control.

High-Resolution Respirometry in Different Respiratory States

Oxygen consumption was measured using intact epimastigotes (5×10^7 parasites/chamber; pTEX-TcIT or pTEX-Ø). Analyses used an O2k-system high-resolution oxygraph (Oroboros Instruments, Innsbruck, Austria). The cells were suspended in 2 ml respiration solution containing 100 mM sucrose, 50 mM KCl, and 50 mM Tris-HCl (pH 7.2) at 28°C with continuous stirring, and 50 µM digitonin was added to permeabilize the parasites. Oxygen concentrations and O_2 consumption were recorded using DatLab software coupled to Oxygraph-2K (basal O_2 consumption). Subsequently, 10 mM succinate and 200 µM ADP were added. Uncoupled respiration was stimulated after adding 3 µM FCCP and respiration was inhibited by adding 2.5 µg/ml antimycin A to measure residual O_2 consumption (Nogueira et al., 2017). In a series of experiments, titration with substrates and inhibitors was not carried out, and O_2 consumption was measured only in the presence of endogenous substrates (basal consumption) over all recordings.

Superoxide Dismutase Activity

Superoxide dismutase (SOD) activity was measured as described in Winterbourn et al. (1975), with modifications, based on SOD inhibiting the reduction of nitro blue tetrazolium (NBT) by O_2^- . Epimastigote cells were harvested by centrifugation, washed three times in cold PBS, and disrupted by freeze-thaw. The protein concentration of the total homogenate was quantified by the Lowry method (Lowry et al., 1951). The homogenates (using known quantities of protein in the range of 10–50 µg) were incubated in reaction medium (200 µl, final volume) containing 45 mM potassium phosphate buffer (pH 7.8), 6.5 mM EDTA, and 50 mM NBT. The reaction was initiated by adding 2 mM riboflavin. After 12 min in a light box, the absorbance of the sample was recorded at 560 nm. The percent inhibition was measured for each amount of protein, and SOD activity was expressed as the amount of enzyme inhibiting NBT reduction by 50%.

Intracellular ATP Quantification

The intracellular ATP was quantified by using an ATP bioluminescent somatic cell assay kit (Sigma-Aldrich). Briefly, mutant epimastigotes (10^7 parasites per tube, 0.1 ml) were incubated in a solution containing 100 mM sucrose, 50 mM KCl, and 50 mM Tris-HCl (pH 7.2 adjusted with HCl). Cellular extracts were prepared by mixing 0.1 ml epimastigotes with 0.1 ml somatic cell ATP releasing reagent and the mixture was left on ice for 1 min. Half of the cellular extract (0.1 ml) was transferred to MTS-11C minitubes (Axygen, Union City, CA, USA) containing 0.1 ml ATP assay mix and stirred for 10 s at room temperature. The total

amount of light emitted was measured with a GloMax Multi JR detection system (Promega, Madison, WI, USA). Total intracellular ATP concentration per cell number was calculated using a standard ATP curve, prepared, and analyzed in each experiment (Carvalho-Kelly et al., 2020).

Amplex Red Peroxidase Assay

The production of H_2O_2 in mutants overexpressing TcIT was assayed by the rate of H_2O_2 reduction to H_2O , which is stoichiometrically coupled (1:1) to the simultaneous oxidation of the non-fluorescent Amplex[®] Red probe to the fluorescent resorufin (Dos-Santos et al., 2019). Briefly, assays containing $0.1 \mu M$ H_2O_2 were incubated with 10^7 parasites/ml for 30 min at room temperature in 5 mM Tris-HCl (pH 7.4), $1.7 \mu M$ Amplex[®] Red (Invitrogen, Carlsbad, CA, USA), and 6.7 U/ml horseradish peroxidase (Sigma-Aldrich) in a final volume of 100 μl . The evolution of fluorescence was followed at excitation/emission wavelengths of 563/587 nm (slit 5 nm).

Interaction of Trypomastigotes With LLC-MK2 Cells

Metacyclogenesis was induced as described above in section 2.1. After 3 days, the parasites were collected and purified using the ion-exchange chromatography technique Sepharose membrane-DEAE (Cruz-Saavedra et al., 2017) to obtain a preparation enriched with metacyclic trypomastigotes. Then, the parasites were incubated with LLC-MK2 cells (CCL-7; ATCC, Rockville, MD, USA) (50 parasites:1 cell) in RPMI 1640 medium supplemented with 10% FBS in a 96-well PS F-bottom microplate (Greiner Bio-One Brazil Ltd., Americana, Brazil) for 24 h at 37°C under 5% CO_2 in air. After removing the medium containing parasites not adhered to the cells, adding the fresh medium, and incubating further (48 h), the cells were fixed with 4% paraformaldehyde in PBS for 10 min. After incubation with Hoechst 33342 (Invitrogen) (1:5,000 dilution) for 60 min at room temperature in the dark, the wells were washed with Milli-Q deionized water and analyzed in a high-content screening system ImageXpress Micro XL (Molecular Devices, San José, CA, USA) using the MetaXpress 6.0 software. The interaction parasites:cells was quantified by counting the respective nuclei.

Statistical Analysis

Data are presented as mean \pm SE. Means were compared by using unpaired Student's *t*-test and GraphPad Prism 7.0 (San Diego, CA, USA). When more than two means were compared, one-way ANOVA followed by Tukey's test or two-way ANOVA with multiple comparisons was used, as indicated in the text or in the figure legends.

3 RESULTS

Identification and Analysis of Iron Transporter Sequence in *Trypanosoma cruzi*

A putative zinc-iron (Zn-Fe) transporter sequence was found in the genome database of *T. cruzi* (TriTrypDB: TCDM_06386) following a BLAST search, using the Fe transporter LIT1 from *L. amazonensis* (TriTrypDB: LmjF.31.3060) (Huynh et al., 2006) as target. The

TCDM_06386 was named TcIT and has 1,119 bp, and the deduced amino-acid sequence of the peptide comprises 372 residues, thus resulting in a predicted molecular mass of 39.8 kDa. The deduced protein TcIT has a structural model (Figure 1A) in which its eight possible transmembrane domains can be seen (TMpred Server) (Hofmann and Stoffel, 1993). TcIT has a highly conserved domain corresponding to the zinc iron permeases (ZIP) superfamily domain (permeases classified as 2.A.5 in the Transporter Classification Database/TCDB, Saier Lab. Bioinformatics Group). We encountered the domain in Zn and Fe transporter proteins by using the Conserved Domain Database (CDD, National Center for Biotechnology Information/NCBI). This domain has conserved amino acids corresponding to Zn/Fe binding, such as those labeled H105, H223, S224, H249, and E253 in Figure 1A, which are located along the inner surface of the channel formed by the transmembrane domains and bind the metal during the transport process (Jacques et al., 2010).

TcIT alignment had 34% identity and 53% similarity to the LIT1 from *L. amazonensis* and 28% identity and 46% similarity to the IRT1 from *A. thaliana* (Figure 1B), with 30% identity between the sequences of *L. amazonensis* and *A. thaliana* (Jacques et al., 2010). Analysis showed that all three sequences have eight transmembrane domains (underlined in Figure 1B) and the same residues for Zn/Fe binding (residues H105, H223, S224, H249, and E253, red boxes in Figure 1B). To analyze the phylogenetic relationship with the ZIP superfamily, we compared the amino-acid sequence of TcIT with sequences of putative and functionally characterized Fe transporters from several organisms, using MEGA 7 software (Figure 1C).

Low Iron Availability Induces the Expression of TcIT

Impaired growth was seen in epimastigotes maintained in IDM compared with those grown in RM (Figure 2A). The decrease in cell number was not due to cell death: MTT assays showed that viability of the cells was similar (Figure 2B). Although cells in IDM possess TcIT transcripts that increased with Fe removal from the culture medium (Figure 2C), this was insufficient for maintaining Fe intracellular content: epimastigotes from IDM had 50% lower intracellular Fe content compared with epimastigotes from RM (Figure 2D). In addition, Fe depletion lowered basal O_2 consumption (representative recordings in Figure 2E), comparatively quantified in Figure 2F.

Plasma Membrane Localization of TcIT

By using immunofluorescence assays, we determined that the labeling of the tagged protein TcIT-HA colocalizes with the labeling of the plasma membrane protein TcSMP, indicating that the Fe transporter is localized in the plasma membrane of epimastigotes (Figure 3A).

As negative control, parasites transfected with pTEX-Ø did not stain with HA. Mutants overexpressing TcIT had a higher Fe intracellular content compared with the basal content of the mutant transfected with pTEX-Ø (Figure 3B), together with very high transcription levels of TcIT (Figure 3C). In agreement with the immunofluorescence results, the plasma membrane-enriched fraction (PM) from pTEX-TcIT had a 39-kDa band corresponding

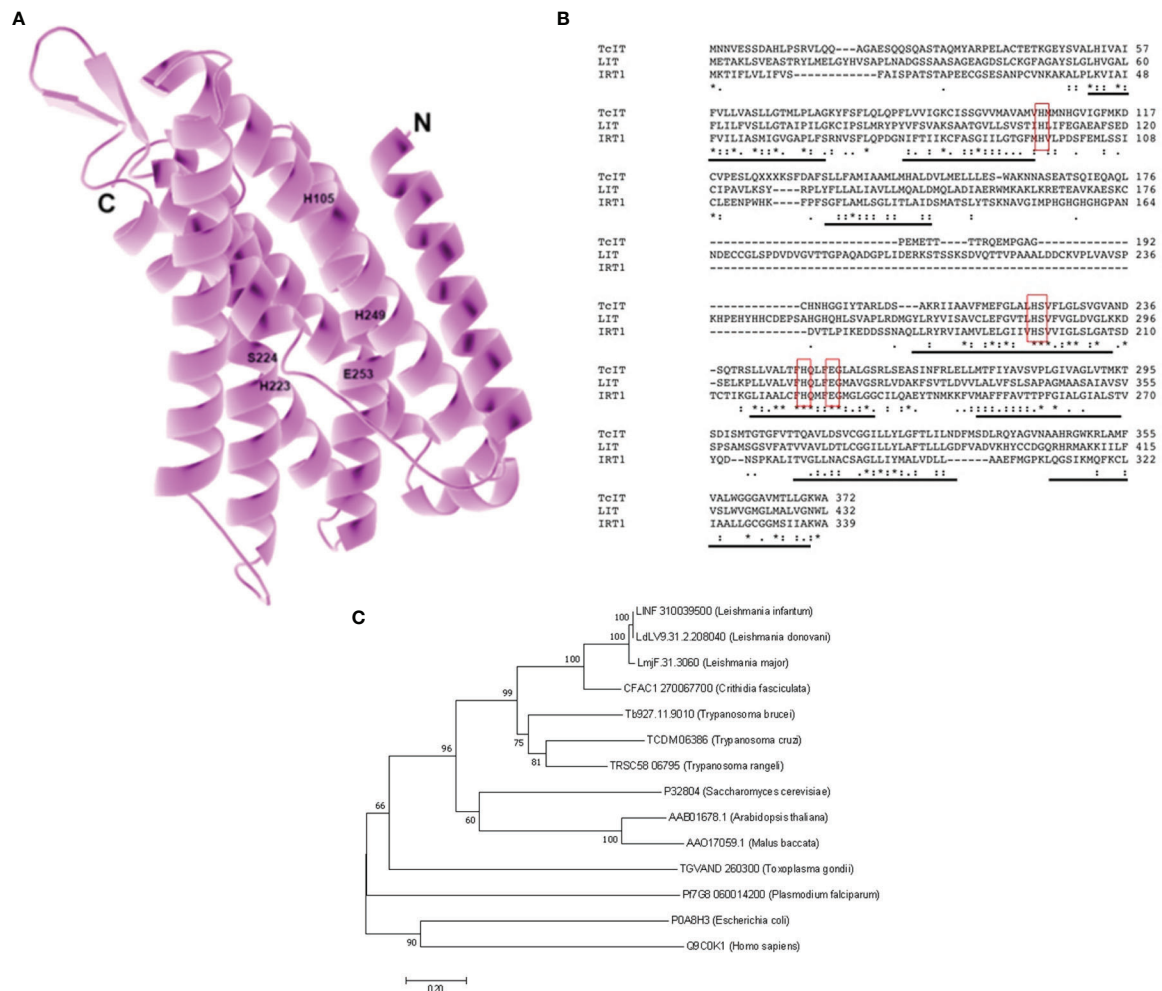


FIGURE 1 | Model for the iron (Fe) transporter TcIT: alignment and phylogenetic analysis for TcIT and ZIP family members from different species. **(A)** Structural model of Fe transporter from *T. cruzi* (TcIT). The model was constructed using the protein structure prediction PHYRE (www.sbg.bio.ic.ac.uk/phyre/) (Kelley and Sternberg, 2009) and visualized with the standard molecular viewer PyMOL 2002 (PyMOL Molecular Graphics System, DeLano Scientific, San Carlos, CA, USA; <http://pymol.sourceforge.net/>). The eight transmembrane helices are shown in pink, and labels highlight the five key residues mentioned in the text. **(B)** Alignment of amino-acid sequences from *T. cruzi* TcIT, DM28c strain (TrTrypDB: TCDM_06386), *L. major* LIT1 (TrTrypDB: LmjF.31.3060), and *Arabidopsis thaliana* IRT1 (GenBank: AAB01678.1). Conserved residues responsible for Fe transport in IRT1 and LIT1 (Jacques et al., 2010) are indicated in red boxes. Predicted transmembrane domains are underlined in black. Alignment used the ClustalW algorithm. Identical amino acids are indicated with an asterisk (*). Conservation between amino acid groups of strongly similar properties is indicated by a colon (:). Conservation between amino acid groups of weakly similar properties is indicated by a period (.). **(C)** Evolutionary relationships of ZIP family members. The evolutionary history was inferred using the neighbor-joining method (Saitou and Nei, 1987). The optimal tree with the sum of branch length = 6.09506879 is shown. The percentage of replicate trees in which the associated taxa clustered together in the bootstrap test (1,000 replicates) is shown at the beginning of each branch (Felsenstein, 1985). The tree is drawn to scale, with branch lengths in the same units as those of the evolutionary distances used to infer the phylogenetic tree. The evolutionary distances were computed using the Poisson correction method and given in the units of the number of amino-acid substitutions per site. All positions containing gaps and missing data have been eliminated. Evolutionary analyses were conducted in MEGA7 (Kumar et al., 2016), which involved 14 amino-acid sequences: *Leishmania infantum* putative sequence (GenBank: LINF310039500), *L. donovani* putative sequence (GenBank: LdLV9.31.2.208040), *L. major* LIT1 (GenBank: LmjF.31.3060), *Crithidia fasciculata* putative sequence (GenBank: CFAC1 270067700), *Trypanosoma brucei* putative sequence (GenBank: Tb927.11.9010), *T. cruzi* TcIT (GenBank: TCDM06386, this work), *T. rangeli* putative sequence (GenBank: TRSC58 06795), *Saccharomyces cerevisiae* ZRT1 (GenBank: P32804), *Arabidopsis thaliana* IRT1 (GenBank: AAB01678.1), *Malus baccata* MblIRT1 (GenBank: AAO17059.1), *Toxoplasma gondii* putative sequence (GenBank: TGVAND 260300), *Plasmodium falciparum* (GenBank: PfG8 0600 14200), *Escherichia coli* ZupT (GenBank: P0A8H3), and *Homo sapiens* SLC39A8 HsZIP8 (GenBank: Q9C0K1).

to TcIT. **Figure 3D** shows a representative Western blot image, where the arrow points to the 39-kDa band; no bands were observed in pTEX-Ø epimastigotes (**Figure 3E**). The densitometric analysis of pTEX-TcIT Western blots ($n = 3$) of the HG, total membranes, and

PM gave, respectively, the following values in arbitrary units: 52.9 ± 8.6 , 59.6 ± 2.4 , and 133.0 ± 2.9 . One-way ANOVA followed by Tukey's test demonstrated that the enrichment of TcIT in PM with respect to HG (160%) and TM (130%) was highly significant

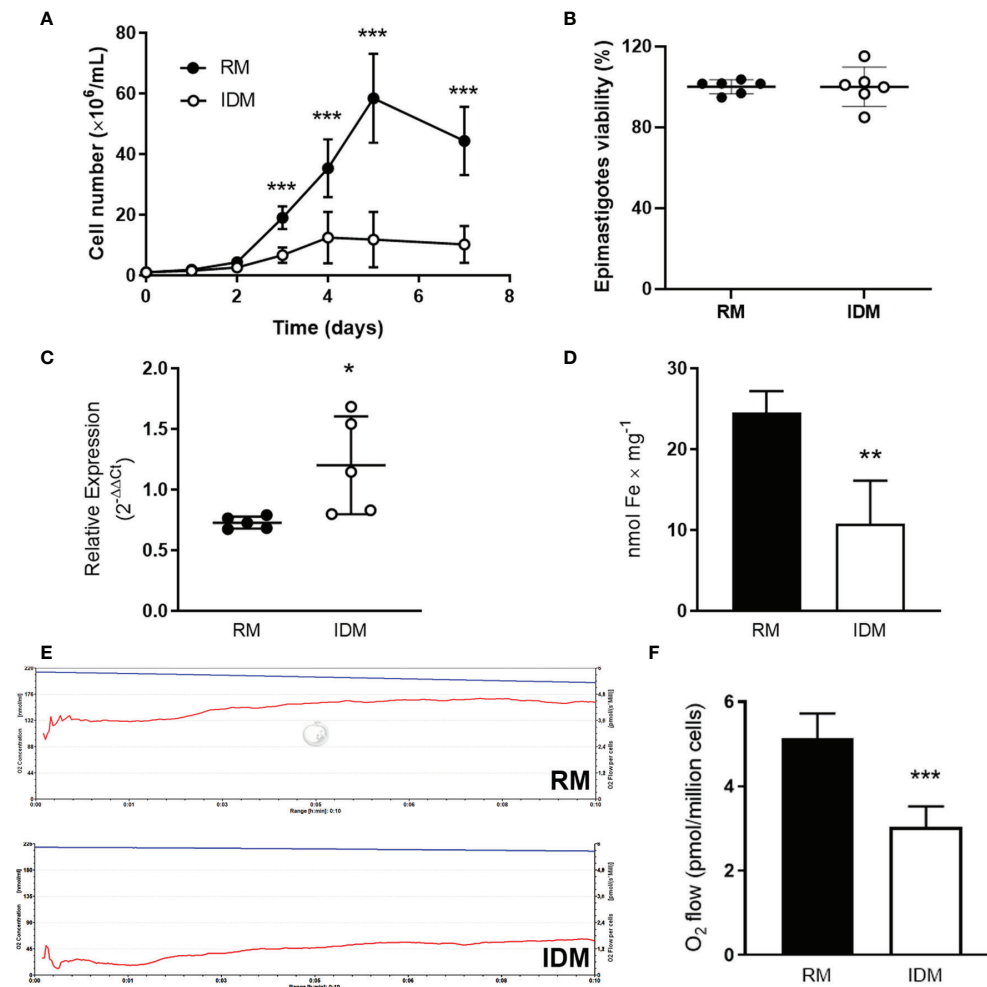


FIGURE 2 | Growth and respiration of wild-type epimastigotes are dependent on Fe content in culture medium and Fe depletion increases the expression of TcIT. **(A)** Influence of culture medium Fe content on *T. cruzi* proliferation. Wild-type epimastigotes of *T. cruzi* at mid-log phase were harvested, washed twice, seeded in fresh medium, and grown for the indicated times in regular medium [RM: brain heart infusion medium (BHI) supplemented with 30 μ M hemin and 10% fetal bovine serum (FBS)] (filled circles) or in iron-depleted medium (IDM: BHI without hemin supplementation and treated with Chelex for ionic Fe depletion plus 10% iron-depleted FBS) (empty circles); *** P < 0.001 (n = 12). **(B)** Viability of epimastigotes incubated in RM (filled circles) or IDM (empty circles) (5×10^7 epimastigotes/ml) was assayed using the MTT assay. **(C)** Quantification of the TcIT transcript in wild-type *T. cruzi* epimastigotes. Quantitative PCR was done using 100 ng cDNA from epimastigotes in mid-log phase when maintained in RM (filled circles) or IDM (empty circles); * P < 0.05 (n = 5). The housekeeping *GADPH* gene was used to normalize qPCR. **(D)** Intracellular Fe content in epimastigotes maintained in RM (black bars) or IDM (empty bars); ** P < 0.01 (n = 6). **(E)** Representative recordings of O₂ consumption rates vs. time (pmol/s per cell; lower traces in both panels) and decrease of O₂ concentration (nmol/ml; upper traces in both panels): 5×10^7 epimastigotes/chamber from RM (upper panel) or IDM (lower panel) were harvested, washed twice, and used to measure O₂ consumption in reaction medium (2 ml) containing 116 mM NaCl, 5.4 mM KCl, 5.5 mM D-glucose, 50 mM HEPES-Tris (pH 7.2). **(F)** Quantification of O₂ consumption by epimastigotes incubated in RM (black bars) or IDM (empty bars) (*** P < 0.001; n = 6). In all cases, using unpaired Student's *t*-test assessed differences between mean values. In **(A)**, the differences were assessed by comparing time-matched determinations.

(P < 0.0001 and P = 0.0001, respectively). Ponceau red loading controls are presented in **Figures 3F** (pTEX-TcIT) and **Figure 3G** (pTEX- \emptyset).

TcIT Transporter Increases Mitochondrial Respiratory Rates in *Trypanosoma cruzi*

In **Figures 2E, F**, we showed that Fe depletion in culture decreases O₂ consumption by *T. cruzi*. **Figures 4A** (representative traces) and **Figure 4B** (quantification of O₂ consumption in different

respiratory states) show that higher respiration rates are encountered—in phosphorylating and uncoupled conditions—when TcIT is overexpressed. Permeabilization with digitonin did not alter the profile of basal respiration (data not shown). After adding succinate (the LEAK O₂ consumption), there was no difference in O₂ consumption between pTEX- \emptyset and pTEX-TcIT epimastigotes, but the subsequent addition of ADP (corresponding to the oxidative phosphorylation—OXPHOS—state) that caused a significant increase of respiration by the two classes of mutants, O₂

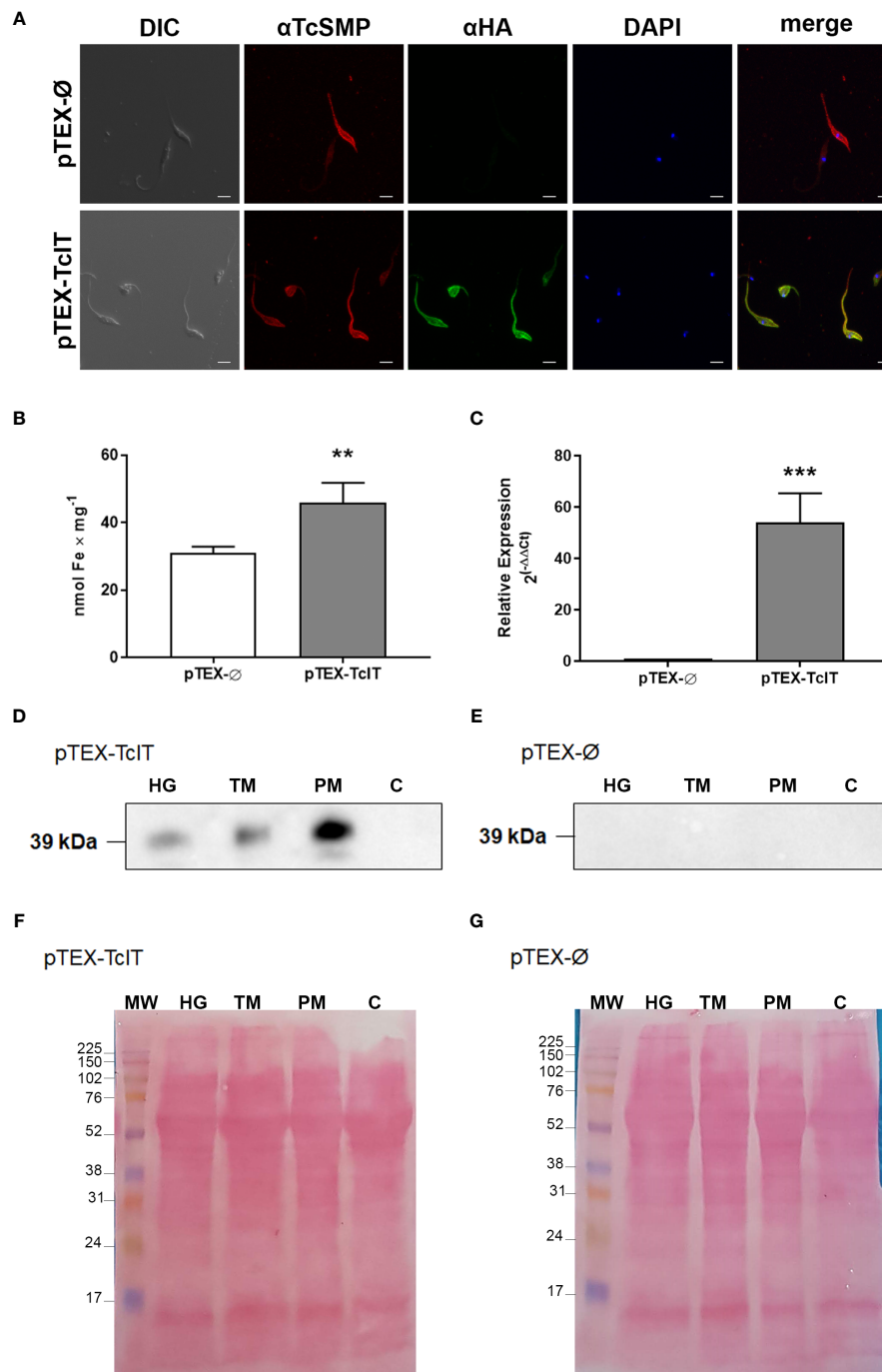


FIGURE 3 | (A) Immunofluorescence of epimastigotes shows TcIT expression in plasma membranes. *Trypanosoma cruzi* epimastigotes were transfected with empty vector (pTEX-Ø) or TcIT tagged with hemagglutinin (pTEX-TcIT). DIC: differential interference contrast microscopy. TcSMP: images using antisera for this surface membrane protein and the secondary anti-mouse-Alexa 546 (red). HA: TcIT expression using anti-HA and secondary anti-rabbit FITC (green). DAPI: nuclei stained with DAPI (blue). In merge, the green fluorescent staining for TcIT overlaps with the red fluorescent signal for TcSMP, suggesting the proteins are in the same region of the plasma membrane; ×60 magnification, scale bar 4 μm. **(B)** Intracellular Fe content is higher in epimastigotes transfected with pTEX-Ø (empty bar) or pTEX-TcIT (gray bar); **P < 0.01 (n = 6). **(C)** Quantification of the TcIT transcript in *T. cruzi* epimastigotes. Quantitative PCR was carried out using 100 ng cDNA from mutants pTEX-Ø (empty bar) or pTEX-TcIT (gray bar); ***P < 0.001 (n = 4). In both cases, using Student's *t*-test assessed differences between mean values. **(D)** Representative Western blot using homogenate (HG), total membrane (TM), plasma membrane (PM), and cytosol (C) fractions from pTEX-TcIT epimastigotes, as indicated in the upper part of the image, and the antibody anti-HA. **(E)** Representative Western blot using HG, TM, PM, and C fractions from pTEX-Ø epimastigotes, as indicated in the upper part of the image, and the antibody anti-HA. The predicted size of TcIT is 39.8 kDa. **(F, G)** Ponceau red loading controls for representative Western blots of membranes from pTEX-TcIT and pTEX-Ø epimastigotes, as indicated in the upper left corners.

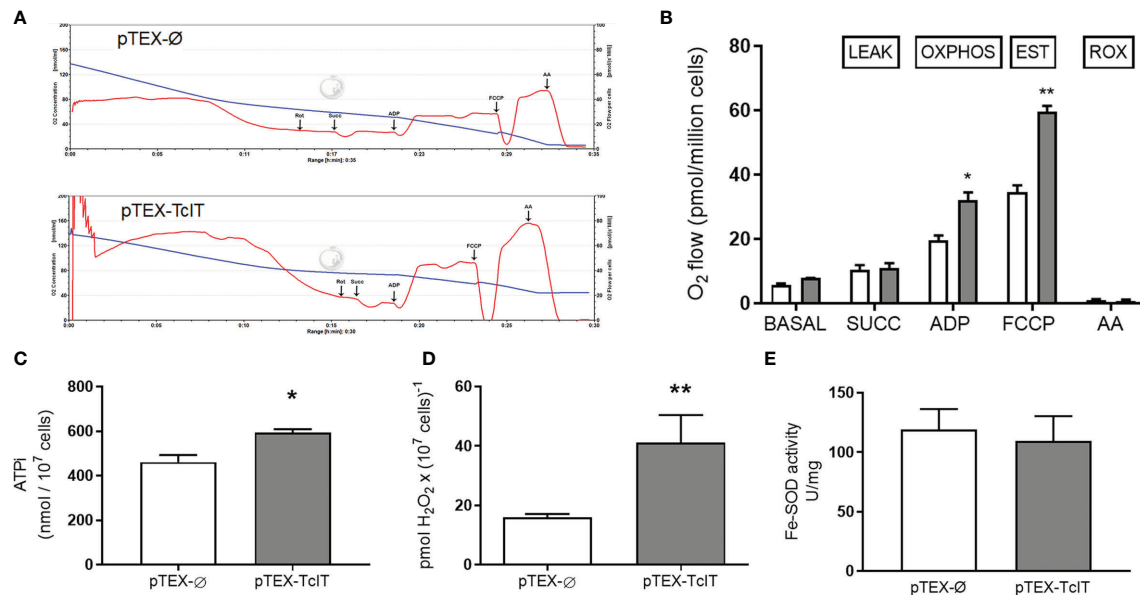


FIGURE 4 | Effect of TcIT overexpression on epimastigote mitochondrial physiology and Fe-SOD activity. **(A)** Representative recordings of O₂ consumption and decrease of O₂ concentration. *Trypanosoma cruzi* epimastigotes transfected with pTEX-Ø empty vector (upper panel) or pTEX-TcIT plasmid (lower panel) were initially tested for respiration of intact epimastigotes. Epimastigotes were then digitonin-permeabilized, as described in Nogueira et al. (2017), to measure mitochondrial activity after the successive additions indicated by arrows: Rot (rotenone), Succ (succinate), ADP, FCCP, and AA (antimycin A). **(B)** Graphic representation of O₂ consumption after the additions shown on the abscissa: SUCC, ADP, FCCP, and AA; **P* < 0.01, ***P* < 0.05 (*n* = 4). **(C)** Intracellular ATP in *T. cruzi* epimastigotes transfected with pTEX-Ø empty vector (empty bar) or pTEX-TcIT plasmid (gray bar) was measured as described in M&M section. **P* < 0.05 (*n* = 3). **(D)** Production of H₂O₂ by living cells of *T. cruzi* epimastigotes transfected with pTEX-Ø empty vector (empty bar) or pTEX-TcIT plasmid (gray bar); ***P* < 0.001 (*n* = 3). **(E)** SOD activity was assessed from epimastigotes transfected with pTEX-Ø empty vector (empty bars) or pTEX-TcIT plasmid (gray bars). The values represent the mean ± SEM. In **(C–E)**, using Student's *t*-test assessed differences between mean values. In **(B)**, differences were assessed by two-way ANOVA followed by Tukey's test. In all cases, the uncoupled respiration (with FCCP) was significantly higher than the respiration in phosphorylating conditions (with ADP). Both stimulated respiratory states were also significantly higher than those obtained only after addition of succinate (at least *P* < 0.05). No differences were found between the respiration of pTEX-Ø pTEX-TcIT epimastigotes in the presence of endogenous substrates or after the addition of succinate.

consumption of TcIT mutants was higher compared with pTEX-Ø mutants. There were a further increase and uncoupled respiration rates (EST, electron transfer system uncoupled from phosphorylation) after the addition of FCCP (a H⁺ ionophore), again higher in overexpressing TcIT. The addition of antimycin A completely abolished mitochondrial respiration in both mutants.

Higher mitochondrial O₂ consumption can be coupled to both increased oxidative phosphorylation and higher ROS production. Therefore, we measured total intracellular ATP concentration (Figure 4C) and H₂O₂ formation (Figure 4D) in both mutants. Parasites overexpressing TcIT had higher intracellular ATP (ATPi) content, as was expected, and a 2-fold higher content of H₂O₂. Nevertheless, there was no difference between the mutants in their activity of the antioxidant enzyme SOD (Figure 4E).

Possible ultrastructural changes in epimastigotes that overexpress TcIT were analyzed by transmission electron microscopy (Figure 5). As control, we used parasites transfected with pTEX-Ø. Control epimastigotes presented normal cell and organelle morphology and positioning (Figures 5A–C). We could not find any alteration in the major cellular organelles, including kinetoplast, nucleus, and organelles of the endocytic pathway such as cytosome–cytopharynx complex and reservosomes. Most organelles had normal morphology and positioning in

epimastigotes that overexpress TcIT (Figures 5D–H), except for the mitochondria. In mutant parasites, we frequently observed mitochondrial swelling, increase in cristae density, inner membrane vesiculation (Figures 5E–G), and mitochondrial disorganization (Figure 5H). These findings may reflect the increase in mitochondrial activity found in the case of parasites overexpressing TcIT.

Identification of the *Trypanosoma cruzi* Epimastigote Phenotype Overexpressing the TcIT Transporter: Stimulus of Differentiation to Trypomastigote and Replication Amastigote Rate

Overexpression of TcIT in *T. cruzi* epimastigotes did not interfere with their in-vitro proliferation (Figure 6A), since these mutants proliferate at the same rate as the epimastigotes transfected with the empty vector pTEX-Ø. However, when epimastigotes transfected with pTEX-TcIT were subjected to in-vitro differentiation in TAU medium, almost 40% of the forms present after 96 h were trypomastigotes, whereas transfection with pTEX-Ø for the same time led to only 20% of the organisms as trypomastigotes (Figure 6B). This indicates that overexpression of the TcIT

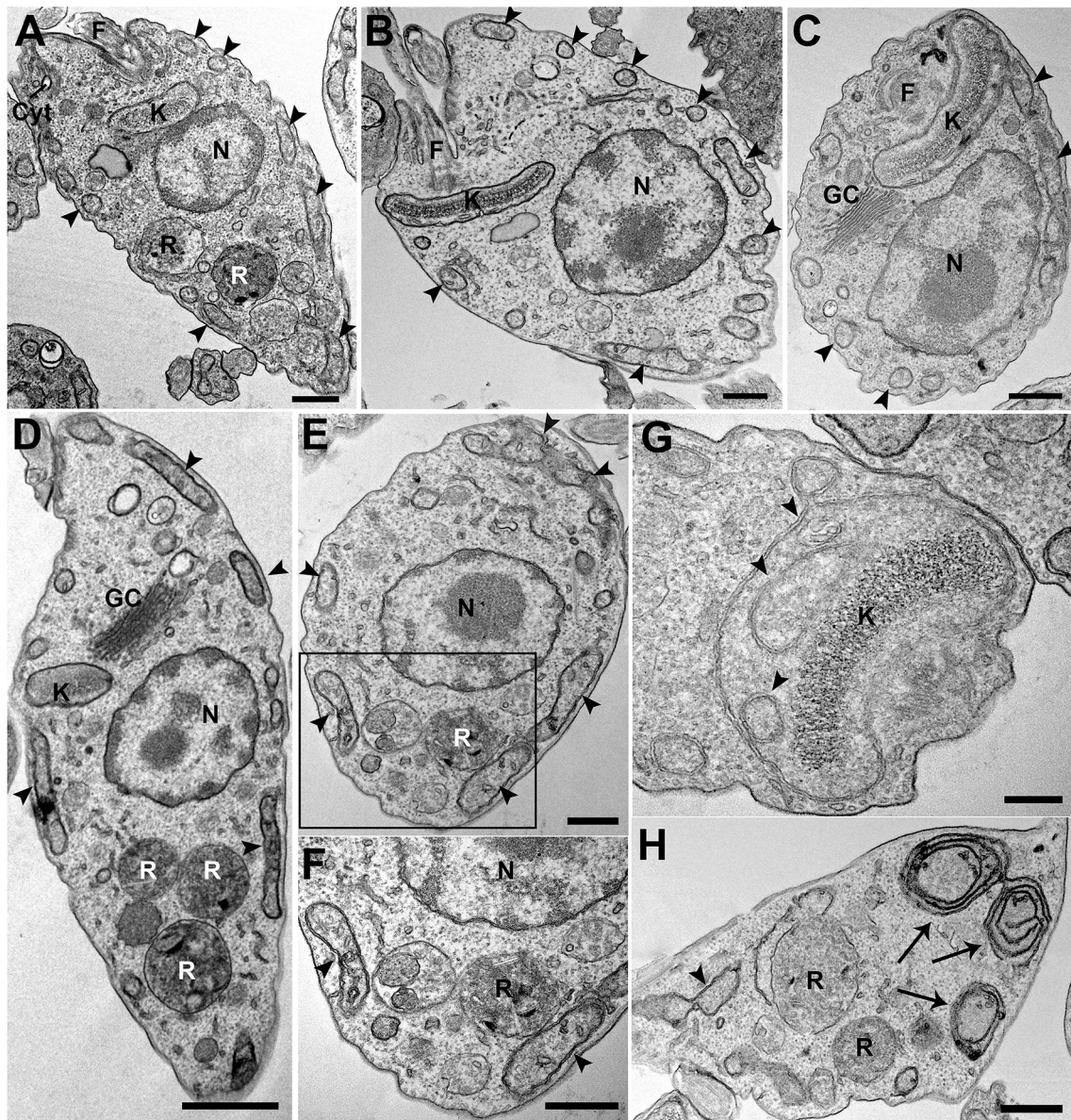


FIGURE 5 | Ultrastructural changes in TcIT-superepressing parasites. pTEX-Ø and epimastigotes overexpressing TcIT were processed and observed by transmission electron microscopy. (A–C) Control pTEX-Ø epimastigotes show normal morphology of major cellular organelles: kinetoplast (K), nucleus (N), Golgi complex (GC), cytosome–cytopharynx complex (Cyt), and reservosomes (R). Mitochondrial branches are seen all along the cell body, juxtaposing the cell membrane (arrowheads), F (flagellum). (D–H) Epimastigotes overexpressing TcIT. (D) Mutants also present normal organelle morphology and positioning when compared with controls, except for the mitochondria. (E) Swollen mitochondrial branches (arrowheads) are observed in overexpressing parasites. (F) Increased magnification of the area delimited by the rectangle in (E) shows an increase in mitochondrial cristae and inner membrane vesiculation (arrowheads). (G) Mitochondrial inner vesiculation was observed at the kinetoplast (K) region (arrowheads). (H) Areas of mitochondrial inner membrane disorganization were also observed (arrows). Bars: (A–C, E, F, H) 500 nm; (D) 1 µm; (G) 200 nm.

transporter favors in-vitro differentiation. The cytometric analysis (Figure 6C) using the 1G7 antibody against the marker of metacyclogenesis GP90 demonstrated, after the 4th day in TAU, a higher number of GP90(+) cells in parasites transfected with TcIT than in those transfected with pTEX-Ø (54.5% vs. 46%). In contrast, the number of GP90(–) cells was higher in pTEX-Ø parasites (54% vs. 46.4%). The hypothesis that TcIT overexpression stimulates metacyclogenesis is also supported by

the fact that trypomastigotes have higher levels of TcIT mRNA than epimastigote forms (Figure 6D). In fact, LLC-MK2 cells infected with metacyclic trypomastigotes derived from epimastigotes pTEX-TcIT present a higher replication rate of amastigotes (parasites/LLC-MK2 cells) when compared with those LLC-MK2 cells infected with pTEX-Ø metacyclics (Figure 6E). Representative images of the amastigote forms inside LLC-MK2 cells are shown in Figure 6F.

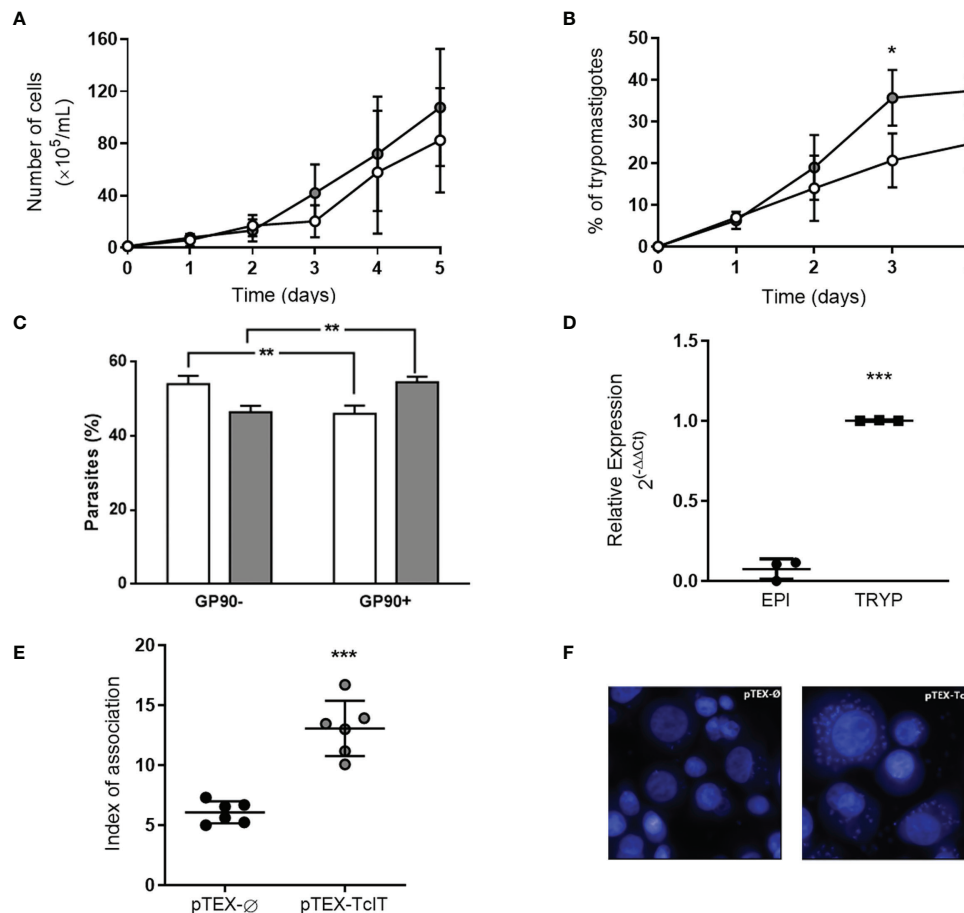


FIGURE 6 | TcIT overexpression influences *T. cruzi* differentiation to trypomastigotes, but not proliferation. **(A)** *T. cruzi* epimastigotes transfected with pTEX-Ø empty vector (white circles) or pTEX-TcIT plasmid (gray circles) proliferation. Epimastigotes of *T. cruzi* at mid-log phase were harvested, washed twice, seeded into fresh medium, and grown for the indicated times in regular medium under the antibiotic pressure of G418 (50 mg/ml) ($n = 6$). **(B)** Transfected epimastigotes with empty vector pTEX-Ø (white circles) or pTEX-TcIT (gray circles) were exposed to *in-vitro* differentiation medium TAU. Each day, epimastigotes and trypomastigotes were differentially counted to determine the percentage of trypomastigotes in culture; * $P < 0.05$ ($n = 4$). **(C)** Cytometric analysis of parasites after the 4th day in TAU **(B)** using the 1G7 antibody against the marker of metacyclogenesis GP90. **(D)** Quantification of the TcIT transcript in *T. cruzi* epimastigotes (EPI) or trypomastigotes (TRYP). Quantitative PCR used 100 ng cDNA from mutants, as indicated on the abscissa; *** $P < 0.001$ ($n = 3$). **(E)** Index of association estimated by total number of intracellular parasites per infected LLC-MK2 cells. *** $P < 0.001$ ($n = 6$). **(F)** Representative images of pTEX-Ø or pTEX-TcIT parasites infection in LLC-MK2 cells, quantitatively compared in **(E)**. Except for **(C)**, using Student's *t*-test assessed the differences between mean values. In **(A, B)**, the differences were assessed by comparing time-matched determinations. In **(C)**, the comparisons were performed by using two-way ANOVA. ** $P < 0.01$ ($n = 3$).

4 DISCUSSION

Trypanosoma cruzi has a high requirement for Fe, mobilizing heme or non-heme Fe, for both *in-vitro* proliferation of epimastigotes and *in-vivo* proliferation in mice (Lalonde and Holbein, 1984). In mammalian cells, Fe is complexed with proteins, e.g., ferritin, which has the highest number of bound Fe per molecule of protein; hemoglobin, which carries the largest amount of Fe in the body; lactoferrin, mainly found in mucosae; and finally, transferrin (Tf), a seric protein responsible for transporting Fe to all cells (Weinberg, 2009). The identification of a Tf receptor in *T. cruzi* amastigote forms (Lima and Villalta, 1990) and the fact that these forms can take up human transferrin directly by the endocytosis pathway *via* the cytostome (Porto-Carreiro et al.,

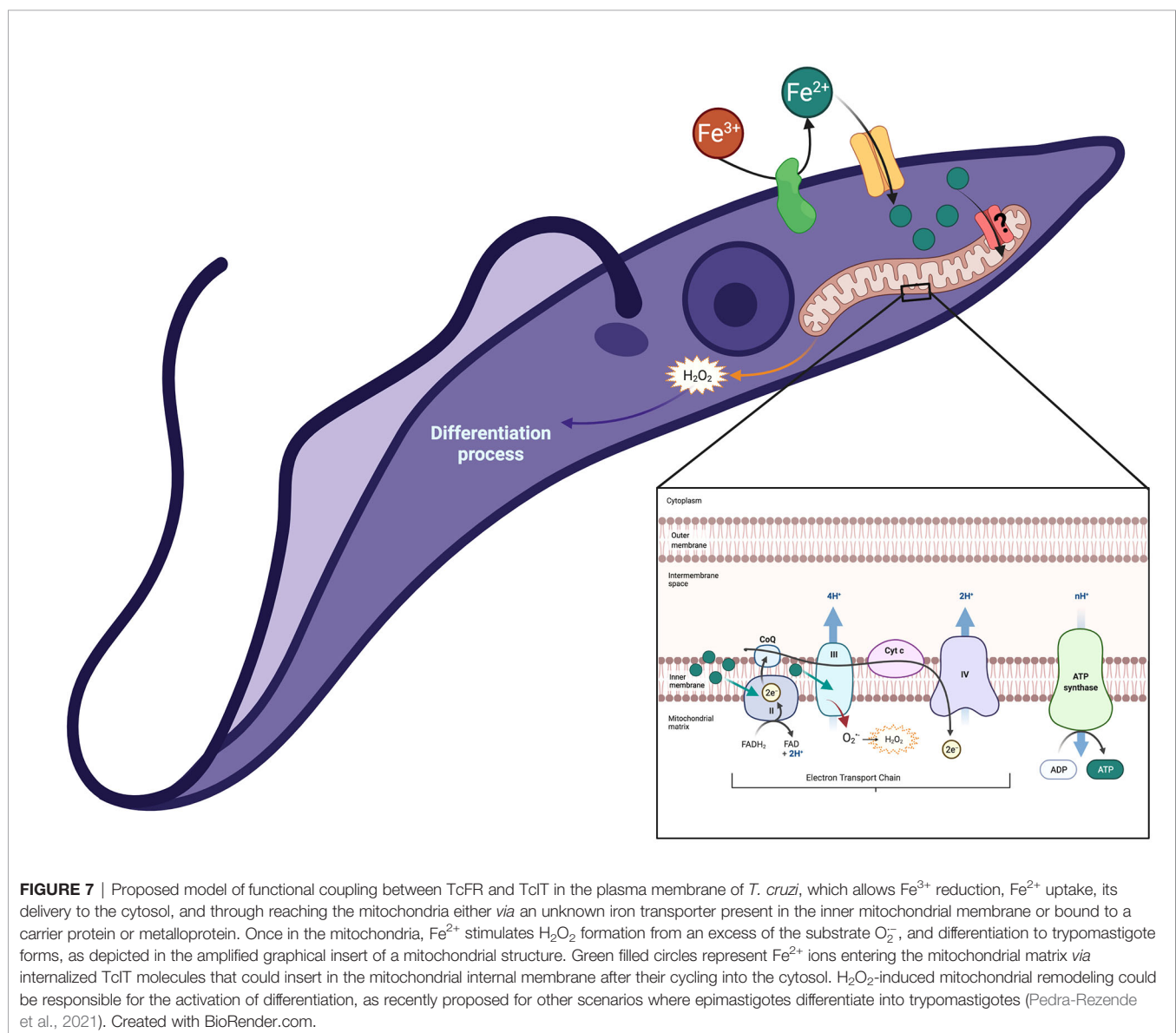
2000; Rocha et al., 2010) indicate that *T. cruzi* amastigotes can use Tf as the major Fe source. *Trypanosoma cruzi* may take up heme through an ABC transporter (Lara et al., 2007; Cupello et al., 2011). Before heme can be utilized, its degradation by heme oxidase (HO) is necessary; however, the *HO* gene is absent in the *T. cruzi* genome (El-Sayed et al., 2005), limiting Fe removal from the heme ring (Taylor and Kelly, 2010). In this way, reducing Fe^{3+} to Fe^{2+} releases the ion from the extracellular heme, thus facilitating Fe uptake by heavy-metal transporters, as proposed for *Leishmania* parasites (Ortiz-Estrada et al., 2012). Identifying Fe-reductase TcFR in *T. cruzi* plasma membranes (Dick et al., 2020) opened up the possibility of the same mechanism being present in the parasite.

Ferric ion reduction to Fe^{2+} by Fe-reductases is usually coupled to Fe^{2+} transport in bacteria, yeasts, plants, and animal cells (Huynh

and Andrews, 2008). The identification of an Fe-reductase in *L. chagasi* (Wilson et al., 2002), *L. amazonensis* (Flannery et al., 2011), and recently, in *T. cruzi* (Dick et al., 2020) strongly suggests that trypanosomatids have Fe^{2+} transport systems. In this way, the identification of a putative Fe transporter in the *T. cruzi* genome, TcIT (TriTrypDB: TCDM_06386) modeled in **Figure 1A**, which is homologous to the newly described Fe transporter in *L. amazonensis*, LIT (TritypDB: LmjF.31.3060), and the *Arabidopsis thaliana* Fe transporter IRT1 (GenBank: AAB01678.1), supports this idea. Indeed, analysis of the predicted amino-acid sequence shows eight transmembrane domains, as shown for TcIT, LIT, and IRT1 sequences (**Figure 1B**). Both *Leishmania* LIT1 and *Arabidopsis* IRT1 are Fe^{2+} transporters from the ZIP family, and the amino- and carboxyl-terminal ends are located on the extracellular side of the plasma membrane. By alignment analysis, we found that, as in LIT1 and IRT1, *T. cruzi* TcIT has the same

features. The most conserved portion of ZIP family proteins is also present; the amphipathic helix of the putative transmembrane domain IV contains a His residue and an adjacent semipolar Ser residue, essential components for heavy-metal binding sites (Guerinot, 2000; Huynh et al., 2006). Thus, TcIT is the first member of the ZIP family to be identified in *T. cruzi*.

A wide range of biological processes, such as electron and O_2 transport and DNA synthesis, depend on Fe content, making Fe homeostasis an ensemble of processes that are essential for all cells, including pathogenic protozoa (Nadadur et al., 2008; Ortiz-Estrada et al., 2012). Upregulation of TcIT mRNA levels in response to Fe depletion (**Figure 2C**) indicated that the parasite has a compensatory mechanism, although insufficient for sustaining the Fe requirement (**Figure 2D**), possibly because the Fe content is very low in IDM. Low O_2 consumption in parasites maintained in Fe-depleted medium (**Figure 2F**) suggests that



Fe depletion arrests mitochondrial function. Plasma membrane immunolocalization (**Figure 3A**) and enrichment in the plasma-membrane fraction (**Figure 3D**) also strongly suggest that TcIT is responsible for Fe uptake in *T. cruzi* epimastigotes, ensuring differentiation to infective trypomastigotes. TcIT could be translocated to the inner mitochondrial membrane *via* an unknown mechanism involving membrane fusion despite the evident immunolocalization in the parasite plasma membrane. In addition, Fe²⁺ could reach the mitochondria through an unknown iron transporter present in the inner mitochondrial membrane or bound to a carrier protein or metalloprotein. This could be one of the ways to allow Fe to interact with the mitochondrial complexes, thus stimulating respiration and H₂O₂ formation.

Parasites overexpressing TcIT (**Figure 6D**) have a higher capacity for differentiating into trypomastigotes *in vitro* (**Figures 6B, C**). These forms express proteins (such as gp83 glycoprotein, cruzipain, oligopeptidase B, and P21) that are involved with host-cell invasion (Burleigh and Andrews, 1998; Yoshida and Cortez, 2008; da Silva et al., 2009; Martins et al., 2020). In this regard, and as an example of maintenance of chronic infection, it is of interest that P21 was recently demonstrated to be important for intracellular confinement of *T. cruzi* amastigotes (Martins et al., 2020). In addition, parasites that overexpress TcIT display an increase in the average number of intracellular parasites per LLC-MK2-infected cells after 48 h post-infection (**Figures 6E, F**), demonstrating the importance of Fe transporter in increasing the rate of amastigote replication.

In *Leishmania*, upregulation of LIT1 expression activates promastigote to amastigote differentiation, mainly *via* Fe-SOD activity. Fe-SOD activity converts O₂⁻ to H₂O₂, a molecule that triggers the generation of infective amastigotes (Mittra et al., 2013). Although H₂O₂ production is very high in parasites that overexpress TcIT (**Figure 4D**), Fe-SOD activity is not modulated by the presence of the gene (**Figure 4E**), indicating that elevated levels of H₂O₂ are the result of accelerated dismutation of an elevated O₂⁻ formation. In *T. cruzi*, the significant increase in H₂O₂ production seems to be due to mitochondrial activity (**Figures 4A, B**). Indeed, the mitochondria were the only organelles where significant changes were observed (**Figure 5**). We propose that the 200% increase in H₂O₂ could be key for *T. cruzi* infectivity and virulence, as demonstrated by the persistence of amastigotes in macrophages of infected mice (Paiva et al., 2012). Since heme induces epimastigote proliferation *via* mitochondrial ROS production without altering ATP production (Nogueira et al., 2017), it may be that TcIT overexpression induces epimastigote to trypomastigote differentiation through a different signaling pathway. Therefore, we conclude that this work presents evidence regarding the possible participation of TcIT in Fe metabolism, proliferation/differentiation processes, infectivity virulence, and maintenance of *T. cruzi* infection. Since the lack of correlation between the increase of TcIT expression in IDM and the Fe content in the parasite raises the question of whether the protein is the only mechanism responsible for Fe uptake in *T. cruzi*, further transport or generation and analysis of mutant cell lines need to be performed in the future.

Finally, **Figure 7** presents a hypothetical mechanistic model for the functional coupling between TcFR (Dick et al., 2020) and

TcIT for Fe²⁺ uptake across the plasma membrane of *T. cruzi*, which increases mitochondrial H₂O₂ formation and stimulates parasite differentiation, thus allowing invasion of the host cells.

DATA AVAILABILITY STATEMENT

The original contributions presented in the study are included in the article/Supplementary Material. Further inquiries can be directed to the corresponding author.

AUTHOR CONTRIBUTIONS

CD conceived, designed, and performed the experiments; analyzed the data; and wrote the manuscript. NR-M, AD-S, LC-K, and CA contributed to the experimental process. CA and NC-S analyzed the data and revised the manuscript. JM-F and AV conceived the experiments, analyzed the data, and revised the manuscript. All authors contributed to the article and approved the submitted version.

FUNDING

This research was funded by the Brazilian National Research Council/CNPq to CD (grant Young Talented People # 300338/2015-5), JM-F (grant # 401134/2014-8), and AV (grant # 307605/2015-9). The support of the Rio de Janeiro State Research Foundation/FAPERJ to CD (grant Grade 10 for Post-doctoral Studies # E-26/202.359/2017), JM-F (grant # E-26/201.300/2014), and AV (grant # E-26/2012.963/2017) is also acknowledged.

ACKNOWLEDGMENTS

The authors are grateful to Dr. José Franco da Silveira for the generous gift of the polyclonal antibody raised in his laboratory (Federal University of São Paulo) against the *T. cruzi* surface membrane protein. The authors recognize Fernando Pereira de Almeida, Renata Travassos de Lima and Rosângela Rosa de Araújo for their excellent technical assistance. The authors also thank BioMedES (United Kingdom) for the preparation of the final draft. The English correction of the revised version by Dr. Martha Sorenson is also acknowledged.

SUPPLEMENTARY MATERIAL

The Supplementary Material for this article can be found online at: <https://www.frontiersin.org/articles/10.3389/fcimb.2021.789401/full#supplementary-material>

Supplementary Figure 1 | (A) 5'-nucleotidase activity in fractions of pTEX-Ø (n = 4). **(B)** 5'-nucleotidase activity in fractions of pTEX-TcIT (n = 4). **(C)** Fe-reductase activity in fractions of pTEX-Ø (n = 3). **(D)** Fe-reductase activity in fractions of pTEX-TcIT (n = 3). HG, total homogenate; TM, total membranes; PM, plasma membranes; C, cytosol. In all cases, differences were assayed by one-way ANOVA following by Tukey's test within each panel. NS, not significant; **P < 0.01; ***P < 0.001.

REFERENCES

- Atkins, P., and de Paula, J. (2006). "Thermodynamics of Ion and Electron Transport," in *Physical Chemistry for the Life Sciences* (Oxford, UK: Oxford University Press), 200–236.
- Bayer-Santos, E., Cunha-e-Silva, N. L., Yoshida, N., and Franco da Silveira, J. (2013). Expression and Cellular Trafficking of GP82 and GP90 Glycoproteins During *Trypanosoma Cruzi* Metacyclogenesis. *Parasit Vectors*. 6, 127. doi: 10.1186/1756-3305-6-127
- Burleigh, B. A., and Andrews, N. W. (1998). Signaling and Host Cell Invasion by *Trypanosoma Cruzi*. *Curr. Opin. Microbiol.* 1, 461–465. doi: 10.1016/s1369-5274(98)80066-0
- Carvalho-Kelly, L. F., Pralon, C. F., Rocco-Machado, N., Nascimento, M. T., Carvalho-de-Araújo, A. D., and Meyer-Fernandes, J. R. (2020). *Acanthamoeba castellanii* Phosphate Transporter (AcPHS) Is Important to Maintain Inorganic Phosphate Influx and Is Related to Trophozoite Metabolic Processes. *J. Bioenerg. Biomembr.* 52, 93–102. doi: 10.1007/s10863-020-09822-y
- Contreras, V. T., Salles, J. M., Thomas, N., Morel, C. M., and Goldenberg, S. (1985). *In Vitro* Differentiation of *Trypanosoma cruzi* Under Chemically Defined Conditions. *Mol. Biochem. Parasitol.* 16, 315–327. doi: 10.1016/0166-6851(85)90073-8
- Cruz-Saavedra, L., Muñoz, M., León, C., Patarroyo, M. A., Arevalo, G., Pavia, P., et al. (2017). Purification of *Trypanosoma cruzi* Metacyclic Trypomastigotes by Ion Exchange Chromatography in Sepharose-DEAE, a Novel Methodology for Host-Pathogen Interaction Studies. *J. Microbiol. Methods* 142, 27–32. doi: 10.1016/j.mimet.2017.08.021
- Cupello, M. P., Souza, C. F., Buchensky, C., Soares, J. B., Laranja, G. A., Coelho, M. G., et al. (2011). The Heme Uptake Process in *Trypanosoma cruzi* Epimastigotes Is Inhibited by Heme Analogues and by Inhibitors of ABC Transporters. *Acta Trop.* 120, 211–218. doi: 10.1016/j.actatropica.2011.08.011
- da Silva, C. V., Kawashita, S. Y., Probst, C. M., Dallagiovanna, B., Cruz, M. C., da Silva, E. A., et al. (1984). Characterization of a 21kDa Protein from *Trypanosoma Cruzi* Associated With Mammalian Cell Invasion. *Microbes Infect.* 11, 563–570. doi: 10.1016/j.micinf.2009.03.007
- de Souza, W. (1984). Cell Biology of *Trypanosoma cruzi*. *Int. Rev. Cytol.* 86, 197–283. doi: 10.1016/s0074-7696(08)60180-1
- Dick, C. F., Guimarães, L. M., Carvalho-Kelly, L. F., Cortes, A. L., Morcillo, L. S. L., Sampaio, L. S., et al. (2020). A Ferric Reductase of *Trypanosoma cruzi* (TcFR) Is Involved in Iron Metabolism in the Parasite. *Exp. Parasitol.* 217, 107962. doi: 10.1016/j.exppara.2020.107962
- Dos-Santos, A. L. A., Dick, C. F., Lopes, L. R., Rocco-Machado, N., Muzi-Filho, H., Freitas-Mesquita, A. L., et al. (2019). Tartrate-Resistant Phosphatase Type 5 in *Trypanosoma cruzi* Is Important for Resistance to Oxidative Stress Promoted by Hydrogen Peroxide. *Exp. Parasitol.* 205, 107748. doi: 10.1016/j.exppara.2019.107748
- El-Sayed, N. M., Myler, P. J., Bartholomeu, D. C., Nilsson, D., Aggarwal, G., Tran, A. N., et al. (2005). The Genome Sequence of *Trypanosoma Cruzi*, Etiologic Agent of Chagas Disease. *Science* 309, 409–415. doi: 10.1126/science.1112631
- Felsenstein, J. (1985). Confidence Limits on Phylogenies: An Approach Using the Bootstrap. *Evolution* 39, 783–791. doi: 10.1111/j.1558-5646.1985.tb00420.x
- Flannery, A. R., Huynh, C., Mittra, B., Mortara, R. A., and Andrews, N. W. (2011). LFR1 Ferric Iron Reductase of *Leishmania amazonensis* Is Essential for the Generation of Infective Parasite Forms. *J. Biol. Chem.* 286, 23266–23279. doi: 10.1074/jbc.M111.229674
- Geslin, C., Llanos, J., Prieur, D., and Jeanthon, C. (2001). The Manganese and Iron Superoxide Dismutases Protect *Escherichia Coli* From Heavy Metal Toxicity. *Res. Microbiol.* 152, 901–905. doi: 10.1016/s0923-2508(01)01273-6
- Gottlieb, E. M., and Dwyer, D. M. (1983). Evidence for Distinct 5'- and 3'-Nucleotidase Activities in the Surface Membrane Fraction of *Leishmania donovani* Promastigotes. *Mol. Biochem. Parasitol.* 7, 303–317. doi: 10.1016/0166-6851(83)90013-0
- Grisard, E. C., Teixeira, S. M., de Almeida, L. G., Stoco, P. H., Gerber, A. L., Talavera-López, C., et al. (2014). *Trypanosoma cruzi* Clone Dm28c Draft Genome Sequence. *Genome Announc.* 2, e01114–e01113. doi: 10.1128/genomeA.01114-13
- Guerinot, M. L. (2000). The ZIP Family of Metal Transporters. *Biochim. Biophys. Acta* 1465, 190–198. doi: 10.1016/s0005-2736(00)00138-3
- Hofmann, K., and Stoffel, W. (1993). TMbase-A Database of Membrane Spanning Proteins Segments. *Biol. Chem. Hoppe Seyler* 347, 166.
- Huynh, C., and Andrews, N. W. (2008). Iron Acquisition Within Host Cells and the Pathogenicity of *Leishmania*. *Cell. Microbiol.* 10, 293–300. doi: 10.1111/j.1462-5822.2007.01095.x
- Huynh, C., Sacks, D. L., and Andrews, N. W. (2006). A *Leishmania amazonensis* ZIP Family Iron Transporter Is Essential for Parasite Replication Within Macrophage Phagolysosomes. *J. Exp. Med.* 203, 2363–2375. doi: 10.1084/jem.20060559
- Jacques, J., Andrews, N. W., and Huynh, C. (2010). Functional Characterization of LIT1, the *Leishmania amazonensis* Ferrous Iron Transport. *Mol. Biochem. Parasitol.* 170, 28–36. doi: 10.1016/j.molbiopara.2009.12.003
- Kelley, L. A., and Sternberg, M. J. E. (2009). Protein Structure Prediction on the Web: A Case Study Using the Phyre Server. *Nat. Protoc.* 4, 363–371. doi: 10.1038/nprot.2009.2
- Kelly, J. M., Ward, H. M., Miles, M. A., and Kendall, G. (1992). A Shuttle Vector Which Facilitates the Expression of Transfected Genes in *Trypanosoma cruzi* and *Leishmania*. *Nucleic Acids Res.* 20, 3963–3969. doi: 10.1093/nar/20.15.3963
- Koeller, C. M., van der Wel, H., Feasley, C. L., Abreu, F., da Rocha, J. D., Montalvão, F., et al. (2014). Golgi UDP-GlcNAc:polypeptide O- α -N-Acetyl-D-Glucosaminyltransferase 2 (TcOGNT2) Regulates Trypomastigote Production and Function in *Trypanosoma cruzi*. *Eukaryot. Cell* 13, 1312–1327. doi: 10.1128/EC.00165-14
- Krumova, K., and Cosa, G. (2016). "Overview of Reactive Oxygen Species", in *Singlet Oxygen: Appl. Biosci. Nanosciences* (London, UK: Royal Society of Chemistry), 1–21. doi: 10.1039/9781782622208
- Kumar, S., Stecher, G., and Tamura, K. (2016). MEGA7: Molecular Evolutionary Genetics Analysis Version 7.0 for Bigger Datasets. *Mol. Biol. Evol.* 33, 1870–1874. doi: 10.1093/molbev/msw054
- Lalonde, R. G., and Holbein, B. E. (1984). Role of Iron in *Trypanosoma Cruzi* Infection of Mice. *J. Clin. Invest.* 73, 470–476. doi: 10.1172/JCI111233
- Lara, F. A., Sant'anna, C., Lemos, D., Laranja, G. A., Coelho, M. G., Reis Salles, I., et al. (2007). Heme Requirement and Intracellular Trafficking in *Trypanosoma cruzi* Epimastigotes. *Biochem. Biophys. Res. Commun.* 355, 16–22. doi: 10.1016/j.bbrc.2006.12.238
- Lima, M. F., and Villalta, F. (1990). *Trypanosoma cruzi* Receptors for Human Transferrin and Their Role. *Mol. Biochem. Parasitol.* 38, 245–252. doi: 10.1016/0166-6851(90)90027-j
- Lowry, O. H., Rosebrough, N. J., Farr, A. L., and Randall, R. J. (1951). Protein Measurement With the Folin Phenol Reagent. *J. Biol. Chem.* 193, 265–275. doi: 10.1016/S0021-9258(19)52451-6
- Martins, F. A., Dos Santos, M. A., Santos, J. G., da Silva, A. A., Borges, B. C., da Costa, M. S., et al. (2020). The Recombinant Form of *Trypanosoma cruzi* P21 Controls Infection by Modulating Host Immune Response. *Front. Immunol.* 11, 1010. doi: 10.3389/fimmu.2020.01010
- Martins, N. O., Souza, R. T., Cordero, E. M., Maldonado, D. C., Cortez, C., Marini, M. M., et al. (2015). Molecular Characterization of a Novel Family of *Trypanosoma cruzi* Surface Membrane Proteins (TcSMP) Involved in Mammalian Host Cell Invasion. *PLoS Negl. Trop. Dis.* 13, e0004216. doi: 10.1371/journal.pntd.0004216
- Mittra, B., Cortez, M., Haydock, A., Ramasamy, G., Myler, P. J., and Andrews, N. W. (2013). Iron Uptake Controls the Generation of *Leishmania* Infective Forms Through Regulation of ROS Levels. *J. Exp. Med.* 210, 401–416. doi: 10.1084/jem.20121368
- Nadadur, S. S., Srirama, K., and Mudipalli, A. (2008). Iron Transport & Homeostasis Mechanisms: Their Role in Health & Disease. *Indian J. Med. Res.* 128, 533–544.
- Nogueira, N. P., Saraiva, F. M. S., Oliveira, M. P., Mendonça, A. P. M., Inacio, J. D. F., Almeida-Amaral, E. E., et al. (2017). Heme Modulates *Trypanosoma cruzi* Bioenergetics Inducing Mitochondrial ROS Production. *Free Radic. Biol. Med.* 108, 183–191. doi: 10.1016/j.freeradbiomed.2017.03.027
- Ortiz-Estrada, G., Luna-Castro, S., Piña-Vázquez, C., Samaniego-Barrón, L., León-Sicairens, N., Serrano-Luna, J., et al. (2012). Iron-Saturated Lactoferrin and Pathogenic Protozoa: Could This Protein be an Iron Source for Their Parasitic Style of Life? *Future Microbiol.* 7, 149–164. doi: 10.2217/fmb.11.140
- Paiva, C. N., Feijó, D. F., Dutra, F. F., Carneiro, V. C., Freitas, G. B., Alves, L. S., et al. (2012). Oxidative Stress Fuels *Trypanosoma cruzi* Infection in Mice. *J. Clin. Invest.* 122, 2531–2542. doi: 10.1172/JCI58525

- Pedra-Rezende, Y., Fernandes, M. C., Mesquita-Rodrigues, C., Stiebler, R., Bombaça, A. C. S., Pinho, N., et al. (2021). Starvation and pH Stress Conditions Induced Mitochondrial Dysfunction, ROS Production and Autophagy in *Trypanosoma cruzi* Epimastigotes. *Biochim. Biophys. Acta Mol. Basis Dis.* 1867, 166028. doi: 10.1016/j.bbdis.2020.166028
- Pinheiro, C. M., Martins-Duarte, E. S., Ferraro, R. B., Fonseca-de-Souza, A. L., Gomes, M. T., Lopes, A. H., et al. (2006). *Leishmania amazonensis*: Biological and Biochemical Characterization of Ecto-Nucleoside Triphosphate Diphosphohydrolase Activities. *Exp. Parasitol.* 114, 16–25. doi: 10.1016/j.exppara.2006.02.007
- Porto-Carreiro, I., Attias, M. A., Miranda, K., de Souza, W., and Cunha-e-Silva, N. (2000). *Trypanosoma Cruzi* Epimastigote Endocytic Pathway: Cargo Enters the Cytostome and Passes Through an Early Endosomal Network Before Storage in Reservoirs. *Eur. J. Cell. Biol.* 70, 858–869. doi: 10.1078/0171-9335-00112
- Rocha, G. M., Seabra, S. H., Miranda, K. R., Cunha-e-Silva, N., Carvalho, T. M. U., and de Souza, W. (2010). Attachment of Flagellum to the Cell Body Is Important to the Kinetics of Transferrin Uptake by *Trypanosoma cruzi*. *Parasitol. Int.* 59, 629–633. doi: 10.1016/j.parint.2010.07.005
- Saitou, N., and Nei, M. (1987). The Neighbor-Joining Method: A New Method for Reconstructing Phylogenetic Trees. *Mol. Biol. Evol.* 4, 406–425. doi: 10.1093/oxfordjournals.molbev.a040454
- Sedláček, V., van Spanning, R. J., and Kucera, I. (2009). Characterization of the Quinone Reductase Activity of the Ferric Reductase B Protein From *Paracoccus denitrificans*. *Arch. Biochem. Biophys.* 483, 29–36. doi: 10.1016/j.abb.2008.12.016
- Sutak, R., Lesuisse, E., Tachezy, J., and Richardson, D. (2008). Crusade for Iron: Iron Uptake in Unicellular Eukaryotes and Its Significance for Virulence. *Trends Microbiol.* 16, 261–268. doi: 10.1016/j.tim.2008.03.005
- Tainer, J., Getzoff, E., Richardson, J., and Richardson, D. (1983). Structure and Mechanism of Copper, Zinc Superoxide Dismutase. *Nature* 306, 284–287. doi: 10.1038/306284a0
- Taylor, M. C., and Kelly, J. M. (2010). Iron Metabolism in Trypanosomatids, and Its Crucial Role in Infection. *Parasitology* 137, 899–917. doi: 10.1017/S0031182009991880
- Vert, G., Grotz, N., Dédaldéchamp, F., Gaymard, F., Guerinot, M. L., Briat, J. F., et al. (2002). IRT1, an *Arabidopsis* Transporter Essential for Iron Uptake From the Soil and for Plant Growth. *Plant Cell.* 14, 1223–1233. doi: 10.1105/tpc.001388
- Weinberg, E. D. (2009). Iron Availability and Infection. *Biochim. Biophys. Acta* 1790, 600–605. doi: 10.1016/j.bbagen.2008.07.002
- Wilkinson, S. R., Prathalingam, S. R., Taylor, M. C., Ahmed, A., Horn, D., and Kelly, J. M. (2006). Functional Characterisation of the Iron Superoxide Dismutase Gene Repertoire in *Trypanosoma brucei*. *Free Radic. Biol. Med.* 40, 198–209. doi: 10.1016/j.freeradbiomed.2005.06.022
- Willingham, M. C., and Rutherford, A. V. (1984). The Use of Osmium-Thiocarbonylhydrazide-Osmium (OTO) and Ferrocyanide-Reduced Osmium Methods to Enhance Membrane Contrast and Preservation in Cultured Cells. *J. Histochem. Cytochem.* 32, 455–460. doi: 10.1177/32.4.6323574
- Wilson, M. E., Lewis, T. S., Miller, M. A., McCormick, M. L., and Britigan, B. E. (2002). *Leishmania Chagasi*: Uptake of Iron Bound to Lactoferrin or Transferrin Requires an Iron Reductase. *Exp. Parasitol.* 100, 196–207. doi: 10.1016/s0014-4894(02)00018-8
- Winterbourn, C. C., Hawkins, R. E., Brian, M., and Carrell, R. W. (1975). The Estimation of Red Cell Superoxide Dismutase Activity. *J. Lab. Clin. Med.* 85, 337–341.
- Yoshida, N., and Cortez, M. (2008). *Trypanosoma cruzi*: Parasite and Host Cell Signaling During the Invasion Process. *Subcell. Biochem.* 47, 82–91. doi: 10.1007/978-0-387-78267-6_6
- Zingales, B., Carniol, C., Abramhamssohn, P. A., and Colli, W. (1979). Purification of an Adenylyl Cyclase-Containing Plasma Membrane Fraction from *Trypanosoma Cruzi*. *Biochim. Biophys. Acta* 550, 233–244. doi: 10.1016/0005-2736(79)90210-4

Conflict of Interest: The authors declare that the research was conducted in the absence of any commercial or financial relationships that could be construed as a potential conflict of interest.

Publisher's Note: All claims expressed in this article are solely those of the authors and do not necessarily represent those of their affiliated organizations, or those of the publisher, the editors and the reviewers. Any product that may be evaluated in this article, or claim that may be made by its manufacturer, is not guaranteed or endorsed by the publisher.

Copyright © 2022 Dick, Rocco-Machado, Dos-Santos, Carvalho-Kelly, Alcantara, Cunha-E-Silva, Meyer-Fernandes and Vieyra. This is an open-access article distributed under the terms of the Creative Commons Attribution License (CC BY). The use, distribution or reproduction in other forums is permitted, provided the original author(s) and the copyright owner(s) are credited and that the original publication in this journal is cited, in accordance with accepted academic practice. No use, distribution or reproduction is permitted which does not comply with these terms.



OPEN ACCESS

Edited by:

Maria E. Francia,
Institut Pasteur de Montevideo,
Uruguay

Reviewed by:

Santuza Maria Ribeiro Teixeira,
Federal University of Minas Gerais,
Brazil
Beatriz Simonsen Stolf,
University of São Paulo, Brazil

***Correspondence:**

Claudio Vieira da Silva
silva_cv@yahoo.com.br
José Franco da Silveira
jose.franco@unifesp.br

[†]Present address:

Éden Ramalho Ferreira,
York Biomedical Research Institute &
Department of Biology, University of
York, York, United Kingdom

Specialty section:

This article was submitted to
Parasite and Host,
a section of the journal
Frontiers in Cellular and
Infection Microbiology

Received: 21 October 2021

Accepted: 25 January 2022

Published: 18 February 2022

Citation:

Teixeira TL, Chiurillo MA, Lander N,
Rodrigues CC, Onofre TS, Ferreira ÉR,
Yonamine CM, Santos JdG,
Mortara RA, da Silva CV and Silveira JF
(2022) Ablation of the P21 Gene of
Trypanosoma cruzi Provides Evidence
of P21 as a Mediator in the Control of
Epimastigote and Intracellular
Amastigote Replication.
Front. Cell. Infect. Microbiol. 12:799668.
doi: 10.3389/fcimb.2022.799668

Ablation of the *P21* Gene of *Trypanosoma cruzi* Provides Evidence of P21 as a Mediator in the Control of Epimastigote and Intracellular Amastigote Replication

Thaise Lara Teixeira¹, Miguel Angel Chiurillo², Noelia Lander²,
Cassiano Costa Rodrigues³, Thiago Souza Onofre¹, Éden Ramalho Ferreira^{1†},
Camila Miyagui Yonamine¹, Júlia de Gouveia Santos³, Renato Arruda Mortara¹,
Claudio Vieira da Silva^{3*} and José Franco da Silveira^{1*}

¹ Departamento de Microbiologia, Imunologia e Parasitologia, Escola Paulista de Medicina, Universidade Federal de São Paulo, São Paulo, Brazil, ² Department of Biological Sciences, University of Cincinnati, Cincinnati, OH, United States,

³ Laboratório de Tripanosomatídeos, Universidade Federal de Uberlândia, Uberlândia, Brazil

P21 is an immunomodulatory protein expressed throughout the life cycle of *Trypanosoma cruzi*, the etiologic agent of Chagas disease. *In vitro* and *in vivo* studies have shown that P21 plays an important role in the invasion of mammalian host cells and establishment of infection in a murine model. P21 functions as a signal transducer, triggering intracellular cascades in host cells and resulting in the remodeling of the actin cytoskeleton and parasite internalization. Furthermore, *in vivo* studies have shown that P21 inhibits angiogenesis, induces inflammation and fibrosis, and regulates intracellular amastigote replication. In this study, we used the CRISPR/Cas9 system for *P21* gene knockout and investigated whether the ablation of *P21* results in changes in the phenotypes associated with this protein. Ablation of *P21* gene resulted in a lower growth rate of epimastigotes and delayed cell cycle progression, accompanied by accumulation of parasites in G1 phase. However, *P21* knockout epimastigotes were viable and able to differentiate into metacyclic trypomastigotes, which are infective to mammalian cells. In comparison with wild-type parasites, *P21* knockout cells showed a reduced cell invasion rate, demonstrating the role of this protein in host cell invasion. However, there was a higher number of intracellular amastigotes per cell, suggesting that P21 is a negative regulator of amastigote proliferation in mammalian cells. Here, for the first time, we demonstrated the direct correlation between P21 and the replication of intracellular amastigotes, which underlies the chronicity of *T. cruzi* infection.

Keywords: *Trypanosoma cruzi*, Chagas disease, chronic phase, P21 protein, CRISPR/Cas9, amastigotes, proliferation, cell cycle

INTRODUCTION

Chagas disease is a potentially life-threatening illness caused by the protozoan parasite *Trypanosoma cruzi*. It has been estimated that 6–7 million people are infected with *T. cruzi* worldwide, mainly in Latin America. Moreover, approximately 10,000 people die from Chagas disease each year, thus constituting an important public health problem (WHO, 2021).

The course of Chagas disease runs from an early phase with clinical symptoms or entirely without them to a latent period (often lasting for decades), which can eventually lead to severe disease. The persistence of the parasite in host tissues could be attributed to the perpetuation of the disease and its chronicity, a stage for which there is no effective treatment. Studies have reported the presence of dormant amastigotes or amastigote nests with a reduced replication rate in host tissues and how the replicative status of these parasites contributes to resistance to benznidazole therapy (Dumoulin and Burleigh, 2018; Sánchez-Valdéz et al., 2018; Ward et al., 2020). However, the mechanisms involved in these processes remain poorly understood.

T. cruzi circulates in the bloodstream of infected humans or reservoir mammals and invades several types of nucleated cells, within which it replicates and remains infectious. *T. cruzi* invasion and replication processes involve interactions between the parasite and host cell molecules in a coevolutionary arms race (Souza et al., 2010; Pech-Canul et al., 2017). In this framework, P21 is a protein secreted by *T. cruzi* and can be detected in the culture supernatant of parasites and in amastigotes nests present in the heart tissue of infected mice (Silva et al., 2009; Martins et al., 2020). Previous studies have shown that P21 is a key protein in the pathogenesis of Chagas disease, inducing the invasion by *T. cruzi* through activation of the chemokine receptor CXCR4, which induces the reorganization of the actin cytoskeleton promoting the parasite internalization (Silva et al., 2009; Rodrigues et al., 2012; Teixeira et al., 2017). Furthermore, recombinant P21 protein was reported to inhibit blood vessel formation by modulating the expression of angiogenesis-associated genes, inducing collagen deposition, leukocyte chemotaxis and reducing the replication of intracellular amastigotes into cardiac tissues, which could favor the permanence of the parasites inside cells and the consequent evasion of host's immune response (Teixeira et al., 2015; Teixeira et al., 2017; Teixeira et al., 2019; Martins et al., 2020). These findings suggest a role for P21 in the chronification process of Chagas disease, in which long-term parasite persistence is determinant of the disease progression (Teixeira et al., 2015; Teixeira et al., 2019; Martins et al., 2020).

The development of molecular tools such as CRISPR/Cas9 (Doudna and Charpentier, 2014) makes it possible to precisely cleave double-stranded DNA using the Cas9 nuclease from a specific gene sequence determined by a single-guide RNA (sgRNA). The repair system allows the precise editing of the target gene, providing a multitude of uses (Knott and Doudna, 2018). For protozoan parasites, the CRISPR/Cas9 system provides the opportunity to gain new insights into parasite biology and allows the development of new approaches to study pathogenesis and parasite-host interactions at the cellular and molecular levels

(Zhang et al., 2014; Sollelis et al., 2015; Lander et al., 2016; Sidik et al., 2016; Lander and Chiurillo, 2019; Young et al., 2019). Several studies have used these tools to deepen the functional understanding of *T. cruzi* and its interaction with host cells (Peng et al., 2014; Lander et al., 2015; Chiurillo et al., 2017; Lander et al., 2017; Costa et al., 2018; Akutsu et al., 2019; Chiurillo et al., 2019; Tavernelli et al., 2019; Chiurillo et al., 2020; Lander et al., 2020; Costa-Silva et al., 2021; Ibarrola-Vannucci et al., 2021; Ramakrishnan et al., 2021).

Here, we generated a *T. cruzi* knockout cell line for the P21 gene using CRISPR/Cas9 and investigated whether P21 deletion changes parasite phenotypes associated with the infection of mammalian host cells and the growth and replication of epimastigotes and intracellular amastigotes. Our results demonstrated the role of P21 in parasite invasion and replication within host cells and showed that CRISPR/Cas9 may be a valuable tool for P21 gene characterization.

MATERIALS AND METHODS

Cell Culture

T. cruzi epimastigotes (Y strain) were grown at 28°C in liver infusion tryptose (LIT) medium supplemented with 10% or 20% fetal bovine serum (FBS; Invitrogen) and manipulated in level 2 biosafety cabinets following institutional safety procedures. To differentiate epimastigotes into metacyclic forms, the epimastigotes were maintained in LIT medium (10% FBS) for 14 days, and metacyclic trypomastigotes were purified as previously described (Teixeira and Yoshida, 1986). Human cervical adenocarcinoma cells (HeLa cells) were cultivated in RPMI 1640 medium (Sigma-Aldrich) supplemented with 10% FBS and an antibiotic solution (10 µg/mL streptomycin, 100 U/mL penicillin, and 40 µg/mL gentamicin) in a humidified atmosphere at 37°C with 5% CO₂.

Determination of Selective Antibiotic Concentration

Wild-type (WT) *T. cruzi* epimastigotes (Y strain) were seeded (2×10^5 cells/well) into a 96-well plate and incubated with 200 µL of LIT medium supplemented with antibiotics (G418, 150–350 µg/mL; blasticidin, 5–25 µg/mL). The parasites were kept at 28°C, and the LIT medium (containing the antibiotics) was replaced as needed. After 10 days of incubation, the number of parasites was determined by counting in a Neubauer chamber.

Gene Knockout by CRISPR/Cas9

To knockout P21 gene we used CRISPR/Cas9-mediated genome editing, as previously described (Lander et al., 2015; Lander et al., 2019). Briefly, the Cas9/pTREX-n vector (Addgene, catalog number: 68708) was used to clone a specific sgRNA sequence to target P21 gene (TriTrypDB ID: TcYC6_0032830), which encodes the *T. cruzi* P21 protein.

Selection of protospacer was performed using EuPaGDT (Eukaryotic Pathogen CRISPR Guide RNA/DNA Design Tool, <http://grna.ctegd.uga.edu/>). This *in silico* analysis allows to

choose a specific protospacer, containing a unique on-target site, and no off-targets in the genome of *T. cruzi* Y C6 TritrypDB-46 release (<https://tritrypdb.org/> dataset). The protospacer sequence is shown in the **Supplementary Material**. Cas9 was expressed in fusion with human influenza virus hemagglutinin (HA) tag, SV40 nuclear localization signal (NLS), and green fluorescent protein (GFP) (Lander et al., 2015). The construct sgRNA/Cas9/pTREX-n, together with DNA donor cassettes for inducing homology-directed repair, was used to transfect *T. cruzi* epimastigotes and disrupt P21 ORF with a blasticidin resistance gene (*Bsd*; gene encoding blasticidin-S-deaminase). In addition, parasites were transfected with Cas9/pTREX-n vector containing Scrambled sgRNA sequence as previously described (Lander et al., 2015). The Scrambled protospacer sequence (GCACTACCAGAGCTAACTCA) does not recognize any target gene in the *T. cruzi* genome. All constructs were confirmed by Sanger sequencing.

The sgRNA was designed to induce a double-stranded break in the *P21* locus sequence using Cas9 nuclease. Chimeric sgRNA was obtained by PCR from plasmid pUC_sgRNA as previously described (Lander et al., 2015; Lander et al., 2019) using the oligonucleotides sgRNA Fw (**Table S1**, primer 1), which included a *Bam*HI restriction site and a 20 nt protospacer region, and sgRNA Rv (**Table S1**, primer 3), a 20 nt sequence that anneals to the sgRNA backbone. Subsequently, this sgRNA (120bp) was cloned into Cas9/pTREX-n (neomycin resistance) through the *Bam*HI site.

To generate a DNA donor cassette containing the *Bsd* gene, the pGEM-*bsd* vector was used. The template for homologous recombination was amplified by PCR using 120 bp ultramers (**Table S1**, primers 4 and 5), consisting of a 100 bp sequence corresponding to regions located upstream or downstream of the Cas9 target site of the *P21* gene, and a 20 bp sequence for annealing on the pGEM-*bsd* vector, which was used as a PCR template (Lander et al., 2015; Lander et al., 2019). PCR was carried out with the following cycling conditions (GoTaq DNA polymerase M7805; Promega): initial denaturation for 2 min at 95°C, followed by 35 cycles for 30 s at 95°C, 20 s at 63°C, and 40 s at 72°C and a final extension for 5 min at 72°C.

Cell Transfection

T. cruzi epimastigotes (Y strain) in the early exponential phase were washed with phosphate-buffered saline (PBS; pH 7.4) and transfected with 25 µg of plasmid (sgRNA/Cas9/pTREX-n) diluted in P3 Primary Cell 4D-Nucleofector (V4XP-3024) solution according to the manufacturer's instructions. The parasites were electroporated with two pulses (EH100 program) delivered by the 4D Nucleofector system (Lonza) (Cordero et al., 2019). Then, the parasites were maintained in LIT medium supplemented with 20% FBS under drug selection (250 µg/mL G418). Transfectant cell lines were sorted based on green fluorescence using the BD FACS Aria II Cell Sorter (BD Biosciences) after selection with G418, cells were electroporated with 25 µg of donor DNA, and selected with blasticidin (25 µg/mL). Next, clonal populations were selected by serial dilutions in 96-well plates. CRISPR mutant cell lines were maintained in LIT medium supplemented with 20% FBS and maintained under

selection with 250 µg/mL G418 and 25 µg/mL blasticidin. The growth rate of mutant epimastigotes was determined by cell counting in a Neubauer chamber performed by two blinded observers every 48 h for 14 days.

Genomic DNA was extracted from WT, Scrambled, and knockout clones using the DNeasy Blood & Tissue Kit (69506; Qiagen) and used in PCR to verify the presence or absence of the *P21* and *Bsd* genes with specific sets of oligonucleotides (**Table S1**, primers 6–11). PCR conditions were as follows: initial denaturation for 3 min at 94°C followed by 30 cycles for 45 s at 94°C, 30 s at 60°C, and 45 s at 72°C and a final extension for 7 min at 72°C. The *P21* locus was sequenced using the Sanger method to ensure that the *Bsd* gene was inserted at the correct location (**Supplementary Material**).

RNA Isolation and cDNA Synthesis by RT-PCR

Total RNA from WT, Scrambled, and knockout clones (1×10^7 epimastigotes) was extracted using the PureLink RNA Mini Kit (12183018A; Invitrogen) and treated with DNase I (Sigma-Aldrich) according to the manufacturer's instructions. First-strand cDNA was synthesized from total RNA (1 µg) and oligo (dT) primers using the Superscript III First-Strand Synthesis System (18080051; Invitrogen) following the manufacturer's instructions. Next, PCR was performed in a separate microtube using the primers listed in **Table S1** (primers 6 and 7; 12 and 13; 14 and 15), which amplify *P21* and the endogenous housekeeping controls TcHGPRT (Murta et al., 2006) and TcMVK (Ferreira et al., 2016). The same PCR conditions were used to analyze the *P21* knockout clones and controls, as described in the previous section.

Immunofluorescence Analysis of P21 Expression

WT and *P21* knockout clones were fixed with 2% paraformaldehyde and washed twice with PBS. The parasites were incubated overnight with anti-P21 polyclonal antibodies produced in mouse (1:2,000) (Silva et al., 2009) diluted in permeabilization solution (PBS pH 7.2, 0.1% gelatin, 0.1% sodium azide, and 0.2% saponin). The parasites were then incubated with anti-mouse secondary antibodies conjugated to Alexa Fluor 568 (1:200) and 4',6-diamidino-2-phenylindole (DAPI; 1:500) for 1 h. Images were acquired in a TCS SP5 II tandem scanner (Leica) confocal microscope with a 63x NA 1.40 PlanApo oil immersion objective, and Imaris software (Bitplane) was used for imaging analysis.

Analysis of Cell Cycle Progression by Flow Cytometry

To evaluate the cell cycle progression, WT and knockout clone parasites in log phase growth were incubated with 20 mM hydroxyurea (HU) for 18 h as previously described (Santos Júnior et al., 2021). Thus, cells were washed three times with PBS and resuspended in LIT medium (10% FBS). Samples were collected each 24 h until 120 h. At each time point parasites were washed with PBS and fixed in 500 µL methanol and PBS (1:1) at

-20°C for 15 min. For DNA staining parasites were incubated with 10 µg/mL RNase A (Invitrogen) and 10 µg/mL propidium iodide and incubated at 37°C for 30 min. Cytometry was performed on a FACSCanto II (BD Bioscience) and analyzed with the FlowJo v10 software.

Western Blotting Analysis

Metacyclic trypomastigotes were obtained from axenic cultures of epimastigotes in the stationary phase maintained in LIT medium (pH 7.2) for 14 days at 28°C. After differentiation, the number of parasites was counted in a Neubauer chamber. Then, the samples were washed twice with PBS, and the pellet was resuspended in 50 µL of lysis buffer (10 mM Tris-HCl pH 7.5, 50 mM NaCl, 5 mM EDTA, 4 mM Na₃VO₄, 2 mM NaF, 20% glycerol, 1% NP-40, and complete-C protease inhibitors). The extracts were incubated on ice for 30 min and centrifuged at 13,000 × g for 10 min at 4°C. The supernatant was recovered and frozen at -20°C.

The protein concentration of the parasite extracts was estimated by Bradford assay, and 40 µg of total protein was loaded onto a 10% SDS-PAGE gel and transferred to a nitrocellulose membrane. The gp82 and α -tubulin proteins were labeled using the monoclonal antibodies 3F6 (1:1,500) (Teixeira and Yoshida, 1986) and anti- α -tubulin (1:2,500; Sigma-Aldrich), respectively, both of which were produced in mice. The membranes were blocked with 5% skimmed milk powder in 0.1% PBS-T solution (PBS containing 0.1% Tween 20) for 1 h under constant agitation at room temperature. After blocking, the membranes were washed three times with PBS-T 0.1% for 10 min and incubated with antibodies against gp82 and α -tubulin, followed by anti-mouse IgG-peroxidase antibodies (1:6,000) in the same blocking solution; the membranes were washed three times before each incubation. Protein bands were detected using Immobilon Western Chemiluminescent HRP Substrate (Millipore) and Amersham HyperfilmTM ECL (GE Healthcare). The intensity of the bands associated with the gp82 and α -tubulin proteins was quantified using GelAnalyzer 19.1 software; the density of each band was converted to peaks, and the area under the peaks was used to determine the pixel intensity. The assays were performed in two independent experiments.

Invasion and Replication Assays

HeLa cells were seeded onto 24-well plates containing 13 mm coverslips to a final density of 1×10^5 cells/well for invasion and 5×10^4 cells/well for replication assays and maintained overnight under optimal conditions for adhesion. Then, the cells were incubated for 2h with purified metacyclic forms of the WT and P21 knockout clones at a multiplicity of infection (MOI) of 20 (20 parasites:1 host cell) for invasion and 10 (10 parasites:1 host cell) for replication.

The cells were washed three times with PBS to remove non-internalized parasites, fixed with Bouin's solution (HT10132; Sigma-Aldrich) for 5 min, washed with PBS, and stained with Giemsa (1:3) (GS500; Sigma-Aldrich) for 1 h. Then, the stained cells were dehydrated sequentially in acetone, acetone:xylol, and xylol and mounted on slides with Entellan[®] (Merck Millipore), and the number of infected cells was quantified for 100 cells.

For the replication assays, after 2 h, HeLa cells were washed and maintained in optimal conditions for 24h, 48h or 72 h. Then, the cells were fixed with 2% paraformaldehyde and incubated with anti-chagasic human serum (1:100) diluted in permeabilization solution overnight. The cells were washed with PBS and incubated with secondary antibodies conjugated to Alexa Fluor 568 (1:200) and DAPI (1:500) for 1 h. The number of parasites per cell was quantified for 100 infected cells. Representative images of intracellular amastigotes were captured using a confocal microscope (Leica SP5), and Imaris software (Bitplane) was used to perform the analysis.

Statistical Analysis

Statistical analyses were performed using GraphPad Prism software version 7.0. All values are expressed as the mean \pm standard deviation of two independent assays performed at least in duplicate. Differences were considered significant at $p < 0.05$. Significant differences were determined by one-way ANOVA and Tukey's test for multiple comparisons of parametric data, Kruskal-Wallis and Dunn's test for multiple comparisons of nonparametric data, or two-way ANOVA and Tukey's or Sidak's test for multiple comparisons.

RESULTS

T. cruzi P21 Gene Knockout Strategy

In this work, gene P21 from strain Y clone C6 (Y C6) (Gene ID: TcYC6_0032830) was selected for functional analysis. The genome of Y C6 was organized into 40 chromosome-scale scaffolds, many of which represent near-complete chromosomes, such as the chromosome 17 where gene P21 has been assigned (Wang et al., 2021). The gene P21 encodes a 154-amino acid protein (TcYC6_0032830-RA) and it was mapped (position:58,538-59,002 nt) near one end of chromosome 17. P21 is located within a polycistronic unit of about 230,000 nt belonging to a syntenic region conserved in different strains of *T. cruzi*. Nucleotide blast analysis demonstrate that P21 protein is coded by a pair of alleles and no orthologs were found in other trypanosomatids (https://tritypdb.org/tritypdb/app/record/gene/TcYC6_0032830).

Firstly, we determined the antibiotic concentration of G418 and blasticidin for selecting the epimastigotes of the Y strain under culture conditions. They were incubated with different concentrations of antibiotics for 10 days, and the number of parasites was estimated by counting in a Neubauer chamber. We found that 250 µg/mL G418 and 25 µg/mL blasticidin could be used to select the parasites after electroporation (**Supplementary Figures 1A, B**).

To obtain P21 knockout clones, we used a single vector for the co-expression of Cas9 and sgRNA. As demonstrated in a previous study, this sgRNA/Cas9/pTREX-n construct can induce the transcription of Cas9 and sgRNA and the translation of Cas9 alone with nuclear import (Cas9-HA-2xNLS-GFP) (Lander et al., 2015). The P21 sgRNA was cloned into the Cas9/pTREX-n vector, which was confirmed by Sanger sequencing (**Supplementary Figure 1C**). We also cloned a non-targeting (Scrambled) sgRNA into the Cas9/pTREX-n vector as the control. Subsequently, donor

DNA (599 bp) was synthesized by PCR using ultramer primers (which contain the homologous recombination sequences plus 20 nt that recognizes the *Bsd* gene) and the pGEM-*Bsd* vector as a template. The plasmids were used to electroporate epimastigotes, generating lines that express the Cas9-GFP fusion protein in the parasite nucleus (**Supplementary Figure 1D**). After the selection with G418 (250 µg/mL), the parasites were electroporated with donor DNA (**Supplementary Figure 1E**), which contained the “homology arms” and the *Bsd* gene, and selected with 25 µg/mL blasticidin and 250 µg/mL G418.

After antibiotic selection, the genomic DNA of transfected parasites was extracted and analyzed by PCR with primers that anneal in the *P21*, *Bsd*, and *P21* UTR regions (**Tables S1, S2**). The gel electrophoresis profile of amplicons found on the transfected population (sgRNA_21) indicated the presence of both the *P21* and *Bsd* genes, suggesting a mixed population (**Supplementary Figure 2**). The mixed population was cloned by limiting dilution at 0.2 parasites/well. We isolated four *P21* knockout clones, which were analyzed by PCR. **Figure 1A** shows a schematic representation of the *P21* WT and *P21* knockout gene locus and the alignment sites of the primers used to screen for knockout clones. We found that DNA from the WT and mixed populations showed amplification of the *P21* gene (392 bp); while the four knockout clones did not show amplification (**Figure 1B**). Furthermore, when we analyzed the amplicons obtained using the UTR primers, we identified a 778 bp band from the WT control and a 904 bp band from the knockout clones. The mixed population showed both bands, suggesting the deletion of a single *P21* allele in this population.

In addition, we analyzed the *Bsd* insertion site in the 4 knockout clones by PCR using the combination of UTR Fw/BSD Rv, and BSD Fw/UTR Rv primers. The results demonstrate that the *Bsd* gene was inserted between the UTR regions of the *P21* gene (**Supplementary Figure 3**). Furthermore, to confirm whether the *Bsd* sequence was correctly inserted in the *P21* locus, amplicons obtained by PCR using UTR primers were purified and sequenced, and the results indicated that homologous recombination with the *Bsd* gene was successful (**Supplementary Material_sequencing**).

Analysis of *P21* Gene Expression in Knockout Clones

To confirm the absence of *P21* transcripts in the *P21* knockout clones, we analyzed cDNA clones synthesized by RT-PCR from total RNA using primers for the *P21* coding sequence. Two housekeeping genes were included as internal controls for the assay: *T. cruzi* mevalonate kinase (TcMVK) (Ferreira et al., 2016) and hypoxanthine-guanine phosphoribosyltransferase (TcHGPRT) (Murta et al., 2006). The results demonstrated that there were no *P21* transcripts in the knockout clones. On the other hand, all clones expressed TcMVK and HGPRT transcripts (**Figure 1C**). We also analyzed the expression of the *P21* protein in parasites by immunofluorescence assay. The parasites were labeled with mouse anti-*P21* primary antibodies and anti-mouse secondary antibodies conjugated to Alexa Fluor 568 and analyzed by confocal microscopy. In WT epimastigotes,

the *P21* protein was clustered at multiple points; however, knockout parasites showed a weak labeling, a nonspecific trace of detection from the polyclonal antibody (**Figure 1D**).

Effects of *P21* Ablation on Epimastigote Growth and Cell Cycle Progression

To investigate whether *P21* deficiency hinders the growth of *T. cruzi*, we evaluated the growth curve of *P21* knockout clones compared with that of WT parasites for 14 days by counting the number of parasites every 2 days. We found that *P21* knockout cells exhibit a slower growth rate than WT parasites (**Figure 2A**). We also compared the growth curve between WT, Scrambled and clone 1 *P21* KO. The data showed that the profile of the curve is similar between WT and Scrambled even though at the times of 10 and 14 days there was a statistical difference. But, similarly to what was found previously, between the 8th and 14th day, clone 1 *P21* KO showed reduced growth rate compared to WT and Scrambled controls (**Supplementary Figure 4**).

Furthermore, we examined the cell cycle progression (24–120 h) of WT and *P21* knockout parasites by flow cytometry after synchronization cells with hydroxyurea treatment. The first graph (0H) demonstrated that most of the parasites from both groups were synchronized in the G1 phase of the cell cycle. At other times the data demonstrated that *P21* ablation altered the cell cycle progression compared with WT parasites. *P21* knockout parasites accumulated in G1 and decreased in S phase throughout the cell cycle while WT cells presented normal progression (**Figure 2B**). These data indicate that *P21* ablation impairs epimastigote replication.

We also investigated the effect of *P21* ablation in *T. cruzi* metacyclogenesis. We analyzed the expression of the glycoprotein gp82, a molecular marker of the differentiation of epimastigotes into metacyclic trypomastigotes, after 14 days of growth. The results showed that there was no difference in the expression of gp82 between the knockout clones and controls (**Figure 3A**).

Effects of *P21* Ablation on Metacyclic Trypomastigote Invasion and Intracellular Amastigote Replication

Previous studies have shown that *P21* plays an important role in the *T. cruzi* invasion process. Therefore, we investigated whether the absence of *P21* transcripts affects the invasion of host cells. We infected HeLa cells with purified metacyclic trypomastigotes for 2 h and analyzed the rate of invasion and the number of internalized parasites by counting 100 cells. *P21* knockout cells showed a significant reduction in the invasion rate compared with that of WT or Scrambled controls (**Figures 3B, C**).

We also investigated the replication pattern of the parasites at 24, 48 and 72 hours after invasion by counting the parasites present in 100 infected cells. The results showed that at the times of 24 and 48 hours there was no difference in replication between the analyzed groups (**Supplementary Figure 5**). However, at the time of 72 hours after invasion the overall replication rate of knockout clones was higher than that of WT and Scrambled parasites (**Figures 4A, B**). Furthermore, we determined the

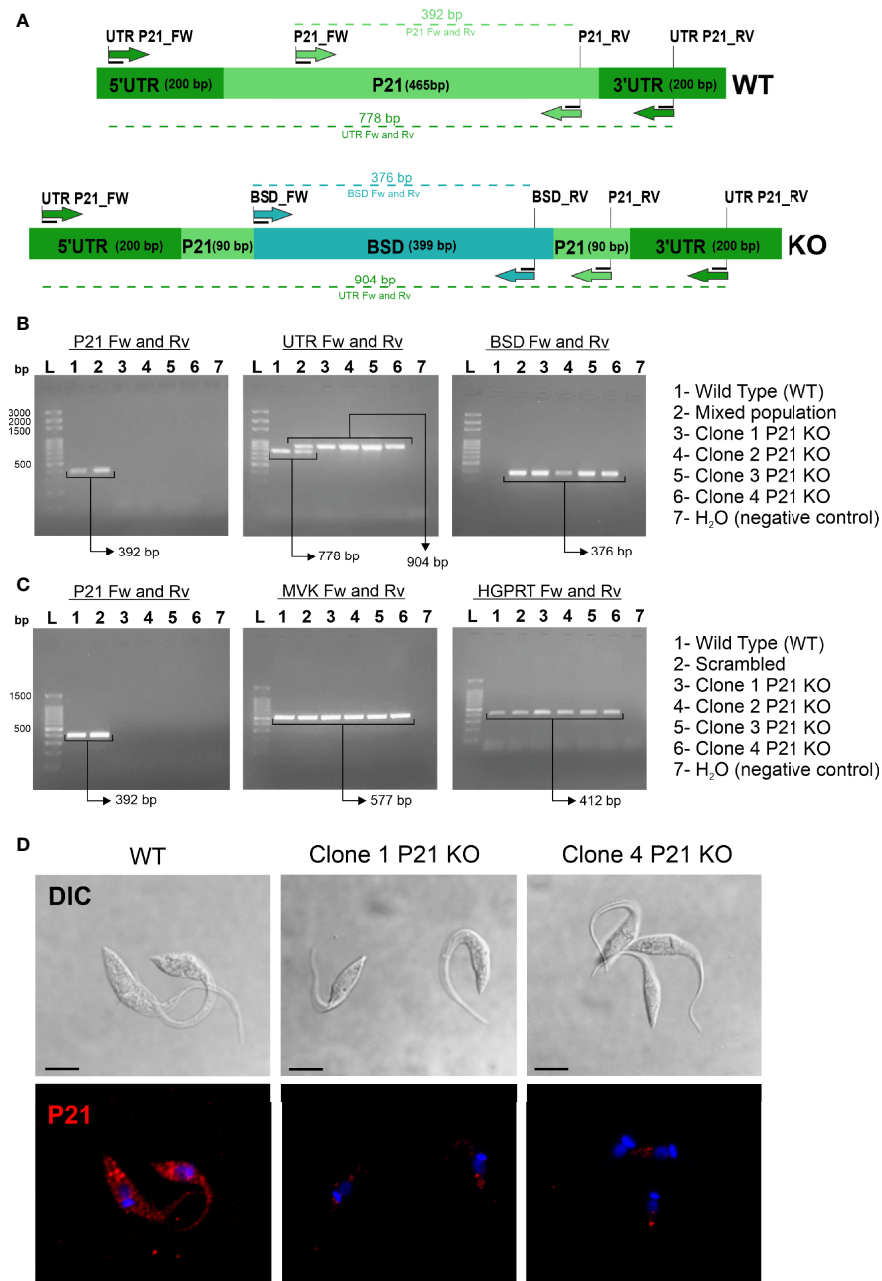


FIGURE 1 | Confirmation of *P21* knockout clones. **(A)** Schematic representation of the *P21* gene locus in WT and knockout clones. The indicated primers are shown in **Table S1**. **(B)** PCR of gDNA isolated from knockout clones and controls (WT and Scrambled) using specific primers for *P21*, the UTR region of the *P21* gene, and the blasticidin resistance gene (*Bsd*). **(C)** PCR of cDNA from knockout clones and controls (WT and Scrambled) by analyzing the expression of *P21* and endogenous TcMVK and TcHGPRT. **(D)** Epimastigotes were incubated with polyclonal anti-*P21* antibodies (mouse) and anti-mouse antibodies conjugated to Alexa Fluor 568 (red). The nucleus and kinetoplast were labeled with DAPI (blue). DIC, differential interference contrast; P21 KO, *P21* knockout. Single plane images were acquired by confocal microscopy. The scale bars represent 5 μ m.

number of parasites per cell for 100 infected cells, and there was a larger number of cells with ≥ 4 parasites among cells infected with knockout clones compared with those infected with controls, as shown in **Figure 4C**. The findings indicated that *P21* ablation impaired metacyclic trypomastigotes invasion and increased the replication rate of intracellular amastigotes.

DISCUSSION

Bioinformatics analysis of the genome of *P21* in different strains of *T. cruzi* has revealed that the *P21* protein is encoded by a single-copy gene, and no orthologs are found in other trypanosomatids. The Y strain (lineage TcII) is homozygous

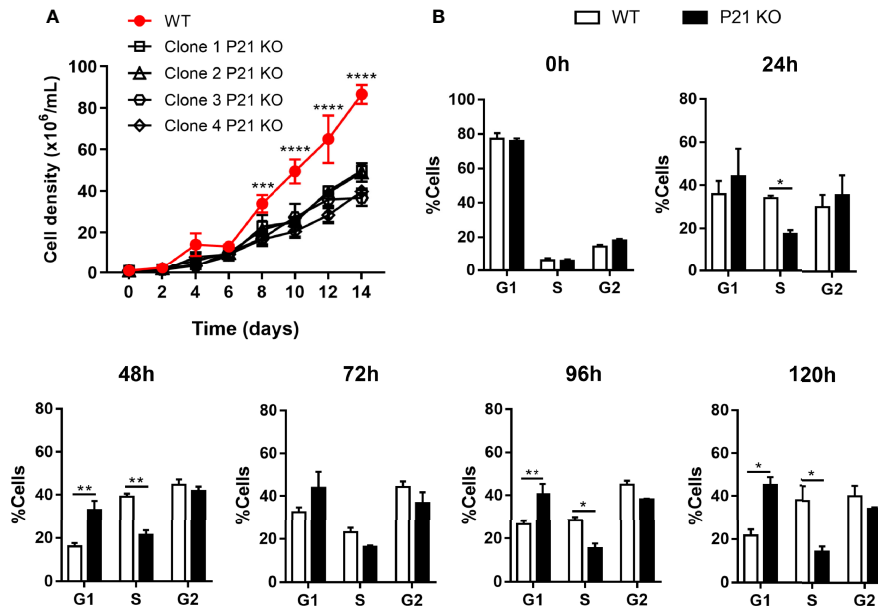


FIGURE 2 | Effects of *P21* ablation on epimastigote growth and cell cycle progression. **(A)** Epimastigote growth curve for 14 days. The graph shows the representative mean \pm SD of one of the two independent experiments performed in quadruplicate. The comparison was performed by two-way ANOVA and Tukey's test for multiple comparisons **(B)** Flow Cytometry analysis of the cell cycle progression, after treatment with hydroxyurea for 18 h. The graphs represent a percentage of parasites in each cell cycle phase per time point (24–120 h). The first graph (0h) represents the synchronization of the parasites in the G1 phase. Data represent the mean \pm SD of one of two independent experiments performed in triplicate. The comparison was performed by two-way ANOVA and Sidak's test for multiple comparisons. Asterisks indicate significant differences. P21 KO, *P21* knockout. *p* value: * < 0.05, ** < 0.01, *** < 0.001, **** < 0.0001.

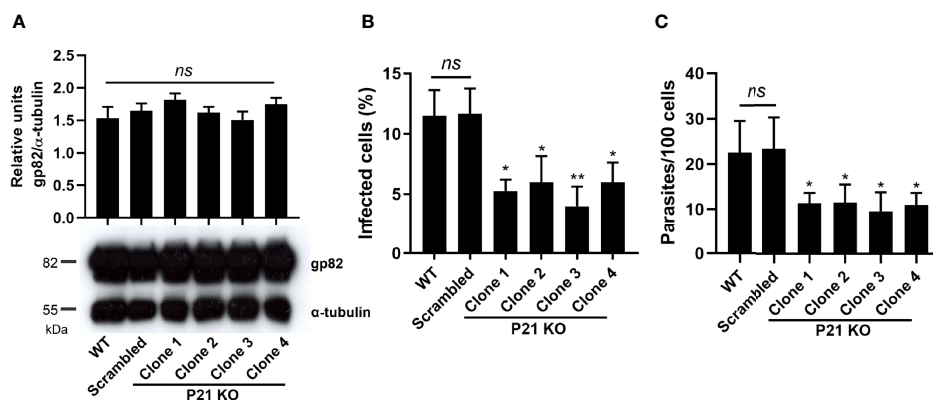


FIGURE 3 | Effects of *P21* ablation on metacyclic forms and its invasion in HeLa cells. **(A)** Western blot and densitometry analysis of WT, Scrambled, and knockout clones. Antibodies for detecting gp82 and α -tubulin (50 kDa, loading control) were used. Densitometry was performed by normalizing the relative expression of gp82 to the control expression, and the graph represents the mean \pm SD of the representative values of one assay performed in duplicate. **(B)** Percentage of infected HeLa cells after 2 h of invasion with purified metacyclic trypomastigotes. **(C)** Number of internalized parasites. The graphs show the representative mean \pm SD of one of the two independent experiments performed in triplicate. The comparison was performed by one-way ANOVA and Tukey's test for multiple comparisons. Asterisks indicate significant differences. P21 KO, *P21* Knockout; ns, no significant differences. *p* value: * < 0.05, ** < 0.01.

for the *P21* locus, which has been assigned to one end of the *in silico* assembled chromosome 17 of the *T. cruzi* Y C6 strain (TriTrypDB ID: TcYC6_0032830). In this study, we used the CRISPR/Cas9 system, a robust genetic tool, to investigate the biological roles of the *P21* protein. We obtained four double-knockout clones, which the *P21* gene locus was sequenced,

confirming the insertion of the *Bsd* gene. No other rearrangements were identified at this particular locus.

We evaluated the growth and differentiation phenotypes of epimastigotes after *P21* ablation. First, we determined the growth curve of knockout clones and WT control for 14 days. From day 8 onwards, knockout clones grew slower than WT parasites, and

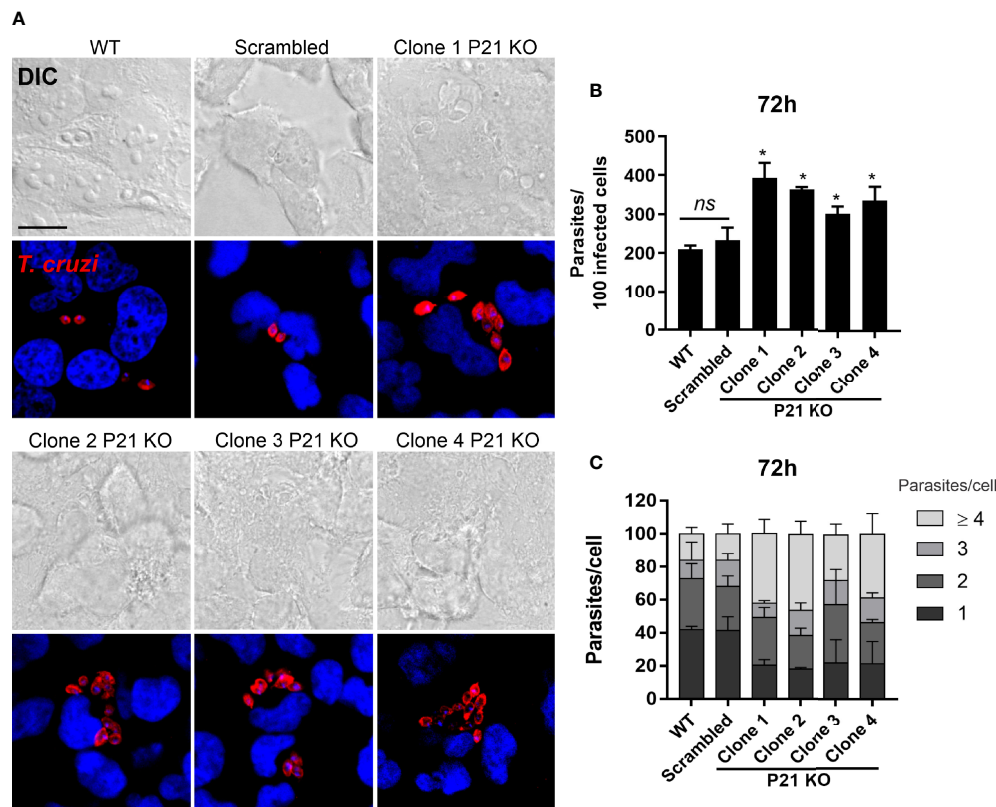


FIGURE 4 | Effects of *P21* ablation on the replication of intracellular amastigotes in HeLa cells. **(A)** Representative confocal microscopy images showing the intracellular replication of amastigotes in HeLa cells after 72 h of invasion. Amastigotes were incubated with chagasic serum and anti-human antibodies conjugated to Alexa Fluor 568 (red). The nucleus and kinetoplast were labeled with DAPI (blue). DIC, differential interference contrast. Single plane images were acquired by confocal microscopy. The scale bar represents 20 μ m. **(B)** Total number of parasites in 100 infected cells. The graph shows the representative mean \pm SD of one of the two independent tests performed in triplicate. **(C)** Number of parasites per cell for 100 infected cells. A total of 100 single-infected cells were analyzed per assay. The bars represent the mean \pm SD of two independent experiments performed in triplicate. The comparison was performed by one-way ANOVA and Tukey's test for multiple comparisons. Asterisks indicate significant differences. P21 KO, *P21* Knockout; ns, no significant differences. *p* value: * < 0.05.

on day 14, their growth rate was around twice slower than that of WT epimastigotes. Interestingly, this result showed that *P21* gene knockout impaired the growth of epimastigotes. We also analyzed the cell cycle progression after synchronization of cells with hydroxyurea treatment. The results showed that *P21* ablation induces an increase in the number of parasites in the G1 and S phases of the cycle at most analyzed times, indicating a delayed cell cycle progression, which corroborates the reduced growth of epimastigotes observed. A previous study reported that the incubation of epimastigotes for 72 h with recombinant *P21* protein (rP21) caused an increase in the number of G1 and S phase parasites with no interference in the G2 phase of the cell cycle (Teixeira et al., 2019). This discrepancy may be attributed to methodological differences, selective pressure, or the study time interval and needs to be further investigated.

T. cruzi epimastigotes survive solely in the gastrointestinal tract of the insect vector where a vigorous immune response may not be mounted in order to avoid eliminating obligate symbiotic microbes on which they rely for survival (Salcedo-Porras and Lowenberger, 2019). In this context, the stressful condition that

triggers epimastigote forms differentiation into metacyclic trypomastigotes is parasite starvation. Martins et al., 2020 demonstrated that epimastigotes undergoing nutritional starvation increased *P21* expression. Here we observed that *P21* knockout parasites showed a lower growth rate compared to controls. This data suggests that *P21* somehow plays a role in epimastigote multiplication. If *P21* is more expressed during parasite starvation, it is reasonable to speculate that the protein has also an impact on parasite metacyclogenesis. The expression of gp82 was not a good parameter to determine the metacyclogenesis process, since we observed similar levels of gp82 among the groups of parasites. This may be explained by the fact that gp82 is also expressed by intermediate forms of the parasite, as shown by Bayer-Santos et al., 2013. From this, the direct impact of *P21* over epimastigote differentiation or an indirect effect due to the lower multiplication rate (lower starvation), will be further studied in future investigations.

As *P21* plays an important role in the invasion of mammalian cells by trypomastigotes (Silva et al., 2009; Rodrigues et al., 2012), we also investigated whether the absence of *P21* transcripts affects the

invasion process. We determined the rate of invasion by metacyclic trypomastigotes by counting the number of HeLa cells infected with parasites. In comparison with WT and Scrambled controls, knockout clones showed a significant reduction in the invasion rate and the number of internalized parasites.

T. cruzi invasion involves surface and secreted parasite molecules that act through complex signaling pathways and trigger cellular responses, leading to the invasion of host cells (reviewed in Caradonna and Burleigh, 2011). Previous studies found that P21 could induce the entry of parasites into HeLa cells and murine macrophages by acting as a signal transducer, triggering intracellular cascades in host cells and resulting in actin cytoskeleton remodeling and parasite internalization through its binding to the CXCR4 receptor (Silva et al., 2009; Rodrigues et al., 2012). Consistent with these findings, we demonstrated that P21 deletion affected the entry of metacyclic forms of the parasites into HeLa cells, decreasing the percentage of infected cells by half and reducing the number of internalized parasites.

It has been reported that rP21 inhibits the intracellular replication of amastigotes by regulating the multiplication of the parasites in host cells (Teixeira et al., 2019; Martins et al., 2020). To investigate whether P21 deletion affects the replication of amastigotes, HeLa cells were infected with P21 knockout metacyclic trypomastigotes, and after 24, 48 or 72 h of growth, the infected cells were immunostained with anti-*T. cruzi* antibodies and counterstained with DAPI. We estimated the number of parasites present in each cell from a sample of 100 infected host cells. The proportion of host cells with ≥ 4 parasites was higher among cells infected with knockout clones compared with those infected with WT and Scrambled controls. In agreement with previous findings, P21 gene knockout produced a result opposite to the inhibitory effect of rP21 in the replication of amastigotes. Taken together, the lack of P21 expression decreased metacyclic trypomastigote cell invasion and increased intracellular amastigote multiplication in a way consistent with our previous data using the recombinant form of P21. Moreover, we believe that the discrepancy concerning the impact of P21 expression in epimastigote and intracellular amastigote multiplication may be due to different signaling events triggered by the different parasite forms. Epimastigote and amastigote are the replicative forms of the parasite. However, many morphological and biochemical differences exist between these evolutionary forms. Epimastigotes infect the gastrointestinal tract of the insect vector and suffer from starvation in order to differentiate into metacyclic trypomastigotes. Amastigotes are found free in the cytosol of mammalian host cell, faces different sources of stressors, differentiates into bloodstream trypomastigote and is responsible for the perpetuation of the infection. These different conditions of life permitted us to envisage that different molecular partners are triggered during P21 signaling pathway in epimastigote and amastigote replication process.

Several studies have examined whether the presence of *T. cruzi* in dormant or low-replication states is related to persistence in host tissues over several years and whether its ability to remain in these states is related to resistance to the

drugs used in the treatment of Chagas disease. Dumoulin and Burleigh (2018) demonstrated that intracellular amastigotes use a strategy referred to as growth plasticity to adapt to and recover from environmental stressors (e.g., nutrient deprivation, metabolism blockers, or exposure to benznidazole). Another study demonstrated that the key to the resistance of *T. cruzi* lies in non-replicating or dormant amastigotes that appear heterogeneously in host cells and resist drug treatment, which may later multiply and generate trypomastigotes capable of invading new cells (Sánchez-Valdéz et al., 2018). On the other hand, Ward et al. (2020) reported that there are more amastigotes in the S phase of the cell cycle in the acute phase than in the chronic phase. Therefore, the parasites can respond to environmental pressure and reduce their replication rate. Furthermore, the authors raised the possibility that the parasites may enter quiescence in the presence of benznidazole due to DNA damage caused by the drug.

Martins et al., 2020 showed that the treatment of C2C12 myoblasts with rP21 reduced the replication rate of intracellular amastigotes and induced an increase in actin polymerization in host cells. Furthermore, mice infected with *T. cruzi* and treated with rP21 exhibited a reduced parasite load in cardiac tissues (Teixeira et al., 2019; Martins et al., 2020). The authors also reported the presence of native P21 secreted by amastigote nests located in the cardiac tissues of infected mice. In addition, intracellular amastigotes were found to express higher levels of P21 when host cells were treated with IFN- γ (Martins et al., 2020). One of the possible explanations for these findings is that P21 may be a pleiotropic protein secreted during parasite cell invasion and acting as a modulator of parasite replication. These attributes may confer the parasite the ability to establish chronic infection and resistance to stress conditions from the mammalian host. The mechanisms beneath these modulation properties will be better studied.

In this work we have provided evidence demonstrating the specific disruption of the TcP21 locus in KO cell lines following a CRISPR/Cas9 strategy that has been successfully used in several studies (reviewed in Lander et al., 2019; Chiurillo and Lander, 2021). To further investigate the physiological function of TcP21 and its role in host cell infection, complementation studies should be performed by restoring the WT P21 gene in KO parasites to confirm and validate our results.

In conclusion, this study demonstrated that P21 ablation could affect epimastigote cell cycle progression, reduce parasite cell invasion, and increase intracellular amastigote replication. Taken together, the results suggest that P21 may play a role in the infectivity of metacyclic trypomastigotes and in the replication rate of amastigotes, which could be crucial for the establishment and perpetuation of infection.

DATA AVAILABILITY STATEMENT

The original contributions presented in the study are included in the article/Supplementary Material. Further inquiries can be directed to the corresponding authors.

AUTHOR CONTRIBUTIONS

TT, MC, NL, CS, and JFS conceived and designed experiments. TT, MC, NL, CR, TO, ÉF, CY, and JGS performed experiments. TT and JFS wrote the manuscript. TT prepared the figures. TT, JFS, CS, and MC discussed the results. All authors reviewed the manuscript. All authors contributed to the article and approved the submitted version.

FUNDING

This study was supported by grants and fellowships from FAPESP, FAPEMIG, CAPES, and CNPq. FAPESP process numbers: 2016/15000-4 (Thematic project) and 2019/05049-4 (Postdoctoral fellowship); FAPEMIG process number: APQ-00971-17.

SUPPLEMENTARY MATERIAL

The Supplementary Material for this article can be found online at: <https://www.frontiersin.org/articles/10.3389/fcimb.2022.799668/full#supplementary-material>

Supplementary Figure 1 | Strategy for obtaining *P21* knockout clones. **(A, B)** Number of wild type Y strain parasites after 10 days of incubation with the antibiotics G418 and blasticidin. The graph represents the mean \pm SD of two independent experiments performed in duplicate. Asterisks indicate statistical significance. The comparison was performed by Kruskal-Wallis test and Dunn's test for multiple comparisons. *p* value: * < 0.05 , ** < 0.01 . **(C)** Representative image of the sequencing of the *P21* sgRNA cloned in pTREX/Cas9. *P21_PS_RC* represents the sequence of

protospacer (query); Seq_2-9-1 and Seq_2-9-2 represent the sequence cloned into a vector, obtained from sequencing, performed in duplicate. **(D)** Representative images of the fluorescence microscopy of parasites electroporated with sgRNA expressing Cas9-EGFP. **(E)** Donor DNA (599 bp) obtained by PCR using ultramer primers (**Table S1**) and the pGEM-*Bsd* vector as a template.

Supplementary Figure 2 | PCR profile of amplicons obtained from a mixed population. **(A)** Schematic representation of the *P21* gene locus in WT and knockout clones. All primer combinations used as well as amplicon sizes are shown in the figure. **(B)** Agarose gels show amplicons obtained by PCR of the WT and sgRNA-*P21* populations using different sets of primers. The results indicated a mixed population, with hemi- or double-knockout parasites prior to cloning by limiting dilution. The schematic representation in **Figure 2** shows the sites of primer annealing, and **Table S2** lists all possible amplicons that can be obtained with the different primer combinations. WT, wild type; sgRNA-*P21*, parasites transfected with sgRNA and DNA donor before cloning (mixed population).

Supplementary Figure 3 | Confirmation of insertion of the *Bsd* gene within the *P21* UTR in knockout clones. Agarose gel shows amplicons obtained by PCR of the WT, Scrambled and 4 knockout clones using UTR Fw/BSD Rv and BSD Fw/UTR Rv primers combination.

Supplementary Figure 4 | Growth curve of epimastigotes comparing WT, Scrambled and Clone 1 *P21* KO groups. Epimastigote growth curve for 14 days comparing WT, Scrambled and Clone 1 *P21* KO parasites. The graph shows the representative mean \pm SD of one experiment performed in sextuplicate. The comparison was performed by two-way ANOVA and Sidak's test for multiple comparisons. *indicated a statistical difference between WT and Scrambled ($p < 0.05$). #indicated a statistical difference between WT, Scrambled and Clone 1 *P21* KO.

Supplementary Figure 5 | Replication of intracellular amastigotes in HeLa cells after 24 and 48 hours of invasion. Total number of parasites in 100 infected cells. The graph shows the representative mean \pm SD of one experiment performed in quintuplicate. The comparison was performed by Kruskal-Wallis test and Dunn's test for multiple comparison. ns, no significant differences.

REFERENCES

- Akutsu, Y., Doi, M., Furukawa, K., and Takagi, Y. (2019). Introducing a Gene Knockout Directly Into the Amastigote Stage of *Trypanosoma Cruzi* Using the CRISPR/Cas9 System. *J. Visual. Experiments. JoVE*. 149, 10.3791/59962. doi: 10.3791/59962
- Bayer-Santos, E., Cunha-e-Silva, N. L., Yoshida, N., and Franco da Silveira, J. (2013). Expression and Cellular Trafficking of GP82 and GP90 Glycoproteins During *Trypanosoma Cruzi* Metacyclogenesis. *Parasit Vectors*. 6, 127. doi: 10.1186/1756-3305-6-127
- Caradonna, K. L., and Burleigh, B. A. (2011). Mechanisms of Host Cell Invasion by *Trypanosoma Cruzi*. *Adv. Parasitol.* 76, 33–61. doi: 10.1016/B978-0-12-385895-5.00002-5
- Chiurillo, M. A., and Lander, N. (2021). The Long and Winding Road of Reverse Genetics in *Trypanosoma Cruzi*. *Microb. Cell* 8, 203–207. doi: 10.15698/mic2021.09.758
- Chiurillo, M. A., Lander, N., Bertolini, M. S., Storey, M., Vercesi, A. E., and Docampo, R. (2017). Different Roles of Mitochondrial Calcium Uniporter Complex Subunits in Growth and Infectivity of *Trypanosoma Cruzi*. *mBio* 8, e00574-17. doi: 10.1128/mBio.00574-17
- Chiurillo, M. A., Lander, N., Bertolini, M. S., Vercesi, A. E., and Docampo, R. (2019). Functional Analysis and Importance for Host Cell Infection of the Ca²⁺-Conducting Subunits of the Mitochondrial Calcium Uniporter of *Trypanosoma Cruzi*. *Mol. Biol. Cell* 30, 1676–1690. doi: 10.1091/mbc.E19-03-0152
- Chiurillo, M. A., Lander, N., Vercesi, A. E., and Docampo, R. (2020). P3 Receptor-Mediated Ca²⁺ Release From Acidocalcisomes Regulates Mitochondrial Bioenergetics and Prevents Autophagy in *Trypanosoma Cruzi*. *Cell Calcium*. 92, 102284. doi: 10.1016/j.ceca.2020.102284
- Cordero, E. M., Cortez, C., Yoshida, N., and da Silveira, J. F. (2019). Signal Peptide Recognition in *Trypanosoma Cruzi* GP82 Adhesin Relies on its Localization at Protein N-Terminus. *Sci. Rep.* 9, 7325. doi: 10.1038/s41598-019-43743-0
- Costa, F. C., Francisco, A. F., Jayawardhana, S., Calderano, S. G., Lewis, M. D., Olmo, F., et al. (2018). Expanding the Toolbox for *Trypanosoma Cruzi*: A Parasite Line Incorporating a Bioluminescence-Fluorescence Dual Reporter and Streamlined CRISPR/Cas9 Functionality for Rapid *In Vivo* Localisation and Phenotyping. *PLoS Neglect. Trop. Dis.* 12, e0006388. doi: 10.1371/journal.pntd.0006388
- Costa-Silva, H. M., Resende, B. C., Umaki, A., Prado, W., da Silva, M. S., Virgílio, S., et al. (2021). DNA Topoisomerase 3 α Is Involved in Homologous Recombination Repair and Replication Stress Response in *Trypanosoma Cruzi*. *Front. Cell Dev. Biol.* 9, 633195w. doi: 10.3389/fcell.2021.633195
- Doudna, J. A., and Charpentier, E. (2014). Genome Editing. The New Frontier of Genome Engineering With CRISPR-Cas9. *Science* 346, 1258096. doi: 10.1126/science.1258096
- Dumoulin, P. C., and Burleigh, B. A. (2018). Stress-Induced Proliferation and Cell Cycle Plasticity of Intracellular *Trypanosoma Cruzi* Amastigotes. *mBio* 9, e00673-18. doi: 10.1128/mBio.00673-18
- Ferreira, E. R., Horjales, E., Bonfim-Melo, A., Cortez, C., Silva, C. V., De Groote, M., et al. (2016). Unique Behavior of *Trypanosoma Cruzi* Mevalonate Kinase: A Conserved Glycosomal Enzyme Involved in Host Cell Invasion and Signaling. *Sci. Rep.* 6, 24610. doi: 10.1038/srep24610
- Ibarrola-Vannucci, A. K., De Pablos, L. M., Retana-Moreira, L., Cornet-Gomez, A., Cruz-Bustos, T., Schijman, A. G., et al. (2021). Characterization and Functional Analysis of the Proteins Prohibitin 1 and 2 in *Trypanosoma Cruzi*. *PLoS Neglect. Trop. Dis.* 15, e0009322. doi: 10.1371/journal.pntd.0009322
- Knott, G. J., and Doudna, J. A. (2018). CRISPR-Cas Guides the Future of Genetic Engineering. *Science* 361, 866–869. doi: 10.1126/science.aat5011

- Lander, N., and Chiurillo, M. A. (2019). State-Of-the-Art CRISPR/Cas9 Technology for Genome Editing in Trypanosomatids. *J. Eukaryot. Microbiol.* 66, 981–991. doi: 10.1111/jeu.12747
- Lander, N., Chiurillo, M. A., and Docampo, R. (2016). Genome Editing by CRISPR/Cas9: A Game Change in the Genetic Manipulation of Protists. *J. Eukaryot. Microbiol.* 63, 679–690. doi: 10.1111/jeu.12338
- Lander, N., Chiurillo, M. A., and Docampo, R. (2019). “Genome Editing by CRISPR/Cas9 in *Trypanosoma Cruzi*,” in *T. Cruzi Infection. Methods in Molecular Biology*, vol. 1955. Eds. K. Gómez and C. Buscaglia (New York, NY: Humana Press). doi: 10.1007/978-1-4939-9148-8_5
- Lander, N., Chiurillo, M. A., Vercesi, A. E., and Docampo, R. (2017). Endogenous C-Terminal Tagging by CRISPR/Cas9 in *Trypanosoma Cruzi*. *Bio-protocol* 7, e2299. doi: 10.21769/BioProtoc.2299
- Lander, N., Cruz-Bustos, T., and Docampo, R. (2020). A CRISPR/Cas9-Riboswitch-Based Method for Downregulation of Gene Expression in *Trypanosoma Cruzi*. *Front. Cell. Infect. Microbiol.* 10. doi: 10.3389/fcimb.2020.00068
- Lander, N., Li, Z. H., Niyogi, S., and Docampo, R. (2015). CRISPR/Cas9-Induced Disruption of Paraflagellar Rod Protein 1 and 2 Genes in *Trypanosoma Cruzi* Reveals Their Role in Flagellar Attachment. *MBio* 6, e01012–e01015. doi: 10.1128/mBio.01012-15
- Martins, F. A., Dos Santos, M. A., Santos, J. G., da Silva, A. A., Borges, B. C., da Costa, M. S., et al. (2020). The Recombinant Form of *Trypanosoma Cruzi* P21 Controls Infection by Modulating Host Immune Response. *Front. Immunol.* 11. doi: 10.3389/fimmu.2020.01010
- Murta, S. M. F., Krieger, M. A., Montenegro, L. R., Campos, F. F. M., Probst, C. M., Avila, A. R., et al. (2006). Deletion of Copies of the Gene Encoding Old Yellow Enzyme (TcOYE), a NAD(P)H Flavin Oxidoreductase, Associates With *In Vitro*-Induced Benznidazole Resistance in *Trypanosoma Cruzi*. *Mol. Biochem. Parasitol.* 146, 151–162. doi: 10.1016/j.molbiopara.2005.12.001
- Pech-Canul, A. C., Monteón, V., and Solís-Oviedo, R. L. (2017). A Brief View of the Surface Membrane Proteins From *Trypanosoma Cruzi*. *J. Parasitol. Res.* 2017, 3751403. doi: 10.1155/2017/3751403
- Peng, D., Kurup, S. P., Yao, P. Y., Minning, T. A., and Tarleton, R. L. (2014). CRISPR-Cas9-Mediated Single-Gene and Gene Family Disruption in *Trypanosoma Cruzi*. *mBio* 6, e02097–14. doi: 10.1128/mBio.02097-14
- Ramakrishnan, S., Unger, L. M., Baptista, R. P., Cruz-Bustos, T., and Docampo, R. (2021). Deletion of a Golgi Protein in *Trypanosoma Cruzi* Reveals a Critical Role for Mn²⁺ in Protein Glycosylation Needed for Host Cell Invasion and Intracellular Replication. *PLoS Pathog.* 17, e1009399. doi: 10.1371/journal.ppat.1009399
- Rodrigues, A. A., Clemente, T. M., Dos Santos, M. A., Machado, F. C., Gomes, R. G. B., Moreira, H. H. T., et al. (2012). A Recombinant Protein Based on *Trypanosoma Cruzi* P21 Enhances Phagocytosis. *PLoS One* 7, e51384. doi: 10.1371/journal.pone.0051384
- Salcedo-Porras, N., and Lowenberger, C. (2019). The Innate Immune System of Kissing Bugs, Vectors of Chagas Disease. *Dev. Comp. Immunol.* 98, 119–128. doi: 10.1016/j.dci.2019.04.007
- Sánchez-Valdéz, F. J., Padilla, A., Wang, W., Orr, D., and Tarleton, R. L. (2018). Spontaneous Dormancy Protects *Trypanosoma Cruzi* During Extended Drug Exposure. *eLife* 7, e34039. doi: 10.7554/eLife.34039
- Santos Júnior, A. C. M. D., Melo, R. M., Ferreira, B. V. G., Pontes, A. H., Lima, C. M. R., Fontes, W., et al. (2021). Quantitative Proteomics and Phosphoproteomics of *Trypanosoma Cruzi* Epimastigote Cell Cycle. *Biochim. Biophys. Acta Proteins Proteom.* 1869, 140619. doi: 10.1016/j.bbapap.2021.140619
- Sidik, S. M., Huet, D., Ganesan, S. M., Huynh, M. H., Wang, T., Nasamu, A. S., et al. (2016). A Genome-Wide CRISPR Screen in *Toxoplasma* Identifies Essential Apicomplexan Genes. *Cell* 166, 1423–1435.e12. doi: 10.1016/j.cell.2016.08.019
- Silva, C. V., Kawashita, S. Y., Probst, C. M., Dallagiovanna, B., Cruz, M. C., Silva, E. A., et al. (2009). Characterization of a 21 kDa Protein From *Trypanosoma Cruzi* Associated With Mammalian Cell Invasion. *Microb. Infect.* 11, 563–570. doi: 10.1016/j.micinf.2009.03.007
- Sollelis, L., Ghorbal, M., MacPherson, C. R., Martins, R. M., Kuk, N., Crobu, L., et al. (2015). First Efficient CRISPR-Cas9-Mediated Genome Editing in Leishmania Parasites. *Cell. Microbiol.* 17, 1405–1412. doi: 10.1111/cmi.12456
- Souza, W. S., Carvalho, T. M. U., and Barrias, E. S. (2010). Review on *Trypanosoma Cruzi*: Host Cell Interaction. *Int. J. Cell Biol.* 295394. doi: 10.1155/2010/295394
- Tavernelli, L. E., Motta, M. C. M., Gonçalves, C. S., da Silva, M. S., Elias, M. C., Alonso, V. L., et al. (2019). Overexpression of *Trypanosoma Cruzi* High Mobility Group B Protein (TcHMGB) Alters the Nuclear Structure, Impairs Cytokinesis and Reduces the Parasite Infectivity. *Sci. Rep.* 9, 192. doi: 10.1038/s41598-018-36718-0
- Teixeira, T. L., Castilhos, P., Rodrigues, C. C., da Silva, A. A., Brígido, R. T., Teixeira, S. C., et al. (2019). Experimental Evidence That P21 Protein Controls *Trypanosoma Cruzi* Replication and Modulates the Pathogenesis of Infection. *Microb. Pathog.* 135, 103618. doi: 10.1016/j.micpath.2019.103618
- Teixeira, S. C., Lopes, D. S., Gimenes, S. N., Teixeira, T. L., da Silva, M. S., Brígido, R. T., et al. (2017). Mechanistic Insights Into the Anti-Angiogenic Activity of *Trypanosoma Cruzi* Protein 21 and its Potential Impact on the Onset of Chagasic Cardiomyopathy. *Sci. Rep.* 7, 44978. doi: 10.1038/srep44978
- Teixeira, T. L., Machado, F. C., Silva, A. A., Teixeira, S. C., Borges, B. C., Dos Santos, M. A., et al. (2015). *Trypanosoma Cruzi* P21: A Potential Novel Target for Chagasic Cardiomyopathy Therapy. *Sci. Rep.* 5, 16877. doi: 10.1038/srep16877
- Teixeira, M. M., and Yoshida, N. (1986). Stage-Specific Surface Antigens of Metacyclic Trypomastigotes of *Trypanosoma Cruzi* Identified by Monoclonal Antibodies. *Mol. Biochem. Parasitol.* 18, 271–282. doi: 10.1016/0166-6851(86)90085-X
- Wang, W., Peng, D., Baptista, R. P., Li, Y., Kissinger, J. C., and Tarleton, R. L. (2021). Strain-Specific Genome Evolution in *Trypanosoma Cruzi*, the Agent of Chagas Disease. *PLoS Pathog.* 17, e1009254. doi: 10.1371/journal.ppat.1009254
- Ward, A. I., Olmo, F., Atherton, R. L., Taylor, M. C., and Kelly, J. M. (2020). *Trypanosoma Cruzi* Amastigotes That Persist in the Colon During Chronic Stage Murine Infections Have a Reduced Replication Rate. *Open Biol.* 10, 200261. doi: 10.1098/rsob.200261
- WHO (2021) *Chagas Disease (American Trypanosomiasis)* (WHO). Available at: [https://www.who.int/news-room/fact-sheets/detail/chagas-disease-\(american-trypanosomiasis\)](https://www.who.int/news-room/fact-sheets/detail/chagas-disease-(american-trypanosomiasis)) (Accessed July 20, 2021).
- Young, J., Dominicus, C., Wagener, J., Butterworth, S., Ye, X., Kelly, G., et al. (2019). A CRISPR Platform for Targeted *In Vivo* Screens Identifies *Toxoplasma Gondii* Virulence Factors in Mice. *Nat. Commun.* 10, 3963. doi: 10.1038/s41467-019-11855-w
- Zhang, C., Xiao, B., Jiang, Y., Zhao, Y., Li, Z., Gao, H., et al. (2014). Efficient Editing of Malaria Parasite Genome Using the CRISPR/Cas9 System. *mBio* 5, e01414-14. doi: 10.1128/mBio.01414-14

Conflict of Interest: The authors declare that the research was conducted in the absence of any commercial or financial relationships that could be construed as a potential conflict of interest.

Publisher's Note: All claims expressed in this article are solely those of the authors and do not necessarily represent those of their affiliated organizations, or those of the publisher, the editors and the reviewers. Any product that may be evaluated in this article, or claim that may be made by its manufacturer, is not guaranteed or endorsed by the publisher.

Copyright © 2022 Teixeira, Chiurillo, Lander, Rodrigues, Onofre, Ferreira, Yonamine, Santos, Mortara, da Silva and Silveira. This is an open-access article distributed under the terms of the Creative Commons Attribution License (CC BY). The use, distribution or reproduction in other forums is permitted, provided the original author(s) and the copyright owner(s) are credited and that the original publication in this journal is cited, in accordance with accepted academic practice. No use, distribution or reproduction is permitted which does not comply with these terms.



Trypanosoma cruzi Genomic Variability: Array Comparative Genomic Hybridization Analysis of Clone and Parental Strain

Danielle Rodrigues Cortez¹, Fabio Mitsuo Lima^{1,2}, João Luís Reis-Cunha³, Daniella Castanheira Bartholomeu³, Rolando Andre Rios Villacis⁴, Silvia Regina Rogatto⁵, André Guilherme Costa-Martins⁶, Fernanda Sycko Marchiano¹, Rafaela Andrade do Carmo¹, Jose Franco da Silveira^{1*} and Marjorie Mendes Marini^{1,2*}

OPEN ACCESS

Edited by:

Natalia de Miguel,
CONICET Instituto Tecnológico de
Chascomús (INTECH), Argentina

Reviewed by:

Michel Tibayrenc,
Institut de Recherche pour le
Développement, Bolivia
Martin M. Edreira,
Universidad de Buenos Aires,
Argentina

*Correspondence:

Marjorie Mendes Marini
marjoriemarini@gmail.com
Jose Franco da Silveira
jose.franco@unifesp.br

Specialty section:

This article was submitted to
Parasite and Host,
a section of the journal
Frontiers in Cellular and
Infection Microbiology

Received: 18 August 2021

Accepted: 25 February 2022

Published: 25 March 2022

Citation:

Cortez DR, Lima FM, Reis-Cunha JL,
Bartholomeu DC, Villacis RAR,
Rogatto SR, Costa-Martins AG,
Marchiano FS, do Carmo RA,
da Silveira JF and Marini MM (2022)
Trypanosoma cruzi Genomic
Variability: Array Comparative
Genomic Hybridization Analysis of
Clone and Parental Strain.
Front. Cell. Infect. Microbiol. 12:760830.
doi: 10.3389/fcimb.2022.760830

¹ Departamento de Microbiologia, Imunologia e Parasitologia, Escola Paulista de Medicina, Universidade Federal de São Paulo, São Paulo, Brazil, ² Centro Universitário São Camilo, Biomedicina, São Paulo, Brazil, ³ Departamento de Parasitologia, Instituto de Ciências Biológicas, Universidade Federal de Minas Gerais, Belo Horizonte, Brazil, ⁴ Departamento de Genética e Morfologia, Instituto de Biologia, Universidade de Brasília, Brasília, Brazil, ⁵ Department of Clinical Genetics, Institute of Regional Health Research, University of Southern Denmark, Vejle, Denmark, ⁶ Department of Clinical and Toxicological Analyses, Faculdade de Ciências Farmacêuticas, Universidade de São Paulo, São Paulo, Brazil

Trypanosoma cruzi, the etiological agent of Chagas disease, exhibits extensive inter- and intrastrain genetic diversity. As we have previously described, there are some genetic differences between the parental G strain and its clone D11, which was isolated by the limiting dilution method and infection of cultured mammalian cells. Electrophoretic karyotyping and Southern blot hybridization of chromosomal bands with specific markers revealed chromosome length polymorphisms of small size with additional chromosomal bands in clone D11 and the maintenance of large syntenic groups. Both G strain and clone D11 belong to the *T. cruzi* lineage TcI. Here, we designed intraspecific array-based comparative genomic hybridization (aCGH) to identify chromosomal regions harboring copy-number variations between clone D11 and the G strain. DNA losses were more extensive than DNA gains in clone D11. Most alterations were flanked by repeated sequences from multigene families that could be involved in the duplication and deletion events. Several rearrangements were detected by chromoblot hybridization and confirmed by aCGH. We have integrated the information of genomic sequence data obtained by aCGH to the electrophoretic karyotype, allowing the reconstruction of possible recombination events that could have generated the karyotype of clone D11. These rearrangements may be explained by unequal crossing over between sister or homologous chromatids mediated by flanking repeated sequences and unequal homologous recombination *via* break-induced replication. The genomic changes detected by aCGH suggest the presence of a dynamic genome that responds to environmental stress by varying the number of gene copies and generating segmental aneuploidy.

Keywords: *Trypanosoma cruzi*, intrastrain variability, parental strain and clone, karyotyping, array comparative genomic hybridization, gene copy number variation, chromosome rearrangement, aneuploidy

INTRODUCTION

Chagas disease is a neglected tropical disease with a global prevalence of 6-7 million infected people that causes more than 10,000 deaths every year (Coura and Viñas, 2010; WHO, 2021). *Trypanosoma cruzi*, the etiological agent of Chagas disease, is a flagellate protozoan of the order Trypanosomatida, which comprises species that diverged from the main eukaryotic lineage early in their evolution. The population structure of *T. cruzi* has been shown to be predominantly clonal, but there is extensive evidence of genetic exchange and natural hybridization, including meiotic sex, between strains (Tibayrenc et al., 1990; Westenberger et al., 2005; de Freitas et al., 2006; Tibayrenc and Ayala, 2013; Berry et al., 2019; Schwabl et al., 2019). Natural populations of *T. cruzi* exhibit a broad spectrum of genotypic and phenotypic traits and have been grouped into six discrete typing units (DTUs) known as lineages TcI-VI (Ackermann et al., 2012; Zingales et al., 2012).

Whole genomic analyses by next-generation sequencing (NGS) technologies have shown extensive genomic variability and aneuploidy among isolates from different *T. cruzi* lineages (Franzén et al., 2011; Ackermann et al., 2012; Reis-Cunha et al., 2015; Bradwell et al., 2018; Berná et al., 2018; Callejas-Hernández et al., 2018) and within isolates of the same lineage (Reis-Cunha et al., 2018). Minning et al. (2011) compared 17 *T. cruzi* strains using array comparative genomic hybridization (aCGH). They observed extensive, widespread gene copy number variation (CNV) among the isolates, suggesting that the parasite is tolerant to CNVs and even aneuploidy. Reis-Cunha et al. (2015) identified notably few aneuploidy events in isolates from the TcI lineage, while isolates from TcII and TcIII lineages had a large number of chromosomal expansions.

Molecular karyotyping analysis by pulsed field gel electrophoresis (PFGE) and hybridization with chromosome-specific markers demonstrated that *T. cruzi* exhibits extensive inter- and intrastrain karyotypic heterogeneities, suggesting gross chromosomal rearrangements (Henriksson et al., 1996; Porcile et al., 2003; Souza et al., 2011; Lima et al., 2013). McDaniel and Dvorak (1993) reported the presence of intrastrain chromosome rearrangements in naturally occurring variants of the Y-02 stock of the *T. cruzi* Y strain. In a previous report, we described differences between the karyotypes of the parental G strain and its clone D11, a clone isolated by the limiting dilution method and by infecting cultured mammalian cells *in vitro* (Lima et al., 2013). The karyotype of clone D11 differs in number and size of chromosomal bands from the karyotype of the G strain, and chromosomal rearrangements were detected by Southern blot hybridizations with chromosome-specific markers. In most cases the chromosome length polymorphisms were small, resulting in the appearance of additional chromosomal bands in clone D11. Despite the karyotypic alterations, large syntenic groups were conserved, suggesting that core genomic regions are essential for development of the parasite (Lima et al., 2013).

The occurrence of intrastrain genetic variability in *T. cruzi* has been investigated by different approaches. Clones derived from the same parental strain can differ from each other in antigenic composition (Brenière et al., 1991); growth and virulence (Postan et al., 1983; Campos and Andrade, 1996); and zymodeme (Dvorak

et al., 1980; Goldberg and Silva Pereira, 1983) and kDNA profiles (Morel et al., 1980). Recently, it has been demonstrated that isogenic clonal cell lines of *T. cruzi* have varying phenotypes, including expression of surface protein and fitness-determining traits (Seco-Hidalgo et al., 2015). Clones CLB and CL-14 of the CL strain display contrasting virulence phenotypes in a murine model of infection. Comparative transcriptome analysis indicates that the avirulent phenotype of CL-14 may be related to reduced or delayed expression of surface protein genes (Belew et al., 2017).

Although several reports have shown the presence of clonal and intrastrain karyotypic differences and CNVs in *T. cruzi*, the clonal heterogeneity in this parasite remains to be explained. In this study, we carried out a more in-depth comparative genomic analysis of the parental G strain and clone D11. By combining aCGH, PFGE karyotyping and hybridization with specific chromosome markers, we identified gene and chromosome copy-number differences between the G strain and clone D11, which could be a source of genomic variation. Our results may help to elucidate *T. cruzi* response to stress and the mechanism responsible for genome plasticity in this parasite.

METHODS

Parasites and DNA Extraction

Clone CL Brener (CLB) (*T. cruzi* Discrete Typing Unit (DTU) VI-lineage TcVI) (Zingales et al., 1997; Zingales et al., 2009; Zingales et al., 2012) and the G strain (*T. cruzi* DTU I - lineageTcI) (Yoshida, 1983; Briones et al., 1999; Zingales et al., 2009; Zingales et al., 2012) in axenic cultures at 28°C in liver-infusion tryptose medium (LIT) containing 10% fetal calf serum. Clone D11, which also belongs to the DTU I - lineageTcI (Lima et al., 2013), was isolated from the G strain by Santori (1991) using the protocol described by Lima and Villalta (1989). Log-phase epimastigotes were washed in phosphate buffered saline (PBS) and collected by centrifugation. Genomic DNA extraction was performed with the DNeasy Blood & Tissue (Qiagen) kit using 5×10^7 cells/mL according to the manufacturer's instructions.

Separation of *T. cruzi* chromosomal bands by pulsed-field gel electrophoresis (PFGE) and Southern blot analysis

Approximately 1×10^7 epimastigotes in exponential phase were washed with PBS and collected by centrifugation; an equal volume of cell suspension and 2% low-melting point agarose were mixed as previously described (Souza et al., 2011). The chromosomes were separated by pulsed-field gel electrophoresis (PFGE) and hybridized with the indicated markers labelled with (Zingales et al., 1997)P as previously described (Cano et al., 1995; Souza et al., 2011). The genes used as probes are indicated in the figure legends.

aCGH Design, Hybridization and Analysis

The 8x60K array was designed and produced by Agilent (Agilent Technologies, Santa Clara, CA,US) based on the *T. cruzi* clone CLB genome, release 6, available in TriTrypDB (<http://tritrypdb>).

org/tritrypdb/; see **Supplementary Table S1**). CLB genomic contigs were assembled into 41 *in silico* chromosome (TcChr) pairs varying in size from 78 kb to 2.3 Mb (Weatherly et al., 2009). Because of the hybrid origin of CLB, the genome of this strain is composed of two parental haplotypes, designated Esmeraldo-like (S) and non-Esmeraldo-like (P) (El-Sayed et al., 2005). Two groups of probes totaling 48,787 probes covering all the *in silico* chromosomes were selected. The first group of probes covered all the chromosomes, including coding and non-coding regions, with an average of one probe every 1.2 kb to give a total of 44,860 probes. To design the second group, we selected 422 specific chromosome markers (i.e., single copy genes present only in the homologous chromosomes). In order to obtain a higher coverage with these markers, probe density was increased to one probe every 120 bp.

Raw data was first normalized using Feature Extraction software (Agilent technologies). Agilent Genomic Workbench Standard Edition 6.5 was then used to perform CNV interval detection. The QC metrics motif of Workbench 6.5 ensured adequate quality control of the hybridization data. In our study, an array signal which met the requirements if intensity value >50 and signal-to-noise ratio >25 was included in the analysis. The Aberration Detection Method 2 algorithm was used with a threshold of 6 and bin size of 10 to identify genomic variation. The aCGH scanning step for data acquisition and extraction was carried out by the Agilent Feature Extraction Software using the default of 0.25 log₂ ratio (log₂ ratio > 0.25 for gains and log₂ ratio < -0.25 for losses). Additionally, we applied a relatively stringent post-analysis filter to ignore small, spurious or low-quality alterations (Wang et al., 2015). We used as defining criteria of copy number alterations the presence of at least four consecutive probes altered in the region, minimum average absolute log₂ ratio 0.5, Log₂ ratios > 0.5 and < -0.5 as the threshold for gain and loss, respectively.

The raw aCGH data and sequence of probes involved in the aCGH design for *Trypanosoma cruzi* have been deposited into the GenBank GEO database (GSE197870). The GenBank GEO accession number (GSE197870) (<http://www.ncbi.nlm.nih.gov/geo/>).

Quantitative Real Time PCR Validation

qPCR was used to validate the aCGH data. Primer amplification efficiency for each gene was determined. Specific sequences of the reference and target genes were cloned into pGEM-T easy vector (Invitrogen). Known amounts of genomic DNA (from clones D11 and CLB and G strain) and recombinant plasmids containing the sequences of interest were incubated with 10 µL SYBR Green-Based Detection (Applied Biosystems), sense and antisense primers and water to a total reaction volume of 20 µL. The reaction mixture was distributed into 0.2 mL tubes and subjected to 40 cycles of amplification in the Rotor-Gene® Q PCR cycler (Qiagen) according to the manufacturer's instructions. The qPCR program was set as follows: initial denaturation at 95°C for 5 min, 40 cycles of denaturation at 95°C for 15 s, annealing and extension at 60°C for 60 s. The results were analyzed with Rotor-Gene 6000 v1.7 software (Qiagen). A standard curve was constructed for each target gene. Data obtained by amplification with genomic DNA samples could

be compared as the amount of genomic DNA was the same for the three *T. cruzi* isolates. To estimate the copy numbers of each target gene in the three isolates, data were normalized separately using the genome size of each *T. cruzi* isolate (Souza et al., 2011). All experiments were performed in triplicate.

Content of Amplified and Deleted Gene Regions and Chromosomal Distribution

To estimate gene content in amplified and deleted regions in clone D11 in relation to that of Esmeraldo-like and Non-Esmeraldo-like haplotypes, the coordinates of the regions that varied in copy numbers were crossed with the gene coordinates in CLB General Feature Format (GFF) files, version 9, downloaded from TriTrypdb (<http://tritrypdb.org/tritrypdb/>) using BEDTools intersect v2.23 (Quinlan and Hall, 2010). Initially, all genes whose coordinates were inside the deleted or amplified regions were counted and classified as follows: 1- Multigene Families (MGFs.) if they were annotated as Trans-sialidase (TS), Mucins (TcMUC), Mucin Associated Surface Proteins (MASP), Retrotransposon Hotspot Protein (RHS), surface glycoprotein gp63 (GP63) or Dispersed Gene Family 1 (DGF-1); 2- Hypothetical if they were annotated as Hypothetical Proteins; and 3- Others if they did not meet any of the above criteria. To compare the MGF content of the amplified or deleted regions, the proportion of each multigene family was determined.

Visualization of the D11 amplified or deleted regions with the Esmeraldo-like or Non-Esmeraldo-like *in silico* chromosomal sequences was performed using Perl scripts and the R libraries grid (<https://stat.ethz.ch/R-manual/R-devel/library/grid/html/00Index.html>), ade4 (<https://cran.r-project.org/web/packages/ade4/index.html>) and genoPlotR (<http://genopltr.r-forge.r-project.org/>). The length of the chromosomes was drawn according to the coordinates in the Esmeraldo-like and Non-Esmeraldo-like genome FASTA files, version 9, downloaded from TriTrypdb (<http://tritrypdb.org/tritrypdb/>). Each gene was drawn in its position and strand based on the GFF file, where grey boxes correspond to housekeeping and hypothetical genes and cyan boxes denote MGF genes. The green and red boxes correspond to deleted and duplicated regions, respectively.

The whole genome sequence (WGS) of *T. cruzi* isolate Dm28c-version 2018 (lineage TcI) was downloaded from <http://tritrypdb.org/tritrypdb/>. Whole genome alignments between CLB chromosomes (TcChr S - Esmeraldo-like haplotype and TcChr P - non-Esmeraldo-like haplotype) and Dm28c contigs were performed using the blastn algorithm and implemented with big_blast.pl script from the Sanger Institute. The annotation and graphical output of chromosome-specific markers were obtained using the Artemis Comparison Tool (ACT) (Carver et al., 2005) (<http://www.sanger.ac.uk/resources/software/act>).

RESULTS

Design of the Array and Experiments

Clone D11 and its parental G strain belong to the DTU I – lineage TcI of *T. cruzi* (Briones et al., 1999; Zingales et al., 2009; Zingales et al., 2012; Lima et al., 2013). The genome of clone CL

Brener (CLB) of lineage TcVI (Zingales et al., 1997; El-Sayed et al., 2005; Zingales et al., 2009; Zingales et al., 2012) was used as the DNA reference in the microarray design because it was the only *T. cruzi* genome assembled into chromosomes (Weatherly et al., 2009). Genomic sequences of clone CLB, the reference strain of the *T. cruzi* genome, have been previously assembled into chromosome-sized scaffolds that allowed the array to be designed. CLB genomic contigs were assembled into 41 *in silico* chromosome (TcChr) pairs that varied in size from 78 kb to 2.3 Mb (El-Sayed et al., 2005). Because of the hybrid nature of CLB, the genome of this strain is composed of two parental haplotypes designated Esmeraldo-like (S) and non-Esmeraldo-like (P). Nearly 50% of the *T. cruzi* genome is comprised of repetitive sequences, such as multigene families (MGFs), retrotransposons and micro- and mini-satellites (El-Sayed et al., 2005). The final assembly of chromosomes was hampered by its hybrid nature and the many repetitive sequences, which means that a considerable number of unassigned contigs are found in the *T. cruzi* database. Although the G strain (TcI) and clone CLB (TcVI) belong to two distantly related lineages, there is evidence that large syntenic regions are conserved among the different *T. cruzi* lineages (Souza et al., 2011). This has recently been confirmed by Next Generation Sequencing (NGS) procedures (Berná et al., 2018; Callejas-Hernández et al., 2018). To compare sequence divergence between the genomes of isolates from TcVI and TcI lineages, we evaluated the homology of individual chromosomes of CLB (TcVI) with their counterparts in Dm28c (TcI) whose assembly in large contigs was recently published (Berná et al., 2018). We confirmed gene sequence identity between CLB and Dm28c, and the conservation of gene order (synteny) in the same relative positions in the chromosomes of these isolates (**Supplementary Figure S1**). The differences found between CLB and Dm28c are usually due to variation in the number of copies of MGFs and genes encoding small RNAs (snRNA, sonRNA, tRNA). These results support our aCGH analysis comparing the genomes of the G strain and clone D11 with that of CLB.

The DNA content of the G strain [genome size=89.8 Mb (Lima et al., 2013)] and clone D11 were assumed to be the reference and test DNAs, respectively. This assumption has taken into account that clone D11 was isolated from strain G. Therefore, alterations related to DNA gains in the G strain that did not occur in clone D11 were assumed to be DNA losses in clone D11; conversely, DNA losses in the G strain were assumed to represent DNA gains in clone D11. We assumed that each clone D11 chromosome is homologous to a CLB chromosome (TcChr). For example, TcChr12 chromosome markers identified DNA gain and loss in the homologous of clone D11, which will be referred to here as a D11 chromosome homologous to TcChr12 of CLB.

Detailed Features of Chromosomal Alterations in Clone D11

aCGH can be used to identify losses and gains, including imbalances associated with apparently balanced translocation, i.e., duplication followed by translocation. However, it is unable

to detect balanced chromosomal rearrangements, e.g., inversions and balanced reciprocal translocations. The bulk of the detailed information on chromosomal alterations found in clone D11 is presented in **Supplementary Table S2**, which includes the *in silico* CLB chromosomes to which they were mapped, the genomic location (the beginning and end of the alteration), the size and type of alteration (DNA loss or gain) and the number of probes for each alteration. Of the 418 chromosomal imbalances identified in clone D11, 144 (34.45%) were classified as DNA gain/amplification, and 274 (65.55%) as DNA loss/deletion. It is interesting to note that the parameters used in our analysis to identify DNA alterations were not equally stringent for defining gain and loss. A more restrictive threshold was used to define DNA gain than DNA loss. To increase the stringency and selection of non-random alterations, we have used at least 4 consecutive altered probes. However, we can not rule out that the high proportion of DNA loss over DNA gain in clone D11 may also be due to a more stringent threshold for defining DNA gain. The average size of chromosomal alterations was 23 kb, the smallest being 1.5 kb, and the largest 405 kb (**Supplementary Figure S2**). Most chromosomal alterations (89.71%) were smaller than 50 kb, and only six were >200 kb.

Chromosomal alterations identified in clone D11 were mapped on both haplotypes (S, Esmeraldo-like and P, Non-Esmeraldo-like) of clone CLB. The proportion of chromosome alterations (loss or gain) in each chromosome was estimated based on the length of CLB chromosomes (Weatherly et al., 2009) (**Supplementary Figure S3**). CNVs were distributed in a heterogeneous manner throughout the D11 genome and their proportion to a given chromosome varied from 1.1% to 89.3%. Deletion and duplication proportions appear to vary among D11 chromosomes; notably, losses (65.55%) prevailed over gains (34.45%). The majority of D11 chromosomes exhibited some alteration, except the chromosome that shares homology with TcChr4 of CLB. Eighteen chromosomes had only DNA losses whereas in four chromosomes only DNA gain was observed. There was no apparent correlation between chromosomal length and number of chromosomal alterations. The proportion of chromosomal alterations in D11 was very similar to that in the haplotypes of CLB.

The distribution of CNVs in the chromosomes is shown in **Figure 1**. The bars are scaled according to chromosome size and show the predominance of DNA loss over DNA gain across the chromosomes. We selected several examples of chromosomes with different CNV profiles for a more comprehensive analysis (**Supplementary Figure S4**). For instance, a profile with a few loss/gain events was detected in the D11 chromosomes homologous to TcChr37, TcChr39 and TcChr8 of CLB.

Chromosomes TcChr4 and TcChr37 are part of a single chromosome and syntenic group that is highly conserved among different *T. cruzi* lineages (Souza et al., 2011). Another syntenic group was identified in TcChr39 (Souza et al., 2011). The syntenic groups (TcChr4+TcChr37) and TcChr39 are much larger than would be expected if rearrangements occurred randomly, suggesting that they have undergone positive selection (Souza et al., 2011). The aCGH analysis agreed with

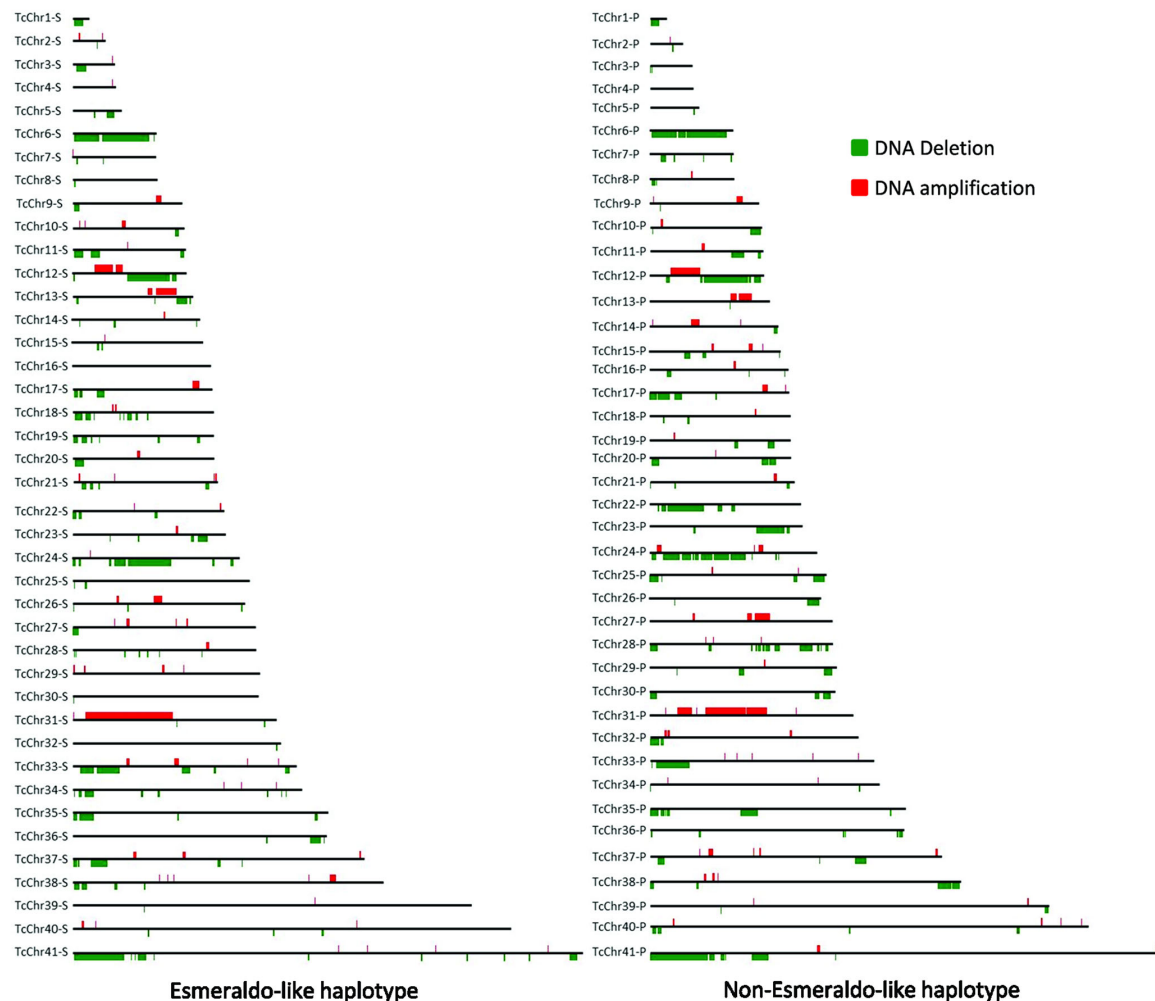


FIGURE 1 | Distribution of CNVs across *T. cruzi* chromosomes. Chromosomal alterations identified in clone D11 were mapped on both haplotypes (S, Esmeraldo-like and P, Non-Esmeraldo-like) on each *in silico* chromosome of the CLB reference genome (Weatherly et al., 2009). *In silico* chromosomes of CLB are numbered 1 to 41, from the smallest, TcChr1 (0.77 Mb), to the largest, TcChr41 (2.37 Mb). Amplification and deletion regions are represented in red and green, respectively. Chromosomes and recombination events are represented to scale.

this hypothesis since chromosomes TcChr39 and (TcChr4+TcChr37) exhibited very few CNVs. In a number of cases, a large part of the chromosome had changed. The D11 chromosome homologous to TcChr6 lost a large region comprising 89% of the entire chromosome whereas the D11 chromosome homologous to TcChr31 showed duplication of a segment covering 41% of the chromosome. A mixed CNV pattern was found in the D11 chromosome that shares homology with TcChr12. This chromosome has a large segment with loss and gain regions that correspond to 80% of the chromosome. Several D11 chromosomes showed different hybridization patterns to those of the haplotypes of CLB. For example, the D11 chromosome homologous to TcChr22-P had a large DNA loss region (32% of the length of the chromosome) that was absent in the TcChr22-S haplotype. Another D11 chromosome had a deletion that corresponded to 36% and

57% of the Tchr24-S and Tchr24-P haplotypes, respectively. Notably, some D11 chromosomes are highly conserved with changes in less than 2% of their lengths, e.g., the D11 chromosomes homologous to TcChr39 and TcChr37. Alterations in TcChr39 correspond to only 0.76% of the whole chromosome (approximately 1.85 Mb). These results agree with previous works that showed a remarkable conservation of TcChr39 and TcChr37 in different *T. cruzi* lineages (Santos et al., 1999; Souza et al., 2011; Lima et al., 2013).

Gene Content of Chromosomal Alterations in Clone D11

To determine the gene content of the chromosomal alterations, we analyzed 418 alterations in clone D11 using gene annotation (**Supplementary Table S3**). We identified 2,199 genes involved in DNA losses: 1,032 genes (of which 18.99% were pseudogenes)

in Esmeraldo haplotypes and 1,167 genes (of which 24.67% were pseudogenes) in non-Esmeraldo haplotypes. A relatively small number of genes were identified in the amplified regions: 353 genes (of which 13.03% were pseudogenes) in Esmeraldo haplotypes and 328 genes (of which 17.68% were pseudogenes) in non-Esmeraldo haplotypes ((**Supplementary Table S3**). The annotated genes were distributed into three groups: a 1st group, consisting of MGFs encoding surface proteins, such as trans-sialidases, MASPs, TcMUC (mucins), GP63 and DGF1 (dispersed gene family 1), and nuclear proteins coded by the RHS gene family (retrotransposon hot spot protein); a 2nd group, consisting of genes encoding hypothetical proteins without an assigned function; and a 3rd group consisting of other genes that do not meet any of the above criteria, such as replication protein genes, kinases and phosphatases (**Supplementary Figure S5**). There was an increase in the proportion of MGFs in clone D11 in relation to the G strain. The gene content of MGFs in DNA gain regions clearly differs from those with DNA loss (**Figure 2**). We observed an increase in MASP, mucins (TcMucII) and Gp63 content in the amplification regions of clone D11 whereas in the deletion

regions there was a decrease in the content of these genes and an increase in RHS and DGF1.

We speculated about a possible association between the presence of MGFs and chromosomal alterations and therefore mapped the alterations (deletions in green and amplifications in red) detected in the D11 clone with the gene annotation (MGFs in light blue and other genes in black) in the *in silico* S and P haplotypes of CLB chromosomes (**Figure 3** and **Supplementary Figure S6**). However, we found that the CNVs were unevenly distributed along the chromosomes, and there seems to be no connection between the abundance or size of multigene family clusters (represented in light blue) and the number and size of chromosomal alterations found in clone D11. For instance, the presence of many members of MGFs throughout chromosomes TcChr18 and TcChr41 was in striking contrast to the small number of alterations in these chromosomes. On the other hand, chromosomes TcChr6 and TcChr31 harbor a small number of genes belonging to MGFs, but many chromosomal alterations could be observed. In agreement with a previous report, the pattern of chromosomal alterations flanked by MGFs was observed (Minning et al., 2011). The authors reported that in

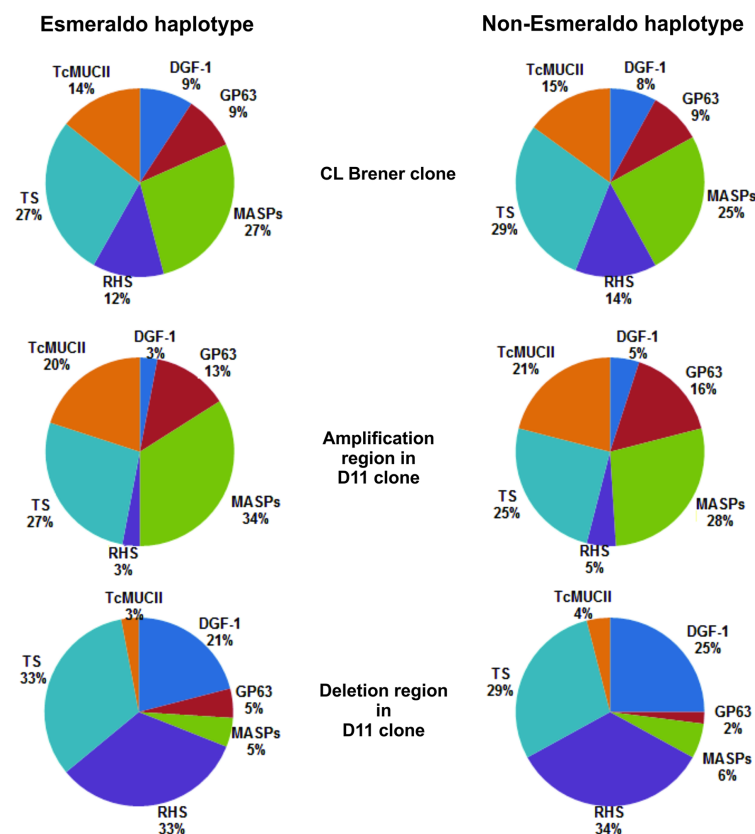


FIGURE 2 | Distribution of multigene families in the chromosomal alterations of clone D11. The distribution of multigene families in amplification and deletion regions was compared with the gene content of both haplotypes (Esmeraldo and non-Esmeraldo) of the CLB reference genome. The CLB gene contents were compared with those in the amplification and deletion regions of clone D11: TS, Trans-Sialidase; TcMUCII – *T. cruzi* Mucin II; DGF-1, Dispersed Gene Family 1; Gp63; MASP – Mucin Associated Surface Protein; RHS, Retrotransposon Hot Spot.



FIGURE 3 | Schematic representation of *in silico* chromosomes of Esmeraldo-like haplotype showing the gene annotation and chromosomal alterations detected by aCGH in clone D11. Annotation of multigene families in CLB is shown in light blue, and the other genes in black. The CNVs detected by aCGH in clone D11 are shown on the *in silico* CLB chromosomes. DNA amplification and deletion are shown in red and green, respectively. Chromosomes and recombination events are shown to scale (Bar=200 kb).

several strains of *T. cruzi*, CNVs were particularly frequent in gene family-rich regions containing mucins and trans-sialidases.

Gross Chromosomal Rearrangements in Clone D11

The electrophoretic karyotypes of clone D11 and the G strain differ in number and size of chromosomes (Lima et al., 2013). To facilitate understanding and comparison of CNVs between the G strain and clone D11, the chromosomal bands of these isolates were separated by PFGE using the electrophoretic conditions established by Lima et al., 2013 (Lima et al., 2013) (**Supplementary Figure S7**). Chromosome size differences between clone D11 and G strain ranged from approximately 40 to 340 kb, suggesting small chromosome rearrangements in clone D11. In this study we carried out Southern blot hybridizations using chromosome-specific markers within or near the chromosomal regions showing alterations detected by aCGH. We also looked for

possible balanced recombination events that could not be identified by aCGH such as translocations.

Representative examples of rearrangements in clone D11 are shown in **Figure 4** (see raw images in **Supplementary Figures S8A-D**). The localization of CNVs in the *in silico* chromosomes and hybridization of chromosomal bands with chromosome-specific markers are shown at the top and bottom in each panel, respectively. **Figure 4A** shows the rearrangement identified with two specific markers from chromosome TcChr8 that hybridized with a single chromosomal band of 0.59 Mb in the G strain and two bands of 0.57 and 0.71 Mb in clone D11, indicating the presence of two homologous chromosomes of the same size (0.59 Mb) in the parental G strain and two different-sized homologous chromosomes in clone D11. Chromoblot hybridization results suggest that the 0.71 Mb chromosome of clone D11 was the result of an internal duplication of a 120 kb region in one of the homologous of the G strain. However, the duplication was not

identified by aCGH in TcChr8 homologues (**Figure 4A**), suggesting that it may have occurred in a region that was not represented in the DNA microarray. For instance, some unresolved gaps located at the subtelomeric and non-syntenic regions of *T. cruzi* genome (El-Sayed et al., 2005; Berná et al., 2018). Only two short chromosomal alterations, a 33.8 kb deletion and a 11.3 kb duplication, were detected by aCGH in the D11 chromosome homologous to TcChr8 (**Figure 4A**).

Taken together, these results suggest the involvement of both homologous chromosomes of the G strain in the chromosomal rearrangement found in clone D11. We also suggest that the 0.71 Mb chromosome of clone D11 was the result of an internal segmental duplication in one of the homologous chromosomes

of the G strain while the 0.57 Mb chromosome of D11 was generated by loss of a (20 kb) fragment in the other homologous chromosome. However, we cannot rule out the possibility of translocation of a 120 kb segment from a nonhomologous chromosome to the 0.59 Mb chromosome of the G strain giving rise to the 0.71 Mb chromosome of D11.

Hybridization of the TcChr12-specific markers identified a single chromosomal band in both isolates, one band of 0.59 Mb in the G strain and another of 0.64 Mb in clone D11 (**Figures 4B** and **Supplementary Figure S8B**). However, the aCGH analysis showed two chromosomal alterations adjacent to each other, a duplicated and a deleted region of approximately 139 kb and 278 kb, respectively. Gain and loss regions are flanked at both sides

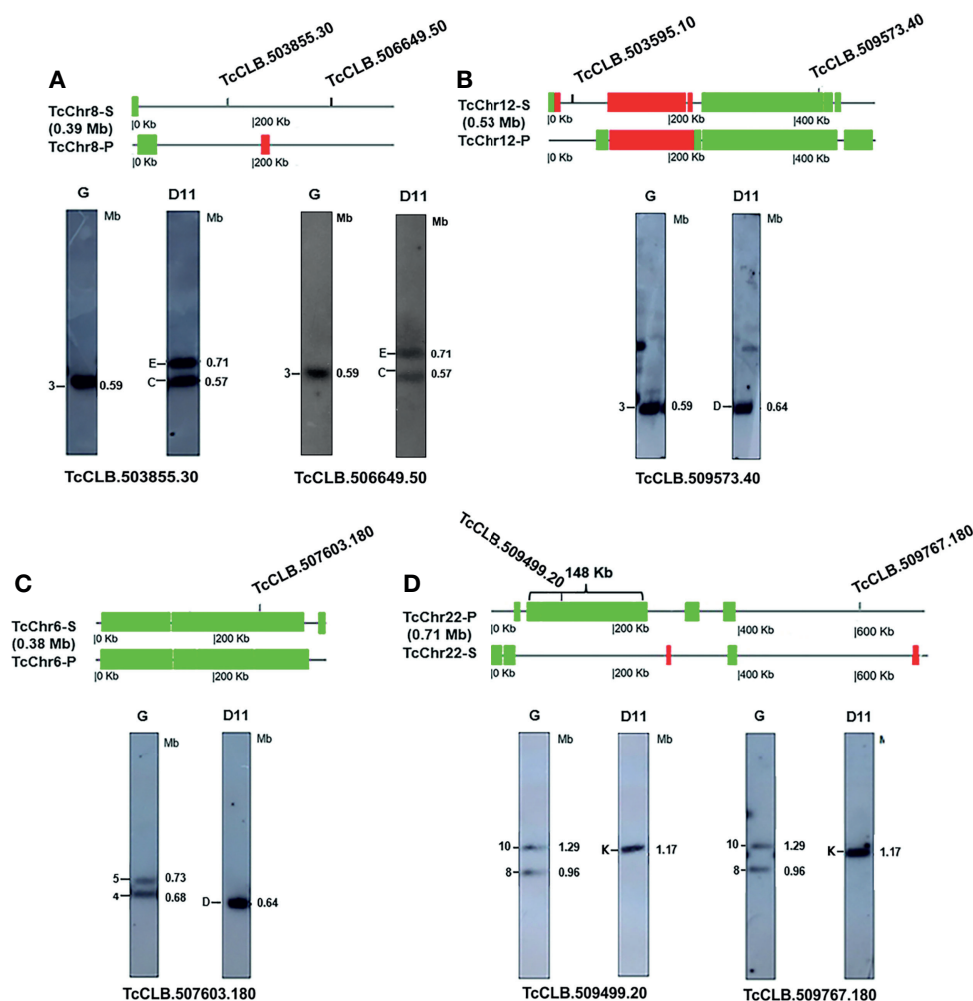


FIGURE 4 | Gross chromosomal rearrangements in clone D11 detected by aCGH and chromoblot hybridization. At the top of each panel there is a schematic representation of *in silico* CLB chromosomes showing the CNVs detected in clone D11 by aCGH. DNA amplification and deletion are shown in red and green, respectively. *In silico* chromosomes and CNVs are shown to scale. Below this is the Southern blot hybridization of chromosomal bands of the G strain and clone D11 separated by PFGE with chromosome-specific markers labeled with (Zingales et al., 1997)P (see the raw image in **Supplementary Figure S8**). The number and size (Mb) of chromosomal bands are indicated. The position of the chromosome-specific marker is indicated in the CLB chromosomes. The *in silico* chromosomes and markers are: **(A)** TcChr8, TcCLB.510337.30 - adenylosuccinate lyase; TcCLB.506649.50 - cytochrome c oxidase assembly factor **(B)** TcChr12, TcCLB.509573.40 - hypothetical protein; TcCLB.503595.10 - hypothetical protein **(C)** TcChr6; TcCLB.507603.180 - ubiquitin hydrolase 6 **(D)** TcChr22; TcCLB.509499.20 - beta propeller protein 1 BPI; T; TcCLB.509767.180 - exosome component CSL4.

by members of MGFs, including pseudogenes of RHS, transsialidases and DGF, allowing misalignment between sister or homologous chromatids. The rearrangement may be explained by unequal sister chromatid exchange that resulted in deletion and duplication of chromosome segments in the same chromatid. As shown in **Figure 5**, an unequal sister chromatid crossing over resulted in two different-sized sister chromatids (**Figure 5A**). The smaller sister chromatid lost an ~250 kb segment (in green) while it gained a segment of ~140 kb, resulting in a duplication of ~280 kb (in red). In the meantime, the larger sister chromatid lost the 140 kb segment and gained 250 kb (**Figure 5A**). At the end of mitotic division there were two sets of homologous chromosomes in the daughter cells (**Figure 5B**). In clone D11, one homologous chromosome was represented by the smaller sister chromatid whereas the other homologous chromosome was similar to the parental chromatid. The use of aCGH allowed the identification of cryptic imbalances, which had not been detected by chromoblot hybridization.

Some considerations need to be made when comparing the size of an in silico chromosome with that of the chromosomal band separated by PFGE. The current sequenced genomes of *T. cruzi* are more complete and precise. However, a very few chromosomes have been finished end to end (telomere to telomere), and some unresolved gaps persist. In this way, in silico chromosomes can be smaller than the chromosomal bands in which they were assigned. The models proposed to explain the chromosomal rearrangements are based on the size of in silico chromosomes that makes difficult to correlate accurately the size of aCGH alterations with the size of chromosomal band.

Regarding the chromosome TcChr6, the deletion identified by aCGH in one of the chromatids could have been balanced by DNA gain of the same size that occurred in the gaps or subtelomeric regions that are not represented in the DNA array. The presence of a single chromosomal band in clone D11 instead of two bands, as expected by the proposed model (**Figure 5**), could be explained by DNA gain occurring in the gaps and/or subtelomeric regions. In a previous work, Lima et al., 2013 (Lima et al., 2013) demonstrated that telomeric regions were involved in the sized-chromosome polymorphism in clone D11. These regions are very polymorphic and for this reason they were not included in the DNA array.

Figure 4C shows the rearrangement found in the D11 chromosome homologous to TcChr6. A specific-chromosome marker of TcChr6 hybridized with two chromosomal bands of 0.73 and 0.68 Mb in the G strain and with a single smaller-sized band of 0.64 Mb in clone D11, indicating the presence of two different-sized homologous chromosomes in the parental strain. Regarding the clone D11, the size of one of the homologous chromosomes can be estimated at 0.64 Mb while the other homologous chromosome would have a smaller size. Chromoblot hybridization corroborated the aCGH finding of a large deletion in TcChr6 ($-1 \log_2$ ratio). This rearrangement may be explained by unequal crossing over between homologous chromatids with deletion of an ~280 kb segment resulting in two different-sized DNA molecules (**Supplementary Figure S9A**). After chromosome segregation, clone D11 receives one recombinant homologous chromosome represented by the smaller chromatid, and the other homologous chromosome is similar to the parental chromatid (**Supplementary Figure S9B**).

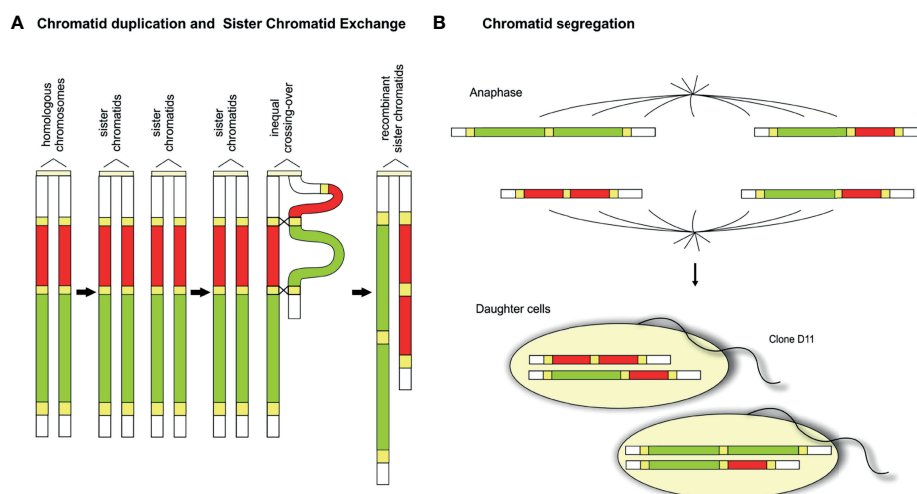


FIGURE 5 | Model of unequal sister chromatid exchange accounting for the rearrangement in the D11 chromosome homologous to TcChr12. **(A)** The pair of parental homologous chromosomes is shown to the left of the duplicated parental sister chromatids. The repeated sequences (pseudogenes RHS, TS and DGF-1) (in yellow) flanking the regions involved in the duplication (red) and deletion (green) recombination events are indicated. After DNA replication, the two sister chromatids are paired with slippage of repeated sequences prior to recombination. Unequal sister chromatid cross over resulting in two chromatids of different sizes. **(B)** At the end of mitotic division two sets of homologous chromosomes are separated from each other in the daughter cells. Each daughter cell receives a sister recombinant chromatid. Clone D11 receives the smaller recombinant chromatid resulting from tandem duplication of a segment (in red) and deletion of the adjacent segment (in green).

TcChr22-chromosome markers hybridized with two chromosomal bands of the parental G strain (1.29 Mb and 0.96 Mb) but with only one band in clone D11 (1.17 Mb) (**Figure 4D**). The assignment of TcChr22 markers into two bands in the G strain indicated the presence of a pair of different-sized homologous chromosomes. The chromosome size differences between clone D11 and the parental strain were 0.12 Mb and 0.21 Mb, suggesting small chromosomal rearrangements. After analyzing the aCGH results, we were able to detect a 148 kb deletion in one of the haplotypes of clone D11. The hybridization of the marker TcCLB.509499.20 to the 1.17 Mb chromosomal band supports that the 148 kb segment identified by aCGH is present in one homologous chromosome of clone D11 (**Figure 4D**). One of the homologous chromosomes of clone D11 may have resulted from a deletion in the 1.29 Mb chromosome of the G strain while the other may have arisen from a segmental duplication in the 0.96 Mb chromosome of the G strain.

Although the chromosomal rearrangement in the D11 chromosome homologous to TcChr22 is quite complex, it allows a comprehensive analysis of the molecular mechanisms involved. The TcChr22-specific markers were mapped to two chromosomal bands of 1.29 and 0.96 Mb in the G strain and to a single band of 1.17 Mb in the clone D11. Lima et al., 2013 (Lima et al., 2013) suggested that fusion of the different-sized homologous chromosomes of 1.29 and 0.94 Mb of the G strain generating a dicentric chromosome was followed by fission,

resulting in two similar-sized homologous chromosomes (1.17 Mb) in clone D11. However, the aCGH analysis showed a 148 kb deletion in one homologous chromosome of clone D11. Since the recombination model proposed by Lima et al., 2013 (Lima et al., 2013) did not foresee a DNA loss, we decided to propose a new model (**Figure 6**), according to which during the cloning process a double-strand break (DSB) occurred in the 1.29 Mb homologous chromosome of the G strain. The break occurred in a region that did not share any homology with the 0.94 Mb homologous chromosome of the G strain. The pairing of homologous chromosomal regions was followed by DNA repair through unequal homologous recombination (HR) *via* break-induced replication (BIR). First, the chromosomal extremity with the DSB recombination annealed with a homologous region of the DNA donor, initiating the replication repair. At the DSB end the strand resection occurred while the other strand invaded the homologous sequence in the intact donor DNA. The repair mechanism generated two homologous chromosomes measuring 1.17 Mb as a result of the addition of a 110 kb region to the donor chromosome.

aCGH Data Validation by qPCR

Quantitative real time PCR (qPCR) was used to validate chromosomal alterations that represent different predicted copy number variations (loss, gain or null) in clone D11 (**Table 1** and **Supplementary Table S4**). Triplicate qPCR

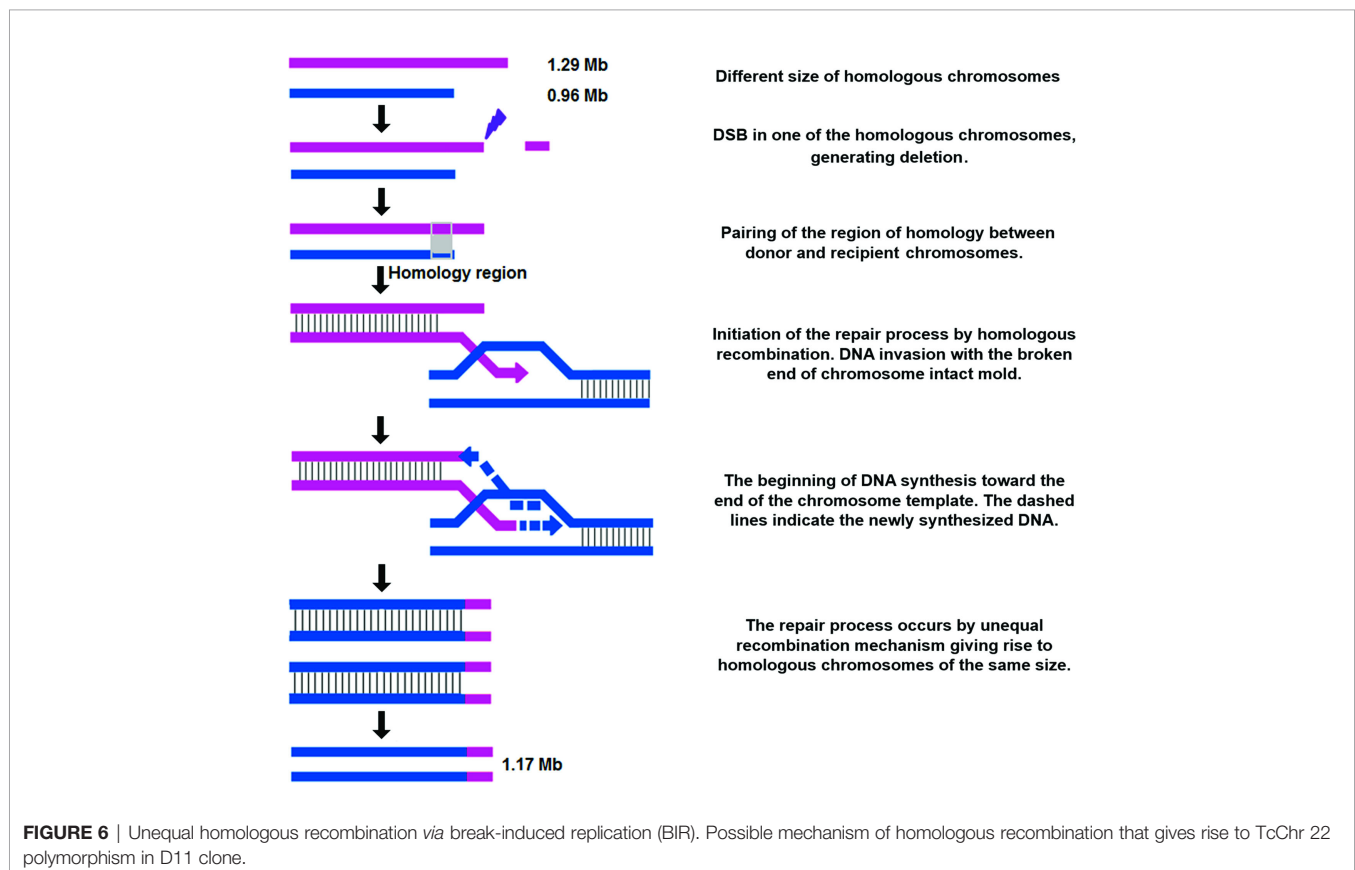


TABLE 1 | Results of quantitative real time PCR analysis for aCGH validation.

TcChr	Alteration			Type*	Validated	Genes		
	Start	End	Frequency			Gene ID	Start	End
6	128524	348838	0,942	loss	no	TcCLB.507603.180	302856	306257
8**			0,026	–	yes	TcCLB.510337.30	146763	148151
12	9715	234335	0,335	gain	yes	TcCLB.503595.10	123806	125734
12	251096	476676	0,528	loss	yes	TcCLB.509573.40	439833	440546
13***	11738	22832	0,202	–	yes	TcCLB.511815.90	200717	202384
13***	379181	475473	0,141	–	yes	TcCLB.511827.50	465082	466506
22	82493	231475	0,311	loss	no	TcCLB.509499.20	118952	120400
22**			0,007	–	yes	TcCLB.504427.170	310344	311150
24	242813	444364	0,203	loss	yes	TcCLB.509123.30	248254	248985

*The minus sign (-) indicates no alteration between parental strain G and clone D11.

**Chromosome region without copy number changes detected by aCGH.

***Chromosome region with copy number changes detected by aCGH.

assays were performed, and the results showed that 7 out of 9 aCGH results (77.7%) were confirmed (**Table 1** and **Supplementary Figure S10**). Two alterations not validated by qPCR correspond to DNA loss and were covered by a large number of probes in the aCGH. These data lead us to suggest that the outcome of aCGH should be considered correct even when it cannot be validated by qPCR.

In our work, the CNV validation rate when we used qPCR was similar to that obtained in mammalian genomes (Li et al., 2012; Wang et al., 2013; Wang et al., 2015; Baldan et al., 2019) observed that the qPCR validation rate is directly related to the number of probes in the region where aCGH detected alterations. They suggested that validation is necessary when the alteration is detected by fewer than 10 probes. Here, two alterations detected by aCGH were not confirmed by qPCR (**Table 1**) but were confirmed by a large number of probes, 257 on chromosome TcChr 22 (TcCLB.509499.20) and 149 on chromosome TcChr 6 (TcCLB.507603.180) (**Supplementary Table S2**). Furthermore, some sequences are known not to amplify in the PCR reaction because Taq polymerase lacks 3'→5' exonuclease activity (Tindall and Kunkel, 1988; Wu et al., 1989). The presence of a mismatch in the last nucleotide at the 3' end of the primer is enough to block the extension of the oligonucleotide by Taq DNA polymerase as there is a lack of 3'→5' exonuclease activity (Wu et al., 1989). It is possible that because of the large size of the probes in aCGH, the chances of finding SNP-type polymorphisms using this technique are higher. This would explain why aCGH is able to detect variants that cannot be detected (amplified) by PCR.

DISCUSSION

Clone D11 is a derived clone of the *T. cruzi* G strain isolated in our laboratory by a limiting dilution method (Santorì, 1991; Lima et al., 2013). The parental G strain was isolated in 1980 from an opossum (*Didelphis marsupialis*) in the Brazilian Amazon (Yoshida, 1983; Yoshida, 2006). Over the years the G strain has shown consistent phenotypic stability for virulence, growth and metacyclogenesis. For instance, the infective metacyclic trypomastigotes display the same profile of cell

surface glycoproteins, as well as the same ability to invade human epithelial cells, which is associated with the expression of cell surface glycoproteins and differential calcium signaling activity (Teixeira and Yoshida, 1986; Mortara et al., 1988; Schenkman et al., 1988; Yoshida et al., 1989; Mortara et al., 1992; Ruiz et al., 1998; Yoshida, 2006; Atayde et al., 2007). Genotyping analysis using 10 different microsatellite loci suggested that the G strain displays a monoclonal population structure (Lima et al., 2013). Clone D11 differs from the parental G strain in five microsatellite loci, suggesting that it might have been generated during the cloning process rather than isolated from a pre-existing mixed population (Lima et al., 2013). On the other hand, we cannot rule out the hypothesis the existence of a multiclonal population structure formed by subpopulations with some differences from the original predominant strain. Taking into account these possibilities, we have assumed that clone D11 is derived from G strain. Here, we designed a high-resolution array based on CLB *in silico* chromosome sequences using the e-array platform from Agilent technologies, Santa Clara, California, USA. The aCGH analysis was performed to compare the chromosomal alterations in the G strain and clone D11, and the CLB genome was used as a reference. The aCGH analysis performed by Minning et al. (2011) highlighted the gene content variability among *T. cruzi* isolates, elucidating the impressive interstrain variation in this parasite. In the present study, we showed intrastrain genetic variability between a clone and its parental strain. We identified a high number of small DNA deletions in clone D11, a finding which is in agreement with previous estimates that the D11 genome (81 Mb) is smaller than the G strain genome (89.8 Mb) (Lima et al., 2013).

Chromosomal alterations (DNA gain or loss) larger than 50 bp between two individuals of the same species are considered the main source of genomic variation (Wang et al., 2015) and are also considered to be an important sources of genetic variation in evolution (Hastings et al., 2009; Anand et al., 2013). Homologous recombination also play a key role to generate genetic exchange and environmental fitness in different organisms and several reports demonstrates homologous recombination also have an important role in *T. cruzi* genetic variability (Chiurillo et al., 2016; Alves et al., 2018). In trypanosomatids, it has been shown that these variations can be due to CNVs that may play an

important role in environmental adaptive response and transcript abundance (De Gaudenzi et al., 2011; Downing et al., 2011; Minning et al., 2011; Sterkers et al., 2012; Real et al., 2013; Reis-Cunha et al., 2015; Belew et al., 2017; Dumetz et al., 2017; Reis-Cunha et al., 2018). Therefore, CNVs can affect not only genomic organization but also gene expression (De Gaudenzi et al., 2011; Reis-Cunha et al., 2015; Belew et al., 2017; Dumetz et al., 2017). Several phenotypic and genotypic differences have been detected between clone D11 and the parental G strain (Mortara, 1991; Santori, 1991; Mortara et al., 1999; Mortara et al., 2005; Lima et al., 2013). For instance, extracellular amastigotes of clone D11 were 10–15% less infective to HeLa cells than those of the G strain (Mortara, 1991; Santori, 1991; Mortara et al., 1999). Although chromosome alterations do not seem to affect the fitness of clone D11, some losses could lead to decreasing virulence, suggesting an adaptive role of chromosome instability. Recently, Dumetz et al. (2017) sequenced the genomes and transcriptomes of *Leishmania donovani* in *in vivo* conditions mimicking the natural vector environment and vertebrate host environment. After passage through the insect vector, karyotype changes and CNVs were detected and correlated with the corresponding transcript levels, confirming the impact of aneuploidy on molecular adaptations and cellular fitness. In *T. cruzi*, Belew et al. (2017) performed a comparative transcriptome analysis of clones CLB and CL-14, both derived from the same parental CL strain of *T. cruzi*. Both clones showed reduced or delayed expression of surface antigen genes, which in clone CL-14 was associated with virulence, as this clone is neither infective nor pathogenic in a murine model.

The identification of chromosomes with large chromosomal alterations (≤ 400 kb) in clone D11 suggests the occurrence of segmental aneuploidy. Although aneuploidy is often considered to be deleterious, some fungi and protozoa seem to benefit from it (Pagès et al., 1989; Sterkers et al., 2011; Sterkers et al., 2012; Hirakawa et al., 2015; Reis-Cunha et al., 2015; Möller et al., 2018; Reis-Cunha et al., 2018). *T. cruzi* is considered to be mainly a diploid organism with different-sized homologous chromosomes, but recent studies have suggested the occurrence of aneuploidy in this parasite (Minning et al., 2011; Reis-Cunha et al., 2015; Reis-Cunha et al., 2018). Our data also suggest that segmental aneuploidy is relatively common in *T. cruzi* and could generate genetic diversity in an organism in which reproduction seems to be predominantly asexual.

The *T. cruzi* genome contains a large number of repetitive sequences (micro and minisatellites, retrotransposons and MGFs) (El-Sayed et al., 2005; Berná et al., 2018; Callejas-Hernández et al., 2018). It has been proposed that the genome is structured in a “core compartment” composed of conserved genes and conserved hypothetical genes, and a nonsyntenic region (“disruptive compartment”) composed of the multigene families TS, MASP and mucins (Berná et al., 2018). Several MGFs (GP63, DGF-1 and RHS) are dispersed throughout both compartments (Berná et al., 2018). These regions of *T. cruzi* rich in repetitive sequences (“disruptive compartments”) could serve as recombination sites for homologous recombination (El-Sayed et al., 2005; Kim et al., 2005; Martins et al., 2008; Bartholomeu

et al., 2009; Moraes Barros et al., 2012; Chiurillo et al., 2016; Talavera-López et al., 2021). Comparison of the gene annotation in altered regions of clone D11 with that of the corresponding regions in CLB indicated an increase in MGFs. When we compared the chromosomal alterations with the gene annotation, we could observe members of MGFs flanking deletions and amplifications in the D11 clone, suggesting that these genes play a role in recombination events. There was an increase in MASP genes and mucin and gp63 in the amplification regions in the D11 clone while in the deletion regions there was a reduction in these genes and an increase in RHS and DGF-1. These results suggest that MGFs may have a role in the homologous recombination, serving as homology site.

Gross chromosome rearrangements in clone D11 were detected by chromoblot hybridization and supported by aCGH. We suggest that mitotic chromosome rearrangements may be explained at molecular and cytological levels by unequal crossing over between sister or homologous chromatids mediated by flanking repeated sequences and unequal homologous recombination *via* break-induced replication. For instance, the rearrangements of chromosomes TcChr12 and TcChr6 may be generated by unequal mitotic crossing over between sister or homologous chromatids which are justified by the rearrangements in chromosomes TcChr12 and TcChr6, respectively. Another mechanism is the unequal HR *via* BIR proposed to explain the TCcr22 rearrangement. Homologous recombination has been demonstrated in *T. cruzi* natural populations and in experimental conditions, in which it mediates the integration of exogenous DNA from the transfection vector into the trypanosome genome (Gaunt et al., 2003; Baptista et al., 2004; Passos-Silva et al., 2010; Ramírez et al., 2013; Chiurillo et al., 2016). One of the best-studied recombination mechanisms is that induced by DNA DSBs (Hastings et al., 2009; Sakofsky et al., 2012; Anand et al., 2013). A DSB is a potentially lethal event that can occur by exposure to ionizing radiation and chemical mutagens, but can also occur spontaneously during DNA replication and segregation (Hastings et al., 2009; Sakofsky et al., 2012; Anand et al., 2013). HR involves the interaction between large homology regions and single strand annealing (SSA), gene conversion or BIR (Hastings et al., 2009; Sakofsky et al., 2012; Anand et al., 2013). The repair occurs by BIR when only one end of a DSB has homology with the donor sequence; one strand is resected, and the other invades the homologous sequence in the intact donor DNA to initiate the repair. BIR repair results in a copy of several kilobases from the donor site and DNA loss.

Accumulating experimental evidence suggests that recombination has driven major genetic alterations in *T. cruzi* (Tibayrenc et al., 1990; Westenberger et al., 2005; de Freitas et al., 2006; Tibayrenc and Ayala, 2013; Berry et al., 2019; Schwabl et al., 2019). Recently, it has been suggested that homologous recombination may play an important role in the dormancy signaling in *T. cruzi*. Sánchez-Valdéz et al. (2018) (Sánchez-Valdéz et al., 2018) described the occurrence of spontaneous dormancy in the amastigote during extended drug exposure in the experimental *T. cruzi* infection. These authors hypothesized

that dormancy could be caused by genetic recombination events in the replicating stages of *T. cruzi* life cycle (Sánchez-Valdéz et al., 2018). Resende et al. (2020) (Resende et al., 2020) demonstrated that homologous recombination plays an important role in the dormancy in *T. cruzi*. They showed that amastigote and epimastigote dormancy is strain-dependent in *T. cruzi* and it is directly correlated with mRNA TcRAD51 levels, a recombination pivot, responsible for strand invasion and search for homology between broken strand and the template (Baumann and West, 1998; Gomes Passos Silva et al., 2018; Resende et al., 2020). Costa-Silva et al. (2021) demonstrated that DNA topoisomerase 3 α (TcTopo3 α) is important for homologous recombination repair and replication stress in *T. cruzi*. TcTopo3 α gene knockout inhibited the amastigote proliferation and a high number of dormant cells was identified. TcTopo3 α knockout parasites treated with methyl methanesulfonate (MMS) showed a slower cell growth and loss their ability to repair damage. Segmental duplication/deletions were associated to the multigene family's regions in the knockout parasites (Costa-Silva et al., 2021).

The genomic changes detected by aCGH suggest the presence of a dynamic genome that responds to environmental stress by varying the number of gene copies and generating segmental aneuploidy.

DATA AVAILABILITY STATEMENT

The original contributions presented in the study are included in the article/**Supplementary Material**. Further inquiries can be directed to the corresponding authors. The raw aCGH data and sequence of probes involved in the aCGH design for *Trypanosoma cruzi* have been deposited into the GenBank GEO database (GSE197870).

AUTHOR CONTRIBUTIONS

Conceived and designed the experiments: MM, JS, DB, and SR. Performed the experiments: DC, MM, FL, JR-C, RC, FM, RV, and AC-M. Analyzed and interpreted the data: MM, DC, and JS. MM and JS wrote the paper with contributions from all authors. All authors read and approved the final manuscript.

FUNDING

This work was supported by the thematic project FAPESP (2016/15000-04) coordinated by Renato Arruda Mortara (RAM), and in this project José Franco da Silveira (JS) participates as deputy coordinator. As recommended by FAPESP, the name of the coordinator must appear together with the process number in the Funding section, as follows: Renato Arruda Mortara (2016/15000-04). AC-M is a postdoctoral fellowship from CAPES/PNPD, Brazil (Coordenação de Aperfeiçoamento de Pessoal de Nível Superior/Programa Nacional de Pós-Doutorado). This study

was also supported by Conselho Nacional de Desenvolvimento Científico e Tecnológico (CNPq), Brazil, as follows: doctoral fellowship for RC (147453/2016-0), postdoctoral fellowship for MM (157637/2015-8) and DC (150526/2017-2) and PQ for JS (306591/2015-4) and DB (309465/2015-0); and in part by CAPES and the Instituto Nacional de Ciência e Tecnologia de Estratégias de Interação Patógeno-Hospedeiro INCT-IPH), CNPq, Fundação à Pesquisa do Estado de Goiás (FAPEG), Brazil.

ACKNOWLEDGMENTS

We would like to thank Dr Yuri Moreira (Agilent Brasil) for his expert advice and technical support for the *T. cruzi*-CGH array, and to Drs Thaise L. Teixeira and Camila M. Yonamine Asanuma for the advice and support in the preparation of the manuscript.

SUPPLEMENTARY MATERIAL

The Supplementary Material for this article can be found online at: <https://www.frontiersin.org/articles/10.3389/fcimb.2022.760830/full#supplementary-material>

Supplementary Figure 1 | Alignment between homologous regions of *T. cruzi* in silico assembled chromosomes of clone CLB (lineage TcVI) and Dm28c (lineage TcI). Pairwise comparisons with ACT (Artemis Comparison Tool) between the chromosomes TcChr4, TcChr6, TcChr8, TcChr12 and TcChr22 ("S" chromosome assigned to the Esmeraldo haplotype and "P" to the non-Esmeraldo haplotype) of the clone CLB and the homologous chromosomes of Dm28c (version 2018). Homologous genes are connected by colored lines. The matches and reverse matches are represented in red and in blue, respectively. Grey blocks represent each chromosome.

Supplementary Figure 2 | The size-class distribution of CNVs identified by aCGH in clone D11. Chromosomal alterations (n=418) were identified in clone D11 by comparison to the parental G strain. On the axes Y and X are shown the number and size (kb) of chromosomal alterations, respectively.

Supplementary Figure 3 | Proportion of total CNVRs length in each *T. cruzi* chromosome that is copy number variable in clone D11. The proportion of chromosome-size alterations (loss or gain) in each chromosome of D11 was determined using the in silico chromosomes of CLB as a reference (Weatherly et al., 2009). Chromosomal alterations identified in clone D11 were mapped on both haplotypes (S, Esmeraldo like and P, Non-Esmeraldo like) on each in silico chromosome of CLB reference genome. The in silico chromosomes of CLB are numbered from 1 to 41, from the smallest TcChr1 (0.77 Mb) to the largest TcChr41 (2.37 Mb). DNA losses or gains are denoted by green and red, respectively. Proportion is on the Y axis.

Supplementary Figure 4 | Schematic representation of the in silico chromosomes TcChr6, TcChr8, TcChr12 and TcChr22 showing the gene annotation and chromosomal alterations detected by aCGH in clone D11. Annotation of multigene families in CLB is shown in light blue and the other genes in black. The CNVs detected by aCGH in the clone D11 are shown on the in silico CLB chromosomes. DNA amplification and deletion are shown in red and green, respectively. S, Esmeraldo- and P, non-Esmeraldo-like.

Supplementary Figure 5 | Gene content in the chromosomal alterations of clone D11. The gene content of amplification and deletion regions of D11 was compared to the gene content of both haplotypes (Esmeraldo and non-Esmeraldo) of the reference genome CLB. The genes annotated in CLB genome were classified into

three groups: Hypothetical - genes encoding hypothetical proteins without assigned function; MGF - multigene families encoding surface proteins, such as, trans-sialidases, MASPs, TcMUC, GP63 and DGF1, and nuclear proteins coded by RHS gene family (retrotransposon hot-spot protein); and others - DNA replication genes, kinases, phosphatases, etc. The CLB gene content was compared with those in the amplification and deletion regions of clone D11 (left).

Supplementary Figure 6 | Schematic representation of the in silico chromosomes of non-Esmeraldo-like haplotype showing the gene annotation and chromosomal alterations detected by aCGH in clone D11. Annotation of multigene families in CLB is shown in light blue and the other genes in black. The CNVs detected by aCGH in the clone D11 are shown on the in silico CLB chromosomes. DNA amplification and deletion are shown in red and green, respectively. The chromosomes and recombination events are shown to scale (Bar=200kb).

Supplementary Figure 7 | Molecular karyotypes of clone D11 and the parental G strain. Panel (A) Chromosomal bands were resolved by PFGE and stained with ethidium bromide. The visualized bands were named using capital letters (21 bands, A – U) (Lima et al., 2013) for clone D11 and Arabic numerals (19 bands, 1 -19) (Souza et al., 2011) for G strain. Panel (B) Schematic representation of the molecular karyotype of clone D11 and G strain showing the molecular weight of each band on the right side of the strip. The thickness of the rectangles represents the thickness of each visualized chromosomal band. C) Raw image showing the pulsed field electrophoresis running gel. Note: The karyotype of D11 and the G strain had already been described by Lima et al., 2013 (Lima et al., 2013). The electrophoretic runs shown in **Figure S7** were performed in the present work. They have included as a **Supplementary Figure** to facilitate the understanding of mapping of aCGH alterations in the chromosomal bands of the G strain and clone D11.

Supplementary Figure 8 | Raw images showing the pulsed field electrophoresis running gels and Southern blot hybridizations from. Upper Panel. Separation of *T. cruzi* chromosomal bands on a pulsed field gel (PFGE). Chromosomal DNA was prepared from *T. cruzi* isolates: clone CL Brener (CLB) used as a reference genome in this study, strain G (parental strain) and clone D11, a single-cell derived of G.

REFERENCES

- Ackermann, A. A., Panunzi, L. G., Cosentino, R. O., Sánchez, D. O., and Agüero, F. (2012). A Genomic Scale Map of Genetic Diversity in *Trypanosoma Cruzi*. *BMC Genomics* 13, 736. doi: 10.1186/1471-2164-13-736
- Alves, C. L., Repolês, B. M., da Silva, M. S., Mendes, I. C., Marin, P. A., Aguiar, P. H. N., et al. (2018). The Recombinase Rad51 Plays a Key Role in Events of Genetic Exchange in *Trypanosoma Cruzi*. *Sci. Rep.* 8, 13335. doi: 10.1038/s41598-018-31541-z
- Anand, R. P., Lovett, S. T., and Haber, J. E. (2013). Break-Induced DNA Replication. *Cold Spring Harb. Perspect. Biol.* 5, a010397–a010397. doi: 10.1101/cshperspect.a010397
- Atayde, V. D., Cortez, M., Souza, R., Silveira, J. F. D., and Yoshida, N. (2007). Expression and Cellular Localization of Molecules of the Gp82 Family in *Trypanosoma Cruzi* Metacyclic Trypomastigotes. *Infect. Immun.* 75, 3264–3270. doi: 10.1128/IAI.00262-07
- Baldan, F., Passon, N., Burra, S., Demori, E., Russo, P. D., and Damante, G. (2019). Quantitative PCR Evaluation of Deletions/Duplications Identified by Array CGH. *Mol. Cell. Probes* 46, 101421. doi: 10.1016/j.mcp.2019.101421
- Baptista, C. S., Vêncio, R. Z., Abdala, S., Valadares, M. P., Martins, C., de Bragança Pereira, C. A., et al. (2004). DNA Microarrays for Comparative Genomics and Analysis of Gene Expression in *Trypanosoma Cruzi*. *Mol. Biochem. Parasitol.* 138, 183–194. doi: 10.1016/j.molbiopara.2004.06.017
- Bartholomeu, D. C., Cerqueira, G. C., Leão, A. C., da Rocha, W. D., Pais, F. S., Macedo, C., et al. (2009). Genomic Organization and Expression Profile of the Mucin-Associated Surface Protein (Masp) Family of the Human Pathogen *Trypanosoma Cruzi*. *Nucleic Acids Res.* 37, 3407–3417. doi: 10.1093/nar/gkp172
- Baumann, P., and West, S. C. (1998). Role of the Human RAD51 Protein in Homologous Recombination and Double-Stranded-Break Repair. *Trends Biochem. Sci.* 23, 247–251. doi: 10.1016/s0968-0004(98)01232-8
- Belew, A. T., Junqueira, C., Rodrigues-Luiz, G. F., Valente, B. M., Oliveira, A. E. R., Polidoro, R. B., et al. (2017). Comparative Transcriptome Profiling of Virulent and non-Virulent *Trypanosoma Cruzi* Underlines the Role of Surface Proteins During Infection. *PLoS Pathog.* 13, 1–23. doi: 10.1371/journal.ppat.1006767
- Berná, L., Rodríguez, M., Chiribao, M. L., Parodi-Talice, A., Pita, S., Rijo, G., et al. (2018). Expanding an Expanded Genome: Long-Read Sequencing of *Trypanosoma Cruzi*. *Microb. Genomics* 4 (5), e000177. doi: 10.1099/mgen.0.000177
- Berry, A. S. F., Salazar-Sánchez, R., Castillo-Neyra, R., Borrini-Mayori, K., Chipana-Ramos, C., Vargas-Maquera, M., et al. (2019). Sexual Reproduction in a Natural *Trypanosoma Cruzi* Population. *PLoS Negl. Trop. Dis.* 13, 1–17. doi: 10.1371/journal.pntd.0007392
- Bradwell, K. R., Koparde, V. N., Matveyev, A. V., Serrano, M. G., Alves, J. M. P., Parikh, H., et al. (2018). Genomic Comparison of *Trypanosoma Conorhini* and *Trypanosoma Rangeli* to *Trypanosoma Cruzi* Strains of High and Low Virulence. *BMC Genomics* 19, 1–20. doi: 10.1186/s12864-018-5112-0
- Brenière, S. F., Araniki, I., Le Ray, D., and Tibayrenc, M. L. (1991). Analyse SDS-PAGE Des Protéines Et Antigènes De Surface Révèle Une Forte Hétérogénéité Chez Les Clones Naturels De *Trypanosoma Cruzi*, Corrélation À La Variabilité Isoenzymatique. *C. R. Acad. Sci. Paris Série III* 312, 449–454.
- Briones, M. R. S., Souto, R. P., Stolf, B. S., and Zingales, B. (1999). The Evolution of Two *Trypanosoma Cruzi* Subgroups Inferred From rRNA Genes can be Correlated With the Interchange of American Mammalian Faunas in the Cenozoic and has Implications to Pathogenicity and Host Specificity. *Mol. Biochem. Parasitol.* 104, 219–232. doi: 10.1016/s0166-6851(99)00155-3
- Callejas-Hernández, F., Rastrojo, A., Poveda, C., Gironès, N., and Fresno, M. (2018). Genomic Assemblies of Newly Sequenced *Trypanosoma Cruzi* Strains Reveal New Genomic Expansion and Greater Complexity. *Sci. Rep.* 8, 1–13. doi: 10.1038/s41598-018-32877-2
- Campos, R. M. F., and Andrade, S. G. (1996). Characterization of Subpopulations (Clones and Subclones) of the 21 SF Strain of *Trypanosoma Cruzi* After Long

- Lasting Maintenance in the Laboratory. *Mem. Inst. Oswaldo Cruz* 91, 795–800. doi: 10.1590/S0074-02761996000600029
- Cano, M. I., Gruber, A., Vazquez, M., Cortés, A., Levin, M. J., González, A., et al. (1995). Molecular Karyotype of Clone CL Brener Chosen for the Trypanosoma Cruzi Genome Project. *Mol. Biochem. Parasitol.* 71, 273–278. doi: 10.1016/0166-6851(95)00066-a
- Carver, T. J., Rutherford, K. M., Berriman, M., Rajandream, M. A., Barrell, B. G., and Parkhill, J. (2005). ACT: The Artemis Comparison Tool. *Bioinform. Oxf. Engl.* 21, 3422–3423. doi: 10.1093/bioinformatics/bti553
- Chiurillo, M. A., Moraes Barros, R. R., Souza, R. T., Marini, M. M., Antonio, C. R., Cortez, D. R., et al. (2016). Subtelomeric I-SceI-Mediated Double-Strand Breaks are Repaired by Homologous Recombination in Trypanosoma Cruzi. *Front. Microbiol.* 7. doi: 10.3389/fmicb.2016.02041
- Costa-Silva, H. M., Resende, B. C., Umaki, A. C. S., Prado, W., da Silva, M. S., Virgilio, S., et al. (2021). DNA Topoisomerase 3 α Is Involved in Homologous Recombination Repair and Replication Stress Response in Trypanosoma Cruzi. *Front. Cell Dev. Biol.* 9, 633195w. doi: 10.3389/fcell.2021.633195
- Coura, J. R., and Viñas, P. A. (2010). Chagas Disease: A New Worldwide Challenge. *Nature* 465, S6–S7. doi: 10.1038/nature09221
- de Freitas, J. M., Augusto-Pinto, L., Pimenta, J. R., Bastos-Rodrigues, L., Gonçalves, V. F., Teixeira, S. M., et al. (2006). Ancestral Genomes, Sex, and the Population Structure of Trypanosoma Cruzi. *PLoS Pathog.* 2, e24. doi: 10.1371/journal.ppat.0020024
- De Gaudenzi, J. G., Noé, G., Campo, V. A., Frasc, A. C., and Cassola, A. (2011). Gene Expression Regulation in Trypanosomatids. *Essays Biochem.* 51, 31–46. doi: 10.1042/bse0510031
- Downing, T., Imamura, H., Decuyper, S., Clark, T. G., Coombs, G. H., Cotton, J. A., et al. (2011). Whole Genome Sequencing of Multiple Leishmania Donovanii Clinical Isolates Provides Insights Into Population Structure and Mechanisms of Drug Resistance. *Genome Res.* 21, 2143–2156. doi: 10.1101/gr.123430.111
- Dumetz, F., Imamura, H., Sanders, M., Seblova, V., Myskova, J., Pescher, P., et al. (2017). Modulation of Aneuploidy in *Leishmania* In Vitro and In Vivo Environments and Its Impact on Gene Expression. *mBio* 8, e00599-17. doi: 10.1128/mBio.00599-17
- Dvorak, J. A., Hartman, D. L., and Miles, M. A. (1980). Trypanosoma Cruzi: Correlation of Growth Kinetics to Zymodeme Type in Clones Derived From Various Sources. *J. Protozool.* 27, 472–474. doi: 10.1111/j.1550-7408.1980.tb05401.x
- El-Sayed, N. M., Myler, P. J., Bartholomeu, D. C., Nilsson, D., Aggarwal, G., Tran, A. N., et al. (2005). The Genome Sequence of Trypanosoma Cruzi, Etiologic Agent of Chagas Disease. *Science* 309, 409–415. doi: 10.1126/science.1112631
- Franzén, O., Ochaya, S., Sherwood, E., Lewis, M. D., Llewellyn, M. S., Miles, M. A., et al. (2011). Shotgun Sequencing Analysis of Trypanosoma Cruzi I Sylvio X10/1 and Comparison With T. Cruzi VI CL Brener. *PLoS Negl. Trop. Dis.* 5, e984. doi: 10.1371/journal.pntd.0000984
- Gaunt, M. W., Yeo, M., Frame, I. A., Stothard, J. R., Carrasco, H. J., Taylor, M. C., et al. (2003). Mechanism of Genetic Exchange in American Trypanosomes. *Nature* 421, 936–939. doi: 10.1038/nature01438
- Goldberg, S. S., and Silva Pereira, A. A. (1983). Enzyme Variation Among Clones of Trypanosoma Cruzi. *J. Parasitol.* 69, 91–96. doi: 10.2307/3281282
- Gomes Passos Silva, D., da Silva Santos, S., Nardelli, S. C., Mendes, I. C., Freire, A. C. G., Repolés, B. M., et al. (2018). The In Vivo and In Vitro Roles of Trypanosoma Cruzi Rad51 in the Repair of DNA Double Strand Breaks and Oxidative Lesions. *PLoS Negl. Trop. Dis.* 12, e0006875. doi: 10.1371/journal.pntd.0006875
- Hastings, P. J., Lupski, J. R., Rosenberg, S. M., and Ira, G. (2009). Mechanisms of Change in Gene Copy Number. *Nat. Rev. Genet.* 10, 551–564. doi: 10.1038/nrg2593
- Henriksson, J., Aslund, L., and Pettersson, U. (1996). Karyotype Variability in Trypanosoma Cruzi. *Parasitol. Today Pers. Ed.* 12, 108–114. doi: 10.1016/0169-4758(96)80670-3
- Hirakawa, M. P., Martinez, D. A., Sakthikumar, S., Anderson, M. Z., Berlin, A., Gujja, S., et al. (2015). Genetic and Phenotypic Intra-Species Variation in Candida Albicans. *Genome Res.* 25, 413–425. doi: 10.1101/gr.174623.114
- Kim, D., Chiurillo, M. A., El-Sayed, N., Jones, K., Santos, M. R., Porcile, P. E., et al. (2005). Telomere and Subtelomere of Trypanosoma Cruzi Chromosomes are Enriched in (Pseudo)Genes of Retrotransposon Hot Spot and Trans-Sialidase-Like Gene Families: The Origins of T. Cruzi Telomeres. *Gene* 346, 153–161. doi: 10.1016/j.gene.2004
- Lima, F. M., Souza, R. T., Santori, F. R., Santos, M. F., Cortez, D. R., Barros, R. M., et al. (2013). Interclonal Variations in the Molecular Karyotype of Trypanosoma Cruzi: Chromosome Rearrangements in a Single Cell-Derived Clone of the G Strain. *PLoS One* 8, e63738. doi: 10.1371/journal.pone.0063738
- Lima, M. F., and Villalta, F. (1989). Trypanosoma Cruzi Trypomastigote Clones Differentially Express a Parasite Cell Adhesion Molecule. *Mol. Biochem. Parasitol.* 33, 159–170. doi: 10.1016/0166-6851(89)90030-3
- Li, Y., Mei, S., Zhang, X., Peng, X., Liu, G., Tao, H., et al. (2012). Identification of Genome-Wide Copy Number Variations Among Diverse Pig Breeds by Array CGH. *BMC Genomics* 13, 725. doi: 10.1186/1471-2164-13-725
- Martins, C., Baptista, C. S., Ienne, S., Cerqueira, G. C., Bartholomeu, D. C., and Zingales, B. (2008). Genomic Organization and Transcription Analysis of the 195-Bp Satellite DNA in Trypanosoma Cruzi. *Mol. Biochem. Parasitol.* 160, 60–64. doi: 10.1016/j.molbiopara.2008.03.004
- McDaniel, J. P., and Dvorak, J. A. (1993). Identification, Isolation, and Characterization of Naturally-Occurring Trypanosoma Cruzi Variants. *Mol. Biochem. Parasitol.* 57, 213–222. doi: 10.1016/0166-6851(93)90197-6
- Minning, T. A., Weatherly, D. B., Flibotte, S., and Tarleton, R. L. (2011). Widespread, Focal Copy Number Variations (CNV) and Whole Chromosome Aneuploidies in Trypanosoma Cruzi Strains Revealed by Array Comparative Genomic Hybridization. *BMC Genomics* 12, 139. doi: 10.1186/1471-2164-12-139
- Möller, M., Habig, M., Freitag, M., and Stukenbrock, E. H. (2018). Extraordinary Genome Instability and Widespread Chromosome Rearrangements During Vegetative Growth. *Genet. Soc. Am.* 210, 517–529. doi: 10.1534/genetics.118.301050
- Moraes Barros, R. R., Marini, M. M., Antônio, C. R., Cortez, D. R., Miyake, A. M., Lima, F. M., et al. (2012). Anatomy and Evolution of Telomeric and Subtelomeric Regions in the Human Protozoan Parasite Trypanosoma Cruzi. *BMC Genomics* 13, 229. doi: 10.1186/1471-2164-13-229
- Morel, C., Chiari, E., Camargo, E. P., Mattei, D. M., Romanha, A. J., and Simpson, L. (1980). Strains and Clones of Trypanosoma Cruzi can be Characterized by Pattern of Restriction Endonuclease Products of Kinetoplast DNA Minicircles. *Proc. Natl. Acad. Sci. U. S. A.* 77, 6810–6814. doi: 10.1073/pnas.77.11.6810
- Mortara, R. A. (1991). Trypanosoma Cruzi: Amastigotes and Trypomastigotes Interact With Different Structures on the Surface of HeLa Cells. *Exp. Parasitol.* 73, 1–14. doi: 10.1016/0014-4894(91)90002-e
- Mortara, R. A., Andreoli, W. K., Taniwaki, N. N., Fernandes, A. B., Silva, C. V., Fernandes, M. C., et al. (2005). Mammalian Cell Invasion and Intracellular Trafficking by Trypanosoma Cruzi Infective Forms. *Acad. Bras. Cienc.* 77, 77–94. doi: 10.1590/s0001-37652005000100006
- Mortara, R. A., Araguth, M. F., and Yoshida, N. (1988). Reactivity of Stage-Specific Monoclonal Antibody 1G7 With Metacyclic Trypomastigotes of Trypanosoma Cruzi Strains: Lytic Property and 90 000 Mol. Wt Surface Antigen Polymorphism. *Parasite Immunol.* 10, 369–378. doi: 10.1111/j.1365-3024.1988.tb00227.x
- Mortara, R. A., da Silva, S. D., Araguth, M. F., Blanco, S. A., and Yoshida, N. (1992). Polymorphism of the 35- and 50-Kilodalton Surface Glycoconjugates of Trypanosoma Cruzi Metacyclic Trypomastigotes. *Infect. Immun.* 60, 4673–4678. doi: 10.1128/iai.60.11.4673-4678.1992
- Mortara, R. A., Procópio, D. O., Barros, H. C., Verbisck, N. V., Andreoli, W. K., Silva, R. B., et al. (1999). Features of Host Cell Invasion by Different Infective Forms of Trypanosoma Cruzi. *Mem. Inst. Oswaldo Cruz* 94, 135–137. doi: 10.1590/s0074-02761999000700014
- Pagès, M., Bastien, P., Veas, F., Rossi, V., Bellis, M., Wincker, P., et al. (1989). Chromosome Size and Number Polymorphisms in Leishmania Infantum Suggest Amplification/Deletion and Possible Genetic Exchange. *Mol. Biochem. Parasitol.* 36, 161–168. doi: 10.1016/0166-6851(89)90188-6
- Passos-Silva, D. G., Rajão, M. A., Nascimento de Aguiar, P. H., Vieira-da-Rocha, J. P., and Machado, C. R. (2010). Furtado C. Overview of DNA Repair in Trypanosoma Cruzi, Trypanosoma Brucei, and Leishmania Major. *J. Nucleic Acids* 2010, 840768. doi: 10.4061/2010/840768
- Porcile, P. E., Santos, M. R., Souza, R. T., Verbisck, N. V., Brandão, A., Urmenyi, T., et al. (2003). A Refined Molecular Karyotype for the Reference Strain of the Trypanosoma Cruzi Genome Project (Clone CL Brener) by Assignment of Chromosome Markers. *Gene* 308, 53–65. doi: 10.1016/s0378-1119(03)00489-x
- Postan, M., Dvorak, J. A., and McDaniel, J. (1983). P. Studies of Trypanosoma Cruzi Clones in Inbred Mice I - A Comparison of Course of Infections of C3H/

- HEN Mice With Two Clones Isolated on a Common Source. *Am. J. Trop. Med. Hyg.* 32, 497–506. doi: 10.4269/ajtmh.1983.32.497
- Quinlan, A. R., and Hall, I. M. (2010). BEDTools: A Flexible Suite of Utilities for Comparing Genomic Features. *Bioinformatics* 26 (6), 841–842. doi: 10.1093/bioinformatics/btq033
- Ramírez, J., Tapia-Calle, G., and Guhl, F. (2013). Genetic Structure of *Trypanosoma Cruzi* in Colombia Revealed by a High-Throughput Nuclear Multilocus Sequence Typing (nMLST) Approach. *BMC Genet.* 14, 96. doi: 10.1186/1471-2156-14-96
- Real, F., Vidal, R. O., Carazzolle, M. F., Mondego, J. M., Costa, G. G., Herai, R. H., et al. (2013). The Genome Sequence of *Leishmania (Leishmania) Amazonensis*: Functional Annotation and Extended Analysis of Gene Models. *DNA Res. Int. J. Rapid Publ. Rep. Genes Genomes* 20, 567–581. doi: 10.1093/dnares/dst031
- Reis-Cunha, J. L., Baptista, R. P., Rodrigues-Luiz, G. F., Coqueiro-Dos-Santos, A., Valdivia, H. O., de Almeida, L. V., et al. (2018). Whole Genome Sequencing of *Trypanosoma Cruzi* Field Isolates Reveals Extensive Genomic Variability and Complex Aneuploidy Patterns Within TcII DTU. *BMC Genomics* 19, 816. doi: 10.1186/s12864-018-5198-4
- Reis-Cunha, J. L., Rodrigues-Luiz, G. F., Valdivia, H. O., Baptista, R. P., Mendes, T. A., de Moraes, G. L., et al. (2015). Chromosomal Copy Number Variation Reveals Differential Levels of Genomic Plasticity in Distinct *Trypanosoma Cruzi* Strains. *BMC Genomics* 16, 499. doi: 10.1186/s12864-015-1680-4
- Resende, B. C., Oliveira, A. C. S., Guañabens, A. C. P., Repolés, B. M., Santana, V., Hiraiwa, P. M., et al. (2020). The Influence of Recombinational Processes to Induce Dormancy in *Trypanosoma Cruzi*. *Front. Cell. Infect. Microbiol.* 28. doi: 10.3389/fcimb.2020.00005
- Ruiz, R. C., Favoreto, S. Jr., Dorta, M. L., Oshiro, M. E., Ferreira, A. T., Manque, P. M., et al. (1998). Infectivity of *Trypanosoma Cruzi* Strains is Associated With Differential Expression of Surface Glycoproteins With Differential Ca²⁺ Signalling Activity. *Biochem. J.* 330, 505–511. doi: 10.1042/bj3300505
- Sakofsky, C. J., Ayyar, S., and Malkova, A. (2012). Break-Induced Replication and Genome Stability. *Biomolecules* 2, 483–504. doi: 10.3390/biom2040483
- Sánchez-Valdéz, F. J., Padilla, A., Wang, W., Orr, D., and Tarleton, R. L. (2018). Spontaneous Dormancy Protects *Trypanosoma Cruzi* During Extended Drug Exposure. *Elife* 7, e34039. doi: 10.7554/eLife.34039
- Santorì, F. R. (1991). *Characterization and Production of Staphylomastigotes of Trypanosoma Cruzi Strain G*. São Paulo: Universidade Federal de São Paulo.
- Santos, M. R., Lorenzi, H., Porcile, P., Carmo, M. S., Schijman, A., Brandão, A., et al. (1999). Physical Mapping of a 670-Kb Region of Chromosomes XVI and XVII From the Human Protozoan Parasite *Trypanosoma Cruzi* Encompassing the Genes for Two Immunodominant Antigens. *Genome Res.* 9, 1268–1276. doi: 10.1101/gr.9.12.1268
- Schenkman, S., Yoshida, N., and Cardoso de Almeida, M. L. (1988). Glycophosphatidylinositol-Anchored Proteins in Metacyclic Trypomastigotes of *Trypanosoma Cruzi*. *Mol. Biochem. Parasitol.* 29, 141–151. doi: 10.1016/0166-6851(88)90069-2
- Schwabl, P., Imamura, H., Van den Broeck, F., Costales, J. A., Maiguashca-Sánchez, J., Miles, M. A., et al. (2019). Meiotic Sex in Chagas Disease Parasite *Trypanosoma Cruzi*. *Nat. Commun.* 10 (1), 3972. doi: 10.1038/s41467-019-11771-z
- Seco-Hidalgo, V., De Pablos, L. M., and Osuna, A. (2015). Transcriptional and Phenotypic Heterogeneity of *Trypanosoma Cruzi* Cell Populations. *Open Biol.* 5 (12), 150190. doi: 10.1098/rsob.150190
- Souza, R. T., Lima, F. M., Barros, R. M., Cortez, D. R., Santos, M. F., Cordero, E. M., et al. (2011). Genome Size, Karyotype Polymorphism and Chromosomal Evolution in *Trypanosoma Cruzi*. *PloS One* 6, e23042. doi: 10.1371/journal.pone.0023042
- Sterkers, Y., Lachaud, L., Bourgeois, N., Crobu, L., Bastien, P., and Pagès, M. (2012). Novel Insights Into Genome Plasticity in Eukaryotes: Mosaic Aneuploidy in *Leishmania*. *Mol. Microbiol.* 86, 15–23. doi: 10.1111/j.1365-2958.2012.08185.x
- Sterkers, Y., Lachaud, L., Crobu, L., Bastien, P., and Pagès, M. (2011). FISH Analysis Reveals Aneuploidy and Continual Generation of Chromosomal Mosaicism in *Leishmania Major*. *Cell. Microbiol.* 13, 274–283. doi: 10.1111/j.1462-5822.2010.01534.x
- Talavera-López, C., Messenger, L. A., Lewis, M. D., Yeo, M., Reis-Cunha, J. L., Matos, G. M., et al. (2021). Repeat-Driven Generation of Antigenic Diversity in a Major Human Pathogen, *Trypanosoma Cruzi*. *Front. Cell Infect. Microbiol.* 11, 614665. doi: 10.3389/fcimb.2021.614665
- Teixeira, M. M. G., and Yoshida, N. (1986). Stage-Specific Surface Antigens of Metacyclic Trypomastigotes of *Trypanosoma Cruzi* Identified by Monoclonal Antibodies. *Mol. Biochem. Parasitol.* 18, 271–282. doi: 10.1016/0166-6851(86)90085-x
- Tibayrenc, M., and Ayala, F. J. (2013). How Clonal are *Trypanosoma* and *Leishmania*? *Trends Parasitol.* 29, 264–269. doi: 10.1016/j.pt.2013.03.007
- Tibayrenc, M., Kjellberg, F., and Ayala, F. J. (1990). A Clonal Theory of Parasitic Protozoa: The Population Structures of *Entamoeba*, *Giardia*, *Leishmania*, *Naegleria*, *Plasmodium*, *Trichomonas*, and *Trypanosoma* and Their Medical and Taxonomical Consequences. *Proc. Natl. Acad. Sci. U. S. A.* 87, 2414–2418. doi: 10.1073/pnas.87.7.2414
- Tindall, K. R., and Kunkel, T. A. (1988). Fidelity of DNA Synthesis by the *Thermus Aquaticus* DNA Polymerase. *Biochemistry* 27, 6008–6013. doi: 10.1021/bi00416a027
- Wang, R., Carter, J., and Lench, N. (2013). Evaluation of Real-Time Quantitative PCR as a Standard Cytogenetic Diagnostic Tool for Confirmation of Microarray (aCGH) Results and Determination of Inheritance. *Genet. Test. Mol. Biomark.* 17, 821–825. doi: 10.1089/gtmb.2013.0284
- Wang, J., Jiang, J., Wang, H., Kang, H., Zhang, Q., and Liu, J. F. (2015). Improved Detection and Characterization of Copy Number Variations Among Diverse Pig Breeds by Array CGH. *G3 Genes Genomes Genet.* 5, 1253–1261. doi: 10.1534/g3.115.018473
- Weatherly, D. B., Boehlke, C., and Tarleton, R. L. (2009). Chromosome Level Assembly of the Hybrid *Trypanosoma Cruzi* Genome. *BMC Genomics* 10, 255. doi: 10.1186/1471-2164-10-255
- Westenberger, S. J., Barnabé, C., Campbell, D. A., and Sturm, N. R. (2005). Two Hybridization Events Define the Population Structure of *Trypanosoma Cruzi*. *Genetics* 171, 527–543. doi: 10.1534/genetics.104.038745
- WHO (2021) *Chagas Disease (American Trypanosomiasis)* (WHO). Available at: [https://www.who.int/news-room/fact-sheets/detail/chagas-disease-\(american-trypanosomiasis\)](https://www.who.int/news-room/fact-sheets/detail/chagas-disease-(american-trypanosomiasis)) (Accessed July 20, 2021).
- Wu, D. Y., Ugozzoli, L., Pal, B. K., and Wallace, R. B. (1989). Allele-Specific Enzymatic Amplification of β -Globin Genomic DNA for Diagnosis of Sickle Cell Anemia. *Proc. Natl. Acad. Sci. U. S. A.* 86, 2757–2760. doi: 10.1073/pnas.86.8.2757
- Yoshida, N. (1983). Surface Antigens of Metacyclic Trypomastigotes of *Trypanosoma Cruzi*. *Infect. Immun.* 40, 836–839. doi: 10.1128/iai.40.2.836-839.1983
- Yoshida, N. (2006). Molecular Basis of Mammalian Cell Invasion by *Trypanosoma Cruzi*. *Acad. Bras. Cienc.* 78, 87–111. doi: 10.1590/s0001-37652006000100010
- Yoshida, N., Mortara, R. A., Araguth, M. F., Gonzalez, J. C., and Russo, M. (1989). Metacyclic Neutralizing Effect of Monoclonal Antibody 10D8 Directed to the 35- and 50-Kilodalton Surface Glycoconjugates of *Trypanosoma Cruzi*. *Infect. Immun.* 57, 1663–1667. doi: 10.1128/iai.57.6.1663-1667.1989
- Zingales, B., Andrade, S. G., Briones, M. R., Campbell, D. A., Chiari, E., Fernandes, O., et al. (2009). A New Consensus for *Trypanosoma Cruzi* Intraspecific Nomenclature: Second Revision Meeting Recommends TcI to TcVI. *Mem. Inst. Oswaldo Cruz* 104, 1051–1054. doi: 10.1590/s0074-02762009000700021
- Zingales, B., Miles, M. A., Campbell, D. A., Tibayrenc, M., Macedo, A. M., Teixeira, M. M., et al. (2012). The Revised *Trypanosoma Cruzi* Subspecific Nomenclature: Rationale, Epidemiological Relevance and Research Applications. *Infect. Genet. Evol. J. Mol. Epidemiol. Evol. Genet. Infect. Dis.* 12, 240–253. doi: 10.1016/j.meegid.2011.12.009
- Zingales, B., Pereira, M. E., Oliveira, R. P., Almeida, K. A., Umezawa, E. S., Souto, R. P., et al. (1997). *Trypanosoma Cruzi* Genome Project: Biological Characteristics and Molecular Typing of Clone CL Brener. *Acta Trop.* 68, 159–175. doi: 10.1016/s0001-706x(97)00088-0

Conflict of Interest: The authors declare that the research was conducted in the absence of any commercial or financial relationships that could be construed as a potential conflict of interest.

Publisher's Note: All claims expressed in this article are solely those of the authors and do not necessarily represent those of their affiliated organizations, or those of

the publisher, the editors and the reviewers. Any product that may be evaluated in this article, or claim that may be made by its manufacturer, is not guaranteed or endorsed by the publisher.

Copyright © 2022 Cortez, Lima, Reis-Cunha, Bartholomeu, Villacis, Rogatto, Costa-Martins, Marchiano, do Carmo, da Silveira and Marini. This is an open-

access article distributed under the terms of the Creative Commons Attribution License (CC BY). The use, distribution or reproduction in other forums is permitted, provided the original author(s) and the copyright owner(s) are credited and that the original publication in this journal is cited, in accordance with accepted academic practice. No use, distribution or reproduction is permitted which does not comply with these terms.

Advantages of publishing in Frontiers



OPEN ACCESS

Articles are free to read
for greatest visibility
and readership



FAST PUBLICATION

Around 90 days
from submission
to decision



HIGH QUALITY PEER-REVIEW

Rigorous, collaborative,
and constructive
peer-review



TRANSPARENT PEER-REVIEW

Editors and reviewers
acknowledged by name
on published articles

Frontiers

Avenue du Tribunal-Fédéral 34
1005 Lausanne | Switzerland

Visit us: www.frontiersin.org

Contact us: frontiersin.org/about/contact



REPRODUCIBILITY OF RESEARCH

Support open data
and methods to enhance
research reproducibility



DIGITAL PUBLISHING

Articles designed
for optimal readership
across devices



FOLLOW US

@frontiersin



IMPACT METRICS

Advanced article metrics
track visibility across
digital media



EXTENSIVE PROMOTION

Marketing
and promotion
of impactful research



LOOP RESEARCH NETWORK

Our network
increases your
article's readership